

https://dspace.org/

Study of bismuth chemistry toward medicinal applications

Billing, Caren

2012-09-12
http://hdl.handle.net/10539/11938

Downloaded from a DSpace repository. https://dspace.org/

Study of bismuth chemistry toward medicinal applications

by

Caren Billing

A thesis submitted in fulfillment of the requirements for the degree of Doctor of Philosophy to the Faculty of Science, University of the Witwatersrand, Johannesburg.

January 2012

DECLARATION

I declare that this thesis is my own, unaided work. It is being submitted for the Degree of Doctor of Philosophy in the University of the Witwatersrand, Johannesburg. It has not been submitted before for any degree or examination in any other University.

_____

(Signature of Candidate)

_____ day of _____ 2012

ABSTRACT

The use of bismuth in medicinal applications has been limited despite the many promising indications of its effectiveness in treatments for a large number of ailments. This is predominantly due to the lack of understanding of bismuth chemistry, including thermodynamic and kinetic aspects, thus hindering the design of improved drugs. This, in turn, is due to the difficulty in studying the complex chemistry of this element.

Bismuth undergoes hydrolysis from below pH 1 and forms precipitates around pH 2 already, thus has to be studied from low pH. The most commonly used technique to determine stability constants, namely glass electrode potentiometry, cannot be employed in very acidic solutions. Complex formation has previously been studied by polarography where potential shifts and changes in current are used to determine solution species and evaluate stability constants. The benefits of employing polarography here are that low bismuth concentrations can be used to postpone precipitation and it can be used across the pH range. However, the diffusion junction potential becomes significant below pH 2 and changes with pH.

Protocols to determine the stability of bismuth complexes using polarography were developed in this study. Firstly, the junction potential cannot be measured directly, so a witness metal ion was introduced into the solution to monitor its magnitude with changing pH. For this thallium (I) was used as it does not readily undergo complexation and hence potential shifts observed with changing pH is due to changes in the junction potential. This process was successfully tested on the cadmium(II)-picolinic acid system. Secondly, it was suggested that the reduction of bismuth(III) is quasi-reversible, so mechanisms of determining the reversible reduction potentials were investigated using the copper(II)-picolinic acid system, as copper(II) has a reduction potential almost identical to bismuth(III) and its reduction is also quasi-reversible. However, it was found that bismuth was reversibly reduced under the polarographic conditions employed. Thirdly, the free bismuth(III) potential had to be

determined in order to calculate potential shifts due to complex formation. This potential cannot be measured directly either, so procedures were developed to determine this value by accounting for both hydrolysis and complex formation with the background electrolyte anion (nitrate). Three bismuth-ligand systems were studied where the ligands were picolinic acid, dipicolinic acid and quinolinic acid. It was necessary to determine the stability constants for these systems by using a combination of direct polarographic data interpretation and the use of virtual potentiometry.

ACKNOWLEDGEMENTS

I thank my supervisor, Prof Ignacy Cukrowski, for his guidance, support and patience throughout my project, as well as the hours spent throwing ideas around.

I also thank my co-supervisor, Prof Helder Marques, for stepping in when requested and spending his holiday proof reading my thesis.

I thank the School of Chemistry and the University of the Witwatersrand for providing me the opportunity to pursue my studies on a part-time basis.

I thank the NRF for their financial support to purchase equipment and for running expenses, without which I would not have been able to complete my degree.

I thank my family, friends and colleagues for their support. In particular, I thank my husband, Dave, for his constant encouragement and willing assistance.

"*After climbing a great hill, one only finds that there are many more hills to climb*."

Nelson Mandela

PUBLICATIONS AND PRESENTATIONS

PUBLICATIONS:

- The crystal structures of two novel cadmium-picolinic acid complexes in relation to the solution species.
  C. Billing, D.C. Levendis, V. Vieira, S. Afr. J. Chem., 64 (2011) 38
- Glass electrode calibration for use in the voltammetric determination of stability constants under extreme acidic conditions
  C. Billing and I. Cukrowski, S. Afr. J. Chem., 62 (2009) 168

CONFERENCES AND SPECIALIST MEETINGS:

- Development of Methodologies to Study Complex Formation with Troublesome Bismuth(III). (Poster)
  By C. Billing and I. Cukrowski
  40th South African Chemical Institute Convention incorporating the 15th Inorganic Conference and the 3rd Federation of African Societies of Chemistry Congress, Johannesburg, 16-21 January 2011
- Use and abuse of glass electrodes in metal ligand equilibria studies. (Poster)
  By C. Billing and I. Cukrowski
  1st International Symposium on Electrochemistry, Cape Town, 9-11 July 2008
- Metal-ligand equilibria studies using polarography. (Oral)
  By C. Billing
  Metrohm Workshop, Johannesburg, 31 May 2007
- Compensation for diffusion junction potentials in complex formation studies by polarography at very low pH values. (Poster)
  By C. Billing and I. Cukrowski
  37th International Conference of Coordination Chemistry, Cape Town, 13-18 Aug 2006

- Compensation for diffusion junction potentials in complex formation studies by polarography at very low pH values. (Oral)
  By C. Billing and I. Cukrowski
  37th National Convention of the South African Chemical Institute, Pretoria, 4-9 July 2004

TABLE OF CONTENTS

Abstract ii
Acknowledgements iv
Publications and Presentations v
Table of Contents vii
List of Figures xii
List of Tables xxi
List of Abbreviations and Symbols xxv

CHAPTER 1: Introduction
1.1) Literature Review 1
1.1.1) Bismuth in medicinal preparations 1
1.1.2) Biochemistry of bismuth 5
1.1.3) Chemistry of bismuth 9
1.1.4) Stability constants 12
1.1.5) Polarography for stability constant determination 14
1.2) Problem Identification and Project Aims 17
1.3) References 20

CHAPTER 2: Experimental
2.1) Introduction 25
2.2) Reagents 28
2.3) Equipment 30
2.4) Experiments 34
2.4.1) GE calibration procedure using strong acid-strong base titration 34
2.4.2) GE calibration procedure using inert solution titration 37
2.4.3) Polarographic measurements 38
2.4.4) Experiments for the determination of stability constants 40
2.5) Processing of Polarographic Data 43
2.5.1) Parameter determination from fitting polarograms 43
2.5.2) Determination of formation constants 46
2.5.3) Virtual potentiometry 50

2.6) References 52

CHAPTER 3: Calibration of the Glass Electrode at Low pH

3.1) Introduction 54
3.1.1) pH and the glass electrode 54
3.1.2) Calibrating the glass electrode for metal-ligand equilibria studies 60
3.2) Aims 68
3.3) Results and Discussion 69
3.3.1) Strong acid-strong base titrations 69
3.3.2) Evaluation of GE performance 85
3.3.3) Alternative approaches to strong acid-strong base titrations 90
3.3.4) Titration of an inert electrolyte 93
3.3.5) Type of hydroxide solution 95
3.3.6) Type of acid 97
3.3.7) Impact of accuracy of pH measurements 97
3.4) Conclusions 100
3.5) References 102

CHAPTER 4: The Diffusion Junction Potential

4.1) Introduction 105
4.1.1) Ion mobilities 105
4.1.2) Diffusion junction potentials 111
4.2) Aims 122
4.3) Results and Discussion 122
4.3.1) Preliminary calculations and measurements 122
4.3.2) Polarographic measurements 131
4.4) Conclusions 141
4.5) References 143

CHAPTER 5: Ligands

5.1) Introduction 145
5.2) Protonation of the ligands 147
5.3) Electrochemical behaviour of the ligands 157

5.3.1) Aims 158
5.3.2) Results and Discussion 158
5.4) Conclusions 163
5.5) References 165

CHAPTER 6: Accounting for the Diffusion Junction Potential – Application to the Cadmium(II) Picolinic Acid System

6.1) Introduction 169
6.2) Aims 172
6.3) Results and Discussion 173
6.3.1) Background electrolyte 173
6.3.2) Fitting polarograms 176
6.3.3) pH Titration – Metal ions only 177
6.3.4) Predicting the free metal ion potential 184
6.3.5) Modelling the half-wave potential data 185
6.3.6) Comparison of models 190
6.3.7) Recommended procedure for modelling the potential data 195
6.3.8) pH titrations: Using the model to evaluate formation constants 196
4.3.9) Ligand titrations 210
6.3.10) Evaluating errors in stability constants caused by errors in junction potential correction 217
6.4) Conclusions 219
6.5) References 221

CHAPTER 7: The Study of Copper(II) Complex Formation with Picolinic Acid – A Quasi-Reversible System

7.1) Introduction 222
7.1.1) Complex formation of Cu(II) with picolinic acid 222
7.1.2) Reduction of Cu(II) 223
7.1.3) Quasi-reversibility 225
7.2) Aims 230
7.3) Results and Discussion 231
7.3.1) Background electrolyte 231
7.3.2) Determining reversible half-wave potentials from quasi-

reversible polarograms 232
7.3.3) Modelling the difference in the half-wave potential for pH titrations in the absence of ligand 238
7.3.4) pH titrations: Using the model to evaluate formation constants 240
7.3.5) Ligand titrations 243
7.4) Conclusions 246
7.5) References 247

CHAPTER 8: The Hydrolysis of Bismuth and the Determination of the Free Bismuth(III) Potential

8.1) Introduction 249
8.1.1) Bismuth(III) hydrolysis 249
8.1.2) Polarographic reduction of bismuth(III) 257
8.2) Aims 260
8.3) Results and Discussion 261
8.3.1) Effects of Bi(III) hydrolysis on polarographic pH titration data 261
8.3.2) Predicting Bi(III) hydroxide formation constants 273
8.3.3) Determining the free Bi(III) potential 279
8.3.4) Aside on Bi(III) hydrolysis 293
8.4) Conclusions 294
8.5) References 296

CHAPTER 9: Complex Formation Studies with Bismuth

9.1) Introduction 298
9.1.1) Electrospray Ionisation-Mass Spectrometry (ESI-MS) 298
9.2) Aims 299
9.3) Results and Discussion 299
9.3.1) Bi(III)-picolinic acid complexes 300
9.3.2) Bi(III)-dipicolinic acid complexes 327
9.3.3) Tl(I)-dipicolinic acid complexes 336
9.3.3) Bi(III)-quinolinic acid complexes 338
9.3.4) Comparison of Bi(III) pyridinecarboxylic acid systems 347
9.4) Conclusions 349
9.5) References 352

CHAPTER 10: Concluding Summary 354

APPENDICES 360

LIST OF FIGURES

1.1) Correlations between log K_1 values for polydentate ligands (DFB and citrate) and log $K_1(OH^-)$ for the metal ions. The estimate for Bi^{3+} is based on log $K(BiOH^{2+})$ = 12.4.

1.2) Distribution of hardness and softness in the periodic table as a function of the donor atom of a ligand according to the HSAB theory.

2.1) Illustration of current maxima. The solid line is an undistorted DC_{TAST} wave and the dashed and dotted lines give examples of the superimposed current maximum of (a) the first and (b) the second kind.

2.2) Schematic diagram of the automated polarographic and potentiometric experimental setup.

2.3) Photograph of the polarographic cell.

2.4) Potential versus time graph representing the DC polarographic parameters used.

2.5) Polarograms in 0.5 M HNO_3 before and after deoxgenation and after Bi(III) (~5 $\times 10^{-5}$ M) and Tl(I) (~1 $\times 10^{-4}$ M) were added to the deoxygenated solution.

3.1) Schematic diagram of an example of a combined glass electrode.

3.2) Schematic diagram of the structure of lithium silicate glass.

3.3) Titration curve for a 0.5 M HNO_3–NaOH titration and the associated buffer values.

3.4) Comparison of (a) the acidic and (b) the basic regions of calibration graphs obtained from HNO_3–NaOH titrations with different concentrations of solutions where [HNO_3] = [NaOH] within a titration and μ = 0.5 M.

3.5) Data showing deviations from linearity when smaller increments of base were added closer to the equivalence point during a 0.5 M HNO_3–NaOH titration.

3.6) Calculated *Ej* values for the junction between 3 M KCl and test solutions of varying composition as would be obtained from HNO_3–NaOH/KOH titrations.

3.7) Comparison of measured CGE potentials and that corrected for junction potentials using calculated *Ej* values. Linear functions were fitted across the entire pH range.

3.8) pH ranges used to calculate linear calibrations. A: All experimental points. B: pH regions according to that found in titrations where the base solution was added at 0.5 mL increments throughout. C: Deleted experimental points above pH 0.6 and below pH 12.8. D: Recommended pH ranges.

3.9) The very acidic region of a CGE calibration showing the departure of the quadratic function from the linear relationship which was extrapolated to lower pH values for comparison.

3.10) Differences in the separate linear correlations for the acid and base regions for a 0.5 M HNO_3–NaOH calibration using a new CGE.

3.11) The (a) acidic and (b) basic regions of the CGE calibration curves (from the titration of 0.5 M HNO_3 by KOH) using different titration procedures.

3.12) Comparison of the variation in ionic strength as a function of pH for the two titration procedures in Figure 3.11.

3.13) Calibration graphs from the titration of 0.5 M $NaNO_3$ by (a) 0.5 M HNO_3 or (b) 0.5 M NaOH. Data points deviating from linearity were omitted when the fitting the linear function as indicated.

3.14) Comparison of the calibrations in the acid and basic regions for the 0.5 M HNO_3–NaOH/KOH titrations.

4.1) Illustration of the "proton jump" mechanism for (a) the H^+ ion and (b) the OH^- ion.

4.2) The limiting ionic conductivity versus the charge-to-radius ratio plot used to estimate the limiting mobility of Bi^{3+}. The radii quoted are the octahedral ionic radii.

4.3) Junction potentials calculated with respect to time between about 0.1 M and 0.05 M NaCl solutions at different Δt values by Hafemann.

4.4) Junction potentials calculated with respect to time between a) 0.5 M, b) 0.05 M, c) 0.005 M and d) 0.0005 M $CaCl_2$ solutions and a 0.1 M KCl solution for a porous plug junction by Sokalski and Lewenstam.

4.5) Comparison of E_j values calculated using the Henderson and Planck equations for the boundary between a test solution and 0.5 M KNO_3 or $NaNO_3$ salt bridge solution. The test solution consisted of 0.5 M HNO_3 after various additions of 0.5 M KOH or NaOH, respectively.

4.6) Comparison of E_j values using the Henderson and Planck equations for the boundary between a test solution and 3 M KCl reference solution. The test solution consists of 0.5 M HNO_3 after various additions of 0.5 M KOH or NaOH.

4.7) Junction potentials calculated using the Henderson equation for the boundary between a test solution and 0.5 M or 1 M KOH salt bridge solution. The test solution consists of 0.5 M HNO_3 after various additions of 0.5 M KOH.

4.8) Comparison of E_j values calculated using the Henderson equation employing either limiting ion conductivities or ion conductivities for the particular ionic strength of the solution.

4.9) Schematic diagram of the continuous flow salt bridge.

4.10) Polarograms showing the reduction of Tl(I): 2.00×10^{-4} M at pH 0.3 and ~1×10^{-4} M at pH 3, and the polarogram in 0.5 M HNO_3 only.

4.11) Polarogram for 2.00×10^{-4} M Tl(I) in 0.5 M HNO_3 fitted using equation 2.14, where the background current is given by equation 4.15. The separate functions are also shown.

4.12) Polarogram for ~1×10^{-4} M Tl(I) in a nitrate solution at pH 3 fitted using equation 2.14, where the background current is a straight line. The separate functions are shown.

4.13) Comparison of experimental diffusion limited currents and those calculated taking dilution into account for the titration of 2.00×10^{-4} M Tl(I) in 0.5 M HNO_3 by 0.5 M NaOH.

4.14) The half-wave potentials as a function of pH where the free Tl(I) potential is indicated by the solid red line.

4.15) Experimentally determined diffusion junction potentials as a function of pH from data in Figure 4.14 and the calculated values using the Henderson equation and the limiting ion mobilities. These calculated values were then amended by subtracting 2.71 mV at each pH.

4.16) Plot as for Figure 4.15 including the amended junction potentials calculated using the Henderson equation and the ion mobilities at 0.1 M and 0.5 M ionic strengths.

4.17) Experimentally determined diffusion junction potentials, for five data sets, as a function of pH. The amended calculated values using the Henderson equation and ion mobilities at different ionic strengths as given in Figure 4.16 are included.

4.18) The difference between the experimentally determined and calculated E_js using limiting ion mobilities for the five data sets in Figure 4.17. The standard deviation for each data set was calculated with respect to these calculated values.

5.1) Structural formulae of the ligands studied in their neutral form.

5.2) Scheme showing equilibria of an aqueous solution of PA.

5.3) Percentage protonation of PA as a function of pH at 25 °C and 0.5 M ionic strength.

5.4) The zwitterion for PA.

5.5) Scheme showing equilibria of an aqueous solution of DPA.

5.6) Percentage protonation of DPA as a function of pH where the value of log K_3 is excluded from or included in the model as 1.36 or 0.49.

5.7) Percentage protonation of QA as a function of pH where the value of log K_3 is excluded from or included in the model.

5.8) Zwitterion of the H_2L form of QA indicating the O–H···O hydrogen bond.

5.9) Polarograms of (i) 0.5 M HNO_3 background solution, (ii) about 1×10^{-5} M Bi(III) and 2×10^{-5} M Tl(I) in 0.5 M HNO_3 and (iii) ligand added to the metal ion solution as indicated.

5.10) DC polarograms recorded at indicated pH values (amended by addition of 0.5 M NaOH) for (a) 9.0×10^{-4} M PA and (b) 3.4×10^{-4} M DPA.

5.11) Cyclic voltammograms at two scan rates for DPA solutions at (i) pH 0.38 (0.5 M HNO_3) and (ii) pH 1.5 (pH adjusted using 0.5 M NaOH).

5.12) DC polarograms of solutions containing about 1×10^{-5} M Bi(III) and 2×10^{-3} M (a) QA or (b) DPA with pH ranging from pH 1.3 to pH 2.8 in steps of about 0.1 pH units.

6.1) Structural representation and ball and stick diagram of $[Cd(NO_3)_2(C_5H_4NCO_2Et)_2]$.

6.2) Structural representation and ball and stick diagram of $[Cd_2(C_5H_4NCO_2)_4]$.

6.3) Coordination modes of picolinate established crystallographically up to 2007 and the Harris notation that describes these modes.

6.4) Species distribution diagrams for (a) Cd(II) and (b) Tl(I) in an aqueous nitrate solution at 25 °C and μ = 1.0 M.

6.5) Diffusion limited current versus pH for Cd(II) and Tl(I) reduction. The dashed lines represent the expected currents when taking dilution into account.

6.6) The half-wave potentials for the reduction of Cd(II) and Tl(I) as a function of pH.

6.7) The half-wave potentials for Cd(II) and the amended values for Tl(I) as a function of pH to highlight the discrepancies in the lowest pH region.

6.8) Fitting data points in a $E_{1/2}$ versus pH curve for Cd(II). An exponential function (—) and a third order polynomial (—) together with a horizontal line were used and the corresponding $E(Cd_{free})$ values are indicated.

6.9) Anomalous trends in the $E_{1/2}$ values for one experiment. The predicted $E_{1/2}$ values are also shown for comparison.

6.10) Comparisons of experimental and predicted $E_{1/2}$ values for Cd(II) and Tl(I) for a different data set.

6.11) Sixth order polynomial fitted to the combined experimentally determined $E_{1/2}(Cd) - E_{1/2}(Tl)$ values as a function of pH. Above pH 3.1, $\Delta E_{1/2}$ was set to −121.4 mV.

6.12) Comparison of the $\Delta E_{1/2}$ versus pH models when using experimental or fitted $E_{1/2}$ values.

6.13) Comparison of the ΔE_j versus pH models when using experimental or fitted $E_{1/2}$ values.

6.14) Comparison of the normalised $\Delta E_{1/2}$ values versus pH models when using experimental or fitted $E_{1/2}$ values and where the normalisation factor is $\Delta E(M_{free})$.

6.15) Comparison of the difference between the normalised $E_{1/2}$ values versus pH models when using experimental or fitted $E_{1/2}$ values.

6.16) Comparison of the experimental and predicted $E_{1/2}(Cd)$ values for one data set using the mConst model and the experimental $E_{1/2}(Tl)$ data.

6.17) Comparison of the experimental and predicted $E_{1/2}(Cd)$ values when applying the mE model and using the three different sixth order polynomials derived from raw or fitted data.

6.18) Tl(I) half-wave potentials as a function of pH indicating no complex formation in a solution with $[PA_T]:[Tl_T] = 50$ and $[L_T] = 0.01003$ M.

6.19) Cd(II) half-wave potentials before and after accounting for the junction potentials. The predicted $E_{1/2}$ values and $E(Cd_{free})$, calculated using the Tl(I) data, are also indicated.

6.20) Experimental currents for the reduction of Cd(II) in the presence of PA and currents expected if no complexation took place. The quotient of these gives the corrected currents.

6.21) ECFC indicating the main region of constant slope as well as the predominant ligand species in solution in various pH ranges.

6.22) ECFC and CCFCs for the two proposed Cd(II)-PA systems.

6.23) The acidic region showing the ECFC and CCFCs in the presence and absence of CdHL. The inset shows the difference between these two calculated curves.

6.24) Species distribution diagram determined using the log β values derived in this work as given in Table 6.11. The CdLH species was both included and excluded.

6.25) ORTEP diagram for the structure $[Cd(NO_3)_2(C_5H_4NHCO_2)(H_2O)_2]$.

6.26) Slight erratic behaviour is seen for Tl(I) half-wave potentials as a function of pH, where $[PA_T]:[Tl(II)_T] = 100$.

6.27) Experimental and corrected $E_{1/2}$ values for Cd(II) where Tl(I) data were used to correct these values in the E_j region only or throughout the entire pH region.

6.28) Variation of the Tl(I) half-wave potentials as a function of pH probably due to the reference system.

6.29) Experimental and corrected Cd(II) $E_{1/2}$ values as a function of pH.

6.30) The ECFCs and CCFCs for the experimental and corrected potential shift data. The inset highlights the acidic region indicating the presence of the CdHL species for the corrected data.

6.31) Comparison of ECFCs for the three titration experiments. The inset highlights the region where CdHL formation would occur.

6.32) Plots of the ECFC showing the slope analysis for three of the ligand titrations at the indicated pH values.

6.33) Representations of species distribution diagrams at the pHs indicated showing the effect of increasing the concentration of PA resulting in [PA]:[Cd] varying from 10 to 200.

6.34) Representation of the species distribution diagram to show the predicted the solution species at pH 2.0 in a ligand titration where [PA]:[Cd] varies from 10 to 200.

6.35) ECFC for the ligand titration at pH 2.0. Various CCFCs were calculated and the log β values are denoted next to the species type.

6.36) Species distribution diagram for the hypothetical metal-ligand system.

7.1) Examples of DC waves showing reversible, quasi-reversible and irreversible electron transfer processes. In all cases the number of electrons transferred is the same. $E^r_{1/2}$, $E^i_{1/2}$ and $E^q_{1/2}$ refer to the reversible, irreversible and quasi-reversible $E_{1/2}$ values, respectively.

7.2) Species distribution diagram for Cu(II) in an aqueous nitrate solution at 25 °C. Precipitation of $Cu(OH)_2$ was predicted using log K_{sp} of −18.9.

7.3) Polarograms for the reduction of Cu(II) and Tl(I) in a nitrate medium at pH 0.25 and 3.28.

7.4) The value of δ illustrating the change in the electron transfer rate for the reduction of Cu(II) in a nitrate background in the absence or presence of PA (where [PA]:[Cu(II)] = 103) as a function of pH.

7.5) Polarogram for the reduction of Cu(II) at pH 1.51. The polarogram was fitted using the DC wave equation through all points or only though the points indicated by ○ and fixing $\delta = 1$ to estimate $E^r_{1/2}$.

7.6) Comparison of $E^q_{1/2}$ and $E^r_{1/2}$ (using the procedure by Cukrowski and Zhang[19]) and the predicted $E_{1/2}$ values (using calculated E_j values and $E(Cu_{free})$ for the reversible potentials).

7.7) Comparison of $E^q_{1/2}$(○), $E^r_{1/2}$ from fitting equation 7.14 and $E^i_{1/2}$ from fitting equation 7.15. The predicted trend in $E_{1/2}$ was calculated as before.

7.8) Log analysis showing two possible asymptotes that could be extrapolated to determine $E^r_{1/2}$. The DC wave with subtracted background current is also displayed.

7.9) Fifth order polynomial fitted to the combined experimentally determined $E_{1/2}(Cu) - E_{1/2}(Tl)$ values as a function of pH. Above pH 2.7, $\Delta E_{1/2}$ was set to 487.7 mV.

7.10) $E^r_{1/2}$ values before and after accounting for E_j for a pH titration with $[PA]_T$:$[Cu(II)]_T$ = 103. The values of $E^q_{1/2}$ *and* $E(Cu_{free})$ are also shown, as well as the predicted $E_{1/2}$ values in the absence of ligand.

7.11) The ECFC and CCFC calculated for the ML and ML_2 species. ($[PA]_T$:$[Cu(II)]_T$ = 103).

7.12) Comparison of the ECFCs and CCFCs for the three ligand-to-metal concentration ratio experiments.

7.13) Species distribution diagrams for aqueous solutions of Cu(II)-PA using the average log β values and [Cu(II)] = 1×10^{-4} M.

7.14) ECFCs and CCFCs for the three ligand titrations at the indicated pHs. The slopes in various regions are also displayed.

7.15) Structure of CuL_2 showing its square-planar arrangement.

8.1) Cuboctahedral structure of $Bi_6(OH)_{12}^{6+}$.

8.2) The aqueous solution equilibria of Bi(III) where A denotes the anion nitrate, perchlorate or chloride.

8.3) The pBi′-pH diagrams for bismuth in the presence of (a) 1 M nitrate and (b) 1 M perchlorate at 23.0 °C as present by Kragten *et al*. The regions of predominance of species above the precipitation regions were calculated using equilibrium constants.

8.4) Plot of log(solubility of $BiONO_3$) in nitric acid solutions at 25 °C as given by Smith and Swinehart and Garrett.

8.5) Stereodiagram of the structure of $Bi_6O_4(OH)_4^{6+}$ by Sundvall. Ellipsoids are scaled to include 50% probability and solid lines between Bi atoms do not indicate bonding.

8.6) Polarograms showing the reduction Bi(III) and Tl(I) in 0.5 M HNO_3. Data points are given as circles and functions are given by the solid lines. The crosses are data points that were deleted in fitting the Bi(III) wave.

8.7) Species distribution diagram for [Bi(III)] = 5×10^{-5} M assuming both $Bi(OH)_2^+$ and $Bi_6(OH)_{12}^{6+}$ are present or only $Bi(OH)_2^+$ is in solution. (Log β values at 25 °C and 0.5 M ionic strength were used).

8.8) Species distribution diagram for [Bi(III)] = 1×10^{-5} M, determined with all possible Bi(III)-hydroxide species included in the model. (Log β values at 25 °C and 0.5 M ionic strength were used).

8.9) Species distribution diagrams for Bi(III) nitrate and hydroxide species with $[NO_3^-]$ = 0.5 M and [Bi(III)] = (a) 5×10^{-5} M or (b) 1×10^{-5} M. (Log β values at 25 °C and 0.5 M ionic strength were used).

8.10) PXRD pattern of the bismuth-oxy-nitrate precipitate formed.

8.11) The value of δ versus pH for the reduction of Bi(III) in a H/$NaNO_3$ solution.

8.12) The change in the diffusion limited currents during a pH titration experiment where initial concentrations of Bi(III) and Tl(I) were 4.99×10^{-5} M and 9.99×10^{-5} M respectively.

8.13) Half-wave potentials versus pH for the reduction of Bi(III) and Tl(I).

8.14) Reduction potentials of Bi(III) (initially at 4.99×10^{-5} M) as a function of pH. Potential shifts due to E_j and $Bi(OH)^{2+}$ formation (using log β = 12.4 or 11.6) were compensated for.

8.15) $U\{Bi(OH)_y\}$ plotted as a function of y using values given in Table 8.5. The trendline was fitted by omitting the value at y = 3.

8.16) $U\{Bi(OH)_y\}$ plotted as a function of y for several trivalent metal ions at 0 M ionic strength and 25 °C. Trendlines were fitted by omitting the value at y = 3.

8.17) Plot of log β_{xy} against y using data in Table 8.7.

8.18) (a) $E_{1/2}$ values of Bi(III) reduction as a function of pH. Potential shifts due to the E_j and ΔE due to $Bi(OH)^{2+}$ and $Bi(OH)_2^+$ in the presence of nitrate, or ΔE due to $Bi(OH)^{2+}$, $Bi(OH)_2^+$ and Bi(III) nitrate species, were compensated for. Initial [Bi(III)] = 4.99×10^{-5} M. (b) Species distribution diagram for the corresponding pH region with $[NO_3^-]$ = 0.5 M and [Bi(III)] = 5×10^{-5} M.

8.19) Polarograms collected directly after Bi(III) addition and again after the specified waiting times for solutions at pH 1.52 and 2.11.

8.20) Compensated reduction potentials of Bi(III) as a function of pH (initial [Bi(III)] = 5×10^{-5} M) for experiments with 20 and 30 minute time intervals.

8.21) Polarograms showing oxygen contamination after 2 mL of 0.5 M KOH was added to a 9.97×10^{-6} M Bi(III) deoxygenated solution at pH 0.3.

8.22) Values of (a) i_d, (b) $E_{1/2}$ and (c) δ or α all plotted as a function of pH obtained by fitting polarograms with the DC wave equation or the Ružić equation (where i_d calculated or fixed). Initial [Bi(III)] = 9.97×10^{-6} M.

8.23) The effect of including or omitting data points that showed the most curvature due to mercury oxidation on the calculated background current and the polarographic parameters.

8.24) (a) $E_{1/2}$ values of Bi(III) reduction as a function of pH. Potential shifts due to the E_j and ΔE due to $Bi(OH)^{2+}$ and $Bi(OH)_2^{+}$ in the presence of nitrate, or ΔE due to $Bi(OH)^{2+}$, $Bi(OH)_2^{+}$ and Bi(III) nitrate species, were compensated for. Initial [Bi(III)] = 9.97×10^{-6} M. (b) Species distribution diagram for the corresponding pH region with $[NO_3^-]$ = 0.5 M and [Bi(III)] = 1×10^{-5} M.

9.1) Differences in the compensated $E_{1/2}$ values when using the two methods indicated to determine E_j. The calculated values of $E(Bi_{free})$ and $E(Bi_{free})_{OH}$ are also plotted. $([PA]_T:[Bi(III)]_T = 197)$.

9.2) Polarograms at pH 0.30 (where [Bi(III)] = 1×10^{-5} M) before and after the addition of PA ([PA] = 2×10^{-3} M), where $[PA]_T:[Bi(III)]_T = 197$. The $E_{1/2}$ values indicate a shift of 1.65 mV.

9.3) $E_{1/2}$ values corrected for E_j (as in Figure 9.1) overlayed with the species distribution diagram (as in Figure 8.9(b)). $E(Bi_{free})$ and $E(Bi_{free})_{OH}$ are also plotted.

9.4) Slope analysis of the ECFC calculated using $E(Bi_{free})_{OH}$, where $[PA]_T:[Bi(III)]_T$ = 197. Specific slopes are highlighted and the pH regions for the predominant forms of the ligand are indicated.

9.5) The ECFC, calculated using $E(Bi_{free})_{OH}$, is plotted with various CCFCs determined by including the species indicated in the models ($[PA]_T:[Bi(III)]_T$ = 197).

9.6) The ECFC, calculated using $E(Bi_{free})$, is plotted with the CCFCs determined by including the species indicated in the models ($[PA]_T:[Bi(III)]_T = 197$).

9.7) The ECFCs (calculated using $E(Bi_{free})$) and CCFCs for the three ligand-to-metal concentration ratio experiments. The species included in the calculating the CCFC are indicated.

9.8) The low pH range is highlighted for the ECFC calculated using $E(Bi_{free})$ and the CCFCs determined by including the species indicated in the models. The ECFC calculated using $E(Bi_{free})_{OH}$ is also shown.

9.9) Species distribution diagrams for aqueous solutions of Bi(III)-PA using the two sets of averaged log β values in Table 9.2. (a) [Bi(III)] = 1×10^{-5} M and [PA] = 2×10^{-3} M and (b) including the $Bi(NO_3)_x^{(3-x)}$ species (where x = 1 – 4) with $[NO_3^-]$ = 0.5 M.

9.10) Structures of two Bi(III) picolinic acid complexes showing (a) a BiL_3 and (b) a BiL_4 arrangement.

9.11) Packing diagram of the BiL_3 arrangement in Figure 9.10(a).

9.12) Species distribution diagrams are compared for aqueous solutions of Bi(III)-PA for species models including and excluding ML_4 and the pH of the solutions measured by ESI-MS are indicated. Log β values in Tables 9.2 and 9.5 were used and [Bi(III)] = 1×10^{-4} M and $[PA]_T:[Bi(III)]_T = 100$.

9.13) Mass spectra for (a) negative and (b) positive ions in a solution containing 10^{-4} M Bi(III) and 10^{-2} M PA at pH 4.0.

9.14) Mass spectra for (a) negative and (b) positive ions in a solution containing 10^{-4} M Bi(III) and 10^{-2} M PA at pH 6.9.

9.15) The ECFC, calculated using $E(Bi_{free})$, is plotted with various CCFC's determined using the species indicated ($[PA]_T$:$[Bi(III)]_T$ = 197).

9.16) Species distribution diagrams for aqueous solutions of Bi(III)-PA using log β values in Table 9.6 and $[PA]_T$:$[Bi(III)]_T$ = 100. (a) Values for the two models determined using $E(Bi_{free})$ are compared and [Bi(III)] = 1×10^{-5} M. (b) Values determined by Cukrowski *et al.*[11] are compared for two Bi(III) concentrations.

9.17) The expected and measured currents for the reduction of Bi(III) in the presence PA ($[PA]_T$:$[Bi(III)]_T$ = 197). The normalised current is the ratio of the measured-to-expected currents.

9.18) Experimental data at low pH values analysed by Cukrowski *et al.*

9.19) The virtual potential plotted against log [M_{free}] showing the trend lines fitted only through the linear data points (for data calculated using $E(Bi_{free})$).

9.20) The polarogram at pH 0.30 was for a solution containing total Bi(III), Tl(I) and DPA having concentrations of about 1×10^{-5} M, 2×10^{-5} M and 1.09×10^{-3} M respectively. After 24.84 mL of KOH was added, the polarogram at pH 4.13 was collected.

9.21) The $E_{1/2}$ values for the reduction of Tl(I) in the presence DPA as a function of pH. $[DPA]_T$:$[Tl(I)]_T$ = 27.

9.22) The discrepancy between the measured and expected diffusion limited currents for the reduction of Bi(III) in the presence DPA ($[DPA]_T$:$[Bi(III)]_T$ = 53). The normalised currents are also plotted.

9.23) Slope analysis of the corrected potential shifts for Bi(III) reduction in the presence DPA ($[DPA]_T$:$[Bi(III)]_T$ = 53). The pH regions for the predominant forms of the ligand are also indicated.

9.24) The ECFC and two different CCFCs calculated using the species indicated ($[DPA]_T$:$[Bi(III)]_T$ = 53).

9.25) Species distribution diagrams for aqueous solutions of Bi(III)-DPA using average log β values in Table 9.10 and [Bi(III)] = 1×10^{-5} M and [DPA] = 1×10^{-3} M. The two possible models are illustrated: including ML_3OH or ML_2OH.

9.26) Two structures showing the ML_2 arrangement for Bi(III)-DPA.

9.27) Structure showing the ML_3 arrangement for Cd(II) with DPA.

9.28) Slope analysis of the corrected potential shifts for Tl(I) reduction in the presence DPA ($[DPA]_T$:$[Tl(I)]_T$ = 40). The CCFC (—) is also shown.

9.29) Structure showing the MLH arrangement for Tl(I) with DPA.

9.30) Species distribution diagrams for aqueous solutions of Tl(I)-DPA using average log β values in Table 9.12 and [Tl(III)] = 2×10^{-5} M and [DPA] = 1×10^{-3} M, where MHL was included or excluded.

9.31) Polarograms at pH 0.30 (where [Bi(III)] = 1×10^{-5} M) before and after the addition of QA, where $[QA]_T$:$[Bi(III)]_T$ = 75. The $E_{1/2}$ values indicate a shift of 2.24 mV.

9.32) Slope analysis for the reduction of Bi(III) in the presence QA ($[QA]_T$:$[Bi(III)]_T$ = 102). The pH regions for the predominant forms of the ligand are indicated.

9.33) The ECFC (calculated using $E(Bi_{free})$) and three different CCFCs calculated using the species indicated ($[QA]_T$:$[Bi(III)]_T$ = 102).

9.34) The ECFCs (calculated using $E(Bi_{free})$) and CCFCs for the three QA-to-Bi(III) concentration ratio experiments using the species model indicated.

9.35) Species distribution diagrams for $[QA]_T$:[Bi(III)] = 100 and [Bi(III)] = 1×10^{-5} M using average log β values in Table 9.14(a). The models including $ML_2(OH)$ or ML_3 and $ML_3(OH)$ are compared.

9.36) The normalised currents, as calculated from the measured and expected i_d values, for the reduction of Bi(III) in the presence QA ($[QA]_T$:$[Bi(III)]_T$ = 102) showing deviations from unity above pH 4.

9.37) Structures showing coordination of QA with (a) nickel in a M_2L arrangement, (b) zinc in a $M(HL)_2$ arrangement and (c) manganese showing the $M(HL)_3$ arrangement.

9.38) The virtual potential plotted against log [M_{free}] showing the trend lines fitted only through the linear data points (for data calculated using $E(Bi_{free})$).

9.39) Species distribution diagram for $[QA]_T$:[Bi(III)] = 100, [Bi(III)] = 1×10^{-5} M and $[NO_3^-]$ = 0.5. Average log β values ML_2 and $ML_2(OH)$ are from Table 9.14(a) and that for ML and MLH are from Table 9.15(b).

9.40) LFER for log β_1(Bi(III)) versus log β_1(Pb(II)) for the three pyridine-carboxylic acid ligands.

LIST OF TABLES

1.1) Structural formulae of various compounds mentioned in this chapter.

2.1) List of reagents used together with the supplier and the manufacturer's assay.

2.2) Metrohm GE characteristics.

2.3) Predicted slopes of the ECFC for the reduction of a dominant solution species for a pH titration experiment. The metal ion is divalent and the prevalent form of the ligand is H_2L.

2.4) Predicted slopes of the ECFC for the reduction of a dominant solution species for a ligand titration experiment. The metal ion is divalent and the prevalent form of the ligand is H_2L.

3.1) Table of pK_w values at different temperatures and ionic strengths.

3.2) pH ranges in which data were collected in HNO_3–NaOH titrations using different concentrations of solutions, but where $[HNO_3] = [NaOH]$ within a titration.

3.3) (a) Linear calibration parameters obtained from data in Figure 3.4 and (b) calculated pH values using these parameters at selected potential values.

3.4) Comparison of pH values calculated using linear parameters derived from fitting data in selected pH ranges to investigate the effect of E_j and alkaline errors in the very acidic and basic regions.

3.5) (a) Linear calibration parameters from data in different pH ranges and (b) calculated pH values using these parameters at selected potential values.

3.6) Calculated pH values at selected potential values in the very acidic region using the quadratic function and linear calibrations presented in Table 3.5(a).

3.7) Comparison of slopes (in mV/pH unit) calculated separately from data in the basic and acidic regions for GE1 and GE2.

3.8) Suggested criteria of the GE performance and suitability for M-L equilibria studies at low pH. Slopes apply to data obtained from a 0.5 M H^+–OH^- titration.

4.1) Limiting ion conductivities and calculated corresponding limiting ion mobilities in water at 25 °C.

4.2) Limiting ion conductivities (in mS m^2 mol^{-1}) in water at 0, 25 and 100 °C. Ratios of these values at different temperatures were also calculated.

4.3) Limiting ion mobilities (in 10^{-8} m^2 s^{-1} V^{-1}) in water at 25 °C and the mobilities calculated using the Onsager limiting law for solutions of ionic strength 0.1 M and 0.5 M. The ratio of mobility in 0.1 M solutions to limiting mobility was also calculated.

5.1) Stepwise protonation constants as log K values for PA in aqueous solutions at 25 °C.

5.2) Stepwise protonation constants (given as log K values) for pyridine-**x**-carboxylic acids at 0.5 M ionic strength and 25 °C. Values given in brackets are uncertain.

5.3) Stepwise protonation constants (as log *K* values) for DPA in aqueous solutions at 25 °C.

5.4) Stepwise protonation constants (given as log *K* values) for QA in aqueous solutions at 25 °C.

5.5) Stepwise protonation constants (given as log *K* values) for (a) pyridine-x,y-dicarboxylic acids at 0.5 M ionic strength and 25 °C and (b) benzene-x,y-dicarboxylic acids at 0.5 M ionic strength and 25 °C. Values given in brackets are uncertain.

6.1) Formation constants, as log β values, for Cd(II) PA species.

6.2) Formation constants, as log β values, for Cd(II) nitrate species at 25 °C.

6.3) Formation constants for Tl(I) species at 25 °C and μ = 1 M.

6.4) Formation constants for Cd(II) and Tl(I) hydroxide species at 25 °C and μ = 3.0 M.

6.5) Half-wave potentials for the reduction of Cu(II), Tl(I) and Cd(II) in 0.50 M and 0.25 M KNO_3 at 25 °C. The standard deviations were calculated from only two data sets.

6.6) Free metal ion potentials for Cd(II) and Tl(I) from pH titration experiments in the absence of ligand.

6.7) Key to names for the models used.

6.8) Table of R^2 values for the various sixth order polynomial models.

6.9) Standard deviations between experimental and predicted $E_{1/2}(Cd)$ values for the $E_{1/2}$ versus pH plots. $E_{1/2}(Cd)$ values were predicted using experimental $E_{1/2}(Tl)$ data and the models derived from (a) experimental and (b) fitted potential data.

6.10) Predicted slopes (in mV per pH unit) of potential versus pH data for the corresponding reduction reactions.

6.11) Formation constants as determined here and from literature. The standard deviations quoted were determined from the mathematical refinement procedure.

6.12) Stability constants using Cd(II) potential data that had been corrected using the mE model and the Tl(I) potential data in either the E_j pH region only or the entire pH range data.

6.13) Stability constants quoted as logβ values using experimental half-wave potentials and potentials corrected using Tl(I) data.

6.14) Log β values for the two proposed Cd(II)-PA systems where CdHL is (a) excluded or (b) included. Processes for the correction of potential data are indicted in each case.

6.15) Average log β values for the two proposed Cd(II)-PA systems.

6.16) Predicted slopes (in mV per log unit) of potential versus log [L_{free}] data for the corresponding reduction reactions.

6.17) Log β values obtained from the ligand titrations at the specified pHs.

7.1) Stability constants for Cu(II)-PA complexes at 25°C as given by the NIST database.

7.2) Formation constants, as log β values, for Cu(II) hydroxide and nitrate species at 25 °C.

7.3) Free metal ion potentials for Cu(II) and Tl(I) from pH titration experiments in the absence of ligand.

7.4) Predicted slopes (in mV per pH unit) of potential versus pH data for the corresponding reduction reactions.

7.5) Log β values for the indicated equilibria at 25 °C and ionic strength between 0.25 and 0.5 M.

7.6) Predicted slopes (in mV per log unit) of potential versus log [L_{free}] data for possible reduction reactions.

7.7) Log β values for the given equilibria at 25 °C and ionic strength between 0.25 and 0.5 M.

8.1) Table of log K values for Bi(III) hydrolysis products at 25 °C.

8.2) Table of log β values for Bi(III) nitrate and chloride species at 25 °C.

8.3) The log K_{SO} values (where K_{SO} is the solubility product) used to calculate the boundary lines in Figures 3(a) and (b).

8.4) Rate constants (k_e) at 20 °C for the reduction of various metal ions from aqueous solution to an amalgam in various supporting electrolytes.

8.5) Experimental log β_{1y} values (at 25 °C and ionic strengths of 0.1 M or 1.0 M) and the calculated log β^*_{1y} and $U\{Bi(OH)_y\}$ values.

8.6) Calculated $U\{Bi(OH)_y\}$, log β^*_{1y} and log β_{1y} values at 0 M ionic strength using the electronegativity of Bi^{3+}. The experimental and recalculated log β_{1y} values for 0 M ionic strength are also given.

8.7) Calculated and literature values for log β_{xy} at 0.1 M and 0.5 M ionic strengths.

8.8) Approximate pHs for the onset of the precipitation of bismuth-oxy-nitrate species for titration experiments with varying time intervals between hydroxide addition and polarographic data collection. (Initial [Bi(III)] = 5×10^{-5} M).

8.9) The free metal ion potentials for Bi(III) and Tl(I) and their difference for titration experiments with varying time intervals. $\Delta E(M_{free})_{OH} = E(Bi_{free})_{OH} - E(Tl_{free})$.

8.10) $\Delta E(M_{free})$ values for titration experiments with initial [Bi(III)] = 9.97×10^{-6} M, where $\Delta E(M_{free})_{OH} = E(Bi_{free})_{OH} - E(Tl_{free})$ and $\Delta E(M_{free}) = E(Bi_{free}) - E(Tl_{free})$.

9.1) Predicted slopes (in mV per pH unit) of potential versus pH data for the corresponding reduction reactions.

9.2) Log β values determined using $E(Bi_{free})$ and $E(Bi_{free})_{OH}$ for the given equilibria, where L = PA, at 25 °C and ionic strength between 0.25 and 0.5 M.

9.3) Assignment of the peaks in the mass spectra in Figure 9.13.

9.4) Assignment of the peaks in the mass spectra in Figure 9.14.

9.5) Log β values determined using $E(Bi_{free})$ and $E(Bi_{free})_{OH}$ for the given equilibria (including BiL_4^-), where L = PA, at 25 °C and ionic strength between 0.25 and 0.5 M.

9.6) Average log β values at 25°C for the proposed equilibria, where L = PA, for this work (0.25 - 0.5 M (K,H)NO_3) and that determined by Cukrowski *et al.* (0.5 M (Na,H)NO_3*).

9.7) The percentage of the corrected potential shift at each step due to the current term, and the values used to calculate it, in the pH range where the measured i_d dropped unexpectedly.

9.8) Log β values for the given equilibria obtained from virtual potentiometry, where L = PA, at 25 °C and ionic strength between 0.25 and 0.5 M.

9.9) Predicted slopes (in mV per pH unit) of potential versus pH data for the corresponding reduction reactions

9.10) Log β values for the given equilibria, where L = DPA, at 25 ^{o}C and ionic strength between 0.25 and 0.5 M. Only one of the $BiL_x(OH)$ species are present, but it is unclear which one.

9.11) Variation in the log β value for ML and the overall fit of the CCFC as the value of log K_3 was changed using data where $[DPA]_T$:$[Bi(III)]_T$ = 80.

9.12) Log β values for the given equilibria with Tl(I), where L = DPA, at 25 ^{o}C and ionic strength between 0.25 and 0.5 M.

9.13) Predicted slopes (in mV per pH unit) of potential versus pH data for the corresponding reduction reactions.

9.14) Table of log β values determined using $E(Bi_{free})$ and $E(Bi_{free})_{OH}$ for the given equilibria, where L = QA, at 25 ^{o}C and ionic strength between 0.25 and 0.5 M.

9.15) Log β values for the given equilibria obtained from virtual potentiometry, where L = QA, at 25 °C and ionic strength between 0.25 and 0.5 M.

9.16) Comparison of log β values for complexation of Bi(III) by the three ligands, PA, QA and DPA at 25 °C and ionic strength between 0.25 and 0.5 M. Charges in equilibria are omitted as they vary depending on L.

LIST OF ABBREVIATIONS AND SYMBOLS

ABBREVIATIONS

AC	-	alternating current
BSI	-	British Standards Institution
BSS	-	bismuth subsalicylate
CBS	-	colloidal bismuth subcitrate
CCFC	-	calculated complex formation curve
CGE	-	combination glass electrode
CE	-	counter electrode
DC	-	direct current
DCP	-	direct current polarography
DME	-	dropping mercury electrode
DPA	-	dipicolinic acid
DPP	-	differential pulse polarography
ECFC	-	experimental complex formation curve
emf	-	electromotive force
ESI-MS	-	electrospray ionisation mass spectrometry
GE	-	glass electrode
GEP	-	glass electrode potentiometry
GUI	-	graphical user interface
IR	-	infra red
ISE	-	ion selective electrode
IUPAC	-	International Union of Pure and Applied Chemistry
LFER	-	linear free energy relationship
MT	-	metallothionein
NIST	-	National Institute of Standards and Technology
PA	-	picolinic acid
QA	-	quinolinic acid
RBC	-	ranitidine bismuth citrate
RE	-	reference electrode
Ref.	-	reference
S.D.	-	standard deviation

TF	-	transferrin
VI	-	virtual instrument
Voltam	-	voltammetry
XRD	-	X-ray diffraction

SYMBOLS

a	-	effective ionic diameter
a_X	-	activity of X
c_a	-	concentration of acid
c_b	-	concentration of base
c_x	-	concentration of X
D	-	diffusion coefficient
E_{cell}	-	cell potential
E	-	potential
$E_{1/2}$	-	half-wave potential
$E^r_{1/2}$	-	reversible half-wave potential
$E^i_{1/2}$	-	irreversible half-wave potential
$E^q_{1/2}$	-	quasi-reversible half-wave potential
E_g	-	glass membrane potential
$E_g{}^o$	-	standard glass membrane potential
E_j	-	diffusion junction potential
$E(M_{free})$	-	free metal ion potential
E_r	-	potential due to internal and external reference electrodes
ΔE		potential shift
i	-	current
i_d	-	diffusion limited current
f	-	fugacity
k	-	constant which denotes the electromotive efficiency of the glass membrane
k^o	-	standard rate constant for electron transfer
K	-	stepwise stability constant
K_w	-	autoprotolysis constant of water
n	-	number of electrons transferred

pa_{H+}	-	–log a_{H+}
pH	-	–log [H^+]
t	-	transport or transference numbers
T	-	absolute temperature
u	-	ionic mobility
u^o	-	limiting ionic mobility
v_a	-	volume of acid
v_b	-	volume of base
v_i	-	volume of inert electrolyte
T	-	temperature in K
[X]	-	concentration of X
z	-	charge on an ion
α	-	transfer coefficient
β	-	overall stability constant
δ	-	slope of the DC wave
γ_X	-	activity coefficient of X
μ	-	ionic strength
λ	-	ionic conductivity
λ^o	-	limiting ionic conductivity
Λ	-	conductance
Λ^o	-	limiting conductance

CHAPTER 1
Introduction

1.1) Literature Review

1.1.1) *Bismuth in medicinal preparations*

Bismuth has been used in medicinal preparations for decades. This has been highlighted in many review articles.[1-5] In the middle ages bismuth subnitrate (BSN) was already used in medicines and in 1786 the first full account was given for its use in treating dyspepsia.[3] (The inclusion of the term "sub" probably designates the high oxygen content of these salts and the presence of Bi–O moieties. These salts can have variable formulae, depending on the method of preparation.[1])

The most widespread use of bismuth compounds is in the treatment of gastric and duodenal ulcers, where colloidal bismuth subcitrate (CBS), bismuth subsalicylate (BSS), and most recently ranitidine bismuth citrate (RBC) are most commonly used.[1] Other gastric ailments such as traveller's diarrhoea and dyspepsia are also treated using bismuth compounds. In the review article by Briand and Burford,[1] a comprehensive table with treatments containing bismuth for various gastrointestinal disorders is given.

CBS is the most extensively studied series of bismuth compounds.[6-12] It is water soluble producing a colloidal solution.[1,3] The empirical formula for CBS is often given as $K_3(NH_4)_2[Bi_6O_3(OH)_5(Hcit)_4]$, where Hcit is the triply deprotonated trianionic form of citric acid. However, by varying the pH of the solution and adding different ratios of bismuth and citrate, various adducts have been isolated and characterised.[3,10,11,13] In acidic solutions, CBS precipitates and it was thought to form bismuth oxychloride (BiOCl) or bismuth citrate,[3,14] but further investigation showed that the white precipitate produced when dilute hydrochloric acid was added to CBS (giving a final pH of 3), was $K(NH_4)[Bi_2(cit)_2(H_2O)_2].4H_2O$.[11] It was initially believed that the precipitate

formed in ulcer craters provided a protective coating. However, BSS did not produce a precipitate. Instead it decomposed in hydrochloric acid solutions at pH less than 3.5 to produce bismuth oxide and salicylic acid.[12,13]

Today evidence shows that bismuth has an antibacterial action which is probably more likely the reason for its healing properties. In treating gastric ulcers, bismuth compounds act against *Helicobacter pylori* (*H. pylori*), previously named *Campylobacter pyloridis*, found in the human gastric mucosa.[3,13,15] *H. pylori* has been named as a category 1 carcinogen by the World Health Organisation as it is a risk factor in developing gastric cancer.[16]

Ranitidine bismuth citrate is a relatively new antimicrobial agent that was developed to treat *H. pylori* infection. It both inhibits gastric secretion and has bactericidal activity against *H. pylori*. Its activity against the bacteria is about twice as effective as an equivalent mixture of ranitidine (see Table 1.1 for the structural formula) and bismuth citrate, which has possibly been attributed to the greater solubility of RBC even at very low pH and thus allows for penetration of the gastric mucous layer.[17-19]

All this being said, the mechanism of action of these bismuth-containing drugs are still not properly understood. It has been suggested that any number of mechanisms could be responsible for its bactericidal properties. It could involve the inhibition of certain functions such as protein synthesis, membrane function, cell wall synthesis and ATP synthesis. It inhibits the number of enzymes produced by *H. pylori* (such as urease, catalase and lipase) which could result in the local environment change affecting the bacteria, and a decrease in the adherence of *H. pylori* to the surface of epithelial cells has been observed.[20,21] Current treatments for the eradication of *H. pylori* involves combination drugs including colloidal bismuth salts, H_2-receptor antagonists or proton-pump inhibitors, and antibiotics.[16-18,22-27]

Due to the antimicrobial and antibacterial effects of bismuth, it is not surprising that bismuth compounds have found other medicinal applications at some time or other. Bismuth has been used, at times in combination with other drugs, to

treat syphilis[1,3] and nasal catarrh,[3] in wound dressings[3,28] and for arterial hypertension.[1,3] The use of bismuth compounds against other bacteria[29] and yeasts[30] have also been investigated.

Certain bismuth complexes exhibit anticancer activity and others inhibit production of the HIV-1 virus from chronically infected H9 cells.[3] There has only been a fairly recent interest in bismuth compounds as antitumour drugs.[1,5,31] This was probably due to the lack of evidence for DNA-binding of bismuth.[31] A short review article[5] about the use of bismuth and antimony compounds in oncology has recently been written, be it an undeveloped field. There have also been indications that pre-treatment with bismuth complexes can prevent the toxic side effects of the anticancer drug cisplatin without compromising it antitumour activity. This probably occurs due to bismuth inducing the synthesis of renal metallothionein to which platinum binds.[1,5,32,33] On the same basis it was investigated whether the bismuth-induced metallothionein would protect against cadmium cytotoxicity, but this was not the case.[34]

^{212}Bi and ^{213}Bi are both α-particle emitters which have great potential therapeutic value.[1,3-5] They have short half-lives of 61 and 46 minutes respectively and can be readily obtained from a ^{224}Ra generator.[3,4] Typical α-particles have kinetic energies of about 5–9 MeV which result in penetration of 50-90 μm into tissue (equivalent to about 2–10 cell diameters). These short range interactions necessitate the radionuclide to be at or close to the targeted cells, but it also results in reduced toxicity to surrounding normal tissue. β-particle emitters have longer range interactions (0.5–12 mm penetration) producing a poor tumour-to-normal-tissue dose ratio.[4] A chelating agent for the bismuth radionuclide is required to bind it to the carrier molecules which specifically target the cancer cells. The complex must be thermodynamically stable, kinetically inert and the preparation should be rapid and efficient.[3,4,35] Ligands such as diethylenetriaminepentaacetate (DTPA), 6-mercaptopurine and thioguanine (see Table 1.1 for the structural formulae) have been

investigated for this purpose.[3] More recently, the investigation into using ^{213}Bi radionucleides for treating ovarian cancer gave promising results.[36]

In the 1960's and 1970's, toxic effects due to the overdose of bismuth compounds were reported, particularly in France and Australia, where people suffered from reversible bismuth-induced encephalopathy (neurotoxicity).[1,37] This was really due to the careless use of bismuth containing medication with doses of about 10 g per day.[3,4] Other side-effects due to the overdose of bismuth compounds in humans include reversible nephrotoxicty [39-41] (toxicity of the kidneys), osteoarthropathy, gingivitis (bad breath), stomatitis (inflammation of the mouth) and colitis (inflammation of the colon or other parts of the intestine).[39] The kidney is the organ shown to contain the highest concentration of bismuth after its intake into the body, followed by the liver. Interestingly, it was not toxic at doses up to 100 μM, whereas zinc, cadmium and mercury exhibited varying degrees of toxicity at the same concentration.[38] Chelators, such as *meso*-2,3-dimercaptosuccinic acid (DMSA) and D,L-2,3-dimercaptopropane-1-sulphonic acid (DMPS) (see Table 1.1 for the structural formulae), have been investigated to remove excess bismuth from the body.[42]

Abrams and Murrer[13] suggest that the diverse applications of metal compounds in treatments reflect the fact that many were serendipitous discoveries. Many bismuth preparations are still not well characterised.[1] It appears that most work has been done on a series of thiolate complexes for which antibacterial, fungicidal and antitumour activity has been reported.[1] Numerous experimental studies on suggested treatments using bismuth salts or coordination compounds are hindered by the complexity of the compounds or the "superficial chemical knowledge base that is currently available for bismuth".[1] The quote below aptly summarises the general situation of bismuth in medicine:

> *Despite the widespread use of bismuth compounds in medicine its chemistry and biochemistry are currently poorly understood.*
>
> P.J. Sadler, H. Li and H. Sun, (1999)[3]

Table 1.1: Structural formulae of various compounds mentioned in this chapter.

Compound	Structural formula
Ranitidine	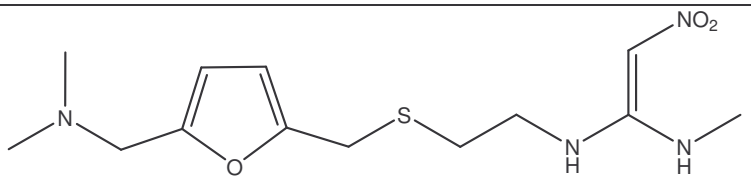
DTPA	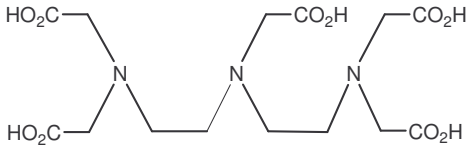
Mercaptopurine	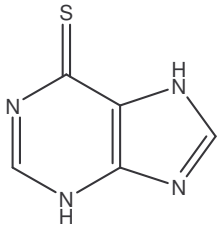
Thioguanine	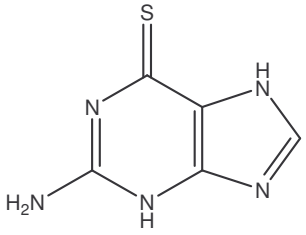
DMSA	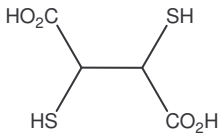
DMPS	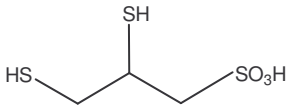
DFB	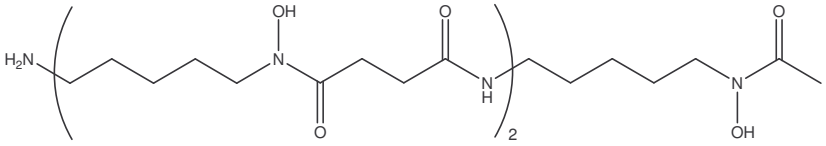

1.1.2) *Biochemistry of bismuth*

The biochemistry of a metal of a particular oxidation state is strongly linked to its affinity for various ligands.[43] Bismuth is not an essential element to human life, so there is no active transport process for the up-take of bismuth or for its transport into the interior of cells.[14] The complexation of bismuth with biomolecules is an important factor in understanding its bioactivity, but studies

involving complexation with amino acids and proteins are rare and characterisation is usually incomplete.[1,3]

The major biological targets for Bi(III) appears to be proteins and enzymes. Bi(III) binds to both Zn(II) sites, such as metallothionein (MT), and Fe(III) sites, such as transferrin (Tf) and lactoferrin (LTf).[1,3]

Metallothioneins are small, widely-distributed proteins made up of only about 60 amino acid residues, about half of these are cysteine residues. This provides seven binding sites for metals where each metal can be bound to four thiolate ligands giving a tetrahedral geometry. The physiological functions of MT involve metabolism and detoxification of essential and nonessential trace metals where the latter includes Cd(II), Hg(II) and Au(I).[3,44] Bismuth also forms the Bi_7MT chelate, but each bismuth is found to bind to only three cysteine sulphur atoms.[32] Bi(III) can displace both Zn(II) and Cd(II) in MT and remains bonded even in strongly acidic solutions (at a pH of about 1), unlike Zn(II) and Cd(II).

Transferrin is a single chain glycoprotein composed of two structurally similar lobes, the N-lobe and the C-lobe (linked by a short peptide) and supplies two metal binding sites. The major role of Tf in blood is to transport Fe(III) to many types of cells in the body.[3,45] After endocytosis and when inside the cell vesicle, the pH drops to 5.5 releasing Fe(III). In human blood, only approximately 30% of the binding sites are occupied by Fe(III), thus allowing other metals to also bind to the unoccupied sites. Bi(III) has been shown to also bind strongly to human Tf (log K_1 = 19.42 and log K_2 = 18.58 at 310 K in 5 mM bicarbonate at pH 7.4).[3] Additionally, Bi(III) binds preferentially to human Tf rather than other scavenger proteins such as albumin (log K = 11.2), even when a large excess of albumin is present.[38,,46] Miquel *et al.*[47] investigated the mechanism of complex formation between Bi(III) and Tf. It appears that when Bi(III) is bound to Tf an open conformation of the protein is retained (unlike with Fe(III)) probably due to its large ionic radius. This could reduce or prevent uptake into the cells and hence justify the low bioavailability of bismuth.[38] Berners-Price and Sadler[2] also noted that the rate of uptake of Bi(III) into red

blood cells and complexation with the thiolate sulphur of glutathione in the cell is comparatively slow (of the order of hours). Since glutathione forms stable complexes with Bi(III) (log K = 29.6 at 298 K and 0.1 M ionic strength in a $NaNO_3$ background), it is thought to play a role in the transport and delivery of this metal ion in cells and biofluids.[3] Due to the strong complexes Bi(III) formed with cysteine and glutathione, CBS does not precipitate at pH 2 when these ligands are present and, furthermore, when bismuth salts are administered orally together with thiolates, a notable increase in the bismuth concentration in blood plasma occurs.[3]

Hernlem *et al.*[48] considered the stability of complexes with the siderophore desferrioxamine B (DFB) (see Table 1.1 for the structural formula) with certain heavy metal ions, including Bi(III). Siderophores are relatively small molecules secreted by microorganisms, such as bacteria, fungi and grasses, to chelate and ultimately transport Fe(III). Siderophores are useful as drugs in facilitating iron mobilization in humans and have been used for iron and aluminium overload therapy.[49] DFB, produced by the bacteria *Streptomyces pilosus* and *Streptomyces coelicolor*, therefore binds to Fe(III) but will also bond to other metal ions. Complexes formed with Bi(III) are very stable with formation constants given as log $\beta([MHL]/[M][HL]) \geq$ ~23.5 and log $\beta([MH_2L]/[M][H_2L]) \geq$ ~19.5 (at 25 °C and 0.5 M ionic strength in a $NaClO_4$ background). These constants were determined using glass electrode potentiometry (GEP) and the authors[48] found it impossible to obtain precise estimates and even said that the "choice of stability constants is somewhat arbitrary". This was due to the strong tendency for bismuth to hydrolyse even at the starting pHs in the acidic region used in the titration. In Figure 1.1,[50] the approximately linear correlation between the log K_1 value for DFB (•) and log $K_1(OH^-)$ for various metal ions is shown. From the NIST database[51] it is seen that log $K_1(OH^-)$ for Bi(III) is about 12.4 implying that the value for log K_1(DFB) should be close to that for Fe(III) and from the correlation this values would be around 32. It is assumed that this value and that quoted as log β([MHL]/[M][HL]) by Hernlem *et al.*[48] is the same, as the structural formula given in Figure 1.1 indicates the terminating amino group as protonated. The value of ~23.5 they quoted was certainly

lower than is indicated here and hence the greater than sign used is appropriate. The linear correlations here may also indicate why Fe(III) binding sites readily bond to Bi(III) in aqueous environments too.

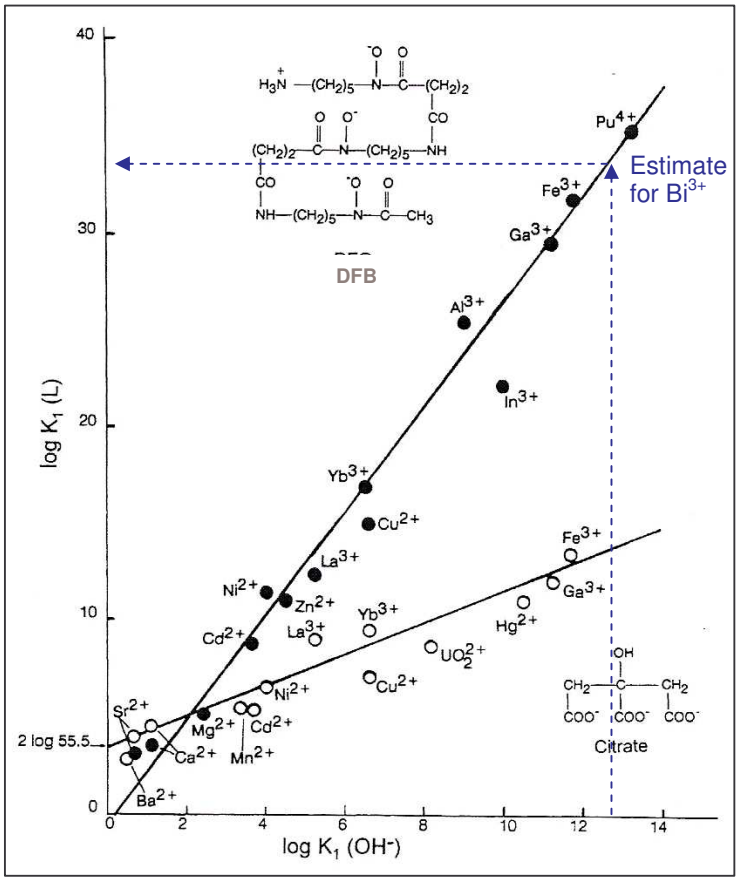

Figure 1.1: Correlations between log K_1 values for polydentate ligands (DFB (•) and citrate (o)) and log $K_1(OH^-)$ for the metal ions.[50] The estimate for Bi^{3+} is based on log $K(BiOH^{2+})$ = 12.4.

Since bismuth preparations are most commonly used in the treatment of gastric ailments, one would assume that most studies have been focused in that direction. Bi(III) has been found to bind strongly to connective tissue proteins, glycoproteins and enzymes in the stomach, but little is known about the binding mode or the kinetic behaviour.[3] This brief look at the biochemical activity of bismuth and its use in medicinal preparations clearly indicates that insufficient knowledge has been accumulated in order to design more effective bismuth-containing drugs while reducing toxic side-effects as far as possible. Before this is considered, however, the chemistry of bismuth needs to be

understood and particularly, for this application, the thermodynamic and kinetic aspects of complexation with various ligands under different conditions.

1.1.3) *Chemistry of bismuth*

Bismuth is the heaviest of the Group 15 elements with an ionic and covalent radius of 1.08 Å (for Bi^{3+}) and 1.52 Å, respectively.[52] Bismuth forms the least stable 5+ oxidation state within the group, with its most stable form being Bi^{3+}.[52] Bismuth forms basic oxides and readily hydrolyses even under very acidic conditions. The hydrolysis of Bi(III) is discussed extensively in Chapter 8.

According to Pearson's Hard and Soft Acid and Base (HSAB) theory[50], soft metal ions prefer ligands with soft donor atoms and hard metal ions prefer ligands with hard donor atoms, thus giving an indication of the type of ligand a metal ion is most likely to prefer. Bi(III) is classified as borderline (between hard and soft) and the classification of some donor atoms are shown in Figure 1.2.[50] Other factors also play a role such as the oxidation state of the element; the presence of strong electron withdrawing groups (such as phenyl) in the ligand which may weaken donor properties; and chelation may enhance the metal-donor interaction.[43] Bi(III) is thus expected to bind strongly to neutral nitrogen, negative sulphur and negative oxygen donor atoms. Due to its large size, Bi(III) also favours the formation of five-membered (rather than six-membered) chelate rings.[50] Bi(III) has a highly variable coordination number, ranging between 3 and 10, and frequently has an irregular coordination geometry.[2,3] Strong intermolecular interactions could result in polymeric structure formation.[2] The kinetics of complex formation has also been described as generally fast or at least within minutes.[3] Bi(V) complexes are not very stable, but the stability can be increased if strong electronegative groups such as substituted aromatic rings or other aromatic ligands are used.[15]

The following quote gives an indication on the position of the chemistry of bismuth at this point:

The chemistry of bismuth is diverse but is perhaps the least well established of the heavier stable elements in terms of a coherent and comprehensive database.

G. Briand and N. Burford, (1999)[1]

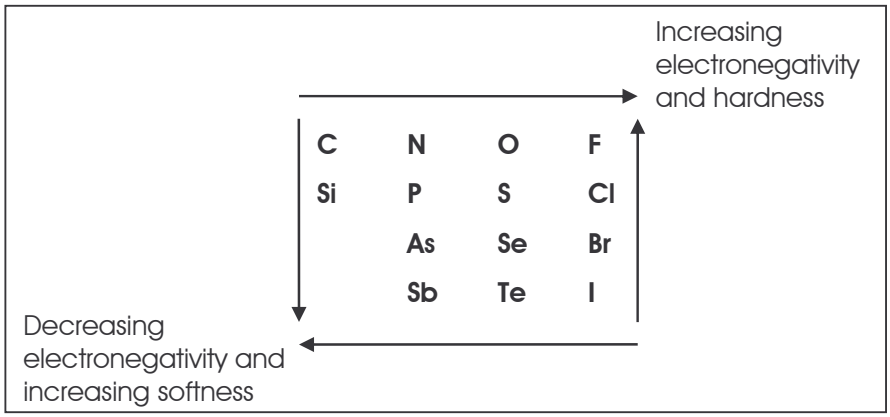

Figure 1.2: Distribution of hardness and softness in the periodic table as a function of the donor atom of a ligand according to the HSAB theory.[50]

Looking at two of the databases that provided information about the thermodynamic stability of complex formation, this was found to be the case. The IUPAC database[53] reports stability constants that have been published in the literature. There are 313 entries for Bi(III) in this database, but these are not necessarily for unique ligands. On closer scrutiny it was found that only 131 different organic and inorganic ligands were studied. The NIST database[51] only publishes critically assessed stability constants and the assessments are performed as indicated in the text by Martell and Hancock.[50] Here, from the 72 Bi(III)-ligand systems which are mentioned, most of these are classified as "published data do not meet criteria for critical selection". Considering that the IUPAC database[53] contains 561 entries for Tl(I), a metal ion which forms extremely weak complexes, the lack of data available for Bi(III) complexation is startling.

The composition of Bi(III) hydrolysis products and their stabilities have been comprehensively investigated. Inorganic ligands such as the halides and pseudohalides, as well as inorganic oxyacids such as NO_3^- and SO_4^{2-} have

also been studied and formation constants with Bi(III) have been determined. The solution species and their formation constants for the binding of Bi(III) with various organic ligands are also given. The organic ligands used are mainly from the classes of carboxylic acids and hydroxycarboxylic acids, biological amino acids, thioketones and thiols, amines, complexones, pyridines etc. and combinations of these.[53]

There are numerous reasons for the lack of data for Bi(III) complexes. There is no real direct probe for bismuth as ^{209}Bi NMR has a large electric quadruple moment which gives broad resonances. NMR studies have thus been done through the ligand nuclei.[2,3]

Many complexes formed by Bi(III) are not very soluble in many solvents and X-ray diffraction (XRD) studies are largely relied upon for characterisation in these cases. Complexation by certain ligands increases solubility allowing for solution studies to take place. These ligands include a number of biologicalll-active molecules such as ascorbic acid, aspirin and tetracyclins to name a few.[1]

As mentioned in the study with DFB,[48] the strong tendency of Bi(III) to hydrolyse causes hydrolysis products to be present in acidic solutions even at a pH less than 1, making many measurements problematic and introducing errors into calculations. To reduce the extent of hydrolysis, studies would have to start in solutions below pH 1; however, it is generally accepted that stability and protonation constants determined below pH 2 carry unacceptably large errors irrespective of the analytical technique used.[54,55] These stability constants are usually not included in critically assessed databases such as the NIST database,[51] or they are given in brackets to indicate values with questionable validity.

Glass electrode potentiometry (GEP) is the technique most used when determining stability constants, but it probably produces the largest errors when applied to solution studies at pH lower than 2. The main source of error is probably because mass-balance equations for the total hydrogen ion

concentration must be solved to obtain the free proton concentration, and the change in the free proton concentration must be predominantly due to the deprotonation of the ligand involved in complex formation reactions. Typical ligand concentrations of 10^{-3} – 10^{-2} M are used in GEP. This concentration is high enough to determine pH as accurately as possible, but still low enough so that it does not contribute significantly to the ionic strength of a solution.[56] In a solution containing high concentrations of strong acid, small pH changes due to the reaction of the ligand therefore become difficult to determine accurately.

1.1.4) *Stability constants*

Stability constants can be quoted as thermodynamic, stoichiometric or "mixed" (also known as Brønsted) constants.[57] As an example, a simple acid dissociation reaction is considered: HL $\rightleftharpoons$ H + L, where charges have been omitted for simplicity. The thermodynamic dissociation constant, K_T, is given in terms of activities as follows

$$K_T = \frac{a_H a_L}{a_{HL}} = \frac{[\mathrm{H}][\mathrm{L}]\gamma_H \gamma_L}{[\mathrm{HL}]\gamma_{HL}} \qquad (1.1)$$

where a_x is the activity coefficient of X, [X] is the concentration of X and γ_X is the activity coefficient of X. The activities of the components in solution have to be measured, which is not always possible, or calculated using the activity coefficients. It is well known that the activity coefficient of a single ion is impossible to measure and thermodynamically meaningless. The coefficients have been calculated using various methods such as the Debye-Hückel equation or its extended version,[54,58,59] the Guggenheim equation,[60] the Davies equation[61] or a series of Pitzer equations[62-64] and so on. The various equations give acceptable values for limited ionic strength solutions only and the values become more uncertain at higher ionic strengths where there are a greater number of interactions between the ions in solution. Certain assumptions also had to be made in deriving these equations, so the accuracy of these coefficients is not really known. The value of K_T is thus independent of the ionic medium and refers to the pure solvent as reference state.[65]

The stoichiometric dissociation constant, K_S, is given in terms of concentrations.

$$K_S = \frac{[H][L]}{[HL]} \tag{1.2}$$

These are probably the most commonly quoted constants as concentrations are more readily determined than activities. The experiments are done under constant ionic strength conditions so that the activity coefficients are constant throughout and hence the values of K_S and K_T vary by a fixed amount.[66] The concentration of the supporting electrolyte needed to maintain the ionic strength is large in comparison to the concentrations of any metal ion, ligand and proton from the system of interest as it would nullify any small variations in ionic strength due to shifts in the reactions being studied. The background electrolyte should also be inert so that it does not induce significant differences in corresponding constants, so ionic salts such as KNO_3 and $NaClO_4$ are often used in aqueous solutions. If the data are to be used for biological applications, it may be more applicable to work under physiological conditions, that is at 37 ^oC and ionic strength 0.15 M NaCl.[65] It is also required that the glass electrode for pH measurement be calibrated in terms of concentration of H^+ at the same ionic strength and temperature. The value of K_s quoted thus only applies to that specific ionic strength and sometimes to the medium in which it was studied.[58,67]

The "mixed" or Brønsted dissociation constant, K_B, is given in terms of concentrations, except for the hydrogen ion which is given in terms of activity as follows

$$K_B = \frac{a_H[L]}{[HL]} \tag{1.3}$$

K_B is determined when the glass electrode is calibrated with buffers and the pH thus measured will give the activity of H^+.[58] This calibration method raises other problems, as will be discussed in Chapter 3, and is generally not recommended.

Berthon[65] emphasised that in order to obtain reliable stability constants it is important to pay attention to experimental technique, computational strategy and the conditions under which these constants have been determined. Additionally, it is possible to obtain more than one set of constants that result in almost identical goodness-of-fit parameters. If so, it is important to know by which criteria the best set were selected.

1.1.5) *Polarography for stability constant determination*

Polarography was created by Jaroslav Heyrovsky in 1922 and in 1959 he received the Nobel Prize in Chemistry for his work in this field.[68] Polarography is a form of voltammetry, where a dropping mercury electrode (DME) is used as the working electrode. Voltammetry involves increasing or decreasing the potential at the working electrode (with respect to the reference electrode) in a regular fashion and the resultant current flowing between the working and counter electrode is measured. The current versus potential plots produced are called voltammograms or polarograms. Background currents, comprised mainly of the capacitance current, are measured until the applied overpotential is sufficient to induce electrons to be transferred and the corresponding increase in current is due to the faradaic current. The potential at which the faradaic process occurs is indicative of the species being oxidised or reduced and the maximum current is an indication of the concentration of the species in solution. It is these properties that are exploited in complex formation studies.

Mercury electrodes have a high hydrogen overpotential and are thus ideal when working in highly acidic solutions, but the anodic region is limited by mercury oxidation. The benefit of using a DME is that the surface is uniform, reproducible and is continually renewed so that oxidation or reduction products do not build up and change the character of the electrode surface. In direct current polarography high charging currents (due to the formation of the double layer) limit the sensitivity of the technique and current maxima have to be suppressed (as discussed in Chapter 2). In the 1970's mercury was designated a toxic and hazardous pollutant and strict control of its use has been implemented.[69] This has lead to the decline in use of polarography. It is

still used in the present studies due to its long term reproducibility in the multi-hour titration experiments employed.

The high concentration of inert supporting electrolyte added to solutions to ensure equilibria studies occur at constant ionic strength is also required when performing voltammetric measurements. The background electrolyte is added to reduce the effect of migration so that the main mode of mass transport is diffusion, for which well-defined mathematical models exist. The concentration of inert electrolyte is usually about a hundred times more than that for the electroactive species. It would thus be more probable that the supporting electrolyte ions migrate rather than the electroactive species.[70] The high concentration of electrolyte also reduces the solution resistance and consequently the iR drop too, allowing the potential at the working electrode to be controlled more accurately. Convection is minimised by making measurements in quiescent solutions.

When polarography is used in complex formation studies, potential and current data are used in conjunction with pH measurements. Both fully labile and non-labile complexes can also be studied using polarography. This distinction can be made by labile complexes resulting in a gradual shift of the metal ion reduction potential to more negative values as the metal ion becomes more extensively complexed by the ligand. Non-labile species require far more energy to reduce the metal ion centre and a separate reduction signal arises at significantly more negative potentials than that of the free metal ion or the labile species. Consequently the current of the labile species' signal decreases more than would be expected from mere dilution (as the titration occurs) due to the diminishing concentrations of these species and the signal of the non-labile species grows as concentration increases. Furthermore, the formation of inert species (or non-electroactive species) can similarly be detected by a larger than expected drop in current signal of the labile species and the extent of the decrease can be directly related to the concentration of the inert species formed.[71,72] Additionally, in studies where a large ligand-to-metal ion ratio is required (for example for weak complexes)[71] polarography is ideal. Low metal ion concentrations can also readily be used which results in

precipitation being postponed to higher pH values if it occurs and also reduces the extent of polymerisation or aggregation.

Lingane was the first to use polarography to study complex formation, but his theory was based solely on a ligand titration experiment and could only handle a single predominant complex in solution at a time.[73] Cukrowski developed the field hugely by introducing a far more general methodology in which either ligand or pH titration experiments can be used and the simultaneous refinement of several formation constants for the various species in solution allowed for the analysis of more complicated metal-ligand equilibria.[74-76] The concept of virtual potentiometry was also introduced where polarographic data can be converted into a form such that it can be analysed utilising software for interpreting potentiometric data.[77,78]

Even though glass electrode potentiometry was not used in this study, it is briefly described here so that clear differences between it and polarography can be seen. GEP is by far the most used technique for determining formation constants so it should be clear why it is necessary to consider other techniques and also to be aware of its limitations. Its wide use has probably to do with the simplicity of the technique, the equipment and the data interpretation, for which various software are available. GEP relies solely on the measurement of the concentration of free H^+ in solution. Ligands, which are generally viewed as Lewis bases, can be protonated to varying degrees. Competing equilibria reactions involving all solution species shift as solution conditions are varied by changing the pH or ligand concentration. Protonated ligands would release hydrogen ions (as free H^+ ions) into solution if they bond preferentially to the metal ions in solution under particular conditions. The glass electrode (GE) only measures the concentration (or activity) of free H^+ ions and thus this measured concentration can be related to the chemistry occurring in solution. This clearly highlights the importance that most of the H^+ ions in solution should arise from the metal-ligand chemistry. This makes working in very acidic solutions impossible as high background concentrations of H^+ would obscure any slight changes due to complex formation and result in large errors in calculated stability constants for species existing in this pH region.

Consequently studies are generally only started from about pH 2. It is also above pH 2 that the diffusion junction potential is insignificant in the measurement. To ensure that the changes in H^+ concentration are sufficient to detect with certainty, the concentrations of the metal ion and ligand have to be high enough. Concentrations of the order of 10^{-3} M are thus generally used. The ligand-to-metal ion concentration ratios are also kept small, ranging from 1:1 and higher so that there is stoichiometrically enough ligand present to form all possible species in solution. A large excess of ligand is avoided as the ligand itself deprotonates under particular right pH conditions and once again this could swamp any changes in H^+ concentration due to complex formation.

1.2) Problem Identification and Project Aims

The study of coordination complexes in aqueous solution is spurred on by the importance of this chemistry to biochemistry, medicine, industry and the environment.[50] In particular, bismuth compounds have been used in many different medicinal preparations, but up until now most of these applications were serendipitous discoveries. This is because relatively little is known about Bi(III) coordination chemistry due to the difficulty in studying these complexes.[50,79] To model and understand the action of bismuth drugs, firstly, thermodynamic stability constants of all probable bismuth species in the system would have to be determined and secondly, the kinetic properties of these complexes would have to be investigated. The design of better bismuth-containing drugs could then be approached from a knowledge-base, rather than from random tests and findings.

GEP has been used to determine approximately 80% of stability constants[50] but it only provides accurate results in solutions with pH values between about 2 and 12. Bi(III), however, is very acidic and undergoes hydrolysis below pH 1, as well as forming precipitates of hydroxo species in solutions at very low pH. In order to study Bi(III) complexation, one generally needs to work in solutions of pH much lower than 2 which rules out the use of GEP.

Polarography is ideal in this case as one can work across the whole pH range, including at very low pH values. The Bi(III) concentration can also be significantly decreased (about 10^{-5} – 10^{-6} M) which shifts precipitation to slightly higher pH values. Using this technique does not come without its own set of challenges. At low pH the diffusion junction potential becomes significant and has to be accounted for. Unfortunately the junction potential cannot be avoided or directly measured and it would impact on both the pH measurement and the polarographic potential measurement as both include a reference electrode with a junction. A dedicated procedure to calibrate the glass electrode would have to be considered as existing protocols only start calibration from about pH 2[54,80,81] thus avoiding the problematic acidic region. The reduction potential of the metal ion being studied would shift due to both complex formation and a changing junction potential when the pH of the solution is changed, but only the overall shift can be measured. A procedure to evaluate and subsequently compensate for the potential shifts due to the junction potential has to be developed. It is proposed that a “witness” metal ion be included in the test solution (which contains the ligand and metal ion of interest), where the witness ion does not undergo complexation itself. Any potential shifts occurring due to the reduction of the witness metal ion would therefore be due to the junction potential alone. It is furthermore proposed that thallium(I) be used as the in-situ witness ion to monitor changes in the junction potential as solution conditions are changed. The recommended methodologies developed here will be applied to known metal-ligand systems to verify the results obtained, but in this study measurements will start in solutions at pH 0.3.

The next challenge is dealing with the hydrolysis of bismuth. Since Bi(III) is already hydrolysed to a small extent at pH 0.3, the free Bi(III) potential cannot be directly measured. The accuracy of this parameter is critical in the calculation of stability constants. It is proposed to use the stability constants already determined for the hydrolysis products to calculate the potential shifts expected as a result of the hydrolysis. The reduction potential measured at pH 0.3 could then be corrected for these shifts (as well as the junction potential shift) and hence the free Bi(III) potential can be estimated.

Once again, the protocols developed would be applied to the study of various Bi(III)-ligand systems where the solution species and their formation constants will be determined. This could contribute to the database of formation constants and to building a knowledge-base for bismuth chemistry. The proposed methodology should generate acceptable results (i.e. correct metal-ligand models and formation constants with small uncertainties) which could then open up a new field in the study of Bi(III) complexes.

1.3) References

1) G. Briand and N. Burford, Chem. Rev., 99 (1999) 2601
2) S. J. Berners-Price and P.J. Sadler, Coord. Chem. Rev., 151 (1996) 1
3) P.J. Sadler, H. Li and H. Sun, Coord. Chem. Rev., 185 (1999) 689
4) S. Hassfjell and M.J. Brechbiel, Chem. Rev., 101 (2001) 2019
5) E.R.T. Tiekink, Crit. Rev. Oncol. Hematol., 42 (2002) 217
6) P.J. Barrie, M.I. Djuran, M.A. Mazid, A. AcParlin, P.J. Sadler, I.J. Scowen and H. Sun, J. Chem. Soc., Dalton Trans. (1996) 2417
7) E. Asato, W.L. Driessen, R.A.G. de Graaff, F.B. Hulsbergen and J. Reedijk, Inorg. Chem., 30 (1991) 4210
8) E. Asato, K. Katsura, M. Mikuriya, T. Fujii and J. Reedijk, Inorg. Chem., 32 (1993) 5322
9) D.R. Williams, J. Inorg. Nucl. Chem., 39 (1977) 711
10) E. Asato, K. Katsura, M. Mikuriya, U. Turpeinen, I. Mutikainen and J. Reedijk, Inorg. Chem., 34 (1995) 2447
11) W. Li, L.Jin, N. Zhu, X. Hou, F. Deng and H. Sun, J. Am. Chem. Soc., 125 (2003) 12408
12) W.A. Herrmann, E. Herdtweck and L. Pajdla, Inorg. Chem., 30 (1991) 2579
13) M.J. Abrams and B.A. Murrer, Science, 261 (1993) 725
14) D.R. Williams, J. Inorg. Biochem., 79 (2000) 275
15) U. Dittes, E. Vogel and B.K. Keppler, Coord. Chem. Rev., 163 (1997) 345
16) T. Alarcón, D. Domingo, I. Sánchez, J.C. Sanz. M.J. Martínez, and M. López-Brea, Eur. J. Clin. Microbiol. Infect. Dis., 17 (1998) 275
17) D.T. Smoot, T. Hinds, H. Ashktorab, J. Jagtap, K.S. Kim and V.F. Scott, Am. J. Gastroenterol., 94 (1999) 955
18) W.A. de Boer, P.W.E. Haeck, M.H. Otten and C.J.J. Mulder, Am. J. Gastroenterol., 7 (1998) 1101
19) P.J. Sadler and H. Sun, J. Chem. Soc., Dalton Trans., (1995) 1395
20) J.R. Lambert and P. Midolo, Aliment Pharmacol. Ther., 11 (1997) 27
21) L. Zhang, S.B. Mulrooney, A.F.K. Leung, Y. Zeng, B.B.C. Ko, R.P. Hausinger and H. Sun, BioMetals, 19 (2006) 503

22) W.A. de Boer, R.J.X.M. van Etten, P.M. Schneeberger and G.N.J. Tytgat, Am. J. Gastroenterol., 95 (2000) 641
23) A. Dubois, D.E. Berg, N. Fiala, L.M. Heman-Ackah, G.I. Perez-Perez and M.J. Blaser, J. Gastroenterol., 33 (1998) 18
24) I. Turel, L. Golič, P. Bukovec and M. Gubina, J. Inorg. Biochem., 71 (1998) 53
25) D. Peura, Am. J. Med., 105 (1998) 424
26) L. Yang, J. Eshraghi and R. Fassihi, J. Control. Release, 57 (1999) 215
27) A. Uygun, A. Kadayifci, M. Safall, S. Ilgan and S. Bagci, J. Dig. Dis., 8 (2007) 211
28) V. Nakhla, Y.M. Takwonoingi and A Sinha, J. Laryngol. Otol. , 121 (2007) 329
29) Ø. Brorson and S.-H. Brorson, Int. Microbiol., 4 (2001) 209
30) T. Murafuji, Y. Miyoshi, M. Ishibashi, A.F.M.M. Rahman, Y. Sugihara, I. Miyakawa and H. Uno, J. Inorg. Biochem., 98 (2004) 547
31) X. Wang, X. Zhang, J. Lin, J. Chen, Q. Xu, and Z. Guo, J. Chem Soc., Dalton Trans., (2003) 2379
32) H. Sun, H. Li, I. Harvey and P.J. Sadler, J. Biol. Chem., 274 (1999) 29094
33) M. Satoh, Y. Aoki and C. Tohyama, Cancer Chemother. Pharmacol., 40 (1997) 358
34) T. Kaji, A. Mishima, C. Yamamoto, Y. Fujiwara, M. Sakamoto, H. Kozuka and F. Koizumi, Bull. Environ. Contam. Toxicol., 56 (1996) 630
35) M.W. Brechbiel and O.A. Gansow, J. Chem. Soc., Perkin Trans., 1 (1992) 1173
36) Y.J. Song, C.F. Qu, S.M.A. Rizvi, Y Li, G. Robertson, C. Raja, A Morgenstern, C. Apostolidis, A.C. Perkins and B.J. Allen, Cancer Letters, 234 (2006) 176
37) J.F. Ross, R.C. Switzer, M.R. Poston and G.T. Lawhorn, Brain Res., 725 (1996) 137
38) V. Rodilla, A.T. Miles, W. Jenner and G.M. Hawksworth, Chem. Biol. Interact., 115 (1998) 71
39) İ. İşlek, S. Uysal, F. Gök, R. Dündaröz and S. Küçüködük, Pediatr. Nephrol., 16 (2001) 510

40) B.T. Leussink, A. Slikkerveer, W.J.J. Krauwinkel, G.B. Van der Voet, E. de Heer, F.A. De Wolff and J.A. Bruijn, Arch. Toxicol., 74 (2000) 349
41) B.T. Leussink, A. Slikkerveer, M.R. Engelbrecht, G.B. van der Voet, E.J. Nouwens, E. de Heer, M.E. de Broe, F.A. de Wolff and J.A. Bruijn, Arch. Toxicol., 74 (2001) 745
42) A. Slikkerveer, L.A. Noach, G.N.T. Tytgat, G.B. Van der Voet and F.A. De Wolff, Analyst, 123 (1998) 91
43) S. Ahrland, Inorg. Chim. Acta, 79 (1983) 154
44) W. Bernhard, M. Good, M. Vašák and J.H.R. Kägi, Inorg. Chim. Acta, 79 (1983) 154
45) H. Sun, H. Li, A.B. Mason, R.C. Woolworth and P.J. Sadler, Biochem., 337 (1999) 105
46) H. Sun and K.Y. Szeto, J. Inorg. Biochem., 94 (2003) 114
47) G. Miquel, T. Nekaa, P.H. Kahn, M. Hémadi and J.-M. El Hage Chahine, Biochem., 43 (2004) 14722
48) B.J. Hernlem, L.M. Vane and G.D. Sayles, Inorg. Chim. Acta, 244 (1996) 179
49) Wikipedia, http://en.wikipedia.org/wiki/Siderophore (accessed 2011-02-17)
50) A.E. Martell and R.D. Hancock, Metal Complexes in Aqueous Solutions, Plenum Press, New York, 1996
51) A.E. Martell, R.M. Smith and R.J. Motekaitis, NIST Standard Reference Database 46 Version 8.0, NIST Critically Selected Stability Constants of Metal Complexes, Gaithersburg, USA, 2004
52) F.A. Cotton and G. Wilkonson, Advanced Inorganic Chemistry - A Comprehensive Text, 4th ed., John Wiley and Sons Inc., New York, 1980
53) L.D. Petit and K.J. Powell, IUPAC Stability Constants Database, IUPAC and Academic Software, 1993-2003
54) G.H. Nancollas, M.B. Tomson, Pure and Appl. Chem., 54 (1982) 2675
55) A. Braibanti, G. Ostacoli, P. Paoletti, L.D. Pettit, S. Sammartano, Pure and Appl. Chem., 59 (1987) 1721
56) C. Billing and I. Cukrowski, S. A. J. Chem., 62 (2009) 168
57) H.M. Irving, M.G. Miles and L.D. Pettit, Anal. Chim. Acta, 38 (1967) 475
58) W.A.E. McBryde, Analyst, 94 (1969) 1118

59) J.I. Partanen, P.M. Juusola and P.O. Minkkinen, J. Soln Chem., 28 (1999) 413
60) E.A. Guggenheim, J. Phys. Chem., 34 (1930) 1758
61) C.W. Davies, Ion Assosciation, Butterworths, London, 1962
62) K.S. Pitzer, Activity coefficients in electrolyte solutions, 2nd ed., CRC Press Boca Raton, FL, 1991
63) J.L. Barriada, I. Brandariz, R Kataky, A.K. Covington and M.E. Sastre de Vicente, J. Chem. Eng. Data, 46 (2001) 1292
64) D.K. Nordstrom, C.N. Alpers, C.J. Ptacek and D.W. Blowes, Environ. Sci. Technol., 34 (2000) 254
65) G. Berthon, Pure & Appl. Chem., 67 (1995) 1117
66) A. Braibanti, G. Ostacoli, P. Paoletti, L.D. Pettit and S. Sammartano, Pure and Appl. Chem., 59 (1987) 1721
67) P.M. May, K. Murray and D.R. Williams, Talanta, 32 (1985) 483
68) Wikipedia, http://en.wikipedia.org/wiki/Jaroslav-Heyrovsk%C3%BD (accessed 2010-09-21)
69) R.G. Compton and C.E. Banks, Understanding Voltammetry, World Scientific Publishing Co., Singapore, 2007
70) P. Zanello, Inorganic Electrochemistry: Theory, Practice and Application, The Royal Society of Chemistry, Padstow UK, 2003
71) I. Cukrowski, R.D. Hancock and R.C. Luckay, Anal. Chim. Acta, 319 (1996) 39
72) R.D. Hancock, I. Cukrowski, J. Baloyi and J. Mashishi, J. Chem Soc., Dalton Trans., (1993) 2895
73) J.J. Lingane, Chem. Rev., 29 (1941) 1
74) I. Cukrowski, Anal. Chim. Acta, 336 (1996) 23
75) I. Cukrowski, Electroanal., 9 (1997) 1167
76) I. Cukrowski, Electroanal., 9 (1997) 699
77) I. Cukrowski and J.M. Zhang, Electroanal., 16 (2004) 612
78) I. Cukrowski, J.M. Zhang and A. van Aswegen, Helv. Chim. Acta, 87 (2004) 1
79) R.D. Hancock, I. Cukrowski, I. Antunes, E. Cukrowska, J. Mashishi and K. Brown, Polyhedron, 14 (1995) 1699

80) I. Brandariz, J.L. Barriada, T. Vilariño and M.E. Sastre de Vicente, Monatshefte für Chemie, 135 (2004) 1475

81) D.I. Hitchcock and A.E. Taylor, J. Am. Chem. Soc., 59 (1937) 1812

CHAPTER 2
Experimental

2.1) Introduction

Lingane[1] used polarography to determine the stability constants of labile metal-ligand systems as early as 1941. He used the potential shift from ligand titration experiments to evaluate stability constants but his work was restricted to systems where only one predominant species was in solution under certain pH conditions. Later DeFord and Hume[2] extended this work and developed a mathematical approach to calculate the formation constants of several major, labile species in solution that were formed successively with increasing ligand concentration. The systems which they could study were therefore severely limited. Cukrowski has developed the methodology whereby the refinement of several formation constants can occur simultaneously thus providing the most rigorous process thus far. This procedure takes both the potential shift and decrease in peak or diffusion limited current into account and will be described in detail later on. Labile and non-labile metal-ligand systems[3-6] can be studied by varying either pH or ligand-to-metal concentration ratios[5-7] in the presence of excess ligand or with the concentrations of the ligand and metal being comparable.[6-8] The presence of excess ligand does however give more reliable data.[8] The species does, however, need to be among the major species in solution for formation constants to be reliable, as it was found that values determined for minor species were generally less certain.[6,9]

Sampled direct current polarography (also called DC_{TAST}) was used in these studies. This was the technique used in the very first application of polarography in complex formation studies[1,10-12] and since then other polarographic techniques such as alternating current (AC)[13-15] and differential pulse polarography (DPP)[3-9,16-20] have also been used. DC_{TAST} was decided on for this study as it is easier to deal with electron transfer processes that are not fully reversible, as will be seen in Chapter 7. DC polarography is the simple procedure of varying the potential in a step-wise fashion while

measuring the resultant current produced. In this case the potential was scanned in a negative direction to promote reduction. In sampled DC polarography, the current is integrated for a short time at the end of the drop life to produce smooth DC waves. If the current is measured constantly, changes in current due to the growing and falling of the mercury drop produces polarograms that have a saw-tooth shape superimposed on the wave. The current is measured at the end of the drop life because the current is greatest when the surface area of the drop is largest; the rate of change of current is lowest due to the area-to-volume ratio decreasing with growth of the drop and also where charging currents (also known as capacitance currents) have decayed to a minimum.

When using polarography in equilibria studies, one needs to consider what is happening in the bulk solution as well as at the electrode-solution interface. Thermodynamic, kinetic and mass transport factors have to be considered. Mass transport is the easiest to control and measurements in quiescent solutions containing high concentrations of background electrolyte ensures that convection and migration are negated, thus leaving diffusion as the main transport mechanism between the bulk solution and the solution at the surface of the electrode. The thermodynamic and kinetic properties for both the solution and the electron transfer processes are a function of the system being studied and, in the case of $DC_{TAST,}$ can only be influenced to a small extent by the measurement parameters.

In DC_{TAST}, a current peak can be superimposed on the wave and is called a current maximum. This is due to an enhanced rate of mass transport at the electrode-solution interface due to the drop growing into the solution. There are two main types of current maxima, the first kind and the second kind, and these are illustrated in Figure 2.1. Maxima of the first kind result from the streaming of the solution around the mercury drop as it grows which causes surface tension differences at various parts of the surface of the mercury drop. Current maxima of the second kind are generally observed in solutions of high ionic strength and although the mechanism is not fully understood, it certainly is also due to increases in convection at the drop surface. Low concentrations

of surfactants can be added to the test solution to suppress these maxima.[21] In this work a few grains of gelatine were added to the test solution to suppress current maxima. Frumkin[22] also described a current maximum of the third kind. This is due to turbulent flow at the surface of the mercury drop arising during the adsorption of sparingly soluble organic substances which form condensed adsorption layers on the mercury if their concentration in solution is high enough.

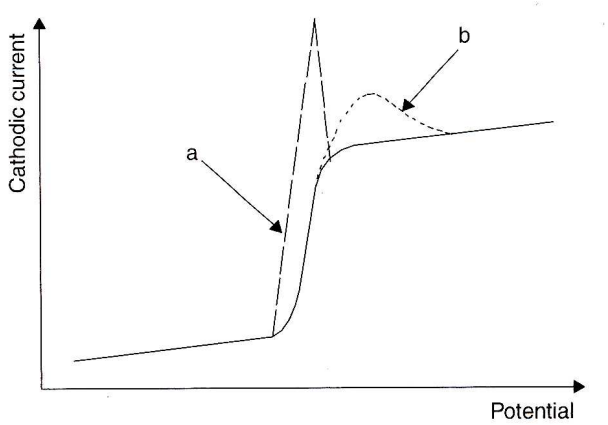

Figure 2.1: Illustration of current maxima. The solid line is an undistorted DC_{TAST} wave and the dashed and dotted lines give examples of the superimposed current maximum of (a) the first and (b) the second kind.[21]

The concentration of oxygen in solution exposed to the atmosphere is relatively large (about 0.5 mM in pure water at 25 °C[23]) and since oxygen is electroactive, large reduction signals are produced which could obscure other signals of interest. The reduction of oxygen proceeds via a hydrogen peroxide intermediate.[24] In acidic solutions the process is

$$O_2 + 2H^+ + 2e^- \rightleftharpoons H_2O_2 \qquad E° = 0.69\ V \qquad (2.1)$$

$$H_2O_2 + 2H^+ + 2e^- \rightleftharpoons 2H_2O \qquad E° = 1.78\ V \qquad (2.2)$$

and the overall reaction is

$$O_2 + 4H^+ + 4e^- \rightleftharpoons 2H_2O \qquad (2.3)$$

In basic solutions the process is

$$O_2 + 2H_2O + 2e^- \rightleftharpoons H_2O_2 + 2OH^- \qquad E° = -0.15\ V \qquad (2.4)$$

$$H_2O_2 + 2e^- \rightleftharpoons 2OH^- \qquad E° = 0.55\ V \qquad (2.5)$$

and the overall reaction is

$$O_2 + 2H_2O + 4e^- \rightleftharpoons 4OH^- \quad (2.6)$$

Not only is the oxygen electroactive, but the H_2O_2 intermediate can function as both an oxidising and reducing agent which could act on other electroactive species present. In unbuffered solutions, pH changes can occur in the vicinity of the electrode due to the electroreduction of oxygen which could lead to precipitation of solution species close to the electrode.[23,25] In our experiments it is critical that the species close to the surface of the mercury drop are the same as those in the bulk of the solution where the pH is measured. In metal-ligand equilibria studies, the actual species (or complex) is dependant on pH and since both polarographic reduction data and pH measurement data are used together, the solution conditions for the GE calibration and the actual titration experiment must be as close as possible for the data to correlate. To remove dissolved oxygen, solutions were purged with moisture-saturated ultra-high purity nitrogen (≥99.999% pure) and an atmosphere of nitrogen was maintained over the solution during polarographic measurements.

2.2) Reagents

A list of reagents used is given in Table 2.1. The way in which they were utilised is discussed below.

All solutions were made up using deionised water (18 MΩ cm) from a Milli-Q water purification unit. Generally 0.5 M HNO_3 and 0.5 M NaOH or KOH solutions were used to calibrate the CGE and in metal-ligand titration experiments. To calculate the required dilutions, the molarities of 14.44 M for the 65% HNO_3 and 11.5 M for the 45% KOH were used. These solutions were transferred to a Dosimat unit for accurate dispensing and the ability to automate the system. Ascarite® or soda lime was used to fill the drying tubes attached to the bottle lid on the Dosimat unit to prevent CO_2 contamination of the hydroxide solutions as far as possible.

Thymol blue indicator was used in the standardisation of acid and base

Table 2.1: List of reagents used together with the supplier and the manufacturer's assay.

Reagent	Supplier	Manufacturer Assay
Mercury Metal, Triply-distilled	Saarchem, UnivAR®	99.8%
Bi(III) Nitrate pentahydrate	Fluka	≥98%
Cd(II) Nitrate tetrahydrate	Fluka	≥99%
Cu(II) Nitrate trihydrate	Fluka	99.0-104%
Tl(I) nitrate	Merck	≥99%
Picolinic acid	Aldrich	99%
Dipicolinic acid	Sigma-Aldrich	99%
Quinolinic acid	Aldrich	99%
Nitric acid	Merck or Saarchem, UnivAR®	≥65%
Sodium hydroxide	Saarchem, UnivAR®	≥98%
Potassium hydroxide solution	Sigma-Aldrich	~45% (≤ 0.3% impurities)
Sodium nitrate	Sigma-Aldrich	≥99.5%
Potassium nitrate	Sigma-Aldrich	≥99.0%
Potassium chloride	Saarchem, UnivAR®	99.0-100.5%
Ascarite®	Fluka	5-20 mesh
Soda lime	Merck, uniLAB®	4-8 mesh
Potassium hydrogen phthalate	Merck	99.9%
Triton® X-100	Fluka	
Gelatine		
Thymol Blue	Sigma-Aldrich	

solutions and was made as suggested by Vogel.[26] About 0.1 g of indicator was dissolved in 2.15 mL of 0.1 M NaOH and diluted to 100 mL with water. The indicator is supplied in the acid form so the NaOH solution is added to neutralise the sulphonic acid groups. The endpoint at about pH 8.9 is indicated by a yellow-blue transition and was used to indicate the endpoint for the acid-base standardisations. Another red-yellow transition occurs at about pH 1.7, but this end point was not utilised here.

Hydroxide solutions were standardised against the primary standard potassium hydrogen phthalate that had been dried at 110 °C for about 2 hours and then stored in a desiccator. For 0.5 M hydroxide solutions, about 0.4 – 0.5 g of potassium hydrogen phthalate was accurately weighed (to 5 decimal places),

added to 5 mL deionised water and dissolved while stirring and purging the solution with nitrogen (about 15 – 20 minutes). Thymol blue indicator was added (3 – 4 drops) and the solution was titrated with the hydroxide solution contained in a Dosimat unit until the required colour change.

Nitric acid solutions were then standardised by adding 3 – 4 drops of thymol blue indicator to a 5 mL aliquot of 0.5 M HNO_3 and stirring and purging for about 10 minutes. These solutions were then titrated with a standardised hydroxide solution until the required colour change. Later a Metrohm 848 Titrino Plus autotitrator was used for these standardisations employing a GE sensor. The instrument parameters used are given in Appendix 1 (A1.1).

The concentrations of the acid and base solutions were calculated to four significant figures and each titration was repeated at least three times, or until the standard deviation gave an uncertainty only on the fourth significant figure. The basic solutions were standardised every two weeks as these solutions could react with CO_2 from the atmosphere. The nitric acid solutions were standardised only when they were replenished or after standing for some time.

Stock solutions of 0.100 M Cd(II), 0.100 M Cu(II) and 0.100 M Tl(I) were made up from their nitrate salts as received by dissolving them in 0.5 M HNO_3. A 0.100 M Bi(III) stock solution was made up in 1 M HNO_3 by first dissolving the nitrate salt in concentrated HNO_3 and then diluting with water. The higher acid concentration was used to prevent hydrolysis of Bi(III). Where required, Bi(III) and Tl(I) stock solutions were diluted to give 0.0100 M solutions, adding HNO_3 to give 1 M and 0.5 M concentrations, respectively. Metal ion stock solutions were not standardised as they were used in the metal-ligand equilibria studies by polarography.

2.3) Equipment

In the study of metal-ligand equilibria using polarography, a combination of both polarographic and potentiometric measurements are made.

For the potentiometric measurements, two types of GE were considered, both manufactured from glass membranes consisting essentially of a silicate framework containing lithium ions and supplied by Metrohm. The characteristics of these electrodes are given in Table 2.2.

Table 2.2: Metrohm GE characteristics.[27]

Electrode	Ecotrode	Unitrode
Shaft material	glass	glass
Membrane material	T-glass	U-glass
Membrane resistance	200-500 MΩ	150-500 MΩ
Diaphragm	Ceramic frit	Fixed ground joint
Diaphragm resistance	0.4-0.9 kΩ	<2 kΩ
Electrolyte flow rate	5-15 /μL hr^{-1}	3-30 /μL hr^{-1}

The Unitrode was designed for alkaline conditions to minimise both the corrosion of the membrane and the alkaline error. This electrode has larger dimensions than the Ecotrode and was difficult to use in the cell together with all electrodes for the polarographic cell. The diaphragm is also higher up the electrode stem requiring extremely careful positioning to ensure that it is submerged by solution and that the stirrer bar does not bump the glass tip. The Ecotrode was therefore mostly used. In both electrodes the outer reference system was combined with the GE and consisted of a “Long Life” Ag/AgCl reference electrode (RE). The RE was filled with 3 M KCl which produces a potential of 207.0 mV at 25 °C and hence the electrode was also stored in a 3 M KCl solution or in a Metrohm storage solution which contains 3 M KCl and other proprietary constituents which are reported to prolong the life of the glass membrane. In the “Long Life” system the silver chloride is contained in a cartridge with a diffusion barrier which is placed around the silver wire.[27] This reduces the AgCl concentration in the filling solution and thus prevents any blockages of the diaphragm due to the precipitation of AgCl. If blockages were to occur, the response times of the electrode would increase. The temperature of the solution was measured using a separate Metrohm Pt 1000 thermocouple with a temperature range of –50 to 180 °C. A

Metrohm 713 pH meter was used to measure the solution temperature and the potential at the combination glass electrode (CGE).

A three electrode polarographic cell was used containing a dropping mercury electrode (DME) as the working electrode, a Ag/AgCl/3 M KCl RE and a platinum wire counter electrode (CE), all supplied by Metrohm. All potentials quoted are with respect to the Ag/AgCl/3 M KCl RE. In order to prevent test solutions being contaminated with chloride, the RE was inserted into a salt bridge containing 0.5 M $NaNO_3$ or KNO_3 solutions (depending whether NaOH or KOH solutions were used in the experiments, respectively).

An automated setup was built[28] using the LabVIEW software package (version 7) that had been programmed in-house, together with the NI-6036-E data acquisition card (National Instruments, Austin, Texas, USA), a homemade interface box and the various components that were controlled by the system. A schematic diagram of the setup is shown in Figure 2.2. A jacketed cell was positioned on a Metrohm 663 VA cell stand and a Labcon CPE 100 thermostat in a homemade water bath maintained the temperature of the cell at 25 ± 0.1 °C (an air-conditioner was used to maintain the room temperature at about 22 °C). For the polarographic measurements, the LabVIEW software controlled a BAS CV27 potentiostat via the interface, which in turn controlled the potential at the DME and measured the resulting current as well as the actual applied potential. The purging gas, the mercury drop knocker and the mercury flow in the DME were all operated using nitrogen gas which was passed through valves on the Metrohm 663 VA cell stand and were also controlled through the interface. The magnetic stirrer was also turned on and off through the interface. Data from the pH meter could be collected by alternating between the various measurement modes, i.e. pH, potential and temperature. Initially when the automated setup was built, it was found that as soon as the three electrodes used for the polarographic cell were connected, a ground loop formed which interfered with the pH measurement. This caused the "measured pH" to drift significantly and it took hours for the GE to stabilise again. To prevent this, the GE was connected to the pH meter via a magnetic

isolator which was sourced by Metrohm. The Dosimat could be set to dispense specified volumes of solution at specified rates, and the volumes at each step throughout a titration were recorded. A photograph of the cell is given in Figure 2.3.

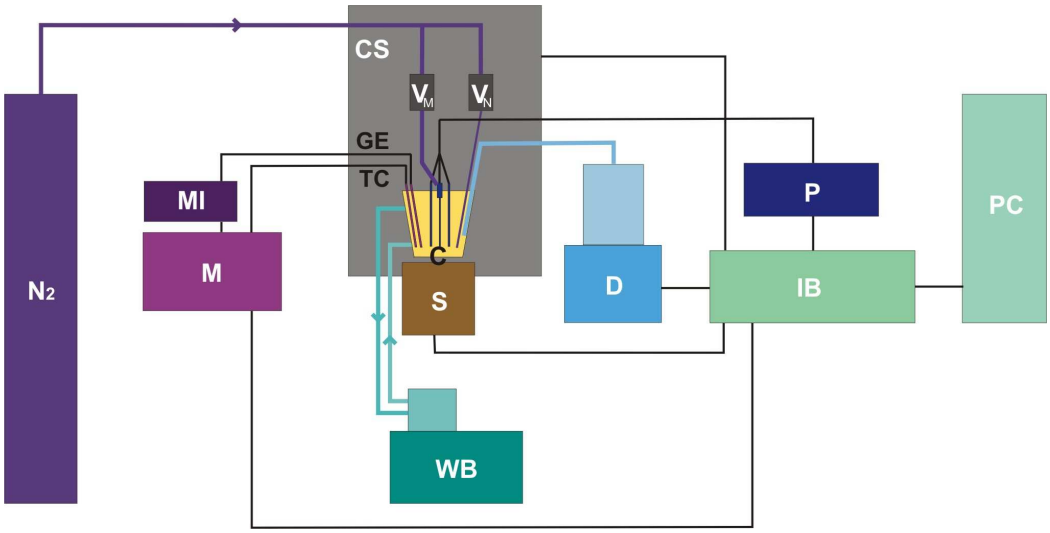

Figure 2.2: Schematic diagram of the automated polarographic and potentiometric experimental setup where the abbreviations stand for the following: N_2 – nitrogen cylinder, V_N – valve that controls nitrogen flow for purging, V_M – valve that controls nitrogen flow for the DME, M – pH meter, MI – magnetic isolator, CS – cell stand, C – cell, GE – connection to the glass electrode, TC – connection to the thermocouple, S – magnetic stirrer, WB – temperature regulated water bath, D – Dosimat, P - potentiostat, IB – interface box, PC – computer containing data acquisition card. (Note, the valve operation the drop knocker is not shown here.)

The LabVIEW software allows one to set up various virtual instruments (VIs) that control the components connected to the interface and can also acquire data as required. VIs were developed to facilitate different automated experiments, for example, potentiometric titrations which were used either to calibrate the GE or titration experiments for metal-ligand equilibria studies using a combination of potentiometric and polarographic measurements. Information collected was saved as ASCII files which could be imported into a Microsoft Excel spreadsheet.

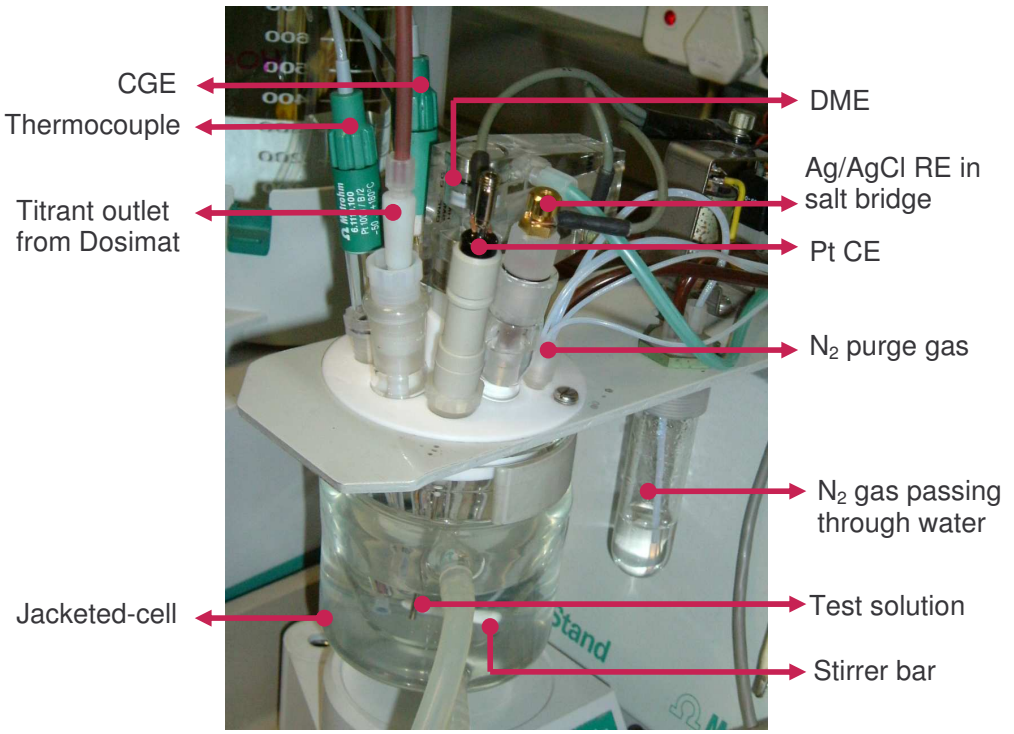

Figure 2.3: Photograph of the polarographic cell.

The sections that follow give general experimental and mathematical approaches that were used. More specific information is given in each chapter where necessary.

2.4) Experiments

2.4.1) *GE calibration procedure using strong acid-strong base titration*

In general, when calibrating a CGE by performing a strong acid-strong base titration (H^+–OH^- titration), 0.5 M standardised acid and base solutions were used. The cell initially contained 25 mL of standardised HNO_3 solution, a magnetic stirrer bar, a thermocouple, a CGE and the delivery tube from the Dosimat through which base solution was added. An anti-diffusion tip was used on the delivery tube which allows solution to be pushed out when needed, but little diffusion into or out of the tube occurs with time. This tip was placed to the right of the GE when stirring in an anticlockwise direction to

reduce a drastic localised increase in pH at the glass membrane as far as possible by first mixing the solutions. All cell components were thoroughly rinsed with deionised water and patted dry (to avoid the build up of static charge) so that no dilution of the solutions occurred since pH was calculated based on the standardised concentrations of acid and base.

The graphical user interface (GUI) of the VI used to calibrate the CGE and parameters used for a typical GE calibration procedure (including the Dosimat settings) are given in Appendix 1, Figure A1.1 and Table A1.2, respectively. Test solutions were stirred and purged throughout the calibration procedure. An initial waiting time of 30 minutes was set to purge solutions sufficiently and to reach thermal equilibrium at 25.0 °C. The 30 minutes purging time was required to remove the dissolved oxygen from solutions for polarographic measurements, and it was decided to keep the calibration and polarographic experimental conditions the same as far as possible. An equilibration time was allowed between each addition of base and the onset of the GE potential measurement. To ensure that test solutions and the GE had equilibrated, the potential was measured at 2 s intervals (the sampling rate) until at least ten readings were recorded. The standard deviation is calculated using the last ten values recorded and compared to the specified stability criterion (the maximum allowed standard deviation). The VI will stop recording the GE potential only when the standard deviation is less than the stability criterion and then the average value of these ten points is taken as the potential reading. The stability criterion was set to 0.040 which implies that from the ten points used to calculate the standard deviation, only one reading can differ by 0.1 mV from the other nine readings which all had to be the same. For all practical purposes, this was regarded as a constant reading. If the stability criterion was not met after the maximum waiting time, the average of the last ten readings was taken and the value was flagged as “timed-out”. This prevented unnecessarily long periods spent collecting data in the low buffer region where readings are generally more unstable and data points are not used in the calibration. If the GE is faulty, the flag does alert one to the problem. The VI terminates the titration when one of the stop conditions is fulfilled, i.e. which ever of the specified potential, pH or volume added value is

reached first. In this case the stop conditions were chosen such that the stop volume was met first. The number of individual potential readings to be saved can be specified so that they can be inspected if required. The 'temperature frequency' (see Figure A1.1) shows after how many titration points the temperature is measured.

The DisC mode on the Dosimat was used as it sums the volume increments added throughout the titration so that the total volume of solution added is displayed. The filling rate was set at the maximum for the exchange unit (e.g. 30 mL min^{-1} for a 10 mL burette) and the addition rate was lower to allow for purging of solutions and to minimise the localised increase in pH near the glass membrane. The base solution was added in 0.50 mL increments, after which the average potential value was determined as described above. A total of one hundred titration points were collected after the entire 50 mL of base had been added, a sufficient number of data points for a calibration.

Once the data for the average potential versus volume of added base had been obtained, the concentration of the hydrogen ions in solution was calculated at each point in the titration as follows:

- before the equivalence point

$$[H^+] = \frac{c_a v_a - c_b v_b}{v_a + v_b} \tag{2.7}$$

- after the equivalence point

$$[H^+] = \frac{K_w (v_a + v_b)}{c_b v_b - c_a v_a} \tag{2.8}$$

where c_a and c_b are the concentrations of the standardised acid and base solutions respectively, v_a and v_b are the total volumes of the acid and base added respectively, and K_w is the autoprotolysis constant of water. The theoretical pH of the solution was calculated and the calibration graph of potential versus pH was then plotted. Thus in this work pH implies –log $[H^+]$, or else it will be signified as pa_{H+} for –log a_{H+}.

Two other amended approaches to the calibration of the CGE using a H^+–OH^- titration were used. The first was simply to reduce the increment size at which the base was added closer to the endpoint to provide more data around the endpoint. Alternatively, after about pH 2.5, the base solution was swopped for a 0.1 M OH^- solution with an ionic strength of 0.5 M, again to supply more data closer to the endpoint and also to avoid the very basic region where the glass membrane corrodes.

It should be mentioned here that when titrating 0.5 M H^+ solution with 0.5 M OH^- solution, the ionic strength varies between 0.5 M and 0.25 M during the titration. It is only when a large concentration of inert salt is added to both acid and base solutions that the ionic strength will remain constant. Unfortunately when working in very acidic solutions at relatively low ionic strengths (ultimately for medicinal purposes), this variation in ionic strength is unavoidable.

2.4.2) *GE calibration procedure using inert solution titration*

Another method for calibrating the CGE was tested where a background electrolyte solution of 0.5 M $NaNO_3$ was titrated separately with either 0.5 M HNO_3 or 0.5 M NaOH. The concentration of the hydrogen ions in solution was calculated after each volume increment as follows:

- in the acidic region

$$[H^+] = \frac{c_a v_a}{v_a + v_i} \tag{2.9}$$

- in the basic region

$$[H^+] = \frac{K_w (v_b + v_i)}{c_b v_b} \tag{2.10}$$

where c_a and c_b are the concentrations of the standardised acid and base solutions respectively, v_a, v_b and v_i are the volumes of the acid, the base and the inert electrolyte, respectively, and all solutions have the same initial ionic strength. The theoretical pH was then calculated and the graph of potential versus pH plotted to determine the calibration.

2.4.3) *Polarographic measurements*

The GUI of the VI which was used to collect DC polarographic data for a single polarogram at a time and the typical settings used for these measurements are given in Appendix 1, Figure A1.2 and Table A1.3, respectively. The initial and final potentials used to collect a DC polarogram varied according to the reduction potentials of the metal ions studied. The time over which the current was integrated at the end of the drop life was initially set to 60 ms, but later changed to 100 ms to give larger and less noisy currents, especially where concentrations of the electroactive species were very low. Figure 2.4 gives a potential versus time graph representing these parameters. Here it can be seen that the initial potential is applied and then decreased by 4 mV at each step until the final potential is reached. Each potential value is applied for 1 s, the drop life. After 1 s the drop is knocked off and a new drop starts growing. For the last 60 – 100 ms of the drop life, the current is measured and integrated. The polarogram is then the plot of the integrated current versus the applied potential at each step. In this case the applied potential is also measured as there could be slight deviations in the sought after potential and the actual potential applied.

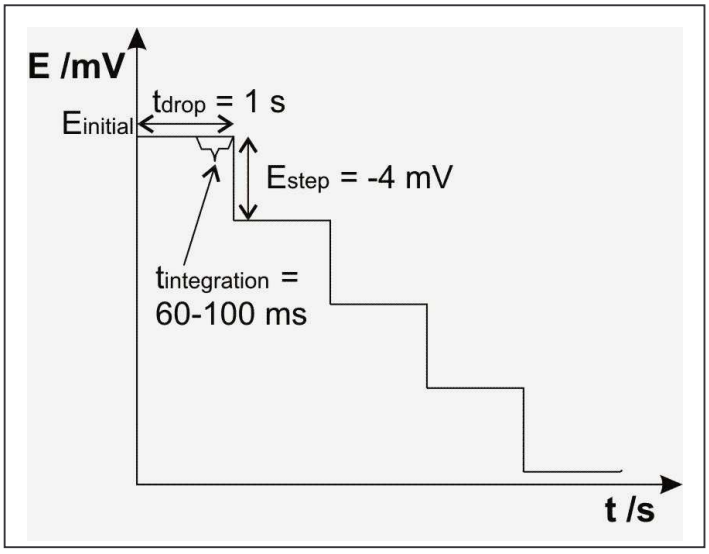

Figure 2.4: Potential versus time graph representing the DC polarographic parameters used.

Since the gain on the BAS CV27 potentiostat could not be controlled digitally, the dial was set manually on the potentiostat and the same value entered as

the CV27 gain in the software to ensure that the correct multiplication factor was used to record the current. The potential and current input ranges controlled the sensitivity of the measurement and were made as small as possible without the collected data moving off scale.

The purge time varied between 30 minutes (1800 s) for a solution that had not been purged before to 5 minutes (300 s) for successive measurements. Figure 2.5 shows the polarographic wave due to the reduction of oxygen to form hydrogen peroxide in a 0.5 M HNO_3 solution as shown in equation 2.1. The further reduction of hydrogen peroxide to form water is not seen here as the onset of hydrogen evolution in the highly acid solution begins at a less negative potential. The onset of hydrogen evolution is clearly demonstrated by the polarogram collected after 30 minutes of purging the solution. The polarogram showing the reduction of Bi(III) and Tl(I) in a deoxygenated 0.5 M HNO_3 solution at concentrations typically used in this work is included to illustrate how critical deoxygenation is just from a wave overlap point of view.

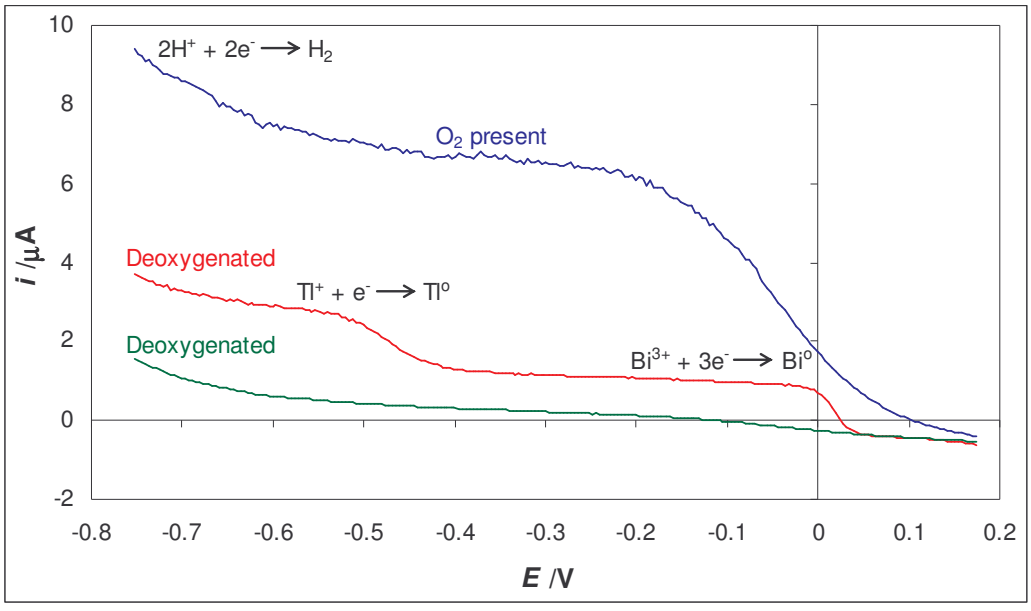

Figure 2.5: Polarograms in 0.5 M HNO_3 before and after deoxgenation and after Bi(III) (~5×10^{-5} M) and Tl(I) (~1×10^{-4} M) were added to the deoxygenated solution.

2.4.4) *Experiments for the determination of stability constants*

There are two main experimental approaches when studying metal-ligand complex formation using polarography: (1) a pH titration and (2) a ligand titration. In a pH titration, the total ligand-to-metal ion concentration ratio ($[L_T]:[M_T]$) is kept constant and the pH of the solution is varied. In a ligand titration, the pH of the solution is kept constant throughout the titration and the ligand-to-metal ion concentration ratio is increased.

(1) pH titration

In general, it is preferred to study metal-ligand equilibria starting from low pH, i.e. from the smallest degree of complexation, toward higher pH that promotes complex formation reactions. For the Bi(III) complexation studies hydrolysis occurs at low pH making it imperative to start experiments at these low pH values.

The CGE was always calibrated before and after the titration to study complexation, using the same acid and base solutions throughout. A typical pH titration experiment is started by collecting a polarogram of the deoxygenated background solution (0.5 M HNO_3) to ensure that no impurities were present in the solution. Small volumes (of the order of microlitres) of the metal ion stock solutions were then added to the background solution using Hamilton micro-syringes such that the final concentration of the metal ions were in the range of 1×10^{-5} to 50×10^{-5} M, depending on the metal ion and the experiment. Polarograms were collected for the reduction of the uncomplexed metal ions. An accurately weighed mass of ligand (using a Mettler Toledo XS105 five decimal place balance) was then added to the solution as the solid and once dissolved, another polarogram were collected.

The single DC polarogram VI was used up till this point and then the automated titration was initiated and the GUI for this VI and the typical settings used are given in Appendix 1, Figure A1.3 and Table A1.4, respectively. In this case the VI combines both potentiometric and polarographic functionalities. The procedure involved measuring the

solution temperature and CGE potential (as before). A polarogram was then recorded using exactly the same parameters as for the initial polarograms. The 0.5 M hydroxide solution, was then added until the change in pH (ΔpH) reached its set value (generally between 0.07 and 0.1). This was achieved by adding the solution in small increments (set from 0.5 mL to 0.01 mL depending on the pH of the solution) and which were periodically changed manually during the titration. Incremental additions were ceased when the specified ΔpH was obtained. The CGE potential and temperature were measured and another polarogram recorded. This procedure continued until one of the stop conditions was met, which was usually defined by the pH value attained in this case.

In order to evaluate the extent by which the diffusion junction potential changes during a pH titration, some pH titrations experiments were performed using solutions containing the metal ions only, without adding the ligand. This will be discussed extensively in proceeding chapters.

(2) Ligand titration

The GE was calibrated as before to determine the exact pH at which a polarogram is recorded. The initial background solution consisted of HNO_3 and hydroxide solution mixed in a ratio to give the required pH and an ionic strength of 0.5 M. Polarograms were recorded on the deoxygenated background solution and the solution after the addition of the metal ion stock solutions.

The titrant was a 0.5 M solution of the ligand adjusted to the pH at which the titration was to be conducted using HNO_3 or OH^-. Titrant was then added to the test solution to give an initial $[L_T]:[M_T]$ of about 20, after which the temperature and CGE potential were measured and a polarogram was collected. An automated titration was then initiated, where a fixed increment of the ligand titrant was added throughout and ΔpH was set to zero. Thus after each addition of the ligand solution, the CGE potential was accurately measured and a polarogram recorded. The volume increment was

calculated such that a minimum of 30 polarograms could be collected as $[L_T]:[M_T]$ was varied from about 20 to 200. Volume increments of about 0.015 – 0.030 mL had to be added for metal ion concentrations of 5×10^{-5} – 1×10^{-4} M, respectively. A 1 mL Dosimat exchange unit was used to add these small volumes as accurately as possible. The titration was ended after the specified volume of titrant was added. Increasing the ligand concentration promotes complex formation, but only complexes stable at that particular pH would be formed.

In both types of titrations, the pH at which each polarogram was recorded was calculated using the CGE potential measurement and the calibration curve as will be discussed in Chapter 3. The polarographic data was analysed as presented below. Both titration methods were repeated at least three times, either at different $[L_T]:[M_T]$ for pH titrations or at different pHs for ligand titrations. Where possible, when studying a particular metal-ligand system, both types of titrations were done. The ligand titration was however only possible when using picolinic acid as dipicolinic acid is not soluble enough to make a ligand solution with a high enough concentration. If the ligand solution is too dilute, a large volume increment would have to be added which would dilute the test solution too much to produce a reasonable polarographic response.

It was suggested that $[L_T]:[M_T]$ should be as large as possible in these studies in order to suppress polynuclear species formation, to shift precipitation of metal hydroxides to higher pH and to regard the concentration of metal ions at the electrode surface as unchanged by the electrochemical reduction process.[9] It was clearly demonstrated that certain species in solution went undetected when very small $[L_T]:[M_T]$ were used, as is required by potentiometry, because precipitation of hydroxides occurred. These species were detected when significantly higher $[L_T]:[M_T]$ were used by postponing precipitation, which is possible when using polarography.[16] Ratios around 100 to 200 are thus used where possible. In certain cases, however, lower $[L_T]:[M_T]$ down to 50 were used to avoid the overlapping of reduction waves.

The pH values at which ligand titrations were performed were chosen based on the analysis of stability constant data obtained from the pH titrations, and hence the pH titrations were always performed first. The pH values were selected such that at least one species formed appreciably at the chosen pH and so that information about all possible species was obtained in at least one of the titration experiments.

In the determination of stability constants, concentrations are generally used instead of activities, but in order to do this, the ionic strength of the solution must be kept constant throughout the titration and this is achieved by having a large concentration of inert electrolyte in the solutions. Since these studies do not occur at fixed ionic strength, the formation constants determined should be quoted for the ionic strength range in which they are determined, i.e. 0.25 – 0.5 M in these studies.

2.5) Processing of Polarographic Data

2.5.1) *Parameter determination from fitting polarograms*

The potential-current relationship for a DC wave is described by the Illkovič-Heyrovsky equation.[29] Considering the reduction process, the equation for a reversible electron transfer process is written as:

$$E = E^{r}_{1/2} + \frac{RT}{nF}\ln\left(\frac{i_d - i}{i}\right) \qquad (2.11)$$

and for an irreversible electron transfer process is written as:

$$E = E^{i}_{1/2} + \frac{RT}{\alpha nF}\ln\left(\frac{i_d - i}{i}\right) \qquad (2.12)$$

where $E^{r}_{1/2}$ and $E^{i}_{1/2}$ are the reversible and irreversible half-wave potentials respectively, i_d is the diffusion limited current, n is the number of electrons transferred and α is the transfer coefficient. The term “reversible” as applied to an electrochemical process implies that the rate of electron transfer must be much faster than the rate of mass transport. For an irreversible electrochemical process the rate of electron transfer is much slower than the

rate of transport. Processes occurring in the transition zone between these two are known as quasi-reversible processes where the rates of electron transfer and mass transport are comparable. The rate at which measurements are made can determine whether a process is seen as reversible or irreversible under those conditions. For quasi-reversible processes, the standard rate constant for the electron transfer ($k°$) lies within the range $2 \times 10^{-7}\ \nu^{1/2} \leq k° \leq 3 \times 10^{-3}\ \nu^{1/2}$ where ν is the scan rate.[30] For both reversible and irreversible DC waves, the value of the ratio $(i_d - i)/i$ would be one at the midpoint of the wave where $i = i_d/2$ which would make the "ln" term zero and the potential at this midpoint corresponds to either the reversible or the irreversible half-wave potential, respectively.[1] The value of i_d is independent of the electron transfer kinetics.

The DC waveform can be described by the following equation:[31,32]

$$E = E_{1/2} + \frac{RT}{\delta nF} \ln\left(\frac{i_d - i}{i}\right) \tag{2.13}$$

where $E_{1/2}$ is the half-wave potential for the experimental wave (be it the reversible, irreversible or quasi-reversible half-wave potential) and δ has no physical meaning but indicates the slope of the wave. When comparing Equations 2.11 and 2.13, it can be seen that for $\delta = 1$, $E_{1/2} = E^r_{1/2}$, indicating a fully reversible electron transfer process. Equation 2.13 can be rearranged such that the dependent variable is i and the independent variable is E which reflects the experimental process of recording a polarogram. The expression becomes:

$$i = \frac{i_d}{10^{\left(\frac{n\delta(E - E_{1/2})}{0.05916} + 1\right)}} \tag{2.14}$$

This relationship only describes the electron transfer process. In DC polarography the capacitance current increases linearly as more negative potentials are applied. The overall current measured is thus the sum of both the faradaic current and the background current as follows:

$$i = \frac{i_d}{10^{\left(\frac{n\delta(E-E_{1/2})}{0.05916}+1\right)}} + i_{bkgnd} \qquad (2.15)$$

If the background current constitutes only the charging current, i_{bkgnd} can be described by the equation for a straight line. The half-wave potential and diffusion limited current, as well as the value of δ, can be obtained by fitting Equation 2.15 to each polarogram using a non-linear curve fitting program.

To assess whether a process is reversible or not, the log analysis approach can be used. This involves plotting E vs $\log\{i/(i_d - i)\}$ where the value of i_d first has to be determined. The slope produced should be equal to $-0.05916/n$ V at 25 °C for a reversible process[1,29] as is evident by rearranging Equation 2.11 to the form:

$$E = E^r_{1/2} - \frac{0.05916}{n}\log\left(\frac{i}{i_d - i}\right) \qquad (2.16)$$

The value of $E^r_{1/2}$ can also be determined from this plot where $i = i_d/2$ and hence $\log\{i/(i_d - i)\} = 0$.[1] In theory this method sounds straight forward, but in practice it seems that the background currents need to be subtracted first to provide meaningful results.

Alternatively the value of δ obtained from fitting the DC wave (Equation 2.13) is a good indication of the reversibility of the electron transfer process. It has been suggested that $1 < \delta < 0.9$ can be regarded to indicate fully reversible processes for our application, $0.9 < \delta < 0.5$ implies a quasi-reversible process and $\delta < 0.5$ implies an irreversible process.[33] Since the value of δ can be directly determined when fitting Equation 2.13 to the polarogram, this value was used to assess the reversibility of the electron transfer process.

In complex formation studies, the reversible half-wave potentials are required in calculations. If a process is quasi-reversible, the reversible half-wave potential for the process first needs to be determined. This is discussed further in Chapter 7 as the reduction of Cu(II) in a nitrate solution is quasi-reversible.

2.5.2) *Determination of formation constants*

The relationship derived by Cukrowski[9] (shown in Appendix 2 (A2.1)) for using polarographic data to determine the type of metal-ligand species present and to evaluate their formation constants is given as:

$$\left\{E(M_{free}) - E(M_{comp})_{(i)}\right\} - \frac{RT}{nF} ln \frac{i(M_{comp})_{(i)}}{i(M_{free})_{(i)}} = \frac{RT}{nF} ln \frac{[M_T]_{(i)}}{[M_{free}]_{(i)}} \qquad (2.17)$$

where $E(M_{free})$ and $E(M_{comp})$ are the half-wave potentials for the free metal ion and the complexed metal ion, respectively; $i(M_{free})$ and $i(M_{comp})$ are diffusion limited currents for the free metal ion and the complexed metal ion, respectively; and $[M_T]$ and $[M_{free}]$ are the total and free metal ion concentrations, respectively. *(i)* implies that these are the values at the ith pH or pL (where pL = $-\log[L_T]$) depending whether a pH or a ligand titration was performed, respectively. The values $i(M_{free})_{(i)}$ and $[M_T]_{(i)}$ are actually independent of the pH or pL of the solution, but these values are recalculated taking dilution effects, due to the addition of the titrant, into account. The relationship in Equation 2.17 also applies to other electrochemical techniques such as normal pulse polarography (NPP) and differential pulse polarography (DPP), where in the latter case the peak potentials (rather than the half-wave potentials) and the peak currents (rather than the diffusion limited currents) would be used.

The left-hand side of Equation 2.17 is calculated from experimental data obtained and is plotted against pH (or pL) to produce the experimental complex formation curve (ECFC) as as follows:[16,17]

$$f(pH) = \left\{E(M_{free}) - E(M_{comp})_{(i)}\right\} - \frac{RT}{nF} \ln \frac{i(M_{comp})_{(i)}}{i(M_{free})_{(i)}} \qquad (2.18)$$

The potential term $\{E(M_{free}) - E(M_{comp})_{(i)}\}$, called the potential shift (ΔE), is the main mechanism of observing changes in species in solution. The more highly complexed the metal ion, the more energy is required to reduce the metal ion centre and thus reduction occurs at more negative potentials as compared to the uncomplexed metal ion. Since ΔE is used to evaluate complex formation and this change is always measured relative to the free metal ion potential, it is critical that $E(M_{free})$ be established as accurately as possible. This value is

usually determined experimentally as the $E_{1/2}$ from the polarograms of solutions containing the metal ion only and no ligand. Generally at least three polarograms are recorded in this solution to ensure $E(M_{free})$ is accurate and the average $E_{1/2}$ value is used. The current term $-RT/nF \ln\{i(M_{comp})_{(i)} / i(M_{free})_{(i)}\}$ is generally close to zero as the $i(M_{comp})_{(i)}$ is calculated at each pH (or pL) taking dilution into account. It is only when there is a big difference in the rate of diffusion of the metal ion complex as compared to that of the free metal ion that this term becomes more significant. When electrochemically inert species are formed, these species can also be accounted for by considering the decrease in $i(M_{comp})_{(i)}$. The potential shift together with this current term (i.e. the left-hand side of Equation 2.17) is also called the corrected potential shift.

The right-hand side of Equation 2.17 is calculated using mass balance equations containing stability constants. Two mass balance equations are involved, namely the mass balance equation for the total metal ion concentration which is:

$$[M_T]_{(i)} = [M_{free}]_{(i)} + \sum_p \sum_q \sum_r p\beta_{M_pL_qH_r} [M_{free}]_{(i)}^{\ p} [L_{free}]_{(i)}^{\ q} [H]_{(i)}^{\ r} + \\ + \sum_x \sum_y x\beta_{M_x(OH)_y} [M_{free}]_{(i)}^{\ x} [OH]_{(i)}^{\ y} \quad (2.19)$$

and that for the total ligand concentration which is:

$$[L_T]_{(i)} = \sum_k \beta_{H_kL} [H]_{(i)}^{\ k} [L_{free}]_{(i)} + \\ + \sum_p \sum_q \sum_r q\beta_{M_pL_qH_r} [M_{free}]_{(i)}^{\ p} [L_{free}]_{(i)}^{\ q} [H]_{(i)}^{\ r} \quad (2.20)$$

where a negative r value indicates OH^-. The computed complex formation curve (CCFC), is the plot of the right-hand side of Equation 2.17 as a function of pH (or pL). For ligand concentrations much larger than the metal ion concentrations, the mass balance equation for the ligand concentration can be simplified by simply taking the protonation of the ligand into account since the concentration of ligand involved in complex formation would be relatively small. When solving the mass balance equations, the total metal ion and total ligand concentrations are known, and the H^+ and OH^- concentrations can be calculated using the measured pH of the solution. The concentrations of the

free metal ion and the free ligand at various pH (or pL) values as well as the stability constants, β, are refined simultaneously. This is achieved by giving initial estimates of the species present and their log β values such that the difference between the ECFC and the CCFC is minimised. In this refinement process, the overall stability constants for the metal-hydroxide complexes, the stepwise protonation constants for the ligand and the dissociation constant for water are all kept constant. This refinement procedure was done using the 3D-CFC software developed by Cukrowski[34] for this purpose which uses a non-linear least-squares refinement process.

For pH titrations, the experimental information for the following initial conditions are needed: the total volume of solution, the total concentrations of metal ion and ligand in the cell and the free metal ion potential and diffusion limited current before ligand is added. For each step in the titration the following information is required: the pH of the solution, the volume of hydroxide solution added and the diffusion limited current and half-wave potential determined from the polarogram. The ECFC can then be plotted using this information.

The type of species in solution and their formation constants have to be speculated as a starting point. The ECFC can be used to deduce which species are in solution by analysing the slopes of the curve in various pH regions. Since the ECFC is the plot of corrected potential versus pH, the slope can be interpreted as follows: [16,17]

$$\text{slope} = \frac{\text{number of protons involved}}{\text{total number of electrons transferred}} \times \text{Nernstian slope}$$

$$slope \approx \frac{no.\ of\ H^+}{no.\ of\ e^-} \times 60 \qquad (2.21)$$

Since this is merely an indication of which species are present, the rounded-off value of 60 for the Nernstian slope is adequate. Table 2.3 gives examples of predicted slopes for the reduction of three different solution species (ML, ML_2 and M_2L) for a divalent metal ion and at a pH where H_2L is the prevalent form of the ligand.

Table 2.3: Predicted slopes of the ECFC for the reduction of a dominant solution species for a pH titration experiment. The metal ion is divalent and the prevalent form of the ligand is H_2L.

Reduction reaction	No. of H^+	No. of e^-	Predicted slope
$ML + 2H^+ + 2e^- \rightleftharpoons M^o + H_2L$	2	2	$\frac{2}{2} \times 60 = 60$
$ML_2 + 4H^+ + 2e^- \rightleftharpoons M^o + 2H_2L$	4	2	$\frac{4}{2} \times 60 = 120$
$M_2L + 2H^+ + 4e^- \rightleftharpoons 2M^o + H_2L$	2	4	$\frac{2}{4} \times 60 = 30$

A plot of the measured half-wave or peak potential versus pH should also give a good indication of the species in solution using this slope analysis, especially when the current term in Equation 2.17 is close to zero. In certain pH ranges there maybe a mixture of species coexisting, as illustrated in species distribution diagrams where the fraction of the various species present is plotted as a function of pH. The slope will then reflect the combination of species present. If the slope is zero, it implies that either no complexes are formed or that no protons are involved in the reaction.[18]

Once the type of species present is approximated, the value of the formation constants can be guessed at for a starting point. Using the 3D-CFC software[34] the CCFC is then compared to the ECFC and the formation constants are varied to ensure a good fit between the two curves. If the CCFC lies below the ECFC, it implies that the formation constant has been under-estimated and the value of the constant has to be increased. Similarly if the CCFC lies above the ECFC, the constants have to be decreased. The pH region in which the CCFC deviates from the ECFC is an indication as to which species' constant has been incorrectly estimated. Once the CCFC reasonably describes the ECFC, the values can then be refined using the fitting procedure utilised by the software.

The 3D-CFC software can plot the species distribution diagrams of the fraction of species present versus pH if the formation constants of all the species, including the metal-hydroxide species, and the protonation constants for the

ligand are provided. These diagrams vary with the total concentrations of ligand and metal ion in solution.

For ligand titrations, the experimental information required is exactly the same as that for the pH titration, except in this case the concentration and volume of ligand added is used and the pH value will be essentially constant. In this case the ECFC is the plot of the corrected potential versus log[L]. The slope analysis of the ECFC is therefore:[18]

$$\text{slope} = \frac{\text{number of ligands involved}}{\text{total number of electrons transferred}} \times \text{Nernstian slope}$$

$$slope \approx \frac{no.\ of\ L}{no.\ of\ e^-} \times 60 \qquad (2.22)$$

Table 2.4 gives examples of predicted slopes for a ligand titration experiment for the reduction of three different solution species as before. Species distribution diagrams can also be plotted for the fraction of the various species present as a function of log[L].

Table 2.4: Predicted slopes of the ECFC for the reduction of a dominant solution species for a ligand titration experiment. The metal ion is divalent and the prevalent form of the ligand is H_2L.

Reduction reaction	No. of L	No. of e^-	Predicted slope
$ML + 2H^+ + 2e^- \rightleftharpoons M^o + H_2L$	1	2	$\frac{1}{2} \times 60 = 30$
$ML_2 + 4H^+ + 2e^- \rightleftharpoons M^o + 2H_2L$	2	2	$\frac{2}{2} \times 60 = 60$
$M_2L + 2H^+ + 4e^- \rightleftharpoons 2M^o + H_2L$	1	4	$\frac{1}{4} \times 60 = 15$

The final stability constants for the species present are then determined by averaging the values determined for all the pH and ligand titration experiments and the standard deviations quoted are then from this averaged data.

2.5.3) *Virtual potentiometry*

Virtual potentiometry is an alternative approach when modelling and refining formation constants in metal-ligand equilibria studies.[31,32,35] This process involves converting polarographic data, from either ligand or pH titration

experiments, into potentiometric data as could be obtained from a virtual free metal ion sensor. The virtual potential, *E(virt)*, is calculated as follows:

$$E(virt)_{(i)} = E(M_{comp})_{(i)} + \frac{RT}{nF}\ln\frac{i(M_{comp})_{(i)}}{i(M_{free})_{(i)}} \qquad (2.23)$$

where the symbols have same meaning as described for Equation 2.17. Software such as ESTA (Equilibrium Simulation and Titration Analysis)[36] which is generally utilised to refine stability constants from potentiometric data, can thus be applied to polarographic data. The slope and y-intercept (E^o) required by the software are obtained from the calibration of the potentiometric sensor. In the case of a virtual potentiometric sensor, these values are obtained from the plot of *E(virt)* against log [M_{free}].

2.6) References

1) J.J. Lingane, Chem. Rev., 29 (1941) 1
2) D.D. DeFord and D.N. Hume, J. Am. Chem. Soc., 73 (1951) 5321
3) R.D. Hancock, I. Cukrowski, J. Baloyi and J. Mashishi, J. Chem. Soc., Dalton Trans. (1993) 2895
4) R.D. Hancock, I. Cukrowski, I. Antunes, E. Cukrowska, J. Mashishi and K. Brown, Polyhedron, 14 (1995) 1699
5) I. Cukrowski, E. Cukrowska, R.D. Hancock and G. Anderegg, Anal. Chim. Acta, 312 (1995) 307
6) I. Cukrowski, F. Marsicano, R.D. Hancock, P.T. Tshetlho and W.A.L. van Otterlo, Polyhedron, 14 (1995) 1661
7) I. Cukrowski, F. Marsicano, R.D. Hancock and E. Cukrowska, Electroanalysis, 7 (1995) 763
8) I. Cukrowski, R.D. Hancock and R.C. Luckay, Anal. Chim. Acta, 319 (1996) 39
9) I. Cukrowski, Anal. Chim. Acta, 336 (1996) 23
10) D.N. Hume, D.D. DeFord and G.C.B. Cave, J. Am. Chem. Soc., 73 (1951) 5323
11) D.N. Hume, and I.M. Kolthoff, J. Am. Chem. Soc., 71 (1949) 867
12) D.N. Hume, and I.M. Kolthoff, J. Am. Chem. Soc., 72 (1950) 4423
13) A.M. Bond, J. Electroanal. Chem., 20 (1969) 223
14) A.M. Bond, J. Electroanal. Chem., 23 (1969) 269
15) A.M. Bond, J. Electrochem. Soc., 117 (1970) 1145
16) I. Cukrowski, Electroanalysis, 9 (1997) 1167
17) I. Cukrowski, Electroanalysis, 9 (1997) 699
18) I. Cukrowski, J.R. Zeevaart and N.V. Jarvis, Anal. Chim. Acta, 379 (1999) 217
19) I. Cukrowski and G. Ngigi, Electroanalysis, 13 (2001) 1242
20) I. Cukrowski and N. Maseko, Electroanalysis, 15 (2003) 1377
21) P.M.S. Monk, Fundamentals of Electroanalytical Chemistry, John Wiley and Sons Ltd, Chichester, UK, 2001
22) A.N. Frumkin, N.V. Fedorovich, B.B. Damaskin, E.V. Stenina and V.S. Krylov, J. Electroanal. Chem., 50 (1974) 103

23) A. Trojánek and K. Holub, Anal. Chim. Acta, 121 (1980) 23
24) C. Colombo and C.M.G. van den Berg, Anal. Chim. Acta, 377 (1998) 229
25) J.J. Pedrotti, L. Angnes and I.G.R. Gutz, Anal. Chim. Acta, 298 (1994) 393
26) A.I. Vogel, A Textbook of Quantitative Inorganic Analysis, Longmans, London, 1961
27) Metrohm, Complete Catalogue Metrosensor Electrodes, Herisau, Switzerland, 1999
28) I. Cukrowski, P. Magampa and T.S. Mkwizu, Helv. Chim. Acta, 89 (2006) 2934
29) C.M.A. Brett and A.M.O. Brett, Electrochemistry Principles, Methods and Applications, Oxford University Press Inc., UK, 1993
30) P. Zanello, Inorganic Chemistry – Theory, Practice and Application, The Royal Society of Chemistry, UK, 2003
31) I. Cukrowski, J.M. Zhang and A. van Aswegen, Helv. Chim. Acta, 87 (2004) 2135
32) I. Cukrowski and J.M. Zhang, Electroanalysis, 16 (2004) 612
33) I. Cukrowski, H.M. Marques, T.S. Mkwizu, P.P. Magampa and C. Serge, Anal. Chim. Acta, 590 (2007) 203
34) I. Cukrowski, 3D-CFC10 software, Version 5.0, 2000
35) I. Cukrowski and J.M. Zhang, Chem. Anal., 50 (2005) 3
36) K. Murray and P. May, Equilibrium Simulation and Titration Analysis (ESTA) User Manual, 1984

CHAPTER 3
Calibration of the Glass Electrode

3.1) Introduction

3.1.1) *pH and the glass electrode*

The concept of pH was first introduced by Sørenson in 1909 when studying enzymes. A paper titled "One Hundred Years of pH" has recently been published by Myers, highlighting how long the concept has endured; although chemists largely ignored pH till the late 1930's.[1] The way in which Sørenson obtained his pH value, however, was neither a measure of concentration nor activity of the hydrogen ion, but rather some conventional scale.[2]

The hydrogen ion activity, or concentration in certain cases, is normally measured using either a hydrogen electrode or a glass electrode (GE). A typical cell setup using a hydrogen electrode could be represented as

$$\mathrm{Pt(s)\,|\,H_2(g,}\ f = 101.325\ \mathrm{kPa)\,|\,Test\ solution}\ \|\ \mathrm{KCl(3\ M)\,|\,AgCl(s)\,|\,Ag(s)}$$

where f is the fugacity of hydrogen. Ideally the glass electrode should behave exactly as the hydrogen electrode to changes in hydrogen ion activity. The ideal or Nernstian response is $(RT/F)\ln(10)$ volts per pH unit, where R, T and F are the gas constant, the absolute temperature and Faraday's constant respectively. This response translates to 0.05916 V per pH unit at 25 °C. This ideal performance is, however, not attainable by a GE over the entire pH range.[1] Even so, the GE is nowadays more frequently utilised than the hydrogen electrode due to its ease of use.

The GE consists of a glass membrane with an inner reference system. The outer reference system can be combined with this into a single electrode and is called a combination glass electrode (CGE). The inner reference system consists of a solution of constant hydrogen ion concentration that is placed in the glass bulb with a reference electrode (RE) immersed into it. These days it will usually be a Ag/AgCl electrode immersed into a dilute hydrochloric acid or

a buffered chloride solution. The buffer capacity of this solution must be fairly high in order to neutralise leachates from the glass. Generally, the inner reference solution is chosen such that an emf of 0 V is produced when the GE is inserted into a commercial buffer solution at pH 7.0.[2] A typical cell setup could be represented as follows:

Ag(s) | AgCl(s) | HCl (0.1 M) | glass | Test solution ‖ KCl (3 M) | AgCl(s) | Ag(s)

A schematic diagram of a combined GE is shown in Figure 3.1.

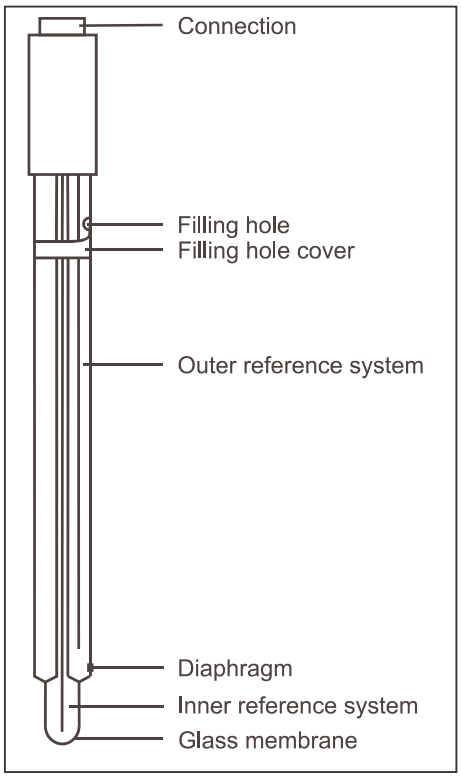

Figure 3.1: Schematic diagram of an example of a combined glass electrode.

The glass membrane consists mainly of a silica framework containing other oxides, predominantly that of the alkali and alkali earth metals. It is the silicate sites that are selective to the hydrogen ions. The most common glass contains SiO_2, CaO and Na_2O, however, other pH-sensitive glasses which contain oxides such as lithium, caesium, barium, lanthanum and so on, have been developed in order to reduce the alkaline error.[2] The membranes of the Metrohm glass electrodes used in this work are a lithium silicate type glass which reduces the alkaline error in the presence of NaOH and KOH.[3]

According to the random-network theory for silicate glasses, each silicon atom is at the centre of a tetrahedron formed by four oxygen atoms, but in glass there is no long-range order in these tetrahedral units. Each oxygen atom is then coordinated to two silicon atoms. In the lithium silicate glass, each singly charged lithium cation gives rise to one singly charged oxygen ion which is coordinated to only one silicon atom.[4] An example of the structure of alkali silicate glass is schematically shown in Figure 3.2.

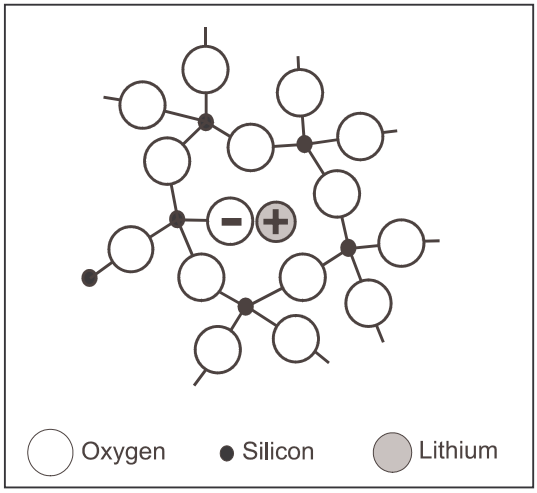

Figure 3.2: Schematic diagram of the structure of lithium silicate glass.

It is essential that the resistance of the cell be much less than that of the electronic circuit of a voltmeter in order to measure the emf of the cell accurately. Thus the resistivity of the glass membrane must be less than about 10^{12} Ω cm, in general.[4] The glass membrane materials for the Metrohm electrodes used have membrane resistances in the range 150 – 500 MΩ for membranes that are 0.2 – 0.5 mm thick,[3] which translates to resistivities of $3 \times 10^6 - 2.5 \times 10^7$ Ω cm and is significantly lower than the limit quoted.

The exact mechanism by which the glass membrane produces the pH response is not fully understood, but some hypotheses based on experimental results have been made. Glass membranes are not semi-permeable, but rather function by developing an interfacial potential difference independently on each membrane surface due to ion exchange reactions with the solutions. From the construction of the electrode, the solution on the one side of the

glass membrane (the inner solution) is kept constant. It is therefore only the change in the composition of the test solution that would result in a variation of the potential difference across the glass membrane.[4] In alkali silicate glass, the current is carried exclusively by the alkali metal ions which move through the immobile silicon-oxygen network. It is speculated that the alkali metal ions close to the membrane surface dissociate from the silicon-oxygen network under the influence of water and pass into the solution. An anionic network thus formed at the membrane surface allows easy passage of hydrogen ions from the solution to the glass surface. The alkali metal ions in the centre of the glass remain intact. It has been shown that the hydrogen ions make almost no contribution to the conduction through the glass as they are probably more strongly bonded in the silicon-oxygen network compared to the alkali metal ions.[2,4] Even so, conduction through the glass is very slight and occurs by the middle alkali metal ion layer moving a little toward one surface or the other with the passage of very small currents, the direction of movement depending upon the direction of the current. It is improbable that anions will be able to occupy space on the membrane surface due to repulsions of the oxygen ions surrounding the interstices of the lattice.[2,4]

As mentioned above, the glass membrane first takes up water which causes the membrane to swell. It is essential that the glass membrane is sufficiently hydrated in order for the electrode to behave accurately as a pH indicator. The exact role of the water in the functioning of the electrode is not known, although it has been suggested that the water may facilitate the movement of ions through the glass or it may lower energy barriers for the transfer of protons from the solution to the gel layer. This is supported by the fact that the resistance of the membrane increases considerably as it becomes dehydrated.[2,4] Glass electrodes are therefore stored in distilled water or buffer solutions, or in the case of a combined outer reference system, in the reference electrode filling solution.

The overall potential measured using a cell containing a GE consists of a combination of potentials as follows:

$$E_{cell} = E_r + E_j + E_g \quad (3.1)$$

E_r is the potential difference due to the use of the internal and the external REs. Each RE should have a potential that is similar in magnitude (provided the two REs are of the same type) and should remain constant throughout a titration. E_j is the diffusion junction potential that is formed between the external RE solution and the test solution. E_g is the potential across the glass membrane and includes the asymmetry potential. The asymmetry potential is due to differences between the inner and outer leached layers of the glass membrane which could stem from, *inter alia*, the manufacturing process, different environments the two layers have experienced or substances adsorbed on either layer.[5] The cell potential expression can be extended to show the pH dependence as follows:

$$E_{cell} = E_r + E_j + E°_g + k\left(\frac{RT}{F}\right) \ln a_{H^+} \quad (3.2)$$

a_{H+} is the hydrogen ion activity and k denotes the electromotive efficiency of the glass membrane and shows how closely the electrode exhibits Nernstian behaviour (for $k = 1$ the electrode behaves in a true Nernstian manner). Glass electrodes have rather been described as sub-Nernstian and k is usually less than 1.[6,7] The value of k is dependant on the ionic strength of the solution, but is approximately equal for all types of glass simply because the inner and outer surfaces of the glass membrane behave the same and thus any influences due to glass composition cancel out.[7] $E°_g$ is the standard glass electrode potential which includes the asymmetry potential. Although the asymmetry potential can drift with time, it does not fluctuate largely or suddenly, thus can be assumed to be stable throughout an experiment.[2]

The values for E_r and $E°_g$ are therefore essentially constant. However, the value of E_j depends on the composition of the test solutions and consequently varies throughout a pH titration. This variation is more pronounced in a very alkaline solutions and even more so in very acidic solutions. GEs are usually used in a pH region where E_j is small, about pH 2-12, and the value of E_j is assumed to be constant. For this pH region the expression can be written as follows:

$$E_{cell} = E_{const} + k\left(\frac{RT}{F}\right) \ln a_{H^+} \tag{3.3}$$

where $E_{const} = E_r + E_j + E^o_g$.

Furthermore, when the ionic strength of the solution is maintained constant, equation 3.3 can be simplified to:

$$E_{cell} = E'_{const} + k\left(\frac{RT}{F}\right) \ln [H^+] \tag{3.4}$$

where $E'_{const} = E_r + E_j + E°_g + k\left(RT/F\right) \ln \gamma_{H^+}$ and γ_{H^+} is the activity coefficient of the hydrogen ion.

It is not always possible to work in the pH region where E_j is constant, so ways to measure or calculate the extent of the value of E_j, or to circumvent this problem have been considered. The use of a cell without a liquid junction such as a Harned cell, which contains a hydrogen electrode, can be used to measure the pH of a solution. This is achieved by including the chloride ions required for the RE in the test solution. The cell can be typically described as:

$$Pt(s) \mid H_2(g, f = 101.325 \text{ kPa}) \mid \text{Test solution, } Cl^-(aq, 3M) \mid AgCl(s) \mid Ag(s)$$

Even though there are advantages to using this cell, it is frequently impractical as one is forced to work in a chloride medium and it introduces other complications such as the dependence of the cell potential on the chloride ion activity.[1]

Since E_j cannot be directly measured, there have been many different approaches to calculate the value of E_j, of which the Henderson equation is the simplest. This will be discussed in more detail in Chapter 4. A reduced form of the Henderson equation, derived for low acid concentrations and univalent electrolytes, has been used[8] to correct for liquid junction potentials when calibrating GEs and is given as:

$$E_j = -\left(\frac{RT}{F}\right) \ln\left(1 + \frac{d[H^+]}{\mu}\right) \tag{3.5}$$

where μ is the ionic strength of the solution. This correction does not apply to the very acidic range, however. In deriving this equation, various assumptions have been made, for example the way in which the diffusion junction is formed, and hence the equation does not apply to all experimental conditions.

3.1.2) *Calibrating the glass electrode for metal-ligand equilibria studies*

Ligands are generally weak acids and the extent of protonation depends on the pH of the solution. Consequently, the type of metal-ligand species present in solution is also dependent on pH, amongst other factors. When determining equilibrium constants, including protonation constants of the ligand and metal-ligand formation constants, it is vital that the pH of the solution be measured as accurately as possible. When using a GE to measure the pH, it needs to be calibrated correctly to reduce errors. The calibration procedure also determines whether it is the hydrogen ion activity or concentration (if the ionic strength is kept constant) that is being measured. Large errors due to inaccuracy in calibration have especially been noted for high ($pK < 3$) or low ($pK > 11$) dissociation constants of acids.[9] This is due mainly to large diffusion junction potentials when there is a large concentration of hydrogen or hydroxide ions present, as well as the glass membrane response to alkali metal ions when there is a deficiency of hydrogen ions in solution. This will be discussed in greater detail below.

Despite many limitations, GEs are still the most frequently used devices to measure pH. Before the pH of a test solution can be measured, the electrode first has to be calibrated so that the measured potential is related to the pH of the solution. There have been a number of proposals on how best to calibrate a glass electrode. The two distinct approaches involve either the use of buffer solutions or an acid-base type titration procedure, of which the latter is preferred for formation constant studies.

Buffers are commonly used to determine the hydronium ion activity in solution. There is a whole range of buffers containing compounds such as oxalates, tartrates, phthalates, acetates, citrates, borates, carbonates, hydroxides, amines and phosphates, to name only a few.[6,10-14] An advantage of using

buffers is that the hydrogen ion concentration is not affected by acid impurities, dissolved carbon dioxide and so on.[15]

There are two approaches to assigning pH values to the buffer solutions.[13,16] Firstly, the British Standards Institution (BSI) has chosen only one reference solution, namely 0.05 mol kg^{-1} potassium hydrogen phthalate. The pH of the solution is measured using a hydrogen electrode in a cell without transference as follows:

$$H_2(g) \mid Pt(s) \mid Buffer, Cl^-(m_{Cl}) \mid AgCl(s) \mid Ag(s)$$

where m_{Cl} is the molality of chloride ions added to the solution. The cell's pH is assigned according to the Bates-Guggenheim convention used to calculate activity coefficients. This convention only holds for solutions of ionic strength less than 0.1 mol kg^{-1} and is a quasi-thermodynamic approach.[2] The pH values of other standards are then derived by measuring cell potentials in a cell with transference employing a capillary diffusion junction as follows:

$$H_2(g) \mid Pt(s) \mid Buffer \parallel KCl(m \geq 3.5 \text{ mol } kg^{-1}) \mid AgCl(s) \mid Ag(s)$$

This standard provides data that is precise, but that lacks thermodynamic meaning.[16]

Secondly, the National Institute of Standards and Technology (NIST) assigned pH values to seven primary and two secondary standard buffer solutions using the cell with transference as given above. Diffusion junction potentials limit the accuracy of the pH measurements. The International Union of Pure and Applied Chemistry (IUPAC) recommends both of these scales simultaneously even though they are mutually exclusive thus one pH standard can have two different values that vary by up to 0.02 pH units.[16]

There are also different procedures to calibrate the GE when using buffers, namely a one-point calibration, a two-point calibration or a multi-point calibration.[6,13,16] In a one-point calibration, the slope of the graph is assumed to be Nernstian and the line will then pass through the point as determined by the measured buffer solution. Most applications use a two-point calibration or "bracketing" procedure, as recommended by IUPAC, where the pH of the

unknown is bracketed by a higher and a lower pH standard. Assuming the calibration line passes through the two points determined by the measured buffer solutions, the slope and the intercept of the line are then calculated. A multi-point calibration uses more than two buffer solutions (usually five buffers are sufficient) and is recommended when a minimum uncertainty and maximum consistency is required over a wide range of pH values.[6,16]

The problem with using buffers to calibrate the GE in formation constant studies is that the protonation constants of the weak acids and bases used in the buffers need to be very accurately known.[15] The junction potential depends on both ionic strength and composition. It is not always possible to calculate the junction potential and hence it cannot be corrected for.[9] Using standards as close to the pH to be measured should reduce the junction potential error somewhat.[13] The hydrogen ion activity coefficient also depends on both ionic strength and composition which may not necessarily be the same for the buffer and test solutions. The ionic strength of the buffer may be adjusted to match that of the test solution provided the ionic strength of the test solution is greater than that of the buffer. It is more problematic when the ionic strength of the solution is significantly lower than that of the buffers.[17] When the ionic strength of the buffer is adjusted, the activity coefficients need to be amended accordingly. These coefficients have been calculated using various methods such as the Debye-Hückel equation recommended for ionic strengths below 0.01 M but used up to 0.1 M,[18,19] the extended form of the Debye-Hückel equation for ionic strengths up to about 0.8 M,[19,20,21] the Guggenheim equation for ionic strengths up to about 0.5 M,[19,22] the Davies equation[23] or the series of Pitzer equations which have been used from moderate to high ionic strengths,[5,21,24-26] to name only a few. All these methods incorporate certain assumptions and thus the accuracy of these activity coefficients is not known. The fact that the determination of a single ion activity coefficient is thermodynamically meaningless and impossible to measure indicates the extent of the assumptions that need to be made. It has been shown that for ionic strengths lower than about 0.05 M, it does not matter which procedure is used to determine the activity coefficients, but these values differ more significantly at higher ionic strengths.[27] The addition of salts to buffer solutions

lowers the pH of the solutions, as would be expected, but it has been shown that the extent to which the pH changes is different for different buffer solutions with the same pH when the same amount of salt is added to them.[28]

Some authors[9,18,29,30] have used buffer solutions for calibrating the GE in stability constant studies. Meinrath and Spitzer[30] used a multi-point calibration procedure with buffer solutions to determine thermodynamic formation constants. Hedwig and Powell[29] used buffer solutions at fixed ionic strength with known hydrogen ion concentration instead of activities for calibrating the glass electrode. A response to the work by Hedwig and Powell however, claims that:

> *… (they) do not appreciate the profound difficulties which are encountered whenever standard buffers are used to calibrate the glass electrode for the determination of stability constants*
>
> and
>
> *They have consequently misjudged the relative importance of the various errors involved.*
>
> P.M. May, (1983)[31]

There have been other attempts to relate the direct measurement from the pH meter to the actual hydrogen ion concentration in solution. McBryde[18] introduced the ratio Γ defined as:

$$\Gamma = \frac{H}{[H^+]} \tag{3.6}$$

where H is determined from the direct pH measurement. The values for Γ were determined by calibrating the glass electrode with four buffers and then taking the pH reading of sets of solutions with differing $[H^+]$, but with a common ionic background. Irving *et al.*[9] introduced the correction factor A, due to the observation that the titration curves of pH versus volume of titrant (for determining protonation constants) that were plotted using 3 different glass electrode calibration procedures, were parallel to one another but slightly displaced along the pH axis. The calibration procedures used (1) a buffer solution, (2) the same buffer solution adjusted to the same ionic strength and

using the background ions as in the test solution and (3) a strong acid-strong base titration as discussed below. The correction factor is defined as:

$$A = p(H) - p[H^+] \tag{3.7}$$

where p(H) is the pH measured directly due to the calibration using a buffer and $p[H^+]$ is the calculated pH from the titration. The values of both Γ and A apply only to a particular cell under a particular set of conditions.

The recommended procedure for the calibration of a GE in stability constant studies at constant ionic strength still remains that of an acid-base titration, and the hydronium ion concentration is determined rather than its activity.[9,20] By using this approach, the composition of the calibration and the test solutions can be as close to each other as possible thus reducing discrepancies in the liquid junction potential. Three different approaches have been taken, namely, the titration of a strong acid with a strong base, the titration of a background electrolyte using a strong acid or a strong base and the titration of a weak acid or base using a strong base or acid respectively. The first approach is the most widely used.

In the strong acid-strong base titration, both solutions are standardized and the acid is titrated by the base. The ionic strengths, adjusted using an excess of background salt electrolyte, are the same for both solutions which results in the ionic strength remaining constant throughout the titration. The concentration of the hydrogen ions in solution can be calculated at each point along the titration curve using equations 2.6 and 2.7 and the measured GE potential is then plotted against the calculated pH and the straight line graph is obtained as given by equation 3.4. When equations 2.6 and 2.7 are substituted into equation 3.4 the following are obtained:

- before the equivalence point

$$E_{cell} = E'_{const} + s \log \left(\frac{c_a v_a - c_b v_b}{v_a + v_b} \right) \tag{3.8}$$

- after the equivalence point

$$E_{cell} = E'_{const} + s \log \left(\frac{K_w (v_a + v_b)}{c_b v_b - c_a v_a} \right) \quad (3.9)$$

where $s = k(RT/F)\ln 10$. Thus in the calibration plot of E versus pH the slope of the graph is affected by systematic errors in the acid and base concentrations.[32,33] Also, linear correlations can be obtained for the acidic region and for the basic region, but often these two regions do not coincide.[15] Generally the best straight line is drawn through the data from both the acidic and basic regions which is some kind of average of the two separate regressions.

The value of K_w depends on both temperature and ionic strength. One would assume that due to the dependence of pH on the value of K_w in the alkaline region, there would be a significant amount of K_w data under various conditions. On the contrary, the only values given in the NIST database[34] are presented in Table 3.1 below, which is by no means a comprehensive list. More than one value is also quoted at a given temperature and ionic strength which makes the selection of these values more difficult. More complete lists of values are given in the IUPAC Stability Constants Database[35] and the help option in the program GLEE (glass electrode evaluation)[36], the latter of which is used in the calibration of a GE by means of a strong acid-strong base titration. Further, as stated with regard to metal complex formation constants and which certainly also applies to the values of K_w:

> *(the) extrapolation of available data to regions of interest is often hampered … by inadequate theory to guide extrapolation …*"
>
> G.H. Nancollas and M.B. Tomson, (1982)[20]

As mentioned, another procedure for the calibration of a GE involves the titration of an inert electrolyte by a strong acid or a strong base. The concentration of hydrogen ions in solution can be calculated at each point along the titration curve using equations 2.8 and 2.9 and when these equations are substituted into equation 3.4, the following are obtained:

- in the acidic region

$$E_{cell} = E'_{const} + s \log\left(\frac{c_a v_a}{v_a + v_i}\right) \tag{3.10}$$

$$E_{cell} = E''_{const} + s \log\left(\frac{v_a}{v_a + v_i}\right) \tag{3.11}$$

- in the basic region

$$E_{cell} = E'_{const} + s \log\left(\frac{K_w (v_b + v_i)}{c_b v_b}\right) \tag{3.12}$$

$$E_{cell} = E''_{const} + s \log\left(\frac{v_b + v_i}{v_b}\right) \tag{3.13}$$

where $E''_{const} = E'_{const} + s \log(c_a)$ and $E''_{const} = E'_{const} + s \log(K_w / c_b)$. The slope in the calibration plot of E versus pH is independent of the concentration of the acid or base used and thus any small errors in the determination of these concentrations do not affect the slope.[32,33] This explains the observation that the slope of the graph is in general also closer to the Nernstian slope when titrating a background electrolyte compared to strong acid-strong base titrations. The errors in the concentrations will, however, be included in the value of E^o (the y-intercept). Frequently, when titrating the background electrolyte, the calibration is done in the acid region only and then extrapolated.[5,32,33] In the titration of a weak acid or a weak base using a strong base or acid respectively, the dissociation constants need to be accurately known in order to calculate the hydrogen ion concentration. The quality of these constants is generally difficult to assess. Calculating the hydrogen ion concentration is also mathematically more complicated. However, a specific pH region can be calibrated by prudent choice of the weak acid or weak base.[33]

In the titration of a weak acid or a weak base using a strong base or acid respectively, the dissociation constants need to be accurately known in order to calculate the hydrogen ion concentration. The quality of these constants is generally difficult to assess. Calculating the hydrogen ion concentration is also mathematically more complicated. However, a specific pH region can be calibrated by prudent choice of the weak acid or weak base.[33]

Table 3.1: Table of pK_w values at different temperatures and ionic strengths.[34]

T / °C	μ / M	pK_w	Background electrolyte
10	0.0	14.533	
25	0.0	13.997 ± 0.003	
40	0.0	13.544	
20	0.1	13.95	
25	0.1	13.78 ± 0.01	
37	0.15	13.36 ± 0.02	
25	0.5	13.69 ± 0.03	NaCl
25	0.5	13.73 ± 0.04	
25	0.5	13.75 ± 0.02	Tetraalkyl ammonium salt
25	0.7	13.75*	
25	1.0	13.71 ± 0.02	NaCl
25	1.0	13.77 ± 0.04	
25	1.0	13.94 ± 0.01	Tetraalkyl ammonium salt
25	2.0	13.82 ± 0.02	NaCl
25	2.0	13.93 ± 0.04	KCl
25	2.0	13.95 ± 0.01	$NaClO_4$
25	3.0	13.87	$LiClO_4$
25	3.0	13.95	$NaNO_3$
25	3.0	13.99 ± 0.03	NaCl
25	3.0	14.15 ± 0.03	KCl
25	3.0	14.20 ± 0.03	$NaClO_4$
25	4.0	14.52	$NaClO_4$
25	5.0	14.47 ± 0.02	NaCl
25	6.0	15.22	$NaClO_4$
25	8.0	15.94	$NaClO_4$

* Value adjusted for compatibility with other values

Background electrolytes often contain alkali metals, but the GE does not produce a linear response for solutions with high concentrations of alkali metals and even alkali earth metals. The potential response to changes in pH drops below the ideal Nernst response and is attributable to the development of a partial response of the glass membrane to cations, especially sodium and to a lesser extent potassium ions.[2,37,38] This deviation in response from ideality is called the alkaline error. It increases rapidly with temperature[38] and may vary with the age and the treatment of the electrode.[12]

3.2) Aims

As the ligands studied in this work are weak acids, the extent of protonation is dependant on the pH of the solution. The pK_a values of these ligands would also influence the type of complex formed under specific solution conditions. The main objective of this study was to investigate metal-ligand equilibria under very acidic conditions by polarography. At each point in the titration experiment information must be acquired from the polarographic reduction wave as well as the p[H] of the solution due to the pH-dependence of the form of the ligand in solution.

In order to determine the pH of the solution, the GE has to be calibrated so that its potential response is related to the concentration of H^+ in solution. As with most analytical techniques it is best to work in the region where the calibration is linear. This is not possible here as studies start in 0.5 M acid solutions and the pH has to be measured as accurately as possible from these values. At these high acid concentrations the liquid junction potential becomes significant which leads to curvature in the calibration and thus needs to be taken into account. GEP measurements generally commence above pH 2, i.e. H^+ concentrations smaller than 0.01 M, so there is not literature on calibrating the GE from pH 0.3. The aim of this work is to establish a rigorous calibration method for the GE to allow complex formation studies to be done at these low pH values.

There are numerous other factors that also need to be considered when calibrating the GE such as the alkaline error since sodium or potassium hydroxide solutions were used to titrate the acid solutions. Unfortunately, commencing work at such low pH and wanting to work at relatively low ionic strengths (for medicinal applications) meant that 0.5 M was the lowest achievable ionic strength. This would imply that no salt is added to the acid and base solutions and as the titration progresses, the ionic strength of the solution would vary. This certainly is not ideal, but the variation in ionic strength will be considered in the calibration procedure and later in the determination of formation constants.

3.3) Results and Discussion

3.3.1) *Strong acid-strong base titrations*

Since species formation studies were to be conducted under very acidic conditions, the CGE needed to be calibrated starting from pH 0.3 (0.5 M H^+). It was decided to use a strong acid-strong base titration (which will be referred to here as an H^+–OH^- titration) as this low pH is accessible when working at 0.5 M ionic strength. It is also best if the GE calibration procedure simulates the titration experiment for the equilibria studies as closely as possible.

As discussed, the potential measured by a GE can be described as:

$$E_{cell} = E_j + E'_{const} + k\left(\frac{RT}{F}\right) \ln a_{H^+} \qquad (3.14)$$

where $E'_{const} = E_r + E°_g$. For an ideal GE the Nernstian relationship should apply and the potential at pH 7.00 should also be 0 mV. The manufacturer of the GEs used allow an error of 0 ± 15 mV at pH 7.[3] A theoretical slope of 59.16 mV per pH unit at 25 °C for the potential vs pH calibration curve results in an ideal y-intercept ($E°$) of 414 (± 15) mV. Since the GE exhibits a slope slightly lower than the Nernstian slope, the value of $E°$ will also be less than the theoretical value. Ideally the value of the diffusion junction potential should also be negligible, which is why the GE is frequently only used between pH 2 and 12.

The cell potential, as described in equation 3.14, varies with the activity of H^+. If the ionic strength is kept constant throughout an acid-base titration, the cell potential would be directly related to the concentration of H^+ since the activity coefficient would be constant. Constant ionic strength experiments are generally adopted in metal-ligand equilibria studies to avoid problems of unknown and erroneous activity coefficients and a calibration graph of potential versus pH may be used. The value of $E°$ in this GE calibration is affected by the activity coefficient and hence the ionic strength of the solution, as shown in equation 3.4.

A GE potential versus pH calibration graph for the titration of 0.1 M HNO_3 by 0.1 M NaOH (0.1M HNO_3–NaOH titration) was plotted where the concentration for H^+ at each point in the titration was calculated using equations 2.6 and 2.7 and hence the pH was determined. A pK_w value of 13.78 for 0.1 M ionic strength at 25 °C was used (see Table 3.1).[34] The potential versus pa_{H+} graph was also plotted using the same data. The H^+ activities were calculated as follows:

- before the equivalence point

$$a_{H^+} = \gamma_{H^+}\left(\frac{c_a v_a - c_b v_b}{v_a + v_b}\right) \tag{3.15}$$

- after the equivalence point

$$a_{H^+} = \frac{K_w'}{\gamma_{OH^-}}\left(\frac{v_a + v_b}{c_b v_b - c_a v_a}\right) \tag{3.16}$$

where the values γ_{H^+} = 0.83 and γ_{OH^-} = 0.76 for the experimental conditions were used.[39] Also, since the value of pK_w used above was for 0.1 M ionic strength, when using activities pK_w' was determined as follows:

$$pK_w' = -\log(\gamma_{H^+}\ \gamma_{OH^-}) + pK_w \tag{3.17}$$

$$\therefore\ pK_w' = 0.20 + 13.78 = 13.98$$

This calculated value is close to the pK_w value of 13.997 determined at 25 °C for solutions at infinite dilution[39] where the activity coefficients would be unity. The resulting straight line calibrations were $y = -58.99x + 397.75$ when using H^+ concentrations and $y = -58.99x + 402.53$ when using H^+ activities. The two calibrations were therefore parallel and the value of $E°$ was closer to the theoretical value when using activities, as would be expected. The potential at pH 7 was -15.17 mV and that at pa_{H+} 7 was -10.40 mV. Since the acceptable error quoted by the manufacturer was for a calibration using buffers, the potential when using activities (i.e. 10.40 mV) would be more directly comparable.

Deviations from linearity in the low buffer region for the H^+–OH^- titration curve have been shown to be unrelated to liquid junction potentials as the same

behaviour was witnessed for cells with and without a liquid junction.[32] It appears that this region is more susceptible to errors in solution concentrations,[32] as well as small errors due to impurities or the presence of carbon dioxide[9] and even having a glass vessel acting as an ion-exchanger.[40] Figure A3.1 (Appendix 3) demonstrates that points closest to pH 7 do not lie on the straight line calibration graph obtained from a 0.5 M HNO_3–NaOH titration. Data points closest to the end point which deviated from linearity were therefore omitted from all calibration graphs.

For strong acids and bases, the total buffer value of water plus completely dissociated acid or base at all pH values can be calculated as follows:[1]

$$\frac{db}{d\text{pH}} = 2.303([H^+] + [OH^-]) \qquad (3.18)$$

The buffer value was calculated for the solution mixture at each stage during a 0.5 M HNO_3–NaOH titration. Figure 3.3 shows that the buffer value is lowest at the equivalence point of the titration where the total concentration of OH^- and H^+ are the lowest. The buffer value then increases as the pH either increases or decreases. The lower the buffer value, the more pronounced the role of impurities or errors in standardised concentrations become.

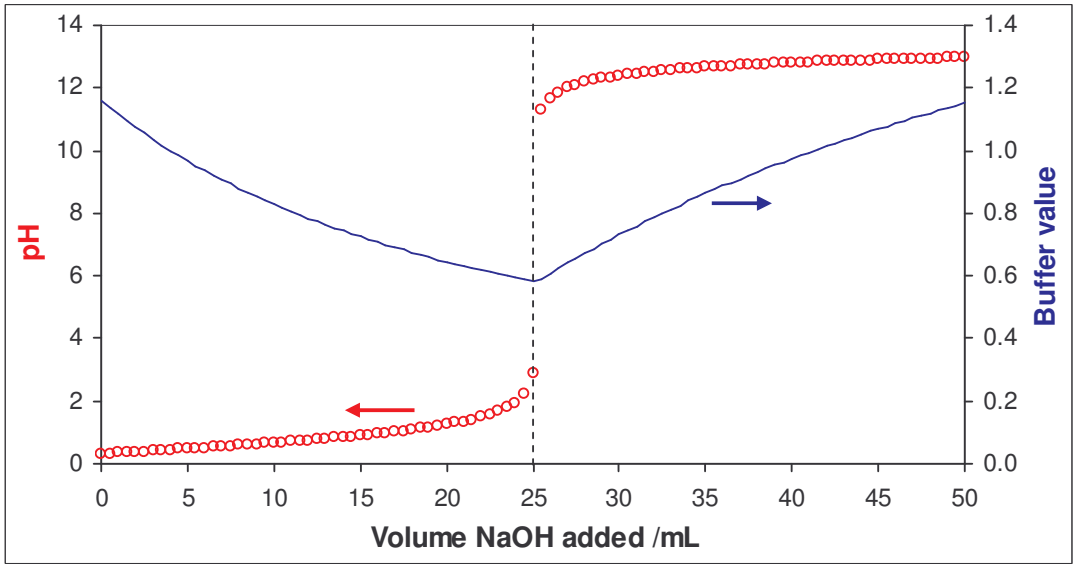

Figure 3.3: Titration curve for a 0.5 M HNO_3–NaOH titration and the associated buffer values.

Various calibrations determined from H^+–OH^- titrations were compared, where HNO_3 and NaOH solutions with concentrations from 0.05 M to 0.5 M were used. The initial volume of acid (25.00 mL), volume increment of added base (0.50 mL) and total volume of base added (50.00 mL) were the same in each case (see Figure A3.2, Appendix 3). As expected, for the more concentrated solutions, lower initial and higher final pH values were attained during the titration. In each titration, the size of the pH region in which data were obtained was about the same in the acidic or the basic region as indicated in Table 3.2. In order to extend the pH range in which data are collected towards the end point, smaller aliquots of base would have to be added closer to the equivalence point or a more dilute base solution would have to be used.

Table 3.2: pH ranges in which data were collected in HNO_3–NaOH titrations using different concentrations of solutions, but where $[HNO_3] = [NaOH]$ within a titration.

	Acidic region		**Basic region**	
Concentration of HNO_3 and NaOH /M	**pH range**	**ΔpH***	**pH range**	**ΔpH***
0.5	0.3 - 1.4	1.1	12.3 - 13.0	0.7
0.2	0.7 - 1.8	1.1	12.0 - 12.6	0.6
0.1	1.0 - 2.1	1.1	11.6 - 12.3	0.7
0.05	1.3 - 2.3	1.0	11.3 - 12.0	0.7

* ΔpH is the number of pH units over which data were collected using the given procedure.

It is generally recommended that the GE be calibrated over very narrow pH ranges in order to obtain a linear response. These have been suggested as pH 2.3 – 2.9 and 10.8 – 11.3[20,33,40] or as pH 2.8 – 3.8 and 10.2 – 11.2[34], which correspond to low acid and base concentrations in the region of 1×10^{-3} to 1.5×10^{-2} M. Errors due to junction potentials and alkaline errors would thus be avoided. It is impractical to calibrate the GE in the suggested pH regions when working under very acidic conditions because the calibration graph would have to be extrapolated into the acidic region where E_j becomes significant and would have to be taken into account. Similarly, if required, extrapolation into the basic region where junction potentials and alkaline errors occur would also result in incorrect calibration.

For the 0.5 M HNO_3–NaOH titration, the pH ranges in which data were obtained were 0.3 – 1.5 and 12.2 – 12.9 for the experimental conditions employed. This certainly lies far from that recommended,[20,33,34,40] hence potential measurements are subject to junction potential and alkaline errors. Since extrapolating a titration curve to more acidic and basic regions is unacceptable, it was questioned whether extrapolating these calibration graphs towards the neutral pH regions would be acceptable.

This was tested by comparing calibration graphs from titrations using 0.5 M solutions and lower concentration solutions, such that the suggested pH regions for calibration were obtained in the latter case. The solutions used in these three separate titrations were:

1) 0.5 M HNO_3 and 0.5 M NaOH
2) 0.01 M HNO_3 and 0.01 M NaOH (both adjusted to μ = 0.5 M with $NaNO_3$)
3) 0.005 M HNO_3 and 0.005 M NaOH (both adjusted to μ = 0.5 M with $NaNO_3$)

The full calibration graphs are given in Figure A3.3 (Appendix 3), but enlargements of the acid and base regions (given in Figures 3.4(a) and (b) respectively) displayed the results more clearly.

Using the calibration parameters in Table 3.3(a), the differences between these calibrations were assessed by calculating pH values at selected potential values from 400 to –350 mV, the extremes of which were only achievable in 0.5 M H^+–OH^- titrations. These results are displayed in Table 3.3(b). Larger variations in the calculated pH values for the three calibrations were observed in the acidic region. The slope for the calibration using 0.5 M solutions was also smaller than that using 0.01 M and 0.005M solutions (which gave almost parallel lines about 0.8 mV apart). The lower slope could be due to the depression of the potential readings in the acidic region resulting from larger junction potentials as well as more curvature in the basic region due to the alkaline error which gives less negative potentials than expected. When some data points at the highest and lowest pH values were removed from the linear

plot (indicated by * in Table 3.3), the slope and the E^o value did increase which emphasises the deviation from linearity at the extreme pH values.

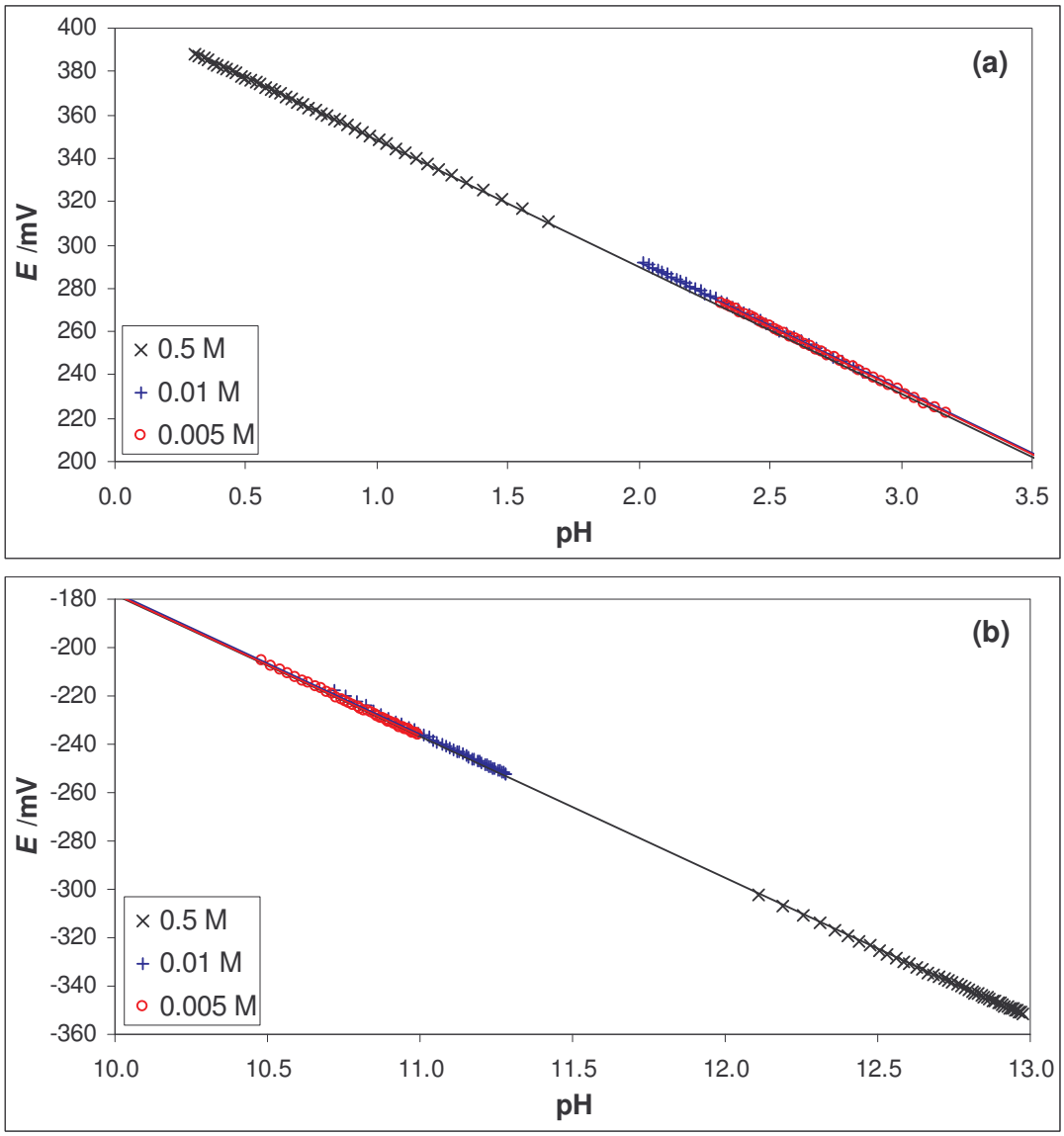

Figure 3.4: Comparison of (a) the acidic and (b) the basic regions of calibration graphs obtained from HNO_3–NaOH titrations with different concentrations of solutions where $[HNO_3]$ = [NaOH] within a titration and μ = 0.5 M.

A similar experiment was repeated using KOH instead of NaOH, as KOH should produce smaller alkaline errors, especially when using lithium silicate type glass membranes. The solutions used to perform two distinct titrations were:

1) 0.5 M HNO_3 and 0.5 M KOH

2) 0.01 M HNO_3 and 0.01 M KOH (both adjusted to μ = 0.5 M with KNO_3)

The acid and base regions of the calibrations are shown in Figures A3.4(a) and (b) (Appendix 3), respectively, and the calibration parameters were again used to calculate pH values at selected potentials (see Table 3.3). In this case larger deviations between the calibrations were observed in the basic region. This was surprising due to the smaller alkaline errors expected. It was therefore concluded that these slight variations in the basic and acidic regions when using KOH or NaOH titrants could simply be due to slight errors in the standardised concentrations of the acid and base solutions which affect the slope of the graph. It was definitely more difficult to detect the end points for the dilute acid and base solutions (i.e. the 0.01 M and 0.005 M solutions) during standardisation when using an indicator. It was also later noted that deviations were witnessed from one calibration to the next, even when the same acid and base solutions were used. These deviations typically resulted in differences in pH values of about 0.002 for successive calibrations, but it increased to as much as 0.03 pH units as the quality of the glass membrane deteriorated. Additionally it should be briefly noted here that a direct comparison between these calibrations is complicated by the fact that the ionic strengths are not the same. The 0.01 M and 0.05 M solutions were adjusted to 0.5 M ionic strength by adding a nitrate salt, but in the case of the 0.5 M solutions no salt was added to the solutions and the ionic strength varied between 0.5 M and 0.25 M during the calibration. This will be discussed in more detail in Section 3.3.3.

A different approach was therefore used to decide whether the extrapolation of the calibration obtained from the 0.5 M HNO_3–NaOH titration, towards the neutral pH region is acceptable. Instead of adding NaOH solution in 0.5 mL aliquots throughout the titration, the aliquot size was reduced close to the equivalence point. In this way more data were acquired as close as possible to the suggested[20,33,34,40] pH ranges for calibration. The resultant calibration graph is given in Figure 3.5 (indicated by ○). Initially it was thought that equilibration had not been established in the low buffer region which resulted in the odd shape of the graph in the basic region. The titration was repeated using longer equilibration times, but the same trend was found.

Table 3.3: (a) Linear calibration parameters obtained from data in Figure 3.4 and (b) calculated pH values using these parameters at selected potential values.

(a)	**Calibration solutions**						
	HNO_3 + NaOH				**HNO_3 + KOH**		
Molarity	0.005	0.01	0.5	0.5*	0.01	0.5	0.5*
pH range:	2.3-11.0	2.0-11.3	0.3-13.0	0.6-12.8	2.0-11.3	0.3-13.0	0.6-12.8
Slope / mV	–58.65 ±0.00(6)	–58.64 ±0.01	–58.47 ±0.01	–58.55 ±0.00(7)	–59.01 ±0.02	–59.15 ±0.00(5)	–59.18 ±0.00(5)
***E*^{o} /mV**	408.72 ±0.05	409.50 ±0.09	406.70 ±0.01	407.17 ±0.06	403.50 ±0.10	402.43 ±0.05	402.59 ±0.04
(b)							
***E* /mV**	**Calculated pH**						
400	0.149	0.162	0.115	0.122	0.059	0.041	0.044
350	1.001	1.015	0.970	0.976	0.907	0.886	0.889
300	1.854	1.867	1.825	1.830	1.754	1.732	1.734
250	2.706	2.720	2.680	2.684	2.601	2.577	2.578
200	3.559	3.573	3.535	3.538	3.449	3.422	3.423
100	5.264	5.278	5.245	5.246	5.143	5.113	5.113
0	6.969	6.984	6.955	6.954	6.838	6.804	6.803
-100	8.674	8.689	8.665	8.662	8.532	8.494	8.493
-200	10.379	10.394	10.376	10.371	10.227	10.185	10.182
-250	11.232	11.247	11.231	11.225	11.074	11.030	11.027
-300	12.084	12.100	12.086	12.079	11.922	11.875	11.872
-350	12.937	12.952	12.941	12.933	12.769	12.721	12.717

* Some experimental points were removed to narrow down the pH ranges.

Another possible reason for these deviations could be attributed to slight errors in the concentrations of the solutions which are more pronounced in the low buffer region. The fact that the point at about pH 5.1 has a negative potential value supported this. However, the same trend was found with a different GE and different solutions (0.5 M HNO_3 and KOH). It could be that this behaviour might be a property of the glass membrane or a systematic error exists when standardising the solutions. In further analyses of these data, the outlying data points were deleted and a straight line fitted through the remainder (see Figure 3.5).

Data were obtained in the 0.3 – 2.9 pH range in the acidic region which incorporated the suggested pH calibration range of 2.3 – 2.9. In the basic

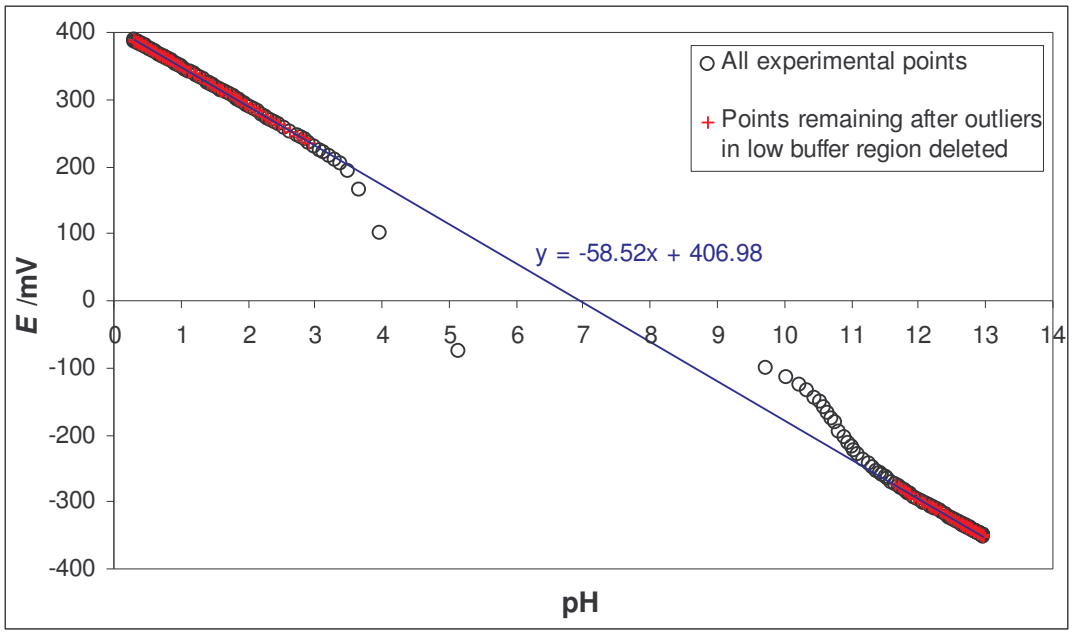

Figure 3.5: Data showing deviations from linearity when smaller increments of base were added closer to the equivalence point during a 0.5 M HNO_3–NaOH titration.

region linear data were obtained in the pH range 11.6 – 13.0, which unfortunately did not include the suggested calibration range of pH 10.8 – 11.3.[20,33,40] This data set was studied in detail to assess the best approach for calibrating the CGE by considering various pH regions.

Since the departure from linearity in the acidic region is due mainly to larger E_j values, it was investigated whether the CGE potential values could be corrected using E_j values calculated by the Henderson equation[1] (as discussed in detail in Chapter 4). The product of the concentration and conductivity (or mobility) of the ions moving across the boundary in both directions are used in this calculation. The theoretical E_j values for the junction between the 3 M KCl solution in the outer RE of the CGE and the test solution at varying concentrations of HNO_3, NaOH (or KOH) and $NaNO_3$ (or KNO_3) as expected in the 0.5 M H^+–OH^- titration to calibrate the CGE. The limiting ionic conductivities used in this calculation are given in Table 4.1 (Chapter 4) and the results are displayed in Figure 3.6. As will be seen in Chapter 4, the junction potentials calculated in this manner adequately predicted E_j values that were measured from polarographic experiments.

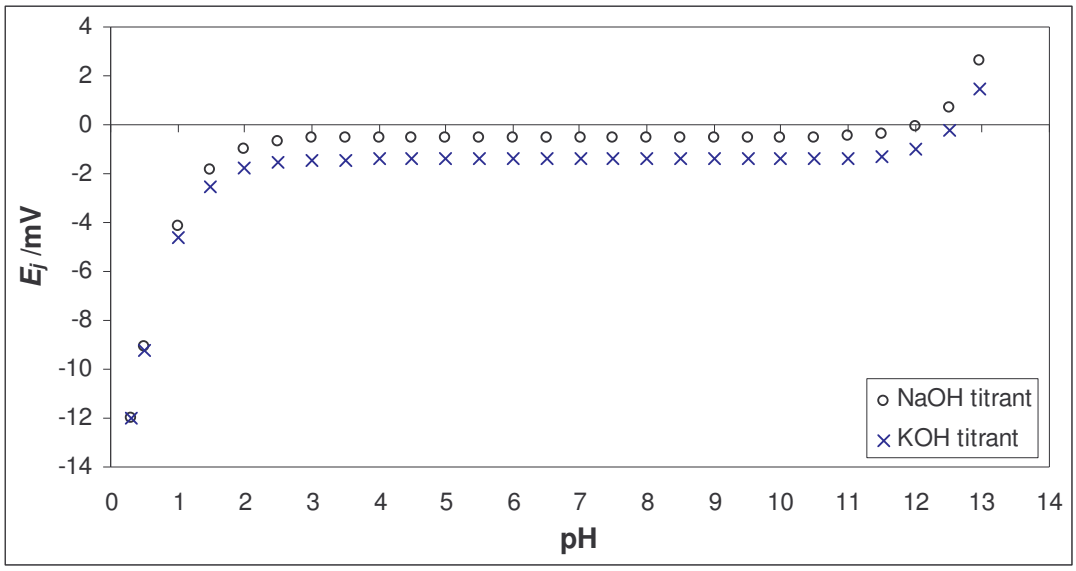

Figure 3.6: Calculated *Ej* values for the junction between 3 M KCl and test solutions of varying composition as would be obtained from HNO_3–NaOH/KOH titrations.

The sign of the E_j value indicates which side of the junction is positive and which is negative. In this case, a negative E_j value implies the RE solution side is positive and the test solution side is negative. The calculated junction potentials were fairly constant between pH 2 and 12 with an average value of about –0.5 mV and –1.4 mV when using titrants of NaOH and KOH respectively. The difference in these E_j values is due to the lower mobility of the Na^+ ion as compared to the K^+ ion.[41] The magnitude of the junction potential increased significantly below pH 2, with a value of about –12.0 mV at pH 0.3 where only HNO_3 was present in the test solution. At pH 13.0 the E_j values were 2.6 mV and 1.5 mV for test solutions containing Na^+ and K^+ respectively. The junction potential results in the overall measured potential of the CGE being less positive in the acidic region and less negative in the basic region, leading to curvature of the calibration graph in these pH regions. The calculated E_j values clearly indicate that the junction potentials need to be accounted for.

When the linear data regions of Figure 3.5 were enlarged (see Figure 3.7 indicated by ○), slight departures from linearity were observed at the extreme pH values. These departures were confirmed by removing experimental points at the very acid and basic pHs and a slight increase in slope and $E°$ value was

observed. The CGE potential data were corrected for junction potentials using the calculated values and are also shown in Figure 3.7 (indicated by ×). This correction resulted in overcompensation especially at the lowest pH values, as seen from the deviation of the points from the linear function fitted to data across the entire pH range. Using calculated values to compensate for the junction potentials is therefore not recommended.

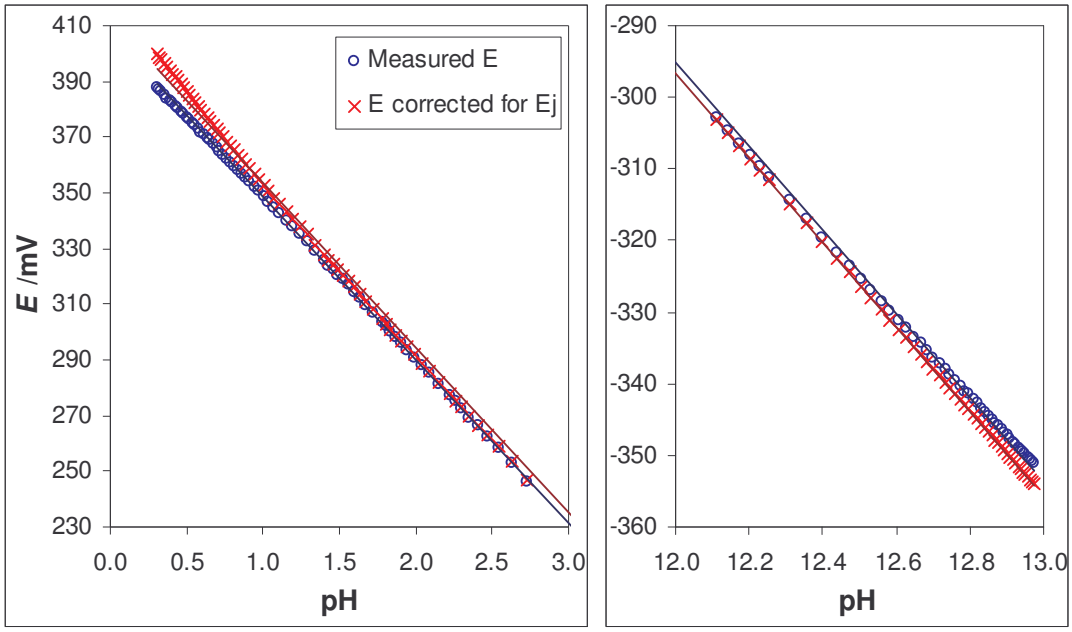

Figure 3.7: Comparison of measured CGE potentials and that corrected for junction potentials using calculated *Ej* values. Linear functions were fitted across the entire pH range.

From all the experiments done so far, it was observed that the CGE did not exhibit the large departures in the very acidic and basic regions as was expected. Junction potentials as well as acid and alkaline errors have somehow been kept to a minimum for these specific CGEs. Since the linear range was fairly large, it was reasonable to use a 0.5 M H^+–OH^- titration to calibrate these CGEs for metal-ligand equilibria studies under acidic conditions down to pH 0.3.

Diffusion junction potential corrections which are included in programs such as ESTA (Equilibrium Simulation and Titration Analysis)[42] used to determine stability constants from GE potentiometric data, should be treated with caution

as the Henderson equation is employed to calculate the junction potential and may then lead to overcompensation. An experimental method to determine and correct for junction potentials for a particular GE used would rather be recommended.

When fitting a linear function through the data points, it was decided to exclude the very acidic and basic points where the most curvature occurred to reduce bias due to the errors in these regions. The question was how many of these points should be removed at the two pH extremes. In order to assess this, data from a 0.5 M HNO_3–NaOH titration (with base added in 0.5 mL increments throughout) was analysed.

Initially a linear calibration was calculated using all data points (except the outliers in the lower buffer region) in the pH range 0.3 – 13.0. Data points were then deleted in the very acidic region so that the lowest pH was 0.4 and the linear function recalculated. This process was repeated by removing points so that the lowest pH was 0.5, then 0.6, 0.7, 0.8, 0.9 and 1.0, and the linear functions calculated for each set of remaining data points. Points were not removed above pH 1.0 as the number of points in the calibration would be too few and the effect of deviations near the low buffer region would become more significant. pH values were calculated at 250 and 350 mV using each of these linear functions and the results are given in Table 3.4(a). The difference between these linear functions were assessed by subtracting each pH value from the corresponding value calculated using data in the pH range 1.0 – 13.0. This difference was 0.007 pH units at 250 mV for the calibration in the pH range 0.3 – 13.0 and was approximately half of this value for the calibration in the pH range 0.6 – 13.0. Data in the basic region was treated in a similar way. Linear functions were determined for data in the pH regions 0.3 up to 13.0, then up to pH 12.9, 12.8, 12.7, 12.6 and 12.5. pH values were then calculated using each of these linear functions at –250 and –350 mV and the results are given in Table 3.4(b). The difference between the pH values calculated using the function in the 0.3 – 12.5 pH range and for each of the other functions was determined. This difference was 0.022 at –250 mV for the calibration including

all points and the difference for the calibration in the pH range 0.3 – 12.8 was 0.011, again about half of that found above. Analogous trends were found for pH values calculated at 350 and –350 mV.

Table 3.4: Comparison of pH values calculated using linear parameters derived from fitting data in selected pH ranges to investigate the effect of E_j and alkaline errors in the very acidic and basic regions.

(a) Omitting data points in the acid region:								
pH range	0.3 – 13.0	0.4 – 13.0	0.5 – 13.0	0.6 – 13.0	0.7 – 13.0	0.8 – 13.0	0.9 – 13.0	1.0 – 13.0
slope	–58.42	–58.43	–58.44	–58.44	–58.45	–58.46	–58.46	–58.46
***E*°**	407.18	407.26	407.34	407.42	407.51	407.62	407.67	407.70
pH at 250 mV	2.690	2.691	2.693	2.694	2.695	2.696	2.697	2.697
ΔpH[a]	0.007	0.006	0.004	0.003	0.002	0.001	0.000	0.000
pH at 350 mV	0.979	0.980	0.981	0.983	0.984	0.986	0.987	0.987
ΔpH[a]	0.008	0.007	0.006	0.004	0.003	0.001	0.000	0.000

(b) Omitting data points in the basic region:						
pH range	0.3 – 13.0	0.3 – 12.9	0.3 – 12.8	0.3 – 12.7	0.3 – 12.6	0.3 – 12.5
slope	–58.42	–58.45	–58.48	–58.50	–58.52	–58.54
***E*°**	407.18	407.20	407.23	407.25	407.27	407.29
pH at –250 mV	11.249	11.245	11.239	11.234	11.231	11.227
ΔpH[b]	0.022	0.018	0.012	0.007	0.004	0.000
pH at –350 mV	12.960	12.955	12.945	12.944	12.940	12.936
ΔpH[b]	0.024	0.019	0.009	0.008	0.004	0.000

[a] Difference between pH value using linear function in pH range 1.0 – 13.0 and pH values for linear functions in other pH ranges.

[b] Difference between pH value using linear function in pH range 0.3 – 12.5 and pH values for linear functions in other pH ranges.

It was therefore decided to omit points below pH 0.6 and above pH 12.8 when fitting the linear calibration so that the pH region close to the end point can be better represented in the calibration. Since the glass membrane changes with time, a periodical check was made to see whether the pH limits determined here were still valid using a similar procedure. This process also highlighted that there is far more curvature in the basic region (due mainly to the alkaline error) than in the acidic region.

Data obtained from 0.5 M HNO_3–NaOH titrations by adding smaller increments of NaOH closer to the equivalence point, were reconsidered as it allowed comparison of data in numerous ways. Figure 3.8 displays the pH ranges used to calculate linear calibrations and the parameters are given in Table 3.5(a). Using each of these functions, pH values were calculated in a potential range of 390 to –350 mV in order to quantify the differences between these calibrations (see Table 3.5(b)).

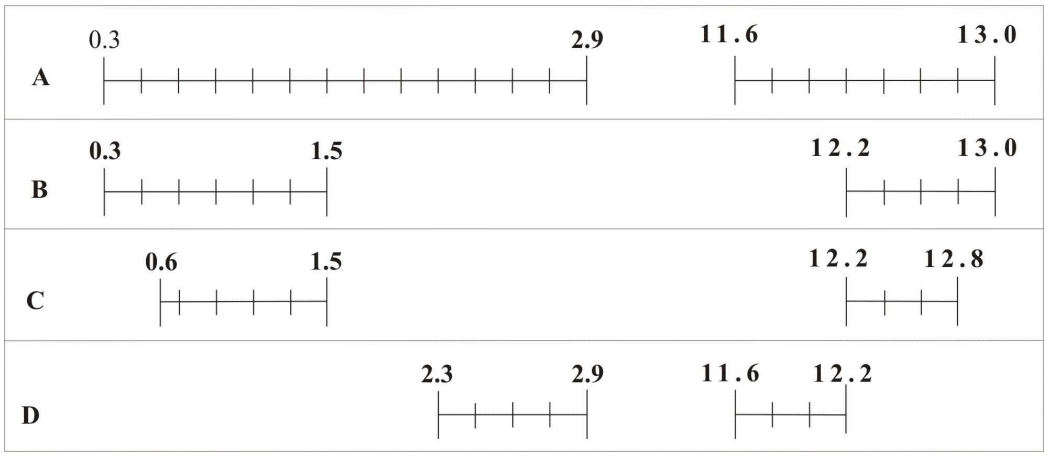

Figure 3.8: pH ranges used to calculate linear calibrations. **A**: All experimental points. **B**: pH regions according to that found in titrations where the base solution was added at 0.5 mL increments throughout. **C**: Deleted experimental points above pH 0.6 and below pH 12.8. **D**: Recommended pH ranges (the basic region was chosen as close to this region as possible).

When comparing calibrations **A** and **B**, it was found that the additional experimental points in the low buffer region did not change the calibration significantly. A larger change was observed for calibration **C**, again illustrating the curvature in the extreme pH regions. Interestingly, the calculated pH values using calibration **D** compared better to those for calibration **C** in the basic region and calibration **B** in the acidic region. The few points used to plot calibration **D** were also the most susceptible to carry error in the low buffer region in this case and the variation in the ionic strength could also influence the calibration. It would rather be suggested that when working in the pH range between 2.3 and 12.2 that lower concentrations of acid and base solutions be used.

Table 3.5: (a) Linear calibration parameters from data in different pH ranges and (b) calculated pH values using these parameters at selected potential values.

(a)				
From Figure 3.8	**A**	**B**	**C**	**D**
pH range	0.3-2.9 11.6-13.0	0.3-1.5 12.2-13.0	0.6-1.5 12.2-12.8	2.3-2.9 11.6-12.2
Slope	–58.52 ± 0.01	–58.49 ± 0.01	–58.58 ± 0.01	–58.54 ± 0.02
***E*° /mV**	406.98 ± 0.09	406.8 ± 0.1	407.4 ± 0.1	406.6 ± 0.2
(b)				
***E* /mV**	**Calculated pH**			
390	0.290	0.288	0.297	0.284
350	0.974	0.972	0.979	0.968
300	1.828	1.827	1.833	1.822
250	2.683	2.682	2.687	2.676
200	3.537	3.536	3.540	3.530
100	5.246	5.246	5.247	5.238
0	6.955	6.956	6.954	6.946
-100	8.664	8.665	8.661	8.655
-200	10.373	10.375	10.369	10.363
-250	11.227	11.230	11.222	11.217
-300	12.082	12.084	12.076	12.071
-350	12.936	12.939	12.929	12.925

In metal-ligand equilibria studies by polarography, the background electrolyte concentration, which is the same as that used to calibrate the GE, is about two orders of magnitude larger than the concentration of ligand in solution. It can therefore be assumed that at the same ionic strength and pH, the junction potential in the calibration solution and the metal-ligand test solution are the same. When measuring the pH of a solution during complex formation studies, the junction potential is also included in the measurement, thus extrapolation of the straight line calibration to more acidic values is not representative of the true behaviour of the GE. The very acidic region was thus considered separately. A quadratic function was fitted to data in the acidic region to account for the curvature. The quadratic calibration was used at the lowest pH values until the straight line calibration intercepted this function. Thereafter the straight line graph was used to calculate pH. Figure 3.9 displays the very acidic region of a calibration graph, showing both the linear and the quadratic

functions. A novel procedure whereby two different functions are used to calibrate the GE over a wider pH range was thus proposed.

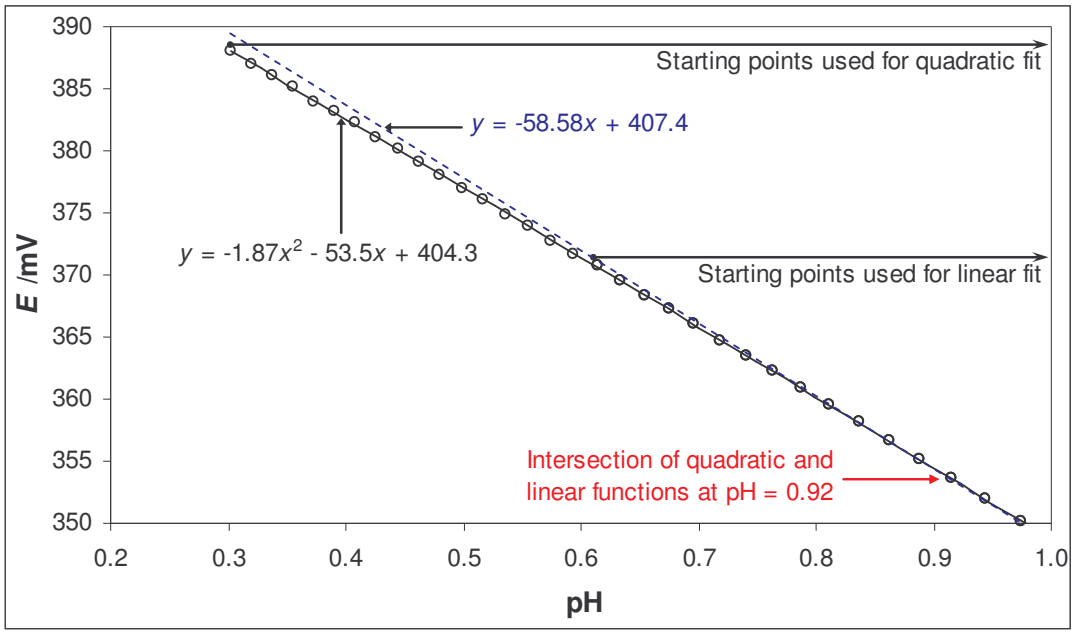

Figure 3.9: The very acidic region of a CGE calibration showing the departure of the quadratic function from the linear relationship which was extrapolated to lower pH values for comparison.

pH values were calculated at selected potential values in the very acidic region using quadratic and linear functions and the results are displayed in Table 3.6. For the most acidic solutions (i.e. at the highest potentials), the calculated pH was significantly different when taking the curvature of the graph into account by using a quadratic function to fit data in the acidic region. At a first glance it appeared that calibration **C** gave the greatest error at high potential values due to the large ΔpH value, but this was due to removing data points which showed significant curvature in this case. Lower slopes in calibration **B** resulted from the best straight line being fitted through points, including those at the extreme pH values which showed curvature. All three linear calibrations clearly demonstrate that merely extrapolating the linear function to very high pH values is insufficient to describe the actual glass membrane response. There was no need to look at the very basic region any further as metal-ligand equilibria studies were not of interest in this region for this work.

Table 3.6: Calculated pH values at selected potential values in the very acidic region using the quadratic function and linear calibrations presented in Table 3.5(a).

From Figure 3.8		**B**		**C**		**D**	
Function	Quadratic	Linear		Linear		Linear	
Calibration pH range	0.3 – 1.5	0.3 – 1.5 12.2 – 13.0		0.6 – 1.5 12.2 – 12.8		2.3 – 2.9 11.6 – 12.2	
***E* /mV**	**Calc pH**	**Calc pH**	**ΔpH ***	**Calc pH**	**ΔpH ***	**Calc pH**	**ΔpH ***
390	0.265	0.288	0.023	0.297	0.032	0.284	0.019
380	0.448	0.459	0.011	0.467	0.021	0.455	0.008
370	0.628	0.630	0.002	0.638	0.010	0.626	-0.002
360	0.806	0.801	-0.005	0.809	0.003	0.797	-0.009
350	0.982	0.972	-0.010	0.979	-0.002	0.968	-0.014
340	1.156	1.143	-0.013	1.150	-0.005	1.138	-0.017
330	1.328	1.314	-0.014	1.321	-0.007	1.309	-0.018
320	1.498	1.485	-0.013	1.492	-0.006	1.480	-0.018
310	1.666	1.656	-0.010	1.662	-0.004	1.651	-0.015
300	1.832	1.827	-0.006	1.833	0.001	1.822	-0.011

* ΔpH is the difference between the calculated pH for each of the linear calibrations and that for the quadratic calibration.

3.3.2) *Evaluation of GE performance*

The separate linear correlations for the acidic and the basic regions often do not coincide.[15] In fact, they never overlapped in this work. This is clearly illustrated in Figure 3.10 where a new CGE was used for a 0.5 M HNO_3–NaOH titration (NaOH added in 0.5 mL increments). When the linear functions were extrapolated it was observed that the acid region line passed near to the basic region data, at pH 7 E = 3.65 mV (i.e. close to 0 mV) and the slope was closer to the Nernstian slope. When extrapolating the linear function for the basic region data, the line diverged from the acidic region. Therefore, by drawing a straight calibration line through both the acidic and basic regions, an error is already being introduced. It is only on closer investigation that these deviations were noticed since frequently the correlation coefficient, R^2, was 1.0000 for the linear fit across the entire pH region.

More curvature was observed in the basic region and this is probably mainly due to the alkaline error and to a lesser extent due to the junction potentials.

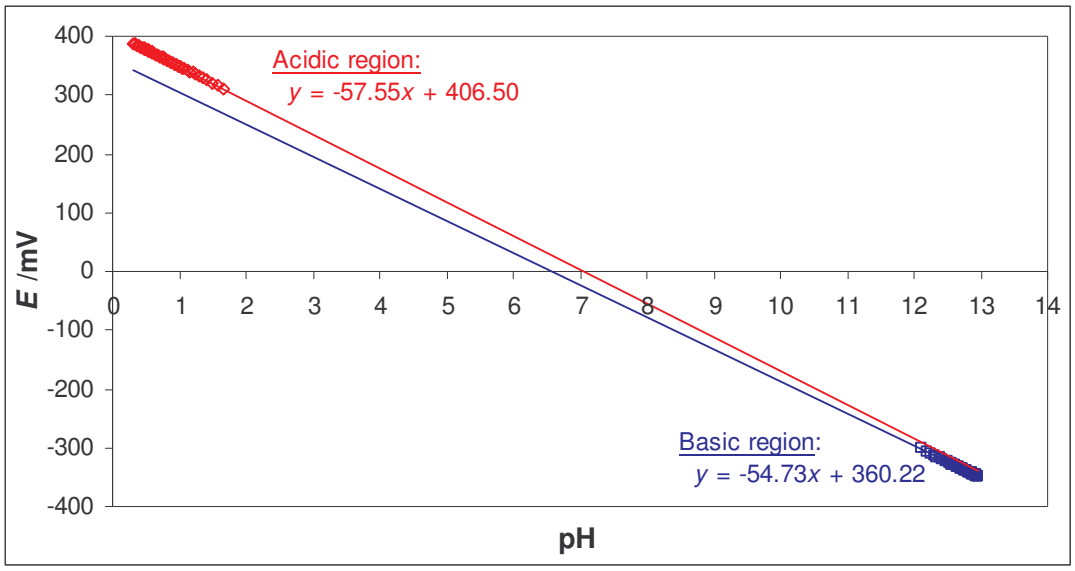

Figure 3.10: Differences in the separate linear correlations for the acid and base regions for a 0.5 M HNO_3–NaOH calibration using a new CGE.

The curvature in this pH region increased significantly when an old CGE was used. It is known that corrosion of the glass surface takes place in solutions with pH greater than about 9 and it has been suggested that a surface reaction occurs between the hydrous silica and sodium hydroxide as follows:[25]

$$H_2SiO_3 + NaOH \rightleftharpoons NaHSiO_3 + H_2O$$

For the calibration using an old CGE, the separate linear correlations were found to be:

$y = -57.65x + 399.58$ for the acidic region, and

$y = -49.93x + 294.78$ for the basic region.

This plot is shown in Figure A3.5 (Appendix 3). The slope for the basic region deviates considerably from the Nernstian slope due to the more pronounced curvature. Thus as the glass membrane degrades, larger alkaline errors are exhibited which affects the calibration. No significant changes were observed in the acid region when comparing a new and old CGE. It is therefore important to ensure that the glass membrane is in good condition for working under very acidic and very basic conditions as the calibration includes both these regions. Omitting data above pH 12.8, where the curvature was most significant, also reduces the extent to which the alkaline error distorts the calibration curve.

These observations led to further testing of CGEs whose glass membranes were at different stages of degradation. A fairly new electrode (called GE1) was used and the same electrode was tested after it had been used for some time (unfortunately this was not quantified). A second electrode (called GE2) that had been left standing in 0.5 M OH^- for some time to corrode the membrane was also tested. Linear correlations for data in various pH regions were determined for each electrode and the slopes obtained are presented in Table 3.7. (The correlations in the basic region for the new and well-used GE1 are illustrated in Figure A3.6(a) and (b) (Appendix 3), respectively.) For GE1, the slopes in the pH range 12.2 – 12.8 only varied by 0.5 mV/pH unit for the new and the well-used glass membrane, but when the pH range was extended to 12.2 – 13.0, the slopes varied by 2.1 mV/ pH unit. Thus the curvature in the 12.8 – 13.0 pH range increased significantly as the membrane degraded. This was also evident when comparing the slopes for the two basic regions considered – the change in slope more than double for the well-used GE1 as compared to the new GE1. For GE2, the slopes in both the basic pH ranges decreased significantly (as compared to GE1) and this electrode would certainly not be recommended for use in the study of metal complexes. Interestingly, the slopes in the acid region did not change much, even for GE2. This behaviour of the glass membranes further supported the decision to omit data above about pH 12.8 when fitting the linear function for calibrating the electrode.

Table 3.7: Comparison of slopes (in mV/pH unit) calculated separately from data in the basic and acidic regions for GE1 and GE2 (see the text for details).

	Basic Region			**Acidic Region**		
pH region	12.2-13.0	12.2-12.8	**Δslope**	0.3-1.5	0.6-1.5	**Δslope**
GE1 slope						
New GE	-55.7	-56.9	1.2	-57.5	-57.9	0.4
Well-used GE	-53.6	-56.4	2.8	-57.8	-58.3	0.6
Δslope	2.1	0.5		-0.3	-0.4	
GE2 slope	-51.9	-53.3	1.4	-57.3	-58.0	0.7

The results observed in Table 3.7 led to a new procedure for testing the suitability in using a GE in experiments for metal-ligand equilibria studies.

Neither the overall linear calibration in the pH range 0.6 – 12.8 nor the data in the acidic region provide sufficient information on the quality of the glass membrane, but the slopes in the base region are a good indicator. Since the alkaline region is generally unavoidable when calibrating the GE, it is critical that the electrode be in good condition. An electrode test, employing a 0.5 M H^+–OH^- titration, can be used to assess the quality of the glass membrane by fitting linear regressions to data in the pH ranges given in Table 3.7 and hence determining the response slope in each pH region. A simple guideline for the acceptable slope ranges is given in Table 3.8, as well as the acceptable difference between the two slopes in the acidic and the basic regions. These guidelines are based purely on experience from the analysis of data from many experiments.

Table 3.8: Suggested criteria of the GE performance and suitability for M-L equilibria studies at low pH. Slopes apply to data obtained from a 0.5 M H^+–OH^- titration.

pH range	**Acceptable slope range**
(1) 12.2 – 12.8	56 – 60
(2) 12.2 – 13.0	55 – 60
Δslope ((2) – (1))	<3
(3) 0.3 – 1.5	57 – 61
(4) 0.6 – 1.5	57 – 61
Δslope ((4) – (3))	< 1
Δslope ((4) – (1))	< 1.5

If an electrode failed the above test, the glass membrane was regenerated by leaching the membrane with HF which improved the performance of the electrode. The procedure used was to treat the glass membrane with 40% HF solution for about 5 s and then rinse it in a 1:1 HCl:H_2O solution for about 10 s. The electrode was then immersed in deionised water at 50°C for 5 hours before the filling solution was removed and replenished with fresh 3 M KCl. The electrode was then left to stand in 3 M KCl storage solution for at least 24 hours before use.

There is no universal criterion for evaluation of GE performance and the suitability of a particular electrode will depend on the purpose of the

experiment and accuracy required. Modern instruments now provide convenient tests for GEs. For instance, the Metrohm 781 pH meter has a built in GE test program which uses buffers of pH 4, 7 and 9 to determine the streaming potential (i.e. the change in potential between stirred and unstirred solutions), the potential drift, the response time, the calibration slope, and the potential offset at pH 7. The manufacturer's preset tolerances for these electrode tests are given in Table A3.1 (Appendix 3).[43] According to the test procedure and these criteria, electrodes which exhibited significant curvature in the basic region were still classified as excellent electrodes, including GE2 that was classified as unsuitable for metal-ligand equilibria studies by the test developed in this work. Even though the manufacturer's criteria can be altered, the behaviour of the GE cannot be established in the extreme pH regions due to the pH of the buffers used. Some of these tests can be useful, but these tests do not provide rigorous enough tests for GEs that are used in the extreme pH regions.

Unfortunately it is impossible to have a constant GE response throughout a multi-hour experiment and GE drift is observed from one calibration to the next. It has been shown that the drift is greater after the electrode was immersed into a very alkaline solution, which is probably due to the deterioration of the glass membrane surface.[20] In order to take this drift into account the GE was always calibrated before and after the titration for metal-ligand equilibria studies and the average pH values for the two calibrations were used. No criterion is available to decide what is the accepted standard deviation of the averaged values and judgement depends to a large degree on the metal-ligand system studied, the pH-range and time the GE spent in solution, as well as the experience of the investigator. As will be seen in Section 3.3.7, the use of polarography is far more tolerant of errors in pH than GEP. Fortunately the equilibria studies done here were not done in the very basic region thereby limiting corrosion of the membrane, but the titration often took more than 12 hours. Initially a maximum standard deviation of 0.03 was tolerated for the pH values calculated using the two calibrations, but this was due to inexperience and an electrode in poor condition being used. A standard deviation less than

0.01 is readily achievable if the GE is in good condition and although a stricter limitation is not needed when using polarography, it is generally achieved.

3.3.3) *Alternative approaches to strong acid-strong base titrations*

In order to avoid severe corrosion of the glass membrane and prolong the lifetime of the GE, as well as to reduce the alkaline error, the GE should not be exposed to extremely basic pH solutions. Since only data up to about pH 12.8 were used in the calibration graph, the 0.5 M HNO_3–OH^- titration could be terminated after adding 42 mL of hydroxide (instead of 50 mL). The calibration is represented by the circles (○) in Figures 3.11(a) and (b).

In order to decrease the final pH still further, smaller increments of base solution could to be added closer to the equivalence point so that sufficient data points are available in the basic region. This was done by initially adding hydroxide in 0.5 mL increments until 22 mL had been added, then adding in 0.2 mL increments until 28 mL had been added and lastly adding in 0.5 mL increments again until a final volume of 35 mL. Thus for 3 mL before and after the equivalence point, the base solution was added in smaller increments thereby collecting more data in this region. This calibration is represented by the crosses (×) in Figures 3.11. An alternative approach used was to again add the base solution in 0.5 mL increments until a volume of 22 mL, but thereafter to added it in 0.1 mL increments until 35 mL had been added. From the calibration in Figures 3.11 (indicated by the plus signs (+)) it was noted that the titration could have been stopped after about pH 12.3 (corresponding to about 29 mL titrant) as there were enough data points in the basic region. This titration process took much longer, which would increase the time of the total experiment and could result in larger deviations in the measured pH throughout the experiment.

Another tactic that was attempted was to use two titrants, where instead of reducing the increment, the concentration of the titrant was reduced. Adding in 0.5 mL increments throughout, 22 mL of a 0.5 M OH^- titrant was added and then a 16 mL of a 0.1 M OH^- titrant (adjusted to an ionic strength of 0.5 M) was

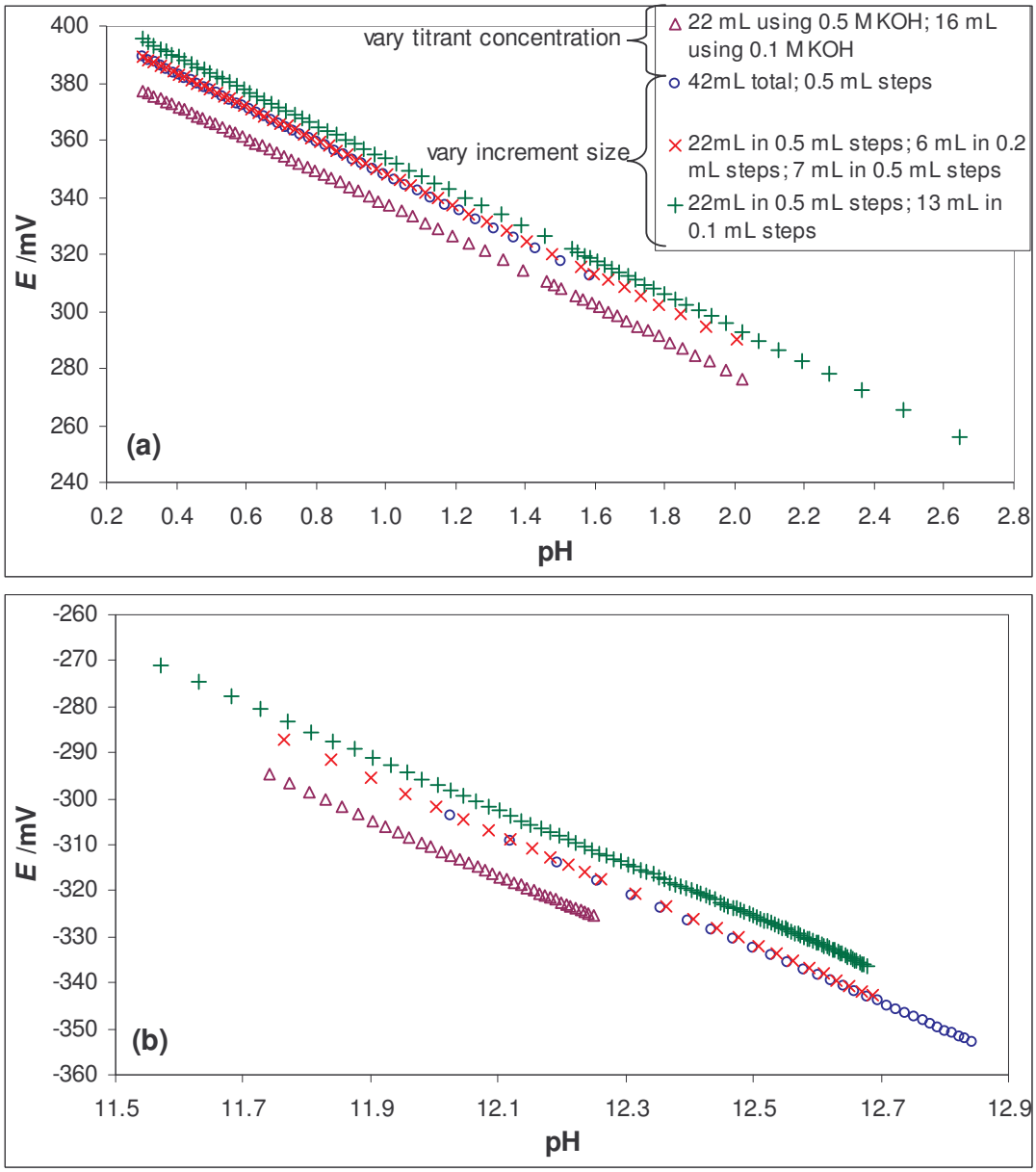

Figure 3.11: The (a) acidic and (b) basic regions of the CGE calibration curves (from the titration of 0.5 M HNO_3 by KOH) using different titration procedures.

then further added. The calibration curve is displayed in Figures 3.11 as the triangles (Δ). Data collected in the basic region were in the pH range 11.7 – 12.2, thus avoiding the higher pH region. Unfortunately this calibration procedure is also time consuming.

As the 0.1 M KOH titrant contained 0.4 M KNO_3 (for the titration using the two titrants at different concentrations), a concern was that the ionic strength would

fluctuate too much and not vary in the same manner as when only 0.5 M KOH was used throughout the titration. The ionic strength was therefore calculated at each point in the titration using the expression:

$$\mu = \sum_i c_i z_i^2 \qquad (3.19)$$

where μ is the ionic strength and c_i and z_i are the concentration and charge for ion i respectively. Ideally molalities should be used in this calculation, but since the molarity values are similar at 25 °C for aqueous solutions, molarities were used for the purpose of this demonstration. For example, at 25 °C a 0.5 g L^{-1} KNO_3 solution has a molarity of 0.509 M,[44] a difference of less than 2%. When calculating ionic strength, H^+ and OH^- concentrations due to the dissociation of water were ignored as these concentrations are low compared to that of the K^+ and NO_3^- ions and the H^+ or OH^- ions (whichever was in excess) from the acid and base solutions. For comparison, the ionic strength was also calculated for the plot represented by (×) in Figure 3.11 and from the results displayed in Figure 3.12 it was noted that there was no significant difference in the trend of the calculated ionic strength for the two approaches in the pH region where the calibration takes place. Small differences in the concentration of acid and base solutions also lead to slight differences in the calculated ionic strength.

The CGE calibration procedure used in the final studies involving Bi(III) complexation is that represented by (×) in Figure 3.11. The membrane showed some degradation over a two month period of regular and prolonged use, where the electrode would be in calibration and test solutions for about five days at a time due to the duration of the experiments and the experiments being run immediately after each other. This was only evident when studying the basic region of the calibration as the overall calibration equation remained surprisingly very much the same. The first calibration equation for this suite of experiments was $y = -59.01x + 407.72$ and after two months of use it was $y = -59.10x + 407.14$. The calibrations before and after each test run always produced calculated pH values with standard deviations well below 0.01 pH units.

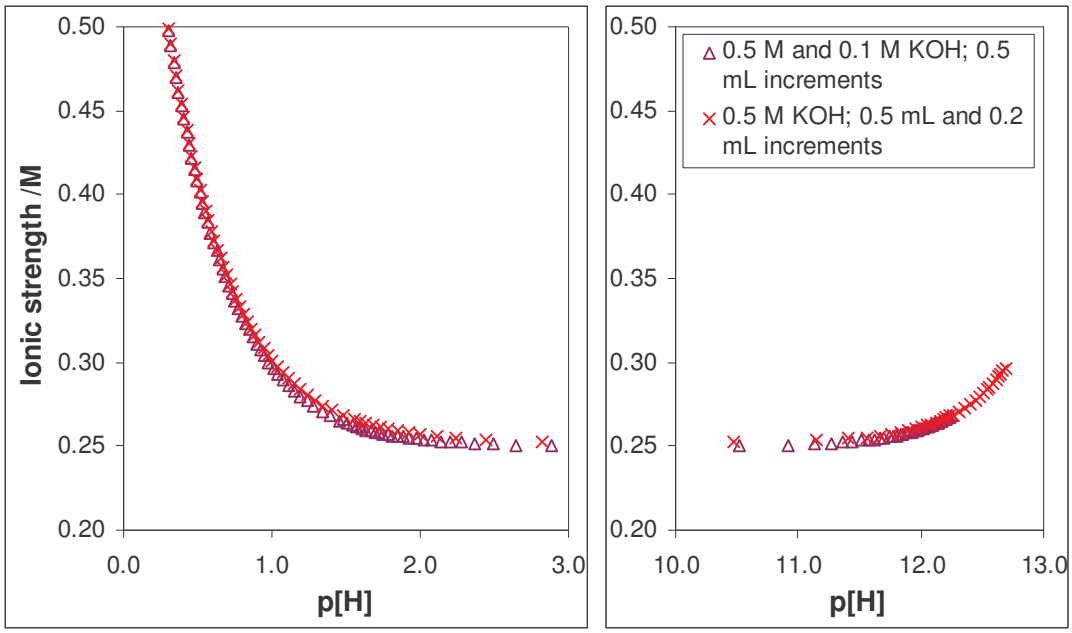

Figure 3.12: Comparison of the variation in ionic strength as a function of pH for the two titration procedures represented by (Δ) and (×) in Figure 3.11.

3.3.4) T*itration of an inert electrolyte*

Another suggested approach to calibrating the glass electrode in metal-ligand equilibria studies is by titrating an inert electrolyte with a strong acid or a strong base. The benefit of using this procedure is that the calibration slope is independent of the concentration of the acid or base solution and deviations from linearity are not observed in the low buffer regions,[32,33] but small errors in the standardised concentrations of these solutions do affect the value of $E°$.

This approach was attempted titrating a 0.5 M $NaNO_3$ solution with 0.5 M HNO_3 or 0.5 M NaOH . The acid or base solutions were initially added in 0.10 mL increments until a volume of 2.00 mL was added, and thereafter in 0.50 mL increments until a total volume of 50.00 mL was added. The calibration graphs (see in Figure 3.13) exhibited significant curvature in both the very acidic and very basic regions. Points which showed the greatest deviation from linearity were omitted when fitting the linear regression and data in the pH regions 1.4 – 2.4 or 11.0 – 12.3 were used. As expected, deviations in the low buffer regions were not observed.

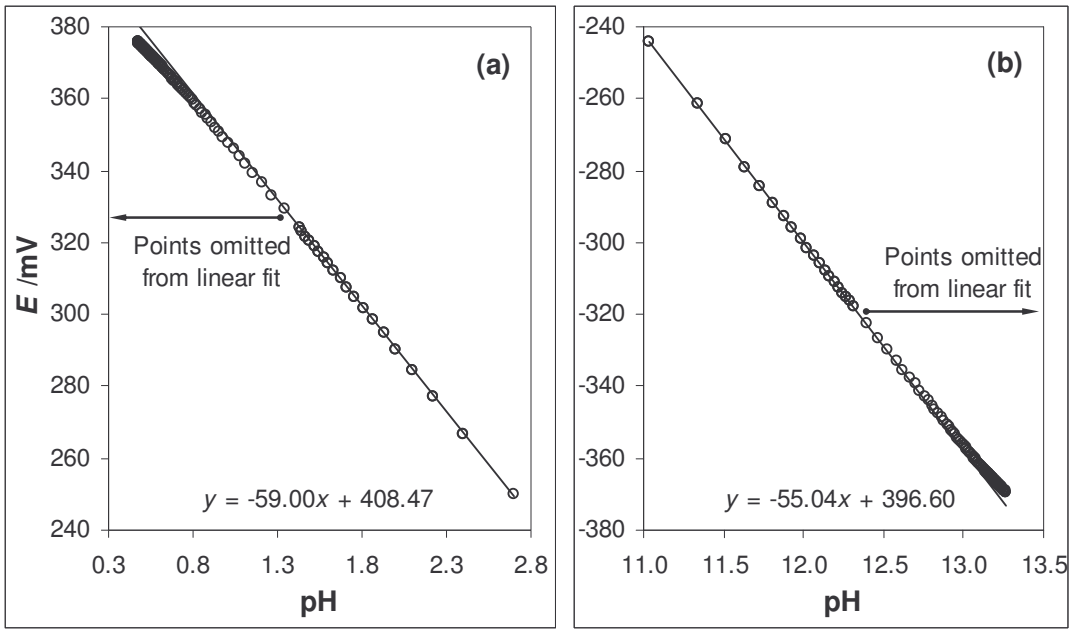

Figure 3.13: Calibration graphs from the titration of 0.5 M $NaNO_3$ by (a) 0.5 M HNO_3 or (b) 0.5 M NaOH. Data points deviating from linearity were omitted when the fitting the linear function as indicated.

When both the acid and base titration data were combined on a single plot, it was noted that the acid and base regions coincided fairly well for data fitted in the narrow pH ranges (see Figure A3.7 in Appendix 3). The two data sets could be combined into a single graph to produce the overall calibration graph, which in this case gave an overall linear calibration of $y = -58.64x + 403.79$. In some cases the acid region calibration is simply extrapolated to the basic region.[5,32,33]

A similar experiment was repeated using 0.5 M KNO_3 which was titrated with 0.5 M HNO_3 or 0.5 M KOH. The linear calibration functions were again fitted after omitting data points from the very acidic and very basic regions, but in this case it was only necessary to omit data below about pH 0.8 and above pH 12.9 (see Figure A3.8 in Appendix 3). A newer CGE was used for this titration, thus the smaller alkaline error observed may not only have been due to the utilisation of potassium solutions, but also the state of the membrane. The calibration using KNO_3 as inert electrolyte displayed similar features to those discussed for the $NaNO_3$ electrolyte.

This titration procedure cannot be used for our studies as the lowest pH value required (i.e. pH 0.3) would not be reached. Only a 0.5 M acid solution would produce a pH of 0.3 and it could not be attained when working at a maximum ionic strength of 0.5 M. As before, the calibration graphs should not be extrapolated into this low pH region due to the large junction potential error and using a quadratic to fit the very acidic region would have to be considered.

This method of calibration does reduce the variation in the ionic strength throughout the titration, but it is important that the calibration procedure simulates the actual conditions of the titration experiment when metal ions and ligand are included as closely as possible. Metal-ligand equilibria titrations generally start at low pH and the pH is then increased to promote complex formation. Reverse titrations could be an option mainly when (i) highly labile metal-ligand systems are investigated, (ii) homogeneous kinetics is very fast, (iii) the solubility of a ligand or complexes formed are not limited, and (iv) metal ions do not undergo hydrolysis. Hydrolysis generally occurs for highly acidic metal ions such as Bi(III), and it would be impossible to start titrations above pH 1. Thus the titration of a strong acid by a strong base appears to be the most suitable, if not the only analytical procedure for acquiring data at very low pH.

3.3.5) *Type of hydroxide solution*

To further investigate the magnitude of the alkaline error, either 0.5 M NaOH or 0.5 M KOH solutions were used to titrate 0.5 M HNO_3. In this case, the two titrations were done straight after each other so that the glass membrane was in as similar condition for the two titrations as possible, thus eliminating one of the parameters affecting the extent of the alkaline error. When comparing the pH values at a particular potential for the two titrations, it was found that the these values differed more in the basic than in the acidic region (see Figure 3.14). For example, at 340 mV the difference was 0.09 pH units and at –340 mV the difference was about 0.22 pH units.

The linear plots in the pH region 0.6 – 12.8 were found to be

$y = -58.55x + 407.17$ for the NaOH titrant and

$y = -59.18x + 402.59$ for the KOH titrant.

The calibration slope when using KOH titrant was closer to the theoretical Nernstian value than that when using NaOH, but departure from theoretical isopotential point (which is 0 mV) was greater when using KOH (11.67 mV at pH 7) than NaOH (2.68 mV at pH 7) as titrant.

When fitting data in the basic region only, the linear calibrations were

$y = -56.18x + 377.52$ for the NaOH titrant and

$y = -57.56x + 382.16$ for the KOH titrant.

Thus data obtained from the titration with NaOH deviated away from the corresponding data in the acidic region to a greater extent than when KOH was used. This confirms the greater alkaline error in the presence of Na^+ ions as compared to K^+ ions. It is also clear that the GE must be calibrated in the same medium as that used in stability constant determinations. This rules out the use of buffer solutions (which are made from various acids and bases) when rigorous data interpretation is required.

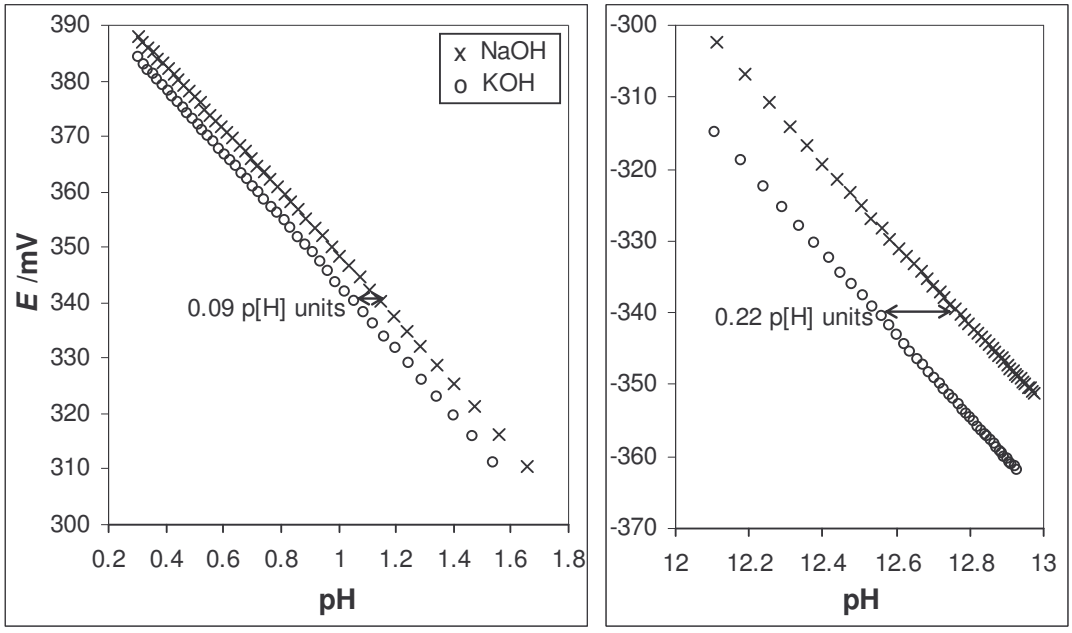

Figure 3.14: Comparison of the calibrations in the acid and basic regions for the 0.5 M HNO_3–NaOH/KOH titrations.

3.3.6) *Type of acid*

Lastly the type of acid that was used was also considered. It was tested whether the use of an oxidising acid like HNO_3 or a more reducing acid such as HCl made any difference when titrated by a strong base such as NaOH. The mobilities of the chloride and nitrate ions are similar,[41] thus the junction potentials do not differ much. The junction potentials were calculated using the Henderson equation[1] for the junction between 3 M KCl in the outer reference electrode and varying mixtures of 0.5 M NaOH and 0.5 M HNO_3 or HCl. It was determined that the maximum difference between the junction potentials was 0.21 mV in the pH range 3 – 10.5. In the more acidic and more basic regions the difference was smaller since the junction potential was due predominantly to the high mobilities of H^+ and OH^- ions respectively, and the NO_3^- and Cl^- ions in the test solution contributed to the junction potential to a lesser extent.

For the 0.5 M H^+-NaOH titrations, the linear calibrations in the 0.6 – 12.8 pH range were

$y = -58.49x + 399.73$ when using HNO_3 and

$y = -58.53x + 397.43$ when using HCl

thus showing no significant difference between the two calibrations. In equilibria studies, however, it should be taken into account that in general, Cl^- ions complex more strongly to metal ions than NO_3^- ions so unless the application for the stability constants derived is specifically for a chloride medium, it would be preferable to work in a nitrate medium.

3.3.7) *Impact of accuracy of pH measurements*

There are several sources of error in determining pH when using a strong acid-strong base titration for calibration. The most significant of the errors would be due to: (i) errors in standardisation of the acid and base solutions; (ii) differences in how the calibration titration was performed, for example using two titrants of different concentration or using different increment additions of one titrant; (iii) the variation in the GE response throughout a titration as seen by comparing the calibrations before and after the complex formation titration experiment and (iv) which data points are included in the linear calibration plot.

For example, point (iv) can be illustrated by data in Table 3.4 where the departure from linearity of the GE response was tested by removing data points in 0.1 pH steps from the GE calibration performed in the 0.3 – 13.0 pH range. From each reduced data set a pH was calculated at 250 mV and –250 mV, the pH values where E_j should be negligible. It was established that removing experimental data points above pH of below 0.6 and above 12.8 changed the calculated pH values at 250 mV and –250 mV by 0.04 and 0.01 pH units respectively.

To demonstrate the impact of error in the pH value on the value of the stability constant determined using these pHs, the following scenario was investigated. Consider a metal-ligand system at pH 2.70 (which corresponds to about 250 mV) and at this pH the ligand is present only as H_2L and the metal exists fully as ML, implying that the formation of ML has already started in 0.1 M acid solution (for simplicity dilution is ignored). An error in pH of 0.04 units (or 2.70 ± 0.02 pH units) is present and hence the absolute error in the proton concentration would be:

$$(2.09 \times 10^{-3})_{pH=2.68} - (1.91 \times 10^{-3})_{pH=2.72} = 1.84 \times 10^{-4} \text{ M } H^+ \qquad (3.20)$$

Firstly, for comparison, conditions used in typical GEP experiments were employed thus the total metal ion concentration ($[M_T]$) and the total ligand concentration ($[L_T]$) were both assumed to be 1×10^{-3} M. From the complex formation reaction:

$$H_2L + M \rightleftharpoons ML + 2H \text{ (charges omitted)}$$

the resulting change in the proton concentration in the sample solution would be 2×10^{-3} M. With the absolute error being 1.84×10^{-4} M H^+, it constitutes 9.2 % of the protons generated from the complexation reaction. This large uncertainty in proton concentration is unacceptable as it could lead to erroneous metal-ligand models or optimisation operations could simply fail since the mass-balance equations for the total hydrogen ion concentration containing this large error would have to be solved. The situation is much worse if the degree of formation of ML at that pH was smaller, i.e. the ML complex starts to form at higher pH. This simplified example clearly indicates

how sensitive the methodology for GEP is towards small errors in pH evaluation. Experimentally, errors in pH should only occur on the third decimal place (preferably within 0.002 pH units).

Secondly, conditions applied in typical polarographic methodologies were used, i.e. low metal ion concentrations and an excess of ligand. Assume $[M_T] = 1 \times 10^{-5}$ M and $[L_T] = 1 \times 10^{-3}$ M, i.e. $[L_T]:[M_T] = 100$. From the complex formation reaction as above, the resulting change in the proton concentration in the sample solution would be 2×10^{-5} M, with the metal ion being the limiting reagent. This change in the proton concentration translates to only about 1% of the total free proton concentration and is much smaller than the error in the free proton measurement by the GE as given in equation 3.20. The determination of stability constants by polarography is far less sensitive to errors in pH than GEP as in the former case (i) mass-balance equations are only solved for $[M_T]$ and $[L_T]$ (not $[H_T]$ as for GEP) and (ii) a large excess of ligand is added. The measured pH, and hence the proton concentration, is used to calculate the free ligand concentration.

In order to investigate the effect of the error on the calculated stability constant for ML and to meet experimental conditions assumed above, the following parameters were set: $pK_a(1) = 12.00$, $pK_a(2) = 7.00$, $pK_a(3) = 0.50$, and $\log K_1 = 19.00$. This resulted in 99.60 % of the total metal ion being in the form of ML and 98.38 % of the total ligand being in the form of H_2L (1 % of the ligand is involved in ML). A change in pH from 2.70 to 2.68 resulted in a decrease of the % ML from 99.597 to 99.558 %. To bring the % ML to its initial value, the value of $\log K_1$ had to be increase from 19.000 to 19.041. The difference in the log value of a 0.041 log units is equivalent to 0.22 % error, a value that can be regarded as much smaller than expected experimental errors typical in the study of metal-ligand equilibria by polarography. A similar procedure was followed for pH = 2.72 and the $\log K_1$ value for the ML complex had to be decreased by 0.040 log units to bring the % ML to its original value.

This simplified but informative example indicates how rigid the polarographic determination of stability constants is where experimental errors in pH

measurements are concerned. Polarography would certainly be the technique of choice, over GEP, for studies in highly acidic media as refined stability constants should have acceptable uncertainties (well below 1% in absolute error).

3.4) Conclusions

From this work it was concluded that the best method for the calibration of the GE for equilibria studies under very acidic conditions is by using a strong acid-strong base titration. Since equilibria studies were done starting in a 0.5 M HNO_3 solution and titrating by a 0.5 M hydroxide solution, the same strategy was applied in the calibration process. It is critical that the calibration method and the titration procedure for the equilibria studies are as similar to each other as possible. This ruled out the use of the calibration process whereby an inert salt solution is titrated by a strong acid or strong base solution because (i) the most acidic pH cannot be attained and (ii) equilibria studies cannot be done via a similar procedure, especially for Bi(III) complex formation studies as the bismuth would have precipitated before the experiment even starts.

The calibration curve (when starting in a 0.5 M HNO_3 solution) was not linear at the lowest pH values due to the diffusion junction potential. Correction of these potential values by adding the diffusion junction potential as calculated using the Henderson equation showed overcompensation for pH values below about 0.8, hence this correction is not recommended. Instead a novel approach of using a combined linear and non-linear calibration of the GE was developed. A quadratic calibration was used in the very acidic region to account for the curvature until this function was intercepted by the straight line calibration which was then used for the remaining pH range. The linear pH range was generally between about pH 0.6 and 12.8, but varied slightly according to the glass membrane condition. A protocol for determining this pH range was suggested.

Curvature of the calibration also occurred at the highest pH values due mainly to the alkaline error. Data points exhibiting deviation from linearity could be

omitted from the calibration as equilibria studies were not attempted in this pH region in this work. However, since corrosion of the glass membrane occurs in basic solutions, it was rather suggested to avoid the very high pH region. This could be achieved by adding a 0.5 M hydroxide solution to the 0.5 M acid solution in 0.5 mL increments until a pH of about 1.5, then either reducing the increment of base addition to 0.2 or 0.1 mL, or reducing the concentration of the hydroxide solution to about 0.1 M.

The extent of the curvature in the basic region especially was an indicator of the condition of a glass membrane. A test was therefore devised, using the titration of the 0.5 M HNO_3 by 0.5 M NaOH, to assess the suitability of the electrode in equilibria studies by polarography. This test should only be done on suspect electrodes as it involves measurements in solutions up to pH 13.0 which should really be avoid as far as possible to prevent corrosion.

No real difference in the calibration was seen when either HCl or HNO_3 solutions were employed. However, significantly large differences in the calibration were noted in the basic region depending on whether KOH or NaOH were used as titrant due to the larger alkaline error in the presence of Na^+, as expected. This highlights problems associated with using buffer solutions for calibrating the GE where the composition of the buffer would be different to that of the test solution and could lead to inaccurate calibration for the intended purpose.

Due to the drift in potential of the GE with time, the GE was calibrated before and after the titration for equilibria studies. The average pH value from the two calibrations was then used. Procedures proposed in this work should significantly minimise errors in pH determination. These values would be suitable for use in polarographic studies of metal complexes, resulting in uncertainties in the log *K* values of less than 1%.

3.5) References

1) R. J. Myers, J. Chem. Ed., 87 (2009) 30
2) R.G. Bates, Determination of pH. Theory and practice, 2nd ed., John Wiley and Sons Inc, New York, 1973
3) Metrohm, Complete Catalogue Metrosensor Electrodes, Herisau, Switzerland, 1999
4) G. Eisenman, Glass electrodes for hydrogen and other cations. Principles and practice, Marcel Dekker Inc, New York, 1967
5) I. Brandariz, T. Vilariño, P. Alonso, R. Herrero, S. Fiol and M.E. Sastre de Vicente, Talanta, 46 (1998) 1469
6) R. Naumann, C. Alexander-Weber, R. Eberhardt, J. Giera and P. Spitzer, Anal. Bioanal. Chem., 374 (2002) 778
7) F.G.K. Baucke, Anal. Chem., 66 (1994) 4519
8) P.M. May, K. Murray and D.R. Williams, Talanta, 32 (1985) 483
9) H.M. Irving, M.G. Miles and L.D. Pettit, Anal. Chim. Acta, 38 (1967) 475
10) A. Avdeef and J.J. Bucher, Anal. Chem., 50 (1978) 2137
11) W.M Tuddenham and D.H. Anderson, Anal. Chem., 22 (1950) 1146
12) M. Filomena, G.F.C. Camoes and A.K. Covington, Anal. Chem., 46 (1974) 1547
13) A.K. Covington, Anal. Chim. Acta, 127 (1981) 1
14) R.G. Bates, R.N. Roy and R.A. Robinson, Anal. Chem., 45 (1973) 1663
15) J.-F. Chen, Y.-X. Xia and G.R. Choppin, Anal. Chem., 68 (1996) 3973
16) F.G.K. Baucke, R. Naumann and C. Alexander-Weber, Anal. Chem., 65 (1993) 3244
17) W. Davison and C. Woof, Anal. Chem., 57 (1985) 2567
18) W.A.E. McBryde, Analyst, 94 (1969) 1118
19) L.D. Petit and K.J. Powell, Sol-Eq, Academic Software, IUPAC, 2002
20) G.H. Nancollas and M.B. Tomson, Pure and Appl. Chem., 54 (1982) 2675
21) J.I. Partanen, P.M. Juusola and P.O. Minkkinen, J. Soln Chem., 28 (1999) 413
22) E.A. Guggenheim, J. Phys. Chem., 34 (1930) 1758
23) C.W. Davies, Ion Assosciation, Butterworths, London, 1962

24) K.S. Pitzer, Activity coefficients in electrolyte solutions, 2nd ed., CRC Press, Boca Raton, FL, 1991
25) J.L. Barriada, I. Brandariz, R Kataky, A.K. Covington and M.E. Sastre de Vicente, J. Chem. Eng. Data, 46 (2001) 1292
26) D.K. Nordstrom, C.N. Alpers, C.J. Ptacek and D.W. Blowes, Environ. Sci. Technol., 34 (2000) 254
27) I. Feldman, Anal. Chem., 28 (1956) 1859
28) E.W. Baumann, Anal. Chim. Acta, 64 (1973) 284
29) G.R. Hedwig and H.K.J. Powell, Anal. Chem., 43 (1971) 1206
30) G. Meinrath and P. Spitzer, Mikrochim. Acta, 135 (2000) 155
31) P.M. May, Talanta, 30 (1983) 889
32) S. Fiol, F. Arce, X.L. Armesto, F. Penedo and M. Sastre de Vicente, Fresenius J. Anal. Chem., 343 (1992) 469
33) I. Brandariz, J.L. Barriada, T. Vilariño and M.E. Sastre de Vicente, Monatshefte für Chemie, 135 (2004) 1475
34) A.E. Martell, R.M. Smith and R.J. Motekaitis, NIST Standard Reference Database 46 Version 8.0, NIST Critically Selected Stability Constants of Metal Complexes, Gaithersburg, USA, 2004
35) L.D. Petit and K.J. Powell, IUPAC Stability Constants Database, IUPAC and Academic Software, 1993-2003
36) P. Gans and B. O'Sullivan, Talanta, 51 (2000) 33
37) M. Dole, J. Am. Chem. Soc., 53 (1931)4260
38) W.C. Gardiner and H.L. Sanders, Ind. Eng. Chem. Anal. Ed., 9 (1937) 274
39) D.A. Skoog, D.M. West and F.J. Holler, Fundementals of Analytical Chemistry, 7th ed., Saunders College Publishing, Florida, 1996
40) D.I. Hitchcock and A.E. Taylor, J. Am. Chem. Soc., 59 (1937) 1812
41) R.A. Robinson and R.H. Stokes, Electrolyte Solutions – The Measurement and Interpretation of Conductance, Chemical Potential and Diffusion in Solutions of Simple Electrolytes, 2nd ed., Butterworth and Co., London, 1959
42) K. Murray and P. May, Equilibrium Simulation and Titration Analysis (ESTA) User Manual, 1984

43) Metrohm, 780 pH Meter - 781 pH/Ion Meter User Manual, Herisau, Switzerland

44) R.C. Weast, CRC Handbook of Chemistry and Physics, 49th ed., The Chemical Rubber Co., Cleveland, Ohio, 1969

CHAPTER 4
The Diffusion Junction Potential

4.1) Introduction

4.1.1) *Ion mobilities*

In any electrochemical cell it is important to consider the motion of ions through the electrolyte solution. In stationary solutions, in the absence of an external field or concentration gradient, the ions have random Brownian motion with instantaneous velocities of the order of 10^{-4} cm s^{-1} through an extremely short path characteristic of the solvent. However, the presence of an external field or a concentration gradient biases the Brownian motion in a particular direction. A field of 1 V cm^{-1} results in a velocity of about 10^{-3} – 10^{-4} cm s^{-1}, which is a very small perturbation on the random motion experienced by the ion. Interestingly, it has been very successful to predict the overall ionic movement by viewing the motion of a particular type of ion as having a fixed velocity in a particular direction instead of the chaotic path actually followed.[1]

Limiting ion mobility ($u°$) refers to the mobility of an ion in a solution at infinite dilution, where interaction between ions in solution is negligible and only interaction with the surrounding solvent needs to be considered. For more concentrated solutions, the ionic mobility (u) is directly proportional to the ionic conductivity (λ) and the relationship between them is:

$$u = \frac{\lambda}{|z|F} \tag{4.1}$$

where z is the charge on the ion and F is Faraday's constant.[2] A table of selected limiting conductivities[1] is given in Table 4.1 to illustrate their relative values and the limiting mobilities were calculated using equation 4.1.

The most outstanding feature in Table 4.1 is the extremely high mobility of the H^+ ion which indicates that there must be another mechanism by which this ion moves. It is unlikely that it is moving as the H_3O^+ ion as this would have

Table 4.1: Limiting ion conductivities[1] and calculated corresponding limiting ion mobilities in water at 25 °C.

Cation	$\lambda°$ /mS m^2 mol^{-1}	$u°$ /10^{-8} m^2 s^{-1} V^{-1}	Anion	$\lambda°$ /mS m^2 mol^{-1}	$u°$ /10^{-8} m^2 s^{-1} V^{-1}
H^+	34.981	36.255	OH^-	19.83	20.55
Li^+	3.868	4.009	F^-	5.54	5.74
Na^+	5.010	5.193	Cl^-	7.635	7.913
K^+	7.350	7.618	Br^-	7.814	8.099
Tl^+	7.47	7.74	I^-	7.684	7.964
Cu^{2+}	10.7	5.56	NO_3^-	7.146	7.406
Pb^{2+}	13.9	7.20	ClO_4^-	6.736	6.981
La^{3+}	20.9	7.22	SO_4^{2-}	16.00	8.294

dimensions similar to that of a water molecule, and the mobility of H_2O is similar to that of K^+ and Cl^- ions. A suggested mechanism is that the proton passes from one water molecule to a favourably oriented neighbouring water molecule, and in so doing leaves these molecules unfavourably oriented for the H^+ ion to move back to the same molecule. This has been called the Grotthuss or "proton jump" mechanism.[3] At any time in the solution most protons are associated with a water molecule forming the H_3O^+ ion, and only a few protons are "jumping" at a time. This mechanism can be represented diagrammatically as given in Figure 4.1(a). The hydroxide ion has the second highest mobility and this can also be accounted for by the "proton jump" mechanism as shown in Figure 4.1(b).

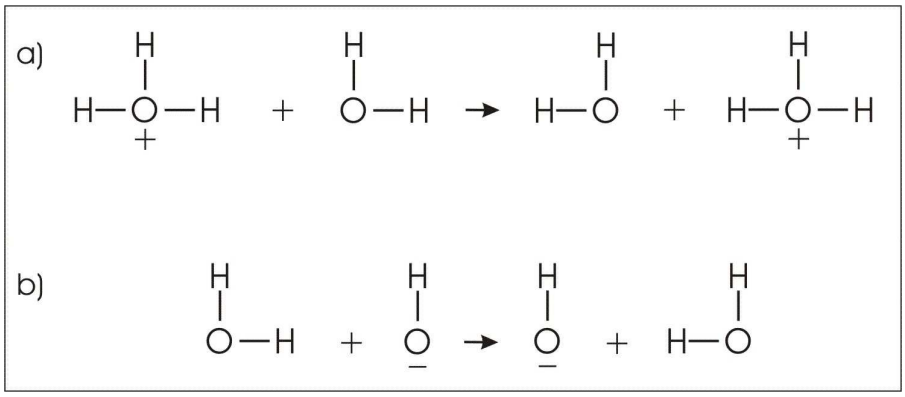

Figure 4.1: Illustration of the "proton jump" mechanism for (a) the H^+ ion and (b) the OH^- ion.[1]

From Table 4.1 it can be seen that the order of mobilities of the alkali-metals is inverse to the order of their ionic radii. This is due to the higher charge density ions being more strongly hydrated. The mobility of the Bi^{3+} ion is not given, but is expected to be similar to that of Pb^{2+} and La^{3+} as it has a similar ionic radius to these ions and has the same charge as the lanthanum ion and thus should be hydrated to the same extent. A plot of the limiting ionic conductivity versus the charge-to-radius ratio gave a linear relationship (see Figure 4.2) which was used to estimate $\lambda°$ as 21.4 mS m^2 mol^{-1} for Bi^{3+} and its corresponding $u°$ as 7.39×10^{-8} m^2 s^{-1} V^{-1}.

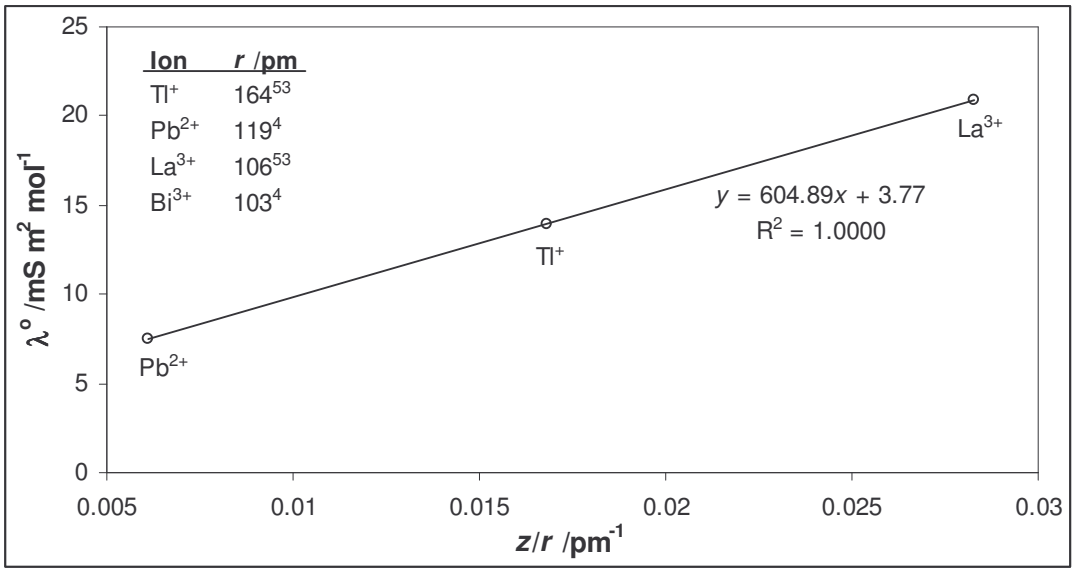

Figure 4.2: The limiting ionic conductivity versus the charge-to-radius ratio plot used to estimate the limiting mobility of Bi^{3+}. The radii quoted are the octahedral ionic radii.

Table 4.2 gives the limiting ion conductivities for various singly charged ions at 0, 25 and 100 °C. The increase in mobility as temperature increases is due mainly to the increasing fluidity of water. Ratios of these values at different temperatures were also calculated and given in the Table 4.2. These ratios indicate that the limiting mobility does not increase by the same extent for the H^+ ion (and to a lesser extent for the OH^- ion) as the temperature is increased as for the other ions. This shows that when the structure of water breaks down at higher temperatures, the abnormally high mobility of the H^+ ion (as well as

the OH^- ion) is reduced, which reinforces the "proton jump" mechanism for these.[1]

Table 4.2: Limiting ion conductivities (in mS m^2 mol^{-1}) in water at 0, 25 and 100 °C.[1] Ratios of these values at different temperatures were also calculated.

Ion	λ° (0 °C)	λ° (25 °C)	λ° (100 °C)	λ° (25 °C) / λ° (0 °C)	λ° (100 °C) / λ° (25 °C)
H^+	22.5	34.98	63.0	1.55	1.80
OH^-	10.5	19.83	45.0	1.89	2.27
Li^+	1.94	6.868	19.5	1.99	2.97
Na^+	2.65	5.010	21.2	1.89	2.89
K^+	4.07	7.350	14.5	1.81	2.65
Cl^-	4.10	7.635	11.5	1.86	2.77
NO_3^-	4.00	7.146	19.5	1.79	2.73
ClO_4^-	3.69	6.736	18.5	1.83	2.75

In electrolyte solutions limiting ion properties would not apply and interionic forces must be accounted for together with Brownian motion. The two main effects that need to be considered in electrolyte solutions are the electrophoretic effect and the relaxation effect, both of which reduce the mobility of the ions. The electrophoretic effect takes into account that an ion is surrounded by an ionic atmosphere due to interionic attractions and repulsions. It is distributed with radial symmetry around the central ion and hence exerts no resultant force on the central ion. Mathematically it is the result of a time averaged distribution of ions. If an external potential is applied to the solution, an ion will tend to move with a velocity that is independent of the presence of other ions, and is determined by the limiting mobility of that ion. However, the ion atmosphere has the opposite charge and it will move in the reverse direction, affecting the overall motion of the central ion. This effect is clearly concentration-dependent and drops to zero at infinite dilution. The relaxation effect considers the motion of the central ion relative to the ionic atmosphere. An external force may cause the central ion to move off-centre from its ionic atmosphere, but it then experiences a restoring force which rapidly disappears as the radial symmetry of the ionic atmosphere is restored by the thermal motion of ions.[1]

The dependence of the actual mobility of ions in a binary electrolyte on the ionic strength of the supporting electrolyte is expressed by the Onsager limiting law which gives the relationship between the actual mobility of the ion and its limiting mobility and takes both the electrophoretic and relaxation effects into account.[4,5] Here it is given for the mobility of a cation:

$$u_+ = u_+^\circ - \left(u_+^\circ z_+ |z_-| B_1 \left(\frac{q}{1+\sqrt{q}} \right) + B_2 z_+ \right) \left(\frac{\sqrt{\mu}}{1+Ba\sqrt{\mu}} \right) \tag{4.2}$$

where u_+ and u_+° are the actual and limiting cation mobilities respectively, and z_+ and z_- are the cation and anion charges respectively. B_1, B_2 and B are constants characteristic of the solvent and temperature. For aqueous solutions at 25 °C they are given as: $B_1 = 0.7817$ M$^{-1/2}$, $B_2 = 3.138 \times 10^{-8}$ m^2 V^{-1} s^{-1} (mol dm^{-3})$^{-1/2}$ and $B = 3.286$ nm^{-1} (mol dm^{-3})$^{-1/2}$.[6] The parameter a is the effective ion diameter which is around 0.3 – 0.5 nm and thus Ba is often approximated by the value 1.5 (mol dm^{-3})$^{-1/2}$.[1,6] q is determined for the background electrolyte and is defined as:

$$q = \left(\frac{z_+ |z_-|}{z_+ + |z_-|} \right) \left(\frac{u_+^\circ + u_-^\circ}{|z_-| u_+^\circ + z_+ u_-^\circ} \right) \tag{4.3}$$

and for symmetrical electrolytes (where $z_+ = z_-$) $q = 0.5$.[6]

The actual mobilities were calculated for several univalent ions (assuming a 1:1 electrolyte) using the Onsager limiting law and limiting ion mobilities given in Table 4.1 for solutions of ionic strength 0.1 M and 0.5 M and the results are given in Table 4.3. The decrease in the mobility of an ion in, for example, a solution at 0.1 M ionic strength compared to solutions at infinite dilution can be clearly seen. The Onsager limiting law is valid for ionic strengths of at most 0.1 mol dm^{-3}. At higher concentrations the experimental mobilities were found to be higher than that predicted.[1] Mobilities calculated for 0.5 M ionic strengths are therefore not reliable. For 2:2 electrolytes and higher valencies, the Onsager limiting law is only obeyed at extremely low concentrations as the formation of ion-pairs is appreciable even in very dilute solutions. At higher concentrations, the experimental mobilities are lower than predicted in these solutions.[1]

Table 4.3: Limiting ion mobilities (in 10^{-8} m^2 s^{-1} V^{-1}) in water at 25 °C[1] and the mobilities calculated using the Onsager limiting law for solutions of ionic strength 0.1 M and 0.5 M. The ratio of mobility in 0.1 M solutions to limiting mobility was also calculated.

Ion	$u°$	u μ = 0.1 M	u μ = 0.5 M *	$u/u°$ μ = 0.1 M
H^+	36.255	33.80	32.33	0.93
Na^+	5.193	4.26	3.71	0.82
K^+	7.618	6.57	5.94	0.86
OH^-	20.55	18.87	17.86	0.92
NO_3^-	7.406	6.37	5.75	0.86
ClO_4^-	6.891	5.97	5.36	0.87

* In reality mobilities would be greater than the values calculated here using the Onsager limiting law.

Ion mobilities are used to calculate the magnitude of diffusion junction potentials. Since the mobility of ions decreases with increasing ionic strength, the extent to which this affects the junction potential would have to be investigated. It may be that the change in mobilities (with change in ionic strength) for the various ions largely cancel out when determining the junction potential and hence has little effect on the actual value. However, from the ratio $u/u°$ in 0.1 M solutions given in Table 4.3, it can be seen that the degree of decrease in the mobility of various ions is not the same, H^+ and OH^- ions having a smaller decrease than the other univalent ions considered.

This observation can be described in another way by considering transport or transference numbers. A transport number (t) is the fraction of the total current carried by one particular charge carrier (ion i) in solution and the limiting transport number ($t°$) is calculated using:

$$t_i° = \frac{\lambda_i°}{\Lambda°} \tag{4.4}$$

for non-associated electrolytes under infinite dilution conditions where $\Lambda°$ is the limiting conductivity of the solution and $\Lambda° = \sum \lambda_i°$. For solutions at higher ionic strengths:

$$t_i = \frac{\lambda_i}{\Lambda} \qquad \text{or} \qquad t_i = \frac{|z_i| u_i c_i}{\sum |z_i| u_i c_i} \tag{4.5}$$

where c_i is the molar concentration of ion i.[1,7]

When considering a HNO_3 solution, $t_+° = 0.8304$ and $t_-° = 0.1696$. For a 0.1 M solution, the transport numbers can be calculated using Equation 4.5 and the values in Table 4.3 to give $t_+ = 0.8412$ and $t_- = 0.1588$. This again demonstrates that the fraction of current carried by the H^+ ion increases slightly as the concentration of the solution is increased.

Very little is actually known about the conductivity in mixed electrolytes, but it appears that ionic mobilities are mainly affected by the ionic strength of the solution and not much affected by the solution composition, recalling that ionic strength is dependent on both the charge and concentration of the ions. It would therefore be justifiable to substitute values for a single pure electrolyte. It has been suggested[8] that simple additivity of the conductivities is sufficient to take mixtures into account as follows:

$$\Lambda_{mixt} = x\Lambda_1 + (1-x)\Lambda_2 \qquad (4.6)$$

where x is the fraction of mixing, solutions 1 and 2 are pure salt solutions and the conductivities, Λ, are at the total ionic strength of the mixture. Departures from this calculated value will occur if there is a large difference between the concentrations of the two solutions.

4.1.2) *Diffusion junction potentials*

The liquid junction is the boundary between two dissimilar solutions (differing in composition and/or concentration) across which ions can diffuse. A potential difference arises due to the difference in the rates of diffusion of oppositely charged ions across this boundary, resulting in the two sides of the boundary being oppositely charged. The diffusion of ions across the boundary is counteracted by the repulsion of like charges and thus a steady state arises when the charges move across the boundary at the same rate. This potential difference is called the liquid or diffusion junction potential.[1] A properly formed junction rapidly reaches a steady state which produces a reproducible, constant potential difference.[9]

For cells with transference (i.e. they contain a liquid junction), the cell potential depends not only on the standard cell potential and the composition of the end solutions, but also on the liquid junction itself. This includes concentration profiles in the liquid junction (which is more important in some cases than others) and the transport and thermodynamic properties in the junction region.

If an acid or base solution is in contact with a salt solution, the junction potential will be greater than if two different salt solutions (of similar concentration to those above) were in contact. This is due to the extremely high mobilities of the hydrogen and hydroxide ions. Consider the example where 0.1 M HNO_3 is in contact with 0.1 M KNO_3. The concentration of nitrate ions is the same on either side of the boundary, thus there is no net change. The hydrogen ion diffuses at a much faster rate than the potassium ion, thus at the boundary the KNO_3 solution becomes positively charged and the HNO_3 solution is left with an overall negative charge. The greater the charge disparity, the greater the potential difference across the boundary. The junction potential is thus a function of pH, ionic strength, the nature of the diffusing ions, the solvent and temperature – anything that affects the mobility of an ion in solution.[10,11]

The two quotes given below indicate the problematic nature of liquid junctions in cells and they are as true today as they were then.

> *Since the days of the first measurements using a cell with transference, the problem of evaluating or eliminating the liquid junction potential has occupied the attention of physical chemists.*
>
> R.G Bates (1973)[9]

> *The potentials of liquid junctions in voltaic cells are sources of perplexity in measurements of the electromotive force of cells and of the single potentials of electrodes, not only because they evade direct observation, they are also a frequent source of considerable experimental uncertainty.*
>
> A.B. Lamb and A.T. Larson (1920)[12]

Experimentally there are various types of liquid junction systems. These were placed into four categories by Guggenheim, namely a continuous mixture junction, a constrained diffusion junction, a flowing junction and a free diffusion junction.[11,13] The *continuous mixture junction* consists of a layer of solution which has a linear concentration profile and varies in composition from the pure solution on the one side to the pure solution of the other. This is extremely difficult to achieve experimentally and can only apply to junctions of the free-flowing capillary type.[14] The *constrained diffusion junction* uses a membrane or other permeable material to separate the two solutions. Ions diffuse freely between the two solutions until a steady state is reached.[13] In a *flowing junction* the two solutions move toward each other and flow away in parallel streams and form a sharp boundary where they meet. A T-piece is used to attain this experimentally.[9] This junction has excellent reproducibility at the correct flow rates.[12,13] Scatchard[15] viewed flowing junctions as continuous flow boundaries because “the time is too short for diffusion to become noticeable”, but there is no way of showing this. In a *free diffusion junction* the two solutions meet to form an initial sharp boundary, after which free diffusion can occur. This junction is most commonly found in practice, it is stable and quite reproducible, but it is not amenable to simple mathematical treatment.[9] The length of the diffusion layer is always increasing, but if there is cylindrical symmetry the junction potential is independent of time after a steady junction has formed.[13]

Another important type of junction not included by Guggenheim is the *restrained flow junction* where the two solutions are separated by, for example, a ceramic plug, and the one solution is allowed to flow into the other at a small but definite rate. This type of junction is reproducible and easy to establish.[11] Other examples of this junction are fibre junctions, glass sleeves, platinum junctions (which consists of a bundle of platinum wires) and so on. Although these types of junctions are frequently used, especially in the case of reference electrodes and salt bridges, they cannot be accurately described by the calculations used for the continuous mixture junction and the complexity of the junctions are difficult to simulate numerically.[14,16] The geometries of these

junctions also vary, thus an experimental approach to determine diffusion junction potentials would certainly be more advantageous.[14]

The liquid junction potential (E_j) is mathematically defined as:

$$E_j = -\frac{RT}{F}\int_1^2 \sum\left(\frac{t_i}{z_i}\right) d\ln a_i \qquad (4.7)$$

where t_i, z_i and a_i are the transport number, ionic charge and activity of the ith ion respectively, and 1 and 2 signifies the two solutions forming the boundary. A number of problems arise in solving this equation. Firstly, the activities of the individual ions are thermodynamically meaningless as they cannot be measured or precisely calculated. Approximations in calculating junction potentials have thus been made such as either adopting a particular activity coefficient convention or using concentrations.[11] One way to calculate the activity of a single ion is to evaluate the junction potential, but in order to evaluate the junction potential the activity of that ion must be known. This is a dilemma from which there is no escape. Secondly, equation 4.7 holds irrespective of the type of junction that is formed, but in order to integrate the function assumptions about the distribution of the ion concentrations in the transition layers (i.e. the concentration profile) between the two boundary solutions have to be made.[8,16] For boundary solutions that consist of the same salt but at different concentrations, or the same concentration with only a single ion different, the potential is independent of the way in which the junction is formed. Otherwise the potential depends on the composition of the transition layers and it is important to be able to reproduce the physical structure of the boundary.[8,9,13,17] Moreover, the transference number is strictly defined as the fraction of current carried by an ion in solutions of uniform composition.[17] This is clearly not the case in the transition layers of the boundary solutions.

When integrating equation 4.7, one of the mathematically easiest approaches is to assume the formation of a continuous mixture junction, not that this is the most commonly formed junction in practice.[9] Henderson derived an equation

to calculate the E_j in this manner.[Original publication: 18] For a diffusion junction occurring between solutions 1 and 2, the Henderson equation is given as:[9]

$$E_j = \frac{RT}{F}\frac{(U_1 - V_1) - (U_2 - V_2)}{\left(U_1' + V_1'\right) - \left(U_2' + V_2'\right)} \ln \frac{\left(U_1' + V_1'\right)}{\left(U_2' + V_2'\right)} \tag{4.8}$$

where $U = \Sigma c_+ \lambda°_+$, $V = \Sigma c_- \lambda°_-$, $U' = \Sigma z_+ c_+ \lambda°_+$ and $V' = \Sigma z_- c_- \lambda°_-$, and c, $\lambda°$ and z are the molar concentration, the limiting conductivity and the magnitude of the charge for each ion, respectively. At a solution temperature of 25 °C this equation can be rewritten as:

$$E_j = 0.05916 \frac{(U_1 - V_1) - (U_2 - V_2)}{\left(U_1' + V_1'\right) - \left(U_2' + V_2'\right)} \log \frac{\left(U_1' + V_1'\right)}{\left(U_2' + V_2'\right)} \tag{4.9}$$

The Henderson equation was originally derived assuming activity coefficients to be unity. It can be shown that the same result will be found if the activity coefficients simply remain constant.[8] This is a reasonable assumption in equilibria studies where the ionic strength of solutions are kept constant. It was also assumed that the mobilities of ions remained constant across the junction[8,19] which again would be valid if the ionic strength of both solutions were kept constant as mobility is dependent more on ionic strength than on composition. The Henderson equation has been shown to predict junction potentials for univalent electrolytes at constant ionic strength rather successfully. Less is known for solutions of different ionic strengths, in which case the junction potentials are generally overestimated by the Henderson equation.[20]

Planck's equation[Original publication: 21] is derived by assuming a constrained diffusion type junction when integrating equation 4.7, which is mathematically more complex to solve but more realistic physically.[8,9] As for the Henderson equation, it was assumed that the solutions were ideal and that the ion mobilities remained constant across the junction.

Additionally, the assumption of electroneutrality throughout the junction is made.[22,23] This seeming self-contradiction is well phased in the following quote:

> *The apparent inconsistency between the existence of a potential difference and the vanishing of the net charge, which gives rise to that potential difference, has been a source of contention and puzzlement to physicists and chemists since Planck's original paper.*
>
> J.L. Jackson (1974)[24]

It had been shown that the electroneutrality assumption is approximately valid for the time scales of the experiments and is only invalid for very sharp junctions.[23-25] If one interprets the charge neutrality to refer to the rate of diffusion of charged ions the assumption makes more sense. Initially the diffusion rates of ions are different due to their different mobilities, but a steady state is reached due to the repulsive electrostatic forces. Once the steady state is attained, the diffusion of the oppositely charge ions must be about equal, i.e. the diffusion of opposite charges balance out and the electroneutrality assumption holds. Leckey and Horne[26] speak about the ions being "coupled" in such a way as to remove their individual identities once the steady state is reached. Hafemann[23] calculated that the steady state is attained after about 10^{-8} s in concentration cells for a free diffusion type junction, the same time frame other authors[24,25] claimed necessary for the electroneutrality assumption to become valid.

The Planck equation was originally used to calculate junction potentials for boundary solutions containing ions of charge ±1.[9,13,22] A more general formula for ions of different valencies was derived by Pleijel[13,Original publication: 27] and more recently by Morf.[22] Morf's equation for the junction potential between solutions 1 and 2 is given by:

$$E_j = \frac{RT}{F}\frac{\bar{u}_+ - \bar{u}_-}{|z_+|\bar{u}_+ + |z_-|\bar{u}_-}\ln\frac{\sum c_i(1)}{\sum c_i(2)} \qquad (4.10)$$

where $\overline{u}_+$ and $\overline{u}_-$ are the mean cation or anion mobilities respectively, and c is the concentration of the ion and the subscript i refers to anions if i is negative and cations if i is positive. The mean ion mobilities can be calculated from the ion mobilities using:

$$\overline{u}_i = \frac{\sum u_i c_i(2)\, e^{z_i F E_j / RT} - \sum u_i c_i(1)}{\sum c_i(2)\, e^{z_i F E_j / RT} - \sum c_i(1)} \tag{4.11}$$

An iterative procedure is required to determine the junction potential as the mean ion mobilities are dependant on this junction potential value. This would require initial values of E_j to be estimated in order to calculate $\overline{u}_+$ and $\overline{u}_-$, and then these values would be used the calculate a more accurate value of E_j, which is then used as the next estimate of E_j until a constant value of E_j is found.

Using equation 4.10 would, however, give a zero junction potential if the concentration of ions in both solutions is the same (i.e. $\Sigma c_i(1) = \Sigma c_i(2)$), which is certainly not the case if the type of ions in the solutions are different. If so, then for $\Sigma c_i(1) = \Sigma c_i(2)$ and $|z_i| = 1$ for all ions, the diffusion junction potential can be implicitly calculated using:[22]

$$E_j = \frac{RT}{F} \ln \frac{\sum u_+ c_+(1) + \sum u_- c_-(2)}{\sum u_+ c_+(2) + \sum u_- c_-(1)} \tag{4.12}$$

This equation corresponds to Goldman's equation for the junction potential of biological membranes.[28]

In both the Henderson and the Planck equation, the type of diffusion junctions assumed are not due to their practical importance, but due to the ease with which mathematical integration can be done. These calculated junction potentials are not very accurate, but provide an idea of the magnitude and sign of the potential. Bates[9] reckoned that it is truly doubtful whether the junction potential will ever be able to be calculated accurately and/or completely eliminated.

Equations for calculating junction potentials have also been simplified for simple junctions. MacInnes[29] showed that a straightforward relationship involving transference numbers can be used to calculate the junction potential if the emf of a cell with transference (E_t) is measured for a junction between two salt solutions of the same type at different concentrations which contain only univalent ions and are both below 0.05 M. The relationship is given as:

$$E_j = E_t\left(1-\frac{1}{2t_+}\right) \tag{4.13}$$

where t_+ is the transference number of the cation. Lewis and Sargent[30] simplified Planck's equation for the junction between equally concentrated solutions of two binary salts having one type of ion in common and is given as:

$$E_j = \frac{RT}{F}\ln\frac{\Lambda_1}{\Lambda_2} \tag{4.14}$$

where Λ is the equivalent conductivity for the solution at the concentration of that solution. MacInnes and Yeh[31] showed that this relationship predicted junction potentials at a flowing junction for chloride solutions of H^+ or other alkali metals of the same concentrations very well, except for junctions where one of the cations was K^+ which they were unable to explain. MacInnes[29] suggested that for slightly more complicated boundaries where neither of the above two relationships holds, they can be combined. For example:

0.01 M NaCl ‖ 0.05 M HCl

can be rearranged as:

0.01 M NaCl ‖ 0.05 M NaCl ‖ 0.05 M HCl

and the junction potential can then be determined by using the sum of the values calculated where equation 4.13 was used for the first junction and equation 4.14 for the second junction.

There are also far more complicated data treatments to calculate junction potentials, most involving some kind of computer simulation.[17,23,29,32-37] Taylor[38] derived an extended form of the Henderson equation which avoids the assumption of uniform mixing and incorporates the ability to use variable mobilities and activity coefficients. The Nernst-Planck-Poisson (NPP) model has been used to study liquid and membrane junctions[32,34] and can be used to

study the time evolution of the membrane potential. The Henderson and Planck equations, which relate to the steady state, produce the same results as the NPP model at infinite time.[34]

It is experimentally important to have an idea of the time required to reach steady junction potentials. Hafemann[23] did some time-related calculations of junction potentials based on a one-dimensional isothermal liquid junction between simple salt solutions. For the junction between about 0.1 M and 0.05 M NaCl solutions he calculated that it takes approximately 6 ns for this junction to reach a steady state as illustrated in Figure 4.3. He also showed that the magnitude of the junction potential is independent of the dielectric constant of the solution, but that the steady state was reached faster for lower dielectric constant solutions. This work was confirmed by Goldberg and Frank[36] for junctions consisting of the same electrolytes at different concentrations in contact with each other. Using the NPP model, Sokalski and Lewenstam[35] calculated that, assuming a porous plug junction is used for the junction between 0.0005 – 0.5 M $CaCl_2$ solutions and a 0.1 M KCl solution, it takes the order of seconds to reach the steady state as demonstrated in Figure 4.4.

Comparing Figures 4.3 and 4.4, the interesting distinction noted is the potential variation before the steady state is attained. Hafemann[23] predicted a rise in potential to the steady state value, while Sokalski and Lewenstam[35] predicted a large initial potential transient where after the potential decreased to the steady state value. The potential of the transient is more-or-less ten times the steady state potential and implies that initially a huge excess of ions traverse the boundary between the two solutions and then slowly diffuses back till a steady state is reached. It is hard to believe that such a large transient can exist when considering that a steady state is reached due the diffusion of ions across the boundary being counteracted by the repulsion of charge at the opposite interface. Irrespective of which timeframe is actually correct in achieving a steady state, the experimental conditions employed in this work give more than sufficient time for this steady state to be reached.

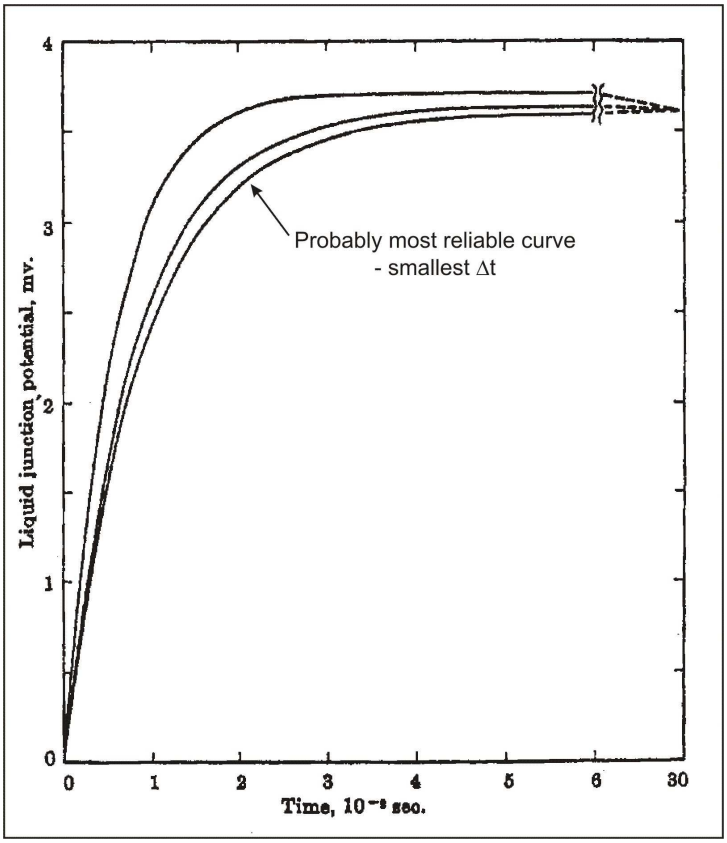

Figure 4.3: Junction potentials calculated with respect to time between about 0.1 M and 0.05 M NaCl solutions at different Δt values by Hafemann.[23]

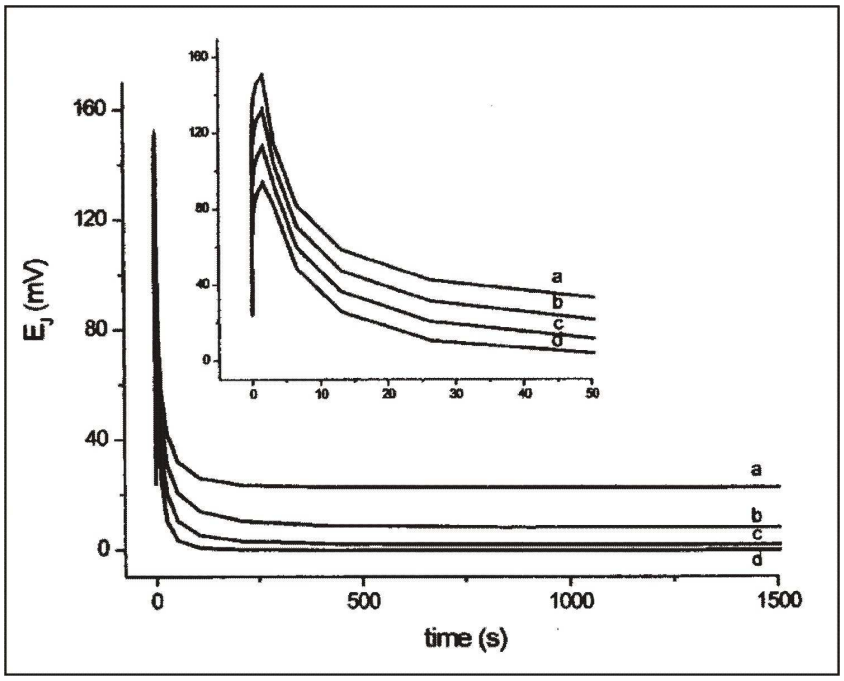

Figure 4.4: Junction potentials calculated with respect to time between a) 0.5 M, b) 0.05 M, c) 0.005 M and d) 0.0005 M $CaCl_2$ solutions and a 0.1 M KCl solution for a porous plug junction by Sokalski and Lewenstam.[35]

The type of junction employed determines which equation is used to calculate the junction potential. It is also important to assess which type of junction gives the most stable and reproducible results experimentally. The flowing junction appears to be the most reproducible provided the solution flow rate is fast enough, but not too fast to produce turbulence.[12,13] and stirred junctions also gave good reproducibility under certain conditions. Lamb and Larson[12] found that junction potentials were different for flowing, stirred and static junctions and also depended on the mode of stirring. Ferguson *et al.*[39] however showed very consistent values when comparing static, flowing (at different flow rates), stirred and stopped flow junctions for the simple junction between 0.01 M and 0.1 M HCl. Guggenheim[13] found that the potential differed by a maximum of 0.5 mV when using continuous mixture or free diffusion junctions for various boundary solutions.

For pH measurements using separate reference electrodes, the lowest uncertainties were found for reference electrodes with capillary junctions and the highest for ceramic junctions. The use of sleeve junctions gave long response times and their quality was variable.[14] It has also been shown that reference electrodes with relatively high KCl flow rates and small junction areas, i.e. with a high flux of KCl, performed the best.[40] The slow flow of KCl into the test solution ensures that the KCl solution is not diluted at the interface of the two solutions. If the junction becomes clogged and prevents the steady flow of KCl solution, the junction potential becomes unstable or fluctuates.[41]

It is important to be aware of any solution chemistry that can take place at the liquid junction and affect the diffusion junction potential. It is well known that the junction between say KCl and $HClO_4$ will result in insoluble $KClO_4$ forming and blocking the junction. $NaClO_4$ is far more soluble and sodium salts should rather be used than potassium salts. When working with sulphates the partially dissociated species HSO_4^- is formed in acid junctions. This affects the junction potential mainly by reducing the concentration of the highly mobile H^+ ion.[33]

4.2) Aims

Since the diffusion junction potential cannot be directly measured, a two pronged approach was considered: firstly, whether it was possible to accurately calculate the junction potential for the experimental conditions used; and secondly, how best to evaluate this parameter from the polarographic measurements. Polarographic experiments were performed by simply looking at the reduction of thallium(I), which does not readily undergo complexation. Polarograms were recorded at different pHs starting from pH 0.3 and increasing to about pH 5, and the half-wave potential data were analysed. The diffusion junction potential varies with pH and this would provide a good comparison to the actual complex formation experiments performed.

Other factors considered were (i) the reproducibility of the experimental junction potential, (ii) whether the two types of salt bridges used in this study affected the magnitude of junction potential, and (iii) if the type and amount of maxima suppressant added to the test solution influences the magnitude of the junction potential by affecting the mobility of the ions.

4.3) Results and Discussion

4.3.1) *Preliminary calculations and measurements*

In this work a combination of a potentiometric cell (using a CGE) and a polarographic cell was used. Diffusion junction potentials are formed in both types of cell. In the potentiometric cell, the junction exists between the outer RE solution of the GE and the test solution and can be represented as:

Ag(s) | AgCl(s) | 3 M KCl ‖ test solution

where ‖ represents the liquid junction.

In the polarographic cell, the RE is inserted into a salt bridge to prevent contamination of the test solution (having a nitrate background electrolyte) with chloride. The salt bridge filling solution was generally a 0.5 M $NaNO_3$ or KNO_3 solution (depending on whether a NaOH or KOH titrant was used, respectively) and at the same ionic strength as the initial test solution. In this case two

junctions are present, one between the RE solution and the salt bridge solution and the other between the salt bridge solution and the test solution and can be represented as:

Ag(s) | AgCl(s) | 3 M KCl ‖ salt bridge solution ‖ test solution

It was assumed that the solution compositions of the RE and the salt bridge remained constant throughout the experiment, as Hefter[8] had also done, and only the test solution composition changed. This implies that the junction potential between the reference and salt bridge solutions remains constant throughout the experiment and was also calculated using the Henderson equation to be relatively small (about 2.8 mV for the junction between 3 M KCl and 0.5 M $NaNO_3$). Thus the main junction to be considered in the polarographic cell is between the salt bridge solution and the test solution.

The E_j values were estimated between typical salt bridge and test solutions as would occur in the polarographic cell. The salt bridge solution (solution 1) was kept constant as (a) 0.5 M KNO_3 or (b) 0.5 M $NaNO_3$. The test solution (solution 2) consisted of a mixture of H^+, NO_3^-, OH^- and (a) K^+ or (b) Na^+ ions of varying concentration, as if 25 mL of 0.5 M HNO_3 solution was titrated with a 0.5 M (a) KOH or (b) NaOH solution. The E_j values were calculated employing both the Henderson and Planck equations where limiting ion mobilities were used, and the results are compared in Figure 4.5. Even though these equations were derived assuming different junction types, the values calculated using the two equations differed by less than 0.6 mV for both sets of solutions and the largest deviations occurred where the E_j s were large. The similar predictions could be due to only univalent ions being present and also NO_3^- existing in both the boundary solutions. The complicating factor in calculating the E_j values is that the test solution was a mixed electrolyte and varied in ionic strength. In Figure 4.5 it can be seen that between about pH 2 to 12 the E_j values are fairly constant, but below about pH 2 and above pH 12 the magnitude of these potentials increase significantly as the concentration of the highly mobile H^+ and OH^- ions in the test solution increase, respectively.

Junction potentials were also calculated for a typical potentiometric cell which involved the junction between the 3 M KCl reference solution and the test solutions which are the same as those described above. The results calculated using both the Henderson and Planck equations are given in Figure 4.6. In this case the deviations were larger between the calculated values using the two equations. This discrepancy appears to be mainly due to the large difference in concentrations between the two solutions (as was also noted by Harper[33]), rather than the fact that Cl^- instead of NO_3^- is present.

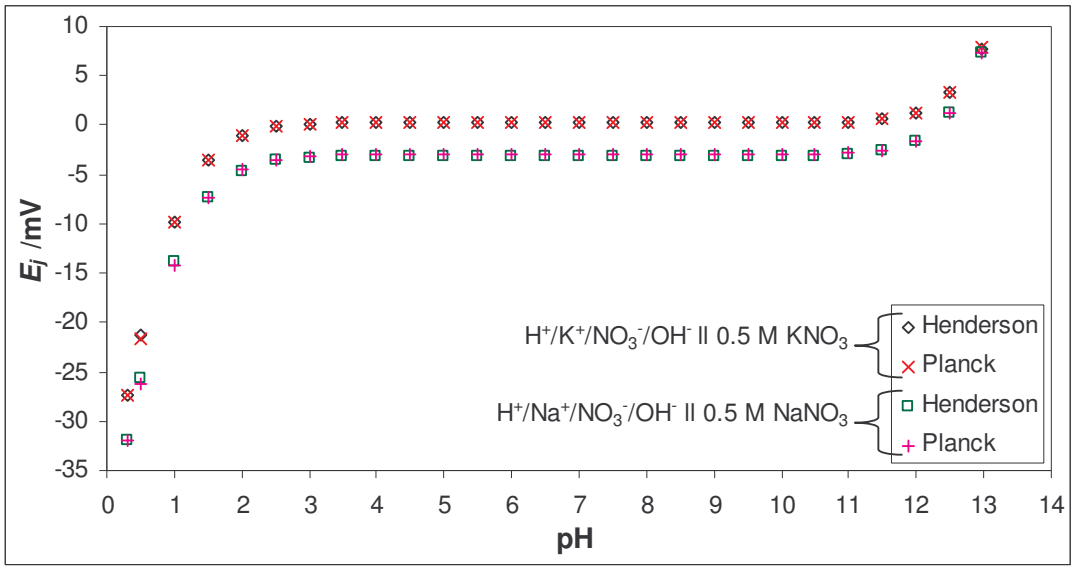

Figure 4.5: Comparison of E_j values calculated using the Henderson and Planck equations for the boundary between a test solution and 0.5 M KNO_3 or $NaNO_3$ salt bridge solution. The test solution consisted of 0.5 M HNO_3 after various additions of 0.5 M KOH or NaOH, respectively.

When junctions between 3 M KNO_3 and the test solutions were calculated, this discrepancy was still noted, although to a slightly lesser extent. What is of importance is the smaller magnitude of the junction potentials in the very acidic and basic regions which is due to the high salt concentration in one of the one boundary solutions. When calculating the junction potentials using an even higher concentration for one of the boundary solutions, these potentials in the very acidic and basic regions decreased further, but at the same time the magnitude of the potential increased in the region where it was approximately constant. The solubility of KCl in water at 20 °C is 34.7g in 100 mL,[42] which

translates to a solution of 4.65 M, so in practice the concentration of the KCl reference solution could be increased if required.

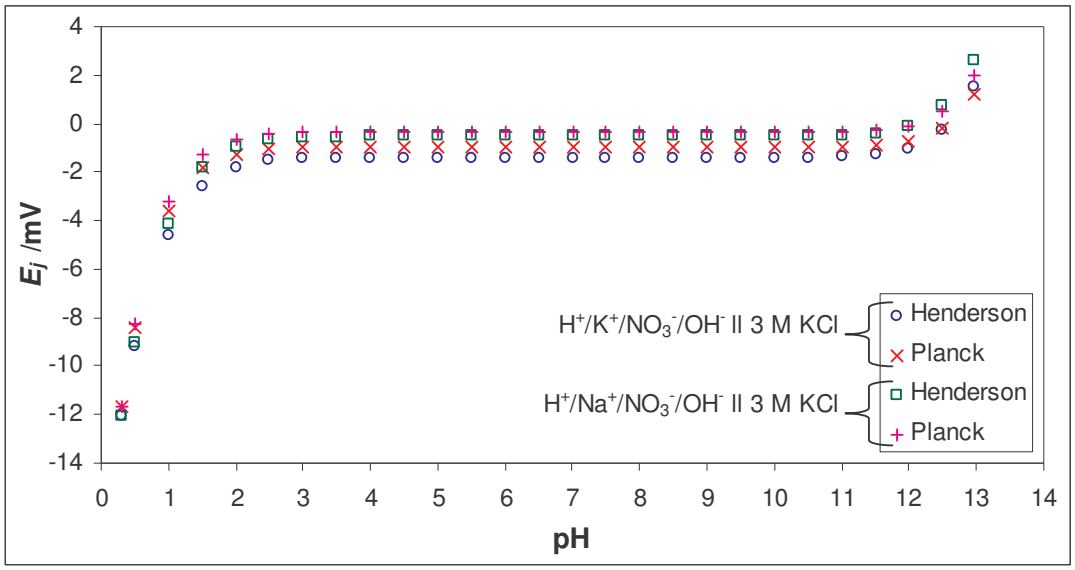

Figure 4.6: Comparison of E_j values using the Henderson and Planck equations for the boundary between a test solution and 3 M KCl reference solution. The test solution consists of 0.5 M HNO_3 after various additions of 0.5 M KOH or NaOH.

The salt bridge solution can be optimised to give the best results for the purpose required. In this work the solution used had a similar ionic strength to the test solution and the type of salt used ensured that both the anion and cation were common to the solutions in contact. Both types of salt bridges used here had restrained flow junctions, resulting in minimal contamination of the test solution. It is critical that minimal contamination takes place in these titration experiments as essentially the same test solution is used in multi-hour experiments. Hefter[8] also found that when restrained flow junctions were used, the values of the junction potential could be calculated with reasonable accuracy. Since our studies start at low pH, the use of an acid solution or a mixture of an acid and a salt solution in the salt bridge was considered. The magnitudes of the junction potentials between the salt bridge and test solution as well as the salt bridge and reference solution would change. However, there would be no additional benefit as we are working across a wide pH range and the change in the junction potential with respect to the change in pH would be about the same for a salt solution alone being used.

A small change in E_j with the change in pH in the acidic region can only be attained if a hydroxide solution is employed in the salt bridge. OH^- is the anion with a mobility closest to that for the H^+ ion that could counteract the charge difference in the junction. The junction potentials will be large in the pH region between 2 and 12 in this case, but will still be constant. If a 0.5 M OH^- solution is used in the salt bridge, the difference in the junction potential between solutions at pH 7 and pH 0.3 is about 9 mV (as shown in Figure 4.7). This difference is still large enough to have to be compensated for in the determination of formation constants for complexes formed at very low pH. A 1 M OH^- salt bridge solution produces much smaller variations in E_j at low pH. The junction potential between the OH^- salt bridge solution and the reference solution is larger (about 5.3 mV for 0.5 M KOH and 8.5 mV for 1 M KOH), but these potentials can be considered as constant throughout the experiment. However, contamination of the test solution by such a relatively large OH^- concentration in the salt bridge could alter the pH of the test solution and lead to unreliable data in the formation constant determination experiments. It could also cause the formation and precipitation of metal hydroxides at the junction, especially when Bi(III) is present, resulting in blocked junctions and unstable potential readings. The use of OH^- solution in the salt bridge is thus not recommended.

In this work it was decided to use salt bridge solutions composed of 0.5 M $NaNO_3$ or KNO_3solutions. In making this selection together with the type of junction used, it was hoped that minimal contamination of the test solution would occur. The diffusion junction potential is small and fairly constant over a wide pH range (above pH 2), but E_j would have to be determined and accounted for below pH 2. The junction potential in the basic region is of no concern here as experiments were terminated at pHs below which the E_j values become significant.

In this work it was decided to use salt bridge solutions composed of 0.5 M $NaNO_3$ or KNO_3solutions. In making this selection together with the type of junction used, it was hoped that minimal contamination of the test solution

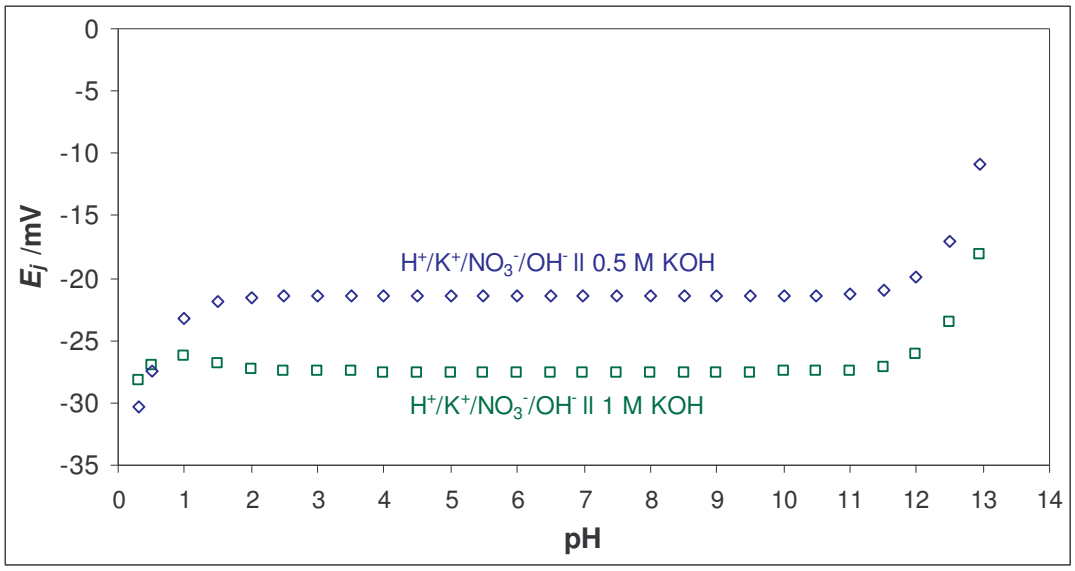

Figure 4.7: Junction potentials calculated using the Henderson equation for the boundary between a test solution and 0.5 M or 1 M KOH salt bridge solution. The test solution consists of 0.5 M HNO_3 after various additions of 0.5 M KOH.

would occur. The diffusion junction potential is small and fairly constant over a wide pH range (above pH 2), but E_j would have to be determined and accounted for below pH 2. The junction potential in the basic region is of no concern here as experiments were terminated at pHs below which the E_j values become significant.

So far limiting ionic conductivities have been used to calculate the diffusion junction potentials, but for the fairly high ionic strength solutions used here, it is not really justifiable using these values, even if there is some cancellation in errors as Hefter[8] suggested. Since ionic mobilities are mainly dependant on ionic strength, the mobilities of each ion in solution was calculated using the Onsager limiting law at the total ionic strength of the solution in which it is present as given in Table 4.3. These values were then used to calculate the diffusion junction potential as before. An example is shown in Figure 4.8 where the Henderson equation was used for the junction between a 0.5 M KNO_3 salt bridge solution and the test solution formed by titrating 0.5 M HNO_3 with 0.5 M KOH. The calculations were repeated for 0.1 M solutions as the ion conductivities determined for 0.5 M ionic strength were not accurate.[1] The largest disparities in the computed E_j values when using limiting ion

conductivities compared to conductivities at a given ionic strength were observed in the very acidic and basic regions. For example, at 0.5 M ionic strength the difference between the E_j values was 2.9 mV at pH 0.3 and 1.4 mV at pH 1, and at 0.1 M ionic strength the difference was 1.7 mV at pH 1. This is due to the transference numbers being greater for the H^+ and OH^- ions at high ionic strengths as compared to the other ions. As seen in Table 4.3 the mobilities of these two ions decreased to less of an extent than for the other ions as the solution concentrations were increased. The predicted mobilities used here at 0.5 M ionic strength are too low, so the difference between the junction potentials at this ionic strength and at infinite dilution should be smaller.

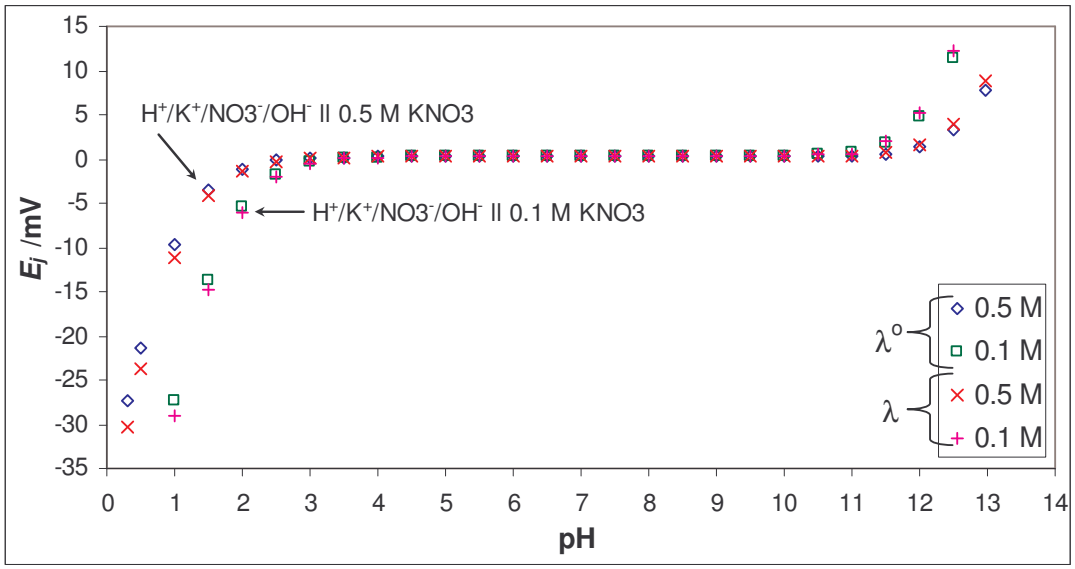

Figure 4.8: Comparison of E_j values calculated using the Henderson equation employing either limiting ion conductivities or ion conductivities for the particular ionic strength of the solution.

Although it was suggested that a flowing junction is the most reproducible (provided the flow rate is optimal),[12,13] it would be impossible to use in this work as measurements in the test solution are made between each step in a titration. A ceramic frit or a ground glass joint (or sleeve) junction was employed in the salt bridge and the Ag/AgCl RE contained a ceramic frit. In the CGE a ceramic frit was at the junction. A separate glass electrode could not be used as a ground loop formed between the potentiometric and

polarographic electrodes in the cell and resulted in nonsensical measurements. Also space was limited in the already full cell. The junctions used were slow flowing junctions to avoid any changes in volume and composition in the cell.

In order to see if there is a significant difference between the different salt bridges, simple potential difference measurements were made using a Uni-T DT830B multimeter. The potential difference between two Ag/AgCl REs was measured as a reference point using the following cells:

Ag | AgCl | 3 M KCl ‖ Solution *X* ‖ 3 M KCl | AgCl | Ag

where solution X was 3 M KCl, 0.1 M KCl or 0.1 M HCl. The order of magnitude of E_j at each junction should be as follows: E_j (3 M KCl) = 0 < E_j (0.1 M KCl) < E_j (0.1 M HCl). The potential difference was measured using a multimeter and was found to be 0.0 mV in all cases. This indicates that the REs had the same potential and the junctions behaved the same.

The one RE was then placed in a salt bridge with a ceramic frit (labelled A) and the other was placed in a salt bridge with a ground glass joint (labelled B). The potential difference between the two electrode systems was then measured as before in the following cell:

AgCl | 3 M KCl ‖ Solution *Y* (A) ‖ 0.1 M HCl ‖ Solution *Y* (B) ‖ 3 M KCl | AgCl | Ag

where solution *Y* was 3 M KCl or 0.1 M KCl. At this stage it had been established that the junction potentials between the reference solution and the salt bridge solution is the same for the two electrodes for the same solution *Y*. Any potential difference measured would thus be at the salt bridge junctions. If the magnitudes at these junctions are the same, an overall zero potential will be measured as the individual potentials will have opposite signs, i.e. for the junctions:

Solution y (A) ‖ 0.1 M HCl ‖ Solution y (B),

the signs will be

$+ \| -$ $\quad\quad$ $- \| +$

The potential difference readings were 0.0 mV indicating that there was no difference in the junction potentials at the two salt bridges.

An “unsymmetrical” cell was also tested where the salted bridge solutions were different in the cell:

$$\text{AgCl}\,|\,\text{3 M KCl} \parallel \text{3 M KCl (A)} \parallel \text{Solution } Z \parallel \text{0.5 M } NaNO_3\text{ (B)} \parallel \text{3 M KCl}\,|\,\text{AgCl}\,|\,\text{Ag}$$

where solution *Z* was 3 M KCl or 0.5 M HNO_3, but the potential difference still remained 0.0 mV. This would be expected due to the additivity of the junction potentials and the end solutions being the same (3 M KCl).

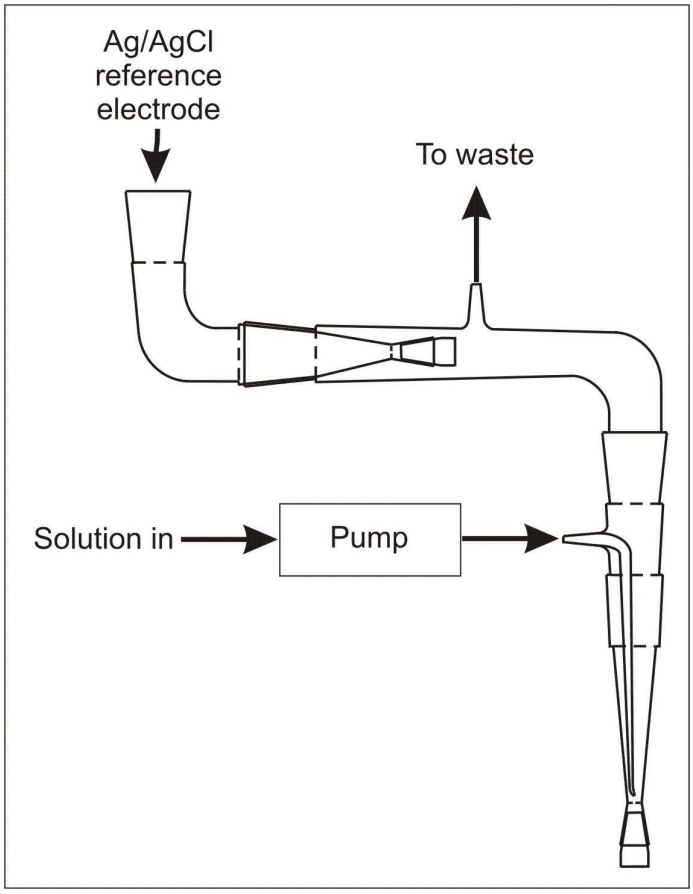

Figure 4.9: Schematic diagram of the continuous flow salt bridge.

A salt bridge with a ground glass joint was designed such that the filling solution was slowly pumped into the bridge close to the joint (labelled C). The salt bridge solution was thus constantly replenished so that the composition of

the inner reference solution remained constant. A schematic diagram of the continuous flow salt bridge is given in Figure 4.9. The potential difference between the two electrode systems was again measured in the following cell:

$$AgCl\,|\,3\ M\ KCl\ \|\ 0.5\ M\ NaNO_3\ (A)\ \|\ 0.5\ M\ HNO_3\ \|\ 0.5\ M\ NaNO_3\ (C)\ \|\ 3\ M\ KCl\,|\,AgCl\,|\,Ag$$

Initially a potential difference of 0.0 mV was measured before pumping of the salt bridge solution was commenced. The reading remained unchanged even after an hour of pumping the solution at a rate of about 1.8 ml min^{-1}. Thus there appeared to be no benefit in using this more complicated salt bridge system.

4.3.2) *Polarographic measurements*

Both the polarographic and potentiometric measurements at low pH incorporate a diffusion junction potential which influences the potential measurement. The GE was calibrated by fitting a quadratic function to the very acidic region to account for the curvature due to the E_j, as discussed in Chapter 3. A similar approach could not be applied to the polarographic potential data. The biggest problem with the pH titration experiments is that the pH is continually changing and hence the magnitude of E_j is also changing, especially below pH 2 as illustrated using calculated values in Figures 4.5 and 4.8. Thallium(I) was introduced into the test solution and used as a witness to monitor the junction potential. Tl(I) generally forms weak complexes, therefore complexation will not occur at low pH with the ligands being studied. This property has previously been exploited by using Tl(I) as an internal standard to correct for current fluctuations in voltammetric analyses.[43]

A typical pH titration experiment was described in Chapter 2. The initial test solution used here consisted of 25.00 mL of 0.5 M HNO_3 solution with 50 μL of 0.100 M Tl(I) stock solution and a few grains of gelatine. The solution was titrated with 0.5 M NaOH solution such that the change in pH was 0.07 between each set of polarographic and potentiometric measurements. The potential range for each polarogram was set from –0.2 to –0.7 V for the reduction of Tl(I) alone and a 60 ms current integration time was used. The

reduction of Tl(I) was fully reversible as the value of $\delta = 1 \pm 0.08$ for each polarogram over the entire pH range was obtained. This δ value was therefore fixed at one thereby eliminating an extra variable that had to be fitted.

Figure 4.10 shows typical polarograms for the reduction of Tl(I) in 0.5 M HNO_3 (i.e. at a pH of 0.3) and at a pH 3 (adjusted by adding 0.5 M NaOH). The lower diffusion limited current displayed in the latter polarogram is due to dilution. A polarogram of the 0.5 M HNO_3 background electrolyte is also included to show that the reduction of the large concentration of H^+ to produce $H_2(g)$ overlaps slightly with the Tl(I) reduction for low pH solutions. At higher pHs where the concentration of H^+ is significantly lower, the hydrogen evolution wave no longer interferes in the potential region studied.

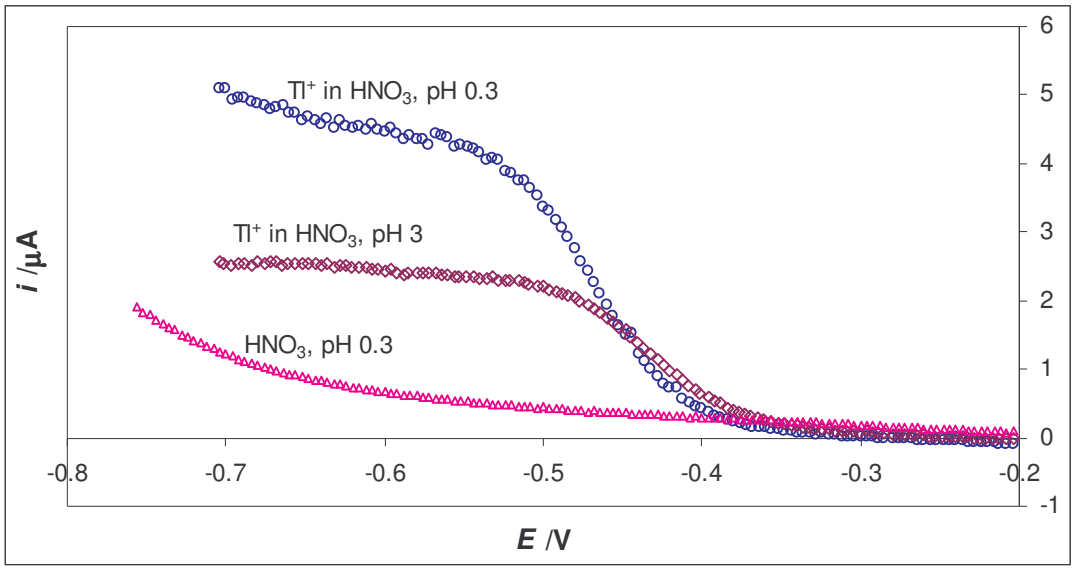

Figure 4.10: Polarograms showing the reduction of Tl(I): 2.00×10^{-4} M at pH 0.3 and ~1×10^{-4} M at pH 3, and the polarogram in 0.5 M HNO_3 only.

For polarograms at low pH, the background current could be fitted using the relationship:

$$i_{bkgnd} = a + bE + c\exp(dE) \qquad (4.15)$$

The straight line terms of the equation describe the capacitance currents and the exponential term describes the H^+ reduction currents. Figure 4.11 gives the separate curves for the background and the DC wave. The fitted curve

(red line) is the sum of these currents and it is shown how it fits through the experimental data.

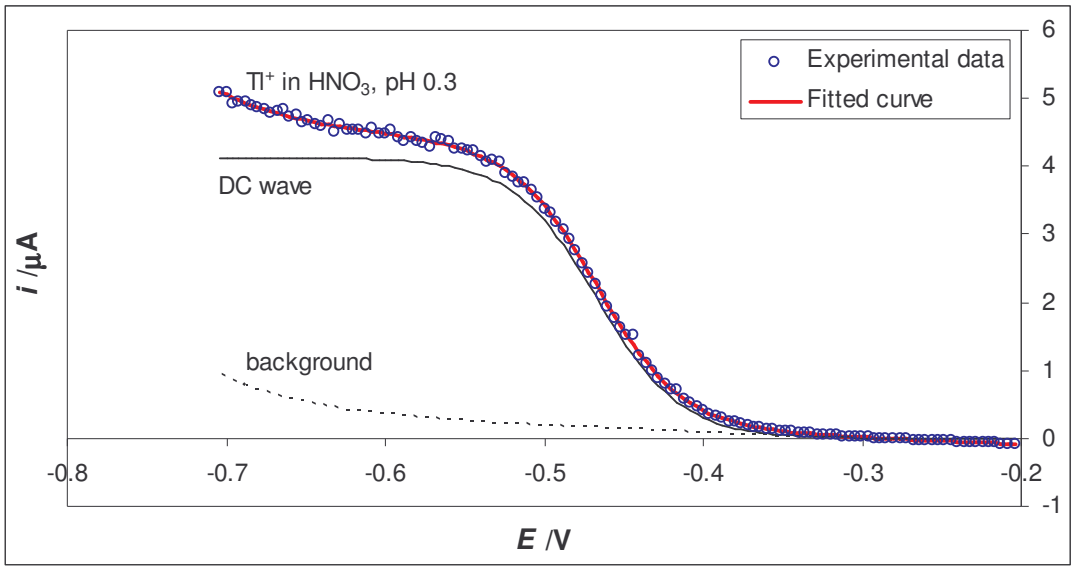

Figure 4.11: Polarogram for 2.00×10^{-4} M Tl(I) in 0.5 M HNO_3 fitted using equation 2.14, where the background current is given by equation 4.15. The separate functions are also shown.

For polarograms at higher pH where the start of the hydrogen evolution wave is absent, the background current only needs to account for the capacitance currents, hence a straight line function is sufficient. An example is given in Figure 4.12 where again the separate currents for the DC wave and the background are displayed, as well as the sum of these currents.

The diffusion limited currents were plotted versus pH and it is shown in Figure 4.13 that the experimentally determined currents and those calculated from the initial value for i_d and the dilution factors correspond extremely well. This "well-behaved" system adds to the strength of using Tl(I) as a witness to monitor the junction potential. The diffusion limited currents (and fitted δ values) for Tl(I) reduction were not used in any further calculations, but were merely inspected to check the integrity of the data.

The half-wave potentials as a function of pH are given in Figure 4.14. These potentials should be independent of pH and the constant value would

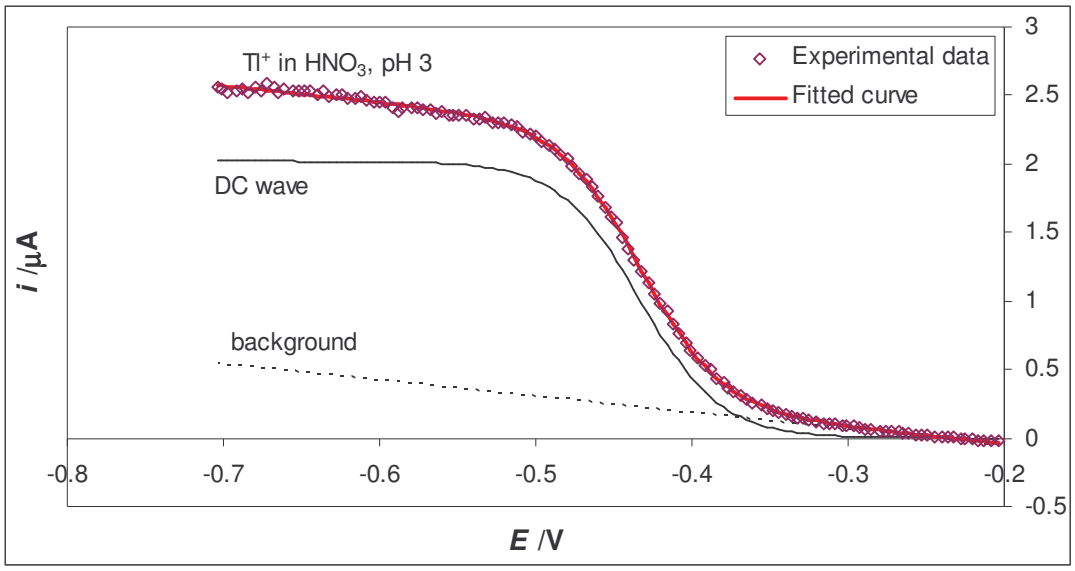

Figure 4.12: Polarogram for ~1 × 10^{-4} M Tl(I) in a nitrate solution at pH 3 fitted using equation 2.14, where the background current is a straight line. The separate functions are shown.

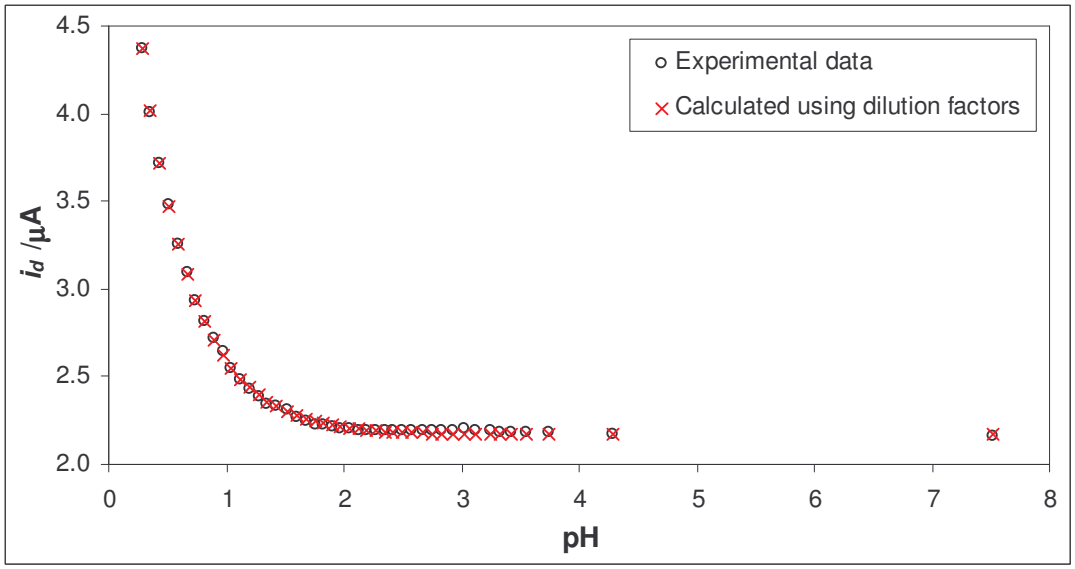

Figure 4.13: Comparison of experimental diffusion limited currents and those calculated taking dilution into account for the titration of 2.00 × 10^{-4} M Tl(I) in 0.5 M HNO_3 by 0.5 M NaOH.

correspond to the free metal ion potential (in a nitrate background electrolyte at about 0.5 M ionic strength). Constant potentials with changing pH were, however, only observed above about pH 2. The free Tl(I) potential ($E(Tl_{free})$) was calculated by averaging the potential values in the pH region where they

were constant and is indicated by the red line in the graph. Below about pH 2, the potentials deviate from $E(Tl_{free})$ due to the large diffusion junction potentials that are incorporated in the potential measurements. The difference between $E(Tl_{free})$ and the recorded half-wave potentials give the magnitude of E_j at each pH (see Figure 4.15).

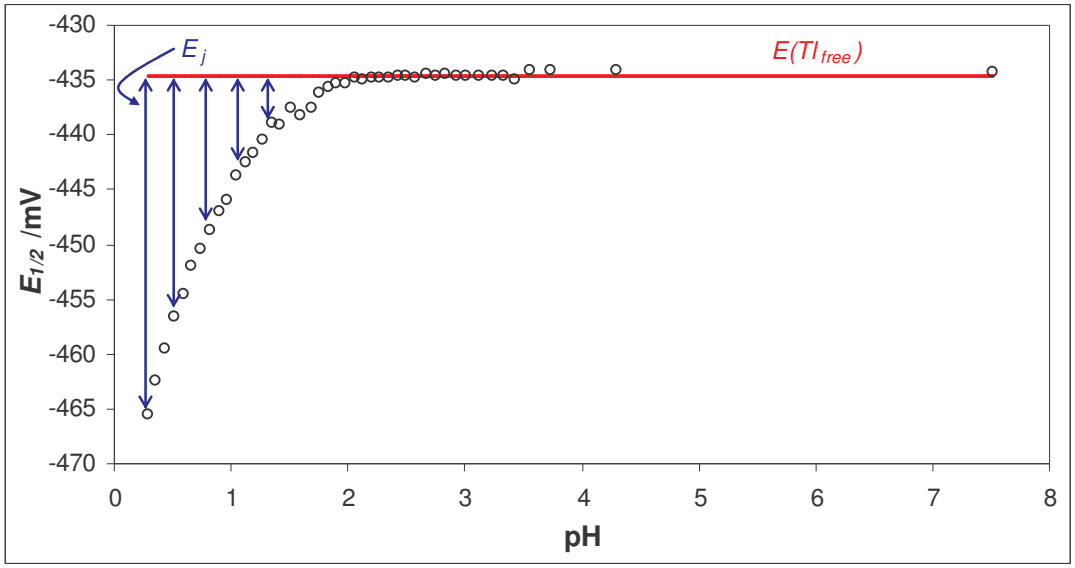

Figure 4.14: The half-wave potentials as a function of pH where the free Tl(I) potential is indicated by the solid red line.

The values of E_j were calculated using the Henderson equation and the limiting ion mobilities and compared to the experimentally determined values in Figure 4.15. Including $TlNO_3$ in the calculation had no effect on the resulting E_j value as the concentrations of these ions were much lower than that of the other ions present. Values of E_j calculated using Planck's equation gave very similar results for the solutions in contact in this case, as seen in Figure 4.5, so either equation could be used. Figure 4.15 shows that the E_j values determined from the polarographic data are not the absolute junction potentials, but rather the change in the junction potential as a function of pH. The diffusion junction potential associated with $E(Tl_{free})$ cannot be directly determined from these experiments and is not accounted for. The junction potential at pH 7 for the solutions used in this experiment was calculated to be 2.71 mV and the value does not deviate significantly in the pH region between 3 and 11. In this work, the exact value for E_j is not important, only the change in the junction potential

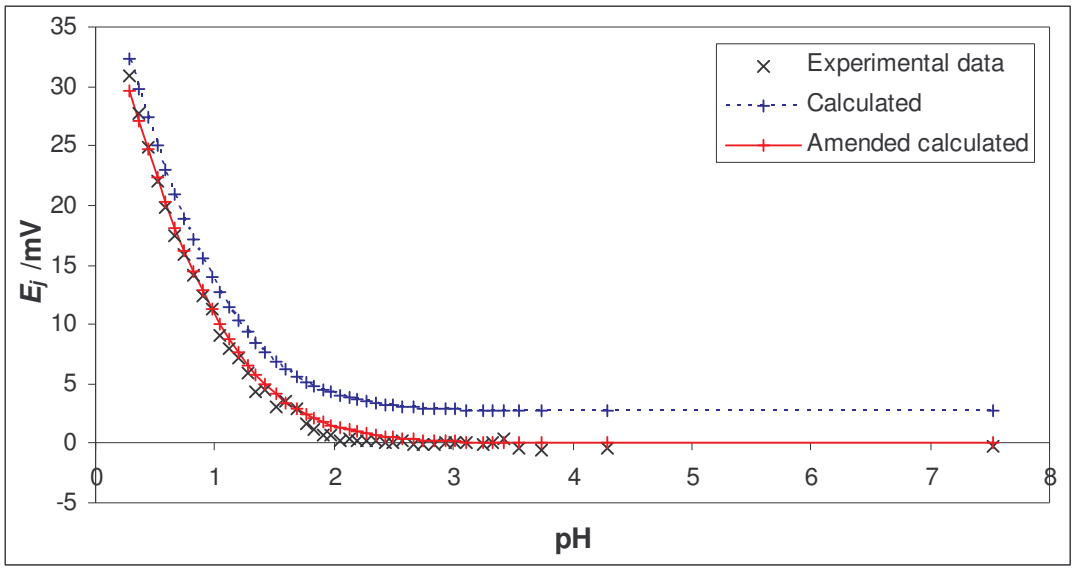

Figure 4.15: Experimentally determined diffusion junction potentials as a function of pH from data in Figure 4.14 and the calculated values using the Henderson equation and the limiting ion mobilities. These calculated values were then amended by subtracting 2.71 mV at each pH (see text).

with pH needs to be accounted for. This is due to the potential shift being employed when calculating formation constants, and as long as the magnitude of E_j is the same for both the free metal ion potential and the potential of the complexed metal ion at each pH, it is cancelled on subtraction. Deducting the value of 2.71 mV from each of the calculated E_j values gave the amended plot in Figure 4.15 which corresponded to the experimental data trend. This is almost surprising considering the use of limiting ion mobilities and the Henderson equation which was derived assuming a continuous mixture junction, whereas a restrained flow junction was actually used and solutions had ionic strengths between 0.5 M and 0.25 M.

Junction potentials were also calculated using the mobilities determined for 0.1 M and 0.5 M ionic strength solutions (from Table 4.3) and amended as before, and the results are presented in Figure 4.16. The standard deviations of the calculated data as compared to the experimental data were calculated using the standard expression:

$$s_{yx} = \sqrt{\frac{\sum_{i=1}^{N} (y_i(obs) - y_i(calc))^2}{N-1}} \qquad (4.16)$$

The s_{yx} values obtained were 0.64, 1.08 and 1.57 for ion mobilities at 0 M, 0.1 M and 0.5 M ionic strength respectively, indicating that the limiting mobilities best predicted the magnitude of the change in the junction potential for this data set.

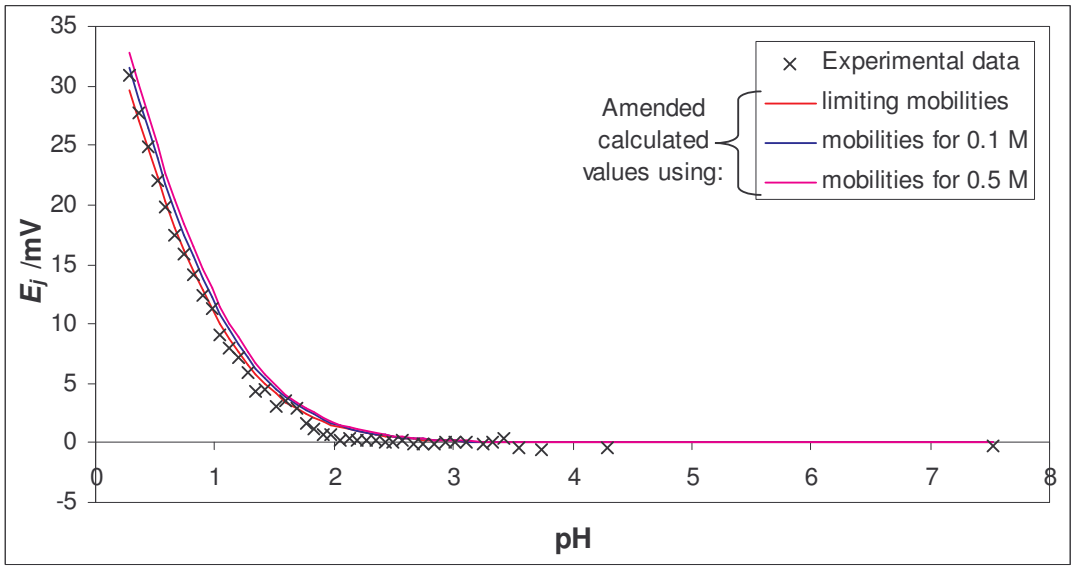

Figure 4.16: Plot as for Figure 4.15 including the amended junction potentials calculated using the Henderson equation and the ion mobilities at 0.1 M and 0.5 M ionic strengths.

The half-wave potential data for the reduction of Tl(I) can therefore be used to determined the change in the junction potential for a pH titration experiment. The proposed approach would be to include Tl(I) in the solution together with the metal ion and ligand that is being studied. Tl(I) would generally remain uncomplexed under the low pH conditions where the junction potential is significant. pH titration experiments are generally started at the lowest pH and then the pH is increased by addition of hydroxide solution. The free metal ion potential is normally determined by finding the half-wave potential in a solution containing the metal ion before the ligand is added. In the case where titrations are started below pH 2, this half-wave potential also carries a large

junction potential which would first have to be corrected for. Also, as the pH is increased during the titration, the decrease in E_j results in a positive potential shift. If labile complexes are formed at low pH between the ligand and the metal ion of interest, the polarographic wave shifts to more negative potentials with increased pH. The net potential shift is the sum of these two effects and if the junction potential is not adequately compensated for, it would result in poor stability constant data. For the metal ion being studied, there is no way to separate the two components of the potential shift directly. However, since Tl(I) does not usually undergo complexation at low pH, the change in magnitude of E_j can be determined for each experiment.

In order to assess the reproducibility of the experimental diffusion junction potential, five data sets were compared and the values are plotted versus pH in Figure 4.17. The values calculated using the Henderson equation and limiting ion mobilities as before, are included in the graph for comparison. This chart illustrates that from one experiment to the next there is a slight variation in the measured E_j. It can also be seen that some data sets would be better described by values calculated using mobilities determined for 0.1 M and 0.5 M ionic strength solutions. Figure 4.18, which is the plot of the difference between the experimentally determined and calculated values as a function of pH, shows this variation more clearly with deviations almost up to 4 mV in the very acidic region. The standard deviations for each data set with respect to the calculated values (using limiting mobilities) were determined using equation 4.16 and are displayed in Figure 4.18.

The variation in junction potentials for the different experiments raises the question as to whether this is due to error in determining the actual half-wave potential values or whether it is due to phenomena occurring at the junction itself. This is discussed in more detail in Chapter 6, where two metal ions are present in the solution simultaneously in the absence of a ligand. If the half-wave potentials as a function of pH for both metal ions show the same trend, then the variations would be due to physical conditions such as the junction or the RE itself. This will be shown to mostly be the case. Calculating E_j, irrespective of how complicated the simulation is, would always give the same

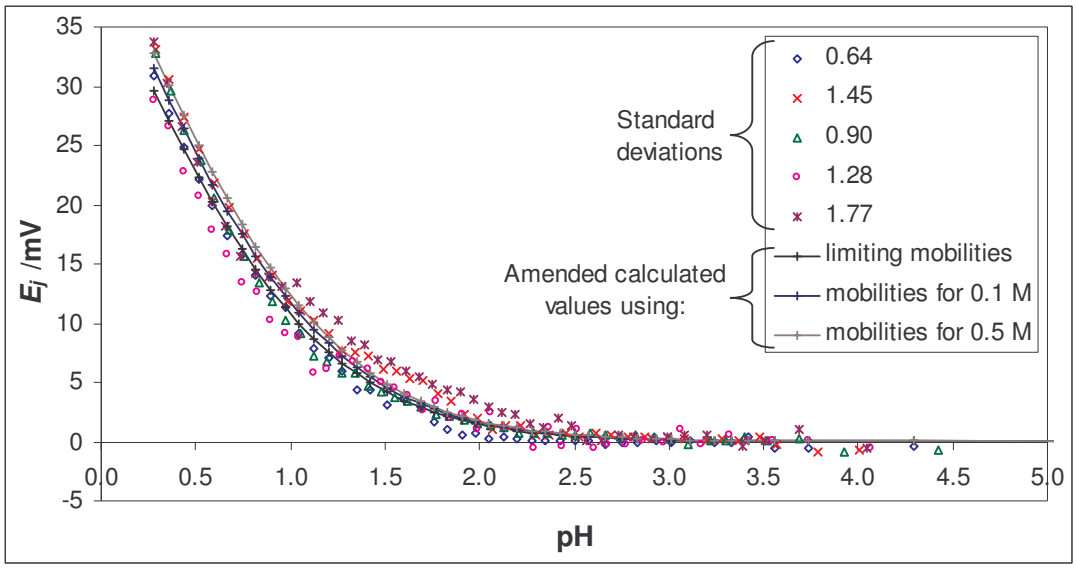

Figure 4.17: Experimentally determined diffusion junction potentials, for five data sets, as a function of pH. The amended calculated values using the Henderson equation and ion mobilities at different ionic strengths as given in Figure 4.16 are included.

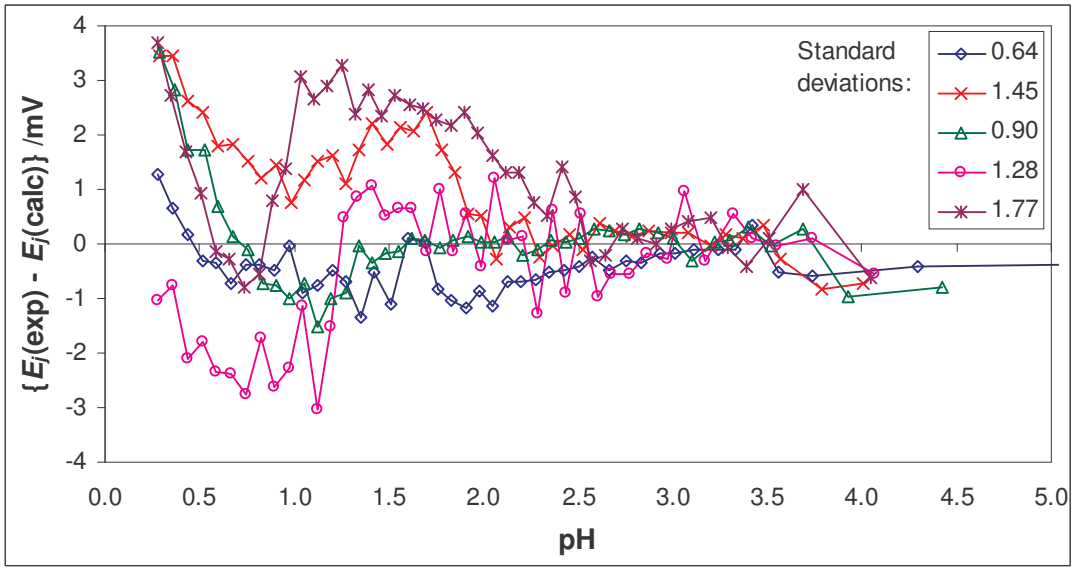

Figure 4.18: The difference between the experimentally determined and calculated E_js using limiting ion mobilities for the five data sets in Figure 4.17. The standard deviation for each data set was calculated with respect to these calculated values.

result for the same solutions and junction type. Calculations would not provide as accurate an assessment as if these potentials were measured for each experiment to account for the variations observed. This is achieved by

including Tl(I) in each test solution so that its reduction potentials can be used to quantify the junction potential for each experiment.

It was investigated whether the experimental conditions could be optimised to give more reproducible junction potentials. Initial titration experiments were performed using a sleeve salt bridge. The tip is removable and contact between the test and salt bridge solutions occurs through the ground glass joint. The tip has to be reseated for each experiment and the reproducibility of this process was questioned as it could affect the diffusion junction potential. A salt bridge with a ceramic frit that was permanently fitted was therefore tested to see whether it delivered more reproducible results. There was, however, no real difference between the magnitudes of the junction potentials measured or the reproducibility of the measurements when comparing these two liquid junctions.

Another factor which could affect the junction potential was the addition of the maxima suppressant. A few grains of gelatine was added to the test solution, but since the mass was less than 10 μg and only a five decimal place balance was available, the mass of gelatine could not be weighed to ensure that a constant amount was added for each experiment. Since the presence of the surfactant in solution could affect the mobility of the ions in solution, it was thought that the slight deviations in the junction potentials between experiments could be due to small variations in the amount of the surfactant used. Triton® X-100 is another commonly used maxima suppressant and it was determined that 10 μL of a 0.3% v/v Triton® X-100 solution added to 25 mL of test solution (instead of the gelatine) was sufficient to eliminate current maxima. A Hamilton microsyringe was used to add the 10 μL to ensure that a consistent amount of surfactant is added for each experiment. Again no real improvement in the reproducibility of the potential data between experiments was observed. This was probably due to the very small concentration of the maxima suppressant not really influencing the mobility of the ions in solution significantly.

4.4) Conclusions

Thallium(I) can be used as a witness ion to determine the magnitude of the change in the diffusion junction potential in a pH titration experiment provided it is not complexed by the ligand below about pH 3. This will allow sufficient data for the free Tl(I) potential to be determined and thereafter the change in the junction potential as a function of pH. In determining the junction potentials for each experiment, the variation in these values due to experimental conditions for each data set can be accounted for.

When calculating the diffusion junction potential it is important to use the expression that was derived for a particular type of junction, however, due to the complexity of the model, expressions have only been derived for junctions that are more readily described mathematically. In the polarographic cell used in this work, the boundary solutions in the cell and salt bridge are fairly simple: they contain essentially only univalent ions with a least one type of ion in common between the two solutions, the ionic strengths do not vary or differ widely and strong electrolytes are used. Additionally all solutions are aqueous solutions so junctions are not complicated by different solvents[44] and all experiments are run at 25 ± 0.1 °C so the temperature dependence of the junction potential[45] is not a factor in this work. It was therefore found that there was no significant difference between the junction potentials calculated using either the Henderson or the Planck equations for the polarographic cell. The discrepancy in the calculated values when using these two equations was larger when employing boundary solutions in the potentiometric cell, which was due to the larger differences in ionic strength between the solutions in contact. Ideally the ion mobilities used to calculate the junction potential should be for the ionic strength of the solution, but using the Onsager limiting law for calculating mobilities at higher ionic strengths is only accurate up to 0.1 M ionic strength.

Comparison between the calculated and experimental junction potential values gave reasonable results considering the derivations of the equations used did not correspond to the actual junction type employed. The calculations could not take variations of the experimental conditions into account, the source of

which could not be established as it was not due to the type of junction or the maxima suppressant that was added.

It was decided to use experimentally determined values of the junction potential, using Tl(I) as the witness ion, for each titration experiment in the determination of formation constants of metal-ligand systems at low pH. The exact implementation of this will be investigated in the subsequent chapters.

4.5) References

1) R.A. Robinson and R.H. Stokes, Electrolyte Solutions – The Measurement and Interpretation of Conductance, Chemical Potential and Diffusion in Solutions of Simple Electrolytes, 2nd ed., Butterworth and Co., London, 1959
2) P.W. Atkins, Physical Chemistry, 6th edition, Oxford University Press, Oxford, 1998
3) J.D. Bernal and R.H. Fowler, J. Chem. Phys., 1 (1933) 515
4) L. Onsager, Phys. Z., 27 (1926) 388
5) L. Onsager, Phys. Z., 28 (1927) 277
6) I. Zusková, A. Novotná, K. Včeláková and B. Gaš, J. Chromatogr. B, 841 (2006) 129
7) K.B. Oldham and J.C. Myland, Fundamentals of Electrochemical Science, Academic Press Inc., San Diego, 1984
8) G.T. Hefter, Anal. Chem., 54 (1982) 2518
9) R.G. Bates, Determination of pH. Theory and practice, 2nd ed., John Wiley and Sons Inc, New York, 1973
10) I. Feldman, Anal. Chem., 28 (1956) 1859
11) G. Eisenman, Glass electrodes for hydrogen and other cations. Principles and practice, Marcel Dekker Inc, New York, 1967
12) A.B. Lamb and A.T. Larson, J. Am. Chem. Soc., 42 (1920) 229
13) E.A. Guggenheim, J. Am. Chem. Soc., 52 (1930) 1315
14) R. Naumann, Ch.Alexander-Weber, R. Eberhardt, J. Giera and P. Spitzer, Anal. Bioanal. Chem., 374 (2002) 778
15) G. Scatchard, J. Am. Chem. Soc., 47 (1925) 696
16) F.G.K. Baucke, R. Naumann and C. Alexander-Weber, Anal. Chem., 65 (1993) 3244
17) W.H. Smyrl and J. Newman, J. Phys. Chem., 72 (1968) 4660
18) (a) P. Henderson, Z. Phys. Chem., 59 (1907) 118; (b) P. Henderson, Z. Phys. Chem., 63 (1908) 325
19) A.K. Covington, Anal. Chim. Acta, 127 (1981) 1
20) P.M. May, K. Murray and D.R. Williams, Talanta, 32 (1985) 483

21) (a) M. Planck, Ann. Phys. Chem., 39 (1890) 161; (b) M. Planck, Ann. Phys. Chem., 40 (1890) 561
22) W.E. Morf, Anal. Chem., 49 (1977) 810
23) D.R. Hafemann, J. Phys. Chem., 69 (1965) 4226
24) J.L. Jackson, J. Phys. Chem., 78 (1974) 2060
25) C.-H. Chen and H.S. Frank, J. Phys. Chem., 77 (1973) 1540
26) J.H. Leckey and F.H. Horne, J. Phys. Chem., 85 (1981) 2504
27) H.Z. Pleijel, Z. Phys. Chem., 72 (1910) 1
28) D.E. Goldman, J. Gen. Physiol., 27 (1943) 37
29) D.A. MacInnes, J. Am. Chem. Soc., 37 (1915) 2301
30) G.N. Lewis and L.W. Sargent, J. Am. Chem. Soc., 31 (1909) 363
31) D.A. MacInnes and Y.L. Yeh, J. Am. Chem. Soc., 43 (1921) 2563
32) O.J. Riveros, J. Phys. Chem., 96 (1992) 6001
33) H.W. Harper, J. Phys. Chem., 89 (1985) 1659
34) T. Sokalski, P. Lingenfelter and A. Lewenstam, J. Phys. Chem. B, 107 (2003) 2443
35) T. Sokalski and A. Lewenstam, Electrochem. Com., 3 (2001) 107
36) R.N Goldberg and H.S. Frank, J. Phys. Chem., 76 (1972) 1758
37) J. Bagg, Electrochim. Acta, 35 (1990) 361
38) P.B. Taylor, J. Phys. Chem., 31 (1927) 1478
39) A.L. Ferguson, K. van Lente and R. Hitchens, J. Am. Chem. Soc., 54 (1932) 1285
40) W. Davison and C. Woof, Anal. Chem., 57 (1985) 2567
41) S. Ito, H. Hachiya, K. Baba, Y. Asano and H. Wada, Talanta, 42 (1995) 1685
42) R.C. Weast, CRC Handbook of Chemistry and Physics, 49th ed., The Chemical Rubber Co., Cleveland, Ohio, 1969
43) I. Pižeta, D. Omanović and M. Branica, Anal. Chim. Acta, 331 (1996) 125
44) G. Cox, A.J. Parker and W.E. Waghorne, J. Am. Chem. Soc., 95 (1973) 1010
45) J. Bagg, Electrochim. Acta, 37 (1992) 719

CHAPTER 5
Ligands

5.1) Introduction

Complex formation using three related pyridinecarboxylic acid ligands were studied: pyridine-2-carboxylic acid (picolinic acid), pyridine-2,6-dicarboxylic acid (dipicolinic acid) and pyridine-2,3-dicarboxylic acid (quinolinic acid). These have been abbreviated PA, DPA and QA respectively. Their structural formulae are given in Figure 5.1. Each consists of a pyridine ring with carboxylic acid groups attached so that they can act as bi- or tridentate ligands by binding to the metal ions through the carboxylate groups and the pyridine nitrogen atom.

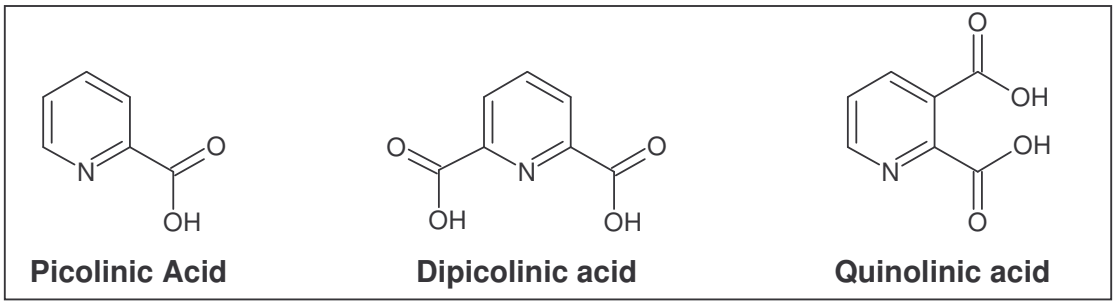

Figure 5.1: Structural formulae of the ligands studied in their neutral form.

Pyridinecarboxylic acids and their derivatives are present in many natural products. The metal complexes of these ligands are of special interest to medicinal chemists because of the wide variety of physiological properties displayed.[1-3]

PA is formed in the body as an intermediate during the degradation of tryptophan, an essential amino acid.[3,4] Chromium picolinate, which has been used as a nutritional supplement, was shown to significantly decrease levels of low density lipoprotein (LDL) cholesterol and apolipoprotein B (the principal protein of the LDL fraction) in human serum, while observing only small increases in concentration of the high density lipoprotein (HDL) cholesterol.[5] However, it was shown to cause chromosome damage in hamster ovary cells

and it was deduced that this was caused by the presence of the picolinate ligand.[6] Speetjens *et al*.[7] demonstrated that it caused DNA damage through the production of hydroxyl radicals. Research also pointed to picolinic acid aiding the absorption of zinc in rats[8] and the high bioavailability of zinc in human milk resulting from the presence of PA which facilitated zinc absorption from the intestine.[9] This was refuted by Rebello *et al*.[10] who said the concentration of PA in human milk was too low and that it was not detected in pancreatic juice or the intestine. Their studies also showed that PA did not increase zinc absorption in cattle. Many other studies involving PA have been undertaken. One of the more recent investigations revealed that PA reduces the amount of replication of the human immunodeficiency virus-1 (HIV-1) and human herpes simplex virus-2 ((HSV-2).[11]

DPA is present in nature as an oxidative degradation product of vitamins, coenzymes and alkaloids.[8] It is a component of fulvic acid[8] and has been used as a simple model for humic acids.[12] It has a diverse biological activity and acts as an inhibitor of the enzymes GA 2β-hydroxylase and proline 4-hydroxylase.[13] The iron-dipicolinic acid complexes are used as electron carriers in some model biological systems.[14-16] Some metal complexes with dipicolinic acid have beneficial effects in normalising elevated blood glucose levels in diabetic rats[17,18] while others showed anti-inflammatory activities.[19]

The DPA content of several species of bacterial spores have been reported to range from 5 – 10% of the dry mass[20] and its calcium salt is thought to be responsible for the heat-resistant property of spores.[21] Since anthrax consists of spores and has been used in biological warfare, the strong chelating property of DPA in these spores has been used in the design of anthrax detectors. A US patent is available for the “method of endospore quantification using lanthanide dipicolinate luminescence” which involves the complexation of lanthanum by DPA.[22] For example, Universal Detection Technology advertises the BSM-2000 Autonomous Anthrax Detector for airborne spores which was developed in conjunction with NASA. This apparatus is described to function as follows: “The device continuously monitors the air for anthrax spores. It then uses heat to “pop” the spores, thus releasing a chemical from

inside the spores called dipicolinic acid (DPA), which is unique to bacterial spores. The DPA instantaneously reacts with the chemical sensor in the solution, which triggers an intense green luminescence when viewed under ultraviolet light. The intensity of the luminescence corresponds to the concentration of bacterial spores in the sample."[23] The La(III)-dipicolinic acid complexes are extremely stable, with the log β values at 25 °C given as 7.94, 13.71 and 17.95 for La(III) chelated by one, two and three dipicolinic acids respectively.[24]

QA is also a metabolite of tryptophan. The neurotoxic effects of quinolinic acid had been well documented and the references listed here[25-32] are only a sample of what is available in literature. QA binds to the *N*-methyl-D-aspatate (NMDA) receptor in the brain and overstimulates it which causes the degeneration of intrinsic neurons. It was thought that the action of QA could be involved in senile dementia of the Alzheimer type or Huntington's disease, but the evidence to support this is not conclusive.[27,33,34] Interestingly, PA, which is also a tryptophan metabolite, can protect against damage done by QA. [25,26]

5.2) Protonation of the ligands

Figure 5.2 shows the equilibria reactions that could occur in an aqueous solution of PA. The cationic species acts a diprotic acid for which two acid dissociation values can be determined. The first proton (process A or B) is lost at a lower pH than the second (process C or D). The equilibrium between the neutral molecule and the zwitterion (process Z) is independent of pH. Using absorption spectroscopy, Green and Tong[35] showed that the zwitterion was the most predominant form of the acid, not the uncharged molecule.

A protonation constant (given the symbol K here) is simply the reciprocal of the corresponding dissociation constant (K_a), i.e. $K = 1/K_a$. For a diprotic acid, $K_1 = 1/K_{a2}$ and $K_2 = 1/K_{a1}$, where K_1 is the first and K_2 is the second protonation constant, or alternatively when using log functions, $\log K_1 = pK_{a2}$ and $\log K_2 = pK_{a1}$. Log K values will be used here instead of pK_a values for consistency as

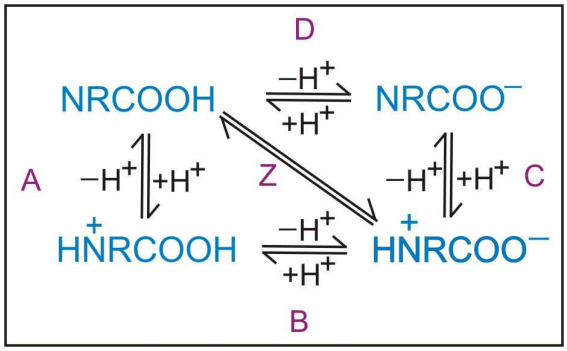

Figure 5.2: Scheme showing equilibria of an aqueous solution of PA.[35]

protonation constants are required by the software used to calculate metal-ligand formation constants and log *K* values are also provided in the NIST[24] and IUPAC[36] databases. Table 5.1 gives values for the stepwise protonation constants as log *K* values for PA. The values used in calculations in this work are log K_1 = 5.18 and log K_2 = 0.86 at 25 °C and 0.5 M ionic strength and come from the critically assessed values in the NIST database.[24] Since the ionic strength in this work was not kept constant and varied between 0.5 M and 0.25 M, it was interesting to see that the values at 0.5 M ionic strength compare well to those at 0.15 M ionic strength (unfortunately no values were available at 0.25 or 0.2 M ionic strength). The graph showing the percentage protonation as a function of pH is given in Figure 5.3. At pH of about 0.9 only 50% of the diprotic cation (H_2L^+) is present and above pH ≈ 3.2 this species is no longer present in solution. In Table 5.1, a larger variation in the log K_2 values measured at the same ionic strength and temperature can be seen, and in some cases it is not measured at all. This is due to deprotonation occurring at low pH and small errors in pH measurement could result in substantial errors in the log *K* values. Above about pH 7.5 the ligand exists in the fully deprotonated form.

Log *K* values for pyridine and benzoic acid at 25 °C and 0.5 M ionic strength are given as 5.22 and 3.95 respectively.[24] This indicates that the pyridine moiety is a stronger base than the carboxylate moiety. For PA, the log K_1 value thus refers to the protonation of the pyridine nitrogen (process C in Figure 5.2) to form the zwitter ion and the log K_2 value refers to the protonation of the carboxylic acid (process B in Figure 5.2). This is supported by the

Table 5.1: Stepwise protonation constants as log *K* values for PA in aqueous solutions at 25 °C.

log K_1	log K_2	Conditions	Tech-nique[a]	Ref.
5.21 ± 0.03	0.95 ± 0.08	0.1 M		24
5.22	1.17	0.1 M KNO_3	Pot	37
5.184 ± 0.001	0.89 ± 0.02	0.15 M KNO_3	Pot	38
5.18 ± 0.03[b]	0.86 ± 0.02[b]	0.5 M		24
5.17 ± 0.01	0.86 ± 0.01	0.5 M KNO_3/$NaClO_4$	Pot	39
5.03 ± 0.04		0.5 M $NaClO_4$	Pot	40
5.28 ± 0.05	1.42 ± 0.05	0.5 M		41
5.18	0.87	0.5 M		42
5.17 ± 0.08		0.5 M	IR	43
5.29 ± 0.03	0.95 ± 0.09	1.0 M		24
5.291 ± 0.005	0.981 ± 0.008	1.5 M	Pot	43
5.20 ± 0.05		1.5 M	IR	43
5.34		2 M $NaClO_4$	Pot	44

[a] Abbreviations for techniques: Pot = Potentiometry, Spec = Spectrophotometry, IR = Infrared spectroscopy
[b] Log *K* values used for this study.

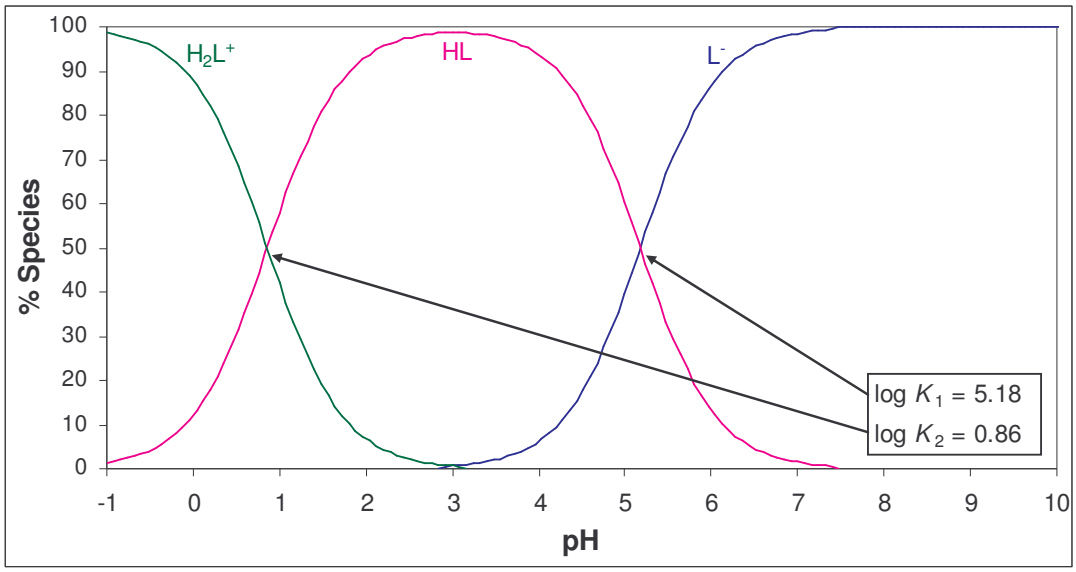

Figure 5.3: Percentage protonation of PA as a function of pH at 25 °C and 0.5 M ionic strength.

findings of Green and Tong.[35] The protonation constant for the nitrogen atom in pyridine and PA is very much the same, but the constant for the carboxylic acid group in benzoic acid and PA differ significantly. The protonation

constants for all the pyridinecarboxylic acids under the same conditions are compared in Table 5.2. For PA, the significantly larger $\Delta\log K$ is due to a larger log K_1 and smaller log K_2 compared to the other two acids, resulting in the zwitterion being in solution over a wider pH range. This indicates that the proximity of the carboxylic acid group to the nitrogen atom plays a role. Other than the carboxylic acid being closer to the electron-withdrawing nitrogen atom, the PA zwitterion (Figure 5.4) could be stabilised by the interaction of the proton and the oxygen atom closest to it. This is not possible for the other pyridinecarboxylic acids.

Table 5.2: Stepwise protonation constants (given as log *K* values) for pyridine-**x**-carboxylic acids at 0.5 M ionic strength and 25 °C.[24] Values given in brackets are uncertain.

Ligand	x	log K_1	log K_2	$\Delta\log K$
Picolinic acid	2	5.18	(0.86)	4.32
Nicotinic acid	3	4.67	2.12	2.55
Isonicotinic acid	4	4.81	1.82	2.99

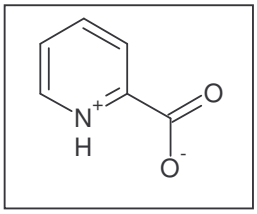

Figure 5.4: The zwitterion for PA.

For interest, the protonation constants of the amino acid glycine (H_2NCH_2COOH) were looked at as it has a similar structure to PA except for the aromatic ring present in the latter. For glycine, log K_1 = 9.54 and log K_2 = 2.39 at 25 °C and 0.5 M ionic strength.[24] Glycine therefore remains protonated at higher pHs than PA indicating the electron-withdrawing ability of the aromatic ring.

A similar scheme of equilibria for DPA was represented by Bridger *et al.*[45] and is shown in Figure 5.5. Here a triprotic cation is present which indicates that three acid dissociation constants can be determined.

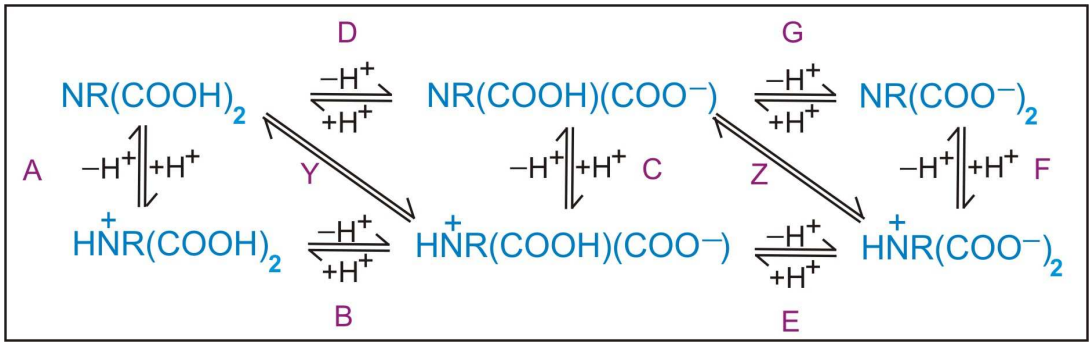

Figure 5.5: Scheme showing equilibria of an aqueous solution of DPA.

Table 5.3 gives the stepwise protonation constants for DPA. Only the first two protonation constants are given in most cases and the critically assessed values of log K_1 = 4.51 and log K_2 = 2.05 at 25 °C and 0.5 M ionic strength[24] were used in this work. Values for log K_3 at 25 °C varied widely and for solutions at 0.1 M, 0.5 M and 1.0 M ionic strength the values are given as 1.36,[37] –1.0[46] and 0.49[47] respectively.

Figure 5.6 shows the extent of protonation of DPA as a function of pH (at 25 °C and 0.5 M ionic strength), where values of log K_3 were either included or excluded. Above pH 7 the ligand is fully deprotonated and above about pH 2.5 the third protonation constant may be neglected for metal-ligand equilibria studies. However, below pH 2.5 the presence of the H_3L^+ form could affect the metal-ligand formation constants. At pH 0.3, the pH at which metal-ligand equilibria studies was commenced in this work, it was found that if log K_3 = 0.49 about 60% of the ligand is in the H_3L^+ form and if log K_3 = 1.36 it increases to about 92%.

This log K_3 value carries a large uncertainty due to the concentration of H^+ from the strong acid in solution being so much higher than that from the equilibria reaction (process A or B in Figure 5.5), especially since mass balance equations only for H^+ concentration are solved when using GEP. Since DPA is only slightly soluble in acidic media[57] and has a solubility of 10 mM in water at 20 °C,[58] it is impossible to try and increase the contribution of H^+ in solution from DPA by increasing it's concentration as far as possible within the experimental constraints. Vargová *et al.*[37] only calibrated the GE

Table 5.3: Stepwise protonation constants (as log K values) for DPA in aqueous solutions at 25 °C.

log K_1	log K_2	Conditions	Tech-nique[a]	Ref
4.66 ± 0.03	2.07 ± 0.03	0.1 M		24
4.53 ± 0.06	2.32 ± 0.05	0.1 M $NaNO_3$	Pot	48
4.701 ± 0.001	2.27 ± 0.01	0.1 M $NaNO_3$	Pot	49
4.7	2.02[b]	0.1 M KNO_3	Pot	37
4.57 ± 0.01	2.06 ± 0.01	0.2 M KCl	Pot	50
4.352 ± 0.005	2.04	0.2 M $NaClO_4$	Pot	51
4.49	2.03	0.4 M KCl	Pot	52
4.51 ± 0.03[c]	2.05 ± 0.05[c]	0.5 M		24
4.532 ± 0.004	2.092 ± 0.006	0.5 M $NaClO_4$	Pot	53
4.50	2.00	0.5 M $NaClO_4$/$LiClO_4$	Pot	54[f]
4.32	2.15[d]	0.5 M $NaClO_4$/$LiClO_4$	Spec	46[f]
4.45 ± 0.03	2.07 ± 0.02	1.0 M		24
4.42	2.09	1.0 M KCl	Pot	55
4.47 ± 0.05	2.05 ± 0.10	1.0 M $NaClO_4$	Pot	45
4.62 ± 0.02	2.18 ± 0.02[e]	1.0 M $NaClO_4$	Pot	47

[a] Abbreviations for techniques: Pot = Potentiometry, Spec = Spectrophotometry
[b] Log K_3 = (1.36)[37]
[c] Log K values used for this study
[d] Log K_3 = (–1.0)[46]
[e] Log K_3 = (0.49 ± 0.02)[47]
[f] Values obtained from IUPAC Stability Constant Database[36]

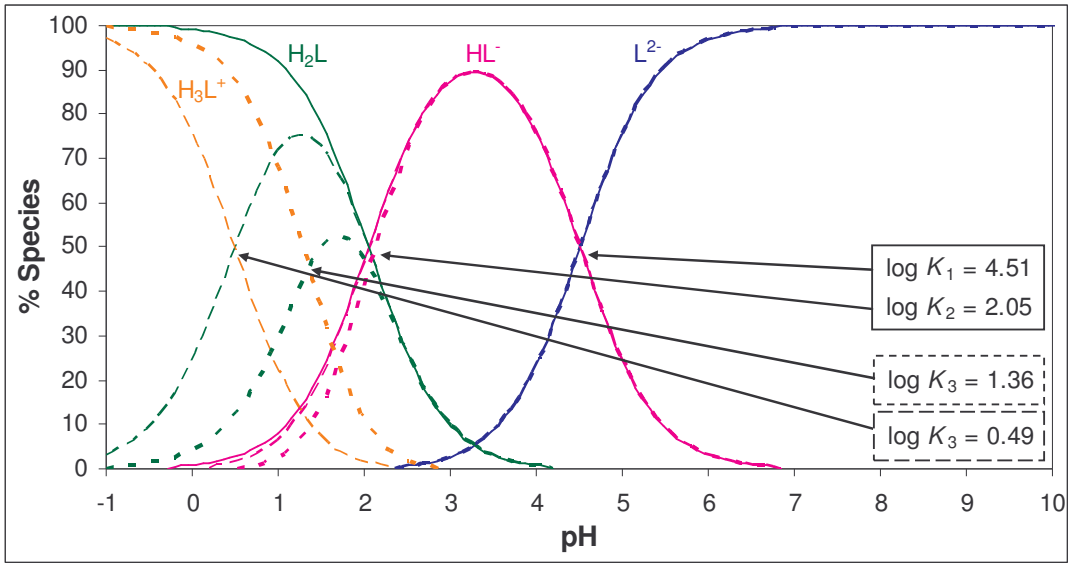

Figure 5.6: Percentage protonation of DPA as a function of pH where the value of log K_3 is excluded from (solid lines) or included in the model as 1.36 (dotted lines) or 0.49 (dashed lines).

from pH 1.8 and would have had to extrapolate the calibration to lower pH values. Both Vargová *et al.*[37] and Funahashi *et al.*[47] corrected for the junction potential in some way which was not described, so it leads to many questions as to the validity of these values. The log K_3 value of −1.0 determined by Chiacchierini *et al.*[46] was determined by a spectrometric technique which is less susceptible to the errors experienced in GEP at low pH. They claim to have used ionic strength of 0.5 M, but even in a strong acid solution of concentration 0.5 M the lowest attainable pH is 0.3. At this pH (assuming log K_3 = −1.0) the fraction of H_3L^+ in solution is negligible. So the validity of this value is also disputed.

The log K_2 value for PA was seen to be lower than that for the other pyridinecarboxylic acids and it was speculated that it could be due to the interaction between the proton on the nitrogen atom and the oxygen on the adjacent carboxylic acid which stabilises the zwitterion form. This would be expected to be the case for DPA too which has two carboxylic acid groups adjacent to the nitrogen atom. Log K_3 values for 3,4- and 3,5-pyridinedicarboxylic acids (which do not have carboxylic acid groups adjacent to the nitrogen atom) are given as 0.6 and 1.1, respectively, at 25 °C and 1 M ionic strength.[24] It would be expected that the log K_3 value for DPA would be somewhat lower than this. The log K_3 values are given for 2,3- and 2,4-pyridinedicarboxylic acids (which have one carboxylic acid group adjacent to the nitrogen atom) as −0.8 and 0.8 at 25 °C[24] respectively, although these values should also be treated with caution.

Iminodiacetic acid ($HOOCCH_2NHCH_2COOH$) is the amino acid with a similar structure to DPA and the protonation constants are given a follows: log K_1 = 9.20, log K_2 = 2.56 and log K_3 = (1.8) at 25 °C and 0.5 M ionic strength.[24] The log K_1 value is significantly lower for the nitrogen atom in the pyridine ring compared to that in the amino acid, as was seen before. It would be expected that the log K_3 value would be lower for DPA as was observed when comparing the log K_2 values for PA and glycine. The log K_3 value of 1.36 for DPA is thus highly doubted.

DPA and QA are structural isomers, where the former is symmetrical but the latter is not. The same equilibria scheme can be used for DPA and QA as given in Figure 5.5. Far fewer investigations have used QA as compared to the other two ligands considered here.

Table 5.4 gives the stepwise protonation constants for QA. Once again, only the first two protonation constants are given in most cases and the critically assessed values of log K_1 = 4.58 and log K_2 = 2.30 at 25 °C and 0.5 M ionic strength[24] were used in this work. A log K_3 value of −0.80 (at 25 °C and 0.5 M ionic strength) was given by Chiacchierini *et al.*[46] and was determined spectrophotometrically, not by GEP. For reasons as discussed above concerning work done by these authors on DPA, this value cannot be accurate.

Table 5.4: Stepwise protonation constants (given as log *K* values) for QA in aqueous solutions at 25 °C.

log K_1	log K_2	Conditions	Tech-nique[a]	Ref
4.72	2.36	0.1 M		24
4.71	2.37	0.1 M KNO_3	Pot	58[d]
4.71	2.35	0.1 M $NaClO_4$/ $LiClO_4$	Pot	59[d]
4.72	2.36	0.1 M KNO_3	Pot	60[d]
4.58[b]	2.30[b]	0.5 M		24
4.65	2.51	0.5 M $NaClO_4$/ $LiClO_4$	Pot	61[d]
4.35	2.30[c]	0.5 M $NaClO_4$/ $LiClO_4$	Spec	46[d]
4.52	2.16	1.33 M NaCl/LiCl	Pot	62[d]

[a] Abbreviations for techniques: Pot = Potentiometry, Spec = Spectrophotometry
[b] Log *K* values used for this study
[c] Log K_3 = −0.80[46]
[d] Values obtained from the IUPAC Stability Constant Database[36]

Figure 5.7 shows the extent of protonation of QA as a function of pH (at 25 °C and 0.5 M ionic strength), where the value of log K_3 was either included or excluded. At pH 0.3, the H_2L form of QA is predominant and only about 8% is in the H_3L^+ form. Some log K_3 values are given in the NIST database[24] for other pyridinedicarboxylic acids, but at ionic strengths of 1 M. The protonation constants for all these ligands are compared in Table 5.5(a). Even though the

ionic strength is different, it can be seen that the log K_3 values for the other pyridinedicarboxylic acids are higher than that for QA. The impact of varying the third protonation constant on the metal-ligand formation constants will have to be evaluated for data at low pH for both QA and DPA.

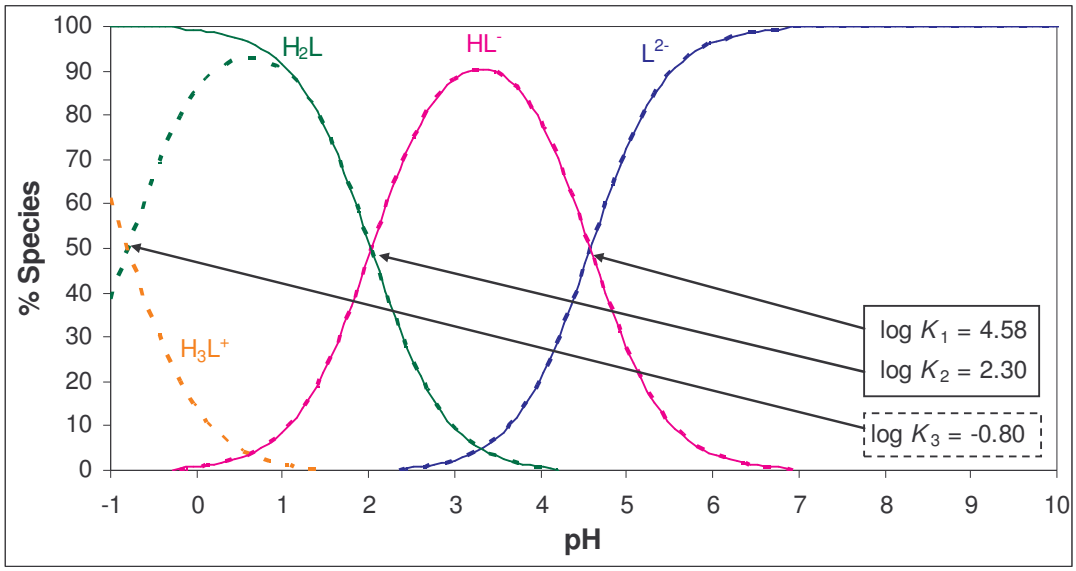

Figure 5.7: Percentage protonation of QA as a function of pH where the value of log K_3 is excluded from (solid lines) or included in (dotted lines) the model.

Table 5.5: Stepwise protonation constants (given as log *K* values) for (a) pyridine-x,y-dicarboxylic acids at 0.5 M ionic strength and 25 °C and (b) benzene-x,y-dicarboxylic acids at 0.5 M ionic strength and 25 °C.[24] Values given in brackets are uncertain.

(a) Pyridine-x,y-dicarboxylic acids					
x,y	**log K_1**	**log K_2**	**log K_3**	**Δlog K (1-2)**	**Δlog K (2-3)**
2,3	4.58	2.30	(–0.80)[b]	2.28	3.1
2,4	4.72	2.20	(0.8)[a]	2.52	1.4
2,5	4.58	2.17		2.41	
2,6	4.51	2.05		2.46	
3,4	4.90	2.70	(0.6)[a]	2.20	2.1
3,5	4.30	2.10	(1.1)[a]	2.20	1.0
(b) Benzene-x,y-dicarboxylic acids					
x,y	**log K_1**	**log K_2**		**Δlog K (1-2)**	
1,2	4.92	2.76		2.16	
1,3	4.38	3.30		1.08	
1,4	4.15	3.38		0.77	

[a] 1 M ionic strength
[b] Reference 46

It has been shown that in aqueous solutions for compounds with carboxylic acid groups on adjacent carbon atoms, as in QA and phthalic acid (benzene-1,2-dicarboxylic acid), intramolecular hydrogen bonding gives a O–H···O interaction resulting in one of the shortest non-bonded O···O distances known. This stabilises the form where only one carboxylic acid group is protonated as can be seen for phthalic acid by the log K_1 value increasing and the log K_2 value decreasing (see Table 5.5(b)), resulting in a larger Δlog K.[63] The scenario is more complicated for QA as the nitrogen atom in the pyridine ring can also be protonated.

Conflicting evidence has been given by Harmon *et al*.[63] and Loring *et al*.[62] on the predominant protonation sites of the of the H_2L and HL^- forms of QA. Harmon *et al*.[63] showed that IR spectra of the solid QA in the H_2L form confirmed the presence of both a N–H bond and a O–H···O hydrogen bond indicating the zwitterion form, but suggested that the zwitterion was not present in solution. Loring *et al*.[62] were unable to confirm whether the zwitterion was present in solution or not by IR spectroscopy. As for the HL^- form, Harmon *et al*.[63] saw only the O–H···O hydrogen bond ruling out the possibility of a zwitterion, whereas Loring *et al*.[62] found evidence for both the zwitterionic and non-zwitterionic forms simultaneously in solution and said that the zwitterion form was most abundant. Considering the argument that indicated the presence of the O–H···O hydrogen bond as applied to phthalic acid, there should be a stabilisation of the HL^- species for QA as compared to its isomers if a carboxylate group is protonated before the nitrogen atom. However, the difference between the log K_1 and log K_2 values is not larger for QA indicating that the O–H···O hydrogen bond is not dominant and supporting the conclusion by Loring *et al*.[62] that the zwitterion is the major species. The difference between the log K_2 and log K_3 values is larger for QA and cinchomeronic acid (pyridine-3,4-dicarboxylic acid) due to a larger log K_2 value and a smaller log K_3 value as compared to the other pyridinedicarboxylic acids. This indicates that there is stabilisation of the H_2L^- form due to the O–H···O interaction which could support zwitterion formation in solution as well, as shown in Figure 5.8.

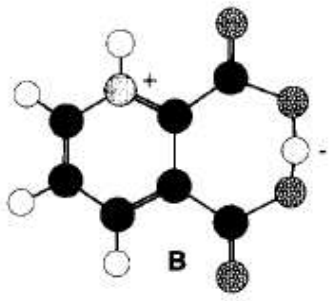

Figure 5.8: Zwitterion of the H_2L form of QA indicating the O–H···O hydrogen bond.[63]

5.3) Electrochemical behaviour of the ligands

In organic electrochemistry it in known that the carboxylic acid group of organic acids can be electrochemically reduced when the energy of the LUMO (lowest unoccupied molecular orbital) is lowered by conjugation with an unsaturated group or by the proximity of an electron withdrawing group. The pyridinecarboxylic acids fall in this category and have been reduced in aqueous media at various pH values.[64] Studies of the reduction of PA by direct current polarography, differential pulse polarography and exhaustive electrolysis, indicated that a two step reduction occurs with an intermediate aldehyde being formed which is then reduced to form the alcohol as follows:[65,66]

$$NRCOOH + 2e^- + 2H^+ \rightarrow NRCHO + H_2O \quad (5.1)$$

$$NRCHO + 2e^- + 2H^+ \rightarrow NRCH_2OH \quad (5.2)$$

The intermediate aldehyde is largely hydrated and dehydration occurs before further reduction to the alcohol takes place.[66] This second reduction step occurs at more positive potentials than that for the first reduction step.[64,65] Studies showed that increasing the acid concentration (of H_2SO_4 in this case) from 0.1 to 1 M favoured the formation of the dehydrated aldehyde.[66]

Not only are these ligands electroactive, but weak adsorption of PA on the mercury electrode was established[65] and strong adsorption of DPA was found in acidic solutions between pH 0 and 4.[57] The predominant form of DPA in this pH region is the zwitterions HL^- and H_2L with the pyridine nitrogen

protonated.[57] It appears that the L^{2-} form is not adsorbed.[67] Buffle *et al*.[68] concluded that the neutral species of PA and DPA, whether they are protonated or complexed to a metal ion, are more strongly adsorbed than the charged species. They interpreted this as adsorption occurring mainly due to the hydrophobic aromatic part of the ligand accumulating on the hydrophobic mercury surface. An electrically charged group would increase hydrophilicity and hence reduce adsorption. This seems to be in stark opposition to having the zwitterion containing at least two charged sites being adsorbed.

5.3.1) *Aims*

In this work the reduction of these ligands was studied not from an empirical point of view, but simply to establish whether it would interfere in any respect with the polarographic determination of stability constants of their metal complexes. Furthermore, since the reduction potentials of both Cu(II) and Bi(III) are positive and close to the potential at which mercury is oxidised, this positive potential region was also briefly explored.

5.3.2) *Results and Discussion*

The reason why the electrochemical behaviour of the ligand became important was due to the observations made particularly for DPA and QA. Figure 5.9 shows polarograms obtained in the study of Bi(III) complex formation. At the most positive potentials in all cases mercury is oxidised to a small extent. Ideally one would want to avoid this, but sufficient data points in this region are required to fit the polarograms properly. The polarogram of the background solution (0.5 M HNO_3) illustrates the linear increasing capacitance current with a negative potential scan. Above about –0.6 V the current increases exponentially due to the reduction of H^+ to form hydrogen gas. Bi(III) and Tl(I) were then added to the background solution and the reduction waves of Bi(III) at about 0.03 V and Tl(I) at about –0.46 V were observed in addition to the mercury oxidation and hydrogen evolution currents. When PA was added to the solution containing the metal ions (the concentration of PA was about 200 times greater than that for Bi(III) here), not much difference was observed when compared to the polarogram without the ligand, except at the most

negative potentials a slightly larger current was recorded. When DPA or QA was added, such that the concentration was about 100 times greater than that for Bi(III), a very sharp rise in current was detected at potentials close to –0.6 V. This was initially thought to be due to hydrogen evolution catalysed by the adsorption of the ligand on the mercury electrode, but on further investigation it was found to be due to the reduction of the ligand itself.

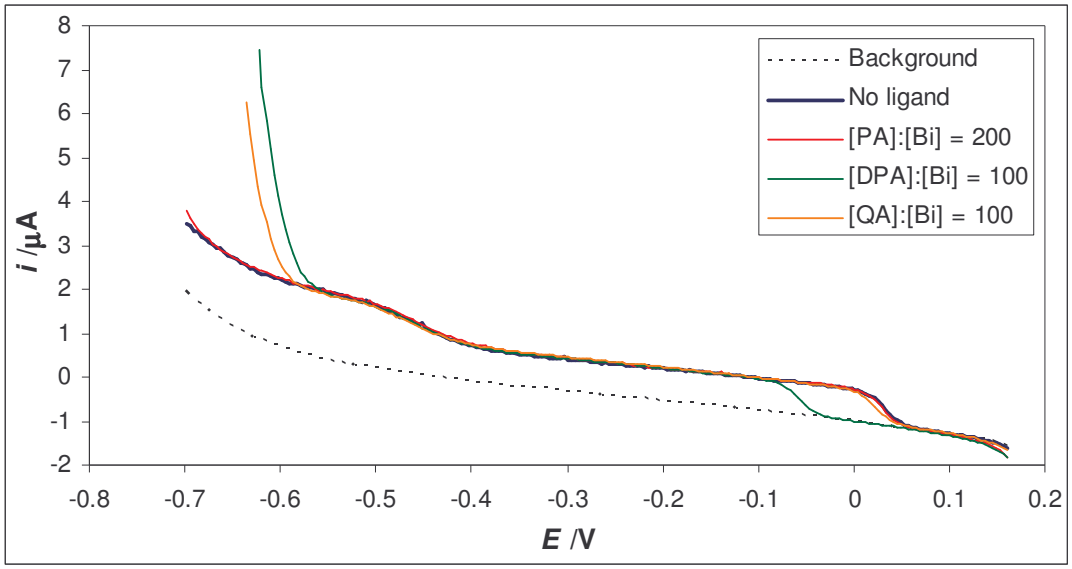

Figure 5.9: Polarograms of (i) 0.5 M HNO_3 background solution, (ii) about 1×10^{-5} M Bi(III) and 2×10^{-5} M Tl(I) in 0.5 M HNO_3 and (iii) ligand added to the metal ion solution as indicated.

The negative potential shift for Bi(III) reduction especially in the presence of DPA was due to complexation with the ligand. Complexation of Tl(I) did not occur at this low pH. The mercury oxidation also seems to be affected by the presence of the ligands to some extent.

The reduction of PA and DPA (examples of mono- and di-substituted pyridines) were further probed by analysing solutions where the metal ions were omitted. DC polarograms given in Figures 5.10 (a) and (b) were collected using the Autolab PGStat 10 where the reduction current is set to be negative, whereas in Figure 5.9 it is positive. Again the polarogram for 0.5 M HNO_3 was included as a reference point. Figure 5.10(a) shows that the reduction of PA commenced just before –0.7 V in the most acidic solution, as

was noted in Figure 5.9 above. As the pH was increased, the onset of PA reduction was shifted to more negative potentials, which fits in with that fact that the reduction process involves the uptake of protons. A similar trend was seen for DPA in Figure 5.10(b), but with reduction starting at about –0.6 V in the most acidic solution, indicating that reduction of a pyridinedicarboxylic acid requires less energy than for a pyridinecarboxylic. This is possibly due to more extensive conjugation when two carboxylic acids are present. The position of the carboxylic acid groups on the pyridine ring also plays a role as reduction of DPA requires slightly lower overpotentials than that for QA. In the former case, both carboxylic acid groups are adjacent to the electron withdrawing nitrogen atom. Also, the greater the extent of protonation of the ligand, the lower the energy required for reduction to occur. In the most acidic solutions, the complete reduction waves of the weak acid were obscured by the hydrogen evolution wave due to the large concentration of strong acid also in solution. Since the objective of this work was not to study the reduction of the ligand, but simply to establish what is causing the reduction and whether it will affect the studies attempted here, measurements were not repeated in solutions without the very large concentration of HNO_3 present.

Cyclic voltammograms of ligand solutions were collected using an EcoChemie Autolab PGStat 10 potentiostat at a hanging mercury drop electrode and employing a platinum CE and Ag/AgCl (3 M KCl) RE as before. The ligand solutions emulated the conditions of the metal-ligand experiments, except no metal ions were added. A 9.0×10^{-4} M PA or 3.4×10^{-4} M DPA solution was made up in 0.5 M HNO_3. These solutions were then titrated with 0.5 M NaOH to adjust the pH of the solution. The GE was calibrated by pH 4 and 7 buffer solutions, so the pH values given are merely estimates.

Selected cyclic voltammograms (CV's) for DPA solutions are given in Figure 5.11. This clearly shows that the reduction of the acid is an irreversible process under these conditions, as was found to be the case for PA. Corredor and Mellado[65] proposed mechanisms for the reduction of PA which depended on the pH of the solution. In the case for the fully protonated H_2L^+ species, a two electron transfer step followed by the reaction with a proton donor in

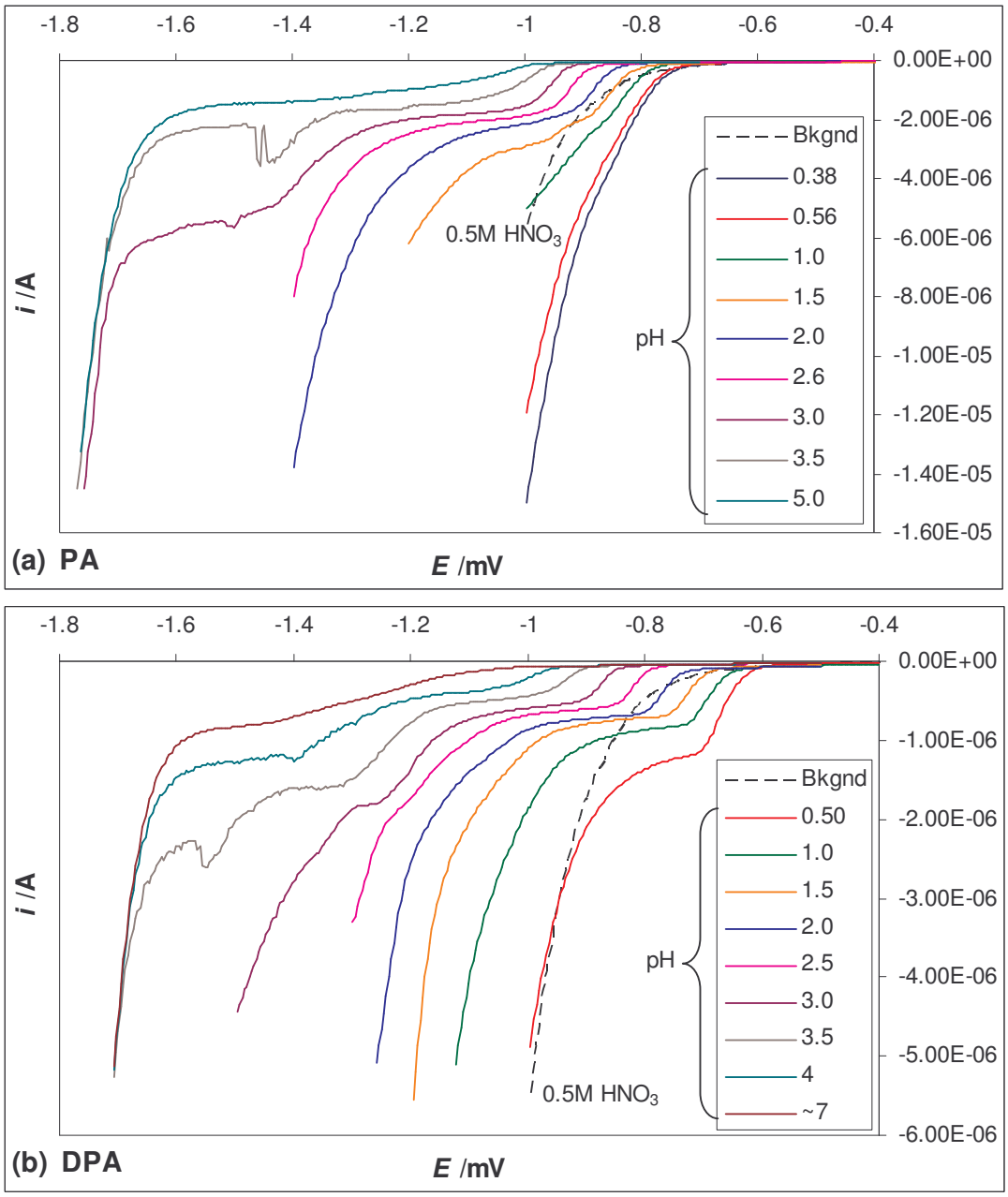

Figure 5.10: DC polarograms recorded at indicated pH values (amended by addition of 0.5 M NaOH) for (a) 9.0×10^{-4} M PA and (b) 3.4×10^{-4} M DPA.

solution converts the acid to the hydrated aldehyde. The aldehyde dehydrates before it is reduced by another two electron transfer to form the alcohol. For the HL species, the first reduction step rather occurs via two one electron transfer steps interspersed by a proton transfer. This could explain the appearance of another reduction wave at more negative potentials in higher pH solutions. However, with the hydrogen evolution wave obstructing much of

the information at low pH, this is merely speculation. Since the reduction of the dehydrated aldehyde to the alcohol occurs at more positive potentials (at –0.59 V in an acetate buffer at pH 4.7[64]) than the reduction of the acid to the aldehyde, it was expected that it would be visible on the second scan of the cv. It was not seen here at any pH investigated and perhaps on further electrolysis the peak would become visible. To unpack each polarogram and CV would require far more investigation than is warranted for our purposes.

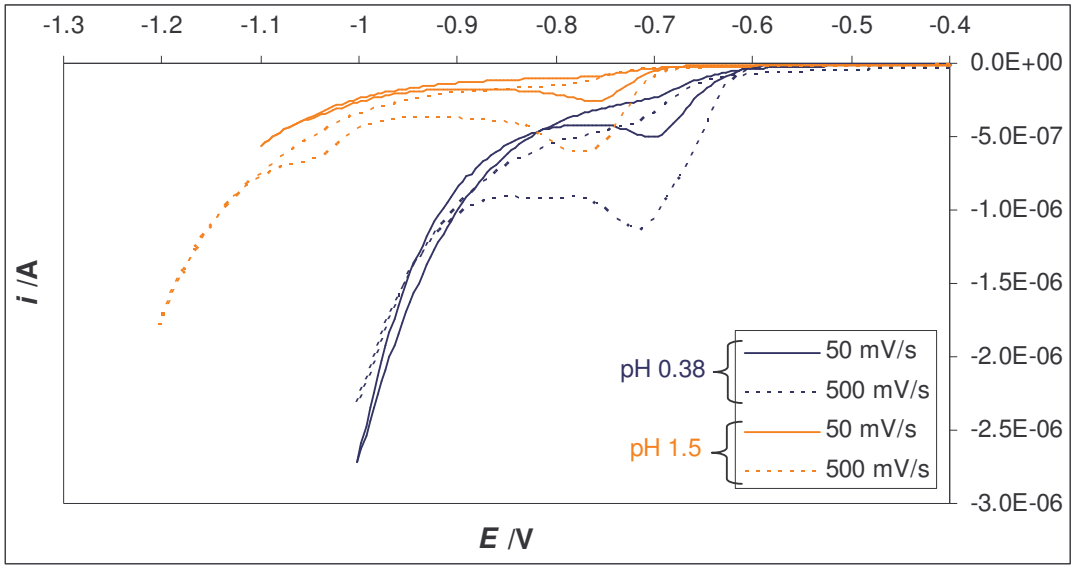

Figure 5.11: Cyclic voltammograms at two scan rates for DPA solutions at (i) pH 0.38 (0.5 M HNO_3) and (ii) pH 1.5 (pH adjusted using 0.5 M NaOH).

Figures 5.12(a) and (b) show that there is a relationship between the negative shift in potential of the Bi(III) reduction wave, which is due to complex formation with ligand, and a negative shift in the mercury oxidation wave. The latter is not simply a pH effect as larger shifts in the mercury wave were observed when DPA was present than either QA or PA. Formation constants indicate that DPA forms far stronger complexes than QA or PA, including complexes formed with Hg(II).[24] This suggests that the oxidised mercury is complexed by the ligand in solution and/or the ligand also adsorbs on the mercury surface. Since the ligand is present in such an excess, this should not affect our calculations of formation constants. For each polarogram that is measured, the amount of substance that is reduced (or oxidised) can be assumed to be negligible as compared to the concentrations in the bulk

solution. Additionally, each time a fresh mercury drop is formed at a more negative potential, it does not carry a memory effect from previous drops.

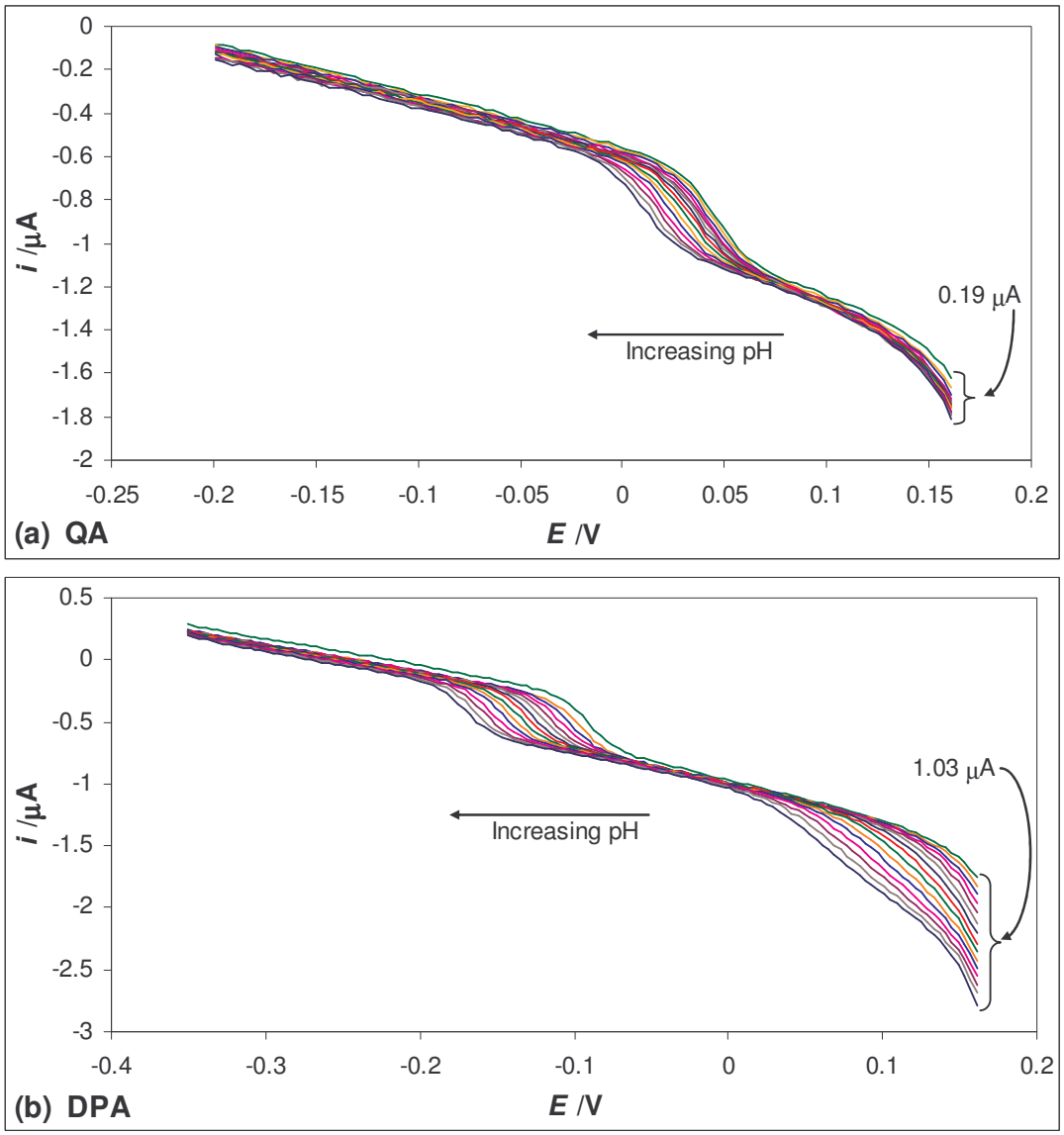

Figure 5.12: DC polarograms of solutions containing about 1×10^{-5} M Bi(III) and 2×10^{-3} M (a) QA or (b) DPA with pH ranging from pH 1.3 to pH 2.8 in steps of about 0.1 pH units.

5.4) Conclusions

The protonation of the three ligands were discussed and for PA the two protonation constants are well established. For DPA and QA, however, the value of the third protonation constant is disputed and although it would not

affect metal-ligand equilibria studies starting at pH 2, as is often the case, it may influence studies starting at lower pH as in this work. GEP cannot be used to accurately determine these values, so other techniques such as NMR (nuclear magnetic resonance) will need to be considered in future. However, NMR requires large concentrations of ligand, which is not possible for ligands with limited solubility such as DPA, and pH still has to be accurately measured. The influence of the value of this protonation constant on formation constants will be considered in following chapters.

The ligands are electroactive and are irreversibly reduced at potentials more negative than Tl(I) so that the Tl(I) wave remains resolved. The reduction of PA which contains one carboxylic acid group requires more energy than for the ligands containing two carboxylic acid groups. As the pH increases, the reduction potentials of the ligands shift to more negative potentials since protons are involved in the reduction process. Even though very small amounts of ligand are reduced during the measurements, it would be best to avoid the very negative potentials.

The mercury oxidation wave is also affected by the ligand in solution or adsorbed on the mercury surface. The wave shifts to more negative potentials with increasing pH and the extent of the shift is related to the complexing ability of the ligand, but the Bi(III) or Cu(II) reduction wave also remains resolved from this wave. Once again, the amount of Hg(II) introduced into solution and able to complex with the ligand is very small and should not affect our studies, nevertheless, this should be avoided as far as possible.

5.5) References

1) K.A. Idriss, M.S. Saleh, H. Seidaira, M.M. Seleim and E.Y. Hashem, Monatsch. Chem., 122 (1991) 507
2) E. Kiss, K. Petrohán, D. Sanna, E. Garribba, G. Micera and T. Kiss, Polyhedron, 19 (2000) 55
3) B.S. Parajón-Costa, C.C. Wagner and E.J. Baran, Z. Anorg. Allg. Chem., 629 (2003) 1085
4) V. Lubes, J. Solution Chem., 34 (2005) 899
5) R.I. Press, J. Geller and G.W. Evans, West J. Med., 152 (1990) 41
6) D.M. Sterns, J.P. Wise, S.R. Patierno and K.E. Wetterhahn, FASEB J., 9 (1995) 1643
7) J.K. Speetjens, R.A. Collins, J.B. Vincent and S.A. Woski, Chem. Res. Toxicol., 12 (1999) 483
8) G.W. Evans and E.C. Johnson, J. Nutr., 110 (1980) 1076
9) G.W. Evans and P.E. Johnson, Pediatr. Res., 14 (1980) 876
10) T. Rebello, B. Lönnerdal and L.S. Hurley, Am. J. Clin. Nutr., 35 (1982) 1
11) J.A. Fernandez-Pol, D.J. Klos and P.D. Hamilton, Anticancer Res., 21 (2001) 3773
12) H.M.V.M. Soares, A.A.N. Almeida, M.P.O. Castro, S.C. Pinho and M.T.S.D. Vasconcelos, Analyst, 123 (1998) 1377
13) D.I. Griggs, P. Heden, K.E. Temple Smith and W. Rademacher, Phytochem., 30 (1991) 2513
14) P. Lainé, A. Gourdon and J.P. Launay, Inorg. Chem., 34 (1995) 5129
15) A.G. Mauk, C.L. Coyle, E, Bardingnon and H.B. Gray, J. Am. Chem. Soc., 101 (1979) 5054
16) P.C. Harrington and R.G. Wilkins, J. Inorg. Biochem., 12 (1980) 107
17) D.C. Crans, J. Inorg. Biochem., 80 (2000) 123
18) L. Yang, D.C. Crans, S.M. Miller, A. la Cour, O.P. Anderson, P.M. Kaszynski, M.E. Godzala, L.D. Austin and G.R. Willsky, Inorg. Chem., 41 (2002) 4859
19) L. Singh, G. Mohan, R.K. Parashar, S.P. Tripathi and R.C. Sharma, Curr. Sci., 55 (1986) 846
20) Y. Hachisuka, K. Tochikubo and T, Murachi, Nature, 207 (1965) 220

21) T. Hasimoto, S.H. Black and P. Gerhardt, Can. J. Microbiol., 6 (1960) 203
22) A. Pons, A.J. Venkateswaran and J.P. Kirby, US Patent 7306930, issued 11 December 2007
23) Universal Detection Technology, http://www.udetection.com (accessed 29 August 2010)
24) A.E. Martell, R.M. Smith and R.J. Motekaitis, NIST Standard Reference Database 46 Version 8.0, NIST Critically Selected Stability Constants of Metal Complexes, Gaithersburg, USA, 2004
25) B.E. Kalisch, K. Jhamandas, R.J. Boegman and R.J. Beninger, Brain Res., 668 (1994) 1
26) K.H. Jhamandas, R.J. Boegman, R.J. Beninger and S. Flesher, Amino Acids, 14 (1998) 257
27) E. Sofic, J. Halket, A. Przyborowska, P. Riederer, H. Beckmann, M. Sandler and K. Jellinger, Eur. Arch. Psychiatr. Neurol. Sci., 239 (1989) 177
28) M.J. During, M.P. Heyes, A. Freese, S.P Markey, J.B. Martin and R.H. Roth, Brain Res., 476 (1989) 384
29) K. Maeda, H. Kaneda, W.O. Whetsell and C.A. Tamminga, Neurosci. Res., 29 (1997) 303
30) J.H. Connick and T.W. Stone, Neurosci. Lett., 101 (1989) 191
31) R.J. Boegman, S.R. El-Defrawy, K. Jhamandas, R.J. Beninger and S.K. Ludwin, Neurobiol. Aging, 6 (1985) 331
32) H. Björkland, L. Olson, D. Dahl and R. Schwarcz, Brain Res., 371 (1986) 267
33) K.L. Haik, D.A. Shear, U. Schroeder, B.A. Sabel and G.L. Dunbar, Exp. Neurol., 163 (2000) 430
34) G.J. Guillemin, B.J. Brew, C.E. Noonan, T.G. Knight, G.A. Smythe and K.M. Cullen, International Congress Series, 1304 (2007) 404
35) R.W. Green and H.K. Tong, J. Am. Chem. Soc., 78 (1956) 4896
36) L.D. Petit and K.J. Powell, IUPAC Stability Constants Database, IUPAC and Academic Software, 1993-2003
37) Z. Vargová, J. Kotek, J, Rudovský, J. Plutnar, R. Gyepes, P. Hermann, K. Györyová and I. Lukeš, Eur. J. Inorg. Chem., 25 (2007) 3974
38) O. Jons and E.S. Johansen, Inorg. Chim. Acta, 151 (1988) 129

39) T.F. Gritmon, M.P. Goedken and G.R. Choppin, J. Inorg. Nucl. Chem., 39 (1977) 2021
40) R.H. Voss and R.B. Jordan, J. Am. Chem. Soc., 98 (1976) 2173
41) A.L. Magri' and A. Napoli, Ann. Chim., 76 (1986) 277
42) J.-P. Scharff and M.R. Paris, Bull. Soc. Chim. France, 8 (1968) 3184
43) J.S. Loring, M. Karlsson, W.R. Fawcett and W.H. Casey, Geochim. Cosmochim. Acta, 64 (2000) 4115
44) H. Yoneda, G.R. Choppin, J.L. Bear and A.J. Graffeo, Inorg. Chem., 4 (1965) 244
45) K. Bridger, R.C. Patel and E. Matijević, Polyhedron, 1 (1982) 269
46) E. Chiacchierini, G. D'Ascenzo et al., Ann. Chim. (Rome), 67 (1977) 195 (as found in IUPAC Stability Constants Database[36])
47) S. Funahashi, K. Haraguchi and M. Tanaka, Inorg. Chem., 16 (1977) 1349
48) M.M. Khalil and A.E. Attia, J. Chem. Eng. Data, 45 (2000) 1108
49) S. Aizawa, T. Natsume, K. Hatano and S. Funahashi, Inorg. Chim. Acta, 248 (1996) 215
50) T. Jakusch, W. Jin, L. Yang, T. Kiss and D.C. Crans, J. Inorg. Biochem., 95 (2003) 1
51) J.G.H. du Preez and B.J.A.M. van Brecht, J. Chem. Soc., Dalton Trans. (1989) 253
52) D.C. Crans, L. Yang, T. Jakusch and T. Kiss, Inorg. Chem., 39 (2000) 4409
53) A. Napoli, Talanta, 15 (1968) 189
54) I. Grenthe and E. Hansson, Acta Chem. Scand., 23 (1969) 611
55) B. Szpoganicz and A.E. Martell, Inorg. Chem., 23 (1984) 4442
56) J. Kragten and L.G. Decnop-Weever, Talanta, 27 (1980) 685
57) S. Ferraro, P. Passamonti, V. Bartocci and F. Pucciarelli, J. Chem. Soc, Faraday Trans., 93 (1997) 289
58) M. Sawhney, D. Joshi et al, Indian J. Chem., 19A (1980) 85 (as found in IUPAC Stability Constants Database[36])
59) D. Shelke and D. Jahagirdar, J. Inorg. Nucl. Chem., 41 (1979) 1635
60) M. Yasuda and K. Yamasaki, Naturwissenschaft, 45 (1958) 84

61) A. Napoli and A. Magri, Ann. Chim. (Rome), 79 (1989) 93 (as found in IUPAC Stability Constants Database[36])
62) J.S. Loring, M. Karlsson, W.R. Fawcett and W.H. Casey, Polyhedron, 20 (2001) 1983
63) K.M. Harmon, P.W. Brown Jr and S.H. Gill, J. Mol. Struct., 448 (1998) 43
64) O.R Brown, J.A. Harrison and K.S. Sastry, Electroanal. Chem., 58 (1975) 387
65) M.C. Corredor and J.M. Rodriguez Mellado, Electrochim. Acta, 49 (2004) 1843
66) A.M. Romulus and A. Savall, Electrochim. Acta, 43 (1998) 1913
67) E. Norkus, I. Stalnioniene and D.C. Crans, Heteroat. Chem., 14 (2003) 625
68) J. Buffle, A.M. Mota and M.L.S. Simoes Goncalves, J. Electroanal. Chem., 223 (1987) 235

CHAPTER 6

Accounting for the Diffusion Junction Potential – Application to the Cadmium(II) Picolinic Acid System

6.1) Introduction

Initial studies of Bi(III) complexation were aborted due to the complex nature of these studies and having to deal with two issues simultaneously, namely the diffusion junction potential and the hydrolysis of Bi(III) hindering the determination of the free Bi(III) potential. Instead, it was decided to first consider a system where the free metal ion potential is readily obtainable and thus only determine how to account for the diffusion junction potential. A well-known system was thus chosen to be studied so that the results obtained here can be compared and the methodology tested. The complexation of Cd(II) by PA has been studied before by both GEP[1-4] and voltammetry.[5,6] The polarographic reduction of the Cd(II) in the absence and presence of PA was fully reversible and the complexes formed were all labile,[5] thus no further complications in data assessment were anticipated. The stability constants reported in literature are given in Table 6.1, which come from the IUPAC Stability Constant Database[7] and are not critically assessed (as in the NIST Database[8]).

Table 6.1: Formation constants, as log β values, for Cd(II) PA species.[7]

Log β_1	Log β_2	Log β_3	T /°C	μ /M	Technique	Ref.
4.34*	8.01*	10.79*	25	0.1[a]	Voltam	5
4.55*	8.16*	10.14	20	0.1[b]	GEP	3
4.36	7.54		25	0.1[b]	GEP	4
		10.3	25	0.32[a]	Voltam	6
4.29*	7.89*	10.49*	25	0.5[b]	Voltam	5
4.18	7.61	10.41	25	0.5[b]	GEP	2
4.47	8.17		25	3[c]	GEP	1

[a] KNO_3
[b] $NaNO_3$
[c] $Na/LiClO_4$
* Values also quoted in the NIST Database[8]

In Chapter 5, when discussing the ligands that were studied, the protonation constants for PA and glycine were compared as they have a similar backbone, with only the aromatic moiety absent in the case of glycine. Although the protonation constants of these two ligands were significantly different, interestingly the log β values for complex formation with Cd(II) were very similar with log β_1 = 4.18, log β_2 = 7.51 and log β_3 = 9.76 for glycine at 25 °C and 0.5 M ionic strength.[8]

It is generally assumed that in solution picolinic acid will bind to Cd(II) through the pyridine nitrogen and one of the carboxylate oxygens to produce a five-membered ring. An octahedral geometry around Cd(II) is achieved by bonding to three ligands in this way. A similar geometry would be expected when only two ligands are bonded to a Cd(II) centre, where the other two binding sites would be occupied by water. The crystal structure obtained by Pons *et al*.[9] for Cd(II) ethyl picolinate (Figure 6.1) shows that two coordinated nitrate ions act as bidentate ligands resulting in Cd(II) having eight coordination sites. It should be noted that these crystals were grown in absolute ethanol and washed with diethyl ether before drying under vacuum. The same structure may not be produced when aqueous solutions are used when growing crystals. Another interesting structure for Cd(II) picolinate obtained by Deloume and Loiseleur[10] (Figure 6.2) shows dimer formation. These crystals were grown by slow evaporation from an aqueous sulphuric acid solution where the concentration ratio of PA:Cd(II) was 2:1. It is difficult to extrapolate the solid state structures to the species present in solution, but the way in which Cd(II) is bonded to PA can also be confirmed in solution studies by other techniques, such as IR and Raman spectroscopy.

Figure 6.3 shows the crystallographically determined coordination modes of picolinate found up until 2007.[11]. In these studies it would not be expected to find more than a single metal bound to the picolinate ligand since the PA concentration is at least one hundred times more than that of Cd(II), leaving the only possibilities of coordination modes demarcated according to the Harris notation,[12] as 1.101 and 1.100 in Figure 6.3. For binding to occur in the 1.100

mode it is suspected that the nitrogen atom would be protonated in solution, implying that this could only occur at low pH.

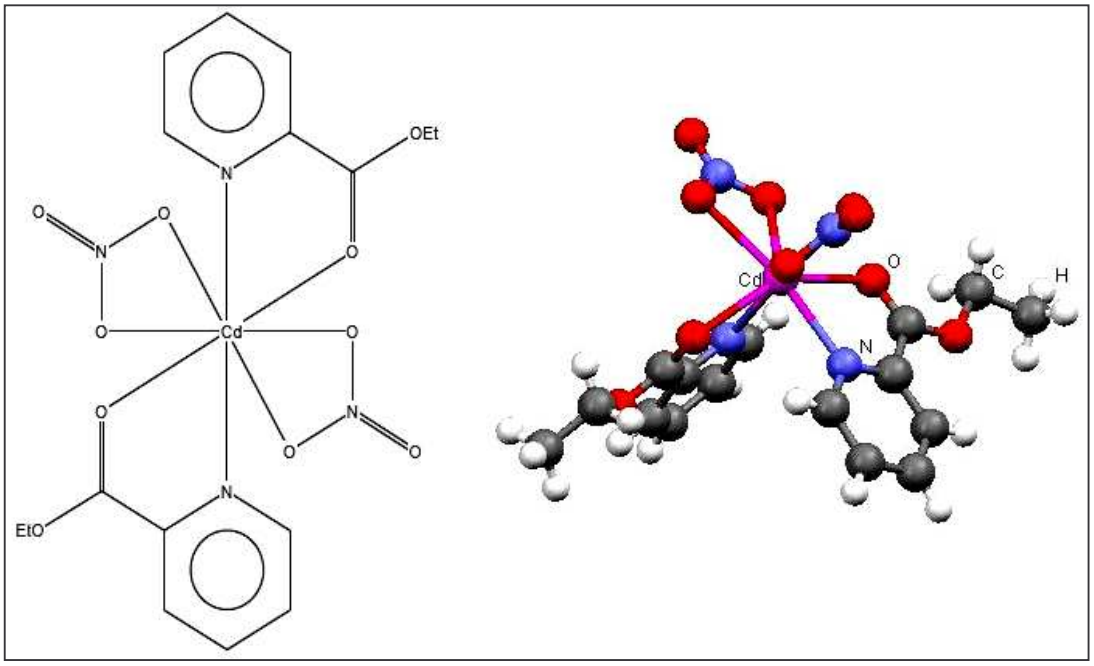

Figure 6.1: Structural representation and ball and stick diagram of $[Cd(NO_3)_2(C_5H_4NCO_2Et)_2]$

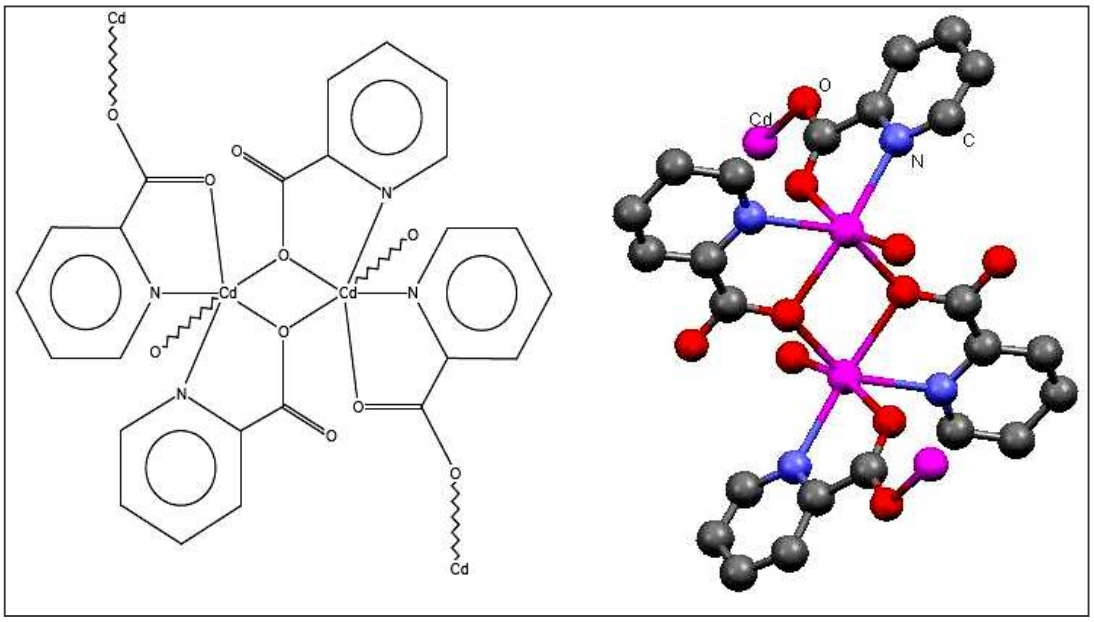

Figure 6.2: Structural representation and ball and stick diagram of $[Cd_2(C_5H_4NCO_2)_4]$

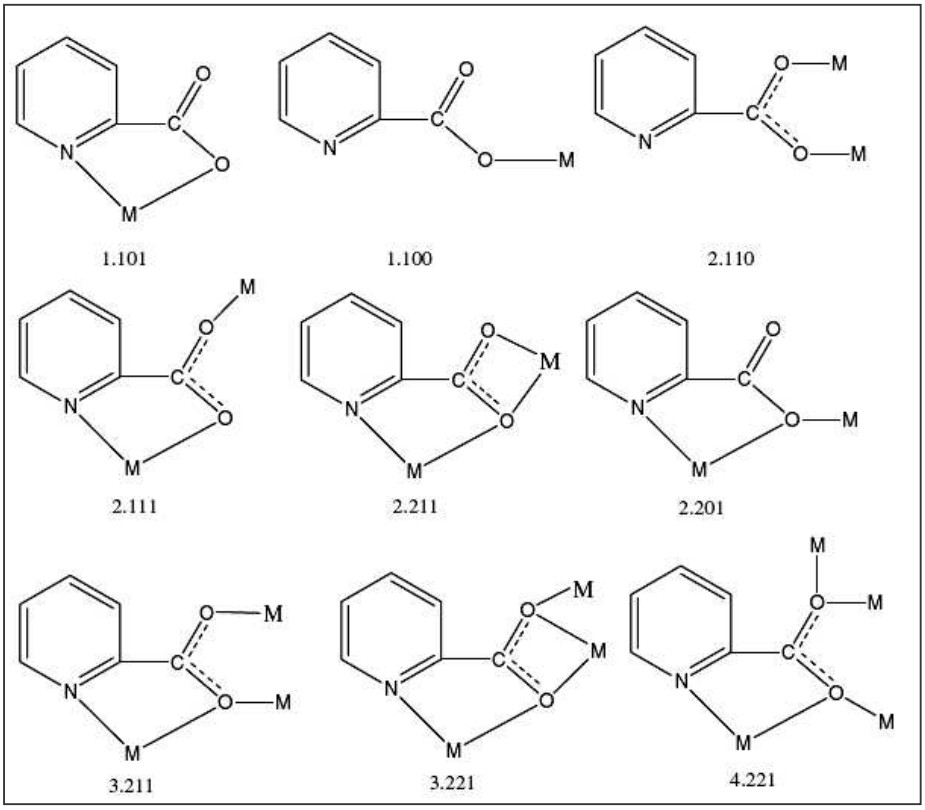

Figure 6.3: Coordination modes of picolinate established crystallographically up to 2007[11] and the Harris notation[12] that describes these modes.

6.2) Aims

As discussed in Chapter 4, the diffusion junction potential must be compensated for when potential measurements are made below about pH 2. When ligand titrations are performed, the pH of a solution is kept constant throughout. Additionally, the concentrations of the ligand and metal ion are significantly lower than that of the background electrolyte when using polarography, so the junction potential would be fairly constant. Since the potential shift ($E(M_{free}) - E(M_{comp})_{(i)}$) is utilised when evaluating formation constants, the junction potential is negated when calculating this difference. However, when pH titrations are performed the solution pH changes throughout the experiment, resulting in the pH of the solution containing the free metal ion and that containing the metal-ligand species being different. The junction potential factor is thus not cancelled when determining the potential shift.

Ideally any shift in the measured $E_{1/2}$ during a pH titration experiment is due to a combination of a change in the diffusion junction potential (below pH 2) and the potential shift due to changes in the metal-ligand species in solution. If the magnitude of the junction potential in known, the extent of the shift in potential due to the variation of species in solution can be monitored and hence formation constants evaluated.

An in-situ monitoring approach of the diffusion junction potential was proposed by including a witness metal ion into the test solution. The witness metal ion should not form complexes with the ligand studied and the polarographic signal should not interfere with that of the metal-ligand system being studied, hence Tl(I) was used. Any variation in the potential of the Tl(I) wave during a pH titration experiment could ideally be attributed to the altered junction potential. By monitoring the junction potential of the witness ion and the overall shift in potential of the metal ion studied in a single solution, an in-situ procedure for predicting the junction potential for the metal ion studied was achieved, hence allowing for the evaluation of complex formation constants accurately even under very acidic condition.

The aim of this work was to test this philosophy to the correction of the diffusion junction potential using the witness ion approach. The procedure was applied to the Cd(II)-PA system which has be studied before[1-6] and hence formation constant data derived here could be compared to literature values to validate the process.

6.3) Results and Discussion

6.3.1) *Background electrolyte*

It is generally assumed that the background electrolyte is non-complexing. This is strictly not true as seen from the formation constants for Cd(II) nitrate species (quoted as log β values in Table 6.2). These values are very small so the nitrate should not really compete with the PA to complex Cd(II). The formation constants quoted in this work are based on the concentration

quotients which would take into account the presence of nitrate and the ionic strength of the solution.

Table 6.2: Formation constants, as log β values, for Cd(II) nitrate species at 25 °C.[8]

Species	Log β	μ /M	Log β	μ /M
$Cd(NO_3)^+$	-0.11	0.5	-0.05	1.0
$Cd(NO_3)_2$			-0.8	1.0

It has been shown that Tl(I) forms stronger complexes with nitrate than with fluoride or perchlorate[13] and values of some formation constants for Tl(I) complexes with anions generally used in background electrolytes are given in Table 6.3. The nitrate complex for Tl(I) is weaker than that for Cd(II) as would be expected.

Table 6.3: Formation constants for Tl(I) species at 25 °C and μ = 1 M.

Species	β_1 [13]	Log β_1
TlF	< 0.32	<-0.49
$TlClO_4$	0.32 ± 0.04	-0.49
$TlNO_3$	0.65 ± 0.05	-0.19
TlCl	2.1 ± 0.1	0.32

Also of importance in aqueous solution are the hydroxide species and the formation constants for both Cd(II) and Tl(I) hydroxides are given in Table 6.4. Unfortunately these values were only available at 3 M ionic strength for the Cd(II) species. Species distribution diagrams for Cd(II) and Tl(I) are presented in Figures 6.4(a) and (b), respectively, to show the fraction of each species present in solution as a function of pH in the absence of an additional ligand. To construct these plots, metal ion and nitrate concentrations were set to typical starting concentrations in experiments performed. Dilution occurs during a titration, but the ratio of total nitrate to metal ion concentrations remains the same.

Under these conditions it was noted that about 33% of Cd(II) is complexed by nitrate up to about pH 7.6 and thereafter various Cd(II) hydroxide species are

Table 6.4: Formation constants for Cd(II) and Tl(I) hydroxide species at 25 °C and μ = 3.0 M.[8]

Species	Log β	Background electrolyte
$Cd(OH)^+$	4.3	$NaClO_4$
$Cd(OH)^+$	3.7	$LiClO_4$
$Cd(OH)_2$	7.7	$NaClO_4$
$Cd(OH)_3^-$	10.3	$NaClO_4$
$Cd(OH)_4^{2-}$	12.0	$NaClO_4$
$Cd_2(OH)^{3+}$	5.06	$LiClO_4$
$Cd_4(OH)_4^{4+}$	23.7	$LiClO_4$
Tl(OH)	0.3[a]	$NaClO_4$

[a] μ= 0.5 M

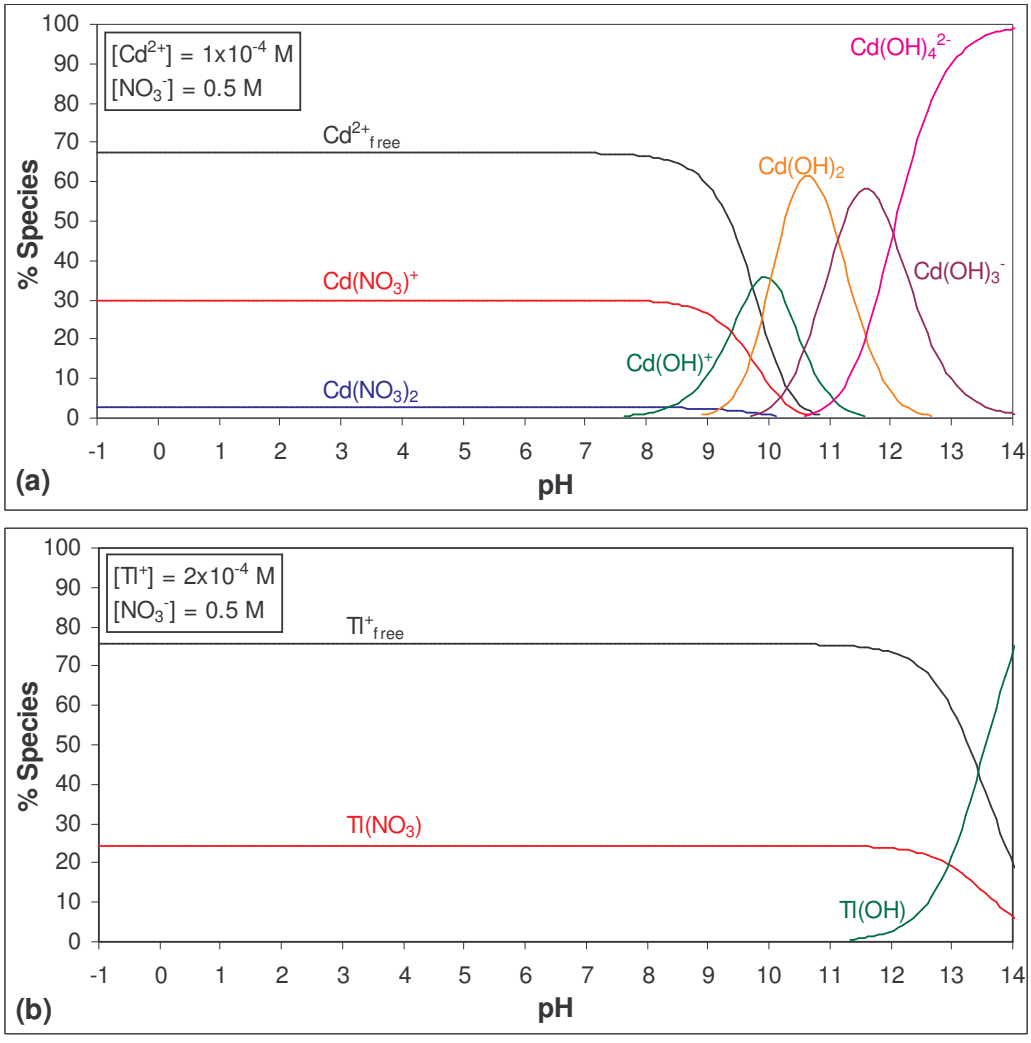

Figure 6.4: Species distribution diagrams for (a) Cd(II) and (b) Tl(I) in an aqueous nitrate solution at 25 °C and μ = 1.0 M.

formed, but neither of the polynuclear hydroxide species are formed at the low Cd(II) concentrations used. Similarly, about 24% of Tl(I) is complexed by nitrate up to a pH of about 12. If the ionic strength is maintained throughout a titration, these values would remain the same and therefore potential shifts with changing pH (between pH 0.3 and 5) would then only be due to the change in the diffusion junction potential. However, since the ionic strength and hence the concentration of nitrate decreased within a titration, it was found that when the concentration of all components were halved, only 19% of the Cd(II) and 14% of the Tl(I) formed nitrate complexes. For both metal ions this refers to a decrease in nitrate complexation of 58%.

6.3.2) *Fitting polarograms*

Polarographic waves are fitted using Equation 2.15. Since the Cd(II) and Tl(I) reduction waves were close together, both waves were fitted simultaneously using the relationship:

$$i = \left[\frac{i_{d,Tl}}{10^{\left(\frac{n_{Tl}\delta_{Tl}(E-E_{1/2,Tl})}{0.05916}\right)}+1}\right] + \left[\frac{i_{d,Cd}}{10^{\left(\frac{n_{Cd}\delta_{Cd}(E-E_{1/2,Cd})}{0.05916}\right)}+1}\right] + i_{bkgnd} \qquad (6.1)$$

where n_{Tl} = 1 and n_{Cd} = 2. For both reduction waves $\delta > 0.9$, indicating reversible reduction processes for both metal ions at all pH values in the presence and absence of PA. At times a δ value slightly greater than one was obtained which is simply an artefact of fitting the data and does not have any physical meaning. To reduce the number of parameters that need to be refined, δ was set equal to one in all cases, thereby improving the fit of the other terms. The background current was fitted using a straight line and an exponential term was included when fitting polarograms collected at low pH where the start of the hydrogen evolution wave was present as given in Equation 4.15. It was found that when the coefficient of the exponential term, *c*, was approximately less than 1×10^{-7}, this term was negligible and could be omitted from the background current expression. Figures A4.1(a) and (b) in Appendix 4 give examples of fitting polarograms where the hydrogen evolution wave is present and absent, respectively.

6.3.3) *pH Titration – Metal ions only*

To assess the change in the magnitude of the diffusion junction potential as a function of pH, pH titrations were performed by titrating a 0.5 M HNO_3 solution containing 9.98×10^{-5} M Cd(II) and 1.99×10^{-4} M Tl(I) with 0.5 M NaOH up to a pH of about 4 using the automated procedure described in Section 2.4.4. Polarograms were collected in the −0.2 to −0.75 V potential range using a current integration time of 60 ms. Eight data sets in total were collected. As hydroxide complexes are not formed by the metal ions in the pH range investigated and no other ligand was present (besides NO_3^-), observed shifts in $E_{1/2}$ values with varying pH were due to changes in the diffusion junction potential.

The decrease in the diffusion limited currents for both Cd(II) and Tl(I) reduction as pH is increased is the trend expected purely due to dilution as the titration proceeds (Figure 6.5). This indicates that the species are fully labile and that inert or nonlabile species are not formed. At low pH large volumes of the NaOH solution are required to increase the pH by about 0.07 pH units, but as the solution becomes less acidic smaller volumes are needed to change the pH by the same amount. The dashed lines in Figure 6.5 depict the calculated current due to dilution using the equation:

$$i_{pH} = i_i \times \frac{v_i}{v_{pH}} \tag{6.2}$$

where i_i and v_i are the initial diffusion limited current and solution volume (before base is added), and i_{pH} and v_{pH} are the current and total solution volume at each step in the titration respectively.

The half-wave potentials were also plotted against pH for the reduction of both metal ions (Figure 6.6). Above pH 2 the junction potential is essentially constant (and was calculated to be small) as indicated by the unchanging half-wave potential which corresponds to the free metal ion potential, $E(M_{free})$, under these conditions. Below pH 2, the change in $E_{1/2}$ as a function of pH was due to the varying diffusion junction potential.

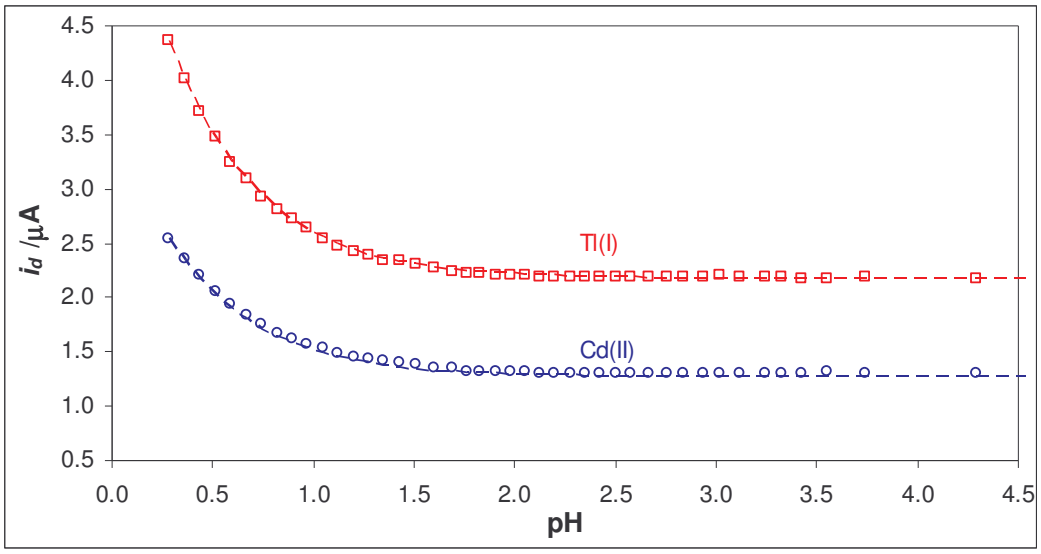

Figure 6.5: Diffusion limited current versus pH for Cd(II) and Tl(I) reduction. The dashed lines represent the expected currents when taking dilution into account.

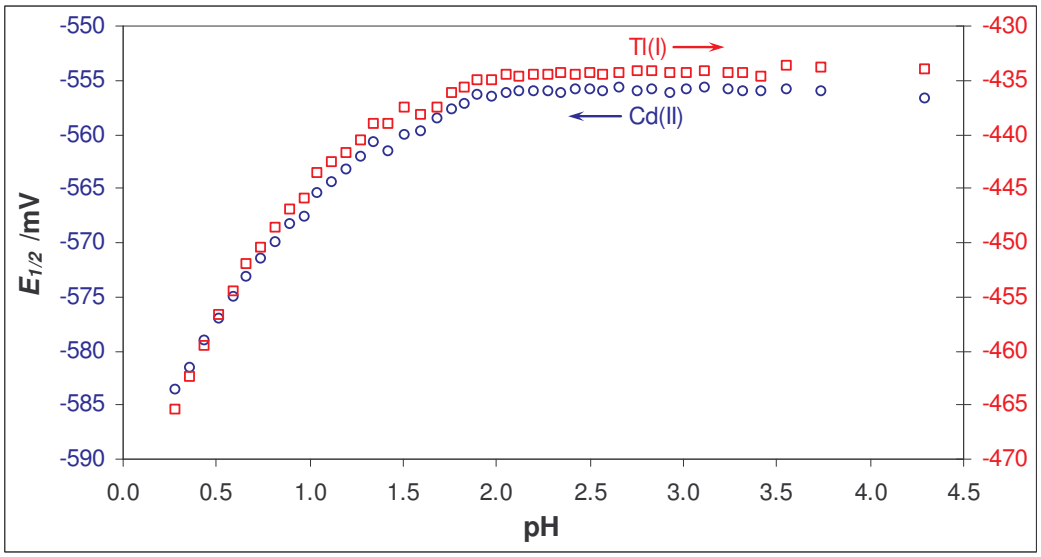

Figure 6.6: The half-wave potentials for the reduction of Cd(II) and Tl(I) as a function of pH.

The junction potential at the interface between the salt bridge solution and the test solution varies with the pH of the test solution and the value for E_j should be the same whether Cd(II) or Tl(I) is being reduced at the DME. The two plots of $E_{1/2}$ versus pH were thus overlayed in Figure 6.7 by adding the value of −121.4 mV to each point on the Tl(I) curve so that the points at the highest pH values were approximately equal for the Tl(I) and Cd(II) curves. (The origin

of the value −121.4 mV will be discussed in Section 6.3.4.) It was noted that $E_{1/2}$ values in the very acidic region did not overlap for the Tl(I) and Cd(II) data. If the junction potential is calculated as the difference between $E(M_{free})$ and $E_{1/2}$ as a function of pH, it would imply that E_j is slightly larger for Tl(I) than for Cd(II), which cannot be true. The discrepancy was relatively small (about 2 – 3 mV at pH 0.3) and as will be seen in Chapter 7, a similar trend was observed between Tl(I) and Cu(II).

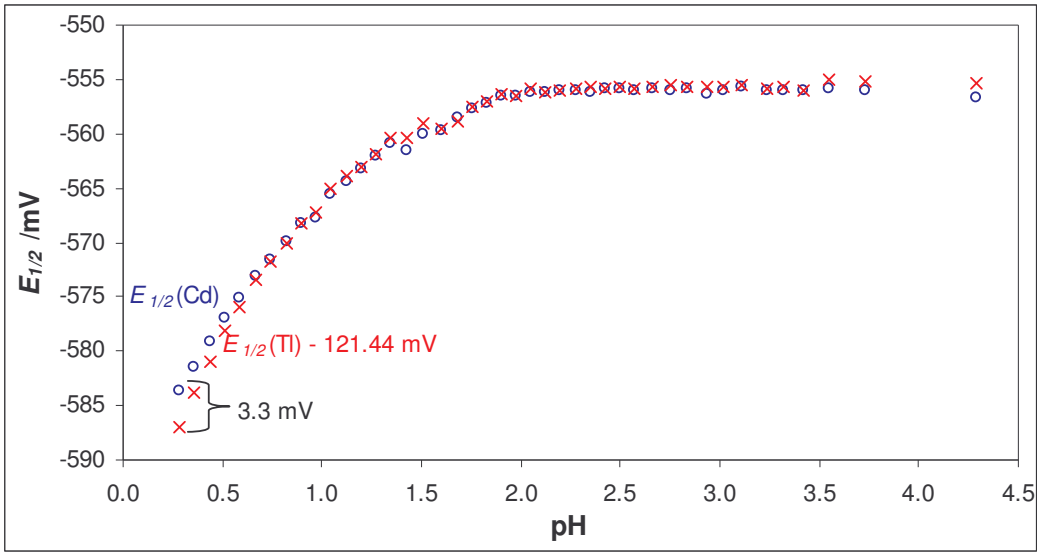

Figure 6.7: The half-wave potentials for Cd(II) and the amended values for Tl(I) as a function of pH to highlight the discrepancies in the lowest pH region.

It was initially thought that the effect was a function of pH and that since hydrogen evolution occurred in the most acidic solutions, this wave could influence the fitting of the reduction waves. As the pH increases, the hydrogen reduction wave diminishes and the $E_{1/2}$ values in Figure 6.7 become comparable. It would be expected that the reduction wave at the most negative potential would be most affected by the hydrogen evolution wave. Cd(II) is reduced at more negative potentials than Tl(I); but Cu(II) is reduced at more positive potentials than Tl(I), thus it was odd that they followed the same trend with the apparent E_j values for Tl(I) being larger than those for Cd(II) and Cu(II) in the most acidic region.

The reason for the observed difference was only found once the older literature by Lingane[14] was reviewed. He described the physical nature of $E_{1/2}$ when considering a reaction occurring at a mercury electrode surface by deriving the expression:

$$E_{1/2} = E_a° - \frac{RT}{nF} ln \frac{\gamma_a kD}{\gamma_s} \quad (6.3)$$

where $E_a°$ is the standard potential of the amalgam for the cell, γ_a and γ_s are the activity coefficients of the metal in the amalgam and the metal ions in solution, respectively, and D is the diffusion constant. The value of $E_{1/2}$ is therefore not equal to $E_a°$ but is also dependent on diffusion rates and activity coefficients. The derivation of this expression is given in Appendix 2 (A2.2). The half-wave potential is therefore dependant on the ionic strength of the solution and in the titration experiments performed here, the ionic strength varied between 0.5 M and 0.25 M.

Solutions containing 2.49×10^{-4} M of Tl(I) and 1.24×10^{-4} M of Cd(II) and Cu(II) were made up in either 0.5 M or 0.25 M KNO_3 with a few grains of gelatine and the $E_{1/2}$ values for the reduction of these metal ions are given in Table 6.5. The shift in $E_{1/2}$ with change in ionic strength for the Cd(II) wave is within the standard deviation (calculated from only two measurements) of the measured values. The higher uncertainty in the $E_{1/2}$ values is probably due to the Cd(II) wave closely following the Tl(I) wave. It is evident that the potential shift due to the change in ionic strength is about 2 mV larger for Tl(I) than Cd(II) or Cu(II) which supports our observations. Further, the shift in $E_{1/2}$ due to the change in ionic strength for Cd(II) and Cu(II) was minimal and within the accepted error for the determination of these values.

Table 6.5: Half-wave potentials for the reduction of Cu(II), Tl(I) and Cd(II) in 0.50 M and 0.25 M KNO_3 at 25 °C. The standard deviations were calculated from only two data sets.

Ionic Strength /M	$E_{1/2}$**(Cu) /mV**	$E_{1/2}$**(Tl) /mV**	$E_{1/2}$**(Cd) /mV**
0.50	44.80 ± 0.04	–436.81 ± 0.10	–555.34 ± 0.50
0.25	45.67 ± 0.18	–434.68 ± 0.03	–555.61 ± 0.29
$E_{1/2}$(0.50 M) – $E_{1/2}$(0.25 M)	–0.87	–2.31	0.26

The potential shift observed for Tl(I) is thus not only due to the junction potential, but a small potential shift also occurs due to the change in ionic strength. The latter is not the same for the metal ion of interest. The aim here is to be able to predict the potential shift for Cd(II) as a function of pH in the absence of a ligand from the $E_{1/2}$ – pH relationship for Tl(I). By modelling the difference between $E_{1/2}$ for Tl(I) and Cd(II) as a function of pH, the discrepancy in the potential shifts for the two metal ions could be accounted for and the Cd(II) $E_{1/2}$ – pH data could be predicted with greater accuracy.

To smooth the $E_{1/2}$ – pH data, it could be fitted by mathematical functions to describe the observed trends and two processes were considered. This was firstly attempted using the exponential function:

$$y = a + b\exp(cx) \tag{6.4}$$

The exponential term would describe the junction potential region and the value of "*a*" would correspond to $E(M_{free})$. However, as shown in Figure 6.8, the $E(M_{free})$ value predicted was too high (and was found to be the case for all data sets), and the function did not fit the raw data very well in certain regions along the curve. A second fitting procedure was investigated where two separate functions were used. The region where E_j was constant was fitted using a straight line with a zero slope (i.e. the average $E_{1/2}$ was calculated) which is equal to $E(M_{free})$ and the junction potential region was fitted using a third order polynomial (see Figure 6.8). The polynomial function did not always meet up adequately with the straight line (especially for noisy data in this pH range), so the number of points around pH 2 used to fit the polynomial was varied till the best possible overall fit was achieved. In general, the value of $E(M_{free})$ for both Cd(II) and Tl(I) was predicted to be about 1 mV lower using this procedure as compared to that when fitting the exponential function.

It is critical that the value of $E(M_{free})$ be as accurate as possible when determining formation constants since every potential shift is calculated relative to this term. The average $E_{1/2}$ value in the region where E_j is constant best described the experimental data in that region and is the value used in all calculations which follow.

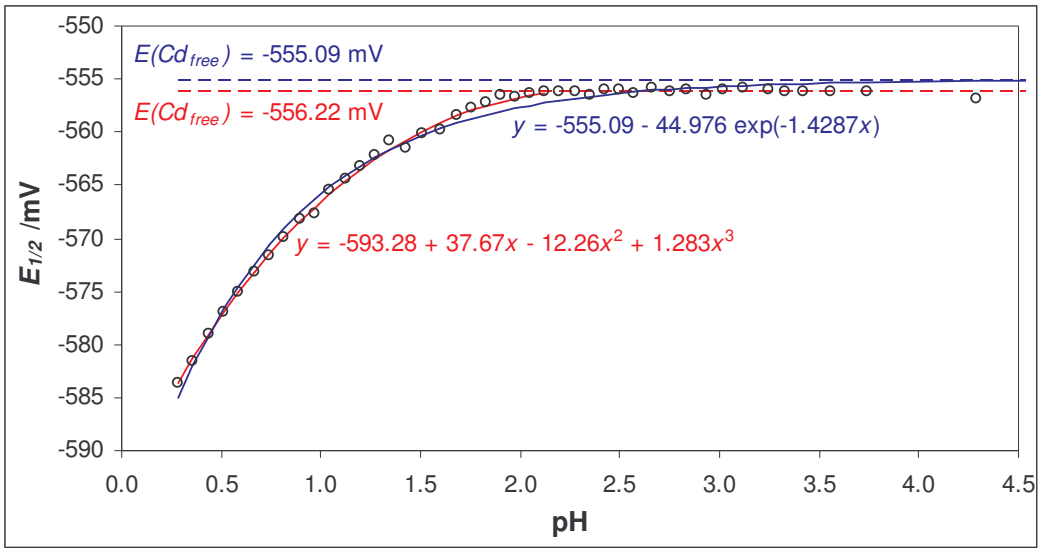

Figure 6.8: Fitting data points in a $E_{1/2}$ versus pH curve for Cd(II). An exponential function (—) and a third order polynomial (—) together with a horizontal line were used and the corresponding $E(Cd_{free})$ values are indicated.

Attempts were made to fit the exponential function given in Equation 6.4 to the experimental data, but setting the value of "*a*" equal to the value of $E(M_{free})$ as determined using the procedure adopted. The exponential function still did not fit the experimental data very well (see Figure A4.2, Appendix 4). Similar fitting trends were observed for the Tl(I) reduction potential data. Thus far the polynomial fit appeared to be best, but it was still further investigated.

Some data sets produced more noisy potential data, probably due to the reference system misbehaving somewhat. The question was how to deal with these data and how to pick up when there is a problem. For example, an anomalous bump was observed in the half-wave potential versus pH plot for both Cd(II) and Tl(I) for one of the experiments (Figure 6.9). The same trend was displayed for both the Cd(II) and Tl(I) curves, reinforcing the concept that the half-wave potentials of the witness metal ion can be used to predict that for the metal ion of interest. In order to assess which points did not fit the trend, the $E_{1/2}$ values were predicted by subtracting the magnitude of the amended E_j values calculated using the Henderson equation[15] (as discussed in Section 4.3.2, Chapter 4) from $E(M_{free})$ in each case. This clearly showed that in the pH region of about 0.8 – 1.5 and below pH 0.5 the reference system did not

behave as expected. As an aside, the predicted half-wave potential versus pH plot was fitted using either an exponential function or a combination of a third order polynomial and a straight line as before. As for the experimental data, it was found that the latter combination produced a better fit (see Figure A4.3 in Appendix 4).

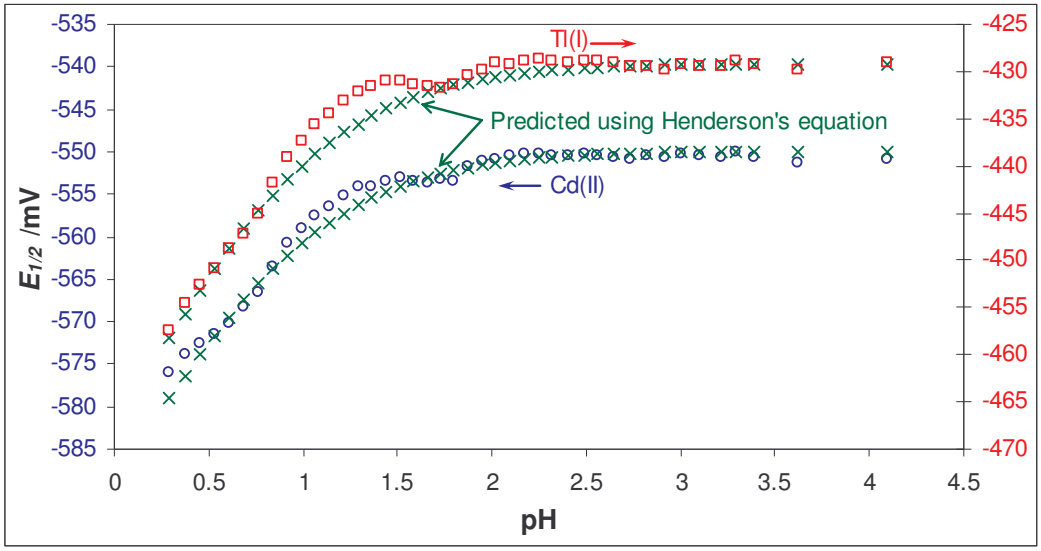

Figure 6.9: Anomalous trends in the $E_{1/2}$ values for one experiment. The predicted $E_{1/2}$ values are also shown for comparison.

Another problematic data set is shown in Figure 6.10 where it was more difficult to detect irregular behaviour. The Cd(II) and Tl(I) data again followed the same trend, but the magnitude of the E_j values were smaller than expected. When these data were compared to the $E_{1/2}$ values calculated employing the Henderson equation[3] as before, this was clearly observed. Data sets which did not show predicted trends were thus not used to model the relationship between the half-wave potentials for Tl(I) and Cd(II). Additionally, when modelling the difference between the Tl(I) and Cd(II) $E_{1/2}$ values for each experiment, similar trends were not obtained for these data sets.

The experimental data points do not necessarily have to be the same as those predicted because the experimental conditions are different to those for which the Henderson equation was derived. The experimental data still best describes the exact behaviour at the liquid junction for a particular experiment

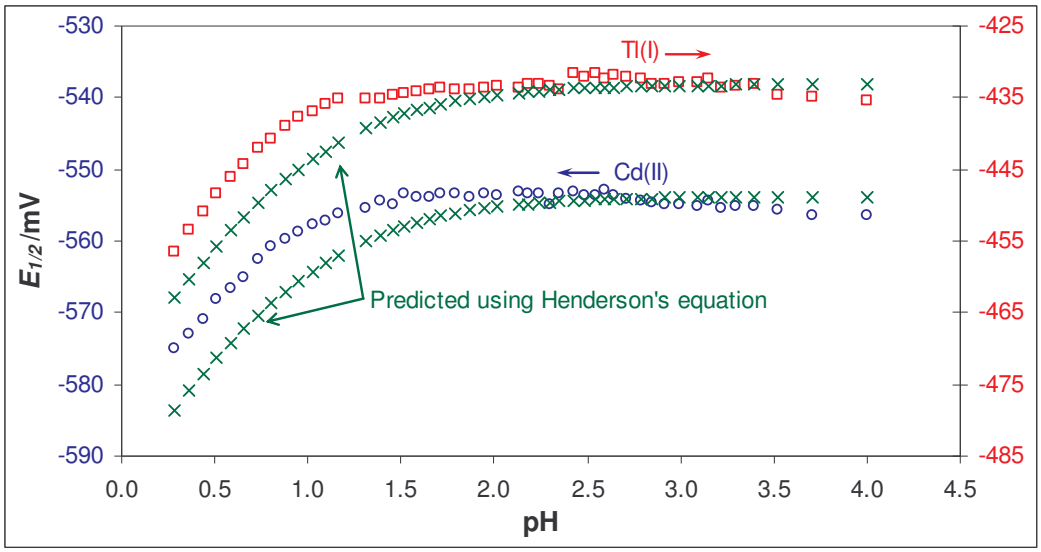

Figure 6.10: Comparisons of experimental and predicted $E_{1/2}$ values for Cd(II) and Tl(I) for a different data set.

and the E_j value is the same whether Tl(I) or Cd(II) reduction is occurring. These predicted values were simply used as a tool to assess the fitness-for-use of the data. Unfortunately, other factors lead to slight differences in the $E_{1/2}$ versus pH trends for the two metal ions.

When ligand is added to the test solution and complex formation with Cd(II) occurs, it is difficult to assess whether there were any problems with the reference system during an experiment. Monitoring the reduction potential behaviour of the witness metal ion, together with the ability to predict trends in potential behaviour using the Henderson equation, provides a powerful tool to assess the validity of the reduction potentials for the Cd(II) complexes.

6.3.4) *Predicting the free metal ion potential*

In metal-ligand equilibria experiments, the free metal ion potential is usually determined by recording polarograms for the reduction of the metal ion studied before the ligand is added to the solution. The half-wave potential then corresponds to $E(M_{free})$ provided there is no hydrolysis occurring at that pH and that it is above a pH of 2 where the diffusion junction potential does not need to be accounted for. In this work, the initial solutions were at about pH 0.3,

resulting in a junction potential of the order of –30 mV which has to be corrected for to give an accurate value of $E(M_{free})$.

One approach to evaluate $E(M_{free})$ in this work was to determine the magnitude of the junction potential as accurately as possible using the Tl(I) potential data and then find a model which relates the half-wave potentials of Cd(II) and Tl(I). This method was not very accurate as the largest uncertainty in the diffusion junction potential was for the most acidic solutions.

When running several experiments with only the metal ions present, the most reproducible value proved to be the difference between the free metal ion potentials for Cd(II) and Tl(I). The actual values of $E(M_{free})$ for both metal ions varied somewhat as the reference system changed, but the difference was found to be constant as shown in Table 6.6. The average difference of –121.4 (± 0.6) mV together with $E(Tl_{free})$, which can also be determined in the presence of the ligand if no complexation takes place, could be used to calculate $E(Cd_{free})$ more accurately using the relationship:

$$E(Cd_{free}) = E(Tl_{free}) - 121.4 \qquad (6.5)$$

This procedure was used in all future experiments.

Table 6.6: Free metal ion potentials for Cd(II) and Tl(I) from pH titration experiments in the absence of ligand.

Data Set	$E(Cd_{free})$ /mV	$E(Tl_{free})$ /mV	$E(Cd_{free}) - E(Tl_{free})$ /mV
1	–550.49	–429.15	–121.34
2	–560.65	–438.55	–122.10
3	–556.22	–434.61	–121.61
6	–544.61	–422.80	–121.81
7	–545.82	–425.48	–120.34
8	–546.98	–425.54	–121.44
Average			–121.4 ± 0.6

6.3.5) *Modelling the half-wave potential data*

A model for the relationship between the half-wave potentials of Cd(II) and Tl(I) with respect to pH (in the absence of ligand) needed to be established so that Tl(I) reduction data could be used to predict the magnitude of the diffusion

junction potential for Cd(II) and thereby could be corrected for in complex formation experiments. Six data sets were used and various models were considered.

Model 1: Constant difference

Here it was assumed that there was a constant difference between the $E_{1/2}$ values for Tl(I) and Cd(II) at all pH values. This would be the case if the change in ionic strength did not lead to slight deviations in this difference, as seen in Figure 6.7. This was a rudimentary approach and subsequent models took this deviation into account.

Model 2: Difference in half-wave potentials

Another straight-forward approach was to find the difference between the half-wave potentials for Cd(II) and Tl(I) as a function of pH. Figure 6.11 shows this difference in the experimental $E_{1/2}$ values for each data set and it clearly demonstrates that the largest difference in the $E_{1/2}$ values occurred in the lowest pH region.

Data sets 7 and 8 showed slightly different trends in this model as compared to the other data sets, but plots of $E_{1/2}$ versus pH for both the Tl(I) and Cd(II) reduction followed a similar trend to that predicted using Henderson's equation. It was therefore decided to keep these data in the overall model as the average correlation was modelled. There would be no other way to judge the data when the ligand was included in the solution and complexation with Cd(II) occurred. A sixth order polynomial was fitted to the combination of all six data sets to determine the average change in $E_{1/2}$ as a function of pH. From pH 3.1 onwards $\Delta E_{1/2}$ was set equal to −121.4 mV, the average difference in the free metal ion potentials for Cd(II) and Tl(I).

Since these plots were very noisy when using the experimental data, the same model was determined for fitted $E_{1/2}$ values, using both the polynomial and straight line combination and the exponential function (where the value of a was fixed to that of the horizontal straight line). These plots are displayed in Figures A4.4(a) and (b) (Appendix 4), respectively. In Figure A4.4(a) the

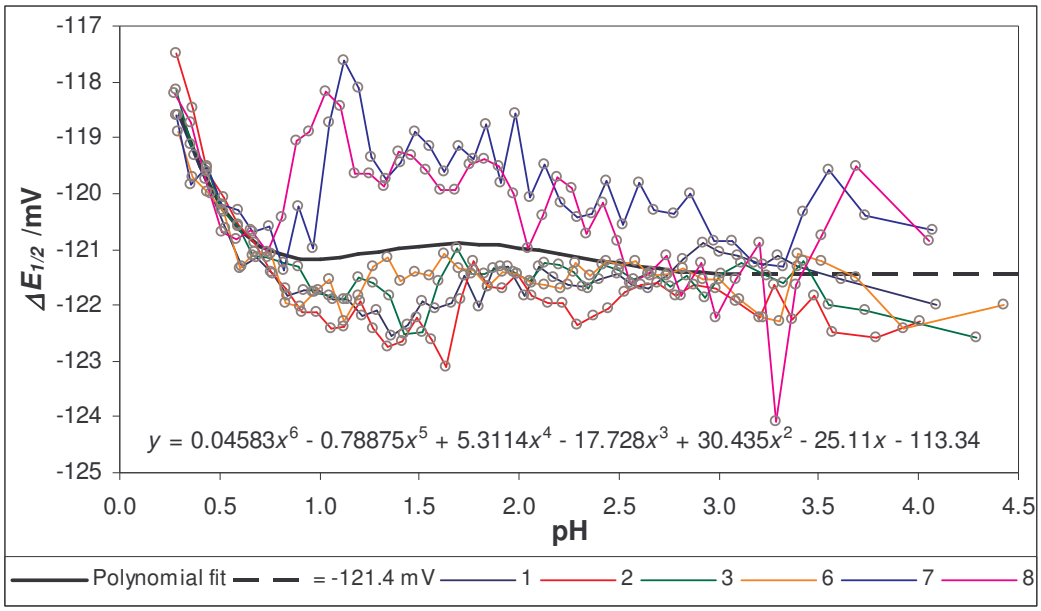

Figure 6.11: Sixth order polynomial fitted to the combined experimentally determined $E_{1/2}(Cd) - E_{1/2}(Tl)$ values as a function of pH. Above pH 3.1, $\Delta E_{1/2}$ was set to –121.4 mV. (The numbers in the legend refer to the data set number.)

individual trends are disjointed due to use of the two separate functions to fit the $E_{1/2}$ versus pH data for the two metal ions. The value of $\Delta E_{1/2}$ was again set equal to –121.4 mV for pH > 2 where the change in the junction potential is negligible and the difference between $E_{1/2}$ for the two metal ions should be constant.

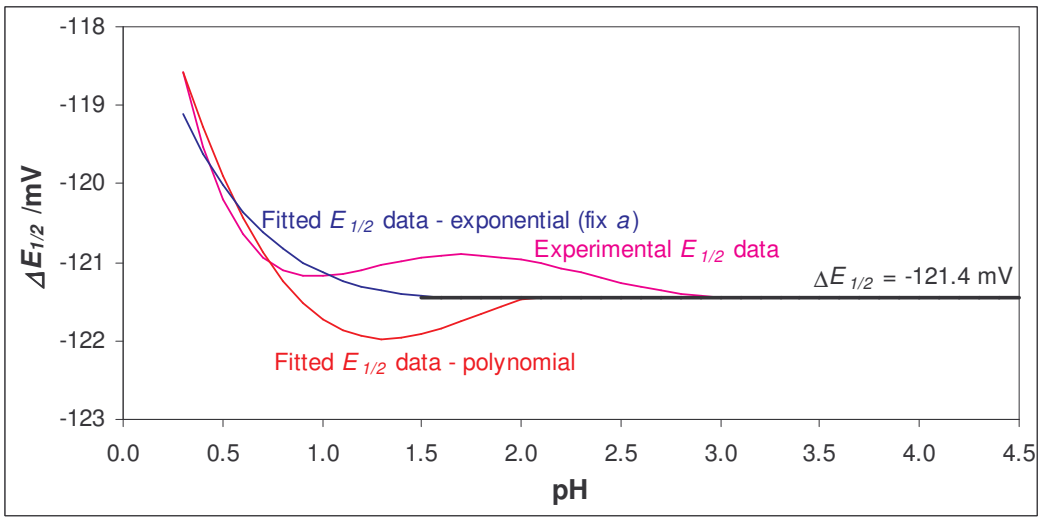

Figure 6.12: Comparison of the $\Delta E_{1/2}$ versus pH models when using experimental or fitted $E_{1/2}$ values.

A comparison of the three ways in which this model was determined is given in Figure 6.12. The fact that there was a difference shows that the two fitting procedures are not exactly the same and that noise in the raw data also affected the model. However, the difference between these approaches was not very significant as at any pH, $\Delta E_{1/2}$ differed by less than 1 mV for these mathematical models.

Model 3: Difference in "diffusion junction" potentials

The "diffusion junction" potentials were calculated for each data set as follows:

$$E_j = E(M_{free}) - E_{1/2} \tag{6.6}$$

Here "diffusion junction" potential is written with quotation marks because, as describe before, this is strictly the change in E_j and also encompasses an additional potential change due to the change in ionic strength of the solution. The difference between these values for Cd(II) and Tl(I) reduction were then plotted against pH for all the data sets and a sixth order polynomial was fitted as before. The graph comparing the models obtained from experimental and fitted $E_{1/2}$ data is given in Figure 6.13. For all these models, ΔE_j was set equal to 0.0 mV at higher pH values where the diffusion junction potential is essentially constant. The difference in the "junction" potentials for the two metal ions is at most 2.9 mV at the lowest pH.

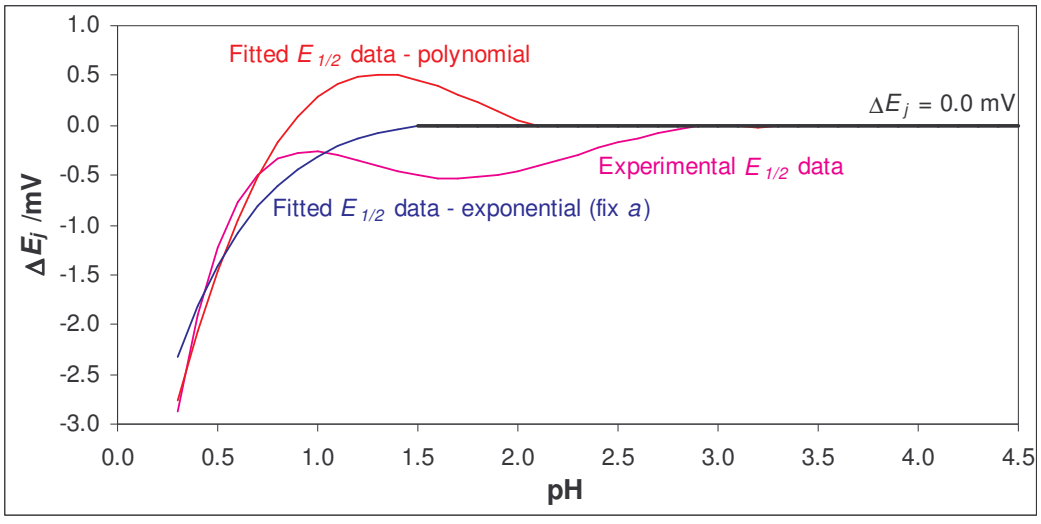

Figure 6.13: Comparison of the ΔE_j versus pH models when using experimental or fitted $E_{1/2}$ values.

Model 4: Normalised difference in half-wave potentials

In this case $\Delta E_{1/2}$ was divided by a normalisation factor, N, which was chosen to be the $\Delta E(M_{free})$ as determined in each experiment, thus giving:

$$\frac{\Delta E_{1/2}}{N} = \frac{\Delta E_{1/2}}{\Delta E(M_{free})} = \frac{E_{1/2}(Cd) - E_{1/2}(Tl)}{E(Cd_{free}) - E(Tl_{free})} \qquad (6.7)$$

The normalisation factor is independent of pH and at higher pH values $\Delta E_{1/2}/\Delta E(M_{free})$ was set equal to one where the diffusion junction potential is negligible and the half-wave potentials are equal to the free metal ion potential. A sixth order polynomial was fitted to the combined data sets and the models derived from experimental and fitted potential data as before and the plots are exhibited in Figure 6.14.

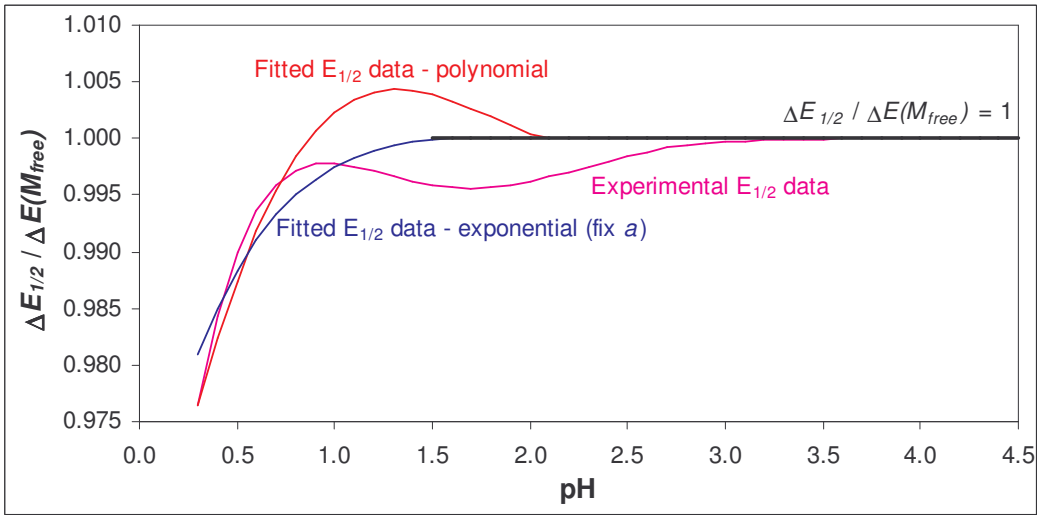

Figure 6.14: Comparison of the normalised $\Delta E_{1/2}$ values versus pH models when using experimental or fitted $E_{1/2}$ values and where the normalisation factor is $\Delta E(M_{free})$.

Model 5: Difference in normalised half-wave potentials

The last model considered entailed normalising the half-wave potential for each metal ion by dividing each by the corresponding free metal ion potential and then finding the difference as a function of pH:

$$\Delta\left(\frac{E_{1/2}}{E(M_{free})}\right) = \frac{E_{1/2}(Cd)}{E(Cd_{free})} - \frac{E_{1/2}(Tl)}{E(Tl_{free})} \qquad (6.8)$$

The combined potential data sets were again fitted by a sixth order polynomial. $\Delta(E_{1/2}/E(M_{free}))$ was set equal to zero at higher pH values where the diffusion junction potential is negligible and the half-wave potentials are equal to the free metal ion potentials for each metal ion, thus both $E_{1/2}/E(M_{free})$ terms were equal to 1.0 and the difference is zero. The modelled data for the experimental and fitted potential values are shown in Figure 6.15.

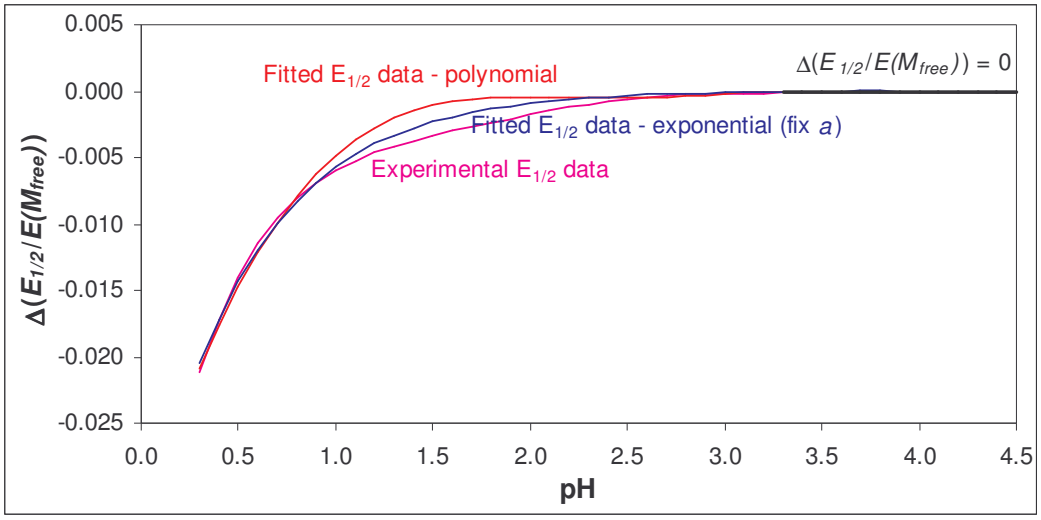

Figure 6.15: Comparison of the difference between the normalised $E_{1/2}$ values versus pH models when using experimental or fitted $E_{1/2}$ values.

The five different models presented here had to be assessed as to determine which would predict the Cd(II) half-wave potentials, using the Tl(I) half-wave potential data and the models relating these two parameters, most accurately. Models 2 – 4 appeared to be essentially equivalent, but they still needed to evaluated more closely.

6.3.6) *Comparison of models*

For ease of discussion and recognition of the five different models, each was named as shown in Table 6.7.

The correlation coefficients, quoted as R^2 values, indicating the goodness-of-fit between the fitted sixth order polynomial and the data from the combined six data sets, were calculated for each model using experimental or fitted $E_{1/2}$

Table 6.7: Key to names for the models used.

Number	Name	Model	Equation
1	mConst	$y = E_{1/2}(Cd) - E_{1/2}(Tl) = -121.4\ mV$	6.9
2	mE	$y = E_{1/2}(Cd) - E_{1/2}(Tl)$	6.10
3	mE_j	$y = E_j(Cd) - E_j(Tl)$	6.11
4	mNorm	$y = \frac{E_{1/2}(Cd) - E_{1/2}(Tl)}{E(Cd_{free}) - E(Tl_{free})}$	6.12
5	mNorm2	$y = \frac{E_{1/2}(Cd)}{E(Cd_{free})} - \frac{E_{1/2}(Tl)}{E(Tl_{free})}$	6.13

values (see Table 6.8). As would be expected, the R^2 values were closer to unity for the fitted $E_{1/2}$ values due to the smoothing of the data, but there was not a significant difference in this case between the two fitting procedures. The R^2 values were similar for the mE, mE_j and mNorm models, but were closer to unity for the mNorm2 model.

Table 6.8: Table of R^2 values for the various sixth order polynomial models.

Model	Experimental $E_{1/2}$	Fitted $E_{1/2}$:	
		Polynomial	Exponential (fixed *a*)
2: mE	0.2857	0.6934	0.6175
3: mE_j	0.3725	0.6835	0.7402
4: mNorm	0.3717	0.7009	0.7397
5: mNorm2	0.8876	0.9571	0.9672

These derived models, together with the Tl(I) potential data, were used to predict the magnitude of the "junction potential" for Cd(II) as a function of pH. The accuracy of using the various models to predict the Cd(II) half-wave potentials was tested by comparing the predicted values to the actual experimental data.

When using the mConst model to predict the $E_{1/2}(Cd)$ values at each pH, as expected, the largest discrepancies between the calculated and experimental values occurred in the lowest pH region as demonstrated in Figure 6.16. Additionally, the magnitude of $\Delta E(M_{free})$ was −122.10 mV for this data set, which generally resulted in slightly lower predicted values throughout.

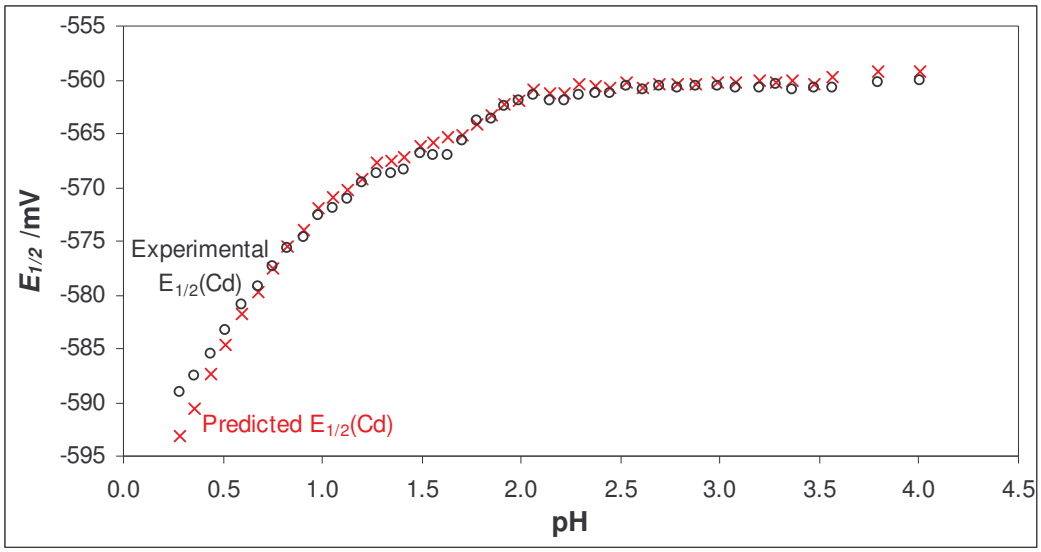

Figure 6.16: Comparison of the experimental and predicted $E_{1/2}(Cd)$ values for one data set using the mConst model and the experimental $E_{1/2}(Tl)$ data.

When using the mE model, the sixth order polynomial obtained from modelling these data were used to calculate the *y*-values at each pH. The half-wave potentials for Cd(II) were calculated using Equation 6.10 rearranged as:

$$E_{1/2}(Cd) = y + E_{1/2}(Tl) \qquad \text{(6.10 rearranged)}$$

At higher pH values *y* was set equal to –121.4 mV as discussed. As expected, the predicted $E_{1/2}(Cd)$ values in the lowest pH region were far closer to the experimental values than when using the mConst model, as shown in Figure 6.17. In this graph, results are shown for the three different sixth order polynomial functions derived from using experimental data (results indicated as Calculated: raw) or fitted potential data employing a polynomial-straight line combination (Calculated: fitted-poly) or the exponential function with a fixed *a* value (Calculated: fitted-exp).

When using the remaining three models to predict the Cd(II) half-wave potentials, the equations became unnecessarily complicated by including the value –121.4 mV in the mE_j model where:

$$E_{1/2}(Cd) = -121.4 + E_{1/2}(Tl) - y \qquad \text{(6.11 rearranged)}$$

and in the mNorm model where:

$$E_{1/2}(Cd) = -121.4y + E_{1/2}(Tl) \qquad \text{(6.12 rearranged)}$$

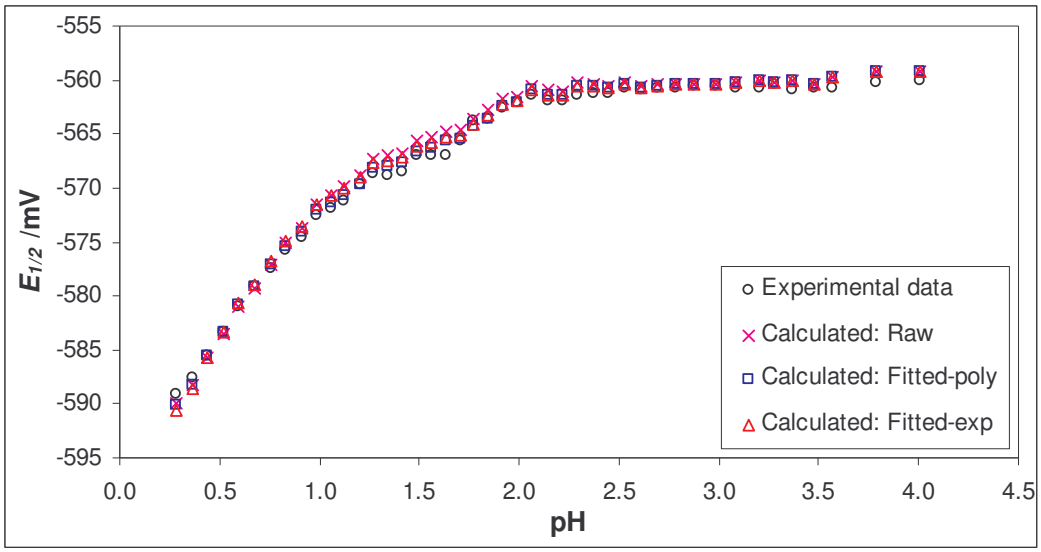

Figure 6.17: Comparison of the experimental and predicted $E_{1/2}(Cd)$ values when applying the mE model and using the three different sixth order polynomials derived from raw or fitted data.

and additionally the value for $E(Tl_{free})$ in the mNorm2 model where:

$$E_{1/2}(Cd) = (-121.4 + E(Tl_{free}))\left(y + \frac{E_{1/2}(Tl)}{E(Tl_{free})}\right) \qquad \text{(6.13 rearranged)}$$

Slight additional uncertainties may be introduced in each case when determining $E_{1/2}(Cd)$.

To assess which model best predicted the Cd(II) reduction potentials, the standard deviation was determined for each curve comparing the experimental and predicted Cd(II) half-wave potentials as a function of pH. The standard deviation was calculated as follows:

$$S.D. = \sqrt{\frac{\sum (E_{obs} - E_{calc})^2}{n-1}} \qquad (6.14)$$

where E_{obs} are the experimental potential values, E_{calc} are the values predicted and n is the number of data points. The standard deviation for each model, whether derived from raw data or fitted data (given in Table 6.9(a) and (b) respectively), was computed.

Table 6.9: Standard deviations between experimental and predicted $E_{1/2}(Cd)$ values for the $E_{1/2}$ versus pH plots. $E_{1/2}(Cd)$ values were predicted using experimental $E_{1/2}(Tl)$ data and the models derived from (a) experimental and (b) fitted potential data

(a) Experimental $E_{1/2}$ values					
Data set	**mConst**	**mE**	**mE_j**	**mNorm**	**mNorm2**
1	0.732	0.661	0.660	0.660	1.110
2	1.088	0.944	0.942	0.947	0.855
3	0.813	0.539	0.538	0.541	0.747
6	0.647	0.506	0.505	0.508	0.599
7	1.788	1.409	1.409	1.406	1.549
8	1.648	1.247	1.247	1.247	1.667

(b) Fitted $E_{1/2}$ values								
Data set	**Polynomial fit:**				**Exponential fit (fixed *a*):**			
	mE	**mE_j**	**mNorm**	**mNorm2**	**mE**	**mE_j**	**mNorm**	**mNorm2**
1	0.317	0.306	0.315	0.612	0.518	0.519	0.518	0.863
2	0.578	0.585	0.570	0.576	0.800	0.801	0.801	0.675
3	0.342	0.341	0.342	0.437	0.450	0.450	0.450	0.538
6	0.435	0.422	0.434	0.464	0.452	0.452	0.451	0.469
7	1.854	1.847	1.854	2.118	1.627	1.623	1.626	1.817
8	1.665	1.662	1.666	2.207	1.428	1.426	1.426	1.905

In all cases the experimentally determined Tl(I) potential data were used, not fitted trends. It was assumed that the reference system must have the same effect on the potential measurements for both ions. This was clearly seen when considering the data set where there was an anomalous hump in the $E_{1/2}$ versus pH plots as shown in Figure 6.9. The predicted potentials followed the same trend as the experimental values, as shown in Figure A4.5 (Appendix 4), using the mE model as an example. However, the reference system is not the only factor that could lead to some variation in the data. Figure A4.6 (Appendix 4) shows that other factors could lead to a slight discrepancy between the Cd(II) and Tl(I) potential data which could result in some error when predicting $E_{1/2}(Cd)$ values. For example, this could be due to variations when fitting polarograms to determine the half-wave potential values, especially for noisy data.

In general, the standard deviations were very similar for models mE, mE_j and mNorm, and were larger for models mConst and mNorm2. The models mE,

mE_j and mNorm were essentially equivalent and any of the three could be used. The mE model was however the simplest to use and also eliminated any small errors associated with determining the free metal ion potentials. The mConst model did not describe the fact that the Cd(II) and Tl(I) potential versus pH curves deviated in the very low pH region. Interestingly, even though the correlation coefficient for fitting the combined six data sets to determined the mNorm2 model was the closest to unity, it did not always predict the Cd(II) reduction potentials as closely as the mE, mE_j and mNorm models. Additionally, the model derived from fitting the potential data with a combination of the polynomial and straight line functions usually produced the best results when predicting the Cd(II) reduction potentials. The combined function described the experimental data more closely than the exponential function and it also eliminated the noisy data when building the models.

6.3.7) *Recommended procedure for modelling the potential data*

The $E_{1/2}$ values from the experiments performed on solutions containing Cd(II) and Tl(I) metal ions in the absence of a complexing ligand, could be used to model the $\Delta E_{1/2}$ values for these metal ions. For experiments including a complexing ligand, this model together with the $E_{1/2}(Tl)$ values, could be used to predict the Cd(II) half-wave potentials for uncomplexed Cd(II). The magnitude of the diffusion junction potential could then be calculated and hence corrected for. The protocols suggested for building the model and predicting the $E_{1/2}(Cd)$ values are given stepwise below.

Building the model

1) Run at least five pH titration experiments as described using solutions containing the metal ion to be studied and Tl(I) with no ligand present.
2) Determine $E_{1/2}$ values for both metal ions at each pH for all experiments and plot the $E_{1/2}$ versus pH curves. Ensure that these curves for both metal ions follow a similar trend to that predicted using the Henderson equation.
3) Fit the $E_{1/2}$ versus pH curves for both metal ions with a third order polynomial function at low pH values to describe the diffusion junction potential region. Average the potential values at higher pH where the

junction potential is constant to determine the free metal ion potential. Use the combination of both these functions to describe the experimental data over the entire pH range.

4) Calculate the average difference between the free metal ion potentials (for the metal ion studied and Tl(I)) for all the data sets.
5) Plot the difference between the half-wave potentials for the metal ion studied and Tl(I) reduction as a function of pH for each data set. Fit an average polynomial to the $\Delta E_{1/2}$ versus pH plots for all the data sets combined to represent the model.

Predicting Cd(II) half-wave potentials

1) Find $E(Cd_{free})$ by adding the average difference between the free metal ion potentials and $E(Tl_{free})$.
2) Calculate the y-value of the sixth order polynomial at each pH.
3) Add the experimental $E_{1/2}(Tl)$ values to this *y*-value at each pH to determine the $E_{1/2}(Cd)$ values as a function of pH.

6.3.8) *pH titrations: Using the model to evaluate formation constants*

Two pH titration experiments were done starting from pH 0.3 with $[PA_T]$:$[Cd_T]$ = 100.5 and 200.0 (i.e. 30.96 mg and 61.63 mg of solid picolinic acid (PA), respectively, were added to the background solution containing 9.98×10^{-5} M Cd(II) and 1.99×10^{-4} M Tl(I)). The process developed to correct for the diffusion junction potential was applied and tested. A third pH titration experiment was done starting from about pH 2 where no correction for the junction potential is necessary with $[PA_T]$:$[Cd_T]$ = 97.2. A 0.02 M NaOH titrant (ionic strength = 0.5 M) was used here so that the pH did not change much for small additions of the base solution. Starting at this high pH was possible for this metal-ligand system as Cd(II)-PA complexes only started forming at higher pH according to literature data.[5,8] The data collection parameters were the same as for the experiments in the absence of ligand, except the final potential was made more negative (up to –0.80 V) as the titration proceeded since the reduction potential of complexed Cd(II) shifted more negative and all titrations were terminated at about pH 7.

From Figure 6.18, it was clear that complexation of Tl(I) by PA did not occur in the pH range studied because the half-wave potential response as a function of pH showed the same trend as when no ligand was added to the solution (see Figure 6.6). The trend was also similar to that predicted using the Henderson equation. Since the ligand concentration is only about an order of magnitude lower than that of the background electrolyte, the presence of the ligand in solution could affect the ionic strength and junction potential value. Since the mobilities of the ligand (at various degrees of protonation) are unknown, the junction potentials cannot be accurately calculated. Once again the importance of determining the junction potential experimentally is illustrated. The Tl(I) potential data were thus used to account for the diffusion junction potential in the Cd(II) reduction potentials.

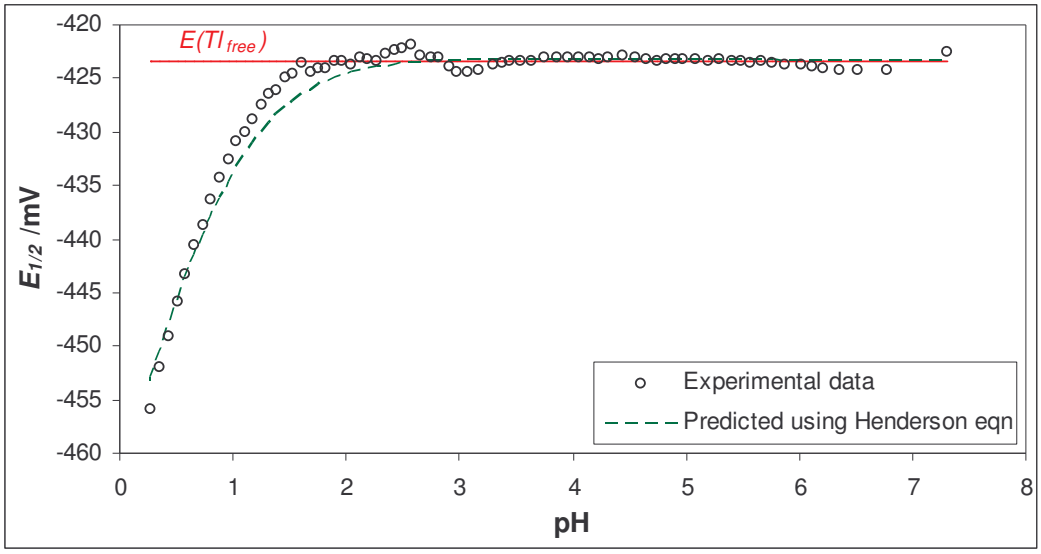

Figure 6.18: Tl(I) half-wave potentials as a function of pH indicating no complex formation in a solution with $[PA_T]:[Tl_T] = 50$ and $[L_T] = 0.01003$ M.

The $E_{1/2}$ versus pH plot for the reduction of Cd(II) in the presence of picolinic acid where $[PA_T]:[Cd_T] = 100.5$ is shown in Figure 6.19. The experimental $E_{1/2}$ values initially increased with an increase in pH indicating the effect of the junction potential. The value of $E(Cd_{free})$ and the predicted $E_{1/2}$ values for Cd(II) in the absence of ligand were calculated using the Tl(I) reduction data (together with the mE polynomial fit model for the latter value) and are also shown in Figure 6.19. The magnitude of E_j was calculated by subtracting the

predicted potential values from $E(Cd_{free})$. The experimental data were then corrected by adding these E_j values. Upon correction of the diffusion junction potential it was observed that the potential actually remained reasonably constant at very low pH which indicates no complex formation in this pH region. The potential then decreases which indicates the formation of Cd(II)-picolinic acid complexes and then tails off around pH 6. For this metal-ligand system, the junction potential and complex formation pH regions appear to be separate.

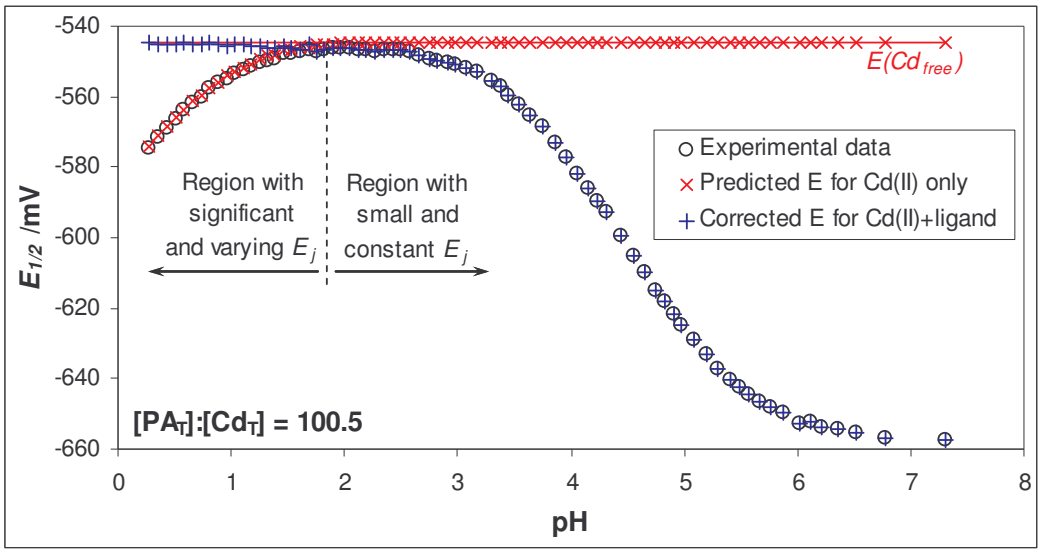

Figure 6.19: Cd(II) half-wave potentials before (experimental data) and after (corrected E) accounting for the junction potentials. The predicted $E_{1/2}$ values and $E(Cd_{free})$, calculated using the Tl(I) data, are also indicated.

To illustrate the importance of correctly compensating for the diffusion junction potential, Figure A4.7 (Appendix 4) highlights the region where E_j is significant and shows the difference between using the mE model as above or simply the mConst model. Over compensation at the lowest pH values occurred when applying the mConst model resulting in a negative value for the potential shift $\{E(M_{free}) - E(M_{comp})_{(i)}\}$ in this case, which is meaningless. For other metal-ligand systems where complexes are formed at this low pH, this overcompensation could affect the value of formation constants and even other proposed species in solution.

Using the corrected $E_{1/2}$ data, the 3D-CFC program was used to assist in predicting the type of metal-ligand species present and refine their stability constants. Since the diffusion limited currents are not affected by junction potentials, experimentally determined current values were used. Figure 6.20 shows the experimentally determined currents ($i(M_{comp})$) and the expected currents, which were calculated using the current of the initial free metal ion ($i(M_{free})$) and taking the dilution factor into account. These two plots did not differ much, thus the normalised currents (i.e. $i(M_{comp})/i(M_{free})$) which are used in Equation 2.17 remain close to unity as would be the case for labile complexes where the diffusion rates for the free and the complexed Cd(II) do not vary much. The term $\ln\{i(M_{comp})/i(M_{free})\}$ is thus close to zero and the potential shift is the predominant factor in determining the formation constants.

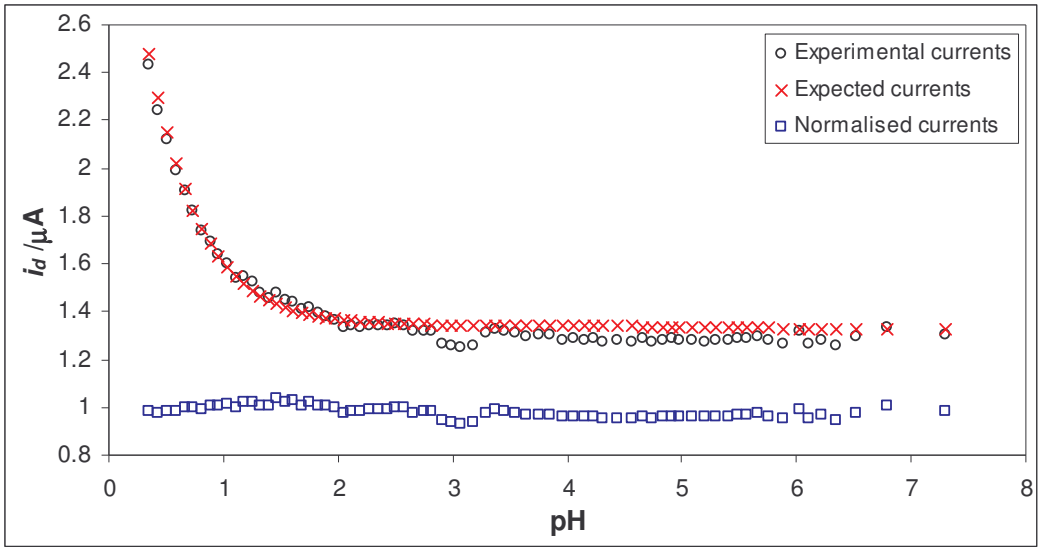

Figure 6.20: Experimental currents for the reduction of Cd(II) in the presence of PA and currents expected if no complexation took place. The quotient of these gives the corrected currents.

To predict which metal-ligand species are in solution, slope analysis was performed on the ECFC plot (as was discussed in Section 2.5.2 using Equation 2.21). Table 6.10 provides the expected slopes for a possible set of reduction reactions. Consolidating this information with the plot in Figure 6.21, a slope of 47 mV/ pH unit in the region where HL is the predominant form of the ligand in solution pointed to a combination of CdL and CdL_2 being formed.

Table 6.10: Predicted slopes (in mV per pH unit) of potential versus pH data for the corresponding reduction reactions.

Reduction reaction	Predicted slope
$CdL^{+} + 2e^{-} + H^{+} \rightleftharpoons Cd^{o} + HL$	30
$CdL_2 + 2e^{-} + 2H^{+} \rightleftharpoons Cd^{o} + 2HL$	60
$CdL_3^{-} + 2e^{-} + 3H^{+} \rightleftharpoons Cd^{o} + 3HL$	90
$CdL_2 + 2e^{-} + 4H^{+} \rightleftharpoons Cd^{o} + 2H_2L^{+}$	120
$CdL_3^{-} + 2e^{-} + 6H^{+} \rightleftharpoons Cd^{o} + 3H_2L^{+}$	180
$CdHL^{2+} + 2e^{-} \rightleftharpoons Cd^{o} + HL$	0 (no H^{+} involved)

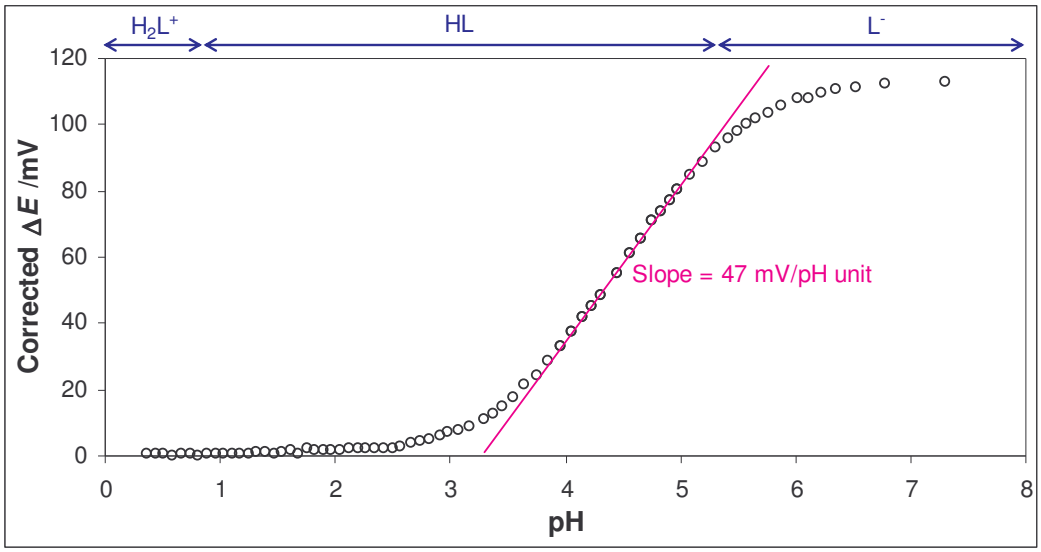

Figure 6.21: ECFC indicating the main region of constant slope as well as the predominant ligand species in solution in various pH ranges.

The CCFC was determined for the CdL and CdL_2 system using refined log β values for these two species and is plotted in Figure 6.22. Clearly this model did not describe the experimentally-derived data sufficiently. When CdL_3 was included in the system, the CCFC tracked the ECFC more closely. Data points at the lowest pH values appeared to be slightly higher than the CCFC predicted, so CdHL was included in the system. From Table 6.10 it is clear that this species cannot be predicted using slope analysis when HL is the main form of the ligand in solution because the slope is zero as there are no protons involved in the reaction. Figure 6.23 highlights the acidic region where the CCFC is affected by the presence of CdHL. Including CdHL improves the fit, but the inset shows that the difference between the potentials calculated in the

presence and in the absence of CdHL is less than 1 mV. This is well within experimental error, especially considering that this is the region for which the junction potential was corrected for.

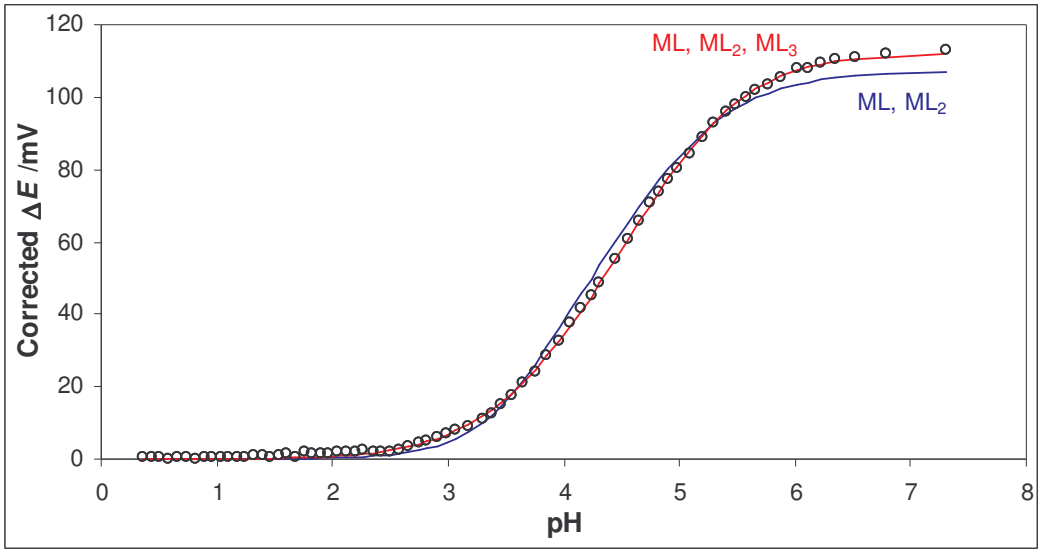

Figure 6.22: ECFC and CCFCs for the two proposed Cd(II)-PA systems.

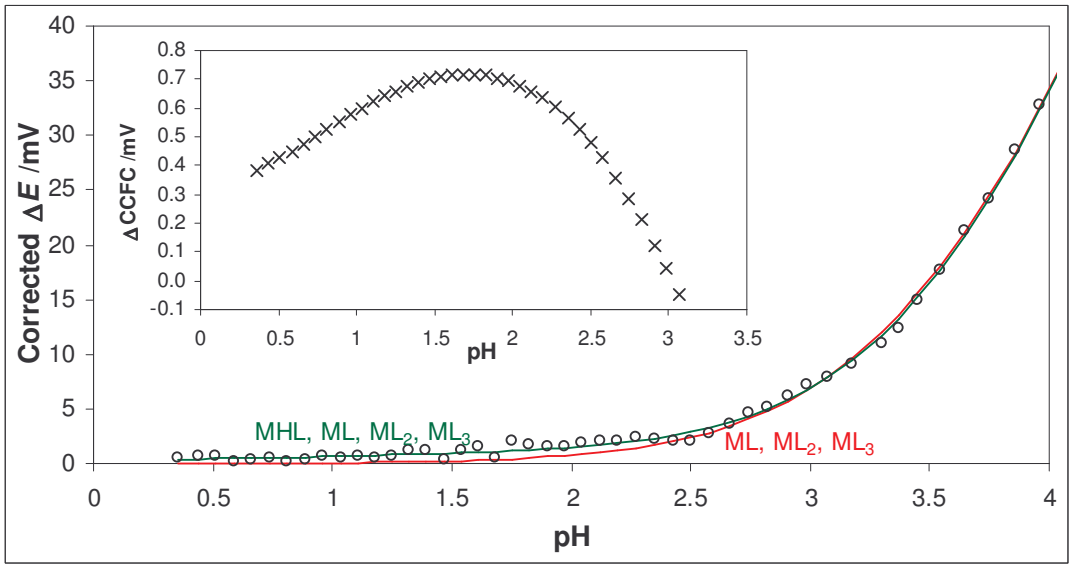

Figure 6.23: The acidic region showing the ECFC and CCFCs in the presence and absence of CdHL. The inset shows the difference between these two calculated curves.

The formation constants determined compare well to the literature values as shown in Table 6.11. The CdHL species has not been suggested before, but

this may simply be due to the experiments always starting above pH 2. The claim that this species exists in solution is still tentative as it is the result of a very small potential shift. Figure 6.24 shows the species distribution diagram determined using the log β values for this work given in Table 6.11 for the two cases where the CdHL species was both included (dotted lines) and excluded (solid lines), and the initial solutions concentrations of Cd(II) and PA were used. A maximum of 11.6% CdHL is formed around pH 1.9 under these conditions showing that this is a minor species. For the higher ligand-to-metal concentration ratio of two hundred, the amount of CdHL formed increases to 19.8%. The experiment was repeated at this higher PA concentration and the results will be discussed shortly.

Table 6.11: Formation constants as determined here and from literature. The standard deviations quoted were determined from the mathematical refinement procedure.

	log β [a]	**log β [a]**	**log β [b]**	**log β [c]**
CdL	4.27 ± 0.03	4.20 ± 0.03	4.29	4.18
CdL_2	7.88 ± 0.03	7.91 ± 0.03	7.89	7.61
CdL_3	10.57 ± 0.02	10.55 ± 0.03	10.49	10.41
CdHL		6.37 ± 0.11		
Overall fit	0.518	0.289		

[a] This work, DCP, 0.25 – 0.5 M H/$NaNO_3$, 25 °C
[b] DPP, 0.5 M H/$NaNO_3$, 25 °C[5] (although the ionic strength should also have been quoted as 0.25 – 0.5 M in this case)
[c] GEP, 0.5 M H/$NaNO_3$, 25 °C[2]

Further work done in this group showed that crystals grown by slow evaporation in diluted nitric acid solutions with pH < 2 containing a 1:1 ratio of $Cd(NO_3)_2$ and PA with initial concentrations of 0.01 M produced $[Cd(NO_3)_2(C_5H_4NHCO_2)(H_2O)_2]$ structures.[18] The ORTEP diagram in Figure 6.25 clearly shows that the pyridine nitrogen atom is protonated and binding to Cd(II) takes place through the two carboxylate oxygen atoms. The species distribution diagrams given in Figure A4.8 (Appendix 4) shows how the percentage CdHL increases in solution as the concentration of both Cd(II) and PA increase which could promote formation of crystallisation of this species on slow evaporation. This structure reinforces the existence of the CdHL species

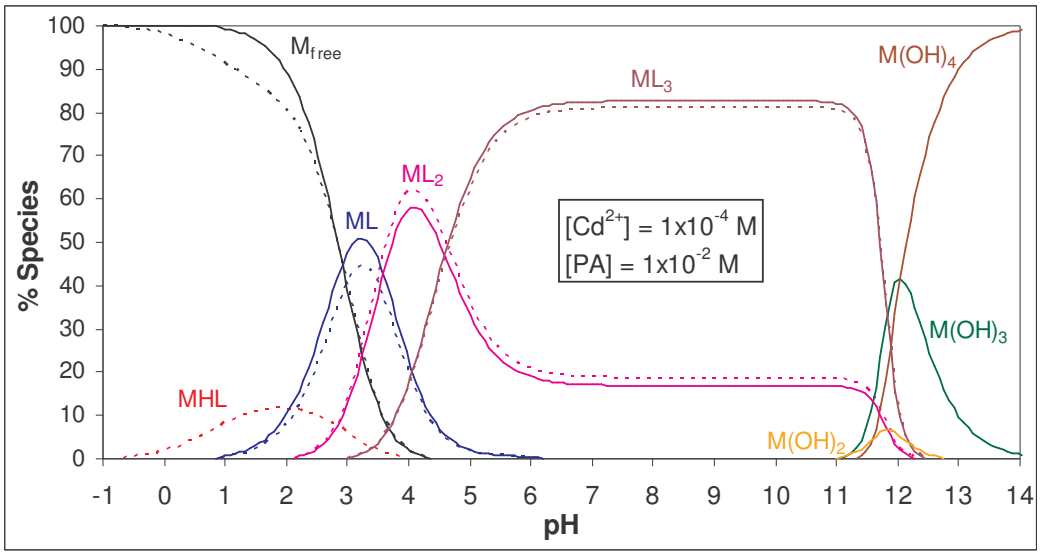

Figure 6.24: Species distribution diagram determined using the log β values derived in this work as given in Table 6.11. The CdLH species was both included (dotted lines) and excluded (solid lines).

in solution. It should be said here that the species distribution curve plotted for the high concentrations may not be totally accurate. It is recommended that these curves be calculated within the limits of the range in which they were determined. Outside this range some additional equilibria may have to be accounted for while others may become negligible.[16]

Shanbhag and Choppin[17] reported on a tracer method that allows for direct measurement of the formation constants for MHL when both ML and MHL are formed. They state[17] that this evaluation is "relatively complicated" when employing potentiometric titrations which, apart from the pH range limitations, is probably why so few values for MHL species are reported. It was interesting to note that for the Eu(III)-malonic acid ($CH_2(COOH)_2$) system they studied, the log β values determined were 4.28 for ML and 6.96 for MHL,[17] which is not too different from those reported here.

In order to assess the other models and approaches considered to account for the junction potential, stability constants were calculated for each case. For the mE models derived from the raw data and data fitted using an exponential function (with the value of *a* fixed), log β values do not deviate by more than

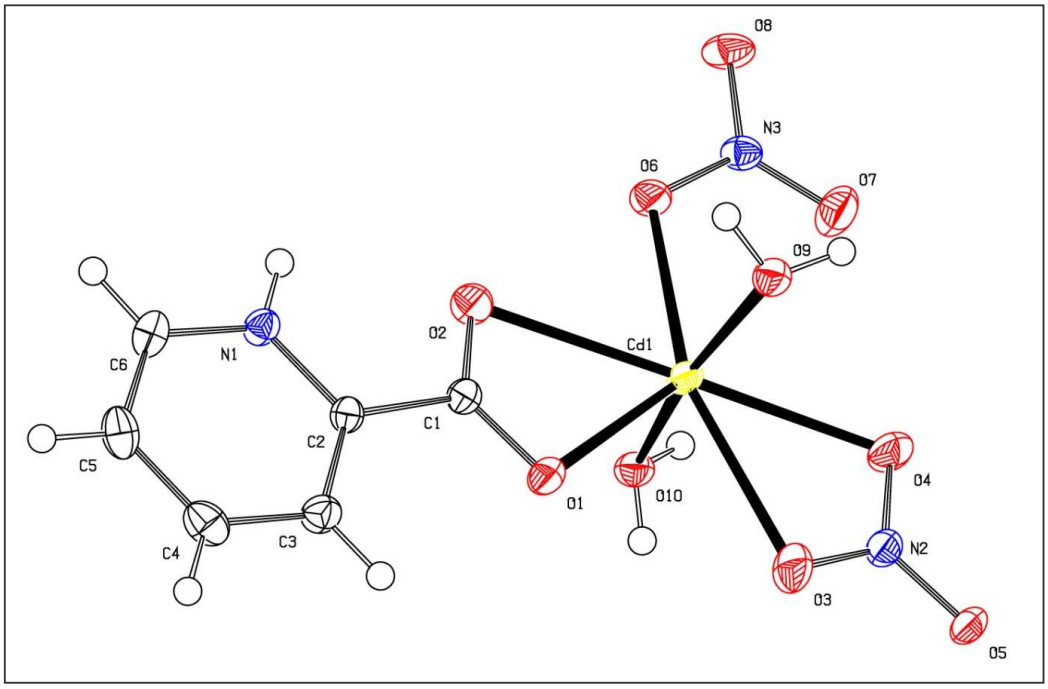

Figure 6.25: ORTEP diagram for the structure $[Cd(NO_3)_2(C_5H_4NHCO_2)(H_2O)_2]$.[18]

0.01 for the CdL, CdL_2 and CdL_3 system which is well within experimental error. However, if CdHL is included in the system the log β values differ by as much as 0.23 for CdHL and 0.08 for CdL. The largest deviations would be expected for these species as they occur in pH regions where corrections to the junction potential are required. The three models mE, mE_j and mNorm produced similar results with log β values within 0.03 of each other for all species. The mNorm2 model values were also comparable except for CdHL which was 0.2 log units larger than from the other models.

In all these cases the free metal ion potential was determined as suggested by using the average difference in $E(M_{free})$ values. For comparison $E(Cd_{free})$ was determined using the half-wave potential of the polarogram collected in solution before ligand was added and then corrected by calculating the magnitude of E_j using the various models. Here again the log β value of CdHL showed the largest variation of up to 1.4 log units which was probably due the percentage change in the shift being greater for this species. Employing the average difference in $E(M_{free})$ values (calculated using data where E_j is negligible) should produce more accurate $E(Cd_{free})$ values than relying on a

single data point and the predicted E_j value at that pH, where E_j is the greatest and the most uncertain.

When the pH titration experiment was repeated, this time with $[PA_T]:[Cd(II)_T]$ = 200.0, the Tl(I) $E_{1/2}$ values gave an unexpected dip between about pH 3 – 6 (see Figure 6.26) which could have been due to the reference system. A question arose as to which points should be averaged to determine the $E(Tl_{free})$. Essentially all points above pH 2.1 were used as the comparison between the predicted and experimental $E_{1/2}$ values were similar to that observed in the previous experiment. Another dilemma was whether the Cd(II) potential data should be corrected in the E_j region only (as before) or could it be assumed that the Cd(II) potentials shifted in a similar manner to the Tl(I) potentials. Both approaches were therefore used to correct Cd(II) potentials (using the mE model derived from the polynomial curve fitting) as shown in Figure 6.27.

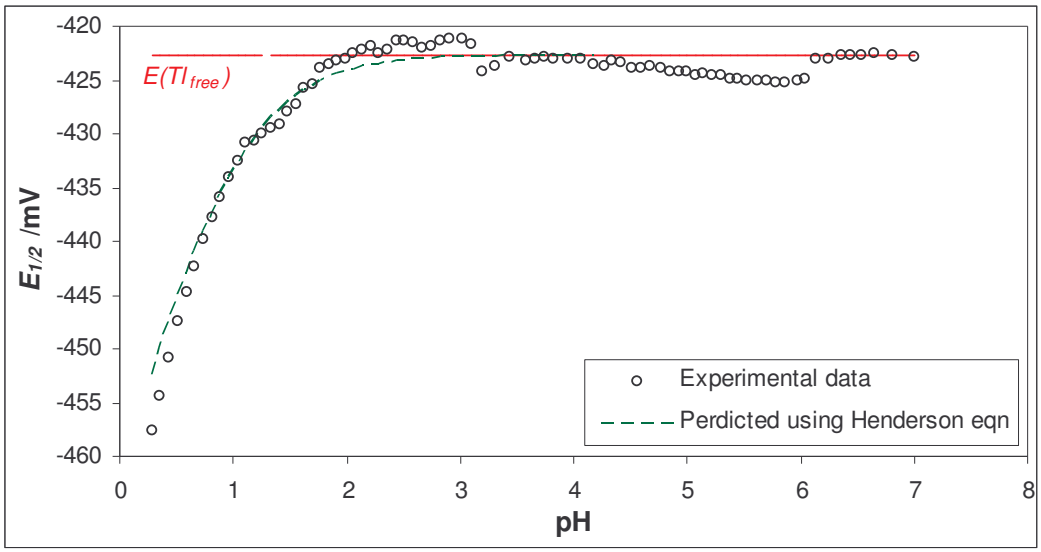

Figure 6.26: Slight erratic behaviour is seen for Tl(I) half-wave potentials as a function of pH, where $[PA_T]:[Tl(II)_T]$ = 100.

The formation constants were assessed as before and the results are given in Table 6.12. There is at most 0.1 log units difference between log β values determined using the two potential correction procedures. Interestingly, the log β values for CdHL determined here were comparable to the values from the

previous experiment which reinforces the presence of this species in solution. Standard deviations for the overall fit were larger when data over the whole pH range was corrected. This was expected since data above pH 2 gave a more erratic trend for the corrected $E_{1/2}$ values than the experimental values (see Figure 6.27). Comparing the log β values also indicated that correcting data in the E_j region only was sufficient in this case.

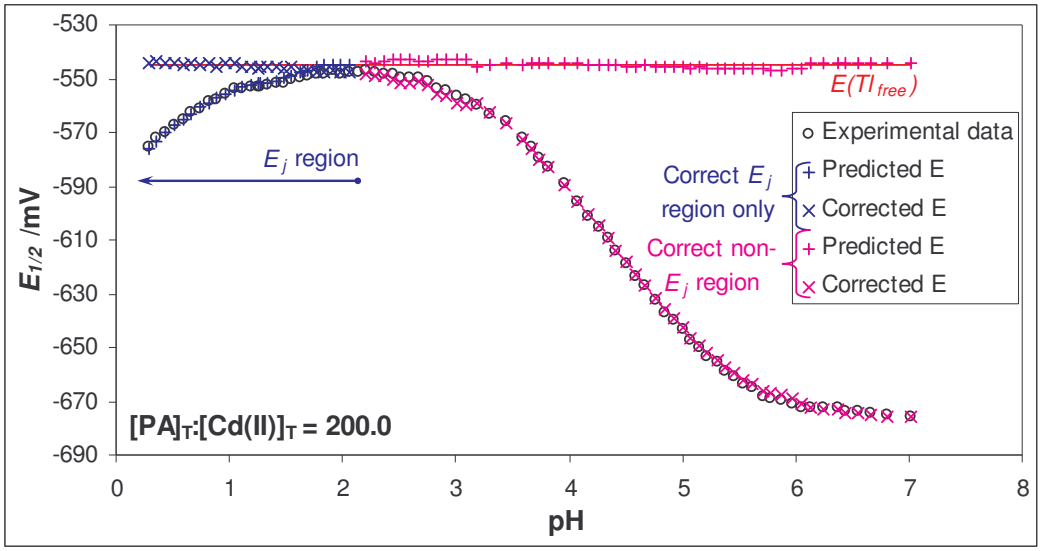

Figure 6.27: Experimental and corrected $E_{1/2}$ values for Cd(II) where Tl(I) data were used to correct these values in the E_j region only or throughout the entire pH region.

Table 6.12: Stability constants using Cd(II) potential data that had been corrected using the mE model and the Tl(I) potential data in either the E_j pH region only or the entire pH range data.

	Corrected $E_{1/2}$(Cd) in E_j region		**Corrected all $E_{1/2}$(Cd) values**	
	log β	**log β**	**log β**	**log β**
CdL	4.29 ± 0.02	4.22 ± 0.03	4.39 ± 0.02	4.32 ± 0.03
CdL_2	7.70 ± 0.03	7.74 ± 0.03	7.62 ± 0.03	7.68 ± 0.03
CdL_3	10.48 ± 0.01	10.47 ± 0.01	10.47 ± 0.01	10.45 ± 0.01
CdHL		6.22 ± 0.10		6.31 ± 0.08
Overall fit	0.622	0.312	1.151	0.705

In the pH titration experiment starting in solutions at pH 2 and with $[PA_T]:[Cd(II)_T]$ = 97.2, Tl(I) was again added to the test solution simply to view the behaviour of the reference system throughout the titration. Figure 6.28 shows that there was some noise in the Tl(I) half-wave potential during the

titration, with values varying between -417.7 and -422.9 mV. This random variation of about ±2.5 mV shows that there was probably some variation in the reference system as it could not be due to any complex formation between Tl(I) and picolinic acid which would be indicated by negative shifts in potential. The value of $E(Tl_{free})$ was determined in two ways, firstly from the measured half-wave potential for the solution at pH 2 before ligand was added, and secondly from the calculated averaged potential values over the entire pH range. These results are also illustrated in Figure 6.28. The measured value for $E(Cd_{free})$ was –541.6 ± 0.8 mV. This value was also calculated by adding -121.4 mV to the calculated value of $E(Tl_{free})$ to give –541 ± 1 mV, which is within the error of the measurement.

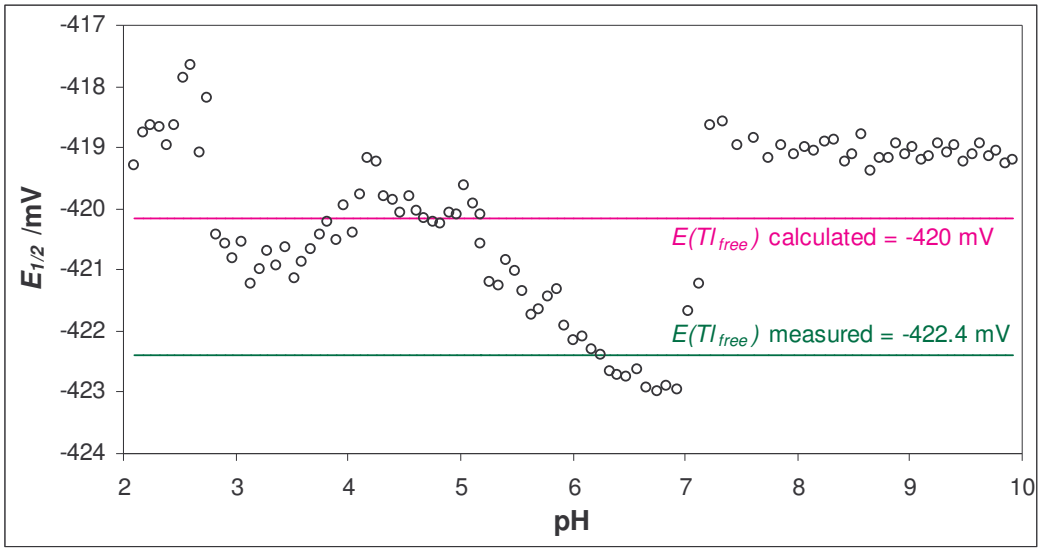

Figure 6.28: Variation of the Tl(I) half-wave potentials as a function of pH probably due to the reference system.

Figure 6.29 shows potential values for the reduction Cd(II) species. Beyond about pH 6 no new species were formed as indicated by the unchanging reduction potentials. These potential values could be used as is, or they could be corrected for the variation observed in the Tl(I) data if it is assumed that the reference system affected the Cd(II) potential data in the same way. Formation constants were determined for both cases and the results are compared in Table 6.13. When experimental data were used, the log β value for CdHL could not be refined, but when the corrected data were used this

value could be refined and was found to be 6.63 ± 0.09. Compared the previous values determined as 6.37 ± 0.11 and 6.22 ± 0.10, this value is about 0.3 log units higher. Considering the species distribution diagram in Figure 6.24 it can be seen that as the pH is raised from pH 2 the amount of CdHL in solution decreases while that of CdL increases rapidly, making the CdHL a minor species in solution and thus more difficult to calculate an accurate log β value. The fact that the values are as close as they are was surprising seen as it was simply based on the variation in $E_{1/2}$ monitored for Tl(I).

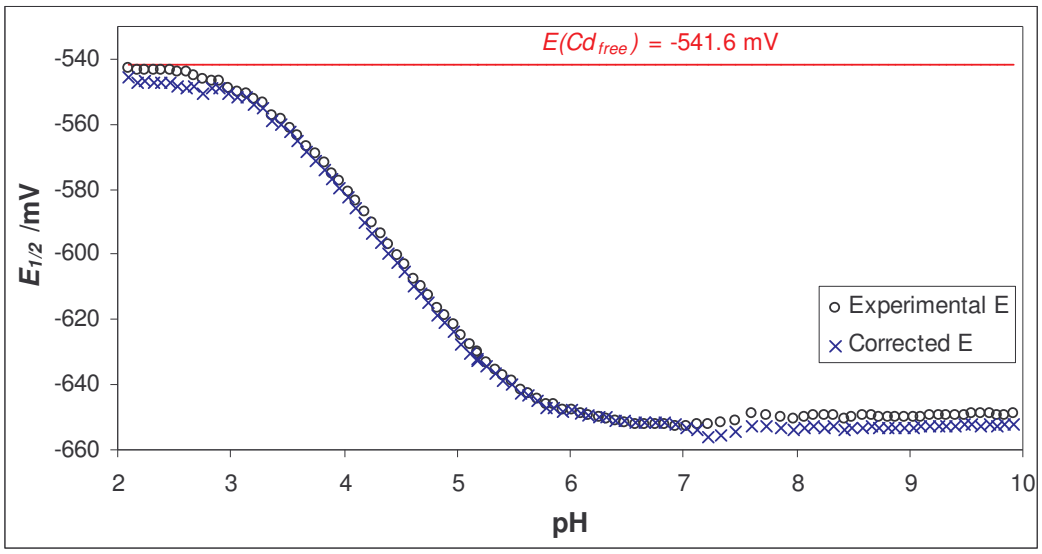

Figure 6.29: Experimental and corrected Cd(II) $E_{1/2}$ values as a function of pH.

Table 6.13: Stability constants quoted as logβ values using experimental half-wave potentials and potentials corrected using Tl(I) data.

Species	Experimental E: log β	Corrected E: log β	log β
CdL	4.21 ± 0.02	4.37 ± 0.02	4.27 ± 0.03
CdL_2	7.62 ± 0.03	7.63 ± 0.03	7.71 ± 0.03
CdL_3	10.41 ± 0.01	10.49 ± 0.01	10.47 ± 0.01
CdHL			6.63 ± 0.09
Overall fit	1.099	1.470	1.208

The ECFCs and CCFCs in Figure 6.30 show the difference for the experimental and corrected data, and the inset highlights the low pH range showing the larger shift that for the corrected data which lead to the inclusion

of the CdHL in the species model. There most definitely was a shift in the reference potential just above pH 7 which resulted in a potential step seen in the experimental Cd(II) data in Figures 6.29 and 6.30, as well as in the Tl(I) data in Figure 6.28. This step disappeared when the Cd(II) potentials were corrected using the Tl(I) data, which gave more confidence to the corrections made in the lower pH range.

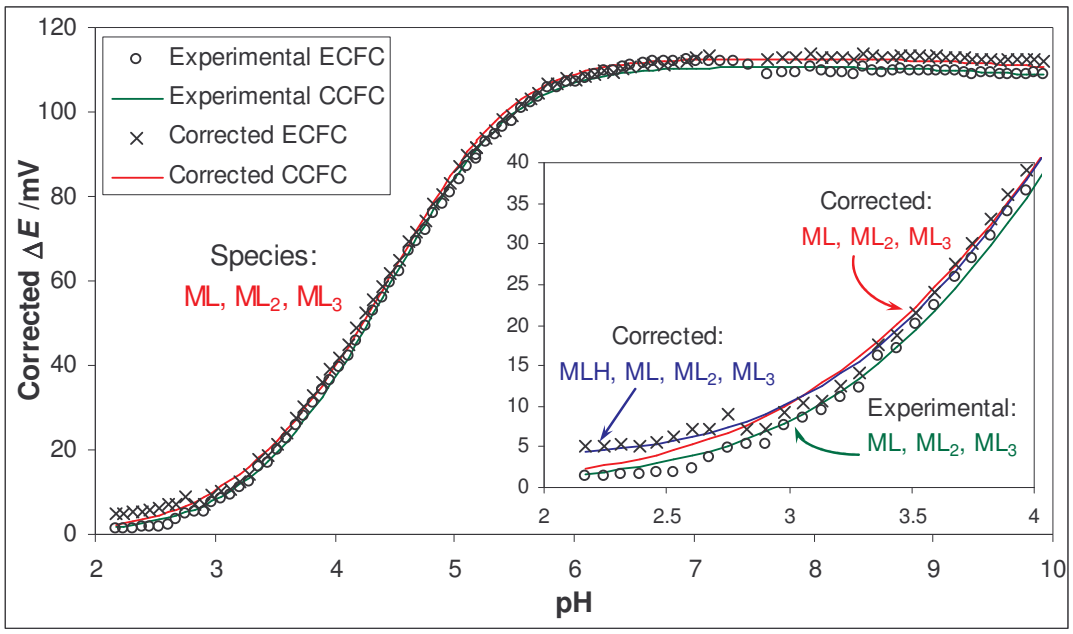

Figure 6.30: The ECFCs and CCFCs for the experimental and corrected potential shift data. The inset highlights the acidic region indicating the presence of the CdHL species for the corrected data.

The results from the three pH titrations were compared and Figure 6.31 shows the ECFC graphs for the three different pH titration experiments. The greater the total ligand-to-metal ion concentration ratio the larger the potential shift, which indicates that higher concentrations of complexes are formed. This ties in with Le Chatelier's Principle as each equilibrium reaction will move to form more products as the concentration of the ligand (a reactant) is increased. Comparing the ECFC's for the titration with $[PA_T]:[Cd_T]$ = 100.5 and for in the titration started at pH 2 $[PA_T]:[Cd_T]$ = 97.2) where the Cd(II) potentials were corrected, it appears from the inset that the potential values at low pH were over corrected. This over correction lead to the comparatively larger log β values for CdL or for CdHL when it was included in the system (see Table

6.14). It is therefore impossible to conclude that all half-wave potentials for Cd(II) follow the same trend as those for Tl(I).

Table 6.14 summarises the log β results for the three pH titration experiments. The standard deviations quoted here were calculated from fitting the CCFC to the ECFC. The average log β values are given in Table 6.15. The averages were calculated for all the values in Table 6.14, as well as for the constants determined using $E_{1/2}(Cd)$ values corrected over whole pH range and then in the E_j pH region only. The standard deviation cited in this table was from averaging the data for the various experiments. The stability constants obtained in this work compared to those in literature under similar conditions[2,5] but their investigation were always started above pH 2.

6.3.9) *Ligand titrations*

Four ligand titration experiments (as described in Section 2.4.4) were performed at pH values of 3.0, 3.8, 5.1 and 2.0. Ligand was added such that the total ligand to metal concentration ratios varied between about 20 and 200. The starting solutions consisted of 25 mL of 9.98×10^{-5} M Cd(II) in a mixture of 0.5 M HNO_3 and 0.5 M NaOH adjusted to the correct pH. For each experiment, a 0.5 M picolinic acid solution was made up and adjusted to the same pH as the starting solution. The picolinic acid solution was added in 0.03 mL increments to ensure about 30 polarograms were collected throughout the titration. Since the pH does not change significantly during these titrations, Tl(I) was omitted from solutions and the half-wave potentials of Cd(II) were used directly to evaluate the formation constants. The graphs of the corrected potential shift versus log [L_{free}] were combined in Figure 6.32. Data from the titration at pH 2.0 will be discussed separately.

To predict which metal-ligand species are in solution, slope analysis was performed on the ECFC plot (as was discussed in Section 2.5.2 using Equation 2.22). Table 6.16 provides the expected slopes for a possible set of reduction reactions and it can be seen that same slope is predicted whether the ligand is in the HL or L form or whether CdL or CdHL is formed. This

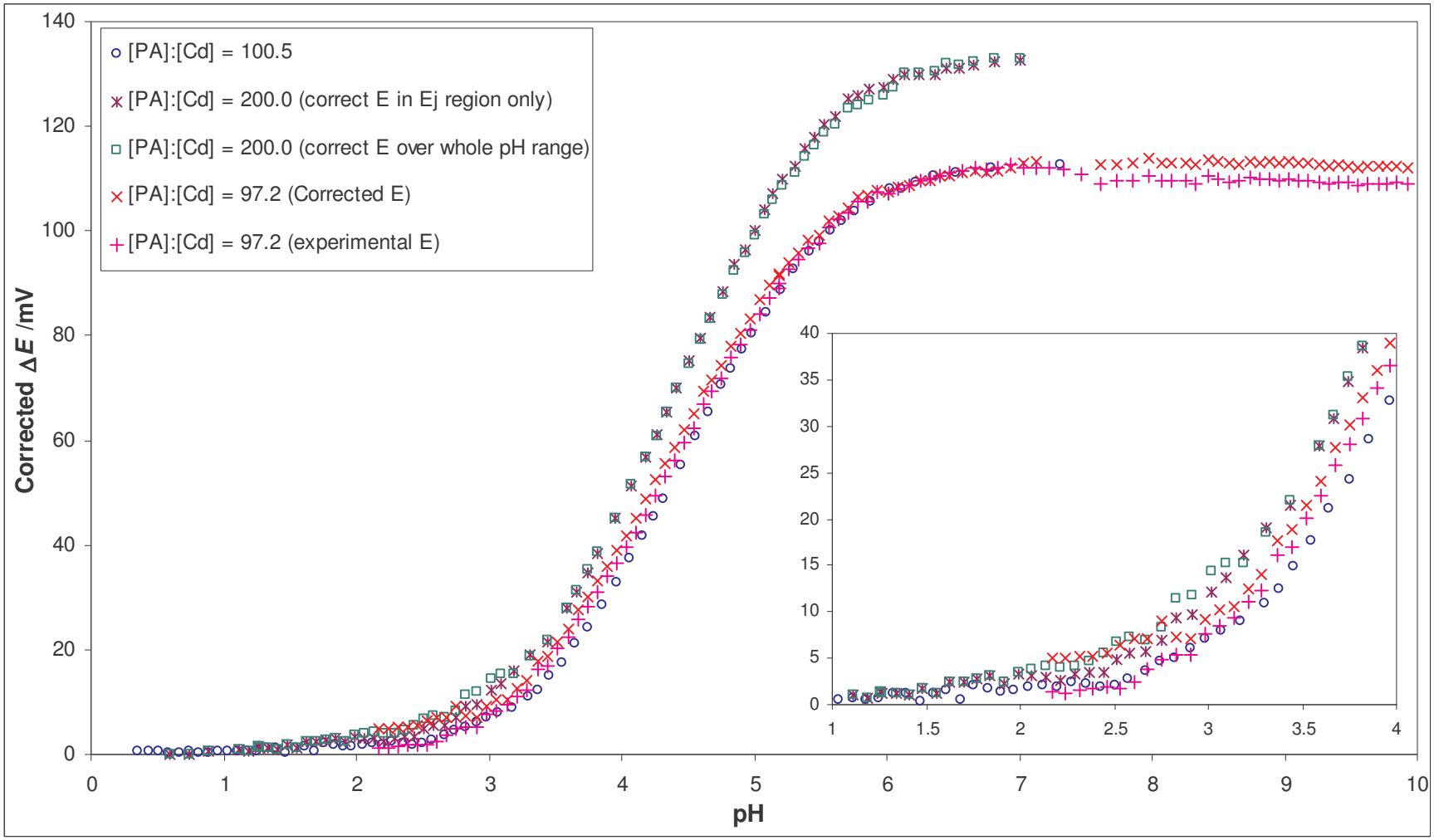

Figure 6.31: Comparison of ECFCs for the three titration experiments. The inset highlights the region where CdHL formation would occur.

Table 6.14: Log β values for the two proposed Cd(II)-PA systems where CdHL is (a) excluded or (b) included. Processes for the correction of potential data are indicted in each case.

$[PA_T]:[Cd_T]$	100.5	100.5	200.0	200.0	97.2	97.2
(a)	**log β [a]**	**log β [b]**	**log β [a]**	**Log β [b]**	**log β [c]**	**log β [b]**
CdL	4.29 ± 0.03	4.27 ± 0.03	4.29 ± 0.02	4.39 ± 0.02	4.21 ± 0.02	4.37 ± 0.02
CdL_2	7.84 ± 0.03	7.88 ± 0.03	7.70 ± 0.03	7.62 ± 0.03	7.62 ± 0.03	7.63 ± 0.03
CdL_3	10.60 ± 0.02	10.57 ± 0.02	10.48 ± 0.01	10.47 ± 0.01	10.41 ± 0.01	10.49 ± 0.01
(b)	**log β [a]**	**log β [b]**	**log β [a]**	**log β [b]**	**log β [c]**	**log β [b]**
CdL	4.24 ± 0.03	4.21 ± 0.03	4.22 ± 0.03	4.32 ± 0.03		4.27 ± 0.03
CdL_2	7.87 ± 0.03	7.91 ± 0.03	7.74 ± 0.03	7.68 ± 0.03		7.71 ± 0.03
CdL_3	10.59 ± 0.02	10.55 ± 0.03	10.47 ± 0.01	10.45 ± 0.01		10.47 ± 0.01
CdHL	6.32 ± 0.13	6.38 ± 0.11	6.22 ± 0.10	6.31 ± 0.08	(not refined)	6.63 ± 0.09

[a] Used Tl(I) data in E_j pH region to correct $E_{1/2}(Cd)$
[b] Used Tl(I) data in whole pH range to correct $E_{1/2}(Cd)$
[c] Used experimental $E_{1/2}(Cd)$

Table 6.15: Average log β values for the two proposed Cd(II)-PA systems.

	log β [a]	**log β [b]**	**log β [c]**	**log β [a]**	**log β [b]**	**log β [c]**	**log β^5**	**log β^2**
CdL	4.30 ± 0.07	4.34 ± 0.06	4.26 ± 0.05	4.25± 0.04	4.27± 0.06	4.23± 0.01	4.29	4.18
CdL_2	7.72 ± 0.12	7.71 ± 0.15	7.72 ± 0.11	7.78 ± 0.10	7.77 ± 0.13	7.81 ± 0.09	7.89	7.61
CdL_3	10.50 ± 0.07	10.51 ± 0.05	10.49 ± 0.10	10.51 ± 0.06	10.49 ± 0.05	10.53 ± 0.08	10.49	10.41
CdHL				6.37 ± 0.16	6.44 ± 0.17	6.27 ± 0.07		

[a] Average of constants in Table 6.14
[b] Average of constants determined using $E_{1/2}(Cd)$ values corrected over whole pH range
[c] Average of constants determined using $E_{1/2}(Cd)$ values corrected in E_j pH region

information was consolidated with the three plots in Figure 6.32. For the titration at pH 3.0 the slope of 30 mV/log unit pointed to CdL being the predominant species in solution which is confirmed by the species distribution diagram in Figure 6.24. At pH 3.8 the slope of 50 mV/log unit indicated the combination of CdL and CdL_2. For the titration at pH 5.1 the slope of 80 mV/log unit at the higher ligand concentrations signified that a combination of CdL_2 and CdL_3 are present but at lower ligand concentrations the slope was closer to 50 mV/ log unit indicating CdL and CdL_2 in solution.

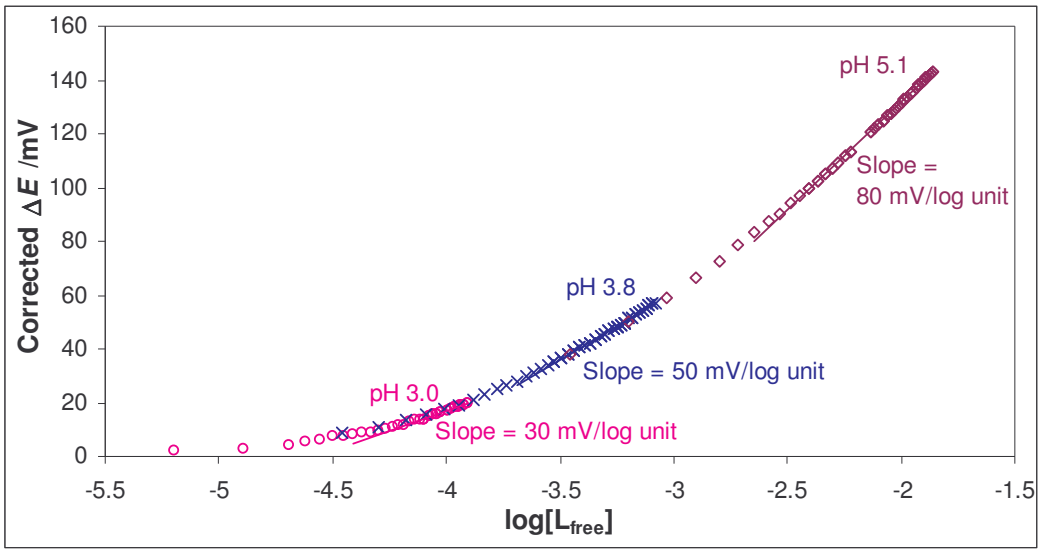

Figure 6.32: Plots of the ECFC showing the slope analysis for three of the ligand titrations at the indicated pH values.

Table 6.16: Predicted slopes (in mV per log unit) of potential versus log [L_{free}] data for the corresponding reduction reactions.

Reduction reaction	Predicted slope
$CdL^{+} + 2e^{-} + H^{+} \rightleftharpoons Cd^{o} + HL$	30
$CdL_2 + 2e^{-} + 2H^{+} \rightleftharpoons Cd^{o} + 2HL$	60
$CdL_3^{-} + 2e^{-} + 3H^{+} \rightleftharpoons Cd^{o} + 3HL$	90
$CdL_2 + 2e^{-} \rightleftharpoons Cd^{o} + 2L^{-}$	60
$CdL_3^{-} + 2e^{-} \rightleftharpoons Cd^{o} + 3L^{-}$	90
$CdHL^{2+} + 2e^{-} \rightleftharpoons Cd^{o} + HL$	30

Using the average of all formation constants as given in Table 6.15 when CdHL was included in the model, the species diagrams of percentage species

versus p[L_T] were plotted (see Figure 6.33) so that the change in solution species could be predicted as ligand is added at each pH. When refining the titration data, stability constants for ML and ML_2 were determined using the pH 3.0 and 3.8 data and for ML, ML_2 and ML_3 when using the pH 5.1 data (see Table 6.17). In the latter case the stability constant for ML was unreliable as this species is only present to a very small extent at this pH. The higher log β value for ML also resulted in a lower log β value for ML_2. Log β values for ML_2 and ML_3 at pH 5.1 were also refined after fixing the log β value for ML as 4.28 (the average of the other two titrations) since this value was not expected to be accurate at pH 5.1. This did result in an increase in the value for ML_2, but it was still lower than that for the other titrations. Plots of the ECFCs and CCFCs are given for each titration in Figure A4.9 (Appendix 4).

Table 6.17: log β values obtained from the ligand titrations at the specified pHs.

pH	3.0	3.8	5.1	5.1
	Log β	**Log β**	**Log β**	**Log β**
CdL	4.26 ± 0.04	4.29 ± 0.03	4.45 ± 0.04	4.28 (fixed)
CdL_2	7.96 ± 0.10	7.99 ± 0.02	7.80 ± 0.04	7.86 ± 0.02
CdL_3			10.33 ± 0.02	10.31 ± 0.01
Overall Fit	0.0827	0.141	0.0448	0.192

To investigate if CdHL is a possible species in solution by ligand titration, an experiment was run at pH 2.0, close to the maximum amount formed in solution according to the species distribution diagram in Figure 6.21. The species distribution diagram with respect to p[L_T] at pH 2.0 (Figure 6.34), also shows that the concentrations of CdL and CdHL would be similar and that the quantities formed in solution would be low.

The ECFC graph was noisy as the largest potential shift measured was about 4.2 mV (see Figure 6.35) and generally an allowance of about 1 mV was permitted for replicate measurements. Accurate stability constants could not be refined from this data, but it was investigated to see whether there is the possibility of the presence of CdHL species at this pH. Log β values were refined either as 4.46 ± 0.04 for CdL or 6.45 ± 0.04 for CdHL, but values for the

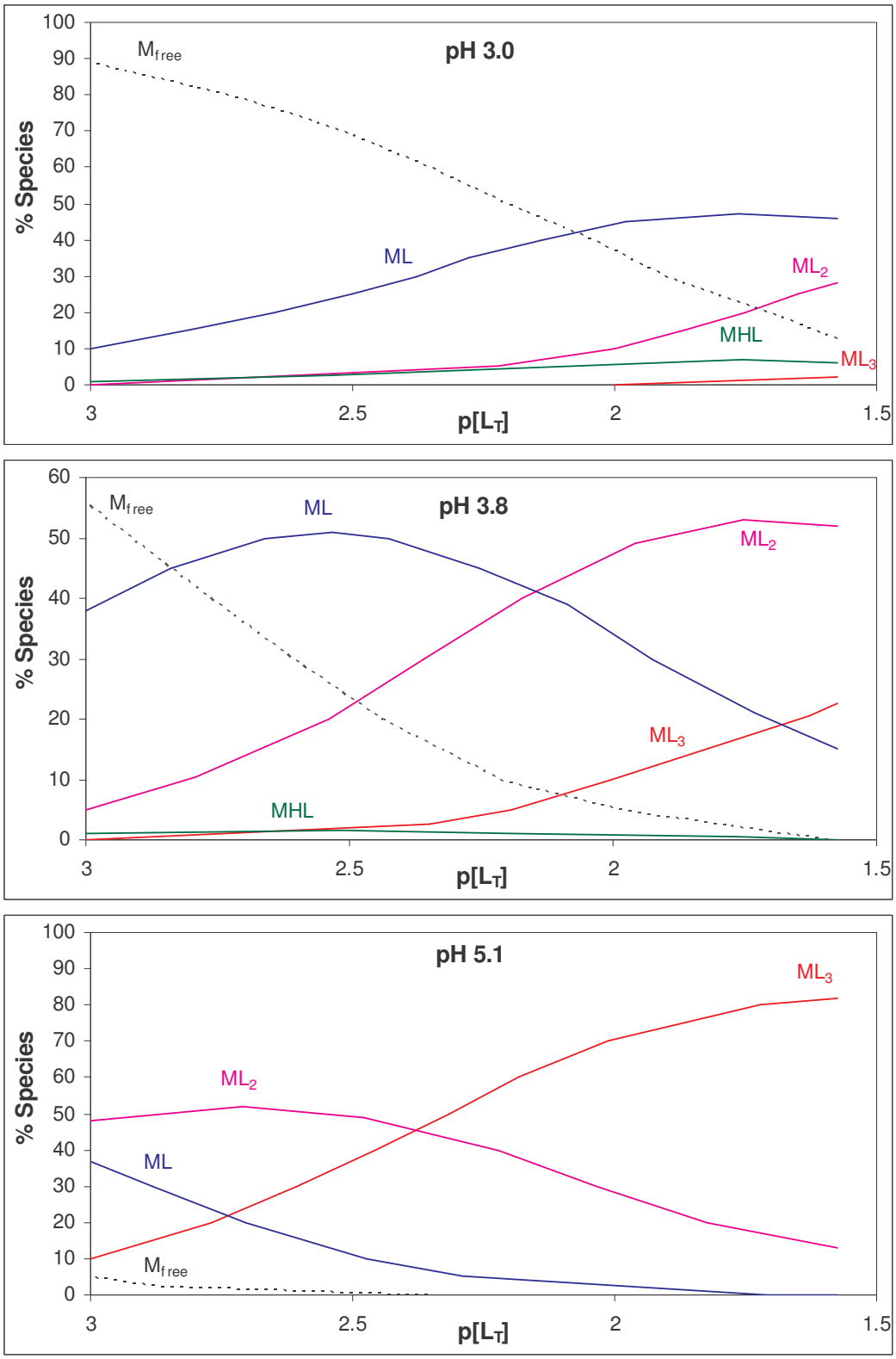

Figure 6.33: Representations of species distribution diagrams at the pHs indicated showing the effect of increasing the concentration of PA resulting in [PA]:[Cd] varying from 10 to 200.

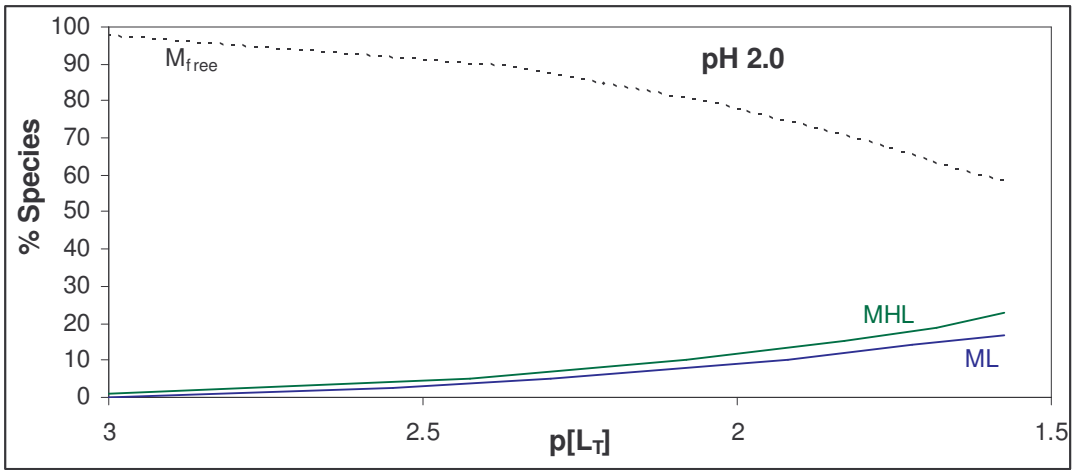

Figure 6.34: Representation of the species distribution diagram to show the predicted the solution species at pH 2.0 in a ligand titration where [PA]:[Cd] varies from 10 to 200.

two species together could not be refined. The ECFC and CCFC's are shown in Appendix 4, Figure A4.10. The value for CdL is higher than determined in other analyses, but when the CFC is calculated using log β values of 4.2 or 4.3, as shown in the same graph, the CCFC is lower than that measured indication that there may be other species in solution. When the CdL_2 species is included in the calculation assuming log β of 8.0, as determined before, only a slight change in the CCFC was observed as shown in Figure 6.35. Log β values 4.3 $\pm$ 0.2 and 9.2 $\pm$ 0.4 were refined simultaneously for the CdL and CdL_2 species respectively. The value for CdL_2 is definitely too high and it was not even predicted to exist in solution at this pH, so this refinement was discarded. Instead, log β values for CdL and CdHL were manually changed and the CCFCs plotted (also shown in Figure 6.35). This seems to indicate that there is a real possibility that the CdHL species is in solution at low pH with a similar log β value predicted from the pH titration experiments. The log β value for CdHL was refined as 6.0 $\pm$ 0.1 when that for ML was fixed at 4.28 (as before).

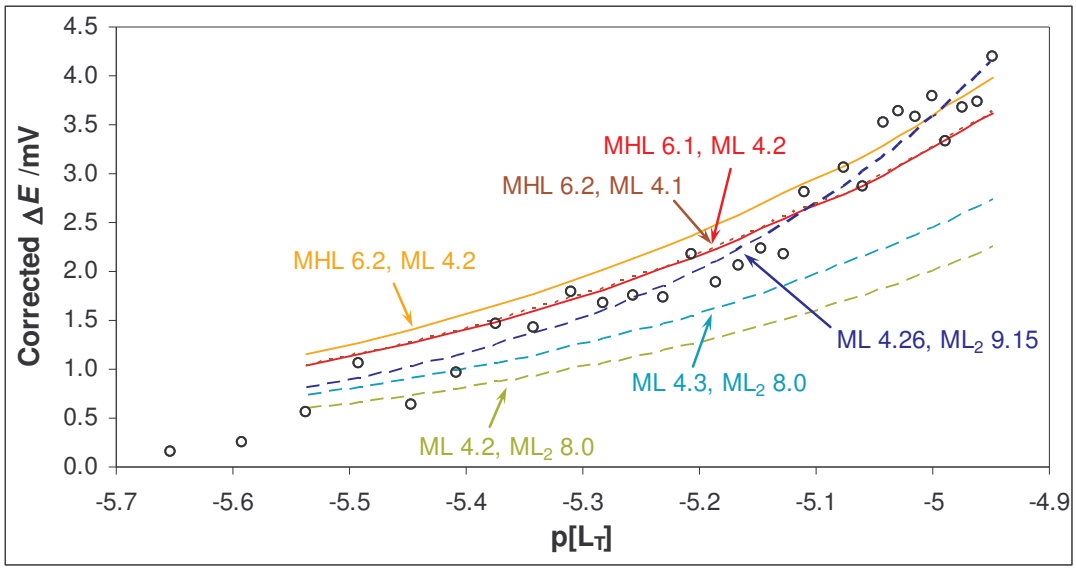

Figure 6.35: ECFC for the ligand titration at pH 2.0. Various CCFCs were calculated and the log β values are denoted next to the species type.

6.3.10) *Evaluating errors in stability constants caused by errors in junction potential correction*

In order to evaluate the error in the stability constants for the procedure developed to correct for the diffusion junction potentials, a hypothetical metal-ligand system was created. Values for stability and protonation constants were loosely based on the Cd(II)-picolinic acid system, but ensuring that complexes exist under more acidic conditions where the junction potential is significant. The species distribution diagram together with the constants used are shown in Figure 6.36. Using conditions similar to those used in the above experiments, current, potential and volume data were simulated for the hypothetical model. Theoretical values for the junction potential were calculated using the Henderson equation and these values were subtracted from the potential data to produce simulated experimental values. Two parameters were evaluated using the witness ion approach when studying metal-ligand equilibria under very acidic conditions, namely the free metal ion potential and the diffusion junction potential. Errors in these parameters were considered separately.

Firstly, the values of the free metal ion potential were varied and the stability constants refined in each case. From experimental data the standard

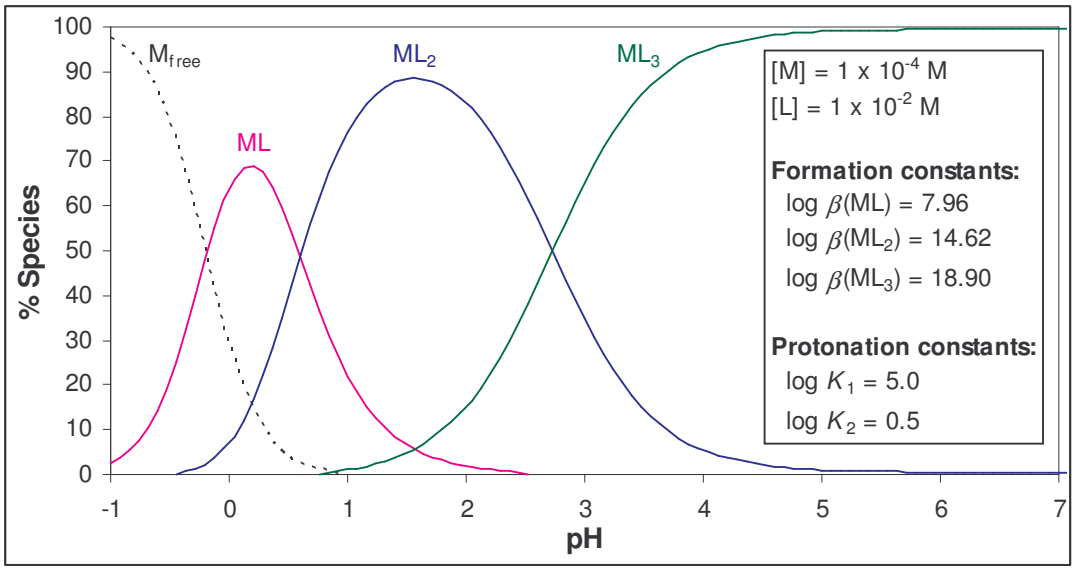

Figure 6.36: Species distribution diagram for the hypothetical metal-ligand system.

deviation for the difference between the $E(Cd_{free})$ and $E(Tl_{free})$ for six data sets was found to be 0.6 mV. Thus the hypothetical value for $E(Cd_{free})$ was varied by ±1 mV and the stability constants refined. The stability constants for all metal-ligand species were affected as the potential shift, i.e. the difference in the free metal ion potential and the potential for the complexed metal ion, is used to assess these constants. A maximum error of ±0.04 log units for the log β values of all the metal-ligand species present was found.

Secondly, the values of the junction potential were varied in a manner observed from experimental data with larger variations at lower pH values. It was previously noted that the maximum difference between the predicted and the experimental Cd(II) potentials for six data sets used to build the ΔE model in the absence of ligand ranged from 0.33 to 1.80 mV. Therefore the calculated junction potential values for Cd(II) were adjusted by ±2 mV at pH 0.3. The adjustments were then slowly reduced such that they approached zero at about pH 2.5 – 3. These adjusted values were then added to the hypothetical experimental potential values as a correction for the junction potential, and the stability constants were then refined. The junction potential adjustment procedure was repeated using slightly different modifications each time according to the behaviour observed with experimental data, but never

adjusting the potential by more than 2 mV. The maximum errors in the log β values were ±0.10 log units for the ML species and ±0.04 log units for the ML_2 species. The ML_3 species was not really affected by the junction potential correction in this case and a maximum error of ±0.01 log units was found. It is therefore extremely important to evaluate the diffusion junction potential as accurately as possible to minimise errors in the stability constants for metal-ligand species formed under very acidic conditions.

6.4) Conclusions

It was found that the diffusion junction potential below about pH 2 becomes significant and has to be taken in to account for metal-ligand equilibria studies. An in-situ monitoring of the junction potential was achieved by introducing a witness metal ion, Tl(I), into the sample solution which did not undergo complexation with the ligand and hence the correction for the diffusion junction potential could be made. An additional potential shift was observed due to the change in ionic strength of the solution throughout the titration and, since the shift was slightly different for Tl(I) and Cd(II), it also had to be accounted for.

Another benefit to the presence of the witness ion was the more accurate calculation of $E(Cd_{free})$ using the $E(Tl_{free})$ value. It is essential that this $E(Cd_{free})$ value be determined as accurately as possible since all potential shifts used to evaluate the formation constants are calculated using this value. A similar approach could also be applied to cases where the free metal ion potential cannot be measured directly at all, such as in the case of Bi(III).

Furthermore, the witness ion could also be used to monitor the performance of the reference system throughout titration experiments under any conditions, not only in the very low pH region. Junction potentials calculated using the Henderson equations gave similar values to those obtained experimentally and hence these calculated values could be used to assess whether the experimental data follows the correct trend.

The junction potential correction using the witness metal ion to monitor and hence correct for the junction potential was successfully applied when investigating the Cd(II)-picolinic acid equilibria and values for the stability constants derived compared very well to those found in the literature.[2,5] An additional minor species, CdHL, was also proposed to exist in the very acidic region. This hypothesis was supported by the ligand titration data at pH 2 and by the crystal structure obtained when the starting liquor solutions were adjusted below pH 2.[18]

The procedures developed here needed to be tested on systems that undergo significant complexation below pH 2 in order to be confident of their validity. The Cu(II)-PA system, which had been studied previously by other techniques, and where the ML species is formed well below pH 2 already, was thus considered.

6.5) References

1) H. Matsui and H. Ohtaki, Bull. Chem. Soc. Jpn, 55 (1982) 2131
2) R. Scharff and M. Paris, Bull. Chem. Soc. Fr., (1968) 3184
3) G. Anderegg, Helv. Chim. Acta, 43 (1960) 414
4) K. Suzuki, M. Yasada, and K. Yamasaki, J. Phys. Chem., 61 (1957) 229
5) I Cukrowski and S.A. Loader, Electroanalysis, 10 (1998) 877
6) J. Ma, J. Wang and N. Li, J. Coord. Chem., 2 (1973) 281
7) L.D. Petit and K.J. Powell, IUPAC Stability Constants Database, IUPAC and Academic Software, 1993-2003
8) A.E. Martell, R.M. Smith and R.J. Motekaitis, NIST Standard Reference Database 46 Version 8.0, NIST Critically Selected Stability Constants of Metal Complexes, Gaithersburg, USA, 2004
9) J. Pons, J. García-Antón, R. Jiménez, X. Solans, M. Font-Bardia and J. Ros, Inorg. Chem. Commun., 10 (2007) 1554
10) J.-P. Deloume and H. Loiseleur, Acta Cryst., B30 (1974) 607
11) C. Papatriantafyllopoulou, C.P. Raptopoulou, A. Terzis, J.F. Janssens, E. Manessi-Zoupa, S.P. Perlepes and J.C. Plakatouras, Polyhedron, 26 (2007) 4053
12) R.A. Coxall, S.G. Harris, D.K. Henderson, S. Parsons, P.A. Tasker and R.E.P. Winpenny, J. Chem. Soc., Dalton Trans. (2000) 2349
13) A.M. Bond, J. Phys. Chem., 74 (1970) 331
14) J.J. Lingane, J. Am. Chem. Soc. 61 (1939) 2099
15) R.A. Robinson and R.H. Stokes, Electrolyte Solutions. The Measurement and Interpretation of Conductance, Chemical Potential and Diffusion in Solutions of Simple Electrolytes, Second Edition, Butterworths, London, 1959
16) G. Berthon, Pure & Appl. Chem., 67 (1995) 1117
17) S.M. Shanbhag and G.R. Choppin, Inorg. Chem., 21 (1982) 1696
18) C. Billing, D.C. Levendis, V. Vieira, S. Afr. J. Chem., 64 (2011) 38

CHAPTER 7

The Study of Copper(II) Complex Formation with Picolinic Acid – A Quasi-Reversible System

7.1) Introduction

7.1.1) *Complex formation of Cu(II) with picolinic acid*

Complex formation of Cu(II) with picolinic acid has been studied in the past and stability constants determined (see Table 7.1).[1] It may therefore be questioned why we are studying these complexes again. Previously techniques such as glass electrode or Cu(II) selective electrode potentiometry and particularly spectrophotometry were used to determine these values. Petitifaux *et al.*[2] determined log β values of 7.9 and 14.75 for the ML and ML_2 species, respectively, by spectrophotometry and 14.88 for ML_2 by polarography at 20 °C and 0.2 M $NaNO_3$. No log β value for ML was obtained by polarography due to the interference of the junction potential.

Table 7.1: Stability constants for Cu(II)-PA complexes at 25°C as given by the NIST database.[1]

Log β_1	Log β_2	Ionic strength /M
7.87	14.78	0.1
	14.70	0.5
7.7	14.5	1.0

Essentially we wanted to test the procedures that were developed thus far for working in very acidic solutions. As will be seen from the species distribution diagram later in this chapter (Figure 7.13), complexation occurs well below pH 2, the pH region of interest in this work. At pH 2 for a ligand-to-metal ratio of 100, 98.5% of Cu(II) is in the CuL_2 form, with the remainder as CuL^+, which starts forming at pH –1 already. In the case of the Cd(II)-PA system under the same conditions, 80 – 89% of Cd(II) was still uncomplexed at pH 2 depending on whether the $CdHL^{2+}$ species was formed or not. The study of the Cu(II) complexes will therefore give a better indication of how well our GE calibration

procedure, the diffusion junction potential correction procedure and the procedure for determining the free metal ion potential performs for very acidic conditions.

7.1.2) *Reduction of Cu(II)*

In complex formation studies in aqueous solutions, background solutions containing perchlorate or nitrate anions are generally used on the assumption that that no complexation or ion paring occurs with the metal ion being studied. At this stage it is known that this is strictly not true. In voltammetry, the interaction of these anions with the metal ion studied has further complications as it could affect the reduction rate of the metal ion. This has been shown to be the case for Cu(II).[3,4] The reduction of Cu(II) in nitrate and perchlorate background electrolytes is dependant on both the pH[4-6] and the ionic strength[3,4] of the solution. Studies have been performed using cyclic voltammetry[3,4] and AC[5] and DC[6] polarography to explain these observations.

Kolthoff and Okinaka[6] showed that Cu(II) was reduced less reversibly in 0.1 M $HClO_4$ than in 0.1 M $NaClO_4$. Hawridge and Bauer[5] suggested that the reduction of Cu(II) in a nitrate background was a "quasi-reversible diffusion-controlled process at high pH" and "a chemical reaction coupled with the electrode process at low pH", where high and low pH refers to pH 5.75 and 1.00, respectively, in that study. At an intermediate pH of 3.40, both processes were significant. Anderson and Shain[4] demonstrated that as the pH was increased, the degree of reversibility also increased for the reduction of Cu(II) in both perchlorate and nitrate media by cyclic voltammetry. The authors did note that the potential shifts observed were greater than would be expected from liquid junction potentials, which was estimated to be about –32 mV at pH 0.

It appears that the mechanism by which the reduction of Cu(II) occurs is complicated, but there is agreement[4-6] agree that the $CuOH^+$ or $Cu(OH)(H_2O)_{5-y}^+$ (where y = 1 to 5) species plays a role at a higher pH. Hawridge and Bauer[5] suggested that the species being reduced would be $Cu(H_2O)_6^{2+}$ in acidic solutions and $Cu(OH)(H_2O)_5^+$ at pH 5.75 (log β for $CuOH^+$ is 6.1)[1], where both

of these species having similar diffusion coefficients (and the assumption was made that nitrate does not complex with Cu(II) significantly). Both species undergo dehydration to various degrees before reduction occurs and at low pH the dehydration reaction is slow enough compared to the rate of electron transfer to result in a quasi-reversible reduction. It appears that $Cu(OH)(H_2O)_5^+$ undergoes more rapid dehydration than the fully aquated form.

Anderson and Shain[4] proposed a more complicated reaction mechanism to explain their observations and the pH dependent reduction of Cu(II). Instead of a one-step two-electron transfer process, they suggested an ECE mechanism that is perturbed by a rapid deaquation prior to charge transfer. The mechanistic scheme was given as follows:[4]

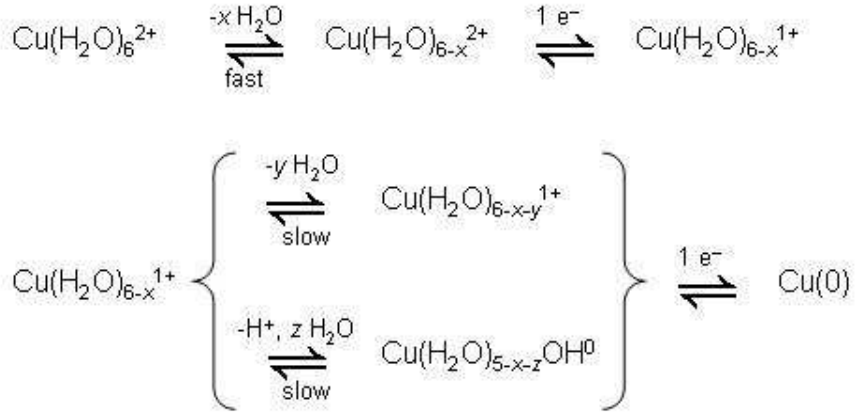

The slow chemical step involves the parallel loss of coordinated water and hydrolysis of Cu(I) with equilibrium favouring the more highly aquated Cu(I) species. Hydrolysis of Cu(II) occurs at higher pH values so it did not play a role in the pH range looked at here. It is likely that in the first fast chemical step, no more than the two Jahn-Teller distorted axial water ligands would be lost before the electron transfer takes place. Additionally, the energy of an ion-water dipole bond in a hydrated metal complex is approximately proportional to the ionic charge and the dipole moment and inversely proportional to the square of the radius of separation. This indicates that the lower charged species are more likely to lose water than the higher charged species.[4] The mechanism was also supported by their studies of oxide films on copper that showed that Cu(I) may hydrolyse at lower pH than Cu(II). It was seen that

Cu_2O formed in the pH range 3 – 5.7 dissolved below pH 3. CuO formed above pH7 and was reduced to Cu_2O as the pH was lowered.[4]

Anderson and Shain[3] also looked at the dependence of Cu(II) reduction with ionic strength in nitrate and perchlorate solutions by cyclic voltammetry. The reduction kinetics of Cu(II) in nitrate solutions is faster than that in the perchlorate solutions and the reduction becomes less reversible in lower ionic strength solutions. This increase in the reduction rate with increasing ionic strength was not large enough to expect a chemical reaction with nitrate to be important.[3] Since nitrate adsorbs more strongly on to the surface of the mercury electrode than perchlorate, it was suggested that an electrostatic interaction of Cu(II) with the adsorbed nitrate ions could also influence the rate of reduction. Alternatively the adsorbed nitrate could act as a conducting bridge between the mercury and the Cu(II), as was previously reported[7] in the case of bridging by carboxylate ions which increased the Cu(II) reduction rate.

Not only does the variation in pH, ionic strength and type of anion in the background solution affect the kinetics of the reduction of Cu(II), but the type of cation ion (where Li^+, Na^+ or K^+ were considered) in the background electrolyte also plays a role at low pH.[5] It was suggested that perhaps the cations affect the preceding chemical reaction and that the more electronegative the cation, the more likely it would interact with or distort the hydration sphere of the Cu(II) species.

7.1.3) *Quasi-reversibility*

The kinetic properties of the electron transfer process have to be considered as the half-wave potential for the reversible reduction is required when evaluating formation constants by the theory employed here. In a reversible electrochemical process, the rate of electron transfer is much faster than the diffusion rate, so the concentrations at the electrode-solution interface are always equal to their equilibrium values and hence the Nernst equation applies.[8] The measured current for a reversible DC wave is thus always diffusion controlled. Delahey[9] suggested that the standard rate constant for the electron transfer process, k^o, should be less than 10^{-2} cm s^{-1}, but as

Gileadi[8] points out, the timescale of the experiment also plays a role. This in reiterated in Bond's[10] description of "practical reversibility" which states that thermodynamic equations (in this case the Nernst equation) apply when signs of disequilibrium cannot be detected, whether this be due to the perturbations applied to the system being small enough or the system reaching equilibrium fast enough as compared to the measurement time.

For an irreversible electrochemical process the rate of electron transfer is much slower than the rate of transport; Delahey[9] suggested $k^o < 5\times10^{-4}$ cm s^{-1}. In quasi-reversible processes the rates of electron transfer and transport are comparable and $10^{-2} < k^o < 5\times10^{-4}$ cm s^{-1}.[9,11] Figure 7.1 illustrates the more drawn out DC waves for slower electron transfer processes, but that at sufficiently high overpotentials the current eventually reaches the diffusion limited current, i_d, irrespective of the electron transfer kinetics.

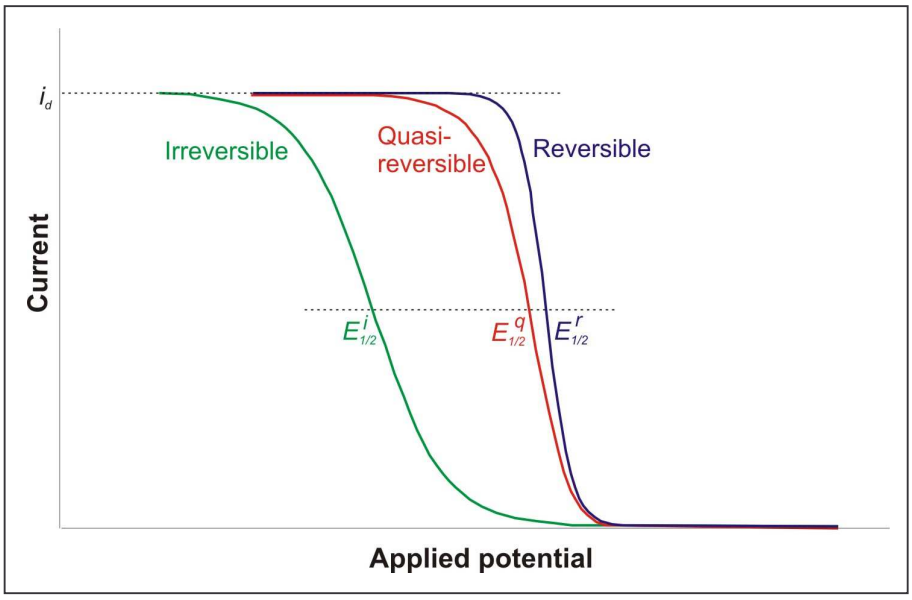

Figure 7.1: Examples of DC waves showing reversible, quasi-reversible and irreversible electron transfer processes. In all cases the number of electrons transferred is the same. $E^r_{1/2}$, $E^i_{1/2}$ and $E^q_{1/2}$ refer to the reversible, irreversible and quasi- reversible $E_{1/2}$ values, respectively.

Dealing with fully reversible processes is straight forward, but it is far more complicated for quasi-reversible processes especially since the extent of "quasi-reversibility" is often pH dependent and thus varies for polarograms

determined throughout a titration experiment. Several approaches to determine the reversible half-wave potential from quasi-reversible DC waves were considered.

Matsuda and Ayabe[12-14] gave the relationship to describe a quasi-reversible DC wave as:

$$\log\left\{\frac{(i_d - i)}{i}\right\} = \log\left\{\exp\left(\frac{nF}{RT}(E - E^r_{1/2})\right) + (1.13/\Lambda\tau^{1/2})\exp\left(\frac{\alpha nF}{RT}(E - E^r_{1/2})\right)\right\} \tag{7.1}$$

where

$$\Lambda = k_s\left(\frac{\gamma_{ox}}{D^{1/2}_{ox}}\right)^{1-\alpha}\left(\frac{\gamma_{red}}{D^{1/2}_{red}}\right)^{\alpha} \tag{7.2}$$

for simple metal ions and $E^r_{1/2}$ is the reversible half-wave potential; τ is the drop life time; α is the cathodic transfer coefficient; k_s is the rate constant for the reduction of the ion; γ is the activity coefficient; D is the diffusion coefficient; and subscripts *ox* and *red* refer to the simple metal ion and the reduced species . For complexed metal ions the value of Λ becomes:

$$\Lambda = (k_s)_B\left(\frac{\gamma_N}{D^{1/2}_N}\right)^{\beta}\left(\frac{\gamma_{red}}{D^{1/2}_{red}}\right)^{\alpha}(f_X c_X)^{-\beta q + p} \tag{7.3}$$

where β is the anodic transfer coefficient; $(k_s)_B$ is the rate constant for the overall electrode reaction of the reduction of the complex ion; c_X is the concentration of the ligand; subscripts *N* and *X* refer to the complex ion and the ligand respectively; and *p* and *q* are the number of ligands in the electroactive and electroinactive complexes, respectively.

The plot of $\log\{(i_d - i)/i\}$ versus E for a quasi-reversible DC polarogram does not produce a straight line (as is the case for reversible or irreversible polarograms), but rather a curve. Graphical methods to determine $E^r_{1/2}$ from this plot for a quasi-reversible processes could be applied. Koryta[15] extrapolated the asymptote from the foot of the wave to the *E*-axis where $\log\{(i_d - i)/i\} = 0$ and the intercept corresponded to $E^r_{1/2}$.[16] Matsuda and

Ayabe[12-14] first determined the irreversible half-wave potential, $E_{1/2}^{i}$, by extrapolating the asymptote from the top of the wave to the *E*-axis and the value of α was determined from the slope of this asymptote as follows:

$$\alpha = \frac{2.303RT}{nF}(\text{slope}) \tag{7.4}$$

The current and potential value at a single point ($E_{1/\gamma+1}$; γ) is taken at the foot of the wave and $E_{1/2}^{r}$ is calculated as follows:

$$E_{1/2}^{r} = E_{1/\gamma+1} - \frac{2.303RT}{nF}\log\left\{\gamma - \exp\left(\frac{\alpha nF}{RT}(E_{1/\gamma+1} - E_{1/2}^{i})\right)\right\} \tag{7.5}$$

Ružić *et al.*[16] proposed a slightly different graphical approach where both $E_{1/2}^{r}$ and α could be evaluated using the entire polarogram. The relationship given is:

$$\log\left\{\frac{(i_d - i)}{i}\right\} = \log\left\{\exp\left(\frac{nF}{RT}(E - E_{1/2}^{r})\right) + \exp\left(\frac{\alpha nF}{RT}(E - E_{1/2}^{i})\right)\right\} \tag{7.6}$$

When comparing equations 7.1 and 7.6 it is seen that:

$$\exp\left(\frac{\alpha nF}{RT}(E - E_{1/2}^{i})\right) = (1.13/\Lambda\tau^{1/2})\exp\left(\frac{\alpha nF}{RT}(E - E_{1/2}^{r})\right) \tag{7.7}$$

From the plot of $\log\{(i_d - i)/i\}$ versus *E*, the way in which α and $E_{1/2}^{r}$ are evaluated depends on the difference between $E_{1/2}^{i}$ and $E_{1/2}^{r}$. For the case where $E_{1/2}^{i} - E_{1/2}^{r} \geq 2RT/nF = 51/n$ mV at 25 °C, the approach is the same as that used by Koryta.[16]

In all these graphical approaches, i_d has to be evaluated initially and the background current also has to be subtracted. These parameters can be determined by fitting equation 2.15 for the DC wave. A number of non-linear curve fitting procedures have also been suggested using these relationships.

Morales *et al.*[11] proposed a slight modification to Ružić's equation[16] by introducing the parameter *f* as follows:

$$\log\left\{\frac{(i_d - i)}{i}\right\} = \log\left\{\exp\left(\frac{nF}{RT}(E - E^r_{1/2})\right) + f\exp\left(\frac{\alpha nF}{RT}(E - E^i_{1/2})\right)\right\} \quad (7.8)$$

where f ranges between 0.77314 and 1.1634 and it is given by:

$$f = \frac{2}{A\sqrt{\pi}}[1 + a(e^{bF(\chi)} - 1)] \quad (7.9)$$

where

$$F(\chi) = \frac{i}{i_d}\left(1 + e^{\frac{nF}{RT}(E - E^r_{1/2})}\right) \quad (7.10)$$

and a = -0.22281, b = 0.91855 and A = 0.96986. Furthermore, a general equation as a function of the quasi-reversible potential, $E^q_{1/2}$, defined as the potential where $i = i_d/2$ holds for polarograms with any degree of reversibility, is given as:

$$\frac{i_d - i}{i} = R\, e^{\frac{nF}{RT}\left(E - E^q_{1/2}\right)} + f\, I\, e^{\frac{\alpha nF}{RT}\left(E - E^q_{1/2}\right)} \quad (7.11)$$

where

$$R = e^{\frac{nF}{RT}(E + E^q_{1/2} - E^r_{1/2})} \quad (7.12)$$

and

$$I = e^{\frac{\alpha nF}{RT}(E + E^q_{1/2} - E^i_{1/2})} \quad (7.13)$$

The values of R and I lie between 0 and 1. Morales *et al.*[11] developed software to determine the values of $E^r_{1/2}$, $E^i_{1/2}$ and α by fitting data from a DC polarogram with this new equation using a non-linear curve fitting method.

Cukrowski *et al.*[17] and Mkwizu[18] also applied non-linear curve fitting to DC polarograms using the relationships by Matsuda and Ayabe[12-14] (equation 7.1) and Ružić *et al.*[16] (equation 7.6) in order to determine the values of i_d and $E^r_{1/2}$ for metal-ligand equilibria studies. To apply the relationships directly to measured polarograms, equations 7.1 and 7.6 were rearranged and a background current included as follows, respectively:

$$i = \frac{i_d}{\exp(nF/RT)(E - E^r_{1/2}) + \Gamma\exp(\alpha nF/RT)(E - E^r_{1/2}) + 1} + i_{bkgnd} \qquad (7.14)$$

where $\Gamma = 1.13/\Lambda\tau^{1/2}$ which was refined as a single value, and

$$i = \frac{i_d}{\exp(nF/RT)(E - E^r_{1/2}) + \exp(\alpha nF/RT)(E - E^i_{1/2}) + 1} + i_{bkgnd} \qquad (7.15)$$

Cukrowski and Zhang[19] estimated the value of $E^r_{1/2}$ from the plot of the quasi-reversible polarogram itself. The polarogram was first fitted using equation 2.15 to obtain the values of i_d and the variables in the background current and for a quasi-reversible reduction, $\delta < 1$. The data were fitted using this equation once more by setting $\delta = 1$ and removing points at the top of the slope of the polarogram so that the fitted curve passes through all remaining points, particularly those at the foot of the wave and where the current is diffusion limited. The only parameter refined in this case is $E_{1/2}$ which should correspond to $E^r_{1/2}$.

7.2) Aims

Picolinic acid complexes Cu(II) below pH 0 already, so it was an ideal system to test the protocols developed for studying complex formation under very acidic conditions. The log β values obtained here could be compared to values in the literature, especially the critically assessed values. Once confidence is gained in these procedures, it could be applied to the unknown Bi(III)-ligand systems. Additionally, it has been reported[20-23] that Bi(III) is not reversibly reduced in "non-complexing" media. Since Cu(II) is also not reduced reversibly, and the potential at which these two metal ions are reduced are very similar, ways of determining the reversible $E_{1/2}$ value can be tested and finalised on a known system.

7.3) Results and Discussion

Experiments were performed as described in Chapter 2. The initial concentrations of Cu(II) and Tl(I) were 9.97×10^{-5} M and 1.99×10^{-4} M, respectively. For the pH titrations the 0.5 M HNO_3 solution containing the metal ions was titrated with 0.5 M NaOH. Polarograms were collected between 0.15 and –0.70 V using a 1 s drop time and a 60 ms current integration time. The reduction of Cu(II) was quasi-reversible both in the presence and absence of picolinic acid. In hindsight, since $E_{1/2}$ is dependent on the drop time for quasi-reversible waves, unlike that for reversible waves,[9,24] a longer drop time could have resulted in the polarograms being more reversible and having values of δ varying over a narrower range closer to unity.

7.3.1) *Background electrolyte*

The species distribution diagram was plotted (Figure 7.2) for Cu(II) in aqueous nitrate background electrolyte using data in Table 7.2. The Cu(II) nitrate species are weak species and about 70% of Cu(II) remains uncomplexed by nitrate in the acidic region. Hydrolysis of Cu(II) starts around pH 5.5 under these conditions, so it does not affect the titration performed in the absence of ligand.

Table 7.2: Formation constants, as log β values, for Cu(II) hydroxide and nitrate species at 25 °C.[1]

Species	Log β	μ /M	Species	Log β	μ /M
$Cu(OH)^+$	6.1	0.1	$Cu(NO_3)^+$	(–0.13)	0.5
	6.1	0.5	$Cu(NO_3)_2$	–0.6	1
$Cu_2(OH)^{3+}$	7.7 [a]	3			
	8.4 [b]	3			
$Cu_2(OH)_2^{2+}$	16.8	0.1			
	16.7	0.5			
$Cu_3(OH)_4^{2+}$	33.7	0.1			

[a] Background electrolyte is $NaClO_4$
[b] Background electrolyte is $LiClO_4$

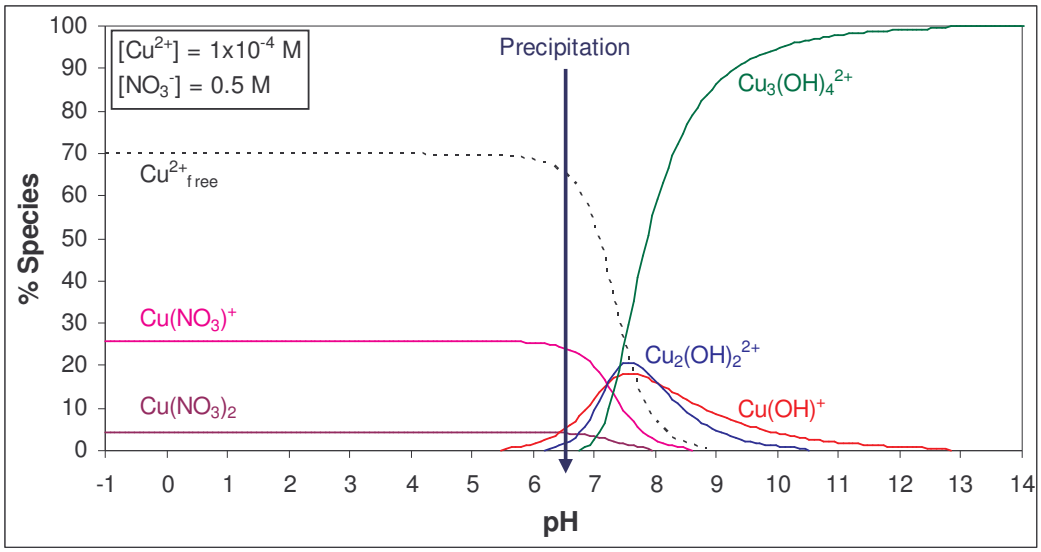

Figure 7.2: Species distribution diagram for Cu(II) in an aqueous nitrate solution at 25 °C. Precipitation of $Cu(OH)_2$ was predicted using log K_{sp} of –18.9.[1]

7.3.2) *Determining reversible half-wave potentials from quasi-reversible polarograms*

The Tl(I) and Cu(II) reduction waves were fitted separately because of the background currents due to hydrogen evolution close to the Tl(I) wave, as well as mercury oxidation close to the Cu(II) wave as indicated in Figure 7.3. Each wave was fitted using the DC wave equation (equation 2.15) where the background current was accounted for by a straight line (for the capacitance current) and an exponential term for the additional Faradaic process in each case. As before, hydrogen evolution was only evident in the low pH solutions. When fitting the Cu(II) reduction wave, points with the most curvature due to mercury oxidation were omitted. The values of $E_{1/2}$, i_d and δ for each reduction process was thus obtained.

In Figure 7.4 it was seen that the value of δ was generally below 0.9 and it decreased as the pH was increased. This indicated that the reduction of Cu(II) in nitrate (under the specific polarographic conditions) was a quasi-reversible process. These titrations were terminated before hydrolysis could occur, so the $Cu(OH)^+$ species did not play a role in the decreasing reversibility, but was probably rather due to the decrease ionic strength on dilution.

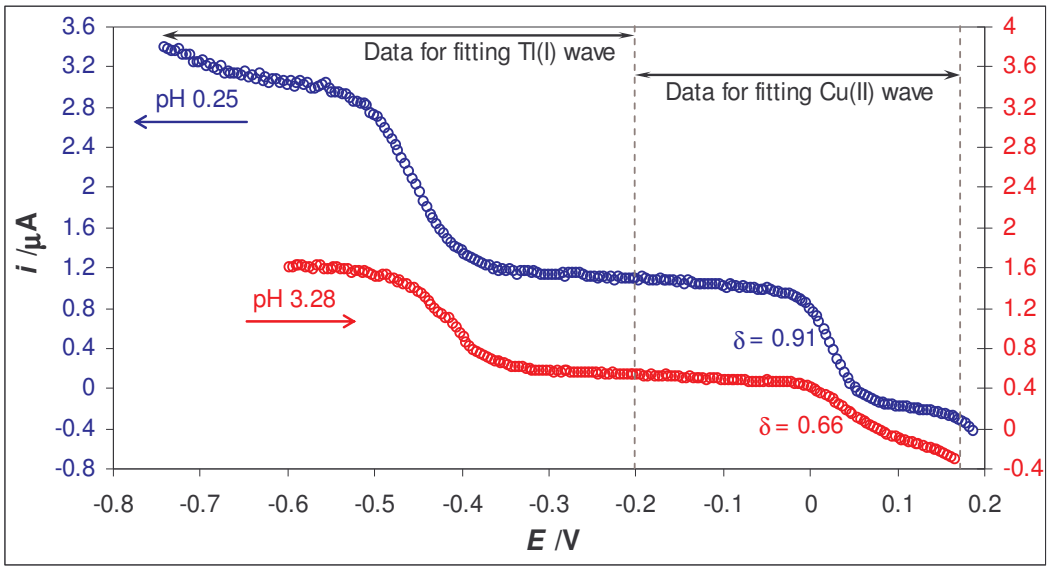

Figure 7.3: Polarograms for the reduction of Cu(II) and Tl(I) in a nitrate medium at pH 0.25 and 3.28.

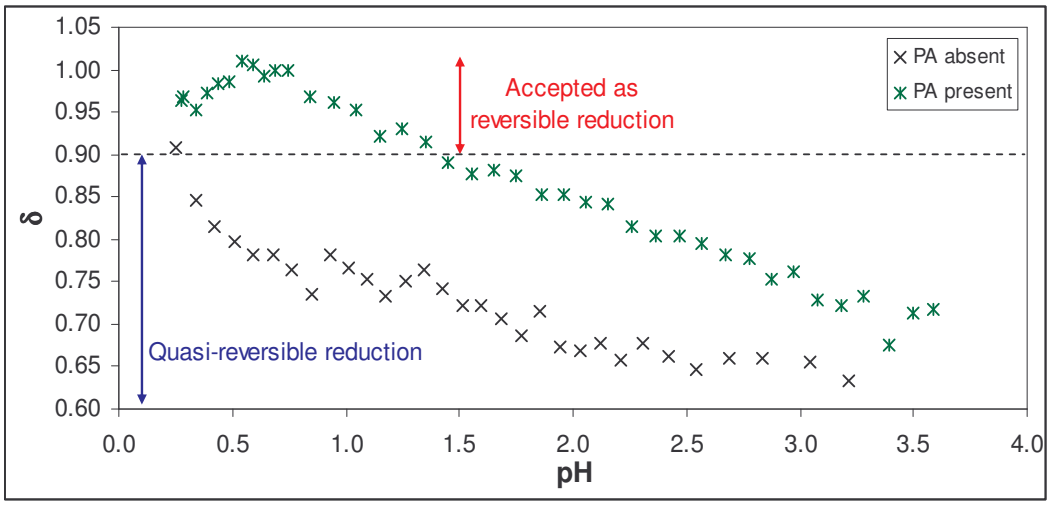

Figure 7.4: The value of δ illustrating the change in the electron transfer rate for the reduction of Cu(II) in a nitrate background in the absence or presence of PA (where [PA]:[Cu(II)] = 103) as a function of pH.

The reduction of the Cu(II)-PA species seemed to be more reversible than the hydrated or $Cu(NO_3)_x^{+(2-x)}$ species (where x = 1 or 2). The amount of gelatine added played a far bigger role in the reduction of Cu(II) than Cd(II). If insufficient gelatine was added, current maxima were formed on the Cu(II) reduction wave, particularly as the solution was diluted during the titration. If too much gelatine was added, it appeared as though the rate of electron

transfer for the Cu(II) reduction was even slower, but it may simply be a distortion of the polarographic wave as suggested by Crow.[25] It has been reported[6] that anionic surface-active substances resulted in the Cu(II) reduction waves being more reversible, whereas cationic and non-ionic suppressants distort the wave and can even split the wave. Gelatin is only negatively charged in neutral and basic solutions and is positively charged in acidic solutions.[6] A maxima suppressant such as sodium dodecyl sulphate (i.e an anionic surface-active agent) should rather be used for the study of complex formation of Cu(II) by polarography in future.

Various ways to determine the reversible half-wave potential ($E^r_{1/2}$) from the quasi-reversible waves were attempted. As i_d is independent of the extent of reversibility, these values, as well as the variables for the background current, were kept the same as that obtained in the initial fitting process using the DC wave equation.

Firstly, the process used by Cukrowski and Zhang[19] was employed to determine $E^r_{1/2}$. Figure 7.5 gives an example of a Cu(II) reduction wave showing the fitted DC wave function (blue line) giving a δ value of 0.722. To determine $E^r_{1/2}$, the value of i_d and the background current parameters were unchanged and the value of δ was set equal to unity. The points indicating a steady state diffusion limited current and the points at the foot of the wave were retained (indicated by ○), but points on the slope of the curve showing the process to be quasi-reversible were deleted (indicated by ×) and the $E_{1/2}$ value was refined. Exactly how many points to delete was decided by ensuring that the fitted curve passed through the remaining points when deleting the fewest possible data points. This process became more challenging when fitting waves collected at higher pH where δ was smaller and the Cu(II) wave laid even closer to the mercury oxidation wave (see Figure A5.1, Appendix 5). The $E_{1/2}$ values determined in this way were taken as $E^r_{1/2}$ values and the results for a pH titration are shown in Figure 7.6 together with the values of $E^q_{1/2}$ determined using the DC wave equation. The $E_{1/2}$ predicted

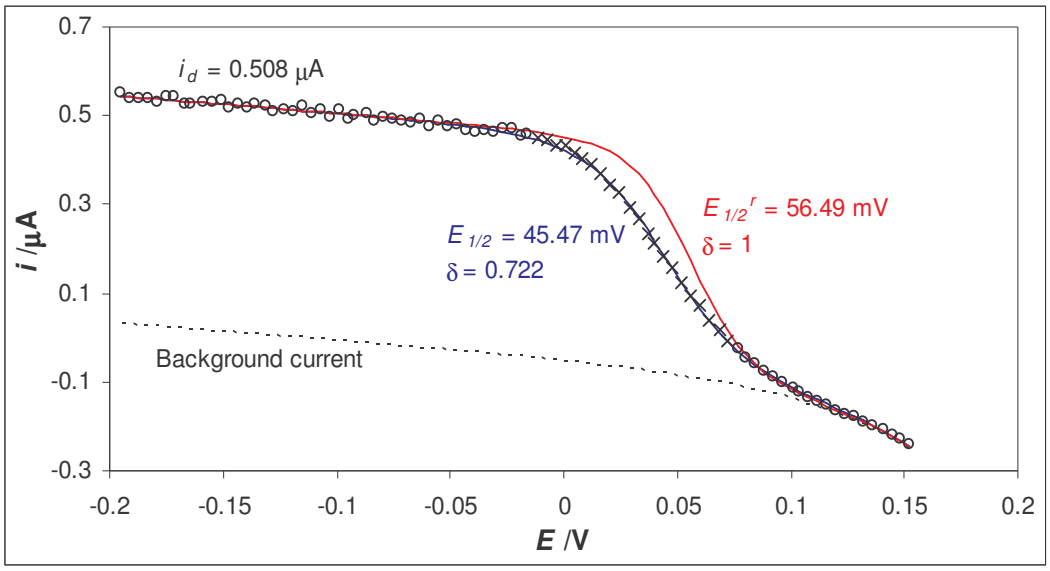

Figure 7.5: Polarogram for the reduction of Cu(II) at pH 1.51. The polarogram was fitted using the DC wave equation through all points (—) or only though the points indicated by ○ (points × were removed) and fixing δ = 1 (—) to estimate $E^{r}_{1/2}$.

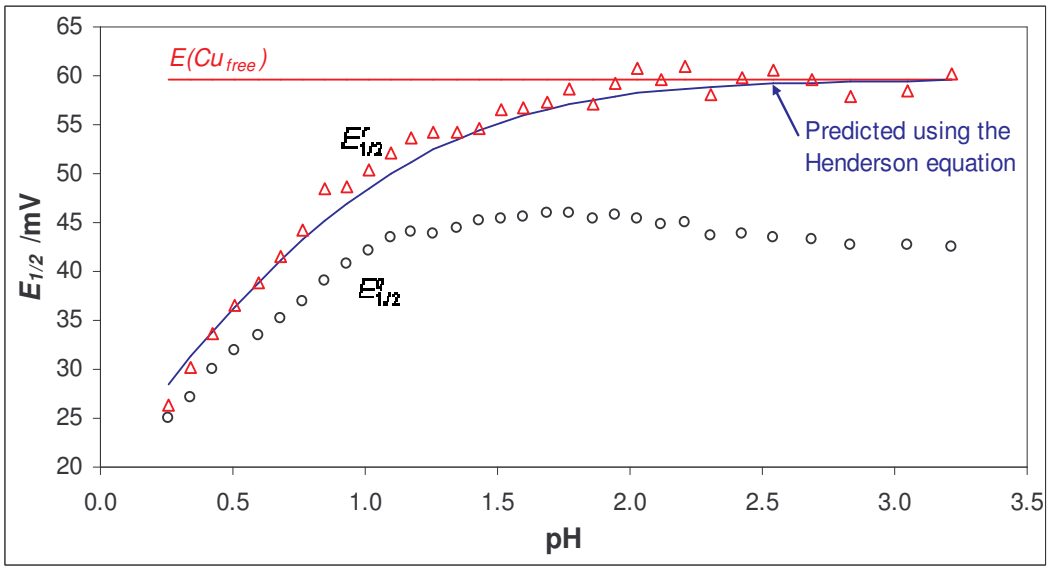

Figure 7.6: Comparison of $E^{q}_{1/2}$ and $E^{r}_{1/2}$ (using the procedure by Cukrowski and Zhang[19]) and the predicted $E_{1/2}$ values (using calculated E_j values and $E(Cu_{free})$ for the reversible potentials).

from calculated E_j values using the Henderson equation and $E(Cu_{free})$ as found for the reversible potentials (as discussed in Chapter 6) were also plotted. The results indicate that the fitting procedure by Cukrowski and Zhang[19] gave results which followed a similar trend to that predicted. Additionally, there is

only a small difference between the $E_{1/2}^{q}$ and $E_{1/2}^{r}$ values (1.4 mV) at the lowest pH where δ = 0.929 and the difference increases with increasing pH, corresponding to decreasing δ values, as expected.

Secondly, the two fitting procedures using equations 7.14 and 7.15 were attempted. The values of i_d and the background current variables were kept the same as those determined when using the DC wave equation to fit the polarogram in order to reduce the number of variables determined. The $E_{1/2}^{r}$ values predicted by the Ružić relationship[16] followed no particular trend and the values were not physically meaningful, giving values as high as 15 V (see Figure A5.2, Appendix 5). However, the $E_{1/2}^{i}$ values were similar to the $E_{1/2}^{q}$ values as shown in Figure 7.7. The $E_{1/2}^{r}$ values predicted by the Matsuda and Ayabe[12-14] relationship produced significantly higher potential values than expected (also shown in Figure 7.7). Neither of the $E_{1/2}$-pH relationships followed the trend predicted from calculated E_j values. Interestingly, the transfer coefficients (α) determined using both equations 7.14 and 7.15 corresponded to the δ value from equation 2.15 as illustrated in Figure A5.3, Appendix 5. The value of Γ in equation 7.14 varied from 4 to 143 with a general increasing trend as the titration proceeded (see Figure A5.4, Appendix 5). Given that $\Gamma = 1.13/\Lambda\tau^{1/2}$ and that the drop time is constant for all measurements made here, the only variable would be Λ which, according to equation 7.2, would be dependent on the diffusion and activity coefficients of the oxidized and reduced species as well as on α and k_s, the rate constant for the reduction of Cu(II) in this case. The diffusion coefficients should remain fairly constant and the activity coefficients would probably increase slightly with the change in ionic strength (from 0.5 M to about 0.25 M). As seen from Figure A5.3, α decreases from about 0.9 to 0.65 and thus (1 – α) increases. With the large variation in α and given that for a quasi-reversible process $10^{-2} < k^o < 5\times10^{-4}$ cm s^{-1},[9,11] it is expected that k_s could decrease somewhat during the titration. Thus overall Γ should increase, as was observed, but the refined values were not meaningful. The reason for these two fitting procedures failing

in this case could be due to the close proximity of the mercury oxidation wave to the reduction wave of Cu(II).

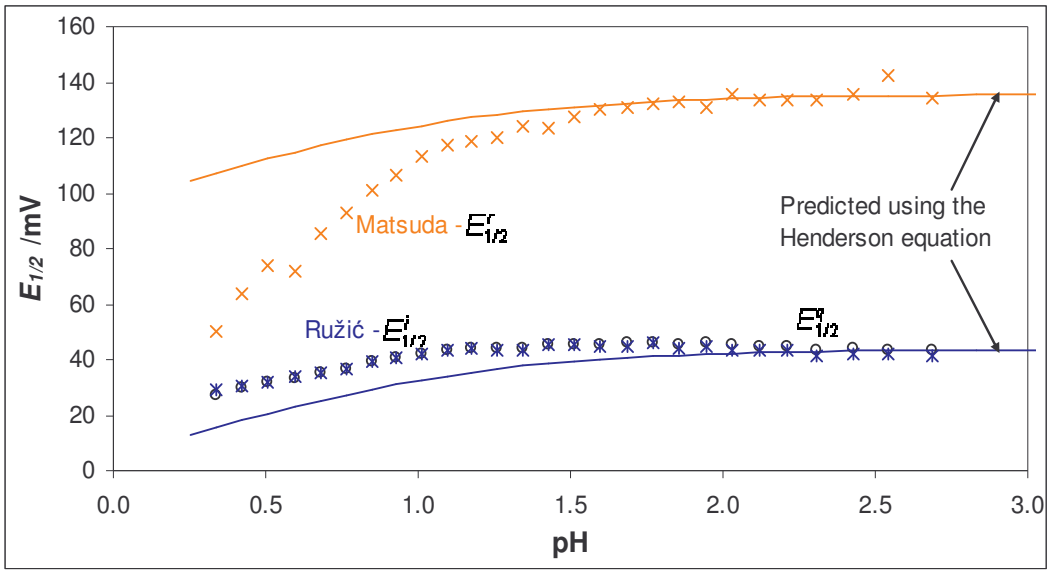

Figure 7.7: Comparison of $E^{q}_{1/2}$(○), $E^{r}_{1/2}$ from fitting equation 7.14 and $E^{i}_{1/2}$ from fitting equation 7.15. The predicted trend in $E_{1/2}$ was calculated as before.

Even though the graphical logarithmic analysis approach is very time consuming, it was considered here due to the fitting procedures failing, but proved to be tricky. This approach involved plotting $\log\{(i_d - i)/i\}$ versus E for each polarogram after the background current was subtracted. According to Koryta[15] $E^{r}_{1/2}$ could be obtained by extrapolating the asymptote from the foot of the wave to the E-axis. Figure 7.8 gives an example where the log analysis was attempted. The polarogram used was that same as that given in Figure 7.5, but after subtraction of the background current. The clear curvature seen in literature examples was not obvious here and deciding where to draw the asymptote was problematic. The asymptote was started where reduction commenced as seen from the increasing current on the DC wave. The pink asymptote was drawn using points up to 77 mV, i.e. up to the same point used to fit the DC wave equation in Figure 7.5 when using the procedure by Cukrowski and Zhang,[19] where $E^{r}_{1/2}$ obtained was 56.5 mV. The graphical approach thus also proved to be inadequate.

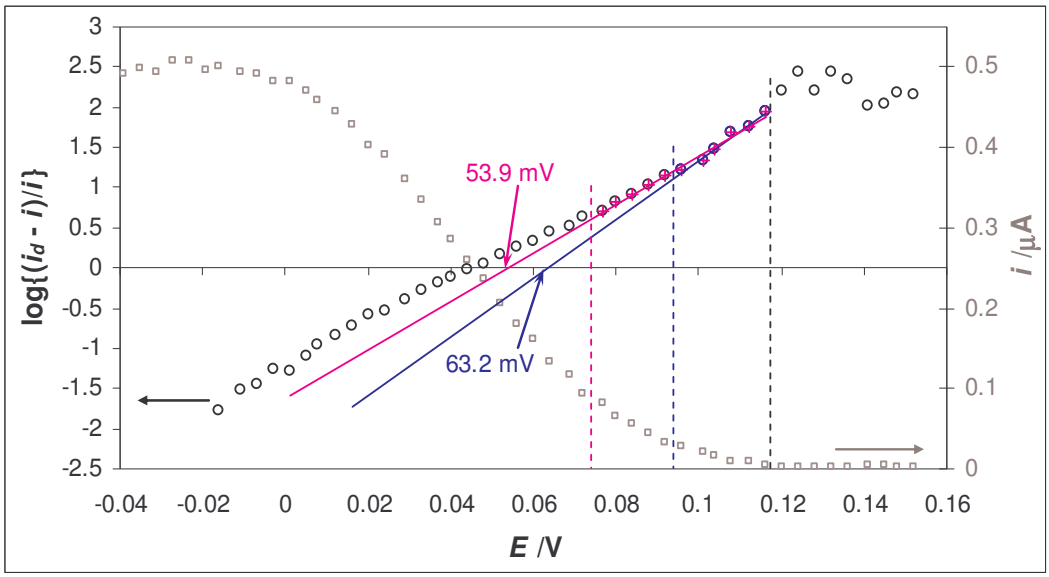

Figure 7.8: Log analysis showing two possible asymptotes that could be extrapolated to determine $E^r_{1/2}$. The DC wave with subtracted background current is also displayed (in grey).

The most successful method for determining $E^r_{1/2}$ from quasi-reversible DC waves in this case was the procedure suggested by Cukrowski and Zhang.[19] This approach was applied to all the Cu(II) reduction waves and the $E_{1/2}$ values used in further calculations refer to the reversible values.

7.3.3) *Modelling the difference in the half-wave potential for pH titrations in the absence of ligand*

Several pH titrations were performed with both Cu(II) and Tl(I) in solution without the addition of PA. The free metal ion potentials were determined for both Cu(II) and Tl(I) by averaging the $E_{1/2}$ values in the pH region where E_j was constant and the results are displayed in Table 7.3. The difference in these values for the two metal ions were evaluated and the average $\Delta E(M_{free})$ value of 487.7 ± 0.3 mV was used in further calculations. Interestingly, the reference electrode used to collect data set 4 was problematic (having a potential shift of almost 200 mV), but the difference in the Cu(II) and Tl(I) reduction potentials were similar to those when using a new reference system. It is again demonstrated how the Tl(I) potential data could act as a "reference" to the potential measurements of the metal ion of interest.

Table 7.3: Free metal ion potentials for Cu(II) and Tl(I) from pH titration experiments in the absence of ligand.

Data Set	$E(Cu_{free})$ /mV	$E(Tl_{free})$ /mV	$E(Cu_{free}) - E(Tl_{free})$ /mV
4	264.76 *	-222.94 *	487.70
5	78.89	-408.73	487.62
6	77.20	-410.83	488.03
7	73.32	-414.43	487.75
8	72.43	-414.75	487.18
Average			487.7 ± 0.3

* Reference system problematic leading to incorrect potential values

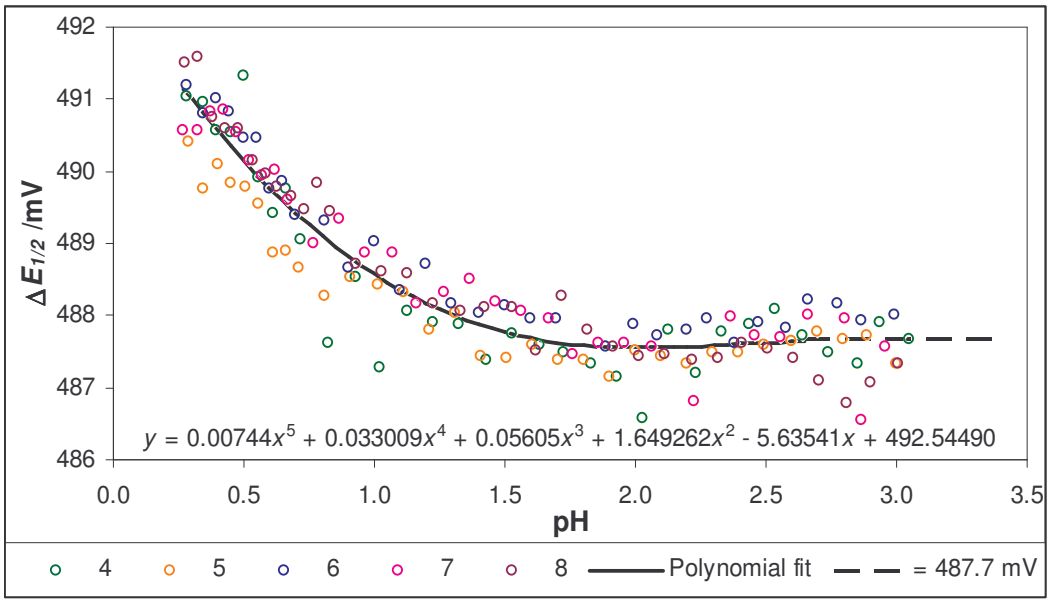

Figure 7.9: Fifth order polynomial fitted to the combined experimentally determined $E_{1/2}(Cu) - E_{1/2}(Tl)$ values as a function of pH. Above pH 2.7, $\Delta E_{1/2}$ was set to 487.7 mV. (The numbers in the legend refer to the data set number.)

As was predicted in Table 6.5, the potential shift due to the change in ionic strength throughout the pH titration was greater for Tl(I) than for Cu(II). This was accounted for by modelling the difference in $E_{1/2}$ for the two metal ions. The average difference for five data sets was determined by fitting a fifth order polynomial to the data as shown in Figure 7.9. Here the difference was calculated from the raw data, but the potential versus pH plots for each metal ion could first be smoothed by fitting a combination of a cubic polynomial in the pH region where E_j varied and a horizontal line where E_j was constant. When comparing the average $\Delta E_{1/2}$ at each pH for the two cases, the values differed

by a maximum of 0.11 mV which was negligible. Thus, using equation 6.10 which employed the $E_{1/2}(Tl)$ values and the *y*-value as determined from the fifth order polynomial, the $E_{1/2}$ values for Cu(II) reduction as a function of pH could be predicted.

7.3.4) *pH titrations: Using the model to evaluate formation constants*

Three pH titrations, each commencing at pH 0.3, were performed with total ligand-to-metal concentration ratios of 32, 103 and 207. The $E(Cu_{free})$ was predicted using the average $\Delta E(M_{free})$ value and this compared well to the value of $E_{1/2}$ before ligand was added which had been corrected for E_j (demarcated • in Figure 7.10). On addition of ligand at pH 0.3 a potential shift was observed, demonstrating that complex formation takes place at this low pH already. Potential shifts due mainly to E_j were predicted from the Tl(I) data and the model above. The $E^r_{1/2}$ values for Cu(II) were corrected for these shifts (as shown in Figure 7.10) and used to determine the species formed and the respective stability constants.

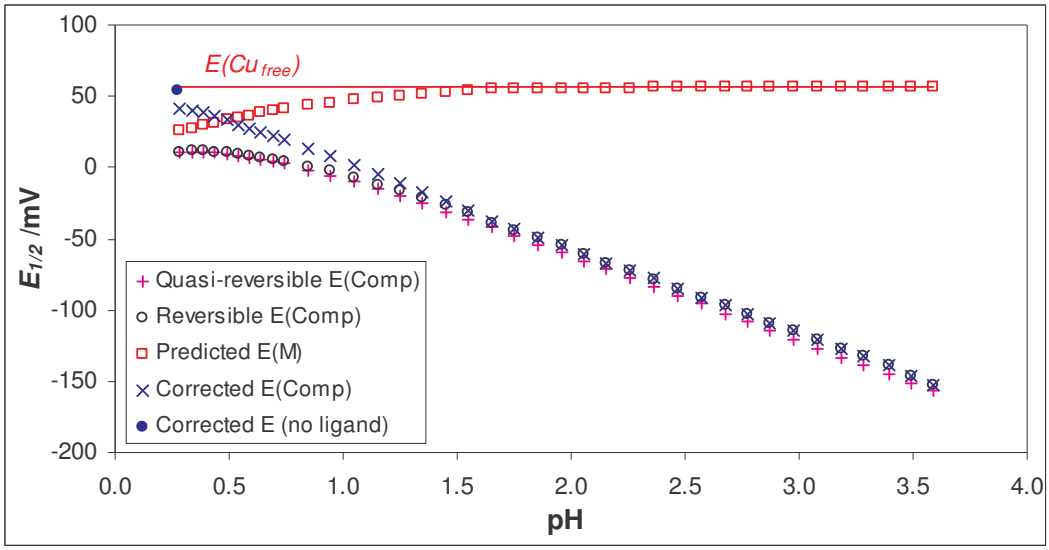

Figure 7.10: $E^r_{1/2}$ values before and after accounting for E_j for a pH titration with $[PA]_T$:$[Cu(II)]_T$ = 103. The values of $E^q_{1/2}$ *and* $E(Cu_{free})$ are also shown, as well as the predicted $E_{1/2}$ values in the absence of ligand.

Slope analysis was done using the ECFC (Figure 7.11) and the slope was found to be 60 mV/pH throughout. Given that the slope is approximately 60/n × number of protons involved in the reaction, some of the possible reduction reactions of solution species that could take place, together with the theoretical slope, are given in Table 7.4. This indicates that CuL^+ forms at low pH where H_2L^+ is the predominant form of the ligand and CuL_2 forms where HL is dominant in solution. The ML and ML_2 species were included in the model to calculate the CCFC and the resultant curve is shown in Figure 7.11. The formation of another species above about pH 3 may be speculated due to the calculated curve being slightly below the experimental values, but this was not the case for the other titrations as shown in Figure 7.12. This slight discrepancy may to due to errors when determining the values of $E^r_{1/2}$ for reduction reactions with the slowest electron transfer rates.

Table 7.4: Predicted slopes (in mV per pH unit) of potential versus pH data for the corresponding reduction reactions.

Reduction reaction	Predicted slope
$CuL^+ + 2e^- + H^+ \rightleftharpoons Cu^o + HL$	30
$CuL^+ + 2e^- + 2H^+ \rightleftharpoons Cu^o + H_2L^+$	60
$CuL_2 + 2e^- + 2H^+ \rightleftharpoons Cu^o + 2HL$	60
$CuL_2 + 2e^- + 4H^+ \rightleftharpoons Cu^o + 2H_2L^+$	120
$CuL_3^- + 2e^- + 3H^+ \rightleftharpoons Cu^o + 3HL$	90

When comparing the diffusion limited currents of the Cu(II)-PA complexes to that expected for uncomplexed Cu(II), the values compared well indicating that the rates of diffusion are very similar. (It is again noted that when referring to the uncomplexed metal ion, it refers to the hydrated form or even complexed by the background electrolyte to an extent.) The potential shift is thus the main factor in establishing the formation constants. The log β values determined for the pH titration are given in Table 7.5 and the averages were also evaluated. These compared well to the literature values in Table 7.1. A larger standard deviation was noted for the average log β value for the CuL^+ species probably due to its formation in the pH region where the junction potential had to be accounted for.

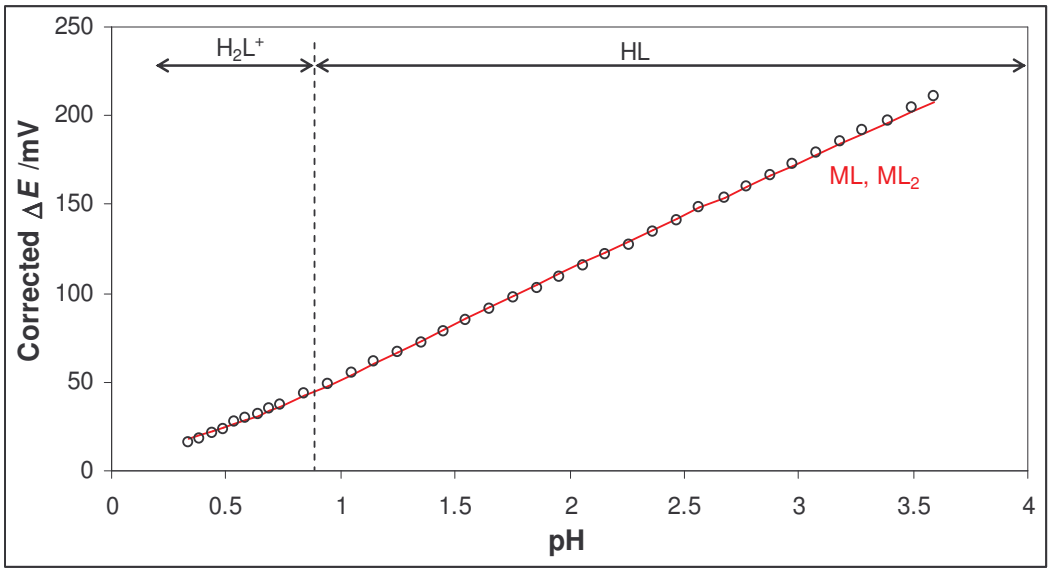

Figure 7.11: The ECFC (○) and CCFC (—) calculated for the ML and ML_2 species. ($[PA]_T$:$[Cu(II)]_T$ = 103).

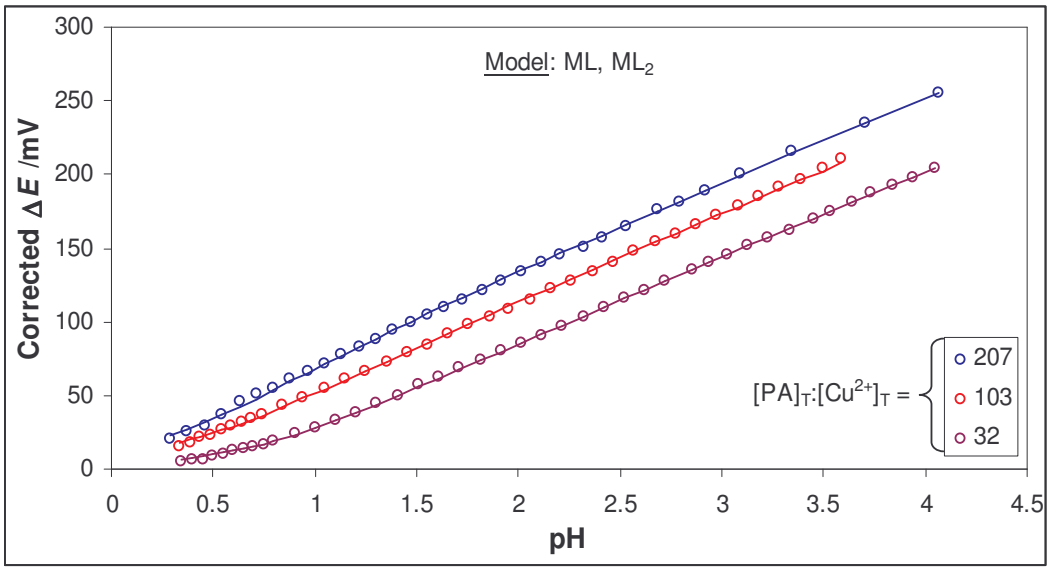

Figure 7.12: Comparison of the ECFCs and CCFCs for the three ligand-to-metal concentration ratio experiments.

The species distribution diagrams in Figure 7.13 shows that the CuL_2 species predominates over a wide pH range. Only at the low ligand-to-metal ratio of 30 does the $Cu_3(OH)_4$ species start forming at around pH 14 under these conditions. CuL^+ is only present under very acidic conditions. It was therefore an ideal metal-ligand system to study to test the protocols developed for working under very acidic conditions.

Table 7.5: Log β values for the indicated equilibria at 25 °C and ionic strength between 0.25 and 0.5 M.

$[PA]_T:[Cu^{2+}]_T$	32 [a]	103 [a]	207 [a]	Average [b]
Equilibrium		**Log β**		
$Cu^{2+} + L^- \rightleftharpoons CuL^+$	7.77 ± 0.02	7.89 ± 0.02	7.61 ± 0.05	7.8 ± 0.1
$Cu^{2+} + 2L^- \rightleftharpoons CuL_2$	14.90 ± 0.01	14.83 ± 0.01	14.91 ± 0.01	14.88 ± 0.04
Overall fit	0.54	1.84	1.94	

[a] Standard deviations of log β values obtained from fitting.
[b] Standard deviations of log β values obtained from averaging.

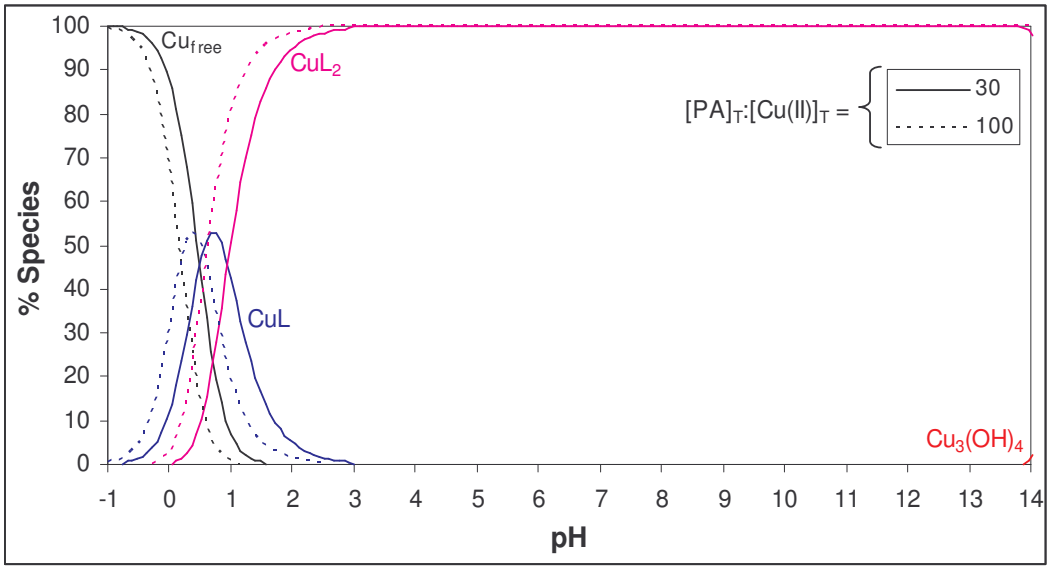

Figure 7.13: Species distribution diagrams for aqueous solutions of Cu(II)-PA using the average log β values and [Cu(II)] = 1×10^{-4} M.

7.3.5) *Ligand titrations*

Three ligand titrations were performed at pH 0.5, 0.9 and 1.4. The very acidic conditions were used in order to glean information about both the ML and ML_2 species. The pH of the solution was adjusted by adding a few µL of 0.5 M NaOH if required to maintain the same pH throughout the titration. A small drift in pH during a ligand titration is often observed and is generally tolerable, but since a fairly big change in E_j is observed with a small change in pH at these very low pHs, the variation was not allowed. Tl(I) was omitted in these titrations, so variations in potential due to the reference system could not be detected or accounted for using this data. The extent of reversibility did not change much during a titration and the δ values were close to 0.9 under these

fairly acidic conditions. The $E^{f}_{1/2}$ determined as before were thus close to the $E^{q}_{1/2}$ values.

Slope analysis on the ECFCs are indicated in Figure 7.14. For ligand titrations, the slope is approximately 60/n × number of free ligand molecules involved in the reaction. The extent of protonation of the ligand is constant due to the constant pH and thus does not affect the slope in a ligand titration. Possible reduction reactions of solution species and the corresponding theoretical slopes for a single complex formed are indicated Table 7.6. The slopes detected thus implied that the major species formed were CuL^{+} and CuL_2. The calculated curves fitted the experimental data when these two species were included. The refined log β values are presented in Table 7.7 and the values compared well with those determined using pH titrations, although the value for ML_2 were 0.19 log units lower here. If all six experimentally determined values were averaged, the log β values for ML was 7.75 ± 0.09 and ML_2 was 14.8 ± 0.1.

Table 7.6: Predicted slopes (in mV per log unit) of potential versus log [L_{free}] data for possible reduction reactions.

Reduction reaction	Predicted slope
$CuL^{+} + 2e^{-} + H^{+} \rightleftharpoons Cu^{o} + HL$	30
$CuL^{+} + 2e^{-} + 2H^{+} \rightleftharpoons Cu^{o} + H_2L^{+}$	30
$CdL_2 + 2e^{-} + 2H^{+} \rightleftharpoons Cd^{o} + 2HL$	60
$CdL_3^{-} + 2e^{-} + 3H^{+} \rightleftharpoons Cd^{o} + 3HL$	90

Table 7.7: Log β values for the given equilibria at 25 °C and ionic strength between 0.25 and 0.5 M.

pH	0.5 [a]	0.9 [a]	1.4 [a]	Average [b]
Equilibrium	**Log β**			
$Cu^{2+} + L^{-} \rightleftharpoons CuL^{+}$	7.69 ± 0.02	7.78 ± 0.02	7.76 ± 0.06	7.74 ± 0.05
$Cu^{2+} + 2L^{-} \rightleftharpoons CuL_2$	14.75 ± 0.04	14.69 ± 0.01	14.63 ± 0.01	14.69 ± 0.06
Overall fit	0.057	0.20	0.044	

[a] Standard deviations of log β values obtained from fitting.
[b] Standard deviations of log β values obtained from averaging.

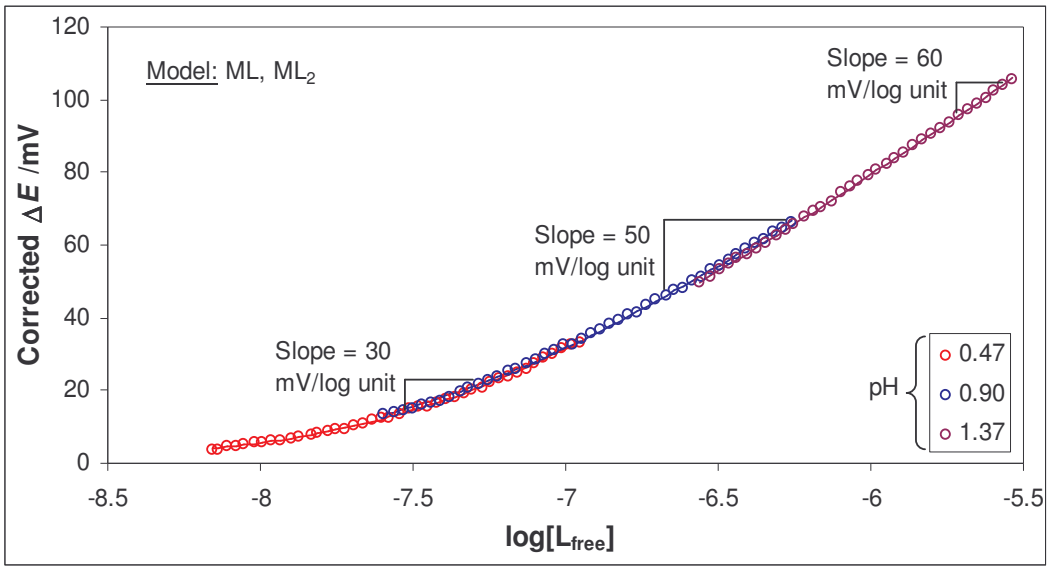

Figure 7.14: ECFCs (○) and CCFCs (—) for the three ligand titrations at the indicated pHs. The slopes in various regions are also displayed.

Unlike the case for the Cd(II)-PA solution species, ML_3 was not detected here, nor was it reported in the NIST database.[1] Additionally, no evidence of an ML_3 species was found in Cambridge Structure Database (CSD)[26] despite many crystals structures for other Cu(II)-PA species being reported. A ball-and-stick diagram (from Mercury[27]) of an example of the CuL_2 arrangement (reference code: CUPICH02) is shown in Figure 7.15. As expected for the Cu(II) centre, a square-planar arrangement is seen due to Jahn Teller distortions resulting in an absence in coordination through the axial positions. In the various crystal structures, the axial positions were either unoccupied or bonded to water or to the oxygen atoms of PA from CuL_2 in parallel layers above and below.

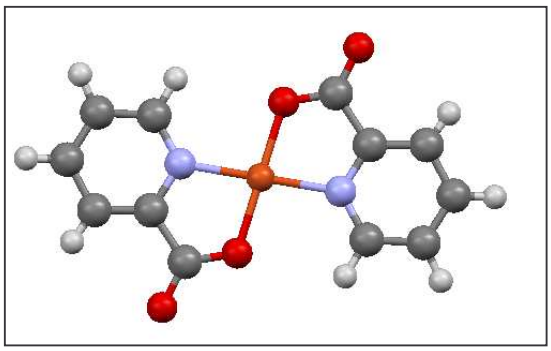

Figure 7.15: Structure of CuL_2 showing its square-planar arrangement.

7.4) Conclusions

The species detected and their stability constants compared well to that determined in literature. Here the log β values were was 7.75 ± 0.09 for ML and 14.8 ± 0.1 for ML_2 at ionic strength between 0.5 and 0.25 M, whereas the values quoted in the NIST database[1] were 7.87 and 7.7 for ML at 0.1 and 1.0 M ionic strength, respectively, and 14.78 and 14.70 for ML_2 at 0.1 and 0.5 M ionic strength, respectively. The closeness of these results were almost surprising due to the fact the potential values used to calculate these stability constants had to be corrected for diffusion junction potentials and reversible $E_{1/2}$ values had to be acquired from quasi-reversible polarograms. This also proved that the procedures developed to study complex formation under very acidic conditions were reliable. This is also the first time the log β value of ML for the Cu(II)-PA system was determined using polarography.

When determining the $E^r_{1/2}$ values for Cu(II) reduction, neither the curve-fitting procedures (using the relationships by Matsuda and Ayabe[12-14] (equation 7.14) and Ružić *et al*.[16] (equation 7.15)) nor the graphical analysis of the logarithmic plots were successful. This was ascribed here to the close proximity of the mercury oxidation wave which limits the amount of data that can be collected at the foot of the wave. However, the approach by Cukrowski and Zhang[19] was used successfully to evaluate $E^r_{1/2}$.

Due to the difficulties experienced in determining $E^r_{1/2}$, it would be suggested to rather increase the extent of reversibility of the measured polarograms as far as possible in future. This could be achieved by extending the drop time, using an anionic maxima suppressant rather than gelatine, quantifying the exact amount of maxima suppressant added so that it is done reproducibly, using high and constant ionic strength solutions and avoiding perchlorate as the background electrolyte (rather use sodium nitrate, as was done here, or possibly even lithium nitrate). The oxidation of mercury should also be avoided as far as possible by reducing the initial potential of the polarogram.

7.5) References

1) A.E. Martell, R.M. Smith and R.J. Motekaitis, NIST Standard Reference Database 46 Version 8.0, NIST Critically Selected Stability Constants of Metal Complexes, USA, 2004
2) C. Petitifaux, J. Barbier and J. Faucherre, Bull. Soc. Chim. Fr., (1970) 3441
3) J.L. Anderson and I. Shain, Anal. Chem. 50 (1978) 163
4) J.L. Anderson and I. Shain, Anal. Chem. 48 (1976) 1274
5) F.M Hawkridge Jr. and H.H. Bauer, Anal. Chem., 44 (1972) 364
6) I.M. Kolthoff and Y. Okinaka, J. Am. Chem. Soc., 81 (1959) 2296
7) S. Fronæus and C.L. Johansson, J. Electroanal. Chem., 60 (1975) 29
8) E. Gileadi, Physical Electrochemistry. Fundamentals, Techniques and Applications, Wiley-VCH, Weinheim, Germany, 2011
9) P. Delahay, J. Am. Chem. Soc., 75 (1953) 1430
10) A.M. Bond, Modern Polarographic Methods in Analytical Chemistry, Marcell Dekker, New York, 1980
11) J.C.R. Morales, J.J.T.J. del Castillo, M.B. Niebla and J.C.R. Placeres, Electroanalysis, 17 (2005) 275
12) H. Matsuda and Y. Ayabe, Bull. Chem. Soc. Japan, 28 (1955) 422
13) H. Matsuda and Y. Ayabe, Bull. Chem. Soc. Japan, 29 (1956) 132
14) H. Matsuda and Y. Ayabe, Z. Elektrochem., 64 (1959) 1164
15) J. Koryta, Electrochim. Acta, 6 (1962) 67
16) I. Ružić, A. Barić and M. Branica, J. Electroanal. Chem., 29 (1971) 411
17) I. Cukrowski, H.M. Marques, T.S. Mkwizu, P.P. Magampa and C. Serge, Anal. Chim. Acta, 590 (2007) 203
18) T.S.P. Mkwizu, MSc Dissertation: A Polarographic and Potentiometric Study of Metal-Ligand Equilibria: Instrumentation and Investigations of Systems with Non-Reversible Electrode Reactions, University of the Witwatersrand, 2006
19) I. Cukrowski and J.M. Zhang, Electroanalysis, 16 (2004) 612
20) A.M Bond, Electrochim. Acta, 17 (1972) 76
21) A.A. Moussa and H.M. Sammour, J. Chem. Soc., (1960) 2151
22) J.E.B. Randles and K.W. Somerton, Trans. Faraday Soc., 48 (1952) 951

23) H.H. Bauer and P.J. Elving, Electrochim. Acta, 2 (1960) 240

24) J.J. Lingane, J. Am. Chem. Soc. 61 (1939) 2099

25) D.R. Crow, Polarography of Metal Complexes, Academic Press, London, 1969

26) F.H. Allen, Acta Cryst., B58 (2002) 380. Cambridge Structural database Version 5.31, November 2008 update

27) MERCURY: C.F. Macrae, P.R. Edgington, P. McCabe, E. Pidcock, G.P. Shields, R. Taylor, M. Towler, and J. van de Streek, *J. Appl. Cryst.*, 39 (2006) 453

CHAPTER 8

The Hydrolysis of Bismuth and the Determination of the Free Bismuth(III) Potential

8.1) Introduction

8.1.1) *Bismuth(III) hydrolysis*

Most cations undergo hydrolysis since most metals form strong bonds with oxygen and hydroxide is always present in aqueous solutions, the concentration of which can vary significantly depending on the pH of the solution. Determining the identity, not to mention the stability, of the hydrolysis species present has been shown to be challenging.

The hydrolytic reactions of many metal ions can simply be written as acid dissociations of the aqua ions, for example:[1]

$$M(OH_2)_x^{n+} \rightleftharpoons M(OH_2)_{x-1}(OH)^{(n-1)+} + H^+$$

A more general formation reaction of a soluble hydrolysis product is given as:[2]

$$xM(OH_2)_w^{z+} + yOH^- + aA^- \rightleftharpoons M_xO_u(OH)_{y-2u}(OH_2)_vA_a^{(xz-y-a)+} + (xw+u-v)H_2O$$

where the ligands O^{2-}, OH^-, H_2O and another anion, A^-, are distinguished. Most techniques cannot discriminate between one O^{2-} and two OH^- ligands, nor can they detect H_2O ligands. The anion A^- is usually that of the supporting electrolyte and is chosen to be non-complexing (or more realistically very weakly complexing). The reaction and formula is thus simplified by considering only the OH^- ligand as follows:[2]

$$xM^{z+} + yOH^- \rightleftharpoons M_x(OH)_y^{(xz-y)}$$

Precipitation of hydroxide or oxide species limits the pH range over which the formation of soluble hydrolysis products can be studied. Also, hydroxide species can often be polynuclear, which results in a large range of possible species that could be formed and a number of them can appear simultaneously. Polynuclear species are generally formed in solutions containing high concentrations of the metal ion. Thus there is often

disagreement about hydrolysis products and the proposed species are treated with skepticism.[2]

Bi(III) is one of the strongest aqua-acids. The hydrolysis of Bi(III) in solution has been extensively studied and has been instrumental in developing techniques to investigate hydrolysis. The formation of the $BiOH^{2+}$ species was readily confirmed.[3-5] Early on evidence of bismuth polynuclear species was found. Graner and Sillén[6] proposed the mechanism:

$$Bi_nO_{n-1}^{n+2} + Bi^{3+} + H_2O \rightleftharpoons Bi_{n+1}O_n^{n+3} + 2H^+$$

thus alluding to the existence of polynuclear species such as Bi_2O^{4+}, $Bi_3O_2^{5+}$, $Bi_4O_3^{6+}$ and so on. Other authors suggested other polynuclear species such as $Bi_2(OH)_5^+$,[7] $Bi_4O_4^{4+}$,[8] $Bi_8(OH)_{20}^{4+}$,[9] and $(BiO)_n^{n+}$ where n=5 or 6.[10]

The initial work by Graner and Sillén[6] was later found to be incorrect due to errors introduced by using a quinhydrone electrode.[4] Corrections made to these data and new data collected in solutions at higher Bi(III) concentrations showed that only two complexes were present, namely $BiOH^{2+}$ and $Bi_6(OH)_{12}^{6+}$.[4,5] With improved analyses, good proof now exists using various techniques to support the presence of the hexamer $Bi_6(OH)_{12}^{6+}$ as the predominant species under the specific experimental conditions.[5,11-14] The uncertainty from Tobias[12] as to whether to call the species $Bi_6(OH)_{12}^{6+}$ or $Bi_6(O)_6^{6+}$ stems from the fact that it is difficult to differentiate whether O^{2-} or OH^- are bound to Bi(III) by numerous experimental techniques, as mentioned.

Olin[5] proposed that the structure of the $Bi_6(OH)_{12}^{6+}$ be very symmetrical which would explain its extreme stability and dominance as a polynuclear species. From Raman spectra, Maroni and Spiro[14] showed that the structure in the solid state and solution were the same. It was proposed that the structure of $Bi_6(OH)_{12}^{6+}$ be cuboctahedral as shown in Figure 8.1.[2]

It was also established that $Bi_6(OH)_{12}^{6+}$ was in equilibrium with larger complexes.[11,15] Sillén proposed a “core and links” approach[2] to explain the formation of polynuclear complexes. This had been applied successfully to the

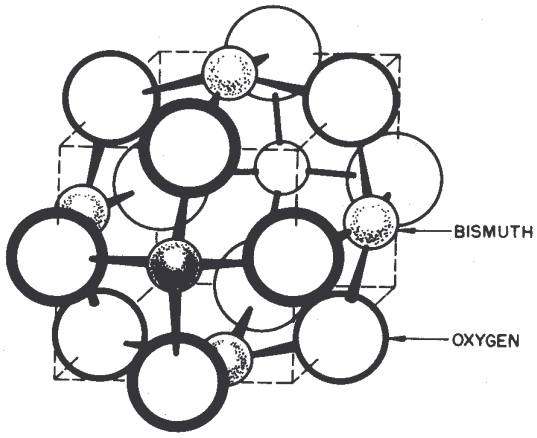

Figure 8.1: Cuboctahedral structure of $Bi_6(OH)_{12}^{6+}$.[2]

hydrolysis of many other metal ions. According to this approach it should be possible to represent the complexes by the formula $Bi_6(OH)_{12}[Bi_6(OH)_{12}(OH)_t]_n$, where *t* is a constant and *n* varies. This theory did not apply to Bi(III), however. The model species $Bi_9(OH)_{20}^{7+}$, $Bi_9(OH)_{21}^{6+}$ and $Bi_9(OH)_{22}^{5+}$ were proposed.[11]

The $Bi(OH)_2^+$ species was not detected by Olin[5] and it was suggested that the hexamer is much more stable than this species, where these two species are stoichiometrically equivalent. Other mononuclear species were also found in solution and Bidleman[16] determined formation constants for $BiOH^{2+}$, $Bi(OH)_3$ and $Bi(OH)_4^-$ for dilute solutions ($<10^{-4}$ M Bi(III)) in a perchlorate background which compared well to other data.[17] He found no evidence for polynuclear species at these Bi(III) concentrations and simply says that formation of $Bi(OH)_2^+$ was not studied. Hataye *et al.*[15] analysed solutions at trace Bi(III) concentrations ($<10^{-7}$ M) using a backward extraction method. They found the species Bi^{3+}, $Bi(OH)^{2+}$, $Bi(OH)_2^+$ and $Bi(OH)_3$ in solution between pH 0 and 5.7, but no polymerised species. It therefore appears that at very low Bi(III) concentrations $Bi(OH)_2^+$ is formed, but at higher concentrations the polymeric species is more stable.

The stability constant data, as given by Martell and Smith in the NIST database,[17] are provided in Table 8.1 for the various Bi(III) hydrolysis products.

The species include those generally accepted as being present in solution. Values of log β at ionic strength 0.5 M were not determined experimentally, but values were calculated using the experimental values and applying the Davies modification of the Debye-Hückel equation by Cukrowski *et al.*[18] and the values are also given in Table 8.1. These values were quoted to two decimal places, but using them to one decimal place is a better indication of the actual precision. The log β values used in this study are marked with an asterisk in the table.

Table 8.1: Table of log *K* values for Bi(III) hydrolysis products at 25 °C.[17]

Species	Reactants	Log *K*	μ /M	Log β [d]
$Bi(OH)^{2+}$	$Bi^{3+} + OH^-$	12.3 [a]	0.5	12.42 *
		12.4	0.1	
		12.3	1.0	
		12.6	3.0	
		12.9	0.0	
$Bi(OH)_2^+$	$Bi^{3+} + 2OH^-$	23.5 *	1.0	
$Bi(OH)_3$	$Bi^{3+} + 3OH^-$	31.9	0.1	31.88 *
		31.3	1.0	
		33.0	0.0	
$Bi(OH)_4^-$	$Bi^{3+} + 4OH^-$	33.6	1.0	32.98 *
		34.8	0.0	
$Bi_6(OH)_{12}^{6+}$	$6Bi^{3+} + 12OH^-$	165.3	1.0	162.78 *
		170.3	3.0	
$Bi_9(OH)_{20}^{7+}$	$Bi_6(OH)_{12}^{6+} + 3Bi^{3+} + 8OH^-$	23.9	0.1	
	$9Bi^{3+} + 20OH^-$	271.9 [b]		266.92 *
$Bi_9(OH)_{21}^{6+}$	$Bi_9(OH)_{20}^{7+} + OH^-$	10.6	0.1	
	$9Bi^{3+} + 21OH^-$	282.5 [c]		276.76 *
$Bi_9(OH)_{22}^{5+}$	$Bi_9(OH)_{21}^{6+} + OH^-$	11.1	0.1	
	$9Bi^{3+} + 22OH^-$	293.6 [c]		287.30 *

[a] at 20 °C
[b] calculated here using log *K* for $Bi_6(OH)_{12}^{6+}$ at 1.0 M ionic strength
[c] calculated here using log *K* for $Bi_9(OH)_{20}^{7+}$ or $Bi_9(OH)_{21}^{6+}$ as required
[d] recalculated for 0.5 M ionic strength[18]

Perchlorates and nitrates are frequently used as background electrolytes as they are very weakly complexing. Maroni and Spiro[14] showed that perchlorate is not bound firmly to the hydrolysed bismuth species. Hataye *et al.*[15] agreed

with this; however they further speculated that nitrate complexes were formed with the hydrolysed bismuth species in 1 M $(H,Na)NO_3$ solutions and represented the species as $Bi(NO_3)_n^{3-n}$, $Bi(OH)(NO_3)_n^{2-n}$, $Bi(OH)_2(NO_3)_n^{1-n}$ and $Bi(OH)_3(NO_3)_n^{-n}$. Similar studies were executed in chloride solutions,[19] which also pointed to the formation of chloride complexes with the hydroysed Bi(III) species. Formation constants for the bismuth nitrate and bismuth chloride species have been determined and the values at an ionic strength close to 0.5 M are presented in Table 8.2.[17] The extent of hydrolysis would be depressed due to the complexing ability of nitrate[20,21] and even more so chloride[20,22,23] with Bi(III) as mononuclear species. This will be illustrated later in this chapter in species distribution diagrams where Bi(III) nitrate and Bi(III) hydroxide species were considered together. Raman spectra showed that the nitrate acted as a bidentate ligand toward Bi(III) (noting that the study was carried out in very acidic solutions) and that the bonds were somewhat covalent in nature.[21]

Table 8.2: Table of log β values for Bi(III) nitrate and chloride species at 25 °C.[17]

Species	**$A^- = NO_3^-$**		**$A^- = Cl^-$**	
	Log β	**μ /M**	**Log β**	**μ /M**
BiA^{2+}	0.72	0.5	2.7	0.5
BiA_2^+	(0.94)	0.5	4.1	0.5
BiA_3	0.7	1.0	5.4	0.5
BiA_4^-	0.6	2.0	6.2	0.5
BiA_5^{2-}			6.7	0.5

Kragten *et al.*[24] also studied the hydrolysis of bismuth in 1 M nitrate and 1 M perchlorate solutions at different bismuth concentrations. They represented the solution equilibria as shown in Figure 8.2. Species distribution diagrams are often a plot of the fraction of species in solution under varying pH conditions for particular concentrations of metal ion and ligand. From the discussion above it is seen that the concentration of Bi(III) also determines which species are present - polynuclear species at high Bi(III) concentrations and mononuclear species at low concentrations. In order to illustrate this, Kragten *et al.*[24] produced pBi′-pH diagrams (where pBi′ refers to $-\log [Bi_{Total}]$)

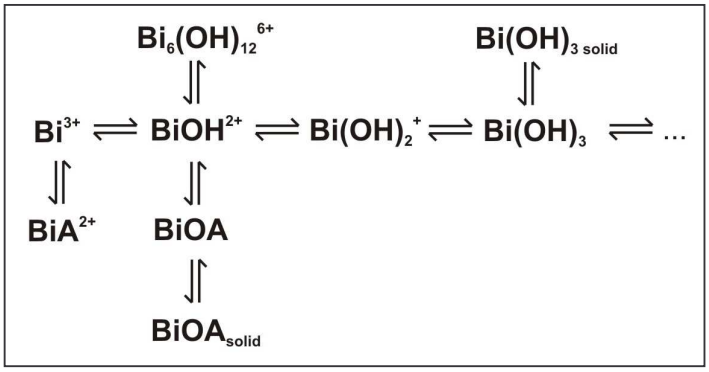

Figure 8.2: The aqueous solution equilibria of Bi(III) where A denotes the anion nitrate, perchlorate or chloride.[24]

given in Figures 8.3(a) and (b) for nitrate and perchlorate solutions respectively. The regions enclosed by borderlines indicate the conditions under which each species is predominant. These plots clearly show that $Bi(OH)_3$ has a limited solubility and precipitates at higher Bi(III) concentrations. The BiOA species also form a precipitate and if placed in a basic solution it slowly recrystallizes to $Bi(OH)_3$.[24] From these plots it is suggested that $BiOClO_4(s)$ is in equilibrium with $Bi_6(OH)_{12}^{6+}$, but that $BiONO_3(s)$ is in equilibrium with $Bi(OH)_2^+$ as $Bi_6(OH)_{12}^{6+}$ does not feature in the plot where the anion is nitrate. Attempts to draw a pBi′-pH diagrams for chloride solutions were aborted as the solubility of BiOCl is very low. The solubility products used to calculate these plots are given in Table 8.3 where the species BiOA is considered as $Bi(OH)_2A$.[24]

Table 8.3: The log K_{SO} values (where K_{SO} is the solubility product) used to calculate the boundary lines in Figures 3(a) and (b).[24]

Equilibrium	log K_{SO} for $A^- = NO_3^-$	log K_{SO} for $A^- = ClO_4^-$
$Bi(OH)_3(s) + 3H^+ \rightleftharpoons Bi^{3+} + 3H_2O$	5.2	5.2
$Bi(OH)_3(s) \rightleftharpoons Bi^{3+} + 3OH^-$	–36.0 [a]	–36.0 [a]
$Bi(OH)_2A(s) + 2H^+ \rightleftharpoons Bi^{3+} + 2H_2O + A^-$	–1.2	–0.9
$Bi(OH)_2A(s) \rightleftharpoons Bi^{3+} + 2OH^- + A^-$	–28.7 [a]	–28.7 [a]

[a] Values converted here using: log K_{SO}^* = log K_{SO} + n log K_w, where n is the number of OH^- groups in the reaction and log K_w = –13.74 (for μ = 1M and at 25.0 °C).[17]

Smith[3] and Swinehart and Garrett[25] determined the solubility (in M) of bismuth oxynitrate, $BiONO_3$, in different concentration of HNO_3 and the results are

plotted in Figure 8.4 (note that no corrections were made for differing ionic strengths). Swinehart and Garrett[25] also considered the solubility of a more basic solid $BiO(OH).BiONO_3$ in the same acid concentration range as for the $BiONO_3$ and found it to be slightly lower up till about 0.065 M HNO_3.

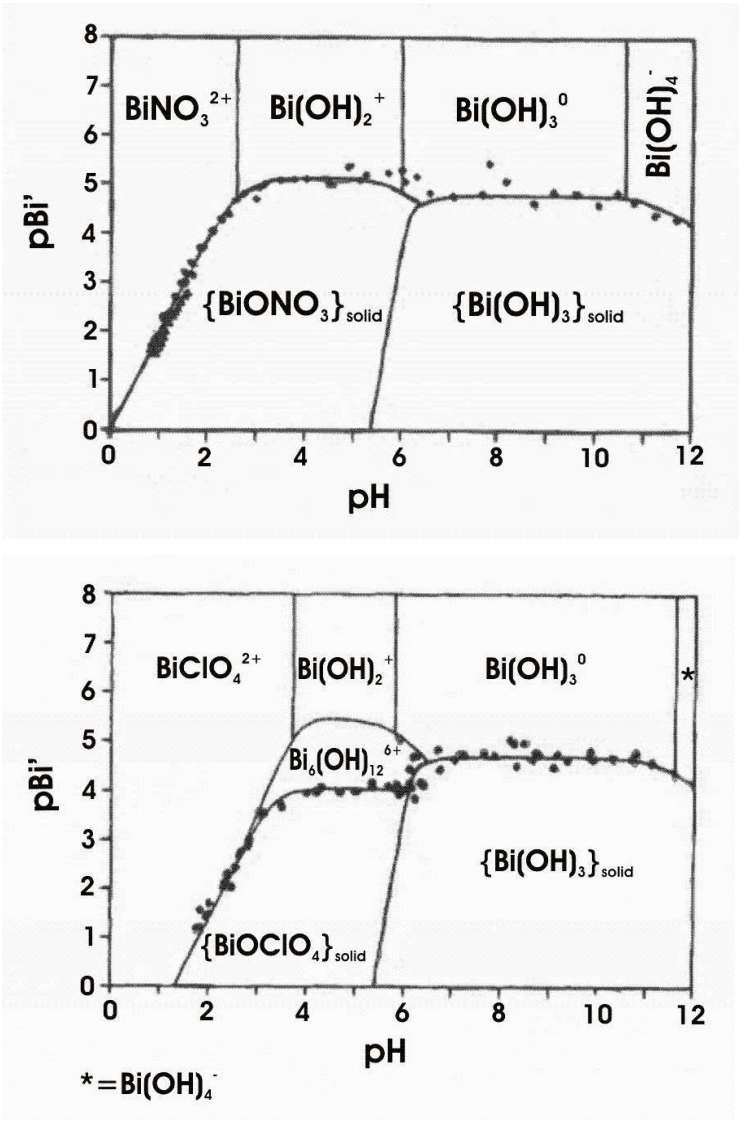

Figure 8.3: The pBi′-pH diagrams for bismuth in the presence of (a) 1 M nitrate and (b) 1 M perchlorate at 23.0 °C as present by Kragten *et al.*[24] ◆: experimental results. The regions of predominance of species above the precipitation regions were calculated using equilibrium constants.

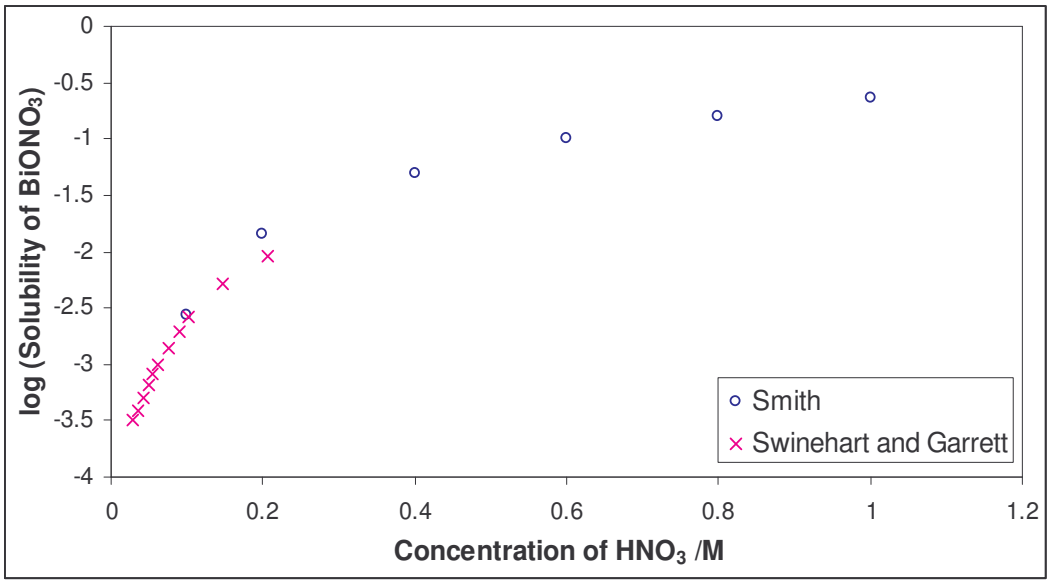

Figure 8.4: Plot of log(solubility of $BiONO_3$) in nitric acid solutions at 25 °C as given by Smith[3] and Swinehart and Garrett.[25]

The $BiONO_3$ species is often referred to, but the solid state study of the precipitates formed sheds some light onto its structure. It was shown that the solid hydrolysis product formed at low pH was a polycondensation of $Bi_6(OH)_{12}^{6+}$ ions in solutions of basic bismuth salts to form the species $[Bi_6O_x(OH)_{8-x}]^{(10-x)+}$.[14,26,27] Henry *et al.*[27] determined the crystal structure for $[Bi_6O_{4.5}(OH)_{3.5}]^{5.5+}$, i.e. the polycations where x = 4 and x = 5 could not be isolated. Both Lazarini[28] and Sundvall[29,30] found that the first hydrolysis product formed below pH 1.2 existed as $Bi_6O_4(OH)_4(A)_6$ for A = NO_3^- or ClO_4^- (i.e. where x = 4) and included waters of hydration. The six bismuth atoms form a slightly distorted octahedron and are bonded to the eight oxygen atoms, each of which is situated above an octahedral face and bound to three bismuth atoms. This can be clearly seen in the stereodiagram given by Sundvall[29] and shown here in Figure 8.5. Lazarini[31] also isolated the x = 5 polycation $Bi_6O_5(OH)_3^{5+}$, which formed between pH 1.2 and 2.4 and determined its crystal structure.

The fact that $Bi_6O_4(OH)_4^{6+}$ exists for both anions indicates that there is a strong probability that this is the species in solution,[29] often referred to as $Bi_6(OH)_{12}^{6+}$. This was confirmed by ^{1}H NMR solution studies by Grenthe and Toth.[32] It is

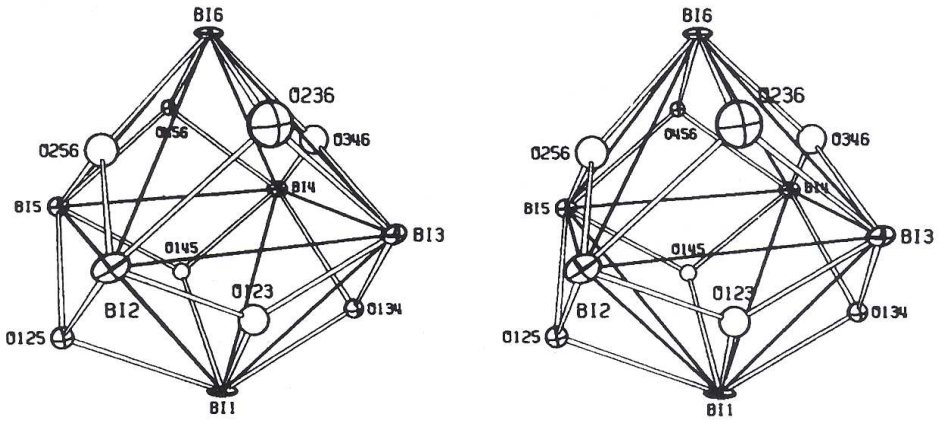

Figure 8.5: Stereodiagram of the structure of $Bi_6O_4(OH)_4^{6+}$ by Sundvall.[29] Ellipsoids are scaled to include 50% probability and solid lines between Bi atoms do not indicate bonding.

noted that $Bi_6O_4(OH)_4(A)_6$ is stoichiometrically equivalent to BiOA or $Bi(OH)_2A$, bearing in mind that many techniques cannot distinguish whether O^{2-} or OH^- is attached to bismuth. Further work on the hydrolysis products of $Bi(NO_3)_3.5H_2O$ has been done using powder X-ray diffraction, thermogravimetric analysis, and so on, which speculate additional slightly different species of the hexa-bismuth ion.[33-35]

As mentioned in Chapter 1, many medicinal papers refer to the hydrolysed bismuth nitrate species as bismuth oxynitrate or more regularly bismuth subnitrate. It was noted that these salts can have variable formulae, depending on the method of preparation.[36]

8.1.2) *Polarographic reduction of bismuth(III)*

In polarography metal ions having an oxidation state of three are not reversibly reduced in “non-complexing” media such as perchlorate.[37] Many studies have shown that this is true for Bi(III).[37-40] The exact reason for this is not fully understood. Intuitively, one may consider the chances of three electrons being transferred fast enough for a reversible process to occur to be remote. Furthermore, it has been suggested that the waters of hydration are probably tightly bound to the triply charged central ion and hence are not very labile, resulting in the slower reduction process.[37] Randles and Somerton[39] attributed

the slow reduction of hydrated Bi(III) in $HClO_4$ to the repulsion of ions from the electrode; a point disputed by Bond[37] in his investigation of other triply charged metals ions such as In(III) and Ga(III).

In the presence of the halides (except fluoride[41]) and certain pseudohalides the reduction of Bi(III) becomes reversible. This was observed even when halides were present at trace levels and much work has been done on the effect of adding chloride to perchlorate solutions containing Bi(III).[37-40] Randles and Somerton[39] speculated that the repulsions between the Bi(III) species in solution and the electrode are diminished probably due to coordination of the chloride to Bi(III) or adsorption of the chloride at the mercury electrode (both are known to occur). The fact that trace concentrations of chloride affect the electron transfer rate significantly, tends to indicate that adsorption plays the key role in this case.[37,39] Bauer and Elving[40] suggested that electron transfer is facilitated through a chloride "bridge" between the electrode and Bi(III) near the electrode surface. Even though reversibility increased significantly on addition of chloride, it is only when all the Bi(III) is complexed that the process becomes fully reversible, thus signifying that complex formation also plays an important role.[37]

This is supported by the observation that the rate of heterogeneous electron transfer also increases in the presence of nitrate which is not strongly adsorbed at the mercury electrode. As seen, the association of Bi(III) with nitrate ions is much stronger than normally associated with metal ion nitrates and exhibits some covalent character, i.e. it is not simply an ion pair. There is even evidence for negatively charged nitrate complexes of Bi(III) in solution.[37] In this instance Bond[37] suggests that the increased rate of electron transfer is due to the formation of covalently bonded nitrate to Bi(III) which disrupts the coordinated water molecules and increases the ease of water removal. The reduction process never reached full reversibility in a nitrate medium, probably due to the nitrate complexes being weaker than the halide Bi(III) complexes, hence there was always some uncomplexed Bi(III). Even an increase in perchlorate concentration resulted in an increased rate of reduction (although

to a lesser extent than for nitrate which forms stronger complexes), which indicates that weak complexes of Bi(III) perchlorate do exist.[37]

Moussa and Sammour[38] also found that in highly acidic solutions where Bi(III) hydrolysis is negligible, the rate of electron transfer for Bi(III) reduction increased with the addition of the following anions in solution: ClO_4^- < SO_4^{2-} < NO_3^- < Cl^-. Since the first three anions listed do not adsorb onto the electrode surface, the fact that the rate of electron transfer varies for these implies that adsorption is not the only factor affecting this process. In the highly acidic conditions SO_4^{2-} is rather present as HSO_4^- (pK_a (HSO_4^-) = –1.08 at 25 °C and 1 M ionic strength[17]). The fact that faster electron transfer occurs in sulphate rather than nitrate solutions was surprising as Bi(III) forms more stable complexes with HSO_4^- than with NO_3^-.[17]

Randles and Somerton[39] measured rate constants (k_e) for the process of the transfer of the metal ion from aqueous solution to the amalgam phase or vice versa in various supporting electrolytes. A selection of their results at 20 °C is given in Table 8.4. These values are quoted as only being reliable to ±30%,[39] but Bauer and Elving[40] have shown how widely these values can differ depending on which technique is used to determine them. Notably, these values display the same trend that has been observed in this work where Tl(I) and Cd(II) were fully reversible, but Cu(II) was not in a nitrate electrolyte.

Table 8.4: Rate constants (k_e) at 20 °C for the reduction of various metal ions from aqueous solution to an amalgam in various supporting electrolytes.[39]

Metal ion	Supporting electrolyte	k_e /cm s^{-1}
Tl^+	1 M KNO_3	>1
Cd^{2+}	1 M KNO_3	~0.6
Cu^{2+}	1 M KNO_3	4.5×10^{-2}
Bi^{3+}	1 M $HClO_4$	3.0×10^{-4}
Bi^{3+}	1 M HCl	>1

Addition of gelatine to the aqueous solutions as a maxima suppressant retards the electron transfer reactions as this is adsorbed onto the electrode surface.

The rate of this reaction decreases to a point and then it becomes stable, probably once the electrode is covered by a monolayer.[39] Randles and Somerton[39] speculate that the higher the charge of the metal ion and the greater the extent of hydration of the metal ion centre, the more difficult it would be to penetrate the gelatine layer making the process slower.

8.2) Aims

Baes and Mesmer[2] made the comment that bismuth hydrolysis has been extensively studied and the summary given in the chapter shows how complicated the system is. Additionally, bismuth interacts relatively strongly with anions such as nitrates and chlorides as compared to most metal ions.

The aim of this work is not to study the hydrolysis of bismuth, but rather to use the given information to understand the aqueous chemistry of bismuth, both in the absence and presence of complexing ligands. This foundation is required when determining one of the most problematic parameters when studying Bi(III)-ligand equilibria by polarography - the free metal ion potential. This parameter can generally be measured directly for most metal ions when measurements start at a pH where the diffusion junction potential can be ignored (above about pH 2). For studies commencing at more acidic pH conditions, the free metal ion potential can no longer be directly measured and protocols for determining this parameter were discussed in Chapter 6. Unfortunately, this process cannot be used in studies with Bi(III) as it is already hydrolysed at pH 0.3, the initial pH of experiments performed in this work. The Bi(III) oxy-nitrate species also precipitates around pH 2 which restricts the pH range in which data can be collected and studied. So investigations into the best procedure to determine the free Bi(III) potential will be investigated here.

8.3) Results and Discussion

8.3.1) *Effects of Bi(III) hydrolysis on polarographic pH titration data*

In this section pH titrations (as described in Chapter 2) of solutions containing only Bi(III) and Tl(I) (and no added ligand) were considered. Initial investigations were performed in solutions starting at 4.99×10^{-5} M Bi(III) (with NaOH as the titrant), but later the concentration was reduced to 9.97×10^{-6} M Bi(III) (using with KOH as the titrant). The concentration of Tl(I) was always approximately twice that of Bi(III) so that the diffusion limited currents were similar for the two reduction waves, although in hindsight more accurate Tl(I) reduction parameters could be obtained if its concentration was higher.

The polarographic parameters were generally the same as those given in Table A1.4 (Appendix 1), but some parameters were changed when the lower concentration Bi(III) solutions were used as given in Table A6.1 (Appendix 6). The solutions with lower Bi(III) concentration were purged longer between the additions of hydroxide solution (due to the introduction of oxygen from the hydroxide solution interfering with the Bi(III) reduction wave), so the equilibration time was lengthened, but in order to reduce the total experimental time, polarograms were only collected at ΔpH intervals of 0.1 instead of 0.07 as before. It was also necessary to increase the current integration times to obtain a reasonable signal throughout the titration for the lower Bi(III) concentrations. To avoid the mercury oxidation region, the initial potentials were made less positive and the final potentials were made less negative as it was sufficient to collect data to -0.70 V.

Figure 8.6 shows the polarograms of Bi(III) and Tl(I) reduction in 0.5 M HNO_3 at different concentrations. The two reduction waves of interest could not be fitted simultaneously due to the background currents; the mercury oxidation wave close to the Bi(III) reduction wave and the hydrogen evolution wave close to the Tl(I) wave. The polarogram was divided into two parts with the separation occurring at –0.2 V. These waves were fitted using equation 2.15 and the function for the background current was:

$$i_{bkgnd} = a + bE + c\exp(dE) \quad (8.1)$$

For the Bi(III) reduction wave the values of *c* and *d* were negative and positive respectively, in order to fit the region where mercury oxidation occurred. For the Tl(I) reduction wave the values of *c* and *d* were positive and negative respectively, to account for the onset of hydrogen evolution. In some cases some data points were removed at the most positive potentials when fitting the Bi(III) wave as indicated in the inset in Figure 8.6. This will be discussed fully later in this section.

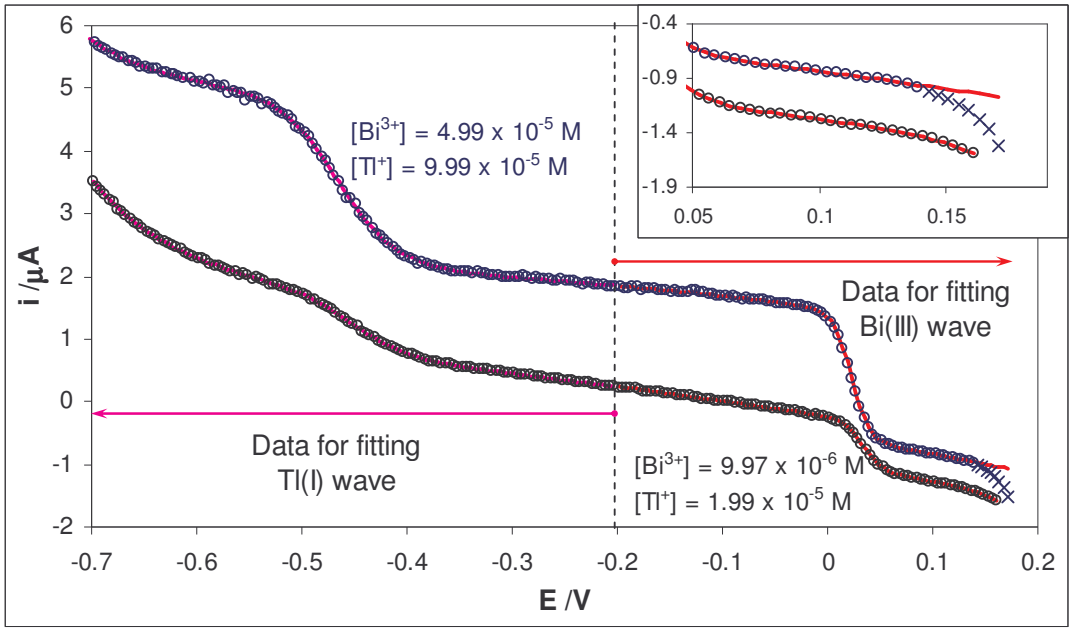

Figure 8.6: Polarograms showing the reduction Bi(III) and Tl(I) in 0.5 M HNO_3. Data points are given as circles and functions are given by the solid lines. The crosses are data points that were deleted in fitting the Bi(III) wave.

To determine the extent of bismuth hydrolysis, especially at low pH values, species distribution diagrams were constructed using formation constants from the literature. The question was whether to consider $Bi(OH)_2^+$ or $Bi_6(OH)_{12}^{6+}$ in solution under the conditions used here, i.e. with Bi(III) concentrations of the order of 10^{-5} M. $Bi(OH)_2^+$ was definitely detected at extremely low Bi(III) concentrations (<10^{-7} M),[15] and Bidleman[16] found no evidence for $Bi_6(OH)_{12}^{6+}$ at Bi(III) concentrations <10^{-4} M. Species distribution diagrams using the log β values at 0.5 M ionic strength (as given in Table 8.1) were plotted by including both the $Bi(OH)_2^+$ and $Bi_6(OH)_{12}^{6+}$ species in the model, as well as only the

$Bi(OH)_2^+$ species, for a Bi(III) concentration of 5×10^{-5} M – the initial concentration of Bi(III) originally used (see Figure 8.7). The species distribution diagram with only the $Bi_6(OH)_{12}^{6+}$ species at the same concentration is given in Figure A6.1 (Appendix 6). By including both the mononuclear and polynuclear species in the model, they become competing species in solution. The two species distribution graphs only differed between about pH 2.5 and 4.5 and $Bi(OH)_2^+$ was clearly the dominant species under these conditions. At this Bi(III) concentration, almost 10% of the Bi(III) exists as $BiOH^{2+}$ at an acid concentration as high as 0.5 M in a non-complexing background solution. The hydroxide ion concentration in an aqueous solution at this pH is only about 2×10^{-14} M, about 10^9 times less than that of the Bi(III) present, proving how strongly acidic the Bi(III) ion is. Precipitation was not indicated on the diagram as $Bi(OH)_3$ is expected to precipitate at about pH 6, but the BiOA species precipitates before then (closer to pH 2 under these conditions) as shown in Figure 8.3.

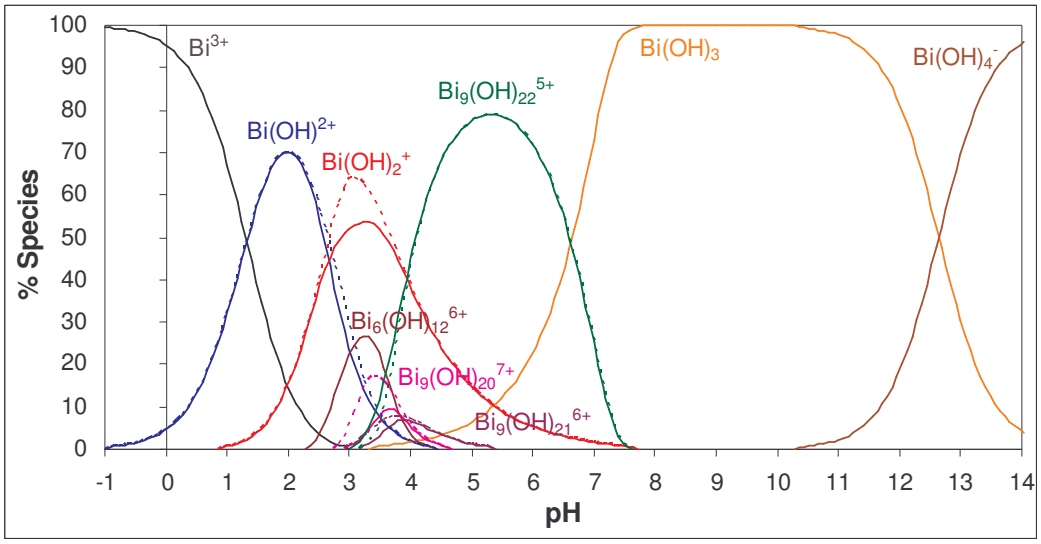

Figure 8.7: Species distribution diagram for [Bi(III)] = 5×10^{-5} M assuming both $Bi(OH)_2^+$ and $Bi_6(OH)_{12}^{6+}$ are present (solid lines) or only $Bi(OH)_2^+$ is in solution (dashed lines). (Log β values at 25 °C and 0.5 M ionic strength were used).

Figure 8.8 was drawn using the same log β values and the model including both the $Bi(OH)_2^+$ and $Bi_6(OH)_{12}^{6+}$ species, but the Bi(III) concentration was set at 1×10^{-5} M – the initial concentration of Bi(III) used in subsequent

experiments. The extent of polymerisation of the Bi(III) hydrolysis products was largely reduced by decreasing the Bi(III) concentration, with only a small amount of $Bi_9(OH)_{22}^{5+}$ and no $Bi_6(OH)_{12}^{6+}$ being formed. In subsequent calculations employing these models, all possible species were included as they compete with one another and the concentration conditions determine which species are present in a significant amount.

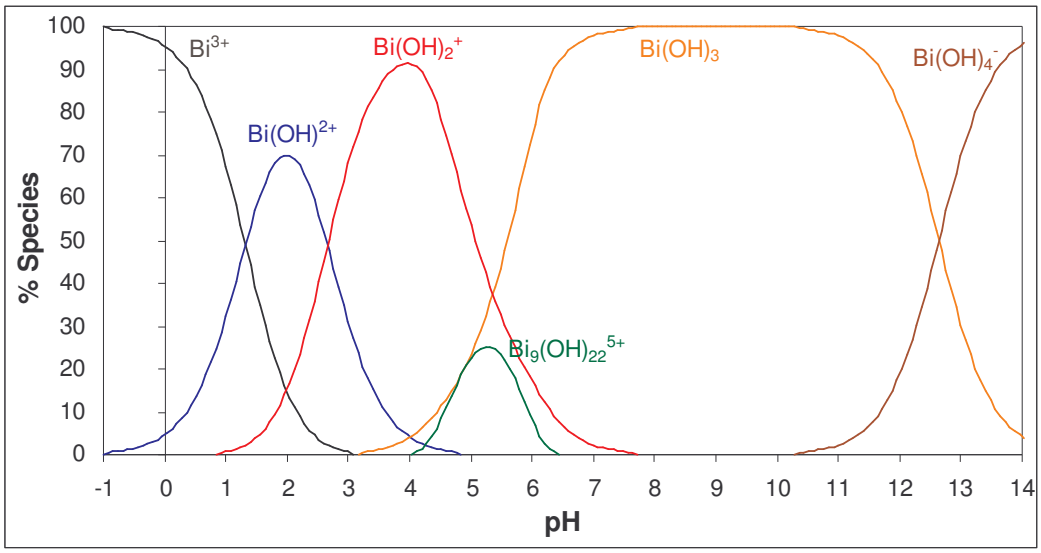

Figure 8.8: Species distribution diagram for [Bi(III)] = 1×10^{-5} M, determined with all possible Bi(III)-hydroxide species included in the model. (Log β values at 25 °C and 0.5 M ionic strength were used).

A nitrate background is often used as it is generally "inert" or not strongly complexing. However, it does form fairly strong complexes with Bi(III). This, together with the fact that there is about 10^4 times more nitrate in solution compared to Bi(III), could result in a significant amount of Bi(III) nitrate species being formed. Species distribution diagrams were therefore plotted as before using stability constants for both the Bi(III) hydroxide and nitrate (as given in Table 8.2) species together at the two different Bi(III) concentrations (see Figures 8.9(a) and (b)). The nitrate competes with the hydroxide under very acidic conditions to complex Bi(III), and the species most influenced by the presence of these high concentrations of nitrate is $Bi(OH)^{2+}$. This was also shown in the pBi′-pH diagram by Kragten *et al.*[24] (Figure 8.3(a)) with $Bi(NO_3)^{2+}$ being the major species below about pH 2.7, not $Bi(OH)^{2+}$ or Bi^{3+}, followed by

$Bi(OH)_2^+$ above this pH. However, in Figure 8.9 it is predicted that $Bi(OH)^{2+}$ would be the dominant species between pH 1.7 and 2.7.

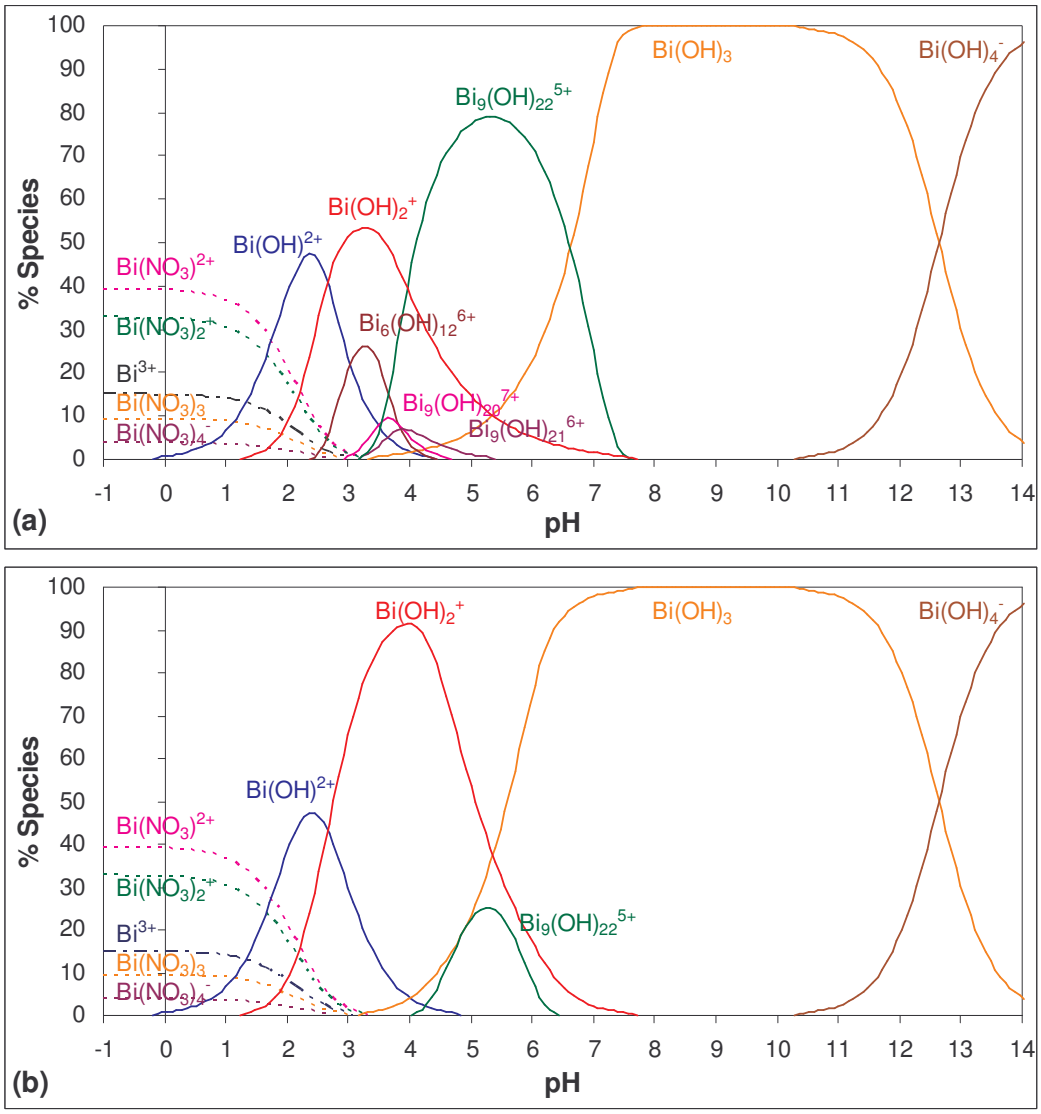

Figure 8.9: Species distribution diagrams for Bi(III) nitrate and hydroxide species with $[NO_3^-]$ = 0.5 M and [Bi(III)] = (a) 5×10^{-5} M or (b) 1×10^{-5} M. (Log β values at 25 °C and 0.5 M ionic strength were used).

The pBi′-pH diagrams presented by Kragten *et al.*[24] (Figure 8.3) display general trends fairly well, but they do raise some questions. For instance, since the $BiClO_4^{2+}$ species is less stable than the $BiNO_3^{2+}$ species (at the same ionic strength) it is doubtful that the former would be predominant in solution to higher pH values than the latter, before $Bi(OH)_2^+$ is formed. The fact that $Bi_6(OH)_{12}^{6+}$ occurs as a major species in perchlorate and not nitrate solutions

could be due to the lower solubility of $BiONO_3$ as compared to $BiOClO_4$, thus Bi(III) concentrations are not high enough for significant polymerisation to occur before precipitation takes place. The experimentally determined points clearly show the conditions under which precipitation occurs and certainly emphasises that it is necessary to work in low Bi(III) concentrations to prevent or postpone precipitation.

This makes polarography an ideal technique to study Bi(III) complexation as it is a fairly sensitive technique which allows us to use low Bi(III) concentrations. In the pH titration experiments, when the initial solutions contained 4.99×10^{-5} M Bi(III), precipitation occurred just before pH 2. It was impossible to actually see the precipitate at this low Bi(III) concentration, so it was deduced from the rapid decrease in the diffusion limited current determined from the polarograms. The onset of precipitation was found to occur at lower pH values if the time between recording polarograms was increased, showing that the precipitate formation process is relatively slow. Moussa and Sammour[38] observed that in solutions containing certain concentrations of Bi(III), $HClO_4$ and chloride, the formation of solid BiOCl occurred at either an immediate or a slow rate, depending on the concentration ratios, and the precipitate only became visible after several hours.

The precipitate formed in this case was assumed to be the Bi(III) oxynitrate species, $BiONO_3$ as predicted by Kragten *et al.*[24] However, other authors[28-30,32] have shown that it exists rather as a hexanuclear bismuth species such as $Bi_6O_4(OH)_4(NO_3)_6$. To test the composition of the precipitate, 0.5 M NaOH was added to a 0.1 M Bi(III) solution in 0.5 M HNO_3 till precipitation occurred below pH 2. The solution was then filtered and allowed to dry. Swinehart and Garrett[25] described the precipitate they formed under acidic conditions as white shiny platelets, which is what was obtained in this case. On analysis of the precipitate by powder X-ray diffraction, the structure was found to correlate with polynuclear species containing bismuth, oxides, hydroxides and nitrates. The powder pattern is given in Figure 8.10 and is superimposed by the powder patterns that were calculated from single crystal data by Lazarini[28,31] (as given in the Inorganic Crystal Structure Database (ICSD)[42]) showing that both

$Bi_6O_4(OH)_4(NO_3)_6(H_2O)_4$ and $Bi_6O_5(OH)_3(NO_3)_5(H_2O)_3$ were present. This is an indication that the precipitate formed does consist of the hexanuclear species. However, this precipitate was formed under relatively high Bi(III) concentrations, about 10^4 time greater than in the polarographic cell, so the stoichiometry may be different. The precipitate will be referred to as a bismuth-oxy-nitrate species in future as the stoichiometry of the products vary and a mixture of these can form. The collodial precipitate is said to react rather slowly and is fairly inert when it sticks to the vessel walls.[24] Glassware was therefore soaked using a 20% nitric acid solution and thoroughly rinsed after use.

A typical set of polarographic results for a pH titration with an initial solution of 0.5 M HNO_3 containing 4.99×10^{-5} M Bi(III) and 9.99×10^{-5} M Tl(I) which was titrated with 0.5 M NaOH will be considered. Figure 8.11 depicts the value of δ at each pH for the reduction of Bi(III), and $\delta = 1.00 \pm 0.04$ for this experiment which would indicate a reversible electron transfer process. From literature[37,41] it is expected that Bi(III) reduction would be quasi-reversible in a nitrate medium. Headridge *et al*.[43] found the reduction of Bi(III) to be reversible in both fluoride and perchlorate media, also contrary to what was expected. Bond[41] suggested that this could be due to the presence of trace quantities of chloride that leaked into the solution from the saturated potassium chloride salt bridge they used. This cannot be the case here as a nitrate solution was used in the salt bridge specifically to avoid chloride contamination.

The observation made here could be explained by the following passage:

> *Current usage of the term "reversibility" in electrochemical literature is generally confusing. Criteria for reversibility are used which depend not only on the system studied, but also on the method of investigation, so that a particular system classified as "reversible" on the basis of one type of investigation may not behave "reversibly" when studied by a different technique.*
>
> Bauer and Elving (1960)[40]

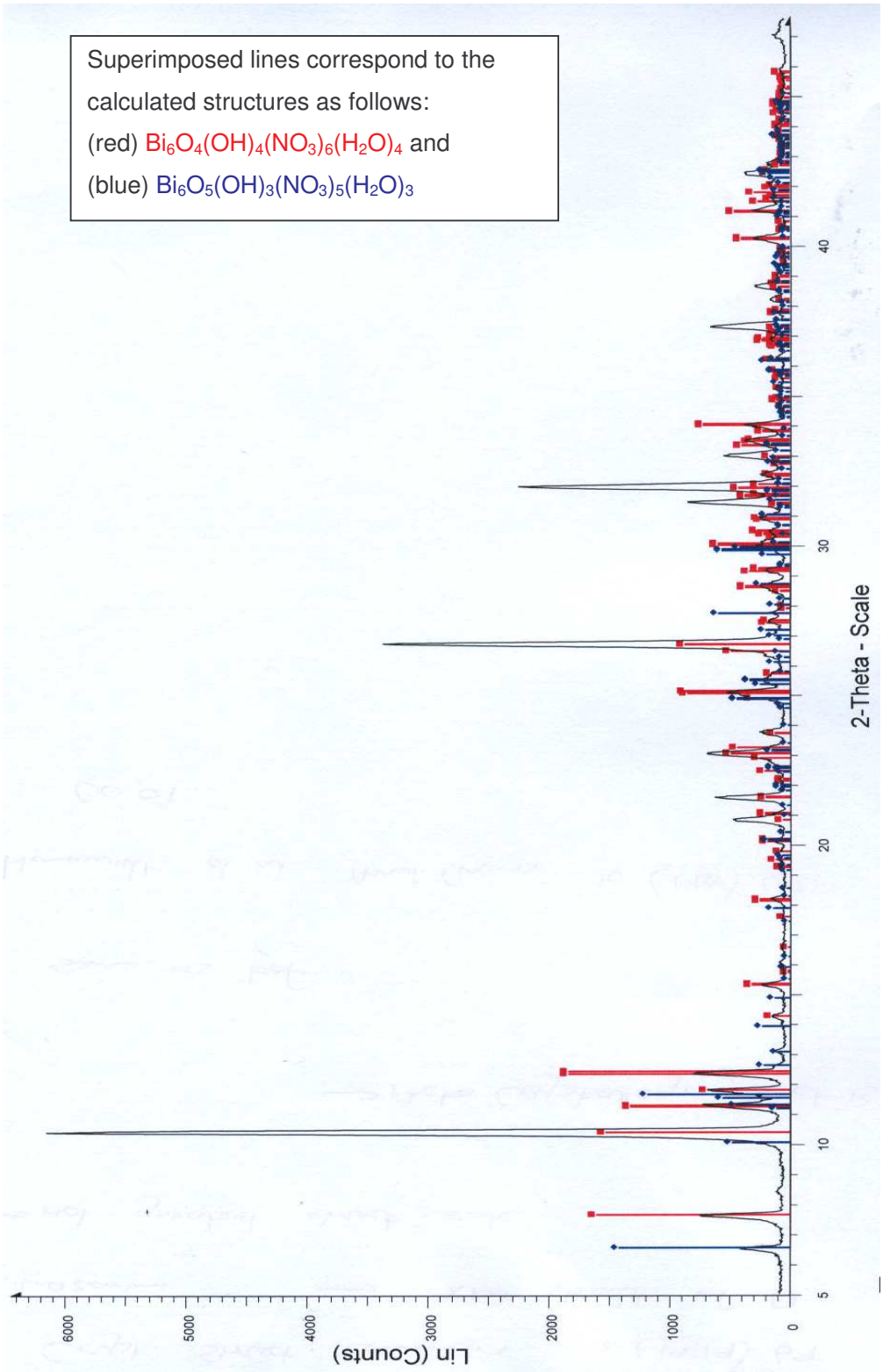

Figure 8.10: PXRD pattern of the bismuth-oxy-nitrate precipitate formed.

They pointed out that the log plots used to determine reversibility for DC polarographic data are not sufficiently sensitive to changes in reversibility. It appears that parameters determined by AC polarography (α, k_e and ρ) change more significantly as the reversibility changes, whereas the slope of the log plots from DC polarography data appears fairly constant.[40]

So what does this mean in terms of this experimental data in this application? Two experimental parameters are used in assessing formation constants from DC polarographic data, namely i_d and $E_{1/2}$. It is well established that i_d does not change with the extent of reversibility. The value of δ is an indication of the slope of the DC polarogram. For $\delta < 1$ the slope would be less than the Nernstian slope and thus $E_{1/2}$ would be more negative than that for a fully reversible process. For DC polarography it was assumed that the reversible $E_{1/2}$ value is determined when δ is unity, even if parameters determined by another technique indicates that it is not fully reversible. In these studies we are interested in the shift in $E_{1/2}$ from the value of the free metal ion to that of the complexed metal ion, and as long as that shift does not include an additional shift due to the change in slope of the DC wave (due to changes in reversibility as measured by δ) it should be adequate for our purpose.

Figure 8.12 shows the plot of the diffusion limited current versus pH for both the reduction of Bi(III) and Tl(I). The data for Tl(I) reduction exhibits (as before) a large drop in current with an initial increase in pH to dilution where large volumes of hydroxide solution are required to change the pH. A very small change in current is observed after about pH 2.5 where only 2 μL of hydroxide was added between each polarogram in this case. A similar behaviour was observed for the Bi(III) reduction waves, but the diffusion limited current dropped rapidly after about pH 1.6 due to precipitation of the bismuth-oxy-nitrate species. This severely limits the pH range in which data for Bi(III) reduction can be collected.

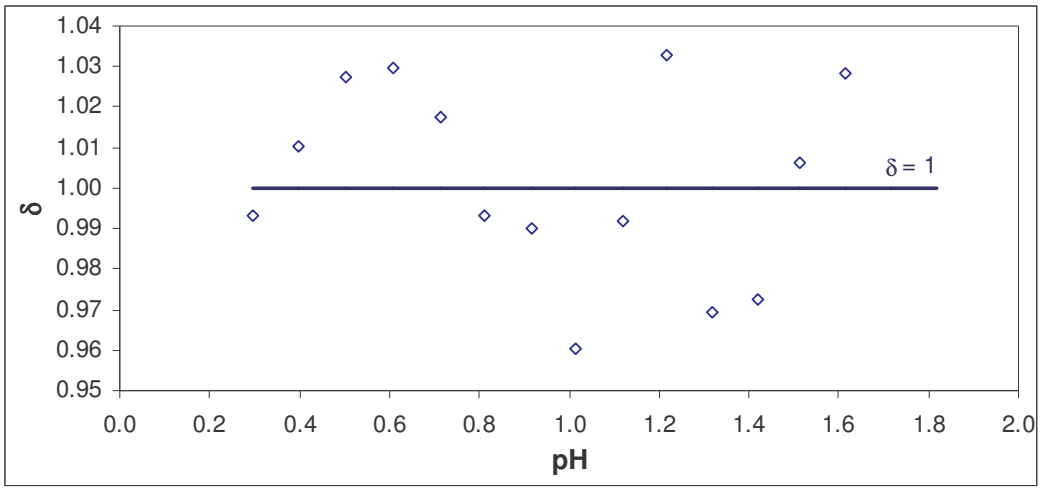

Figure 8.11: The value of δ versus pH for the reduction of Bi(III) in a H/$NaNO_3$ solution.

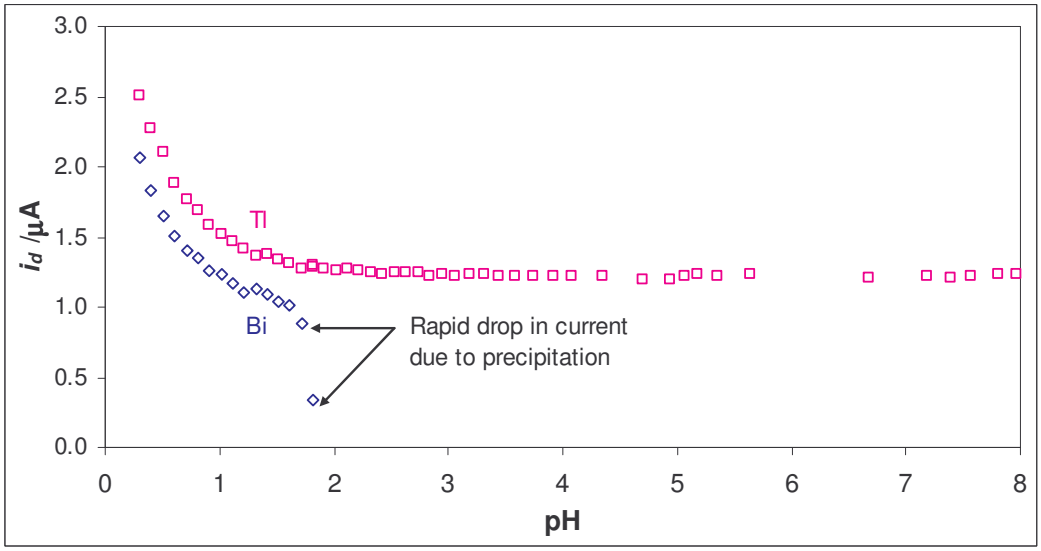

Figure 8.12: The change in the diffusion limited currents during a pH titration experiment where initial concentrations of Bi(III) and Tl(I) were 4.99×10^{-5} M and 9.99×10^{-5} M respectively.

Figure 8.13 shows the graph of the half-wave potential versus pH for the reduction of Tl(I) and Bi(III). The variation in the potential below about pH 2 for the Tl(I) data is due to the diffusion junction potential. The free Tl(I) potential corresponds to the average potential where the change in the junction potential in negligible, as before. The Bi(III) reduction potentials are shown until precipitation occurs. The potential intervals in the graph are the same on both axes (40 mV overall) so that the relative shifts for the two metal ions can

be compared. It can be seen that the Bi(III) reduction potential is influenced by both the junction potential and complex formation with nitrate and/or hydroxide. It is also clear that there is no way to directly determine the free Bi(III) potential from this data as was done with the Tl(I) data and that for the other metal ions studied.

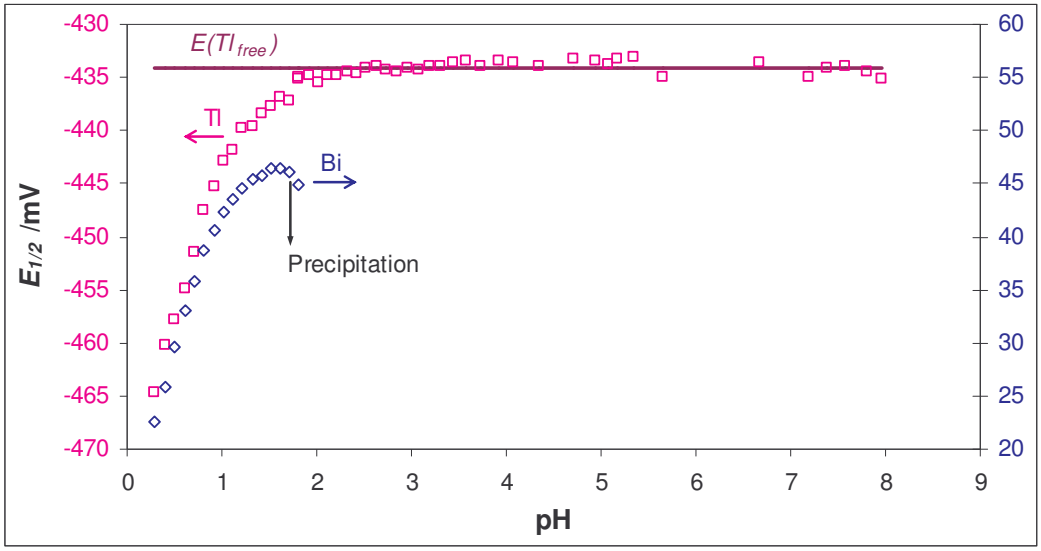

Figure 8.13: Half-wave potentials versus pH for the reduction of Bi(III) and Tl(I).

Thallium was included in the experiment so that the Bi(III) data could be corrected for any change in E_j using Tl(I) as the witness. The change in E_j, as a function of pH, was determined by subtracting each $E_{1/2}$ value from $E(Tl_{free})$. In the pH region where the change in E_j with pH was significant, data points were fitted using a third order polynomial to smooth the data and the $E_{1/2}$ values for the function were used rather than the raw data values (as described in Chapter 6).

In order to determine the free Bi(III) potential, potential shifts due to both E_j and the formation of Bi(III)-hydroxide species (particularly $Bi(OH)^{2+}$ in the pH range considered) would have to be compensated for. Once these compensations were taken into account, a straight horizontal line was expected which would be equal to the free Bi(III) potential. The potential shifts due to Bi(III) hydrolysis ($\Delta E(OH)$) were calculated at each pH value using the 3D-CFC software[44] employing the log β values for the Bi(III)-hydroxide species (as was

used to produce Figure 8.7). Figure 8.14 shows the Bi(III) reduction potentials together with the compensated values. Unfortunately, the horizontal line expected from the points demarcated by × was not produced. It appeared as though there was overcompensation at the higher pH values, which lead to the speculation that the formation constant for $Bi(OH)^{2+}$ was too high. Reducing the log β value from 12.4 to 11.8 yielded a better horizontal line as demarcated by the points + and this was illustrated by plotting the average of these corrected values as a straight solid line to.

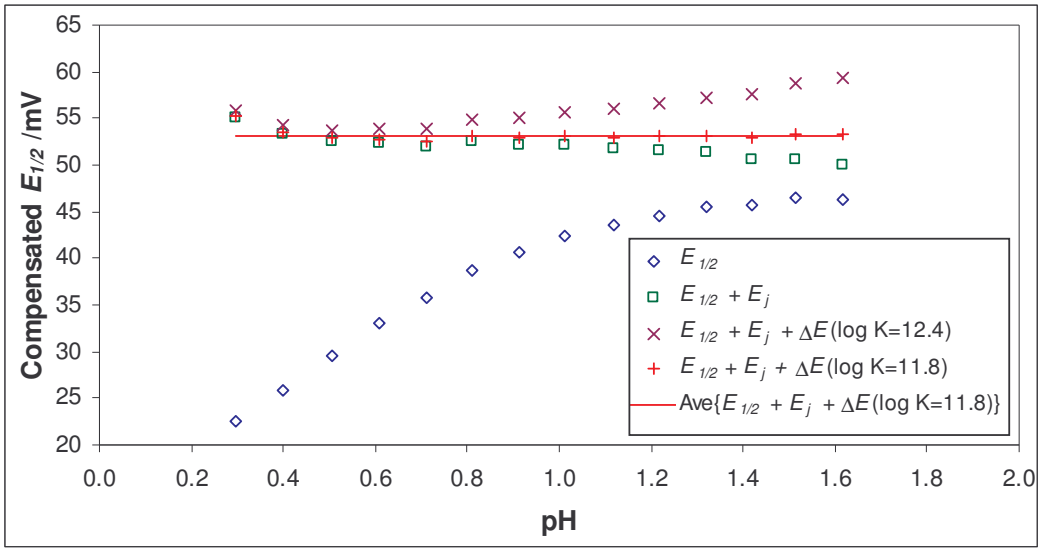

Figure 8.14: Reduction potentials of Bi(III) (initially at 4.99×10^{-5} M) as a function of pH. Potential shifts due to E_j and $Bi(OH)^{2+}$ formation (using log β = 12.4 or 11.6) were compensated for.

However, there were no firm grounds on which to simply reduce the value of the formation constant for the $Bi(OH)^{2+}$ species. An article by Barnum[45] describes general trends in hydrolysis data, as well as mechanisms by which to estimate these formation constants for both mononuclear and polynuclear complexes if they are not available. These theories were applied to the Bi(III) hydrolysis data to assess the accuracy of the formation constants used here and in particular to determine if there is possibly an error in the first hydrolysis constant.

8.3.2) *Predicting Bi(III) hydroxide formation constants*

Barnum[45] found that for most metal ions, the standard free energy of formation of their mononuclear hydroxide species versus the number of coordinated hydroxide ions produced a smooth curve which could be fitted by the relationship:

$$\Delta G_f^{\,o}\{M(OH)_y\} = \Delta G_f^{\,o}\{M\} + By + Cy^2 + D/y \qquad (8.2)$$

where *B*, *C* and *D* are empirical constants determined by fitting experimental data and y is the number of coordinated hydroxide ions. The value of *D* was found to be 8.37 kJ.mol^{-1} for di- and trivalent metal ions and *D* is zero for tetravalent metal ions. By rearranging of the expression, Barnum[45] defined a function $U\{M(OH)_y\}$ as:

$$\left[\Delta G_f^{\,o}\{M(OH)_y\} - \Delta G_f^{\,o}\{M\} - D/y\right] \Big/ y = B + Cy = U\{M(OH)_y\} \qquad (8.3)$$

For the reaction:

$$xM^{n+} + yH_2O \rightleftharpoons M_x(OH)_y + yH^+$$

the formation constant is β^*_{xy} and in particular for the mononuclear hydroxide species the formation constant would be β^*_{1y}. In this case

$$\Delta G^o = -RT\ln K_{1y} = \Delta G_f^{\,o}\{M(OH)_y\} - \Delta G_f^{\,o}\{M^{n+}\} - y\Delta G_f^{\,o}\{H_2O\} \qquad (8.4)$$

Therefore

$$U\{M(OH)_y\} = \Delta G_f^{\,o}\{H_2O\} - D/y^2 - (2.303RT\log\beta^*_{1y})/y \qquad (8.5)$$

Equation 8.3 shows that the graph of *U* versus y gives a straight line with slope *C* and intercept (on the U-axis) *B*. The value for *U* could be calculated using the standard free energy of formation data as in equation 8.3 or using the stability constant as in equation 8.5. The graph could be used to predict unknown formation constants or to highlight disparate data. Disparity may point to experimental error in data, but it may also simply indicate the failure of the empirical equations or that there could be something unusual about the structure or stability of the complex.

Considering the hydrolysis constants of the mononuclear Bi(III) species, the values for log β_{1y} (at 25 °C and ionic strengths of 0.1 M or 1.0 M) were converted to log β^*_{1y} values by applying the following relationship:

$$\log \beta^* = \log \beta + y \log K_w \qquad (8.6)$$

where the values of log K_w used were −13.71 for ionic strength 0.1 M and −13.81 for ionic strength 1.0 M.[17] The values for $U\{M(OH)_y\}$ were calculated using equation 8.5 and a value of −237.19 (±0.025) kJ.mol^{-1} at 25 °C for $\Delta G_f^o\{H_2O(\ell)\}$.[45] These data are given in Table 8.5.

Table 8.5: Experimental log β_{1y} values (at 25 °C and ionic strengths of 0.1 M [a] or 1.0 M [b]) and the calculated log β^*_{1y} and $U\{Bi(OH)_y\}$ values.

y	log β_{1y} [18]	log β^*_{1y}	$U\{Bi(OH)_y\}$
1	12.4[a]	−1.31	−238.91
2	23.5[b]	−4.12	−227.53
3	31.9[a]	−9.23	−220.56
4	33.6[b]	−21.64	−206.84

Figure 8.15 gives the plot of $U\{Bi(OH)_y\}$ versus y. A straight line was fitted through the points by omitting the point at y = 3 which did not follow the trend. The plot gave confidence in the log β_{11} value and thus our speculation that it should be lower is unfounded. It also showed that the log β_{13} value may be too high and was predicted to be about 30.1 using the straight line equation. However, as Barnum[45] pointed out, the experimental value for log β_{13} could simply indicate unusual stability of this species and this could be due to the electroneutrality of this species in this case. Similar plots for other metal ions with a 3+ charge were also calculated (for log β values at 25 °C and 0 M ionic strength and hence the value of log K_w used was −13.997)[17] and are displayed in Figure 8.16. With the exception of Fe(III), the other plots all showed a lower than predicted value for log β_{13}, once again giving confidence in the formations constants found for mononuclear Bi(III) hydrolysis products. This procedure suggested by Barnum[45] does seem to be a useful tool in assessing the validity of metal hydroxide formation constants.

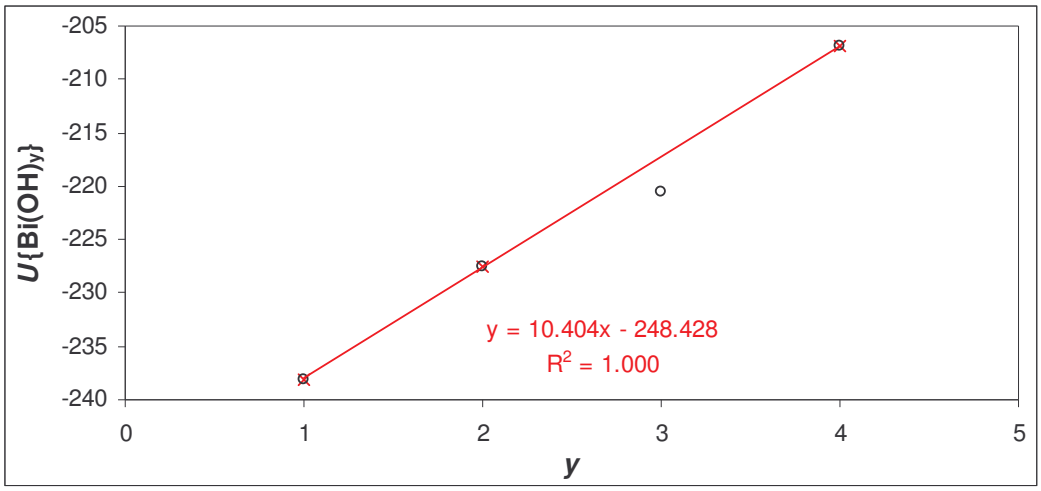

Figure 8.15: $U\{Bi(OH)_y\}$ plotted as a function of y using values given in Table 8.5. The trendline was fitted by omitting the value at y = 3.

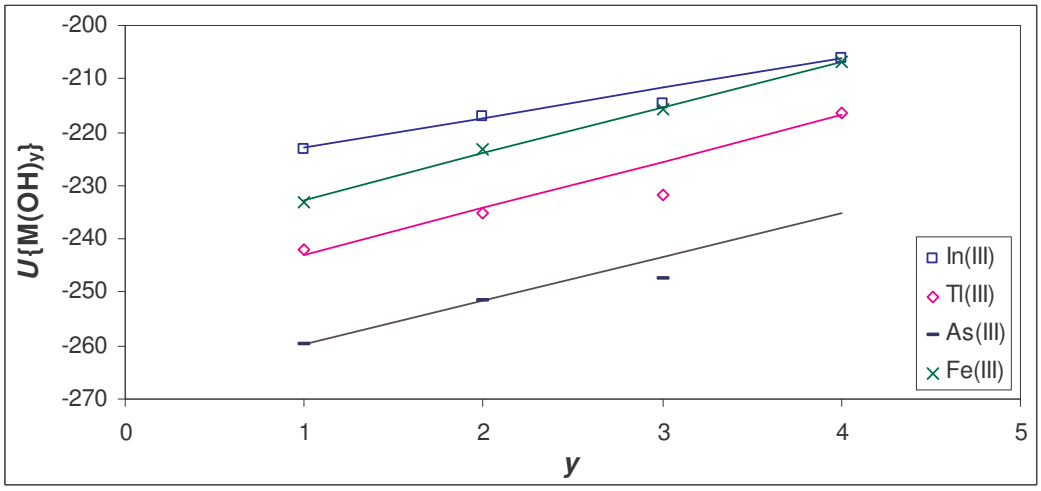

Figure 8.16: $U\{Bi(OH)_y\}$ plotted as a function of y for several trivalent metal ions at 0 M ionic strength and 25 °C. Trendlines were fitted by omitting the value at y = 3.

Barnum[45] also considered the strong dependence of the acidity of the metal aqua ions on the electronegativity (χ) of the metal ion. If the electronegativity of the metal ion is known, the values of B and C in equation 8.3 can be predicted and the formation constants calculated. The electronegativity for Bi^{3+} obtained by Pauling's method is given as 2.02.[45] The following relationships for di- and trivalent metal ions were determined for standard free energies of formation and stability constants at 25 °C and zero ionic strength:[45]

$$B = -189.63 + 14.21\chi - 20.89\chi^2 \qquad (8.7)$$

and

$$C = -0.1318B - 23.21 \quad (8.8)$$

Using the values of B = –246.17 and C = 9.235 for Bi(III) determined from equations 8.7 and 8.8, $U\{M(OH)_y\}$ could be calculated using equation 8.3 and hence applying equations 8.5 and 8.6 (where log K_w is –13.997 for zero ionic strength at 25 °C[17]) the log $\beta^*_{1y}{}^o$ and log $\beta_{1y}{}^o$ values were calculated respectively. The results for Bi(III) are displayed in Table 8.6. Since these relationships were applied to zero ionic strength conditions, the results were compared to literature values under the same conditions where possible.

Table 8.6: Calculated $U\{Bi(OH)_y\}$, log β^*_{1y} and log β_{1y} values at 0 M ionic strength using the electronegativity of Bi^{3+}. The experimental and recalculated log β_{1y} values for 0 M ionic strength are also given.

y	$U\{Bi(OH)_y\}$	log $\beta^*_{1y}{}^o$	log $\beta_{1y}{}^o$		
			Calculated	**Experimental**	**From Davies**
1	–236.93	–1.51	12.5 ± 0.5	12.9	13.0
2	–227.70	–4.06	23.9 ± 1.0	23.5 [a]	24.5
3	–218.46	–10.33	31.7 ± 1.5	33.0	33.2
4	–209.23	–19.97	36.0 ± 2.0	34.8	34.8

[a] Ionic strength of 1.0 M (no values available for 0 M ionic strength)

The log β_{1y} values at zero ionic strength could also be predicted using the Davies equation. This was done using data at 0.1 M ionic strength (or 1 M where no other data were available) and the Sol-Eq software.[46] This software makes use of the relationship between β (at a particular ionic strength) and β^o (at 0 M ionic strength) for the equilibrium:

$$pM + qH + rL \rightleftharpoons M^pH^qL^r$$

being:

$$\beta = \frac{[M_pH_qL_r]}{[M]^p[H]^q[L]^r} = \frac{\beta^o}{\left(\frac{\gamma_{M_pH_qL_r}}{\gamma_M{}^p\gamma_H{}^q\gamma_L{}^r}\right)} \quad (8.9)$$

The Davies equation is used to calculate the mean ionic coefficient and is given as:

$$\log \gamma_i = -Az_i^2 \left[\mu^{2/3} \Big/ (1+\mu^{2/3}) + 0.3\mu \right] \tag{8.10}$$

where A is the Debye-Hückel limiting slope (and is 0.51 at 25 °C), μ is the ionic strength and z_i is the charge of the ion.[46] By substituting equation 8.10 into equation 8.9, the relationship between β and β^o can be given as:

$$\log \beta = \log \beta^o + a_i \left[\mu^{2/3} \Big/ (1+\mu^{2/3}) + 0.3\mu \right] \tag{8.11}$$

where $a_i = A\,\Delta z^2$ and Δz^2 is the square of the charge on each species summed over the formation reaction.[46] The $\log\beta_{1y}^o$ values predicted using the Davies equation compared well to the values given in the NIST database[17] and it also allowed log β_{12}^o to be predicted where no data were available, although the Davies equation is only reliable up to an ionic strength of 0.1 M. These values also compared well to those calculated using the electronegativity of Bi^{3+}, as noted in Table 8.6.

The uncertainty in the calculated log β_{1y}^o values was given as $\pm 0.5y$ [45] and it can be seen that when this error is accounted for, the calculated values compare to those determined experimentally. It should also be kept in mind that the experimental data also carries an error. The large uncertainties in these calculated values make them impractical to use in complex formation studies, but it gives an estimate if these values are not known. It should also be said that considering the only data being used is the electronegativity of the metal ion and applying trends applicable to both di- and trivalent metal ions, it is a good approximation of these formation constants.

Barnum[45] also proposed a method to calculate the formation constants for polynuclear species if the value for log β_{11} is known. The calculation is as follows:

$$\log \beta^*_{xy} = y\left(\log K_q + \log \beta^*_{11}\right) \tag{8.12}$$

where log K_q applies to the reaction:

$$MOH \rightleftharpoons (1/y)M_x(OH)_y + [(y-x)/y]M$$

The average value for log K_q for trivalent ions was found to be 1.15 ± 0.65.[45] Substituting equation 8.6 into equation 8.12 gives:

$$\log \beta_{xy} = y(\log K_q + \log \beta^*_{11} - \log K_w) = y(\log K_q + \log \beta_{11}) \quad (8.13)$$

Since log β_{11} was 12.4 at both 0.1 M and 0.5 M ionic strengths, the predicted log β_{xy} values were the same. Log β_{11} was 12.9 at 0 M ionic strength. The calculated values were once again compared to those from literature at various ionic strengths and the results are given in Table 8.7. Considering the complex species, the simplistic calculation and an average value of log K_q with a large uncertainty used, the calculated log β_{xy} values compared surprisingly well to the literature values. The value of log K_q used is probably for 0 M ionic strength at 25 °C which explains why the log β_{xy} values predicted are closer than those for 0.1 M ionic strength. It also gives an indication of the magnitude of log β at 0.1 M ionic strength for $Bi_6(OH)_{12}$ which is not available in literature. Of course the stoichiometry of the polynuclear species have to be determined experimentally.

Table 8.7: Calculated and literature values for log β_{xy} at 0.1 M and 0.5 M ionic strengths.

Species	**y**	**Calculated μ = 0**	**Calculated μ = 0.1 or 0.5**	**Literature[17] μ = 0.1**	**Literature[18] μ = 0.5**
		log β^o_{xy}	**log β_{xy}**	**log β_{xy}**	**log β_{xy}**
$Bi_6(OH)_{12}$	12	168.6	162.6	165.3 [a]	162.8
$Bi_9(OH)_{20}$	20	281.0	271.0	271.9	266.9
$Bi_9(OH)_{21}$	21	295.1	284.6	282.5	276.8
$Bi_9(OH)_{22}$	22	309.1	298.1	293.6	287.3

[a] μ =1.0 M

Equation 8.13 implies that a plot of log β_{xy} against y would give a straight line passing through the origin and slope of (log K_q + log β_{11}). This is plotted in Figure 8.17 for the values in Table 8.7. The literature data did show the linear trend with the log β_{xy} -intercept close to zero, especially when considering that the value of log K_q is quoted as to be between 0.5 and 1.8[45] and this value is multiplied by y which is relatively large in this case. This alone could result in an error of the slope being ±0.65.

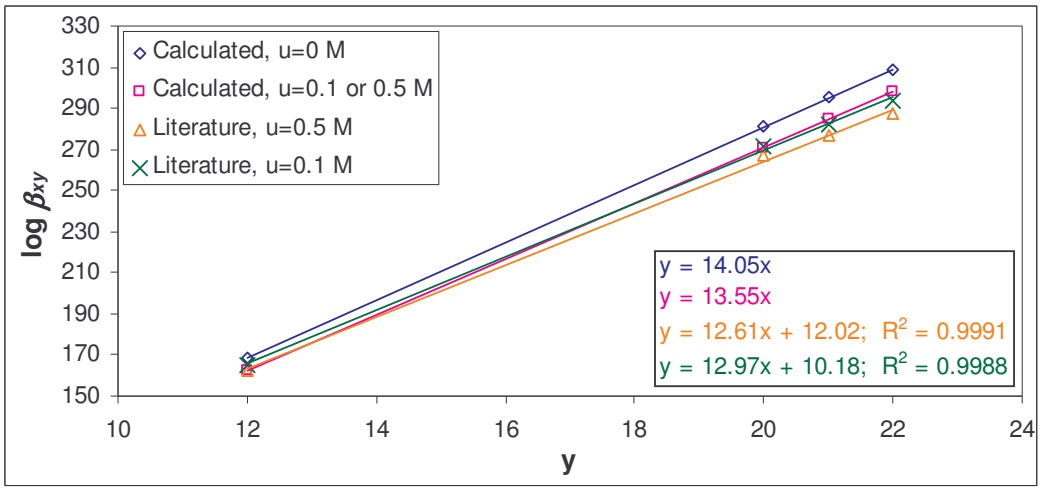

Figure 8.17: Plot of log β_{xy} against y using data in Table 8.7.

This process of comparing the literature values for log β for the hydrolysis products of Bi(III) gave some confidence to the experimentally determined values and therefore querying the validity of the log β value for $Bi(OH)^{2+}$ was unfounded. The process used to determine the free Bi(III) potential, which lead to the questioning of the accuracy of the log β_{11} value, was therefore reconsidered.

8.3.3) *Determining the free Bi(III) potential*

From the discussion earlier, it is noted that at very low pH nitrate complexes formed, rather than the hydroxide complexes, which in effect reduces the extent of hydrolysis below about pH 3. This is why the smaller log β value for $Bi(OH)^{2+}$ appeared to produce better results when compensating for the potential shifts. The 3D-CFC software[44] was again employed to determine potential shifts due to Bi(III) hydrolysis but now also accounting for the presence of Bi(III) nitrate complexes. Log β values for both the Bi(III) hydroxide species and the Bi(III) nitrate species were entered, where nitrate was regarded as the ligand. At each pH, where experimental half-wave potential values were obtained, the concentrations of total Bi(III) and nitrate were calculated, accounting for dilution due to hydroxide solution addition. The potential shifts, as well as the percentage of the various species formed in solution (particularly the hydroxide species), were thus calculated at each pH

under the experimental conditions of the solution at that point. The decreasing Bi(III) concentration did not affect the calculated values much but it was critical to take the changing nitrate concentration into account because nitrate was in such a large excess compared to Bi(III).

An example of a set of results produced is illustrated in Figure 8.18(a). The experimentally determined $E_{1/2}$ values and the resulting potential values after correction for E_j are the same as that given in Figure 8.14. The potential shifts determined using the model which incorporated both nitrate and hydroxide species, were relatively large (between 12.0 and 16.5 mV in this pH range) and were predominantly due to the formation of Bi(III) nitrate species at the lowest pH values, as indicated in the enlarged species distribution diagram for this region (Figure 8.18(b)). These shifts were added to the $E_{1/2} + E_j$ values and the resulting potentials are given as × in Figure 8.18(a). These potential values initially decreased as the pH increased which was unexpected as the change in nitrate concentration was accounted for in the calculation of the potential shifts. It was anticipated that the resulting potential values would produce a horizontal straight line corresponding to the true free metal ion potential. The value of $E(Bi_{free})$ was estimated as the average potential after the $E_{1/2} + E_j$ values were corrected for potential shifts due to nitrate and hydroxide formation (see — in Figure 8.18(a)). Points at the lowest pHs which were significantly higher than the others, were excluded such that the standard deviation of the average was ≤ 1 mV.

The potential shifts due to the formation of only the Bi(III) hydroxide species in the nitrate supporting electrolyte were also considered (as was attempted in Figure 8.14). These were calculated by establishing the percentage of $Bi(OH)^{2+}$ and $Bi(OH)_2^{+}$ formed at each pH using the 3D-CFC software[44] as before. The Bi(III) hydroxide species form ion pairs with nitrate in solution to give species as indicated by the general formula given by Baes and Mesmer[2] as $M_xO_u(OH)_{y-2u}(OH_2)_vA_a^{(xz-y-a)+}$ where A^- would refer to nitrate in this case.

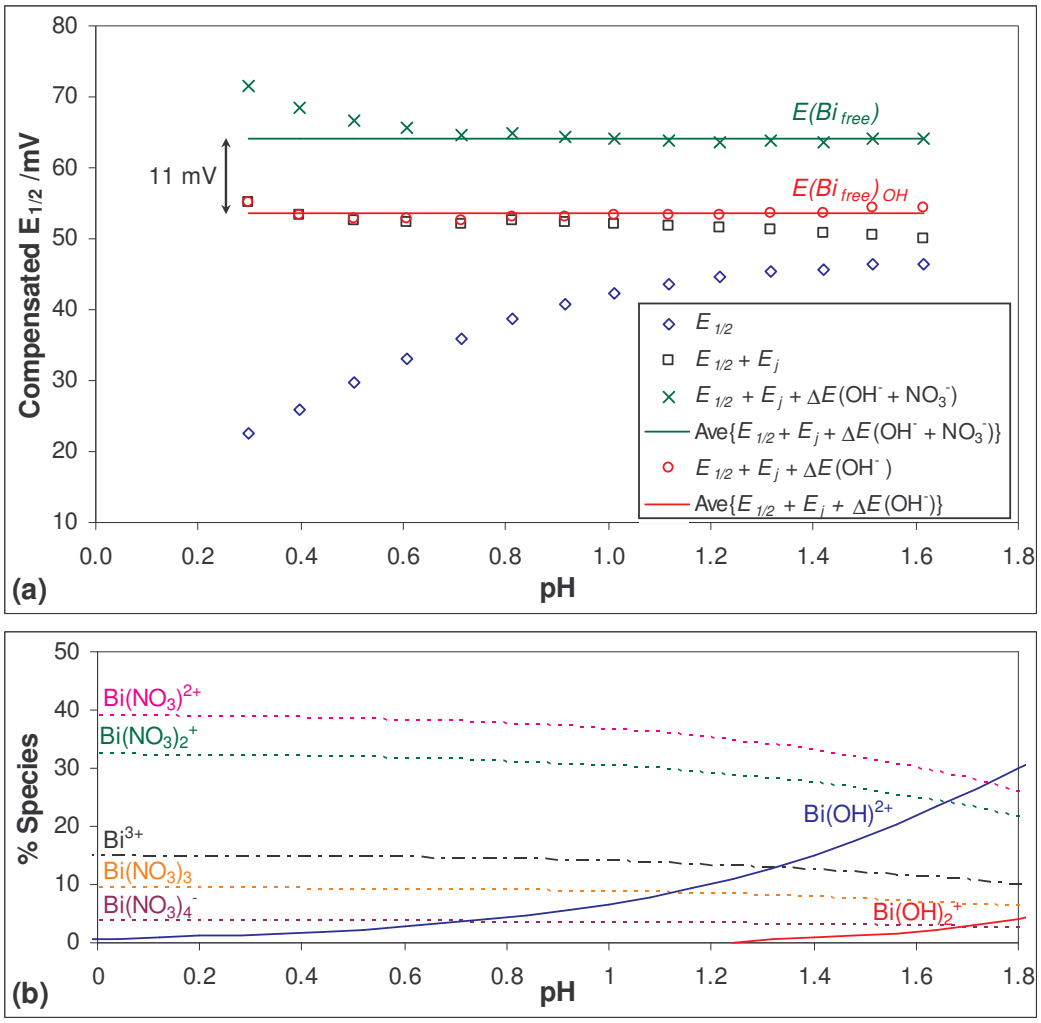

Figure 8.18: (a) $E_{1/2}$ values of Bi(III) reduction as a function of pH. Potential shifts due to the E_j and ΔE due to $Bi(OH)^{2+}$ and $Bi(OH)_2^+$ in the presence of nitrate, or ΔE due to $Bi(OH)^{2+}$, $Bi(OH)_2^+$ and Bi(III) nitrate species, were compensated for. Initial [Bi(III)] = 4.99×10^{-5} M. (b) Species distribution diagram for the corresponding pH region with $[NO_3^-]$ = 0.5 M and [Bi(III)] = 5×10^{-5} M.

The potential shift for the formation of the Bi(III) hydroxides (which includes all hydroxide species present at the specific pH), $\Delta E(OH)$, was calculated using the equation:

$$\Delta E(OH)_{(i)} - \frac{RT}{nF} ln \frac{i(M_{comp})_{(i)}}{i(M_{free})_{(i)}} = \frac{RT}{nF} ln \frac{[M_T]_{(i)}}{[M_{free}]_{(i)}} \qquad (8.14)$$

as would be used to determine the formation constants of metal-ligand complexes (see equation 2.17). It was assumed that the rate of diffusion of the free metal ion (or actually the hydrated metal ion) and that of the hydroxide

complexes is the same and that all hydroxide species were fully labile. Therefore $i(M_{comp})_{(i)} = i(M_{free})_{(i)}$ and:

$$\Delta E(OH)_{(i)} = \frac{RT}{nF} \ln \frac{[M_T]_{(i)}}{[M_{free}]_{(i)}} \qquad (8.15)$$

The total Bi(III) concentration can readily be calculated at each pH by taking the dilution into account. The concentration of $Bi(OH)^{2+}$ and $Bi(OH)_2^{+}$ were determined by multiplying the total Bi(III) concentration at each pH by the fraction of the species found. The free Bi(III) concentration was then calculated by subtracting the concentration of $Bi(OH)^{2+}$ and $Bi(OH)_2^{+}$ from the total Bi(III) concentration, thus ignoring the Bi(III)-nitrate species. The values were then substituted into equation 8.15 to determine $\Delta E(OH)$ at each pH. These $\Delta E(OH)$ values were added to the $E_{1/2} + E_j$ values in Figure 8.18(a) to give the points indicated by ○ and the average value across all pHs is shown as —. It can be seen that these data points do lie closer to a horizontal line, as expected. This average value was thus used as the "free" Bi(III) potential in the presence of nitrate in the low pH region and given the symbol $E(Bi_{free})_{OH}$. The slight overcompensation of E_j at the very low pHs was expected as Tl(I) reduction potentials were used to calculate the E_j values. As was seen for Cd(II) and Cu(II), the change in ionic strength during the titration lead to slightly larger potential shifts for Tl(I), by about 2 – 3 mV at pH 0.3. It appears that this is the case here too.

The difference between $E(Bi_{free})$ and $E(Bi_{free})_{OH}$ was 11 mV for this data set which shows the effect of the formation of nitrate species. The reason for even considering $E(Bi_{free})_{OH}$ will become evident in Chapter 9. It will be seen that the restricting factor is the 3D-CFC[44] software which only allows for only a single ligand (apart from hydroxide) to be considered at a time and hence a model incorporating both nitrate and the ligand that is being investigated is unfortunately not possible.

It was observed that, depending on how fast the titration experiment was performed, the pH at which precipitation occurs varies. A set of experiments was designed to check if this was merely due to kinetically slow precipitate

formation, as suggested by Moussa and Sammour.[38] The time interval between addition of the hydroxide solution to the test solution and the collection of polarographic data was set to range from 10 minutes to 60 minutes for different titration experiments. The approximate pH at which precipitation starts is given in Table 8.8 and clearly indicates that the bismuth-oxy-nitrate precipitate can already start forming below pH 1 given enough time. The plot of the diffusion limited current versus pH for each titration experiment at the various time intervals is also shown in Figure A6.2 (Appendix 6), where the onset of precipitation occurs when there is a sudden drop in current. The disparity in current between titration experiments at the lowest pH could be due to slight variations in the concentration of Bi(III) added, the mercury drop size which varied with the nitrogen pressure and/or the amount of gelatine added. After precipitation commences, the decrease in current is also "slow" and does not drop to zero immediately which would indicate that all the Bi(III) had precipitated.

Table 8.8: Approximate pHs for the onset of the precipitation of bismuth-oxy-nitrate species for titration experiments with varying time intervals between hydroxide addition and polarographic data collection. (Initial [Bi(III)] = 5×10^{-5} M).

Time interval /min	Approximate pH of precipitation
0	>2.1
10	1.7
20	1.5
30	1.3
45	1.3
60	1.0

To test the kinetics of precipitate formation further, an experiment was run as fast as possible. This was achieved by making up acid solutions between about pH 0.3 and 2.1, deoxygenating them and then just before a polarogram was collected, the Bi(III) solution was added. No precipitation was evident up to pH 2.11, even with the concentration of Bi(III) kept constant at about 5×10^{-5} M for all solutions (i.e. no dilution occurs as would be the case in a titration). This experimental procedure is not feasible to run on a routine basis as it took about 24 hours to do and cannot be automated. Additionally, when complex

formation between another ligand and Bi(III) is investigated, the system has to reach equilibrium and unless this happens extremely fast, an experiment like this is not appropriate. Figure 8.19 shows two of the polarograms that were collected directly after Bi(III) and Tl(I) addition to HNO_3 solutions, the one at pH 1.52 and the other at 2.11. After measuring the polarogram and waiting for 2 minutes, another polarogram was collected. It was observed that the current drops in both cases for the second polarogram indicating precipitation, and that this drop is far larger at the higher pH. After another 2 minute waiting time, a third polarogram was collected for the pH 2.11 solution and another dramatic drop in current was observed. This clearly indicates slow precipitate formation and that the process is driven by an increase in pH.

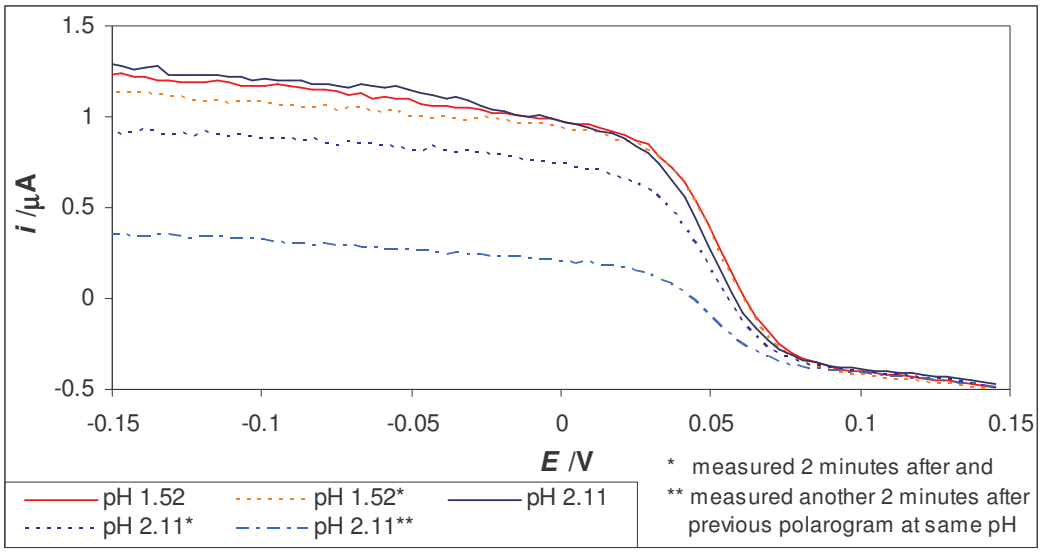

Figure 8.19: Polarograms collected directly after Bi(III) addition and again after the specified waiting times for solutions at pH 1.52 and 2.11.

The question remained whether the rate at which the experiment was performed affected the calculated value of $E(Bi_{free})$. The difference between the free metal ion potentials for Tl(I) and Bi(III) was rather considered since it was found that this difference remained constant even if the absolute $E(M_{free})$ values varied slightly from one experiment to the other. From the results in Table 8.9 it was noted that as the time interval between addition of hydroxide and the collection of the polarographic data increased, the difference between the free metal ion potentials for Bi(III) and Tl(I) decreased. Here only the value

of $E(Bi_{free})_{OH}$ is indicated as the difference between $E(Bi_{free})_{OH}$ and $E(Bi_{free})$ is also a constant value.

Table 8.9: The free metal ion potentials for Bi(III) and Tl(I) and their difference for titration experiments with varying time intervals. $\Delta E(M_{free})_{OH} = E(Bi_{free})_{OH} - E(Tl_{free})$.

Time interval /min	$E(Bi_{free})_{OH}$ /mV	$E(Tl_{free})$ /mV	$\Delta E(M_{free})_{OH}$ /mV
0	59.7 ± 0.9	–432.7 ± 0.6	492.4
10	63.3 ± 0.5	–428.6 ± 0.5	491.9
20	62.8 ± 0.6	–427.3 ± 0.3	490.1
30	56.4 ± 0.6	–428.6 ± 0.6	485.0
45	53.0 ± 0.9	–431.6 ± 0.5	484.6
60	51.7 ± 0.8	–430.9 ± 0.7	482.6

It appears rather that the formation of the bismuth-oxy-nitrate species initially in solution (before precipitation) is slow and not merely the formation of the precipitate itself. The higher the concentration of this species in solution, the greater the shift of the Bi(III) reduction potentials to less positive values. Since this species was not accounted for in the model used to correct the potential shifts, it would make $E(Bi_{free})$ (or $E(Bi_{free})_{OH}$) less positive and hence $\Delta E(M_{free})$ smaller. This was reinforced by the compensated potential versus pH plots and examples are given in Figure 8.20. For time intervals of 0 – 20 minutes, the $E_{1/2}$ values corrected for E_j and $\Delta E(OH)$ produced relatively constant potentials across the pH range, which were averaged to give $E(Bi_{free})_{OH}$. For time intervals of 30 – 60 minutes, the first two or three points at the lowest pH were significantly higher than the rest of the points and these were not used in calculating the average. It was initially assumed that E_j was overcompensated, but it appears that given sufficient time, the bismuth-oxy-nitrate species in solution formed at pH < 1 (resulting in negative potential shifts) and thus precipitation also occurred at lower pH. When $\Delta E(M_{free})_{OH}$ was calculated using only the corrected $E_{1/2}$ value at pH 0.3 for Bi(III), it was found that for the 30, 45 and 60 minute intervals these values were 489.7, 491.2 and 486.9 mV, respectively. Theses values are closer to the values determined for the shorter time intervals (see Table 8.9).

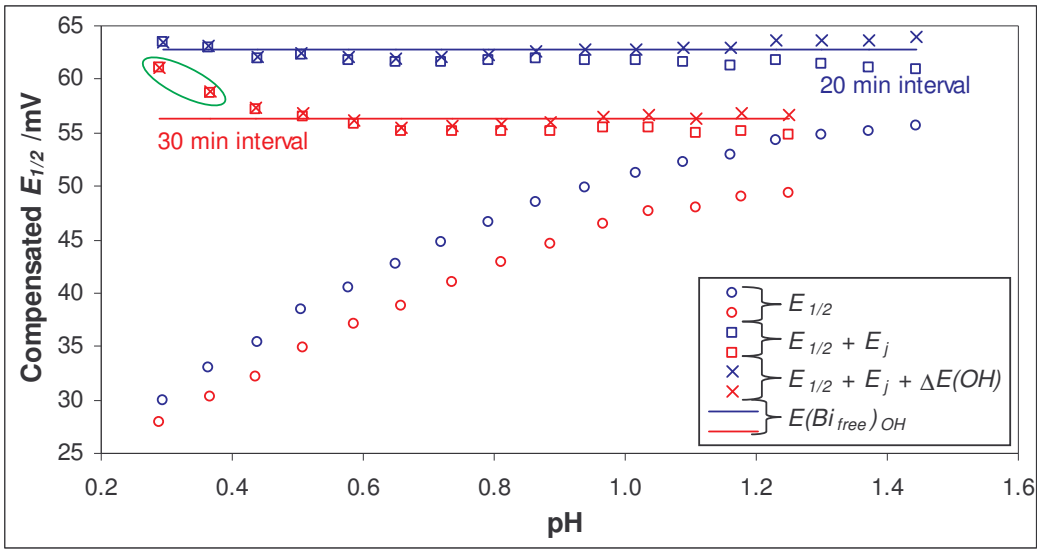

Figure 8.20: Compensated reduction potentials of Bi(III) as a function of pH (initial [Bi(III)] = 5×10^{-5} M) for experiments with 20 and 30 minute time intervals.

In order to postpone precipitation and increase the pH range in which data could be collected, the concentration of Bi(III) was decreased five times to an initial concentration of 9.97×10^{-6} M. According to the pBi′-pH diagram by Kragten *et al.*[24] (Figure 8.3a), by changing the pBi′ from 4.3 to 5, the pH at which the precipitation starts shifts by almost a pH unit. However, oxygen contamination was more evident at this low Bi(III) concentration. Figure 8.21 shows the polarogram for the reduction of Bi(III) in 0.5 M HNO_3 (pH 0.3) after 30 minutes of purging. Then 2 mL of 0.5 M KOH, that was not deoxygenated, was added (in 0.5 mL increments) to adjust the solution to pH 0.37. The solution was purged while the base additions were made, for a 15 s equilibration time and for the accurate pH measurement before the nitrogen was turned off and the polarogram was collected. The current increased due to the first oxygen reduction wave (equation 2.1) overlapping with the Bi(III) reduction wave. The currents were actually expected to decrease slightly due to dilution. It was thus necessary to increase the equilibration time to allow for longer purging times. This required a careful balance between sufficient purging but also minimal bismuth-oxy-nitrate formation. In future, it would be better to purge the KOH solution with nitrogen before addition to minimise purging time in the cell.

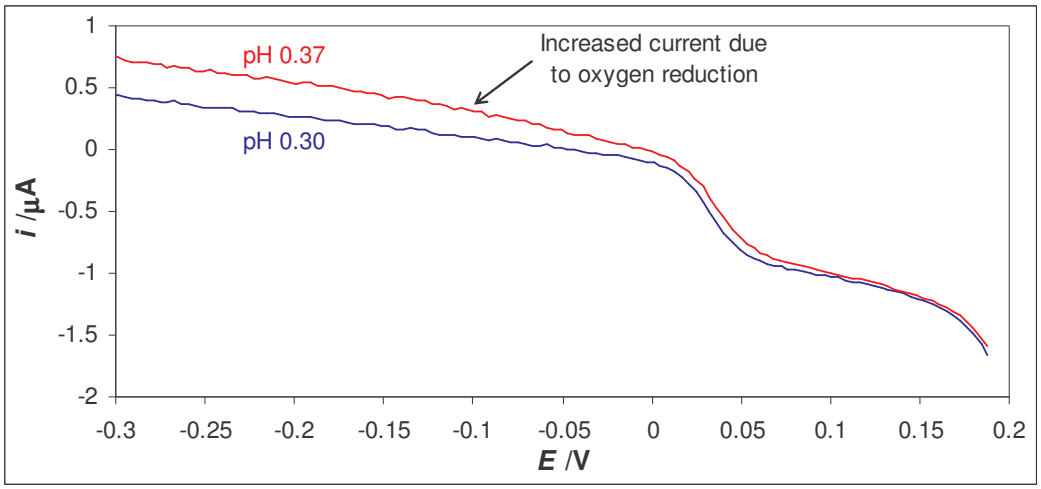

Figure 8.21: Polarograms showing oxygen contamination after 2 mL of 0.5 M KOH was added to a 9.97×10^{-6} M Bi(III) deoxygenated solution at pH 0.3.

When the polarograms from the lower Bi(III) concentration solutions were fitted, it was found that the value of δ was no longer unity and varied between 0.75 and 0.9 for all datasets. This would imply that the reduction was quasi-reversible. The waves were therefore fitted with the relationship given by Ružić *et al.*[47] and rearranged by Cukrowski *et al.*[48] (equation 7.15), with the background current described by equation 8.1. The diffusion limited currents determined were significantly higher when using this Ružić equation as compared to when fitting the DC wave equation, and the i_d versus pH trends were more erratic in the former case (see Figure 8.22(a)). Since i_d is independent of the extent reversibility, it indicated that some other factor was influencing the fitting process. The i_d values were therefore set equal to those determined from the DC wave equation and the polarograms were again fitted using the Ružić equation. In doing so, from Figure 8.22(c) it seemed that the value of α was correlated to i_d. It was also found that the reversible (from the Ružić equation) and the quasi-reversible (from the DC wave equation) half-wave potentials differed by less than 1 mV (see Figure 8.22(b)). So is this reduction process really quasi-reversible?

A correlation matrix of a typical polarogram is given below where the parameters fitted (by the DC wave equation) are indicated on the side of the matrix and since the matrix is symmetrical, only half of the matrix is shown.

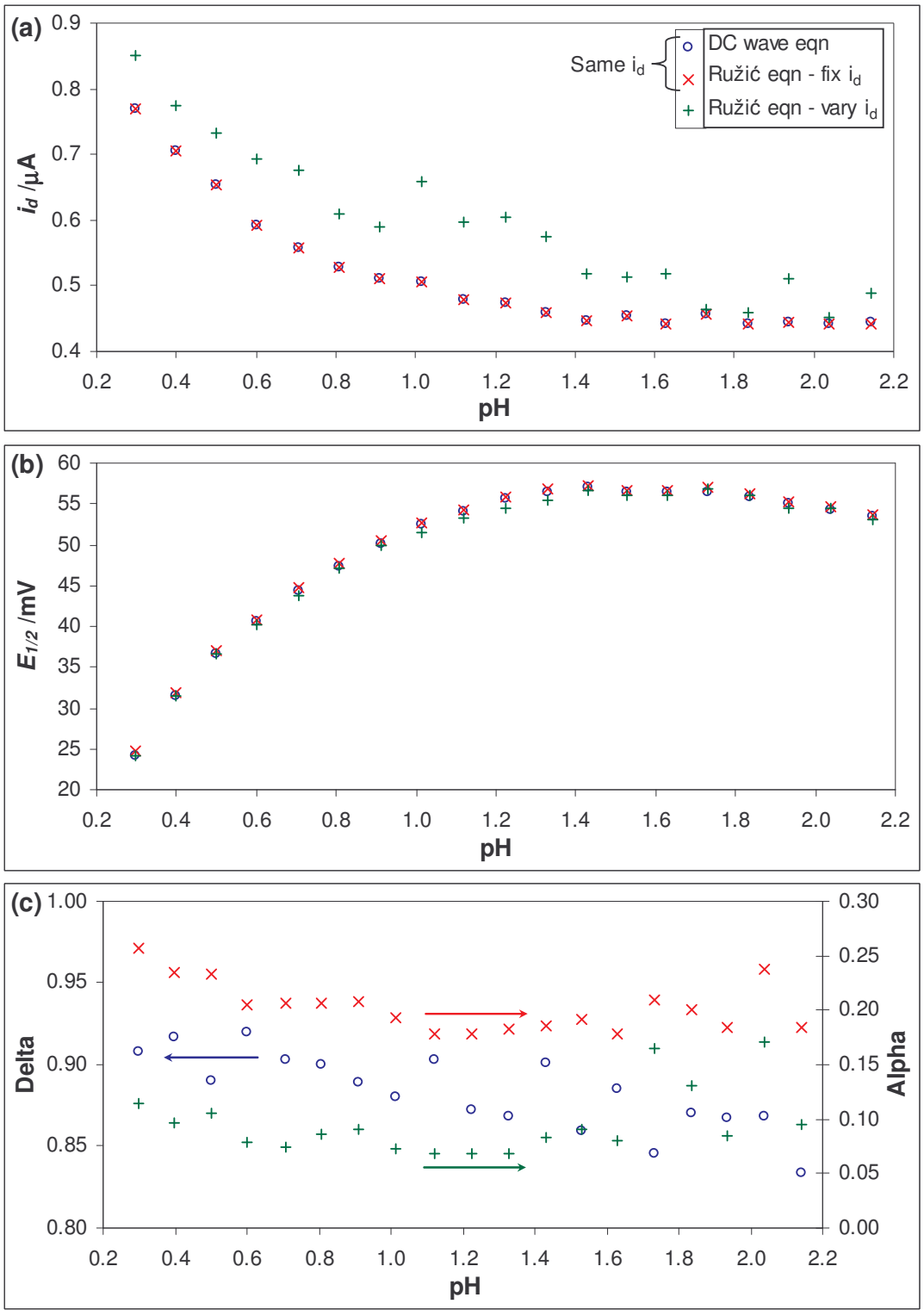

Figure 8.22: Values of (a) i_d, (b) $E_{1/2}$ and (c) δ or α all plotted as a function of pH obtained by fitting polarograms with the DC wave equation or the Ružić equation (where i_d calculated or fixed). Initial [Bi(III)] = 9.97×10^{-6} M.

$$\begin{array}{c} \\ i_d \\ \delta \\ E_{1/2} \\ a \\ b \\ c \\ d \end{array} \begin{bmatrix} 1 & -0.763 & -0.047 & -0.783 & -0.749 & -0.761 & 0.724 \\ & 1 & 0.0005 & 0.521 & 0.489 & -0.501 & -0.471 \\ & & 1 & 0.248 & 0.238 & -0.262 & -0.296 \\ & & & 1 & 0.997 & -0.999 & -0.994 \\ & & & & 1 & -0.998 & -0.992 \\ & & & & & 1 & -0.997 \\ & & & & & & 1 \end{bmatrix}$$

The only truly uncorrelated variables are $E_{1/2}$ and δ and to a lesser extent $E_{1/2}$ and i_d. Values of δ and i_d are correlated, with the negative value signifying that as one variable increases the other decreases and vice versa. The background variables *a*, *b*, *c* and *d* are highly correlated to each other and are also strongly correlated to i_d and somewhat correlated to δ. Least affected by the background parameters was $E_{1/2}$.

Since there was a correlation between the background variables and the values of i_d and δ, it was decided to fit the polarograms by removing the points that showed the most curvature due to mercury oxidation. Figure 8.23 shows that the resultant background currents, by including or deleting these points, differed not only at the most positive potentials, but throughout the potential range. The difference in background currents affected not only the i_d values, but the values of δ were also close to unity when the first few points were deleted. As expected from the correlation matrix, $E_{1/2}$ only change by 0.18 mV in this case, which is well within experimental error. For all polarograms, from the several datasets that were collected and were fitted by removing the points showing the most curvature at the positive potentials, the values of δ calculated were close to unity. Thus δ was set to equal one in all cases to reduce the number of variables determined and eliminate the variation of i_d with the value of δ. Therefore, the half-wave potentials were regarded as reversible for this work.

When assessing the $E_{1/2}$ data obtained from the lower Bi(III) concentration solutions, the same procedures were applied to determine both $E(Bi_{free})$ and $E(Bi_{free})_{OH}$ as before. Figure 8.24(a) gives an example of the $E_{1/2}$ values determined for the reduction of Bi(III) to just before precipitation, as well as the

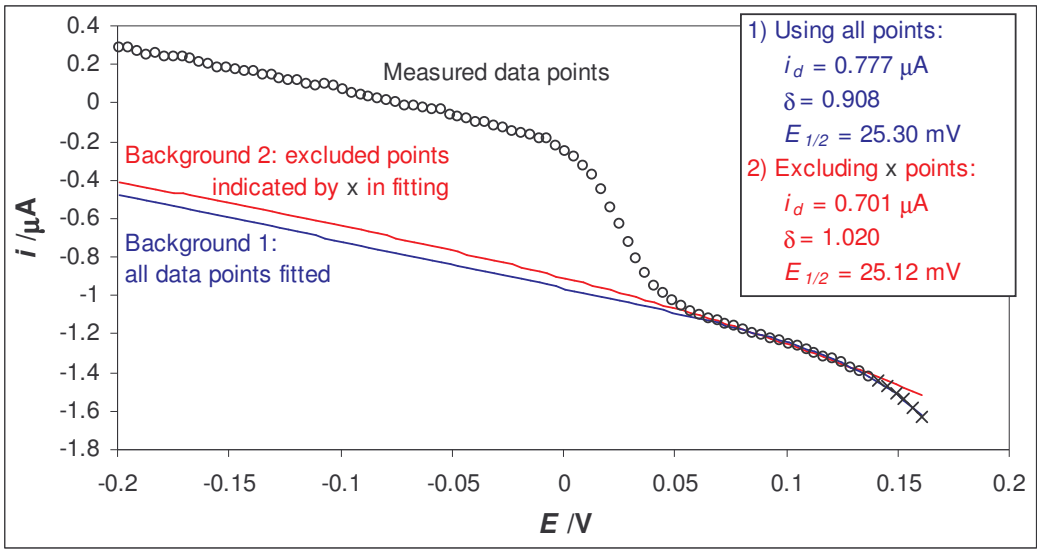

Figure 8.23: The effect of including or omitting data points that showed the most curvature due to mercury oxidation (indicated by ×) on the calculated background current and the polarographic parameters.

potentials that have been compensated for E_j and $\Delta E(OH + NO_3^-)$ or $\Delta E(OH)$ in the presence of nitrate. In this titration experiment a pH of 2.2 was attained before precipitation started. The last 2 to 4 points (i.e. those at the highest pH) that had been corrected for both E_j and $\Delta E(OH)$ appeared to be slightly too high. It was initially thought that this could be due to the formation constant used for the $Bi(OH)_2^-$ species being for 1.0 M ionic strength solutions (log β_2 = 23.5). The value was recalculated for 0.5 M ionic strength using the Davies equation, although this is strictly not the best approach at these relatively high ionic strengths, and a log β_2 value of 23.2 was obtained. This value fits the linear trend for the $U\{Bi(OH)_y\}$ versus y plot for data at 0.5 M ionic strength. However, using this recalculated log β_2 value only made a slight difference in the data at the highest pHs, but still it was decided to use log β_2 = 23.2 for 0.5 M ionic strength from now on. These points were thus ignored when calculating $E(Bi_{free})_{OH}$.

When comparing the potential values to the species distribution diagram in the same pH range (Figures 8.24(a) and (b) respectively) it became evident that the increase in potential for the last few points at the highest pH was due to the fraction of Bi(III) nitrate species in solution decreasing and that of the Bi(III)

hydroxide species increasing. At pHs where no more Bi(III) nitrate species are in solution, the $E_{1/2}$ values compensated for $\Delta E(OH)$ should be equal to $E(Bi_{free})$. Unfortunately data could not be collected to sufficiently high pHs to confirm this.

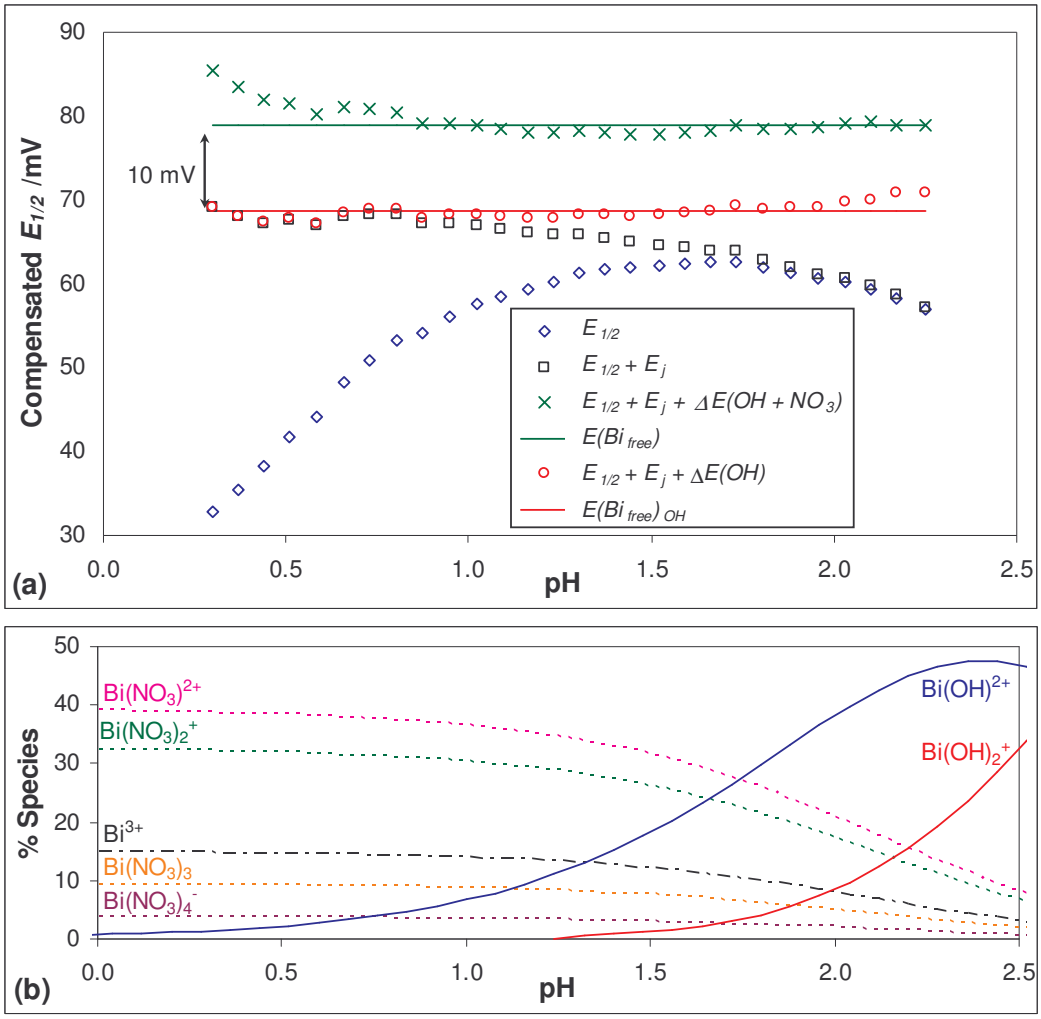

Figure 8.24: (a) $E_{1/2}$ values of Bi(III) reduction as a function of pH. Potential shifts due to the E_j and ΔE due to $Bi(OH)^{2+}$ and $Bi(OH)_2^{+}$ in the presence of nitrate, or ΔE due to $Bi(OH)^{2+}$, $Bi(OH)_2^{+}$ and Bi(III) nitrate species, were compensated for. Initial [Bi(III)] = 9.97×10^{-6} M. (b) Species distribution diagram for the corresponding pH region with $[NO_3^-]$ = 0.5 M and [Bi(III)] = 1×10^{-5} M.

In some cases, the compensated $E_{1/2}$ values at the lowest pHs were somewhat lower than the average value. These points, together with the points at the highest pHs that were above the average, were omitted when calculating the $E(Bi_{free})_{OH}$ value (see Figure A6.3 (Appendix 6)). Neglecting these points only

changed the calculated $E(Bi_{free})_{OH}$ value by at most 0.3 mV for all datasets. The difference between the calculated $E(Bi_{free})$ and $E(Bi_{free})_{OH}$ was 10 mV, which compares well to the 11 mV obtained for the titration employing a higher Bi(III) concentration.

It was again tested if the purging time affected the free Bi(III) potential value for solutions with an initial Bi(III) concentration of 9.97×10^{-6} M by calculating $\Delta E(M_{free})$. Experiments were performed using reasonable purge times of 5, 10 and 20 minutes and the results are given in Table 8.10. For these relatively short time intervals, the $\Delta E(M_{free})$ values could be considered within experimental error of each other (as was really the case for the values in Table 8.9 for intervals up to 20 minutes). The purging time interval was still kept to a minimum of 5 minutes allowing for the required deoxygenation, but limiting the amount of bismuth-oxy-nitrate formation.

Table 8.10: $\Delta E(M_{free})$ values for titration experiments with initial [Bi(III)] = 9.97×10^{-6} M, where $\Delta E(M_{free})_{OH} = E(Bi_{free})_{OH} - E(Tl_{free})$ and $\Delta E(M_{free}) = E(Bi_{free}) - E(Tl_{free})$.

Time interval /min	$\Delta E(M_{free})_{OH}$ /mV	$\Delta E(M_{free})$ /mV
5	485 ± 2 *	495 ± 2 *
10	486.6	496.9
20	485.6	496.0

* Average of 5 determinations

These $\Delta E(M_{free})_{OH}$ values correspond to those given in Table 8.9 with 30 and 45 minute intervals. Here the Bi(III) concentration was decreased which should slow down the formation of the Bi(III)-oxy-nitrate species, but the ratio of Bi(III)-to-hydroxide and nitrate concentrations was also decreased which would favour the formation of these species. Interplay between the thermodynamic and kinetic processes could thus lead to the observations noted. Since these experiments were interspersed by titrations including ligand to determine formation constants of the Bi(III)-ligand systems studied and the same conditions were used in both cases, the average $\Delta E(M_{free})_{OH}$ and $\Delta E(M_{free})$ values determined for the 5 minute interval were used in the Bi(III)-ligand studies presented in the next chapter. The value of $E(M_{free})$ or

$E(M_{free})_{OH}$ for each ligand experiment could therefore be calculated from the sum of this difference and $E(Tl_{free})$ as determined for that titration. The standard deviation of $E(M_{free})$ is greater than that determined when using other metal ions, but it is still only 2 mV, even when having so many factors affecting the Bi(III) $E_{1/2}$ values measured.

8.3.4) *Aside on Bi(III) hydrolysis*

As a brief aside, when looking for methods to standardise the concentration of Bi(III) solutions (since $Bi(NO_3)_3$ occurs as a pentahydrate salt), a complexometric titration using an EDTA titrant was one of the methods suggested by Vogel,[49] where either bromopyrogallol red or Xylenol orange were employed as indicators. This book of quantitative inorganic analysis by Vogel is extensively used by analytical chemists particularly for its wet chemical methods. It was thus surprising to see the method called for the careful addition of ammonia to adjust the pH of the bismuth nitrate solution to between 2 and 3, especially with Bi(III) concentrations above 2×10^{-3} M. This was attempted and as expected the Bi(III) precipitated out of solution. On very slow addition of EDTA, the Bi(III) could still be complexed and redissolved, but this is not the best analytical practice. When the titration was repeated using a solution at pH 1 no precipitation occurred and the results were comparable to those performed as suggested and with very cautious addition of EDTA.

8.4) Conclusions

Since the value of $E(Bi_{free})$ cannot be directly measured, protocols were developed to calculate this value by employing an average $\Delta E(M_{free})$ value and $E(Tl_{free})$, where the latter is determined from the pH titration experiments where the ligand is present (provided Tl(I) is not complexed). To find the $\Delta E(M_{free})$ value, $E(Bi_{free})$ had to be calculated from experiments performed without ligand in solution. To do this, the measured $E_{1/2}$ values were compensated for potential shifts due to E_j and shifts due to both hydrolysis and Bi(III) nitrate formation. The value of $E(Bi_{free})_{OH}$ was also calculated at low pHs where only the potential shift due to hydrolysis of Bi(III) was accounted for in the nitrate

background. It was critical that the extent of complexation by nitrate be considered as, even though they are weak complexes, the large concentration of nitrate led to the fraction of these complexes being significant especially below pH 3. The values of both $\Delta E(M_{free})$ and $\Delta E(M_{free})_{OH}$ determined here were used in the Bi(III)-ligand studies tackled in the next chapter. The validity of these values was nominally assessed in this work, as will be discussed.

A precipitate formed around pH 2 which was confirmed to contain both $Bi_6O_4(OH)_4(NO_3)_6(H_2O)_4$ and $Bi_6O_5(OH)_3(NO_3)_5(H_2O)_3$. It appears that the formation of these species in solution and subsequent precipitation are kinetically slow. Experiments were thus run as fast as possible, but still allowing time for sufficient deoxygenation, and the Bi(III) concentration was made as low as possible to postpone precipitation.

Through comparing species distribution diagrams, it was demonstrated that polynuclear hydrolysis products did not form significantly at the low concentration range used. Also, by applying procedures suggested by Barnum,[45] confidence was given to the log β values for the mononuclear hydrolysis products of Bi(III) as well as for the polynuclear species.

Contrary to literature,[41] the reduction of Bi(III) was found to be reversible for our purposes. A δ value close to unity was obtained provided as little curvature (due to the adjacent mercury oxidation wave) was included when fitting data to determine the polarographic parameters. In future it is suggested that mercury oxidation be avoided as it affects the fitted parameters of the Bi(III) reduction wave, as well as to prevent introduction of Hg(II) into solution.

It can finally be concluded that the chemistry of Bi(III) in aqueous solutions is extremely complicated. It is complicated even further but the relatively strong interactions between Bi(III) and nitrate which cannot be ignored in the excess nitrate present. Why is it then that we chose to work in a nitrate rather than a perchlorate background? Perchlorate forms weaker complexes with Bi(III) and thus may not need to be accounted for when calculating $E(Bi_{free})$. Although

according to Kragten *et al.*[24] $BiClO_4^{2+}$ forms at low pHs and a Bi(III)-oxy-perchlorate precipitate is also formed, but at higher pHs and higher Bi(III) concentrations as compared to the Bi(III)-oxy-nitrate precipitate (see Figure 8.3). However, the reduction of Bi(III) was quasi-reversible in a perchlorate solution, even under the conditions applied here. Determining the reversible reduction potentials would be more challenging and introduce even further uncertainty in the measurement. Additionally, from considering the quasi-reversible reduction of Cu(II) in Chapter 7, which has similar reduction potentials to that for Bi(III), it was seen that determining the reversible half-wave potentials was especially difficult when the wave was close to the mercury oxidation wave (or any other wave). It was therefore decided to rather continue using a nitrate background.

8.5) References

1) F.A. Cotton, G. Wilkinson and P.L. Gaus, Basic Inorganic Chemistry, 2nd ed., John Wiley and Sons Inc., New York, USA, 1987
2) C.F. Baes Jr and R.E. Mesmer, The Hydrolysis of Cations, John Wiley and Sons Inc., New York, USA, 1976
3) D.F. Smith, J. Am. Chem. Soc., 45 (1923) 360
4) F. Graner, A. Olin and L.G. Sillén, Acta Chem. Scand., 10 (1956) 476
5) A. Olin, Acta Chem. Scand., 11 (1957) 1445
6) F. Graner and L.G. Sillén, Acta Chem. Scand., 1 (1947) 631
7) A. Holmqvist, Svensk. Kem. Tidskr., 48 (1936) 106
8) P. Souchay and D. Peschanski, Bull. Soc. Chim. Fr., (1948) 439
9) J. Faucherre, Bull. Soc. Chim. Fr., (1954) 253
10) R.W. Holmberg, K.A. Kraus and J.S. Johnson, J. Am. Chem. Soc., 78 (1956) 5506
11) A. Olin, Acta Chem. Scand., 13 (1959) 1791
12) S. Tobias, J. Am. Chem. Soc., 82 (1960) 1070
13) S. Tobias and S.Y. Tyree, J. Am. Chem. Soc., 82 (1960) 3244
14) V.A. Maroni and T.G. Spiro, J. Am. Chem. Soc., 88 (1966) 1410
15) I. Hataye, H. Suganuma, H. Ikegami and T. Kuchiki, Bull. Chem. Soc. Jpn., 55 (1982) 1475
16) T.F. Bidleman, Anal. Chim. Acta, 56 (1971) 221
17) A.E. Martell, R.M. Smith and R.J. Motekaitis, NIST Standard Reference Database 46 Version 8.0. NIST Critically Selected Stability Constants of Metal Complexes Database, Gaithersburg, USA, 2004
18) I. Cukrowski, R.D. Hancock and R.C. Luckay, Anal. Chim. Acta, 319 (1996) 39
19) H. Suganuma, I. Shimizu and I. Hataye, Bull. Chem. Soc. Jpn., 60 (1987) 877
20) H. Suganuma, K. Ono and I. Hataye, J. Radioanal. Nucl. Chem., Letters, 145 (1990) 167
21) R.P. Oertel and R.A. Plane, Inorg. Chem., 7 (1968) 1192
22) L. Johansson, Acta Chem. Scand., 23 (1969) 548
23) L. Newman and D.N. Hume, J. Am. Chem. Soc., 79 (1957) 4576

24) J. Kragten, L.G. Decnop-Weever and P. Gründler, Talanta, 40 (1993) 485
25) D.F. Swinehart and A.B. Garrett, J. Am. Chem. Soc., 73 (1951) 507
26) H.A. Levy, M.D. Danfold and P.P. Argon, J. Chem. Phys., 31 (1959) 1458
27) N. Henry, M. Evain, P. Deniard, S. Jobic, O. Mentré and F. Abraham, J. Solid State Chem., 176 (2003) 127
28) F. Lazarini, Acta Cryst., B35 (1979) 448
29) B. Sundvall, Acta Chem. Scand., A33 (1979) 219
30) B. Sundvall, Inorg. Chem., 22 (1983) 1906
31) F. Lazarini, Acta Cryst., B34 (1978) 3169
32) I. Grenthe and I. Toth, Inorg. Chem., 24 (1985) 2405
33) G. Gattow and D. Schott, Z. Anorg. Allg. Chem., 324 (1963) 31
34) B.S. Brčić, D. Kolar, F. Lazarini and M. Malešič, Monatsh. Chem., 104 (1973) 365
35) A.N. Christensen, M.-A. Chevallier, J. Skibsted and B.B. Iversen, J. Chem. Soc., Dalton Trans. (2000) 265
36) G. Briand and N. Burford, Chem. Rev., 99 (1999) 2601
37) A.M Bond, Electrochim. Acta, 17 (1972) 76
38) A.A. Moussa and H.M. Sammour, J. Chem. Soc., (1960) 2151
39) J.E.B. Randles and K.W. Somerton, Trans. Faraday Soc., 48 (1952) 951
40) H.H. Bauer and P.J. Elving, Electrochim. Acta, 2 (1960) 240
41) A.M Bond, J. Electroanal. Chem., 23 (1969) 269
42) A. Belsky, M. Hellenbrandt, V.L. Karen, and P. Luksch, Acta Cryst., B58 (2002) 364
43) J.B. Headridge, A.G. Hamza, D.P. Hubbard and M.S. Taylor in G.J. Hills (Ed.), Polarography 1964, Proc. Third Intern. Conf., Southampton, Vol. 1, Macmillan London, 1966
44) I. Cukrowski, 3D-CFC10 software, Version 5.0, 2000
45) D.W. Barnum, Inorg. Chem., 22 (1983) 2297
46) L.D. Petit and K.J. Powell, Sol-Eq, Academic Software, IUPAC, 2002
47) I. Ružić, A. Barić and M. Branica, J. Electroanal. Chem., 29 (1971) 411
48) I. Cukrowski, H.M. Marques, T.S. Mkwizu, P.P. Magampa and C. Serge, Anal. Chim. Acta, 590 (2007) 203
49) A.I. Vogel, A Text-book of Quantitative Inorganic Analysis Including Elementary Instrumental Analysis, 3rd ed., Longmans, London, UK, 1962

CHAPTER 9
Complex Formation Studies with Bismuth

9.1) Introduction

The difficulties in studying complex formation of Bi(III) has been discussed in Chapter 1 and further in Chapter 8, so no further introduction is required. A brief introduction to electrospray ionisation-mass spectrometry is given here as it was used to a small extent in this work.

9.1.1) *Electrospray Ionisation-Mass Spectrometry (ESI-MS)*

Fenn and Tanaka shared the Nobel Prize for Chemistry in 2002 for developing MS methods such as ESI for analysing large biological molecules.[1] ESI is a "soft" ionisation technique as it does not fragment large molecules. Fenn called it the "wings for molecular elephants".[2] Although the niche area for ESI-MS has been for the analysis of very large chargeable molecules such as proteins and nuclei acid polymers, it can also be used for the analysis of ionic metal complexes and other inorganic analytes.[2] It is an ideal technique to determine the stoichiometry of complexes.[3] Burford *et al.*[3-9] used this technique to identify complexes of Bi(III) with many amino acids and thiol ligands, among others.

The fundamental principles of MS are to generate ions, separate these ions by their mass-to-charge ratio (m/z) and then detect the m/z abundances.[2] Of interest here is the way in which the ions are produced. The sample solution is sprayed from a fine capillary by action of a strong electric field and is dispersed into a mist of charged droplets into an inert gas. The gas is at a temperature high enough to evaporate the solvent without freezing the droplets. As solvent evaporation occurs, the droplets shrink until the Rayleigh limit is reached where the surface tension of the droplet is overcome by the electrostatic repulsion of the ions. The droplets then break apart and the process is repeated until ultimately, only the ions in the gas phase are left. It was found that if an induction electrode with a high applied voltage (± 3500 V) is placed

close to the atomising zone, droplets and ions that are only positive or negative are produced, depending on the selected polarity. Ions are then driven into a vacuum chamber containing the mass analyser and then to the detector.[1,2,10]

The question is whether the species in the gas phase have a direct relationship to the solution composition. Burford *et al.*[7] claimed that it offered a close relationship with the solution chemistry, however, it was noted that more ligand was sometimes bound to protein receptors which was probably due to aggregation in the gas phase.[3]

9.2) Aims

The study of Bi(III) complex formation is the culmination of the work done up till now. Procedures developed thus far include calibrating the glass electrode for studies in very acidic solutions; the insitu monitoring the diffusion junction potential using Tl(I) as the witness ion and determining the free metal ion potential for Bi(III) in a nitrate background solution. All these procedures were applied to determine the stability constants of Bi(III) with three pyridinecarboxylic acids, namely, picolinic acid, dipicolinic acid and quinolinic acid. Only studies of Bi(III) with picolinic acid have been previously attempted,[11] so these values will be compared.

9.3) Results and Discussion

When studying the complexation of Bi(III) by various ligands using polarography, the presence of Tl(I) as a witness is essential. Not only is it used in each experiment to monitor the diffusion junction potential, but without it determining the free Bi(III) potential would be near impossible. Additionally, the $E_{1/2}$ values of the Tl(I) wave also monitor the performance of the reference system as problems could otherwise go undetected.

Experiments were run as described in Chapter 8 using the lower concentration of metal ions, i.e. the initial concentrations of Bi(III) and Tl(I) were 9.97×10^{-6} M and 1.99×10^{-5} M respectively. The ligand studied was added in the solid form

to the 0.5 M HNO_3 solution containing the metal ions before titrating with 0.5 M KOH.

In general, each polarogram was also divided into two parts so that the Bi(III) and Tl(I) reduction waves could be fitted separately, but this split did not always occur at –0.20 V (as was the case when no ligand was present) due to the large negative potential shifts caused by some Bi(III) complexes. As discussed in section 8.3, it was necessary to remove data points at the most positive potentials where the most curvature occurred due to mercury oxidation to ensure the δ values were close to unity. Only then were the polarograms were refitted by setting $\delta = 1$ to reduce the number of variables determined in the non-linear least squares process, especially since there was a large interdependence between the values of δ and i_d.

9.3.1) *Bi(III)-picolinic acid complexes*

Three pH titrations were performed with total ligand-to-metal concentration ratios of 94, 148 and 197, with each titration starting at pH 0.3. The diffusion junction potential was calculated using the Tl(I) potential data as described in Chapter 6, where the $E_{1/2}$ versus pH data was fitted by a combination of a cubic polynomial (in the region of changing E_j) and a straight line with zero slope (where the E_j remained fairly constant). In this case the calculated E_j from the Tl(I) data was set equal to that for the Bi(III) data since a model including the potential shift due to the change in the ionic strength was impossible to model with certainty because of the hydrolysis of Bi(III). The experimentally determined E_j was compared to that calculated using the Henderson equation, but here the measured E_j values were slightly greater than those calculated although a similar trend was followed (see Figure A7.1, Appendix 7). It was consistently the case for this set of experiments, whether ligand was included in the titration or not. Theoretically, if the concentration of KNO_3 in the salt bridge was halved, the calculated values were similar to the experimental data, but whether this was actually the case was not confirmed. This highlights the importance of measuring E_j for each experiment, rather than calculating it or using a once off measurement.

An example of the measured $E_{1/2}$ values and those values compensated for E_j (as determined when using Tl(I) potential data or calculated using the Henderson equation) is given in Figure 9.1. The potentials corrected using the E_j values calculated by the Henderson equation show a slight increase with increasing pH in the lowest pH range, which indicates insufficient compensation. When the potentials were corrected using the Tl(I) data, this slight increase was no longer observed, thus giving confidence to the measured E_j values. The values of both $E(Bi_{free})$ and $E(Bi_{free})_{OH}$ are also plotted in Figure 9.1. These values were calculated by summing the value of $E(Tl_{free})$ and $\Delta E(M_{free})_T$ = 495 mV or $\Delta E(M_{free})_{OH}$ = 485 mV (from Table 8.10), respectively. The compensated $E_{1/2}$ values (×) were similar to $E(Bi_{free})_{OH}$ in the lowest pH range which would indicate no complex formation here. However, a 9 mV difference at the lowest pH was observed between the compensated $E_{1/2}$ values (×) and $E(Bi_{free})$, indicating that complex formation has already taken place at pH 0.3. Further clarification regarding these observations is required.

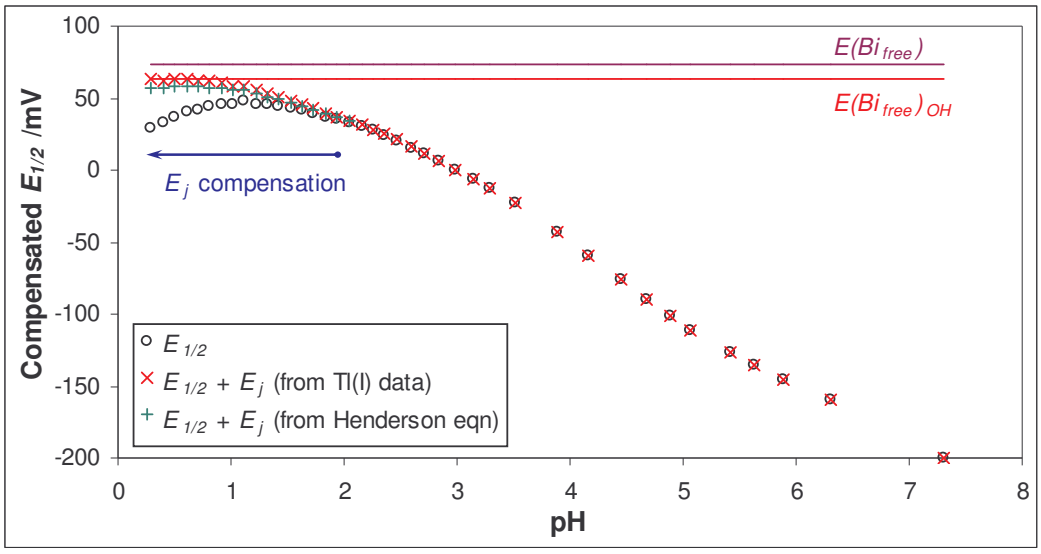

Figure 9.1: Differences in the compensated $E_{1/2}$ values when using the two methods indicated to determine E_j. The calculated values of $E(Bi_{free})$ and $E(Bi_{free})_{OH}$ are also plotted. ($[PA]_T$:$[Bi(III)]_T$ = 197).

Figure 9.2 compares the polarograms of Bi(III) reduction before and after the addition of PA at pH 0.3. A shift in $E_{1/2}$ of less than 2 mV is observed signifying minimal (if any) complexation of Bi(III) by PA at this pH. This implies that the

~9 mV shift between $E(Bi_{free})$ and the compensated $E_{1/2}$ values below pH ~0.7 is not due to the formation of Bi(III) PA species, but rather the formation of Bi(III) nitrate species, which are still present in solution after PA addition. The negligible shift between $E(Bi_{free})_{OH}$ and the compensated $E_{1/2}$ values at low pH shows that there are no "new" complexes being formed.

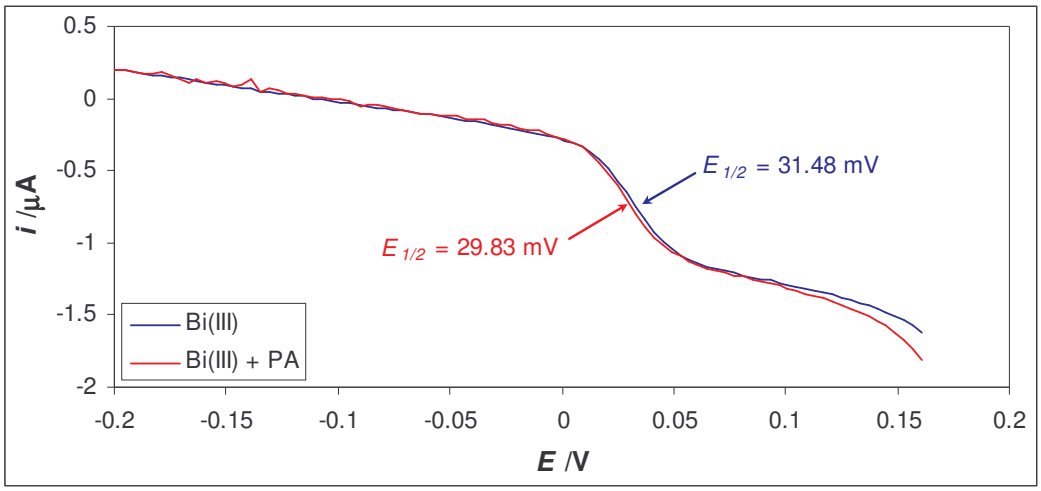

Figure 9.2: Polarograms at pH 0.30 (where [Bi(III)] = 1×10^{-5} M) before and after the addition of PA ([PA] = 2×10^{-3} M), where $[PA]_T$:$[Bi(III)]_T$ = 197. The $E_{1/2}$ values indicate a shift of 1.65 mV.

As the extent of complexation of Bi(III) by PA increases with increasing pH (as observed by the negative shift in the compensated $E_{1/2}$ values in Figure 9.1), the extent of complexation of Bi(III) by nitrate decreases. Ideally one would take the competitive behaviour between these two ligands (as well as hydroxide) into account. Mass balance equations should be solved by keeping the stability constants of both Bi(III) hydroxide and nitrate species constant, while those for Bi(III) PA species would be refined. Unfortunately, the 3D-CFC software[12] can only accommodate two ligands simultaneously, one of which is always hydroxide and the other is the ligand being studied. Thus to fully account for the competition between all potential ligands in solution, the software has to be developed further.

Under the given constraints, to deal with the situation as best as possible, Figure 9.3 shows the compensated $E_{1/2}$ values as a function of pH in the presence of PA (as given in Figure 9.1) overlaid by the species distribution

diagram for Bi(III) nitrate and hydroxide species (as given in Figure 8.9(b)). From the species distribution it can be seen that where the concentration of Bi(III) nitrates are highest and relatively constant (I.e. below pH ~1) using $E(Bi_{free})_{OH}$ to calculate the Bi(III) PA stability constants would give more accurate results. This corresponds to the region where very small potential shifts were observed when PA was added to the solution. If $E(Bi_{free})$ is used in the determination of the log β values for Bi(III) PA species in a pH range where Bi(III) nitrates are still in solution, larger values would be obtained for these species or additional species could be predicted. However, in the pH range where Bi(III) PA species become significant in solution, using $E(Bi_{free})_{OH}$ would produce log β values that are too small. The true stability constants would lie somewhere between the values calculated using $E(Bi_{free})$ and $E(Bi_{free})_{OH}$ if there are any Bi(III) nitrates in solution. Where the Bi(III) nitrates are negligible in solution, $E(Bi_{free})$ must be used.

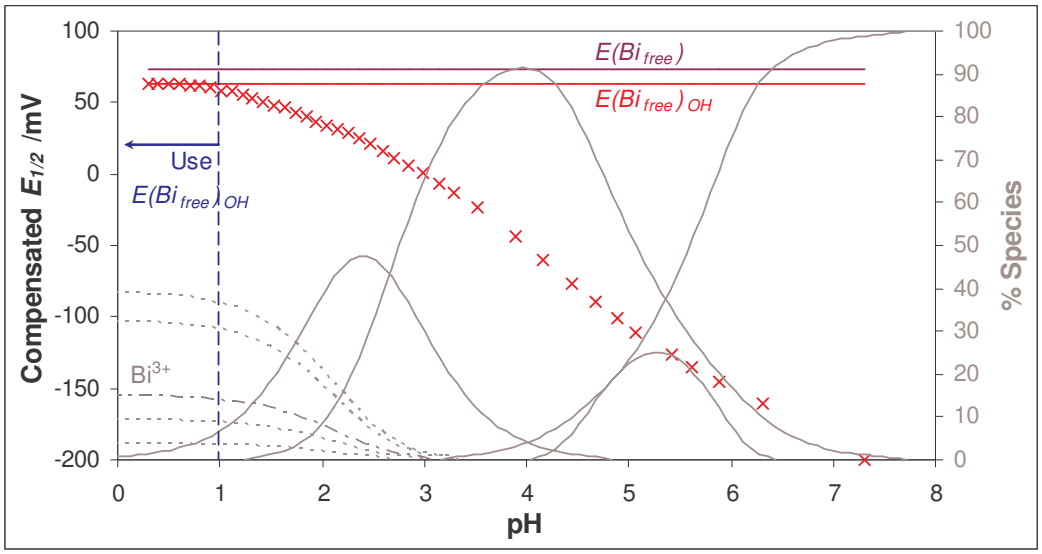

Figure 9.3: $E_{1/2}$ values corrected for E_j (as in Figure 9.1) overlayed with the species distribution diagram (as in Figure 8.9(b)) where (---) and (—) indicate the various nitrate and hydroxide species with Bi(III), respectively. $E(Bi_{free})$ and $E(Bi_{free})_{OH}$ are also plotted.

Slope analysis was done to predict the solution species by considering the reduction reactions taking place and the associated slope of the potential-pH graph, where the slope is approximately $60/n \times$ number of protons involved in the reaction. Possible reductions and the predicted slopes are indicated in

Table 9.1 for this system. As seen in Figure 9.4, the ECFC (for $[PA]_T$:$[Bi(III)]_T$ = 197) in the region between pH 0.86 and 5.18 where HL is the dominant form of the ligand, the ML, ML_2 and ML_3 species are predicted. $E(Bi_{free})_{OH}$ was used to calculate the ECFC here as the slopes do not change with a change in the $E(Bi_{free})$ value, it merely moves the data along the y-axis.

Table 9.1: Predicted slopes (in mV per pH unit) of potential versus pH data for the corresponding reduction reactions.

Reduction reaction	Predicted slope
$BiL^{2+} + 3e^- + 2H^+ \rightleftharpoons Bi^o + H_2L^+$	40
$BiL^{2+} + 3e^- + H^+ \rightleftharpoons Bi^o + HL$	20
$BiL_2^+ + 3e^- + 2H^+ \rightleftharpoons Bi^o + 2HL$	40
$BiL_3 + 3e^- + 3H^+ \rightleftharpoons Bi^o + 3HL$	60
$BiL_4^- + 3e^- + 4H^+ \rightleftharpoons Bi^o + 4HL$	80
$BiL_4^- + 3e^- \rightleftharpoons Bi^o + 4L^-$	0 (no H^+ involved)

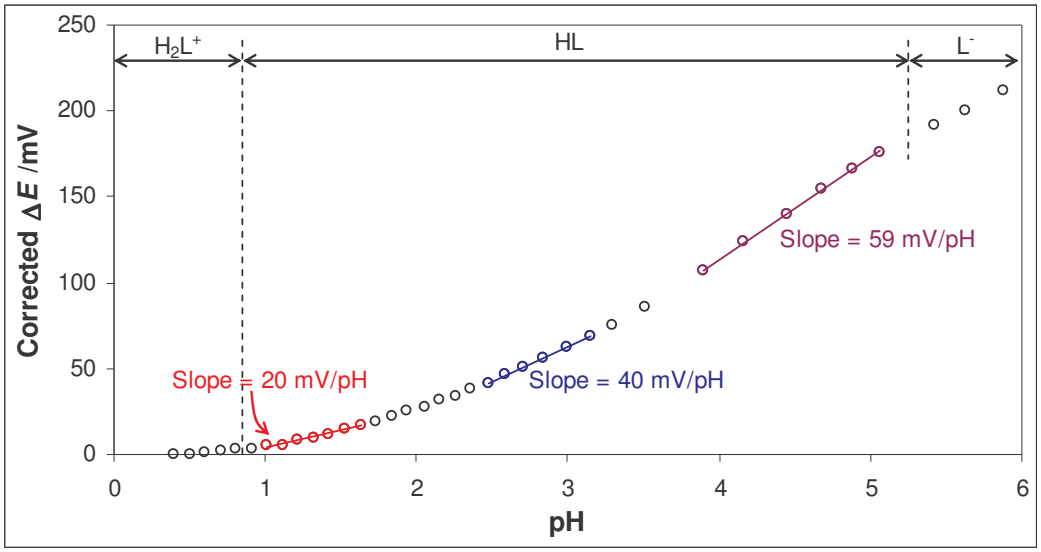

Figure 9.4: Slope analysis of the ECFC calculated using $E(Bi_{free})_{OH}$, where $[PA]_T$:$[Bi(III)]_T$ = 197. Specific slopes are highlighted and the pH regions for the predominant forms of the ligand are indicated.

When including the ML, ML_2 and ML_3 species in the model to calculate the CCFC two resultant curves are shown in Figure 9.5. The dotted line (···) was calculated using the averaged refined values and it lies above the experimental values in one region and below in another. The dashed line (---) was calculated using log β values such that the CCFC either overlapped with

the ECFC or was below it. Here it is seen that the calculated curve does not fit the experimental data above about pH 4 and hence there must be additional species in solution in this region. When the ML_4 species was included in the model, the CCFC fitted the experimental data more closely but only until about pH 5. Instead of ML_4, $ML_3(OH)$ was included in the model which led to the CCFC fitting the experimental data well up until pH 6. It was impossible to refine log β values for both ML_4 and $ML_3(OH)$ simultaneously.

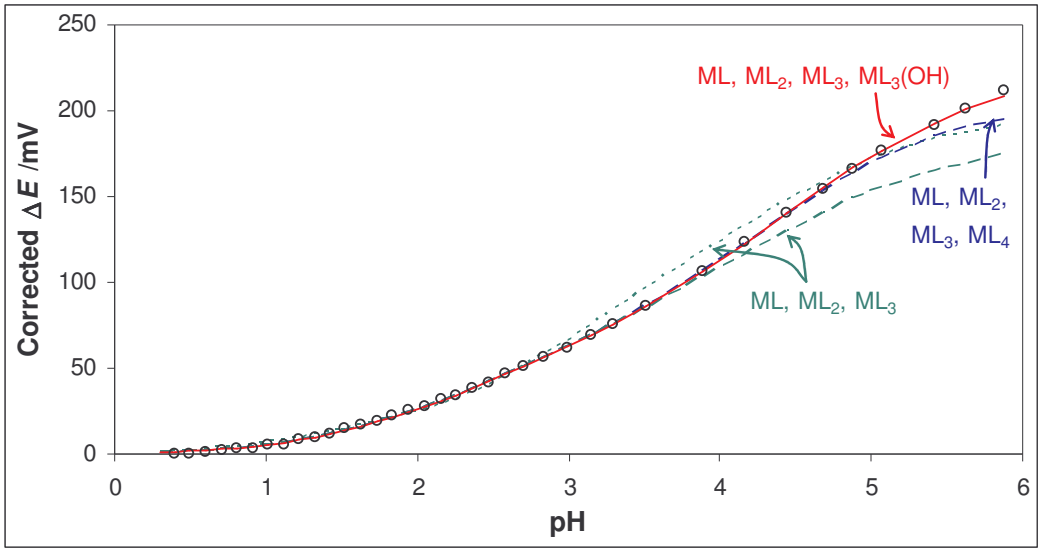

Figure 9.5: The ECFC (○), calculated using $E(Bi_{free})_{OH}$, is plotted with various CCFCs determined by including the species indicated in the models ($[PA]_T$:$[Bi(III)]_T$ = 197).

As expected, a similar behaviour was observed for the ECFC plot calculated using $E(Bi_{free})$ and the model including the ML, ML_2, ML_3 and $ML_3(OH)$ species fitted the ECFC well, except at the lowest pHs (see Figure 9.6). MLH could be included in the model to improve the fit, but it is known that this shift is due to Bi(III) nitrate formation. The MLH species thus compensates for the potential shifts due to the Bi(III) nitrates to some degree. This model was consistent with the data for the other ligand-to-metal concentration ratios and the ECFCs and CCFCs of each ratio is shown in Figure 9.7.

In Figure 9.8 the region below pH 3 is highlighted. The one CCFC plotted (—) shows the model excluding MLH as fitted in Figure 9.6. The other CCFC was calculated using the log β values obtained when MLH was included in the

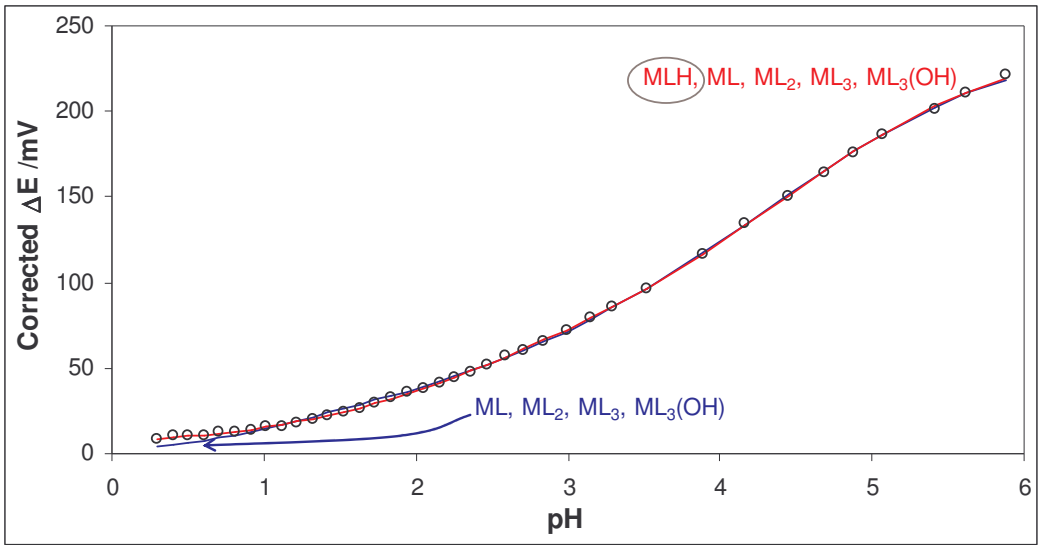

Figure 9.6: The ECFC (○), calculated using *E(Bi$_{free}$)*, is plotted with the CCFCs determined by including the species indicated in the models ([PA]$_T$:[Bi(III)]$_T$ = 197).

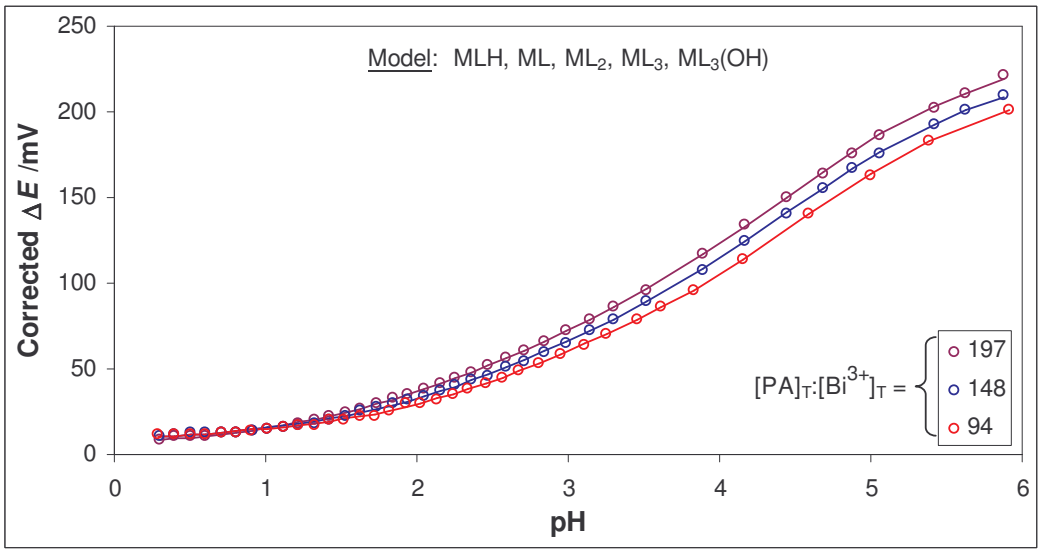

Figure 9.7: The ECFCs (calculated using *E(Bi$_{free}$)*) and CCFCs for the three ligand-to-metal concentration ratio experiments. The species included in the calculating the CCFC are indicated.

model, but the value for the fictitious MLH species was omitted. At the lowest pHs, this CCFC (—) lies closer to the ECFC values calculated using *E(Bi$_{free}$)$_{OH}$*. It was therefore decided to use the model including the MLH species to fit the ECFC (calculated using *E(Bi$_{free}$)*), but the log β value of MLH is meaningless as the species is not actually present in solution and only compensates to some extent for the Bi(III) nitrate species present.

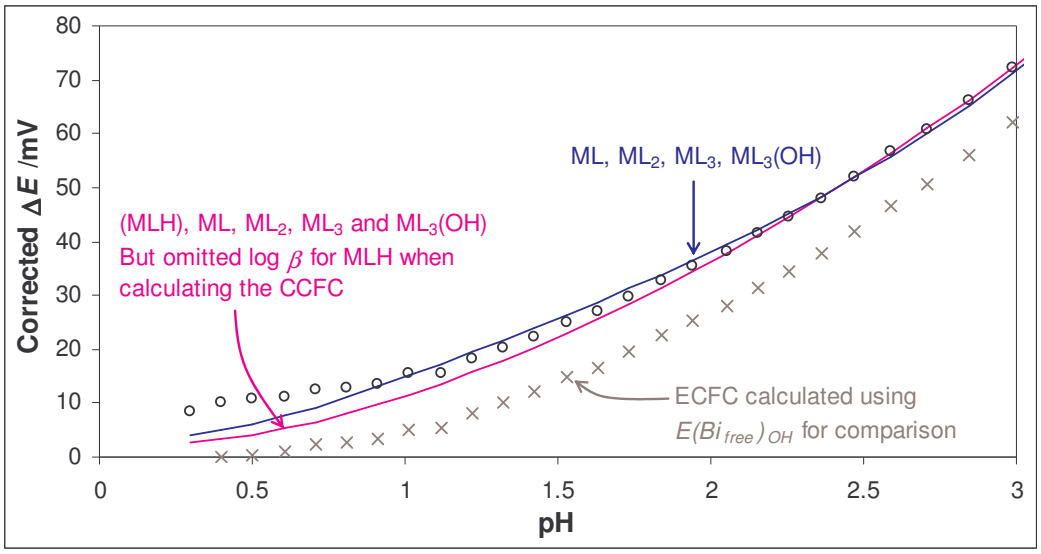

Figure 9.8: The low pH range is highlighted for the ECFC calculated using $E(Bi_{free})$ (○) and the CCFCs determined by including the species indicated in the models. The ECFC calculated using $E(Bi_{free})_{OH}$ (×) is also shown.

The log β values refined when using either $E(Bi_{free})$ or $E(Bi_{free})_{OH}$ to calculate the ECFC are given in Table 9.2 and the average values were also calculated. (The average for MLH is not given as this is not a real species in this case.) Comparing the results determined using the two $E(Bi_{free})$ values shows that the difference in the log β values for all species is about 0.5 except for the ML species where the difference is 0.76. The log β values for ML_3 and $ML_3(OH)$ should be accurate when refined using ECFC data calculated using $E(Bi_{free})$ as these species are dominant above about pH 3 (as will be seen in the species distribution diagram in Figure 9.9(b)). That for ML_2 should also be reasonable as it predominates in a pH region where the Bi(III) nitrate concentration is fairly low. However, significant concentrations of BiL^{2+} and Bi(III) nitrates occur in the same pH range and hence carries the greatest uncertainty in its log β value (even though including MLH in the refinement may compensate somewhat for the Bi(III) nitrate species at the lowest pHs). The systematic decrease in the log β values for MLH with increasing Bi(III)-to-PA concentration ratios indicates that the concentration of Bi(III) nitrates decreases with the increasing PA concentration.

Table 9.2: Log β values determined using $E(Bi_{free})$ and $E(Bi_{free})_{OH}$ for the given equilibria, where L = PA, at 25 °C and ionic strength between 0.25 and 0.5 M.

$[L]_T:[Bi^{3+}]_T$ =	94 [a]	148 [a]	197 [a]	Average [b]
Equilibrium		**Log β**		
(a) Using $E(Bi_{free})$				
$Bi^{3+} + HL \rightleftharpoons BiLH^{3+}$	9.21 ± 0.03	8.99 ± 0.03	8.71 ± 0.05	
$Bi^{3+} + L^{-} \rightleftharpoons BiL^{2+}$	7.59 ± 0.07	7.61 ± 0.06	7.66 ± 0.05	7.62 ± 0.04
$Bi^{3+} + 2L^{-} \rightleftharpoons BiL_2^{+}$	13.96 ± 0.04	13.86 ± 0.04	13.95 ± 0.03	13.92 ± 0.06
$Bi^{3+} + 3L^{-} \rightleftharpoons BiL_3$	18.4 ± 0.2	18.47 ± 0.09	18.51 ± 0.08	18.46 ± 0.06
$Bi^{3+} + 3L^{-} + OH^{-} \rightleftharpoons BiL_3(OH)^{-}$	28.24 ± 0.03	28.10 ± 0.03	28.23 ± 0.02	28.19 ± 0.08
Overall fit	0.31	0.55	0.44	
(b) Using $E(Bi_{free})_{OH}$				
$Bi^{3+} + L^{-} \rightleftharpoons BiL^{2+}$	6.79 ± 0.10	6.93 ± 0.06	6.87 ± 0.07	6.86 ± 0.07
$Bi^{3+} + 2L^{-} \rightleftharpoons BiL_2^{+}$	13.31 ± 0.05	13.28 ± 0.04	13.44 ± 0.03	13.34 ± 0.09
$Bi^{3+} + 3L^{-} \rightleftharpoons BiL_3$	17.96 ± 0.13	17.99 ± 0.08	17.97 ± 0.03	18.00 ± 0.05
$Bi^{3+} + 3L^{-} + OH^{-} \rightleftharpoons BiL_3(OH)^{-}$	27.71 ± 0.03	27.57 ± 0.03	27.72 ± 0.02	27.67 ± 0.08
Overall fit	0.29	0.32	0.87	

[a] Standard deviations of log β values obtained from fitting.
[b] Standard deviations of log β values obtained from averaging.

The species distribution diagrams for both sets of averaged log β values were plotted for a ligand-to-metal concentration ratio of 197 (Figure 9.9). In Figure 9.9(a) the species are shown for the model resolved as given in Table 9.2, but with the MLH species was omitted. (The plot including MLH can be seen in Figure A7.2, Appendix 7.) By comparing the two plots indicated it was seen that they were similar for the ML_2, ML_3, and ML_3OH species, but a large difference is seen for the ML, M_{free} and M(OH) species. For a clearer idea of the actual solution species, a plot including the nitrate species (using Sol-Eq software[13]) is given (Figure 9.9(b)). The distribution of ML_2, ML_3, and ML_3OH species were similar in both diagrams ((a) and (b)), but the fraction of ML, MOH and especially M_{free} was lower when including the bismuth nitrate species. The correlation between the pH range in which the species are found as given in the species distribution diagrams and in the slope analysis plot (Figure 9.4) was also evident.

The Bi(III)-PA system has been studied once before by Cukrowski *et al.*[11] also using polarography. The actual results determined will be discussed shortly,

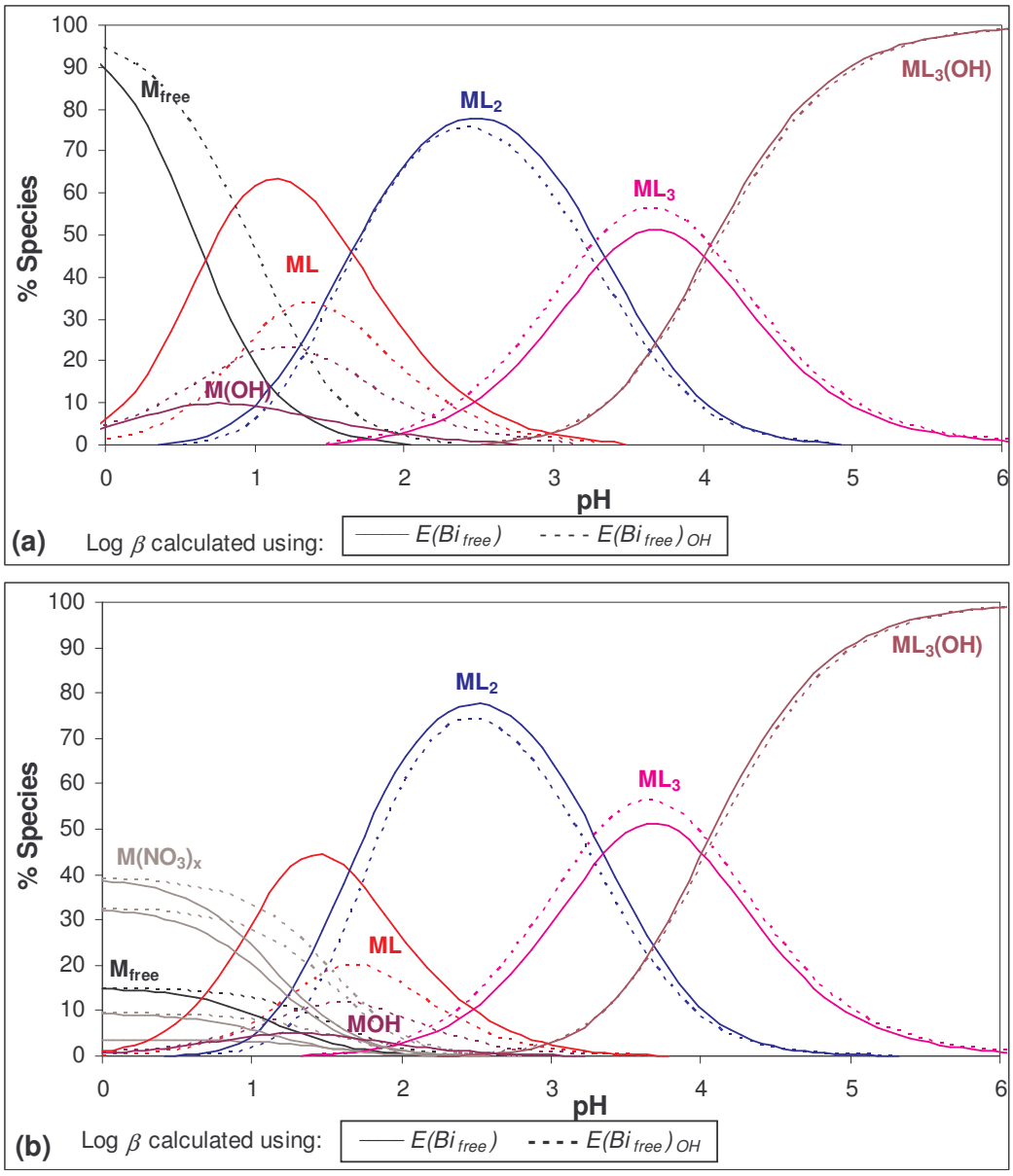

Figure 9.9: Species distribution diagrams for aqueous solutions of Bi(III)-PA using the two sets of averaged log β values in Table 9.2. (a) [Bi(III)] = 1×10^{-5} M and [PA] = 2×10^{-3} M and (b) including the $Bi(NO_3)_x^{(3-x)}$ species (where x = 1 – 4) with [NO_3^-] = 0.5 M.

but what was striking was that they proposed a model consisting of the ML, ML_2, ML_3, ML_4 and $ML_3(OH)$ species. To determine if there was any evidence for the formation of ML_4, the Cambridge Structure Database (CSD)[14] was searched. Two structures containing PA and Bi(III) were found (reference codes: (a) YIZVEJ and (b) YIZVAF) and are presented in Figure 9.10 which shows Bi(III) coordinated to three and four PA ligands, respectively. In Figure

9.10(a) it can be seen that Bi(III) (labelled Bi1) is bonded bidentately to three PA ligands through the carboxylate oxygen and the pyridyl nitrogen atoms. The Bi1A atom bonded to the carboxylate oxygens of two PA ligands shows the packing arrangement and a packing diagram is given in Figure 9.11 to illustrate this more clearly. The Bi1A bond lengths to O2 and O4 (2.649 and 2.574 Å respectively) are also longer than the Bi1 bond lengths to O2 and O4 (2.473 and 2.531 Å respectively). In Figure 9.10(b), Na^+ is included in the structure where each Na^+ is bonded to two carboxylate oxygen atoms on adjacent PA ligands which could stabilise the BiL_4^- arrangement. It is possible that there could be similar interactions in solution with the cation of the background electrolyte, which was K^+ in this work and Na^+ in that of Cukrowski *et al.*[11] The presence of the BiL_4^- arrangement in the solid state indicates that it is also likely to be present in solution, especially at the high ligand-to-metal ratios used here.

In order to further support or refute the existence of ML_4 in solution, electrospray ionisation-mass spectrometry (ESI-MS) was used as an independent technique to analyse particular solutions. Since the solutions

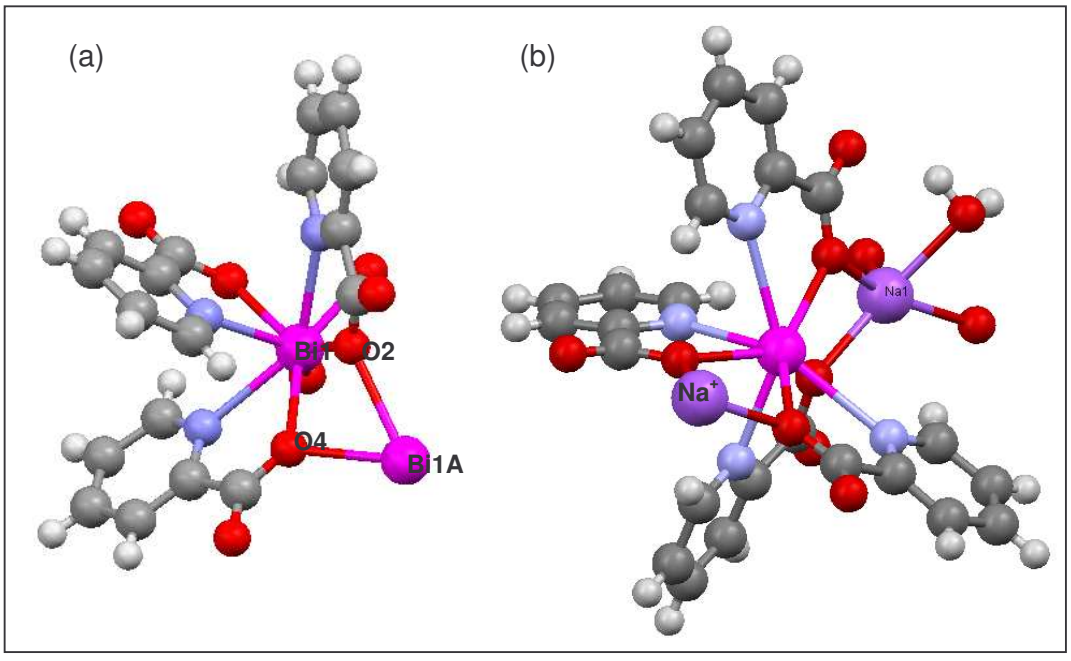

Figure 9.10: Structures of two Bi(III) picolinic acid complexes showing (a) a BiL_3 and (b) a BiL_4 arrangement.

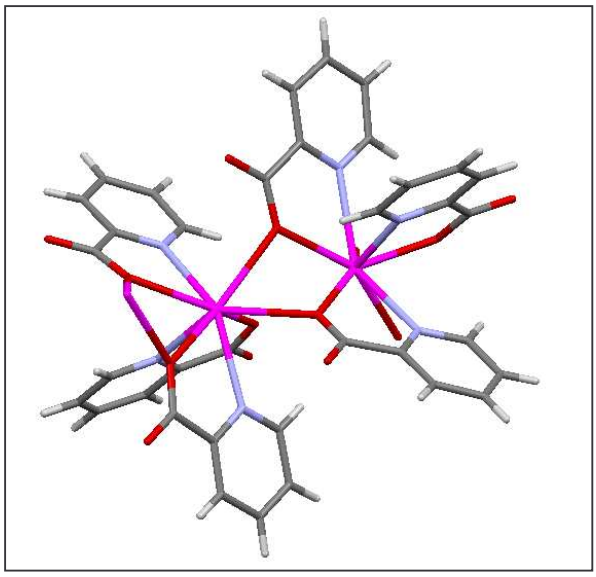

Figure 9.11: Packing diagram of the BiL_3 arrangement in Figure 9.10(a) (drawn using Mercury[15]).

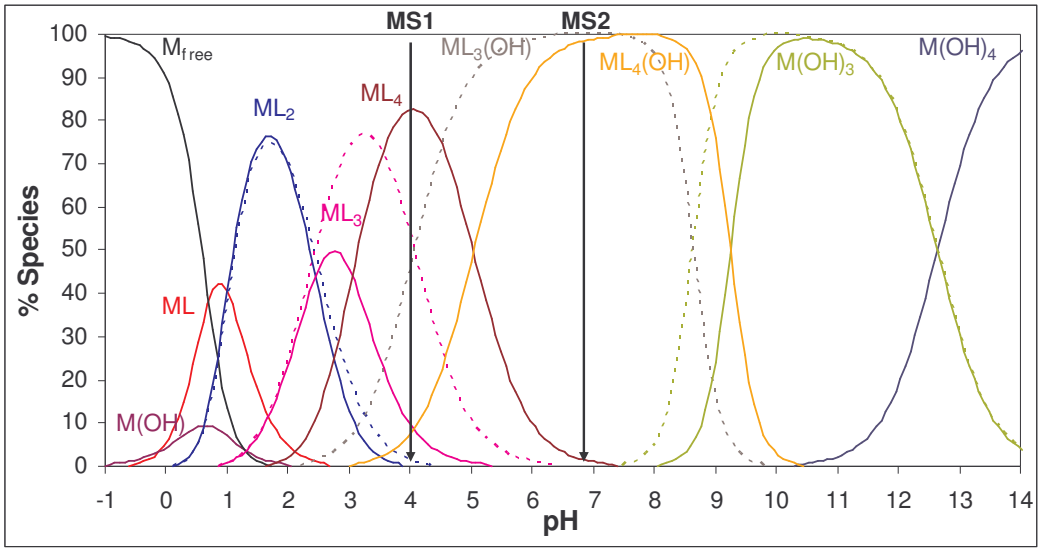

Figure 9.12: Species distribution diagrams are compared for aqueous solutions of Bi(III)-PA for species models including (solid lines) and excluding ML_4 (dotted lines) and the pH of the solutions measured by ESI-MS are indicated. Log β values in Tables 9.2 and 9.5 were used and $[Bi(III)] = 1 \times 10^{-4}$ M and $[PA]_T:[Bi(III)]_T = 100$.

were analysed to particularly detect if ML_4 is present, solution conditions were optimised to promote the formation of this species based on formation constants calculated (see Table 9.5). Additionally, only aqueous solutions were used so that the solution conditions were kept as close to those in the polarographic experiments. Due to the poor sensitivity of the particular

instrument used, it was recommended that higher concentrations of Bi(III) be used. Solutions of a maximum of 1×10^{-4} M Bi(III) could be prepared with excess PA present, else precipitation occurred. The excess PA (100 times more than Bi(III)) was required for ML_4 to be dominant in solution at pH 4, if it is formed, as seen in the species distribution diagram in Figure 9.12. At pH 7 either $ML_3(OH)$ or $ML_4(OH)$ would be dominant. The same solution was analysed, firstly adjusted to pH 4.0 (using 0.5 M KOH) and secondly to pH 6.9.

The mass spectra obtained for the solution at pH 4.0 are given in Figures 9.13 (a) and (b) for the detection of the negative and positive ions respectively, and

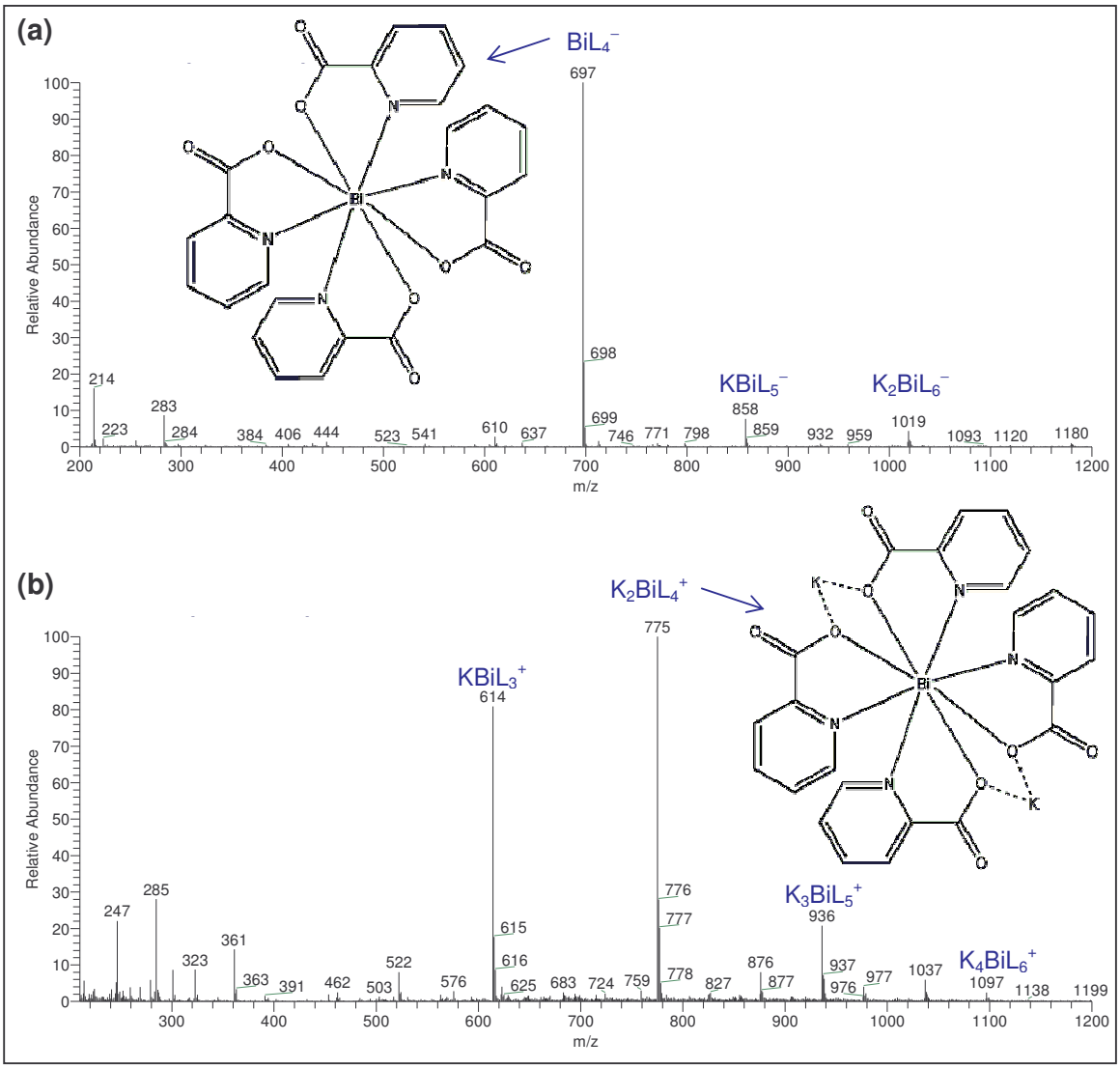

Figure 9.13: Mass spectra for (a) negative and (b) positive ions in a solution containing 10^{-4} M Bi(III) and 10^{-2} M PA at pH 4.0.

the assignment of the peaks are given in Table 9.3. In the assignment, only the mass-charge ratio (m/z) of the most abundant isotope is quoted. Thus, for example, the BiL_4^- species would produce relative abundances of 100.0% at m/z of 697, 26.4% at m/z of 698 and 5.3% at m/z of 699 (as determined from ChemDraw[16]), all of which are clearly seen in the spectrum. With the excess ligand present, large peaks due to the ligand were observed, so the (m/z) range in which data was obtained was reduced to exclude these peaks as far as possible. The spectra, together with the peak assignments, from the ESI-MS analysis of solutions containing only 10^{-2} M PA at pH 4.0 are displayed in Appendix 7 (Figure A7.3). The presence of ML_4 was clearly seen as the anion BiL_4^- and the cation $K_2BiL_4^+$, where the latter could be directly correlated to the structure diagram given in Figure 9.10(b). ML_3 is present in the form $KBiL_3^+$, but is not observed in the spectra for negative ions due to BiL_3 being neutral and no further protons can be lost to produce an anion. In both spectra, species with the stoichiometry ML_5 and ML_6 were also detected. Unfortunately the relative abundance is not necessarily an indication of the concentration of the species, but it depends on many factors such as the efficiency of ionisation, the mechanism of detection and factors leading to disproportionate transmission of the ions between the ionisation source and the detector.

Table 9.3: Assignment of the peaks in the mass spectra in Figure 9.13.

Positive ions:		**Negative ions:**	
m/z	**Assignment**	***m/z***	**Assignment**
614	$KBiL_3^+$	697	BiL_4^-
775	$K_2BiL_4^+$	858	$KBiL_5^-$
936	$K_3BiL_5^+$	1019	$K_2BiL_6^-$
1097	$K_4BiL_6^+$		
876	$K_3BiL_4(NO_3)^+$		
977	$K_4BiL_4(NO_3)_2^+$		
1037	$K_4BiL_5(NO_3)^+$		
247	$H_3L_2^+$	214	$KL(OH)(H_2O)_2^-$
285	$H_2KL_2^+$	283	KL_2^-
323	$HK_2L_2^+$		
361	$K_3L_2^+$		
522	$K_4L_3^+$		

The spectra and the peak assignments for the analysis of the solution at pH 6.9 are given in Figure 9.14 and Table 9.4, respectively. It was expected that either $BiL_3(OH)^-$ or $BiL_4(OH)^{2-}$ would be detected at this pH, as indicated in the species distribution diagram (Figure 9.12), depending which model was correct. As seen in Figure 9.14(a), a small peak at m/z of 357 indicated the presence of $BiL_4(OH)^{2-}$, but no peak was found at m/z of 592 to denote $BiL_3(OH)^-$. Unfortunately the ligand appeared to undergo extensive polymerisation (of some form) at this pH which clutters the spectra. It was noted that when using ESI, adducts could form with other solute or solvent

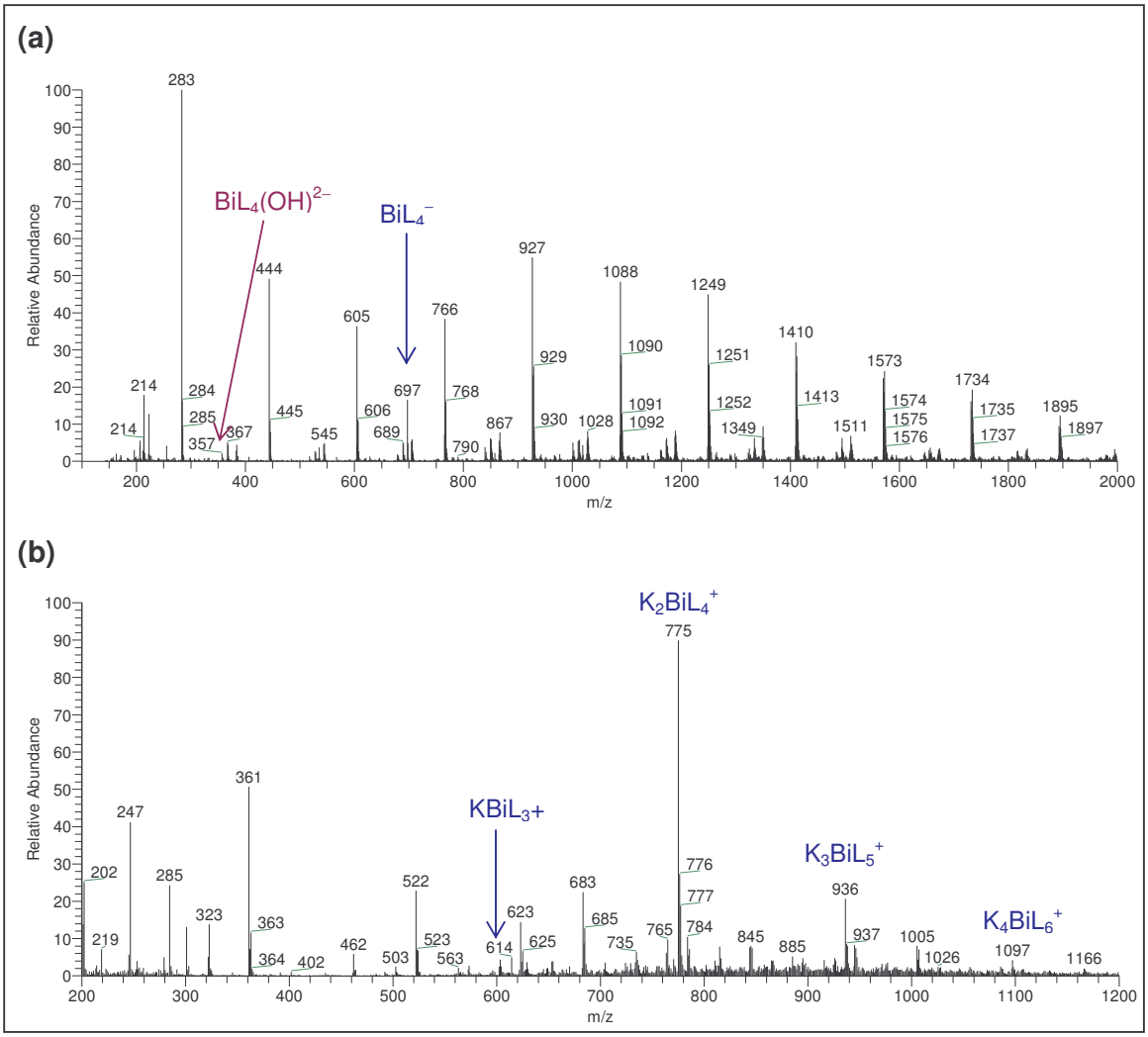

Figure 9.14: Mass spectra for (a) negative and (b) positive ions in a solution containing 10^{-4} M Bi(III) and 10^{-2} M PA at pH 6.9.

species.[10] The polymerisation of PA could be due to the higher concentration of K^+ present and the almost complete deprotonation of the ligand at this pH (see Figure 5.3). The K^+ could act as a bridge between two PA ligands (as illustrated in the structure in Figure 9.10(b)) or it could also be coordinated to the PA through the pyridine nitrogen atom and a carboxylate oxygen atom. To achieve the K^+-to-L^- ratios observed, it is speculated that both processes occur to produce the cations, but possibly only bridging occurs in the anions. This could perhaps be confirmed by growing single crystals at pH 7 in a PA-KOH solution, but it certainly was not the focus of this project.

Table 9.4: Assignment of the peaks in the mass spectra in Figure 9.14.

Positive ions:		**Negative ions:**	
m*/*z	**Assignment**	***m*/*z***	**Assignment**
614	$KBiL_3^+$	697	BiL_4^-
775	$K_2BiL_4^+$	357	$BiL_4(OH)^{2-}$
936	$K_3BiL_5^+$		
1097	$K_4BiL_6^+$		
247	$H_3L_2^+$	214	$KL(OH)(H_2O)_2^-$
285	$H_2KL_2^+$	283	KL_2^-
323	$HK_2L_2^+$	444	$K_2L_3^-$
361	$K_3L_2^+$	605	$K_3L_4^-$
522	$K_4L_3^+$	766	$K_4L_5^-$
623	$K_5L_3(NO_3)^+$	927	$K_5L_6^-$
683	$K_5L_4^+$	1088	$K_6L_7^-$
784	$K_6L_4(NO_3)^+$	1249	$K_7L_8^-$
845 (844)*	$K_6L_5^+$	1410	$K_8L_9^-$
1005	$K_7L_6^+$	1573 (1571)*	$K_9L_{10}^-$
		1734 (1732)*	$K_{10}L_{11}^-$
		1895 (1893)*	$K_{11}L_{12}^-$

* Actual values calculated are given in brackets. In the mass spectrum it was noted that the most abundant value was quoted, but there was a peak just before this which probably corresponded to the *m*/*z* value in brackets.

Due to the results obtained in the mass spectrometry analyses of these solutions and the crystal structure evidence, the polarographic data was reanalysed to include ML_4 as a solution species. Direct correlation between the MS results and the solution species should be treated with caution as the temperature and concentrations conditions (among others) experienced by the

complexes change as evaporation of the solvent occurs before the ions are left in a gas phase and analysed. The fact that the crystal structure of the ML_4 was also found gave additional credibility of the species existing in solution.

From Figure 9.5 it was seen that ML_4 could be included in the model to fit the ECFC, but data between pH 5 to 6 was not predicted well by the CCFC indicating another species in solution. This region could be fitted by including the hydroxide species $ML_4(OH)$ as shown in Figure 9.15 (as previously mentioned, the log β values could not be refined simultaneously for ML_4 and $ML_3(OH)$). Since the ML_5 and ML_6 species were also clearly present in the mass spectra, it was also attempted to include these species in the model, but log β values could not be refined for these species. If they were present under the solution conditions for the polarographic experiments, they were certainly minor species. The log β values obtained using the model including ML_4 and $ML_4(OH)$ are presented in Table 9.5 for all three experiments and the average was calculated. Only values for ML and ML_2 are shown when $E(Bi_{free})_{OH}$ was used to calculate the ECFC as they are the only values that could be influenced by the presence of Bi(III) nitrate species. The standard deviations of the log β values for the ML_3 and ML_4 in each experiment was relatively high, indicating that ML_4 is possibly not formed to a great extent under the solution conditions used here.

Table 9.6 gives a comparison of the log β values obtained by Cukrowski *et al.*[11] and those for both models (using $E(Bi_{free})$ and $E(Bi_{free})_{OH}$ where appropriate) determined in this work. The log β values obtained by the auhtors[11] compare better to those obtained using $E(Bi_{free})$ (rather than $E(Bi_{free})_{OH}$) in this work. Interestingly, log β for ML_2 is the same when determined by Cukrowski *et al.*[11] and in this work using $E(Bi_{free})$, and that for ML only differs by about 0.1 log units. Disparities in the formation constants for the remaining species are expected as different species models were refined. It was impossible to refine the data obtained here using the same model as Cukrowski *et al.*[11]

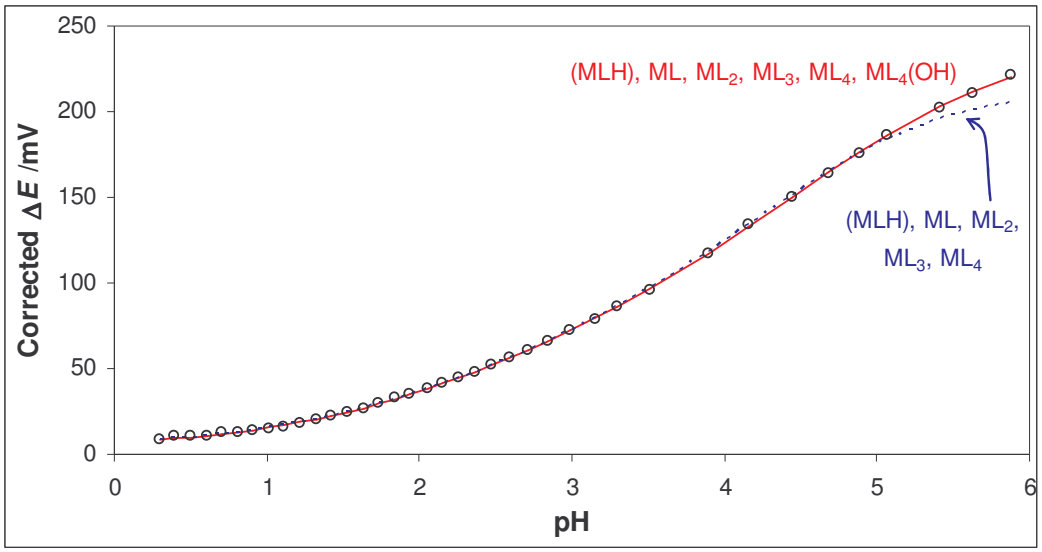

Figure 9.15: The ECFC (○), calculated using $E(Bi_{free})$, is plotted with various CCFC's determined using the species indicated ($[PA]_T$:$[Bi(III)]_T$ = 197).

Table 9.5: Log β values determined using $E(Bi_{free})$ and $E(Bi_{free})_{OH}$ for the given equilibria (including BiL_4^-), where L = PA, at 25 °C and ionic strength between 0.25 and 0.5 M.

$[L]_T$:$[Bi^{3+}]_T$ =	94 [a]	148 [a]	197 [a]	Average [b]
Equilibrium		**Log β**		
(a) Using $E(Bi_{free})$				
$Bi^{3+} + HL \rightleftharpoons BiLH^{3+}$	9.21 ± 0.03	8.99 ± 0.03	8.71 ± 0.05	
$Bi^{3+} + L^- \rightleftharpoons BiL^{2+}$	7.60 ± 0.07	7.62 ± 0.06	7.68 ± 0.05	7.63 ± 0.03
$Bi^{3+} + 2L^- \rightleftharpoons BiL_2^+$	13.96 ± 0.04	13.85 ± 0.04	13.92 ± 0.04	13.91 ± 0.08
$Bi^{3+} + 3L^- \rightleftharpoons BiL_3$	18.4 ± 0.2	18.5 ± 0.1	18.63 ± 0.09	18.5 ± 0.1
$Bi^{3+} + 4L^- \rightleftharpoons BiL_4^-$	23.0 ± 0.1	22.6 ± 0.1	22.6 ± 0.1	22.7 ± 0.2
$Bi^{3+} + 4L^- + OH^- \rightleftharpoons BiL_4(OH)^{2-}$	31.62 ± 0.02	31.28 ± 0.05	31.32 ± 0.05	31.4 ± 0.2
Overall fit	0.31	0.53	0.36	
(b) Using $E(Bi_{free})_{OH}$				
$Bi^{3+} + L^- \rightleftharpoons BiL^{2+}$	6.8 ± 0.1	6.95 ± 0.06	6.89 ± 0.06	6.88 ± 0.08
$Bi^{3+} + 2L^- \rightleftharpoons BiL_2^+$	13.29 ± 0.06	13.26 ± 0.05	13.42 ± 0.03	13.32 ± 0.09

[a] Standard deviations of log β values obtained from fitting.
[b] Standard deviations of log β values obtained from averaging.

Species distribution diagrams are plotted in Figure 9.16 from the results in Table 9.6. The Bi(III) nitrate species are recognised in this work and hence represented in the Figure 9.16(a). It is clear that refining the model containing $ML_3(OH)$ or ML_4 and $ML_4(OH)$ gives a similar species distribution for all other

Table 9.6: Average log β values at 25°C for the proposed equilibria, where L = PA, for this work (0.25 - 0.5 M (K,H)NO_3) and that determined by Cukrowski *et al.*[11] (0.5 M (Na,H)NO_3*).

Species	**log β** (this work)		**log β** (this work)		**log β**[11]
using:	$E(Bi_{free})$	$E(Bi_{free})_{OH}$	$E(Bi_{free})$	$E(Bi_{free})_{OH}$	
BiL^{2+}	7.62 ± 0.04	6.86 ± 0.07	7.63 ± 0.03	6.88 ± 0.08	7.48 ± 0.01
BiL_2^{+}	13.92 ± 0.06	13.34 ± 0.09	13.91 ± 0.05	13.32 ± 0.09	13.94 ± 0.01
BiL_3	18.46 ± 0.06		18.5 ± 0.1		18.10 ± 0.04
BiL_4^{-}			22.7 ± 0.2		20.47 ± 0.25
$BiL_3(OH)^{-}$	28.19 ± 0.08				26.65 ± 0.03
$BiL_4(OH)^{-}$			31.4 ± 0.2		

* The ionic strength was quoted as 0.5 M, but the titration procedure would also lead to the ionic strength varying between 0.25 and 0.5 M.

species present and it would be impossible, based solely on the polarographic data, to conclusively decide whether ML_4 is present in solution or not. It is therefore important to consult other independent techniques to support the species model predicted; however, unless the solution conditions are the same it is difficult to make a definitive correlation between the speculated species. In Figure 9.16(b) the results obtained by Cukrowski *et al.*[11] are used to plot the species distributions at the initial Bi(III) concentration they used (5×10^{-5} M) and that used in this work (1×10^{-5} M), both at a ligand-to-metal ratio of 100. At 5×10^{-5} M Bi(III), ML_4 is a minor species but still gives a maximum of about 33%. At 1×10^{-5} M Bi(III), ML_4 is hardly formed at all and hence it is not surprising that the log β values for ML_4 and $ML_3(OH)$ could not be refined together in this work.

In the three pH titrations performed here, only data up till about pH 6 were analysed and the last four data points were discarded due to the pH changing by almost 1 pH unit between each point. If these were included in the analysis, the additional species $BiL_3(OH)_2^{2-}$ and $BiL_3(OH)_3^{3-}$ were speculated when ML_4 was omitted from the model, or $BiL_4(OH)_2^{3-}$ and $BiL_4(OH)_3^{4-}$ were speculated when ML_4 was included (see Figure A7.4, Appendix 7). The log β values for $BiL_3(OH)_2^{2-}$ and $BiL_3(OH)_3^{3-}$ were estimated to be 35.7 ± 0.1 and 42.5 ± 0.03, respectively, or for $BiL_4(OH)_2^{3-}$ and $BiL_4(OH)_3^{4-}$ they were 38.8 ± 0.1 and 45.8

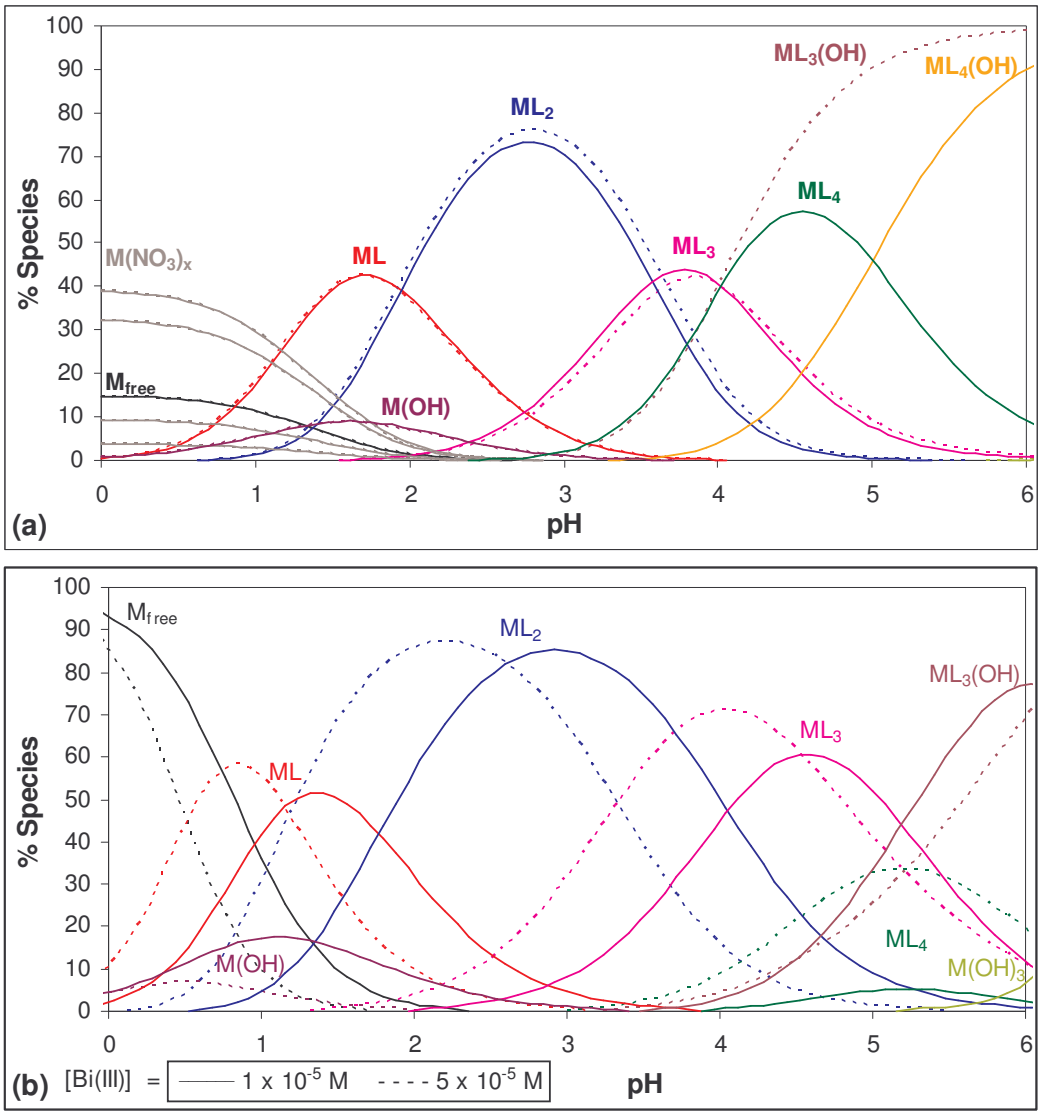

Figure 9.16: Species distribution diagrams for aqueous solutions of Bi(III)-PA using log β values in Table 9.6 and $[PA]_T$:$[Bi(III)]_T$ = 100. (a) Values for the two models determined using $E(Bi_{free})$ are compared and [Bi(III)] = 1×10^{-5} M. (b) Values determined by Cukrowski *et al.*[11] are compared for two Bi(III) concentrations.

± 0.1, respectively. Due to the large uncertainty in these values (as well as the questionable existence of these complexes which are stericly hindered), they were not included in any further calculations. In order to obtain more data points in this region a KOH titrant with a lower concentration (such as 0.1 M or 0.05 M) would have to be used from pH 6 onwards.

The corrected potential shifts are calculated by subtracting the current term, $RT/nF \ln\{i(M_{comp})_{(i)}/i(M_{free})_{(i)}\}$, from the potential shift as shown in equation 2.17.

In this study it is important to consider the diffusion limited current for the Bi(III) wave in the presence of PA as shown in Figure 9.17. The expected currents were calculated using i_d for the free metal ion (measured before ligand was added) and taking the dilution into account. The expected and measured values were essentially the same up to a pH of about 4, implying that the current term (in equation 2.17) is negligible. Above pH 4 the measured i_d values started dropping and around pH 8 the Bi(III) reduction wave disappeared totally. The unexpected decrease in i_d could be due to one of three factors, namely, precipitation (which could not readily be detected visually here due to the low concentrations), a decrease in the diffusion rates of the species or the formation of non-labile species. Cukrowski *et al.*[11] observed precipitation at about pH 6.5 for 5×10^{-5} M Bi(III) solutions containing PA, so precipitation should occur at slightly higher pHs for the lower Bi(III) concentration used here, which would correspond with the disappearance of the reduction wave. It is unlikely that precipitation caused the decrease in current as it was observed over at least 3 pH units. It was also not expected that the diffusion rates of the Bi(III)-PA-hydroxide species should be significantly lower than that for BiL_3.

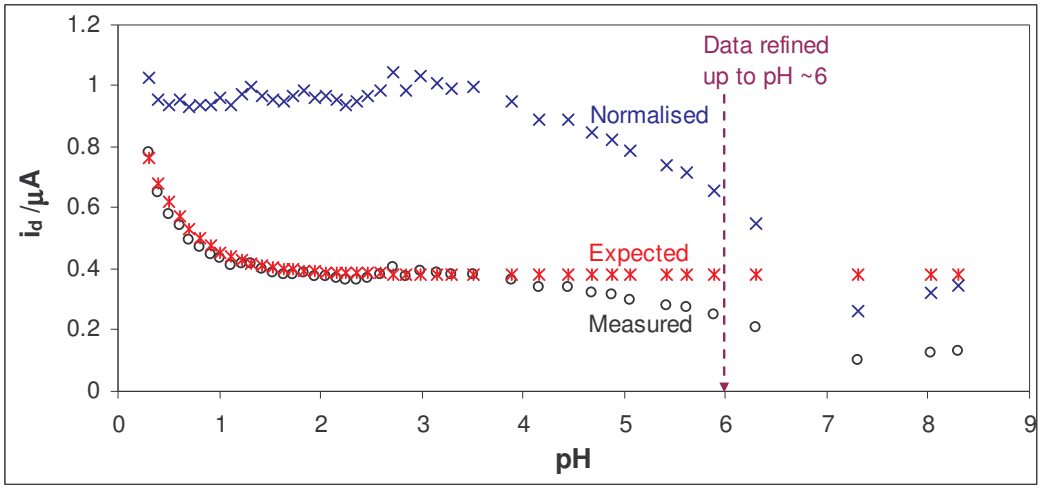

Figure 9.17: The expected and measured currents for the reduction of Bi(III) in the presence PA ($[PA]_T$:$[Bi(III)]_T$ = 197). The normalised current is the ratio of the measured-to-expected currents.

The onset of the drop in current coincides either with the start of formation of $BiL_4(OH)^{2-}$ or where $BiL_3(OH)^-$ becomes significant in solution (about 30% of

Bi(III) exists as $BiL_3(OH)^-$ at pH 4), depending on the species model. Further current drops were observed when the additional $BiL_x(OH)_y$ (where x = 3 or 4 and y = 2 or 3) species were speculated. It is suggested that these Bi(III)-PA-hydroxide species are not labile. Another wave at more negative potentials was not observed here as was the case for the complexation studies of Bi(III)-THETAC (N,N′,N″-tris(hydroxyethyl)triaza-cyclononane)[17] and Bi(III)-cyclen (1,4,7,10- tetraaza-cyclodecane)[18] by DPP. In the complex formation study of Bi(III)-THP-cyclen (1,4,7,10-tetrakis(2-hydroxypropyl)-1,4,7,10-tetraazacyclo-decane)[18] by DPP, no additional peak was observed so the complex was either polarographically inactive or inaccessible in the potential range of the mercury electrode. Previously,[17,18] stability constants had been estimated for non-labile or inert complexes by simply considering the decrease in the current of the signal of the labile complexes.

The corrected potential shifts (ΔE_{corr}) and the normalised currents (i_{norm}) are given in Table 9.7 from about pH 4 where the unexpected drop in the measured i_d values was observed. The current term in equation 2.17 was calculated using these normalised currents and the percentage of the corrected potential shift at each step due to this current term was evaluated. The percentage of the stepwise corrected potential shift due to the current term at pH 5.9 was 33%, which indicates that the Bi(III)-PA-hydroxides may be non-labile species. Irrespective of the reason for the current drop, it is accounted for when calculating the corrected potential shifts and the formation of these species can still be indirectly observed.

Since a different process to calculate the stability constants for Bi(III) PA was employed by Cukrowski *et al.*,[11] their approach is considered. They performed two consecutive pH titrations under the same conditions, the one omitting the ligand and the other including the ligand. The expected potential shift due to hydrolysis of Bi(III) across the pH range was calculated and added to the $E_{1/2}$ values for Bi(III) reduction in the absence of ligand. As shown in Figure 9.18, this new potential versus pH relationship was fitted using a third order polynomial (given as the solid line) and the difference between this polynomial

Table 9.7: The percentage of the corrected potential shift at each step due to the current term, and the values used to calculate it, in the pH range where the measured i_d dropped unexpectedly.

pH	ΔE_{corr} /mV	Stepwise ΔE_{corr} /mV	i_{norm}	$(-RT/nF)\ln(i_{norm})$ /mV	% stepwise ΔE_{corr} due to i_{norm}
3.89	116.85		0.949	0.44	
4.17	134.01	17.16	0.887	1.03	6.0
4.44	150.44	16.43	0.892	0.97	5.9
4.68	164.32	13.88	0.848	1.41	10.2
4.88	176.00	11.68	0.825	1.65	14.1
5.07	186.24	10.24	0.786	2.06	20.1
5.42	201.67	15.43	0.739	2.59	16.8
5.62	210.72	9.05	0.718	2.83	31.3
5.88	221.54	10.82	0.656	3.61	33.4
6.31	238.18	16.64	0.549	5.14	30.9
7.30	283.82	45.64	0.264	11.40	25.0
8.02	325.48	41.66	0.322	9.70	23.3
8.30	346.86	21.38	0.348	9.04	42.3

and the $E_{1/2}$ values in the presence of ligand were therefore considered to be the potential shift due to complex formation. According to the authors, the solid line represented the change in the diffusion junction potential with pH and it approached a constant value of about 85.3 mV (taken as $E(Bi_{free})$) at pH 2.5. The difference between $E(Bi_{free})$ and the solid line was regarded as the magnitude of the diffusion junction potential.

There are a number of possible sources of error when using their approach. (i) The GE was calibrated by an acid-base titration using 0.5 M HNO_3 and 0.5 M NaOH and a straight line relationship was assumed over the entire pH range. This has been shown not to be the case at the lowest pH values, but this calibration should only introduce small errors. (ii) The $Bi(OH)_2^+$ species was not considered as one of the hydrolysis products and as seen in the species distribution diagram in Figure 8.7, some $Bi(OH)_2^+$ does form below pH 2 (the pH up to where experimental data was obtained in the absence of PA in Figure 9.18) at the Bi(III) concentration used in these experiments. However, this would again only have a minimal effect on the results as the $Bi(OH)_2^+$

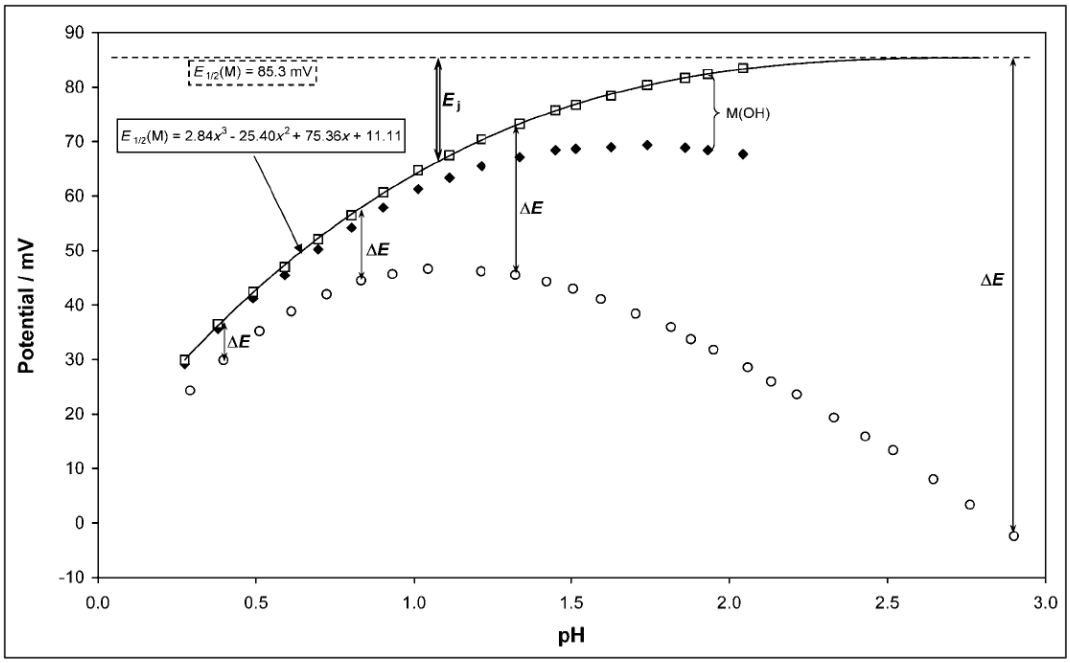

Figure 9.18: Experimental data at low pH values analysed by Cukrowski *et al.*[11] ◆: represents the shift in $E_{1/2}$ values obtained from the Bi(III) solution without ligand. □: represent the corrected $E_{1/2}$ values – the distance between the ◆ and □ represents the contribution made by the formation of Bi(OH). — (fitted □): shows the variation in the diffusion junction potential, E_j, versus pH – it is used to predict the E(M_{free}) value of 85.3 mV. ○: represent the experimental points obtained from the acid titration of a sample containing Bi(III) and the ligand. Shifts in $E_{1/2}$ due to the formation of bismuth complexes are indicated by ΔE.

concentrations are small (about 15% of the Bi(III) exists $Bi(OH)_2^+$ at pH 2 for [Bi(III)] = 5×10^{-5} M). (iii) The formation of Bi(III) nitrate complexes was not considered explicitly, although their procedure appears to compensate for this to an extent since the potential shifts due to complex formation were considered to be the difference between the solid line and the potential values when ligand was added (○) shown as ΔE in the figure. However, the potential shifts calculated due to hydrolysis (resulting in the values indicated by □) are too large (as was shown in this work) and the log β value for particularly ML would be too high. (iv) No measurement nor calculation of the diffusion junction potential was made. From Figure 9.18 it can be seen that at pH ~0.3 the junction potential was given as approximately 55 mV (the difference between 85.3 mV and the value at the point indicated by □ at pH 0.3). This value was overestimated by about 20 mV. The 55 mV shift should rather be regarded as the combination of the shifts due to the junction potential and the

formation of Bi(III) nitrates. (v) The separate pH titrations of solutions containing Bi(III) without ligand followed by that containing Bi(III) with ligand may also lead to incorrect results. From Figure 9.18, for $[PA]_T$:$[Bi(III)]_T$ = 132, the shift at pH ~0.3 simply due to the addition of picolinic acid was about 5 mV (i.e. the difference in potential between the points □ and ○ at pH 0.3). A shift of this magnitude was never observed in this work as shown by the two polarograms of the reduction of Bi(III) that were collected before and just after the addition of picolinic acid for $[PA]_T$:$[Bi(III)]_T$ = 197 (see Figure 9.2). When expected potential shifts were calculated for Bi(III) concentrations of 5×10^{-5} M and $[PA]_T$:$[Bi(III)]_T$ = 132, it was found to be 6.7 mV, within experimental error. However, a slight change in the reference system (electrode and/or salt bridge) from one experiment to the next could lead to error in this approach. Introducing a witness ion such as Tl(I) could assist in monitoring the reference system in this case. Thus the approach by Cukrowski *et al.*[11] inadvertently accounted for shifts due to Bi(III) nitrate formation to an extent, leading to comparative values for the ML, ML_2 and ML_3 species, but the same species model could not be refined in this work as they did. It should be mentioned that one of the limitations used in this work is relying on the log β values for the Bi(III) nitrate species which are small and difficult to determine accurately.

Cukrowski *et al.*[11] also performed three ligand titrations at pH 0.9, 1.37 and 1.85 and obtained log β values for BiL^{2+} of 7.50, 7.66 and 7.89, respectively. Since these titrations were done at fixed pH, the E_j should remain the same throughout the titration so it does not have to be compensated for. However, these titrations were done at different pHs which would result in different degrees of hydrolysis of Bi(III) in the initial solutions and again, the free metal ion potential cannot be directly measured. It was speculated that the systematic error they observed was due to the formation constant for $BiOH^{2+}$ being too high,[11] as was also initially contemplated in Chapter 8 and was shown not to be the case. The source of this error is once again due to the oversight of the presence of the Bi(III) nitrates. Exactly how the authors[11] determined the value of $E(Bi_{free})$ for these experiments was not specified.

Cukrowski *et al*.[11] also used the data from the both the ligand and pH titrations for analysis by virtual potentiometry as described in Chapter 2, Section 2.5.3. When calculating *E(virt)* (equation 2.23), the free metal ion potential is not required. Since the most difficult parameter to determine is $E(Bi_{free})$, it appeared that this approach may be the answer to studying Bi(III) complexation. Additionally, the ESTA software[19] allows for the inclusion of nitrates in the species model, which the polarographic software does not.

The slope and y-intercept (E^o) from the plot of *E(virt)* against log [M_{free}] are required for estimates in the potentiometric software. Such plots were prepared from the three sets of pH titration data collected in this work (see Figure 9.19). The non-linearity of the data below pH 2 could be due to the nitrate species not being accounted for in the model in this region (because of software limitations). The slopes from the linear data were equal to the theoretical slope of 19.71 mV for a three electron reduction at 25 °C. In the refinement procedure, the slope is generally set to the theoretical value, whereas the E^o value is refined. The value of E^o, however, carries with it a history of previous data calculations and refinements. This is due to the values of [M_{free}] being calculated using the mass balance equation given in equation 2.19 which incorporates the mass balance equation for [L_{free}] (equation 2.20) and the log β values for the various metal-ligand species. The log β values were in turn refined from experimental data which included the value of $E(Bi_{free})$. By using the value of E^o it is not a purely independent method for calculating formation constants, however, this value is generally refined.

In this work it was impossible to refine the entire model using virtual potentiometry. Only data up to about pH 2.3 could be refined for all three datasets to give log β values for ML and ML_2, and only if the species model included the Bi(III) nitrate species (where their log β values were kept fixed). Since the E^o value was calculated based on log [M_{free}] values using $E(Bi_{free})$, incorporating the nitrate species in the model should give an indication of the competition between the nitrate and PA ligands. Unfortunately, the concentration of nitrate in the vessel has to be specified, and thus the varying

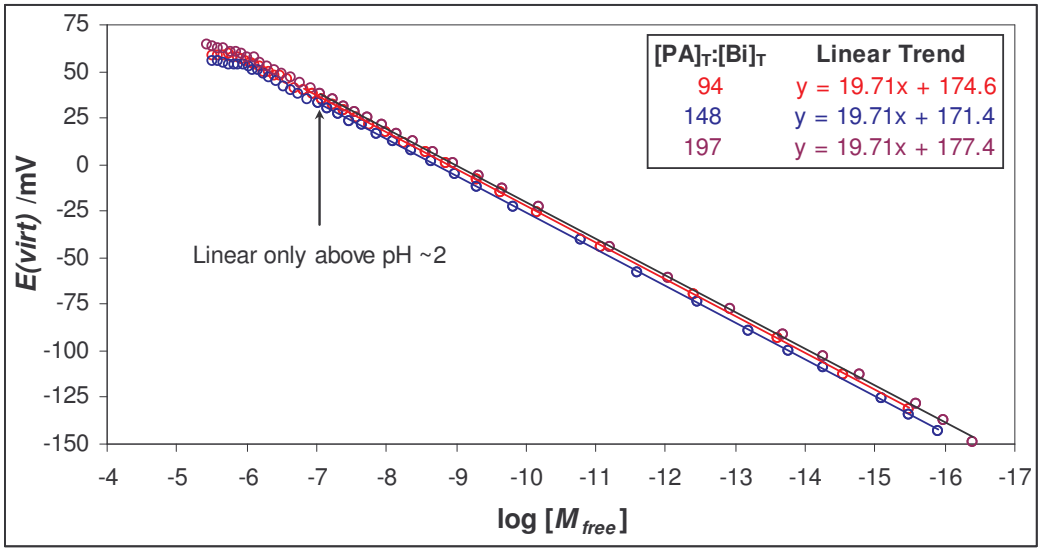

Figure 9.19: The virtual potential plotted against log [M_{free}] showing the trend lines fitted only through the linear data points (for data calculated using $E(Bi_{free})$).

nitrate concentration cannot be taken into account. A concentration of 0.3 M nitrate was used, which corresponds to the average concentration in the region up to pH ~2.3. A typical ESTA file used here is shown in Table A7.1, Appendix 7. The OBJE optimisation module[19] was employed, which optimises the titration parameters using the sum of squares of errors of the emf residues, and unweighted values were used.

The log β values obtained for ML and ML_2 by virtual potentiometry are given in Table 9.8 for all three experiments and the average was calculated because the three datasets could not be refined together (as is standard practice in potentiometry). The value for ML_2 is directly comparable to the polarographic results and the value for ML lies between those calculated when using $E(Bi_{free})$ and $E(Bi_{free})_{OH}$, as expected. Employing virtual potentiometry does take the competition from the nitrate into account in a feasible way. It also appears that the presence of the nitrate species does not affect the stability constant for ML_2. Thus, the final log β values quoted here are those calculated using $E(Bi_{free})$ for ML_2 and all other species formed at higher pHs and that for ML calculated by virtual potentiometry. The best approach would be to work in solutions with a constant ionic strength so that the nitrate concentration does

not have to be estimated. When the nitrate concentration was set to 0.4 M, log β(ML) = 7.5 ± 0.2. Seen as the result of log β(ML) = 7.48 determined by Cukrowski *et al.*[11] was suggested to be too high, the value given in Table 9.8 is a good estimate. The MLH species could also be included in the model and refined, producing log β(MLH) = 8.7 ± 0.4, but it is difficult to assess whether this is a real species. The species distributions given in Figure A7.5 (Appendix 7) show that MHL would complete with the Bi(III) nitrate species and has little effect on the other Bi(III) PA species. The case for speculating the presence of the CdLH species for PA (in Chapter 6) was more straight-forward as there were not additional uncertainties as when dealing with Bi(III), such as Bi(III) nitrate formation and the larger uncertainly in the value of $E(Bi_{free})$. Even though the complete model could not be refined using virtual potentiometry and the standard deviations for the average log β values were relatively high, the close correlation between these values and those determined directly from polarographic data is illustrated.

Table 9.8: Log β values for the given equilibria obtained from virtual potentiometry, where L = PA, at 25 °C and ionic strength between 0.25 and 0.5 M.

$[L]_T:[Bi^{3+}]_T$ =	94 [a]	148 [a]	197 [a]	Average [b]
Equilibrium		**Log β**		
$Bi^{3+} + L^- \rightleftharpoons BiL^{2+}$	7.22 ± 0.10	7.09 ± 0.05	7.44 ± 0.04	7.3 ± 0.2
$Bi^{3+} + 2L^- \rightleftharpoons BiL_2^+$	14.09 ± 0.06	13.86 ± 0.01	13.93 ± 0.02	14.0 ± 0.1
E^o /mV	168.4 ± 0.2	164.8 ± 0.1	173.0 ± 0.2	
Hamiltonian R-factor	0.013	0.0095	0.0087	

9.3.2) *Bi(III)-dipicolinic acid complexes*

Three pH titrations were performed with total DPA-to-Bi(III) concentration ratios of 53, 80 and 109. Since the concentrations of the DPA were very low, it dissolved completely. The reduction wave for DPA occurred at less negative potentials in more acidic solutions, as discussed in Chapter 5, but it was sufficiently resolved from the Tl(I) wave as observed in Figure 9.20 for the polarogram collected at pH 0.3. In this example, the Bi(III) wave was fitted using data in the potential range 0.10 to –0.30 V and the Tl(I) wave using data in the range –0.20 to –0.58 V. The onset of the DPA reduction wave was fitted

by the exponential function (c.exp(dx)) as was previously done for the hydrogen evolution wave. The higher the concentration of DPA, the closer the reduction wave was to that for Tl(I), so lower ligand-to-metal ion ratios were used here. The same applied to the quinolinic acid studies.

Due to the strong complexes formed by Bi(III) with DPA, the potential shifts were large and at higher pHs it was impossible to fit the Tl(I) and Bi(III) reduction waves separately, as indicated by the polarogram at pH 4.13 in Figure 9.20. Fortunately there were no other waves nearby from other electron transfer reactions with H^+, mercury or DPA, so fitting the two reduction waves together was straightforward.

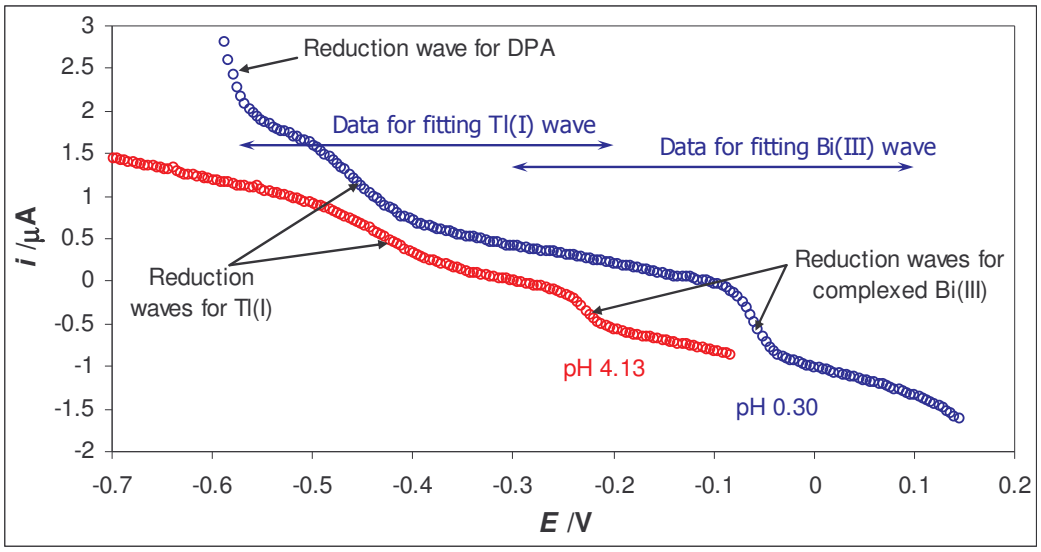

Figure 9.20: The polarogram at pH 0.30 was for a solution containing total Bi(III), Tl(I) and DPA having concentrations of about 1×10^{-5} M, 2×10^{-5} M and 1.09×10^{-3} M respectively. After 24.84 mL of KOH was added, the polarogram at pH 4.13 was collected.

With DPA being such a strong complexing agent, it was found to also complex Tl(I). This was detected by the negative shift in potential with increasing pH as shown in Figure 9.21. Fortunately complexation started above pH 2.5, which left sufficient data to still evaluate the diffusion junction potential and $E(Tl_{free})$. The $E_{1/2}$ values for the reduction of Bi(III) in the presence of DPA could therefore be corrected for E_j and $E(Bi_{free})$ could also be determined. Since large potential shifts were already observed for Bi(III) reduction at pH 0.3 after

the addition of DPA (over 90 mV), it indicated that the effect of Bi(III) nitrate species would be negligible and hence log β values were calculated using only $E(Bi_{free})$ ($E(Bi_{free})_{OH}$ was not considered at all.)

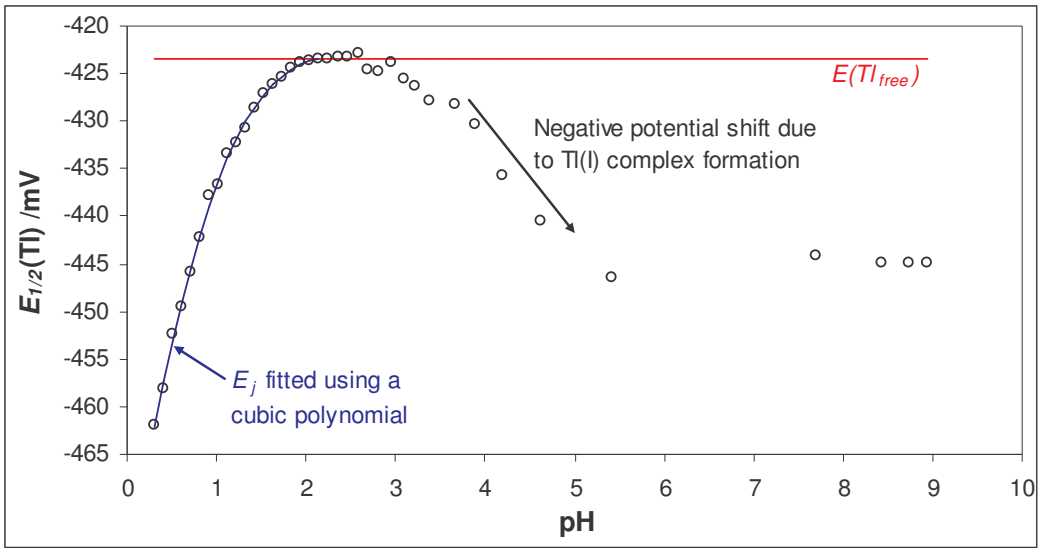

Figure 9.21: The $E_{1/2}$ values for the reduction of Tl(I) in the presence DPA as a function of pH. $[DPA]_T$:$[Tl(I)]_T$ = 27.

The measured and expected diffusion limited currents differed throughout the pH range in this case, with the measured values being lower than those calculated for the free metal ion (see Figure 9.22). This is probably due to slower diffusion rates of the complex since DPA is a fairly bulky ligand. The normalised current value (i.e. the ratio $i_{measured}$ / $i_{expected}$) was fairly constant at 0.78 ± 0.02 for all pHs in Figure 9.22 which, when converted to a potential value using the current term in equation 2.17, would be equivalent to about 2 mV. For the experiments with higher ligand-to-metal concentration ratios, the normalised current was closer to 0.6 resulting in a calculated potential shift of about 4 mV.

Slope analysis was done using the graph of corrected potential shift versus pH and an example is given in Figure 9.23. Slope analysis could also be done using half-wave potentials (instead of the corrected shift) since the current term is generally small and in this case the current term remains essentially constant throughout the pH range. Considering possible reactions and the

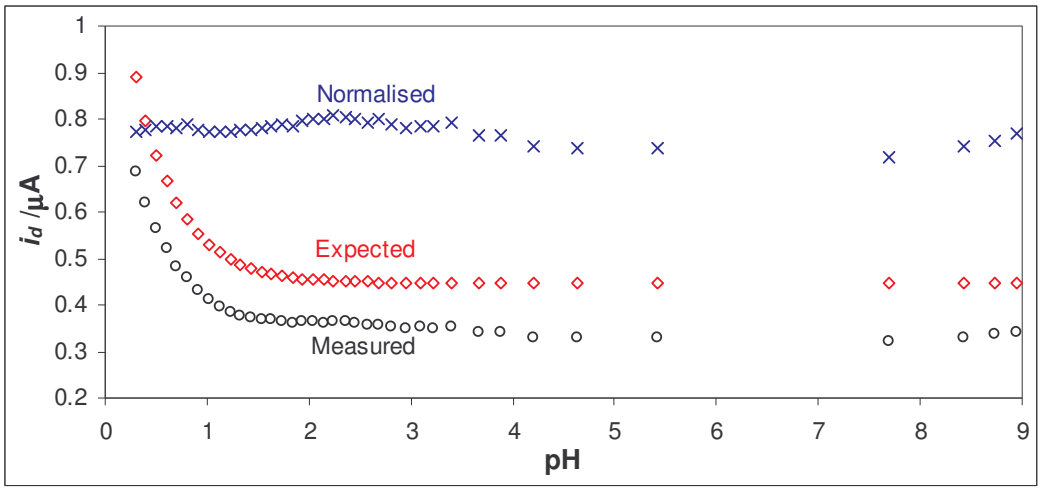

Figure 9.22: The discrepancy between the measured and expected diffusion limited currents for the reduction of Bi(III) in the presence DPA ($[DPA]_T$:$[Bi(III)]_T$ = 53). The normalised currents are also plotted.

associated slope calculated using equation 2.21, the reactions taking place were speculated and are displayed in Table 9.9. In the region below pH 2.05, where H_2L is the dominant form of the ligand, the slopes of 56 and 65 mV/pH were found which would indicate a mixture of BiL^+ and BiL_2^- in solution. In the pH range between 2.05 and 4.51, where HL^- predominates, the slope of 44 mV/pH points to BiL_2^- being prevalent in this region with perhaps some BiL_3^{3-} forming. Above pH 4.51 where L^{2-} is the main form of the ligand, the use of slope analysis is limited as no protons are involved in the reaction. The increase in slope above pH 8 was hypothesised to be due to the formation of hydroxide species.

Table 9.9: Predicted slopes (in mV per pH unit) of potential versus pH data for the corresponding reduction reactions.

Reduction reaction	Predicted slope
$BiL^+ + 3e^- + 2H^+ \rightleftharpoons Bi^o + H_2L$	40
$BiL_2^- + 3e^- + 4H^+ \rightleftharpoons Bi^o + 2H_2L$	80
$BiL_2^- + 3e^- + 2H^+ \rightleftharpoons Bi^o + 2HL^-$	40
$BiL_3^{3-} + 3e^- + 3H^+ \rightleftharpoons Bi^o + 3HL^-$	60
$BiL_3^{3-} + 3e^- \rightleftharpoons Bi^o + 3L^{2-}$	0 (no protons involved)

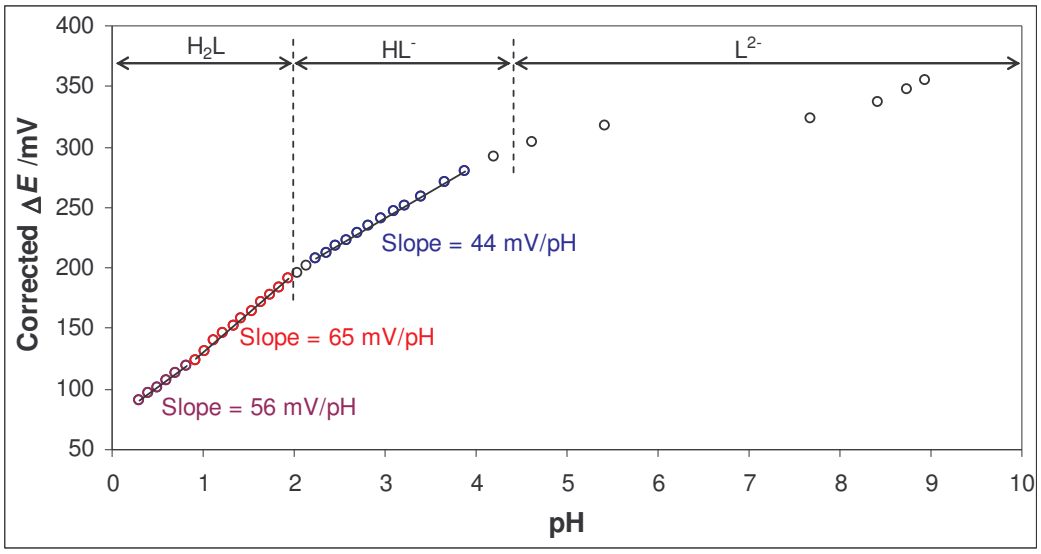

Figure 9.23: Slope analysis of the corrected potential shifts for Bi(III) reduction in the presence DPA ($[DPA]_T$:$[Bi(III)]_T$ = 53). The pH regions for the predominant forms of the ligand are also indicated.

The CCFC calculated using ML, ML_2 and ML_3 species in the model were sufficient to fit the ECFC up to pH of about 5, but data points in the more basic region were not very well predicted as seen in Figure 9.24. Since the CCFC was slightly lower than these data points it was considered that the formation constant for $Bi(OH)_3$ was too low, as could be suggested from Figure 8.16. This value was therefore also refined, but it did not improve the fit. This indicated that there could be some $ML_x(OH)_y$ species in solution. By including $ML_2(OH)$ or $ML_3(OH)$ in the model, the data points in the basic region were better fitted by the CCFC and it was reproducible for the three separate titrations. However, it is impossible say exactly which of the species was actually in solution. Since dipicolinic acid acts as a tridentate ligand and is a rigid, planar structure, the $ML_3(OH)$ species would be stericly hindered but Bi(III) has been known to have coordination numbers up to 10.[20,21] Irrespective of the $ML_x(OH)$ species included (where x = 2 or 3), the log β values for ML, ML_2 and ML_3 were unchanged.

Table 9.10 shows the log β values calculated for the suggested species for each ligand-to-metal concentration ratio as well as the average values for these. The ECFCs and CCFCs plotted for each of the concentration ratios is

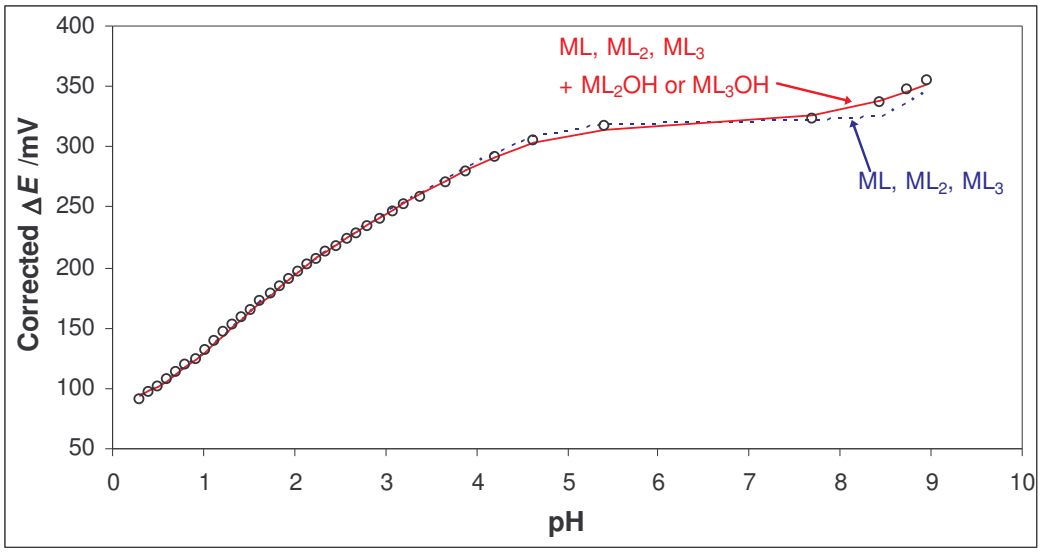

Figure 9.24: The ECFC and two different CCFCs calculated using the species indicated ($[DPA]_T$:$[Bi(III)]_T$ = 53).

given in Figure A7.6, Appendix 7. A comparatively large variation in log β values occurred for the ML species. This could be expected as ML is formed in the pH region where the largest junction potential corrections had to be made. To obtain log β(ML) = 14.06 for the $[DPA]_T$:$[Bi(III)]_T$ = 53 data set, only the first three data points would have to be increased by 2 mV. The standard deviations the log β values of the $ML_x(OH)$ species for the $[DPA]_T$:$[Bi(III)]_T$ = 109 experiment were large due to these values being determined by essentially fitting two data points.

Table 9.10: Log β values for the given equilibria, where L = DPA, at 25 °C and ionic strength between 0.25 and 0.5 M. Only one of the $BiL_x(OH)$ species are present, but it is unclear which one.

$[L]_T$:$[Bi^{3+}]_T$ =	53 [a]	80 [a]	109 [a]	Average [b]
Equilibrium		**Log β**		
$Bi^{3+} + L^{2-} \rightleftharpoons BiL^{+}$	13.88 ± 0.04	14.06 ± 0.04	14.10 ± 0.04	14.0 ± 0.1
$Bi^{3+} + 2L^{2-} \rightleftharpoons BiL_2^{-}$	22.66 ± 0.01	22.65 ± 0.01	22.53 ± 0.01	22.61 ± 0.07
$Bi^{3+} + 3L^{2-} \rightleftharpoons BiL_3^{3-}$	26.73 ± 0.05	26.78 ± 0.03	26.63 ± 0.03	26.71 ± 0.08
$Bi^{3+} + 2L^{2-} + OH^{-} \rightleftharpoons BiL_2(OH)^{2-}$	29.58 ± 0.04	29.47 ± 0.03	29.1 ± 0.1	29.4 ± 0.2
$Bi^{3+} + 3L^{2-} + OH^{-} \rightleftharpoons BiL_3(OH)^{4-}$	33.19 ± 0.04	32.89 ± 0.03	32.4 ± 0.1	32.8 ± 0.4

[a] Standard deviations of log β values obtained from fitting.
[b] Standard deviations of log β values obtained from averaging.

The species distribution diagrams plotted in Figure 9.25 include both of the possible $BiL_x(OH)$ species. The ML species was fully formed before pH 0 and ML_2 was fully formed at pH 2 already. Including the Bi(III) nitrate species in the model did not change the species distribution diagram at all, showing that these species are not present even at the lowest pH after DPA is added. Studying complex formation of other metal ions with dipicolinic acid would thus most likely have to be performed under very acidic conditions and protocols developed in this work could be applied.

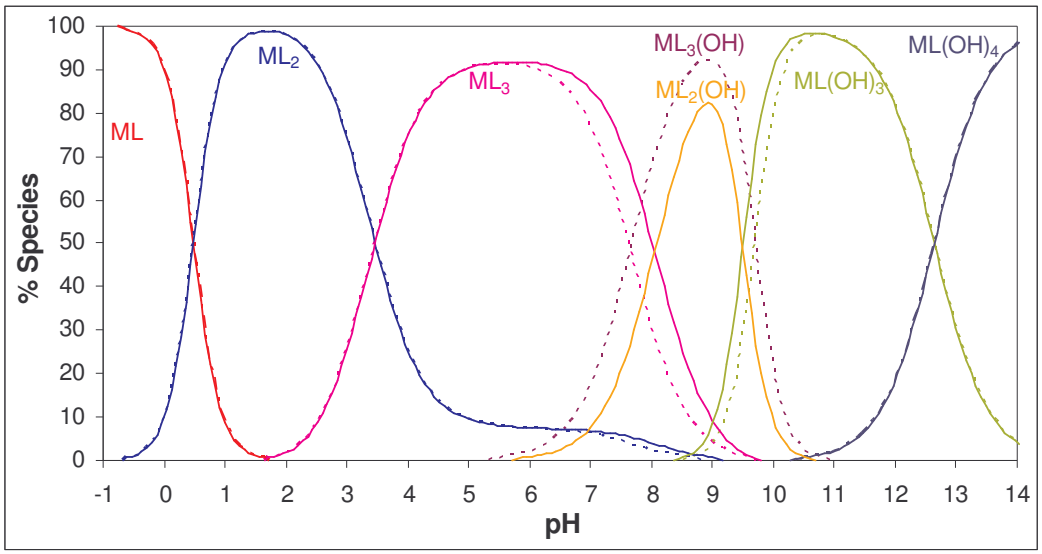

Figure 9.25: Species distribution diagrams for aqueous solutions of Bi(III)-DPA using average log β values in Table 9.10 and [Bi(III)] = 1×10^{-5} M and [DPA] = 1×10^{-3} M. The two possible models are illustrated: including ML_3OH (dotted lines) or ML_2OH (solid lines).

The CSD[14] was again searched for confirmation of the existence of the proposed species in solution. Figure 9.26 gives two examples of a ML_2 arrangement for Bi(III) and DPA (Reference codes: (a) ETAQUL and (b) LAYLUT). The interactions that form a dimeric unit are different in the two examples and are dependent on the liquor from which these crystals were grown. This merely serves to show the possible bonding arrangement on the ML_2 species here. No ML_3 arrangement for Bi(III) and DPA was found in the database, but an example of Cd(II) with DPA is shown in Figure 9.27 (Reference codes: OBUZOB or CEBPEF). The ML_3 arrangement has also been shown for Ce(IV) with DPA,[22] among others. Bi(III) would be nine-

coordinate in the ML_3 complex, within the range that has been observed for Bi(III).[20,21] An example of a Bi(III) structure with an ML arrangement was also found (Reference code: MIPLUS) but it is not shown here. The existence of the particular arrangement around the metal ion centre being present in the crystal structure gives confidence that the species is probably also present in solution.

In Chapter 5 the value of the third protonation constant for DPA was discussed and although the validity of these values was questioned, they were considered here to determine the effect on the formation constants. The log K_3 values tested were 0.49[23] and 1.36,[24] which would affect the calculations for data in the lower pH region. Considering that the dominant form of the ligand

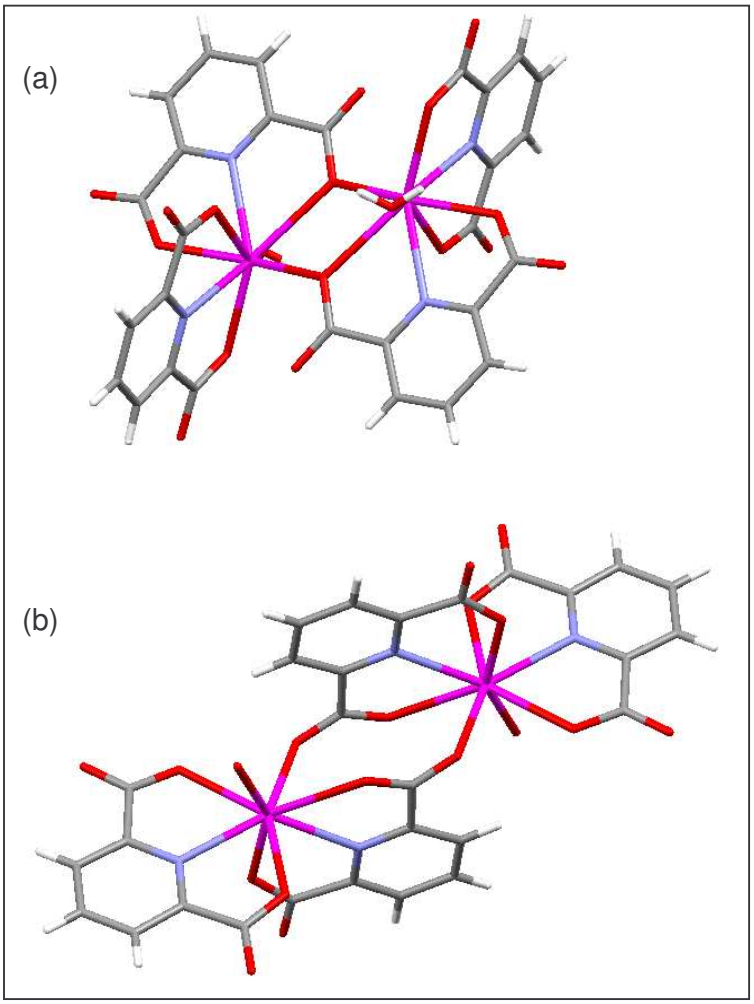

Figure 9.26: Two structures showing the ML_2 arrangement for Bi(III)-DPA.

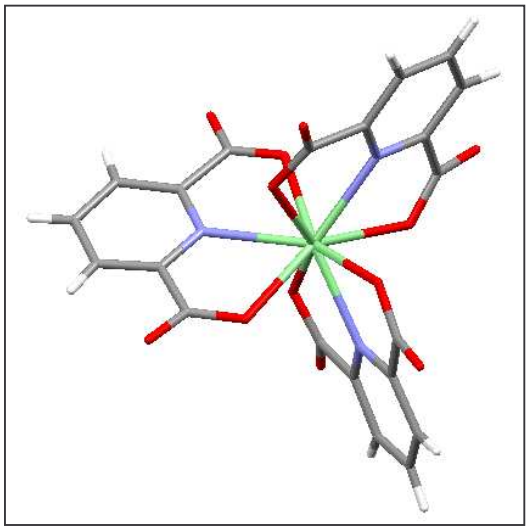

Figure 9.27: Structure showing the ML_3 arrangement for Cd(II) with DPA.

would be H_3L^+ below pH 0.49 or 1.36 respectively, the slope analysis in these pH ranges could be reassessed. Where H_3L^+ is in solution, possible reduction reactions are:

$$BiL^+ + 3e^- + 3H^+ \rightleftharpoons Bi^o + H_3L^+ \qquad \text{slope} \approx 60$$

$$BiHL^{2+} + 3e^- + 2H^+ \rightleftharpoons Bi^o + H_3L^+ \qquad \text{slope} \approx 40$$

From the slope of 56 mV/pH in Figure 9.23, it was deduced that BiL^+ and possibly some $BiHL^{2+}$ would be in solution. When the data was analysed including the log K_3 values, it was impossible to refine a log β value for MHL and only the log β value for ML was affected (that for ML_2 and ML_3 remained essentially the same). Results for the one dataset are present in Table 9.11 and these reflect the trends for the other concentration ratios. As the value of log K_3 increased, so the log β value for ML also increased. Of particular interest was the increase in the overall fit of the CCFC to the ECFC. For a low standard deviation of the overall fit, the model used to calculate the curve must approach the experimental data more closely. This again indicated the dubious quality of the log K_3 values. It is suspected that H_3L^+ is not present in significant concentrations in the pH range studied.

Table 9.11: Variation in the log β value for ML and the overall fit of the CCFC as the value of log K_3 was changed using data where $[DPA]_T:[Bi(III)]_T = 80$.

log K_3	log β(ML)	Overall fit
none	14.06 ± 0.04	2.41
0.49	14.56 ± 0.02	2.90
1.36	15.30 ± 0.02	5.10

9.3.3) *Tl(I)-dipicolinic acid complexes*

As a brief aside, the Tl(I) data collected in the analysis of the Bi(III)-DPA system was further analysed to determine which complex/es are being formed between Tl(I) and DPA. This is certainly not ideal data and should rather be collected from about pH 2. Higher concentrations of DPA could then also be used as the DPA reduction wave is shifted more negative with increasing pH. The only hydrolysis product formed with Tl(I) is Tl(OH), with log β = 0.30 at 25 °C and 0.5 M ionic strength.[2]

Slope analysis was done using the ECFC and an example is given in Figure 9.28 for the DPA-to-Tl(I) concentration ratio of 40. Only one significant slope of 11 mV/pH occurred in the region where HL^- is predominant. Possible reduction reactions are:

$$TlL^- + e^- + H^+ \rightleftharpoons Tl^o + HL^- \qquad \text{slope} \approx 60$$

$$TlLH + e^- \rightleftharpoons Tl^o + 2HL^- \qquad \text{slope} \approx 0$$

A mixture of these two species could therefore form in solution. The CCFC (red line) also plotted in Figure 9.28, was obtained by only including the ML species in the model. Log β values for MLH could only be refined for two of the datasets, but using data that was very noisy. Including MHL in the model did not affect the value of log β for ML. The stability constants obtained are presented in Table 9.12. A comparison of the ECFC and CCFC plots for the three experiments are presented in Figure A7.7, Appendix 7. The log β values for ML were surprisingly reproducible for the three datasets, especially considering the non-ideal analysis conditions for this system.

A structure for TlLH was found in the CSD[14] (Reference codes: DEBVOW or GIZKEG) and is shown in Figure 9.29. The one carboxylic acid moiety is

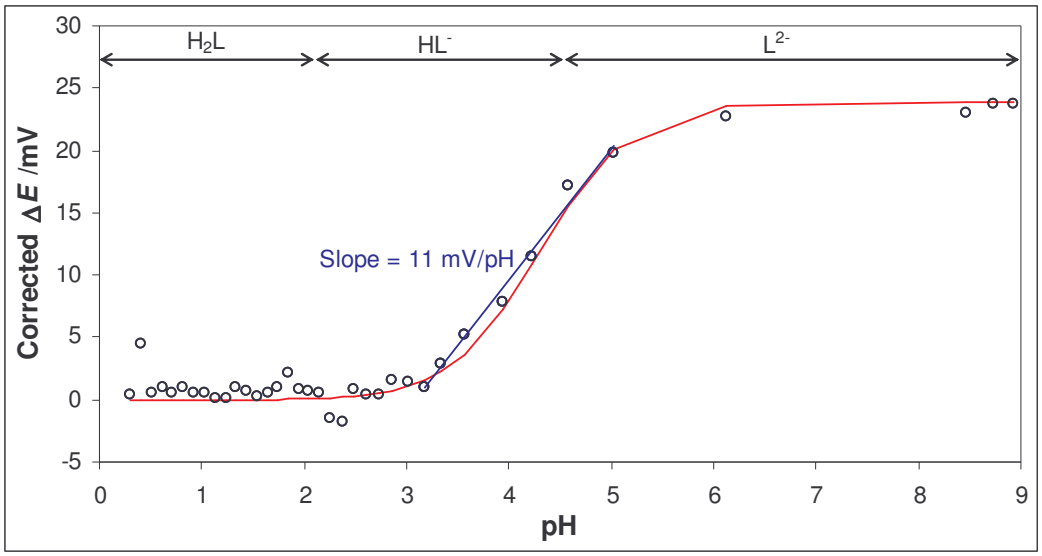

Figure 9.28: Slope analysis of the corrected potential shifts for Tl(I) reduction in the presence DPA ($[DPA]_T$:$[Tl(I)]_T$ = 40). The CCFC (—) is also shown.

Table 9.12: Log β values for the given equilibria with Tl(I), where L = DPA, at 25 °C and ionic strength between 0.25 and 0.5 M.

$[L]_T$:$[Tl^+]_T$ =	27 [a]	40 [a]	55 [a]	Average [b]
Equilibrium		**Log β**		
$Tl^+ + L^{2-} \rightleftharpoons TlL^-$	3.53 ± 0.02	3.59 ± 0.01	3.56 ± 0.01	3.56 ± 0.03
$Tl^+ + HL^- \rightleftharpoons TlLH$		6.2 ± 0.3	6.5 ± 0.1	6.4 ± 0.2

[a] Standard deviations of log β values obtained from fitting.
[b] Standard deviations of log β values obtained from averaging.

protonated and interestingly, the Tl(I) ion is only coordinated through one oxygen atom of the other carboxylate moiety. This again points to the probability of MLH existing in solution. From the species distribution diagram (see Figure 9.30), under conditions similar to those used here, MLH is only a minor species (if the log β value is approximately correct) and it is thus not surprising that it was difficult to determine the value accurately. If the concentrations of both DPA and Tl(I) are increased (even if the ratio remains the same), the percentage of MLH will increase in solution and the log β value could be more accurately determined (see Figure A7.8, Appendix 7). The percentage ML in solution also increased (due to a decreasing free metal ion concentration) which would make these stability constants easier to determine.

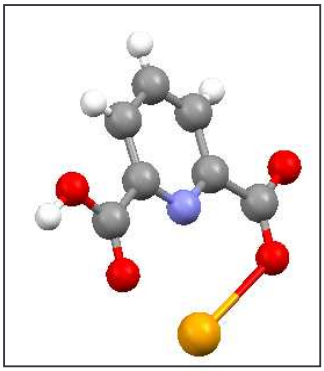

Figure 9.29: Structure showing the MLH arrangement for Tl(I) with DPA.

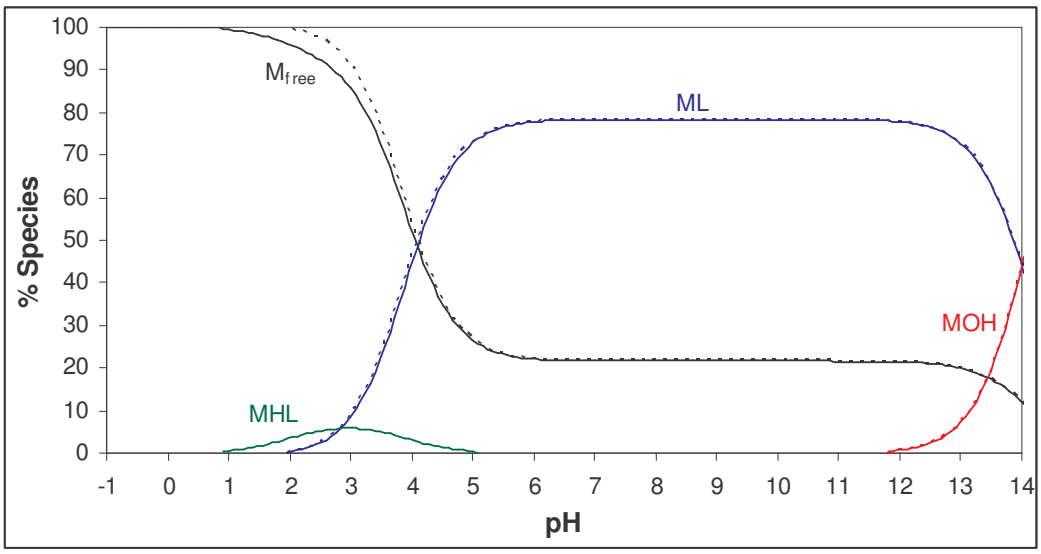

Figure 9.30: Species distribution diagrams for aqueous solutions of Tl(I)-DPA using average log β values in Table 9.12 and [Tl(III)] = 2×10^{-5} M and [DPA] = 1×10^{-3} M, where MHL was included (solid lines) or excluded (dotted lines).

9.3.4) *Bi(III)-quinolinic acid complexes*

Once again three pH titrations were performed with total QA-to-Bi(III) concentration ratios of 47, 75 and 102 with each titration starting at pH 0.3. Larger ratios were not used due to the reduction wave of quinolinic acid lying close to that for Tl(I) in the highly acidic solutions and increasing the ligand concentration could lead to insufficient resolution of the waves. Data could only be collected to pH ~5 before the Bi(III) reduction peak disappeared, most probably due to precipitation.

As with PA, very small shifts were observed when QA was added to the Bi(III) solution at pH 0.3 (see Figure 9.31), thus the Bi(III) nitrate species would still be significant at low pH and need to be considered. Data were therefore analysed using both $E(Bi_{free})$ and $E(Bi_{free})_{OH}$, as well as applying virtual potentiometry where the nitrate species could be included in the model.

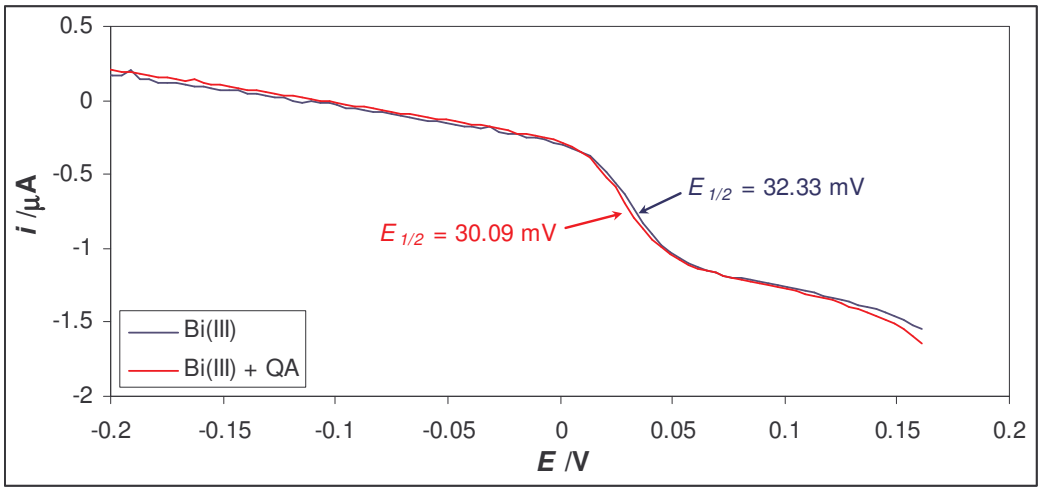

Figure 9.31: Polarograms at pH 0.30 (where [Bi(III)] = 1×10^{-5} M) before and after the addition of QA, where $[QA]_T:[Bi(III)]_T = 75$. The $E_{1/2}$ values indicate a shift of 2.24 mV.

Slope analysis was done using the plot of the corrected potential shift versus pH and the possible reactions that could occur are displayed in Table 9.13. In Figure 9.32, the slope in the pH range where HL^- is predominant clearly indicated the formation of BiL_2^-. From the slope analysis there is no indication of the formation of BiL_3^{3-}. The pH region where the slope is 30 mV/pH suggests the formation of BiL^+ where both HL^- and H_2L are present in significant concentrations and the slope is therefore an average value. The slope of 20 mV/pH could indicate the formation of $BiLH^{2+}$ in the region where H_2L is dominant.

Using information from the slope analysis, the complex formation curves were plotted. From Figure 9.33 it was clear that the ML and ML_2 species were not sufficient to describe the entire ECFC. Excluding MLH from the model resulted in the CCFC being too low all the way up to pH 2. This is far more pronounced

Table 9.13: Predicted slopes (in mV per pH unit) of potential versus pH data for the corresponding reduction reactions.

Reduction reaction	Predicted slope
$BiLH^{2+} + 3e^- + H^+ \rightleftharpoons Bi^o + H_2L^+$	20
$BiL^+ + 3e^- + 2H^+ \rightleftharpoons Bi^o + H_2L^+$	40
$BiL^+ + 3e^- + H^+ \rightleftharpoons Bi^o + HL^-$	20
$BiL_2^- + 3e^- + 2H^+ \rightleftharpoons Bi^o + 2HL^-$	40
$BiL_3^{3-} + 3e^- + 3H^+ \rightleftharpoons Bi^o + 3HL^-$	60

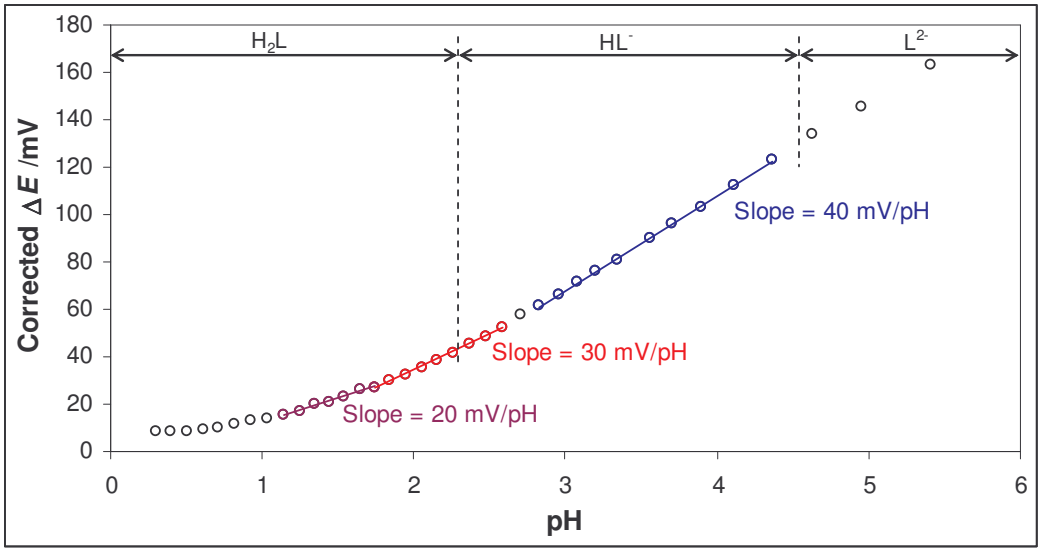

Figure 9.32: Slope analysis for the reduction of Bi(III) in the presence QA ($[QA]_T$:$[Bi(III)]_T$ = 102). The pH regions for the predominant forms of the ligand are indicated.

than in the case of PA, indicating that the MLH species does not merely compensate for shifts due to the formation of Bi(III) nitrate species in solution (as was speculated for PA), but is actually present. Above pH ~4, data could be fitted by including $ML_2(OH)$. Alternatively, ML_3 and ML_3OH would also fit the data, but the values could not be refined simultaneously (one value was fixed while the other refined). ML_3 would be a minor species in the latter case as the standard deviations of these log β values were high and is shown in the species distribution diagram (see Figure 9.35). If ML_4 was included in the model, the value for ML_3 was not refined and hence it was not considered. The most likely species model would be MLH, ML, ML_2 and $ML_2(OH)$. Figure 9.34 shows ECFCs and CCFCs for experiments at each ligand-to-metal concentration ratio fitted using this model.

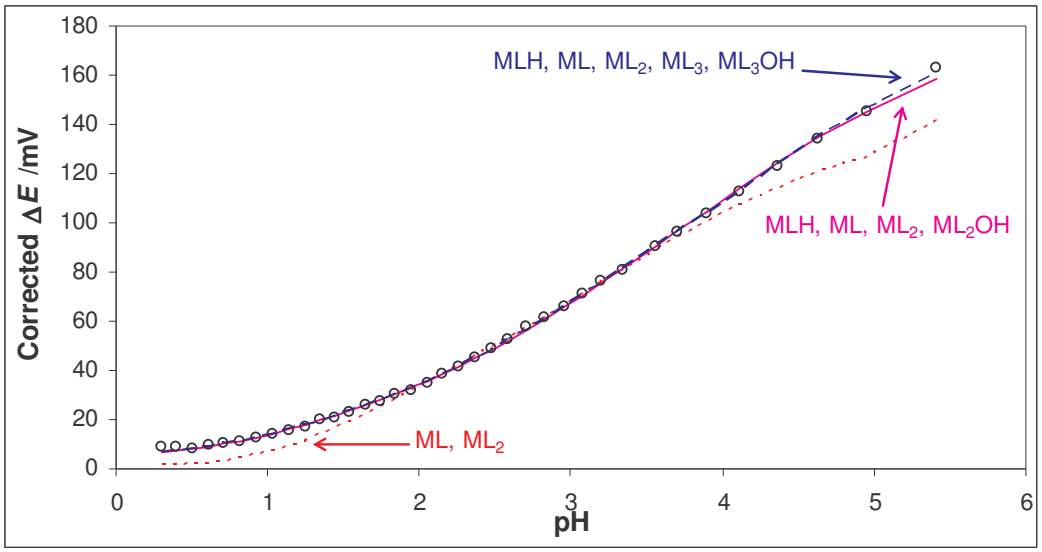

Figure 9.33: The ECFC (calculated using $E(Bi_{free})$) and three different CCFCs calculated using the species indicated ($[QA]_T$:$[Bi(III)]_T$ = 102).

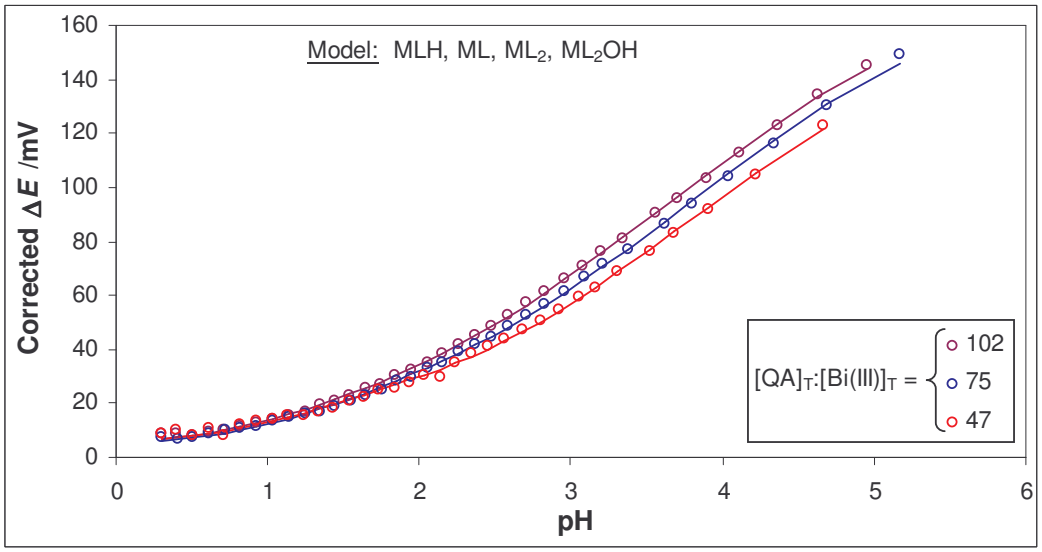

Figure 9.34: The ECFCs (calculated using $E(Bi_{free})$) and CCFCs for the three QA-to-Bi(III) concentration ratio experiments using the species model indicated.

The log β values determined at each ligand-to-metal concentration ratio when using $E(Bi_{free})$ to calculate the ECFC, are given in Table 9.14(a) together with the average values. The large average standard deviations for ML and ML_2 are due to the log β value for $[QA]_T$:$[Bi(III)]_T$ = 47 being too high for the MLH species and thus leading to a lower value for ML. For interest, the average log β values obtained for the model containing ML_3 and $ML_3(OH)$ were 16.8 ± 0.4

and 26.6 ± 0.1, respectively, and the species distribution diagrams for both species models are compared in Figure 9.35.

Table 9.14: Table of log β values determined using $E(Bi_{free})$ and $E(Bi_{free})_{OH}$ for the given equilibria, where L = QA, at 25 °C and ionic strength between 0.25 and 0.5 M.

$[L]_T:[Bi^{3+}]_T$ =	47 [a]	75 [a]	102 [a]	Average [b]
Equilibrium		**Log β**		
(a) Using $E(Bi_{free})$				
$Bi^{3+} + HL^{2-} \rightleftharpoons BiLH^{+}$	9.94 ± 0.02	9.63 ± 0.04	9.61 ± 0.03	9.7 ± 0.2
$Bi^{3+} + L^{2-} \rightleftharpoons BiL^{+}$	7.58 ± 0.07	7.74 ± 0.05	7.78 ± 0.04	7.7 ± 0.1
$Bi^{3+} + 2L^{2-} \rightleftharpoons BiL_2^{-}$	13.25 ± 0.05	13.13 ± 0.05	13.19 ± 0.04	13.19 ± 0.06
$Bi^{3+} + 2L^{2-} + OH^{-} \rightleftharpoons BiL_2(OH)^{2-}$	22.90 ± 0.06	22.91 ± 0.05	22.88 ± 0.05	22.90 ± 0.02
Overall fit	1.44	0.39	0.43	
(b) Using $E(Bi_{free})_{OH}$				
$Bi^{3+} + L^{2-} \rightleftharpoons BiL^{+}$	7.11 ± 0.05	7.19 ± 0.04	7.32 ± 0.03	7.2 ± 0.1
$Bi^{3+} + 2L^{2-} \rightleftharpoons BiL_2^{-}$	12.49 ± 0.08	12.53 ± 0.05	12.60 ± 0.04	12.54 ± 0.06

[a] Standard deviations of log β values obtained from fitting.
[b] Standard deviations of log β values obtained from averaging.

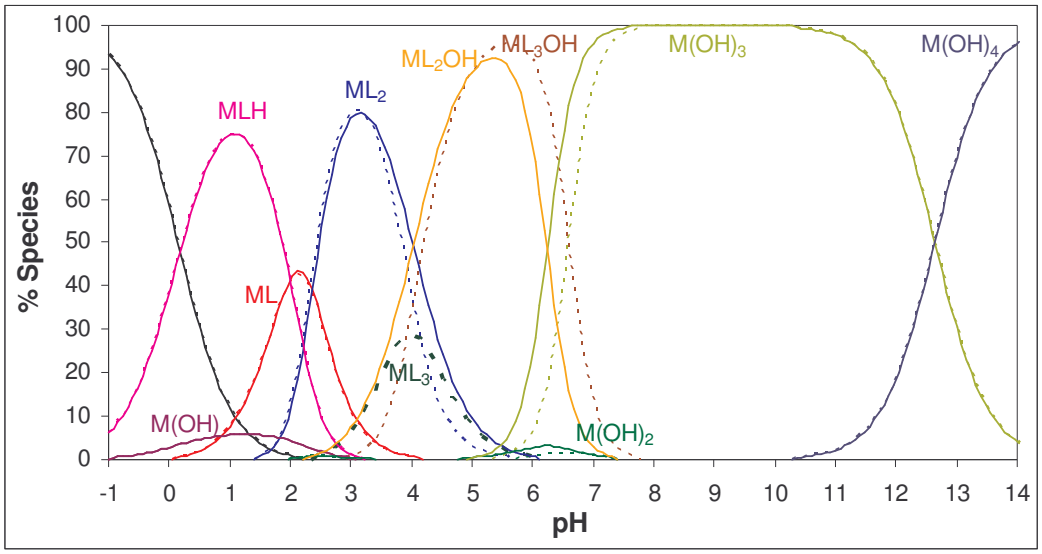

Figure 9.35: Species distribution diagrams for $[QA]_T:[Bi(III)]$ = 100 and [Bi(III)] = 1×10^{-5} M using average log β values in Table 9.14(a). The models including $ML_2(OH)$ (solid lines) or ML_3 and $ML_3(OH)$ (dotted lines) are compared.

When using $E(Bi_{free})_{OH}$ to calculate the ECFC, there was no needed to include MLH to fit data in the low pH region. The log β values only for ML and ML_2 are

shown in this case (Table 9.14(b)) as these would be the only species possibly affected by the Bi(III) nitrate species, although this would be unlikely for ML_2. It was noted that for each ECFC calculated using $E(Bi_{free})_{OH}$, three to four points at the lowest pHs were small negative values, with –3 mV being the largest. The cause of these negative potential shifts could be that the predicted value of $E(Bi_{free})_{OH}$ was too low, or that the diffusion junction potentials were overcompensated. This problem was not encountered when using the same method for determining the $E(Bi_{free})_{OH}$ for the PA studies. Additionally, two of the pH titration experiments without ligand present were performed directly before these experiments with QA and the data was included in the calculation of $\Delta E(M_{free})_{OH}$ in Table 8.10. The standard deviation of $\Delta E(M_{free})_{OH}$ was 2 mV, so the negative potential data points in the ECFC were ignored and the data fitted as presented.

The plot of i_d versus pH for the measured, expected and normalised currents is given in Figure 9.36. The pH at which a significant deviation from unity for the normalised current occurs, is similar to that for the PA system and corresponds to the formation of the ML_2OH species, again indicating that this hydroxide species may be non-labile or else slow precipitation is occurring.

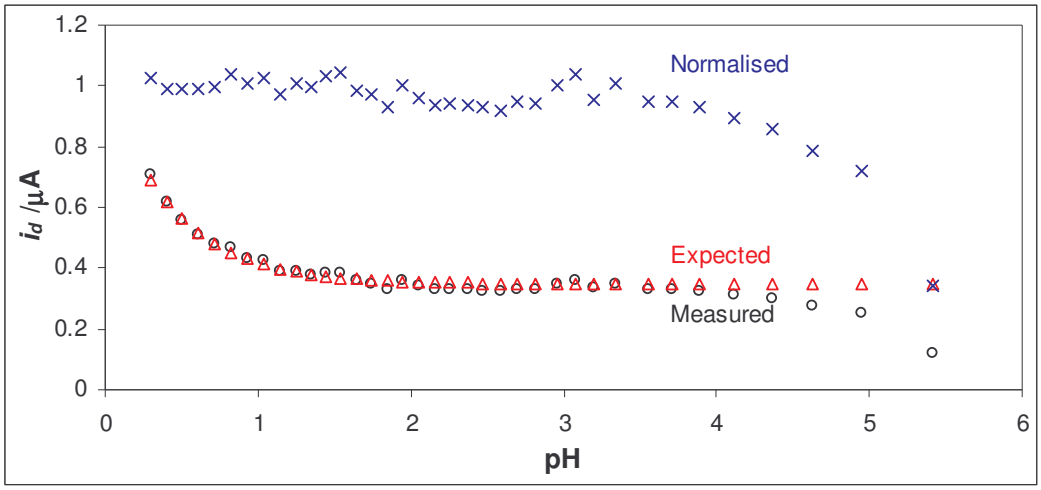

Figure 9.36: The normalised currents, as calculated from the measured and expected i_d values, for the reduction of Bi(III) in the presence QA ($[QA]_T$:$[Bi(III)]_T$ = 102) showing deviations from unity above pH 4.

No structures were found with Bi(III) and QA in the CSD.[14] A search was done for QA bound to any metal ion and a range of structures were found. Examples showing M_2L, $M(HL)_2$ and $M(HL)_3$ arrangements (Ref Codes: VEKVIR01, YIDSEK and HASZIK, respectively) are shown in Figure 9.37. QA shows a range of bonding modes especially since the metal ion can be coordinated through the pyridine nitrogen and oxygen of the adjacent carboxylate group, or through the oxygen atoms of the carboxylate group in position 3 on the ring (as shown in Figure 9.37(a)). With the high ligand-to-metal ratios used in these solution studies, the formation of polynuclear species would be highly unlikely. Figures 9.37 (b) and (c) show the coordinated ligand in the HL^- form. If $M(HL)_2$ and $M(HL)_3$ occur in the pH region where HL^- is the dominant form of the ligand, no protons are involved in the reaction. If H_2L predominates, the predicted slopes would be 40 and 60 mV/pH, respectively, which was not observed in Figure 9.32. A model including $Bi(HL)_2^+$, $Bi(HL)_3$ and even $Bi(HL)_4^-$ was still considered. Incorporating all these species only shifted the CCFC sufficiently to overlap the ECFC up until pH 2.5 (where H_2L is the dominant form of the ligand). If another species was added to the model to fit the ECFC above pH 2.5, the log β values could not be refined. If these species are present, they are minor species under the conditions used here. The presence of $Bi(HL)^{2+}$ is speculated, however.

Virtual potentiometry was applied so that the Bi(III) nitrates formed at low pH could be accommodated in the model, thus determining more accurate stability constants for the Bi(III) QA species at the low pH range. Plots of *E(virt)* against log [M_{free}] used to estimate E^o values are given in Figure 9.38 and again show non-linearity below pH ~1.8. Data only up to pH ~2.4 could be fitted using ESTA and the results are shown in Table 9.15 where two species models were fitted (a) ML only and (b) ML and MLH together. A concentration of 0.3 M nitrate was assumed as before. Log β values for ML_2 or any other species could not be refined. As expected, the log β value determined for ML by virtual potentiometry lies between the values determined directly from the polarographic data when using $E(Bi_{free})$ and $E(Bi_{free})_{OH}$ to calculate the

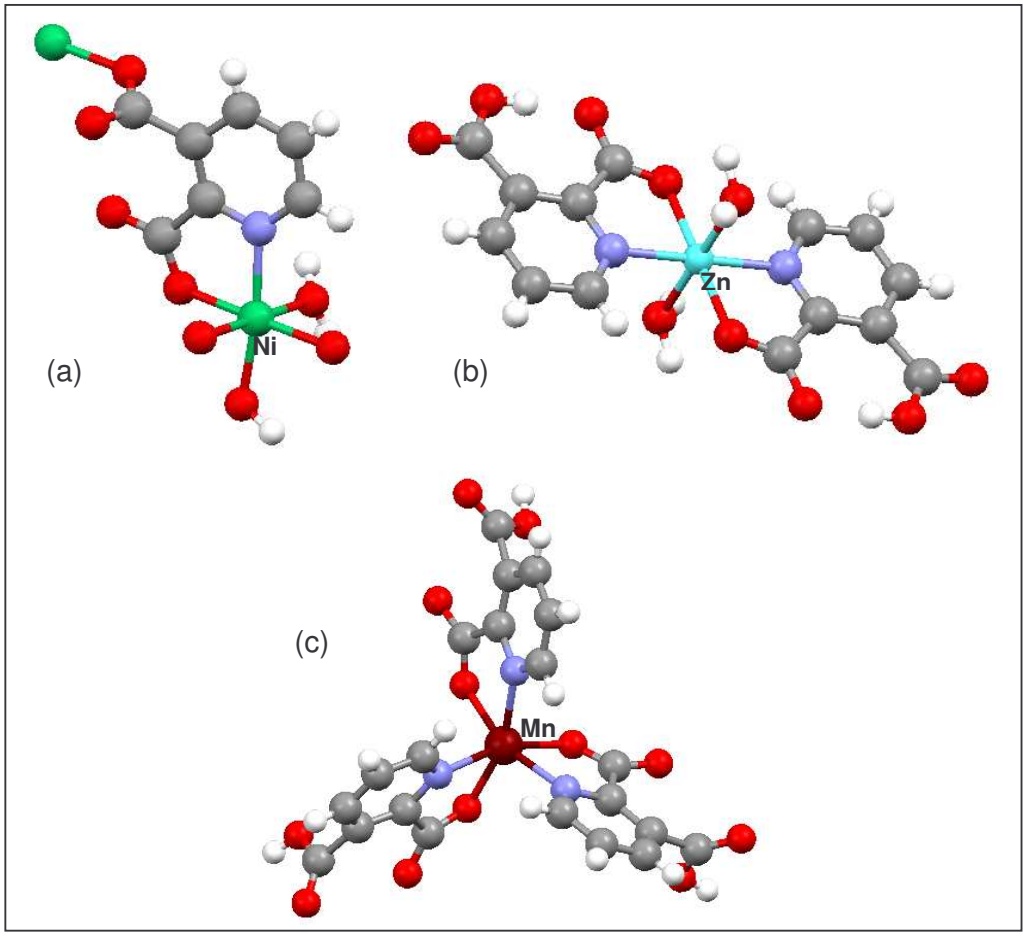

Figure 9.37: Structures showing coordination of QA with (a) nickel in a M_2L arrangement, (b) zinc in a $M(HL)_2$ arrangement and (c) manganese showing the $M(HL)_3$ arrangement.

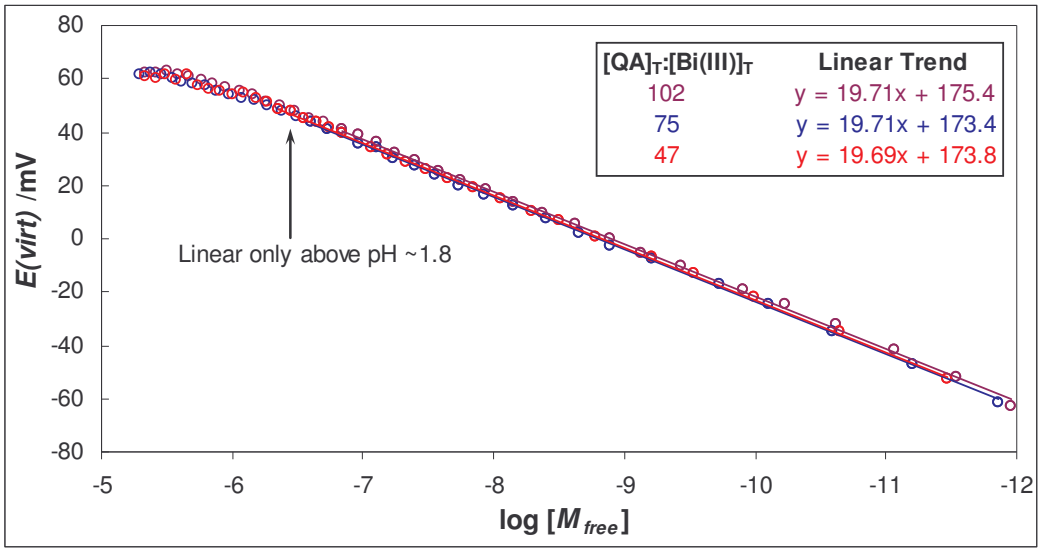

Figure 9.38: The virtual potential plotted against log [M_{free}] showing the trend lines fitted only through the linear data points (for data calculated using $E(Bi_{free})$).

potential shifts. Due to the Bi(III) nitrate species being incorporated in the virtual potentiometry calculations, the log β value refined for MLH is lower than given in Table 9.14. If a concentration of 0.4 M nitrate is used, log β values for ML and MLH were 7.61 ± 0.07 and 9.3 ± 0.1, respectively.

Table 9.15: Log β values for the given equilibria obtained from virtual potentiometry, where L = QA, at 25 °C and ionic strength between 0.25 and 0.5 M.

$[L]_T:[Bi^{3+}]_T$ =	47 [a]	75 [a]	102 [a]	Average [b]
Equilibrium		**Log β**		
(a) Species Model 1				
$Bi^{3+} + L^{2-} \rightleftharpoons BiL^{+}$	7.35 ± 0.05	7.42 ± 0.03	7.45 ±0.02	7.41 ± 0.05
R-factor	0.026	0.024	0.026	
(b) Species Model 2				
$Bi^{3+} + HL^{-} \rightleftharpoons BiLH^{2+}$	9.53 ± 0.03	9.24 ± 0.02	9.08 ± 0.02	9.3 ± 0.2
$Bi^{3+} + L^{-} \rightleftharpoons BiL^{2+}$	7.43 ± 0.04	7.51 ± 0.01	7.57 ± 0.01	7.50 ± 0.07
Hamiltonian R-factor	0.019	0.010	0.011	

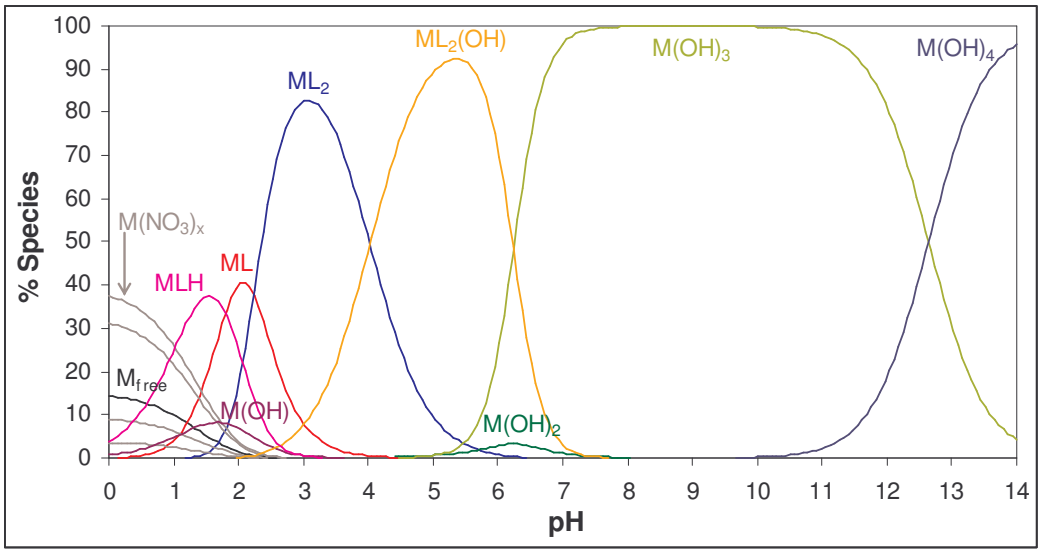

Figure 9.39: Species distribution diagram for $[QA]_T:[Bi(III)] = 100$, $[Bi(III)] = 1 \times 10^{-5}$ M and $[NO_3^-] = 0.5$. Average log β values ML_2 and $ML_2(OH)$ are from Table 9.14(a) and that for ML and MLH are from Table 9.15(b).

The species distribution diagram is given in Figure 9.39, where values for ML and MLH are from Table 9.15(b). This clearly shows the Bi(III) nitrate species in solution at low pH, as suggested by the observed potential shifts. If MLH is excluded from the species model, the nitrate species and ML are affected to

some extent (see Figure A7.9, Appendix 7). This makes it extremely difficult to conclude that MLH is a species in solution under these conditions, but it is more likely to be present in the case of QA than for PA.

9.3.5) *Comparison of Bi(III) pyridinecarboxylic acid systems*

A comparison of the log β values for the complexation of Bi(III) by the three ligands studies here is given in Table 9.16. In each case the two alternative species models are presented ((a) and (b)), as confirmation of the one or other is extremely difficult. Complexes formed with DPA are far more stable than those with PA and QA due to DPA acting as a tridentate ligand, where bonding occurs through an oxygen from both carboxylate groups and through the pyridine nitrogen. PA is generally a bidentate ligand which bonds through the carboxylate oxygen and the pyridine nitrogen. In the case of quinolinic acid, Bi(III) can either bond to the ligand in the same way as PA, forming a 5-member ring, or it can bond through an oxygen atom from each of the adjacent carboxylate groups, forming a 7-membered ring. The log β values for PA and QA are comparable, indicating that complexation most likely involves the pyridine nitrogen for QA. This was substantiated by the crystal structures found.[14] The smaller ring size is also preferred. For the MLH species involving QA, the carboxylate group not bonded to Bi(III) would be protonated.

The $Bi(PA)_4^-$ species may not be a major species under the solution conditions used in these polarographic experiments, but there is strong evidence to support its existence. It was interesting to note that no stability constants have been reported in the NIST database[25] for $M(PA)_4$ other than for all the lanthanides. A similar phenomenon was noticed where the only formation constants for $M(DPA)_3$ species were reported for the lanthanide metal ions. Unfortunately very little work has been done using QA and only stability constants for the M(QA) species were reported for the lanthanides. Since the interaction of PA and QA with Bi(III) were similar, it was surprising that the species models predicted were slightly different, although precipitation did occur at lower pHs for the QA species. The fact that the carboxylate group in position 3, which in not involved in complexation, contributes to more

complicated chemistry may be the reason for this. This moiety's role can be seen by the use of QA in assembling metal-organic frameworks.

Table 9.16: Comparison of log β values for complexation of Bi(III) by the three ligands, PA, QA and DPA at 25 °C and ionic strength between 0.25 and 0.5 M. Charges in equilibria are omitted as they vary depending on L.

L =	**PA** 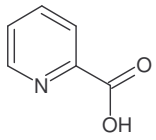	**QA** 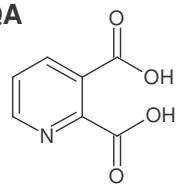	**DPA** 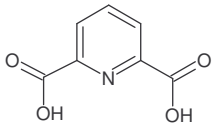
Equilibrium		**Log K**	
$L + H^+ \rightleftharpoons HL$	5.18	4.58	4.51
$HL + H^+ \rightleftharpoons H_2L$	0.86	2.30	2.05
Equilibrium		**Log β**	
(a) Species Model 1			
$Bi + HL \rightleftharpoons BiLH$		9.3 ± 0.2	
$Bi + L \rightleftharpoons BiL$	7.3 ± 0.2	7.50 ± 0.07	14.0 ± 0.1
$Bi + 2L \rightleftharpoons BiL_2$	13.92 ± 0.06	13.19 ± 0.06	22.61 ± 0.07
$Bi + 3L \rightleftharpoons BiL_3$	18.46 ± 0.06		26.71 ± 0.08
$Bi + 2L + OH \rightleftharpoons BiL_2(OH)$		22.90 ± 0.02	29.4 ± 0.2
$Bi + 3L + OH \rightleftharpoons BiL_3(OH)$	28.19 ± 0.08		
(b) Species Model 2			
$Bi + L \rightleftharpoons BiL$	7.3 ± 0.2	7.41 ± 0.05	14.0 ± 0.1
$Bi + 2L \rightleftharpoons BiL_2$	13.91 ± 0.08	13.23 ± 0.04	22.61 ± 0.07
$Bi + 3L \rightleftharpoons BiL_3$	18.5 ± 0.1	16.8 ± 0.4	26.71 ± 0.08
$Bi + 4L \rightleftharpoons BiL_4$	22.7 ± 0.2		
$Bi + 3L + OH \rightleftharpoons BiL_3(OH)$		26.6 ± 0.1	32.8 ± 0.4
$Bi + 4L + OH \rightleftharpoons BiL_4(OH)$	31.4 ± 0.2		

Since Pb(II) and Bi(III) are isoelectronic, it was investigated whether there was a linear free energy relationship (LFER) between the log β values for the ML species (called log β_1) for the ligands studied here. LFERs cannot be derived directly from thermodynamic processes and are thus called "extra-thermodynamic relationships".[26] The log β_1 values for Pb(II) with PA, DPA and QA are 4.49,[25] 8.66[25] and 4.7,[27] respectively, at 25° C and 0.5 M ionic strength. From Figure 9.40 it can be seen that the relationship log β_1(Bi(III)) = 1.61 log β_1(Pb(II)) exists for pyridinecarboxylic acid ligands, but whether it can

be extrapolated to ligands with other donor atoms will have to be tested. Pb(II) and Bi(III) are both classified as borderline according to Pearson's Hard and Soft Acid and Base theory,[26] with Bi(III) probably being harder than Pb(II), thus they should have an affinity for similar ligands. The linear relationship also gave confidence to the actual log β_1 values determined in this work.

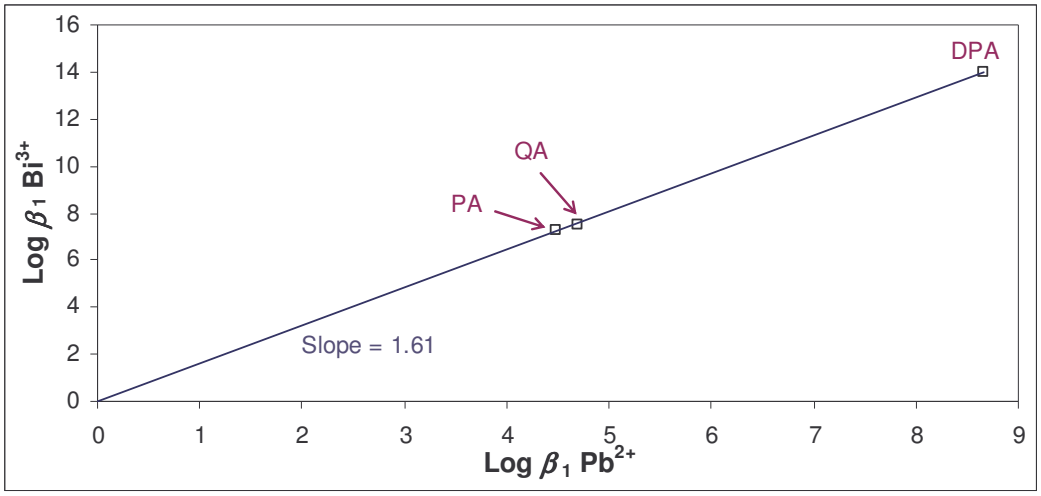

Figure 9.40: LFER for log β_1(Bi(III)) versus log β_1(Pb(II)) for the three pyridine-carboxylic acid ligands.

9.4) Conclusions

It was established that Bi(III) complex formation can be studied by polarography when applying the procedures developed in the previous chapters. This included the GE calibration, the correction for the diffusion junction potential using information from the Tl(I) witness ion and the determination of $E(Bi_{free})$. It was demonstrated that not only do the Bi(III) nitrate species need to be considered when calculating the value of $E(Bi_{free})$, but also where complexation by the ligand of interest does not occur significantly in the lowest pH range.

Unfortunately, limitations in the 3D-CFC software[12] do not allow for these nitrate complexes to be accounted for. $E(Bi_{free})_{OH}$ was thus also used to determine the log β values for species formed at the low pHs. The true log β values would the lie between those determined using $E(Bi_{free})$ and $E(Bi_{free})_{OH}$.

To obtain more accurate log β values for the species in the very acidic region, virtual potentiometry was used. The ESTA software[19] used to refine the stability constants allowed for the Bi(III) nitrates to be included in the model and the results obtained fitted in the range established by the direct polarographic determinations. Only data in the very acidic region could be refined when using virtual potentiometry in this work. This was sufficient for the immediate needs of gaining a better insight into the very acidic region, but further work has to be done to understand why this is the case.

The solution species were predicted and stability constants determined for three Bi(III) pyridinecarboxylic acid systems. Two possible species models were presented in Table 9.16 for each Bi(III)-ligand system, where the exact species, generally occurring in the higher pH regions, could not be stipulated. This is due to the few data points in this region and the ligand generally being in the fully deprotonated form at that stage. For the PA system both single crystal data from the CSD and ESI-MS data indicated that the ML_4 species exists. This species could be included in the model and the stability constant refined for the polarographic data, but the standard deviations were higher than if the species was omitted. ML_4 is certainly formed in solution, but it may not occur to a significant extent in the solution conditions employed here. Independent techniques to verify a species model can be used, but unless the solution conditions are identical, a one-to-one correlation cannot be made.

Only results for the Bi(III)-PA system were found in literature.[11] The results determined here compare to some extent with these, but the authors presented a different species model that could not be refined here. The polarographic procedures used by the authors are somewhat different to that used here and the main oversight on their part was not recognising the presence of the Bi(III) nitrate species.

A linear free energy relationship was demonstrated for the log β_1 values for Bi(III) and Pb(II) with the ligands studied here. Far more work has to be done to make these relationships valuable as a predictive tool. The similarity in the stability constants for PA and QA indicated that in both cases bonding to Bi(III)

occurred through the carboxylate oxygen and the pyridine nitrogen. This was confirmed by the crystal structures found.

The use of Tl(I) to monitor the diffusion junction potential is limited to the cases where it remains uncomplexed by the ligand below pH 2.5. As observed, it was not complexed by PA or QA below pH 7, but ML and small amounts of MLH were formed with DPA. Fortunately, complexation of Tl(I) was only observed above pH 2.5 so it could still be employed in this case. Additionally, lower ligand-to-metal concentration ratios were used for DPA and QA studies to prevent the reduction waves of these ligands from interfering with the Tl(I) reduction wave.

9.5) References

1) R.M. Smith, Understanding Mass Spectra, 2nd ed., John Wiley and Sons, New Jersey, USA, 2004
2) J.H. Gross, Mass Spectrometry – A Textbook, Springer-Verlag, Berlin, Germany, 2004
3) H.A. Phillips and N. Burford, Inorg. Chem., 47 (2008) 2428
4) G.G. Briand, N. Burford, M.D. Eelman, N. Aumeerally, L. Chen, T.S. Cameron and K.N. Robertson, Inorg. Chem., 43 (2004) 6495
5) L. Agocs, N. Burford, T.S. Cameron J.M. Curtis, J.F. Richardson, K.N. Robertson and G.B. Yhard, J.Am. Chem. Soc., 118 (1996) 3225
6) H.A. Phillips, M.D. Eelman and N. Burford, J. Inorg. Biochem., 101 (2007) 736
7) N. Burford, M.D. Eelman and K. Groom, J. Inorg. Biochem., 99 (2005) 1992
8) N. Burford, M.D. Eelman, D.E. Mahony and M. Morash, Chem. Commun., (2003) 146
9) N. Burford, M.D. Eelman and T.S. Cameron, Chem. Commun., (2002) 1402
10) J.B. Fenn, M. Mann, C.K. Meng, S.F. Wong and C.M. Whitehouse, Mass Spec. Rev., 9 (1990) 37
11) I. Cukrowski, J.M. Zhang and A. van Aswegen, Helv. Chim. Acta, 87 (2004) 2135
12) I. Cukrowski, 3D-CFC10 software, Version 5.0, 2000
13) L.D. Petit and K.J. Powell, Sol-Eq, Academic Software, IUPAC, 2002
14) F.H. Allen, Acta Cryst., B58 (2002) 380. Cambridge Structural database Version 5.31, November 2008 update
15) MERCURY: C.F. Macrae, P.R. Edgington, P. McCabe, E. Pidcock, G.P. Shields, R. Taylor, M. Towler, and J. van de Streek, J. Appl. Cryst., 39 (2006) 453
16) ChemDraw Ultra 8.0, CambridgeSoft Corporation, Cambrigde, USA, 2003
17) I. Cukrowski, R.D. Hancock and R.C. Luckay, Anal. Chim. Acta, 319 (1996) 39

18) I. Cukrowski and R.C. Luckay, Anal. Chim. Acta, 372 (1998) 323
19) K. Murray and P. May, Equilibrium Simulation and Titration Analysis (ESTA) User Manual, 1984
20) S. J. Berners-Price and P.J. Sadler, Coord Chem. Rev., 151 (1996) 1
21) P.J. Sadler, H. Li and H. Sun, Coord Chem. Rev., 185 (1999) 689
22) T.K. Prasad and M.V. Rajasekharan, Polyhedron, 26 (2007) 1364
23) S. Funahashi, K. Haraguchi and M. Tanaka, Inorg. Chem., 16 (1977) 1349
24) Z. Vargová, J. Kotek, J, Rudovský, J. Plutnar, R. Gyepes, P. Hermann, K. Györyová and I. Lukeš, Eur. J. Inorg. Chem., (2007) 3974
25) A.E. Martell, R.M. Smith and R.J. Motekaitis, NIST Standard Reference Database 46 Version 8.0, NIST Critically Selected Stability Constants of Metal Complexes, USA, 2004
26) A.E. Martell and R.D. Hancock, Metal Complexes in Aqueous Solutions, Plenum Press, New York, 1996
27) L.D. Petit and K.J. Powell, IUPAC Stability Constants Database, IUPAC and Academic Software, 1993-2003

CHAPTER 10
Concluding Summary

The main objective of this project was to develop a method that would enable the study of Bi(III) complex formation and to determine the stability constants of solution species formed with reasonable certainty. Since Bi(III) undergoes hydrolysis below pH 2, these studies were performed from low pH and at low Bi(III) concentrations. Polarography was thus used to study these systems.

The calibration of the GE below pH 2 was investigated. It is generally recommended to avoid this region as the electrode no longer gives a linear response. However, in this work it was necessary to calibrate in the same pH range as polarographic measurements were made as the solution pH is still required to solve the mass balance equations to refine the stability constants. A combination of a linear and a quadratic function was used to describe the potential-pH relationship, where the latter accounted for the curvature in the acidic region which is mainly due to the diffusion junction potential. The very basic region was avoided as far as possible since it too displayed curvature, which was predominantly due to the alkaline error in this case, and degradation of the glass membrane was accelerated by the basic solutions. It was demonstrated that the GE response in the very basic region was a good indicator of the quality of the membrane and a test was developed to evaluate its condition. It should be highlighted that the same conditions which apply to the GE calibration when using GEP cannot be imposed here. Firstly, the errors in the stability constants incurred by errors in pH measurement are significantly smaller when using polarography than potentiometry, as was demonstrated. Secondly, the low pH region has been avoided thus far (mainly by GEP, but by other techniques too) due to the difficulties in studying these solutions, but a mechanism to do so as accurately as possible is provided here rather than simply ignoring it.

The diffusion junction potential for the polarographic data was more complicated to deal with than simply applying a mathematical function to describe it. It could be calculated by existing equations, such as the Henderson and Planck equations, but due to the complexity of integrating the true expression of the junction potential, assumptions were made in their derivation which does not necessarily apply to the particular conditions of the experiment. Additionally, values for the mobilities for the ions under the particular solution conditions used (such as ionic strength) are not always available. That being said, the values calculated (using many assumptions) compared fairly well to those obtained experimentally. The calculated values of E_j were only used to ensure the experimental data gave the correct trends expected since it could not take any slight variations in the experiment into account as could be done with measured data.

The experimental E_j values were obtained by monitoring the change in $E_{1/2}$ of Tl(I) as the pH of the solution was varied. The change in potential would be dependent on E_j only provided that the temperature and ionic strength of the solution is kept constant. Unfortunately, when working under very acidic conditions where relatively high concentrations of acid are required, it is impossible to keep the ionic strength constant without working at very high ionic strengths where additional complexities arise. It was decided to rather deal with the change in ionic strength, although it is not ideal when determining stability constants under concentration conditions. When comparing log β values in literature at ionic strengths of 0.5 and 0.2 M (or even 0.1 M), generally there were not large discrepancies between the values. Although E_j is the same for all ions in the same solution, it was found that the change in $E_{1/2}$ with ionic strength was different for different metal ions. The difference in $E_{1/2}$ as a function of pH was modelled for Tl(I) (as the witness or reference ion) and the metal ion being studied in the absence of ligand. Establishing this model was, however, not possible with Bi(III) due to the added complication associated with its hydrolysis and it was assumed that Tl(I) and Bi(III) gave the same potential-pH relationship in the absence of a ligand.

Tl(I) was chosen as the witness ion as it does not undergo complexation readily and when ligand is added to the solution, the Tl(I) $E_{1/2}$ data should still reflect the junction potential. In the case of strong complexing ligands such as DPA, Tl(I) did undergo complexation, but above pH 2.5 so that E_j could still be determined. The formation constants for Tl(I) with DPA were estimated, but the experimental conditions employed were not optimal and more appropriate conditions were suggested.

Apart from being able to predict the potential shifts due to E_j and the varying ionic strength, it was also established that the difference in the $E(M_{free})$ for Tl(I) and the metal ion being studied was constant and could be determined from the experiments omitting the ligand. Since Bi(III) undergoes hydrolysis to some extent over the whole pH range investigated, it was impossible to measure $E(Bi_{free})$. This value was calculated by accounting for the potential shifts due to hydrolysis, which in turn were calculated from the already established stability constants of the hydrolysis products. Since Bi(III) also forms unusually strong complexes with nitrate and since nitrate was in such a large excess, both the completing complexation of nitrate with bismuth and the hydrolysis reactions had to be considered and included in the potential shift calculations. It was also concluded that the Bi(III) concentration should be as low as possible and the titration experiments run as fast as possible (under the constraints of the measurement parameters) in order to postpone precipitation to higher pHs. The standard deviation of the average difference in $E(M_{free})$ for Tl(I) and Bi(III) was greater than for the other metal ions studied, but considering all the factors affecting the determination of $E(Bi_{free})$ and the lack of data in the pH range where E_j was constant, it was remarkable that the standard deviation was only $\pm$ 2 mV.

The protocols developed to study complex formation under acidic conditions were applied firstly to the Cd(II) and Cu(II) picolinic acid systems, where stability constant data was available in literature and thus the procedures could be verified. In the case of Cd(II), a CdHL species was proposed which was not reported before, probably due to the system not being studied at such low pHs before. It was, however, only a minor species under the solution conditions

used here. In another study, a crystal structure of this species was determined when the liquor from which the crystals were grown was acidified to predicted pH values using the stability data determined here. The investigation with Cu(II) included dealing with a quasi-reversible reduction process. The reversible $E_{1/2}$ values are required when calculating the formation constants, thus the best procedure to evaluate the reversible potentials was explored. In this case only the very rudimentary process of refitting the polarographic wave by forcing the δ value to be unity and removing points on the wave that did not display reversible behaviour was successful. This was established by comparing the potential-pH relationship for Cu(II) (in the absence of ligand) to that predicted from the calculation of E_j. It was suggested that the other methods attempted did not work in this case due to the close proximity of the Cu(II) reduction wave to the mercury oxidation wave. Conditions for studies with Cu(II) in future were recommended in order to increase the extent of reversibility which would make the determination of the reversible potential more accurate. Since the formation constants of the solution species were comparable to literature data in both studies, the procedures were regarded as validated and could be applied to the study of Bi(III) complexation.

It was anticipated that the reduction of Bi(III) would also be quasi-reversible and that similar strategies employed to determine the reversible $E_{1/2}$ values for Cu(II) would have to be used as the reduction potential for the two metal ions are almost identical. Fortunately, under the conditions used here, Bi(III) reduction was reversible in the presence and absence of ligand. In perchlorate solutions Bi(III) reduction is less reversible, but perchlorate binds more weakly to Bi(III) than nitrate. A bismuth-oxy-perchlorate precipitate is also formed (similar to the bismuth-oxy-nitrate) but at slightly higher pHs. The pros and cons of working in nitrate versus perchlorate solutions were considered, but the extremely time-consuming and very rudimentary approach that would be needed to determine the reversible $E_{1/2}$ values in perchlorate solutions made the nitrate option far more attractive. Using a sodium chloride electrolyte will also need to be explored further due to it biological applications.

The polarographic study of Bi(III) complex formation with PA, DPA and QA were successfully completed. In developing the methods to do so, a far greater understanding of working in the acidic region was gained, as well as dealing with metals ions that undergo hydrolysis under acidic conditions. Additionally, Bi(III) nitrate formation needed to be considered. Ideally the formation constants for Bi(III) hydroxides and nitrates would be included in the species models (and kept constant) when refining stability constants for the Bi(III)-ligand system being studied. The limitation imposed by the software employed which interprets the polarographic data directly, prevented this. $E(Bi_{free})$ was used to calculate potential shifts from which to compute stability constants in the pH range where no Bi(III) nitrates are present. Both $E(Bi_{free})$ and $E(Bi_{free})_{OH}$ were used to determine log β values in the pH region where the Bi(III) nitrates were still in solution. This provided a range in which the true log β values would be. Virtual potentiometry was utilised to determine the log β values for species in the acidic region where Bi(III) nitrates were present as their stability constants could be included in the potentiometric software employed. A full understanding still needs to be gained of the application of virtual potentiometry where high proton concentrations and low ligand and metal ion concentrations are present.

Although this work was geared towards the study of Bi(III), it could also be applied or used as a starting point to the study of other metal ions under similar conditions. One limitation in this work was the lack of the ability to accurately determine the ligand protonation constants under very acidic conditions at this stage. Since GEP cannot be used meaningfully in the pH range below about 2, other techniques such as NMR or spectrophotometry would have to be used. This still has to be investigated.

The methods to study the metal-ligand chemistry of Bi(III) have been developed and tested in this work. Now the challenge of applying these procedures to gain a quantitative thermodynamic understanding of this chemistry lies ahead. Burford, one of the current forerunners in bismuth chemistry, has taken a more qualitative approach thus far to understanding the Bi(III)-ligand interactions. This work would compliment that already done in the

field. Bismuth is used mainly in drugs for the treatment of gastric ulcers at this stage, but has shown potential in so many other medicinal applications. It is hoped that by providing these tools and contributing to the knowledge base of bismuth chemistry, these applications could come to fruition.

One of the additional aspects that came to the fore in this work was the close relationship between simple crystal structures showing metal-ligand interactions and the stoichiometry of the solution species. It was therefore questioned to what extent it would be possible, by knowing the stability constants of the solution species, to manipulate the structure of the crystal grown by controlling the conditions of the liquor from which they are grown. Another aspect briefly touched on here was how comparable are the solution species under polarographic conditions, which are very dilute, to those determined by ESI-MS in which concentrations are significantly reduced before the ions are left in the gas phase. These are complimentary techniques that could be used to support the polarographic data and assist in elucidating the stoichiometry of species in solution.

APPENDICES

1) Experimental Parameters 361

A1.1) Autotitrator Procedures

A1.2) Potentiometric and Polarographic Experimental Details

2) Derivations 367

A2.1) Derivation of the equation used to determine stability constants

A2.2) Derivation of the expression for the half-wave potential

A2.3) References

3) Supplementary information for Chapter 3 371

4) Supplementary information for Chapter 6 378

5) Supplementary information for Chapter 7 385

6) Supplementary information for Chapter 8 387

7) Supplementary information for Chapter 9 389

APPENDIX 1
Experimental Parameters

A1.1) Autotitrator Procedures

Procedures to standardise to acid and hydroxide solutions using the Metrohm 848 Titrino Plus autotitrator were developed and the parameters used are given in Table A1.1. These parameters were used for the standardisation of both the acid and the hydroxide solutions and the hydroxide was always kept as the titrant.

In the case of the standardisation of the hydroxide solutions, the concentration was calculated as follows:

$$\frac{C00 \times 1000}{204.23 \times EP1}$$

where C00 is the sample size entered as the mass of potassium hydrogen phthalate weighed and EP1 is the volume of titrant added at the end-point. The notation is kept the same as that used by the autotitrator. The value 204.23 is the molar mass of potassium hydrogen phthalate.

For the standardisation of the acid solutions, the concentration was calculated as follows:

$$\frac{conc \times EP1}{C00}$$

where C00 is the sample size entered as the volume of the acid solution (added using a Dosimat unit), EP1 is again the volume of titrant added at the end-point and conc is the concentration of the titrant. This concentration can be edited in the solution list which links a specific Dosimat unit to the solution inside. The hydroxide solutions were therefore always standardised first so that the accurate concentration was known.

Table A1.1: Parameters used by the autotitrator for the standardisation of acid and hydroxide solutions. (EP refers to the endpoint)

Parameter	Setting
Start conditions:	
Start delay time	30 s
Start volume	0 mL
Dosing rate	1 mL min^{-1}
Pause	5 s
Titration parameters:	
Titration rate	slow
Temperature	25.0 ^{o}C
Sensor	pH electrode
Solution	0.5 M OH^{-}
Stirrer	on
Stirring rate	5
Stop conditions:	
Stop volume	10 mL
Stop EP	1
Volume after EP	1 mL
Filling rate	max.
Evaluation:	
EP criterion	25
EP recognition	all

A1.2) Potentiometric and Polarographic Experimental Details

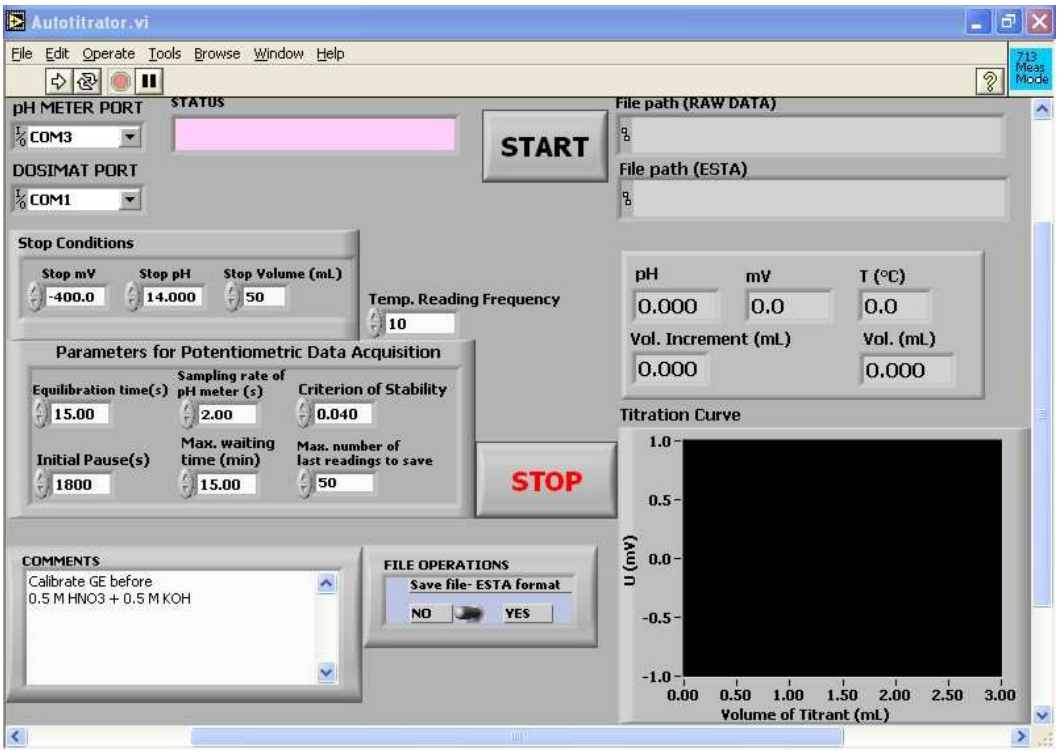

Figure A1.1: Graphical user interface (GUI) of the VI used to calibrate the GE.

Table A1.2: Parameters for a typical GE calibration.

Parameter	Setting
Potentiometric data:	
Initial pause	1800 s
Equilibration time	15 s
Sampling rate	2 s
Maximum waiting time	15 min
Stability criterion	0.040
Number of readings saved	50
Temperature reading frequency	10
Stop conditions:	
E	-400 mV
pH	14
Volume	50 mL
Dosimat configuration:	
Mode	DisC
Volume increment	0.5 mL
Rate of addition	5 mL min^{-1}
Rate of filling	30 mL min^{-1}

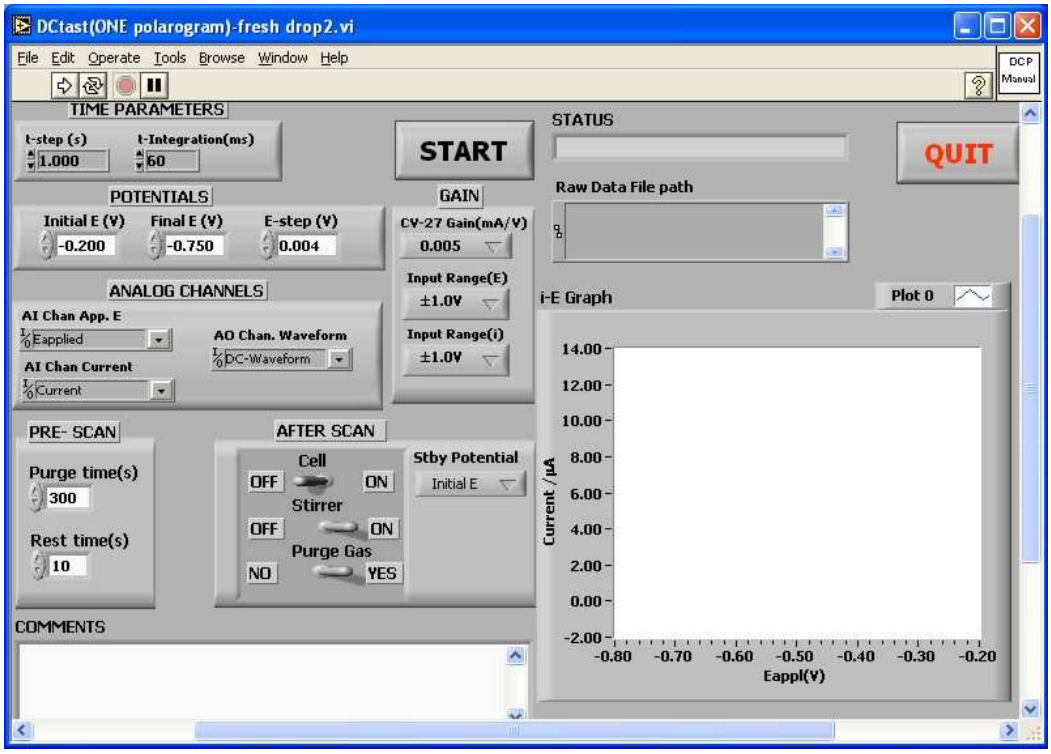

Figure A1.2: GUI of the VI for the collection of a single DC polarogram.

Table A1.3: Typical values for the parameters required for the single DC polarogram VI.

Parameter	Setting
Initial potential	varied
Final potential	varied
Step potential	-4 mV
Step time (drop life)	1 s
Current integration time	60 – 100 ms
CV-gain	0.005 mA V^{-1}
Potential input range	± 1.0 V
Current input range	± 1.0 V
Purge time	varied
Rest time	10 s

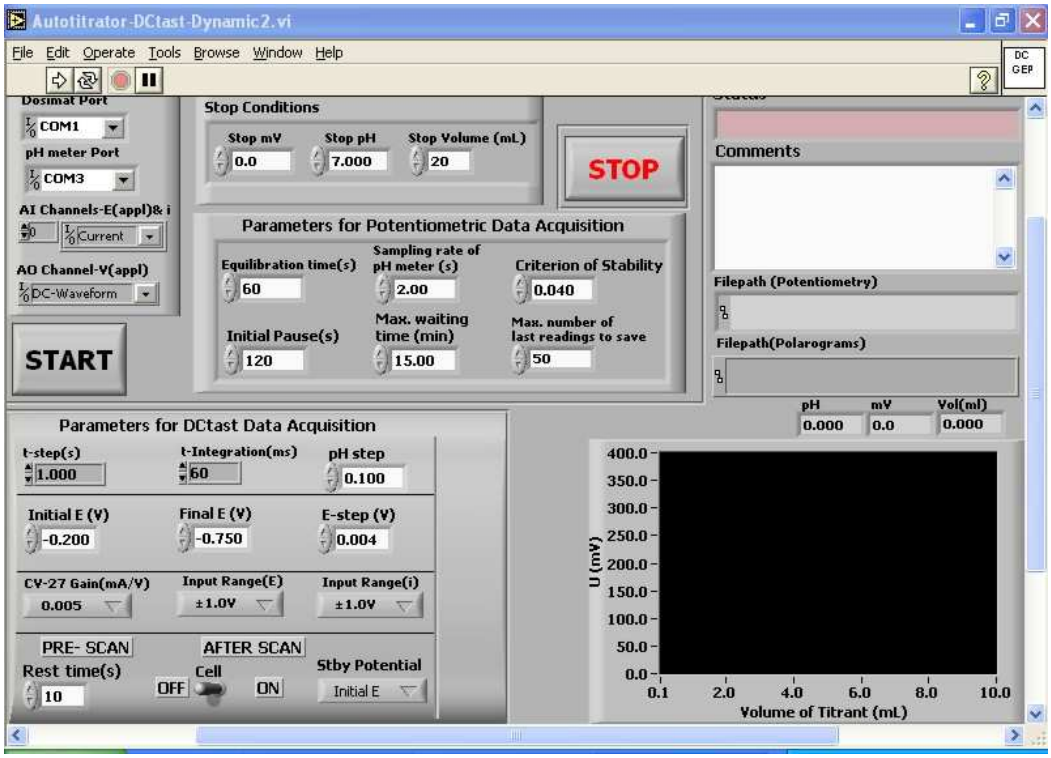

Figure A1.3: GUI of the VI for the automated titration collecting both potentiometric and polarographic data.

Table A1.4: Values for the parameters required for the automated DC polarogram VI.

Parameter	Setting
Potentiometric data:	
Initial pause	120 s
Equilibration time	60 s
Sample rate	2 s
Criterion for stability	0.04
Maximum waiting time	15 min
Number of readings saved	50
Polarographic data:	
Initial potential	varied
Final potential	varied
Step potential	-4 mV
Step time (drop life)	1 s
Current integration time	60 – 100 ms
pH step	0.07 – 0.1
CV-gain	0.005 mA V^{-1}
Potential input range	± 1.0 V
Current input range	± 1.0 V
Purge time	varied
Rest time	10 s
Stop conditions:	
Stop potential	0 mV
Stop pH	7
Stop volume	30 mL
Dosimat configuration:	
Mode	DisC
Rate of addition	5 mL min^{-1}
Rate of filling	30 mL min^{-1} (for a 10 mL burette)
Volume increment	Ranged from 0.5 mL to 0.01 mL throughout the titration

APPENDIX 2
Derivations

A2.1) Derivation of the equation used to determine stability constants[1]

Consider the reduction of an uncomplexed metal ion at a DME:

$$M^{n+} + ne^- \rightleftharpoons M(Hg)$$

The potential at which this occurs can be described by the Nernst equation for a reversible electron transfer process and under diffusion controlled conditions. This can be written as:

$$E(M_{free}) = E' - \frac{RT}{nF} ln \frac{[M_{Hg}(1)]}{[M_{free}(1)]} \qquad \text{(A2.1)}$$

where $E(M_{free})$ is the peak or half-wave potential for the reduction of the free metal ion (in the absence of a complexing ligand), E' is the formal potential and $[M_{free}(1)]$ and $[M_{Hg}(1)]$ are the concentrations of the free metal ion at the electrode surface and in the mercury drop, respectively. Concentrations and formal potentials are used as experiments are conducted at constant ionic strength and temperature.

If ligand is added and complexes with the metal ions, the amount of free metal ion is reduced and the concentration of metal in the mercury drop could also vary as the rate of diffusion of the free metal ion could be different to that of the complexed metal ion. The Nernst equation can again be written in this case as:

$$E(M_{comp}) = E' - \frac{RT}{nF} ln \frac{[M_{Hg}(2)]}{[M_{free}(2)]} \qquad \text{(A2.2)}$$

where $E(M_{comp})$ is the peak or half-wave potential for the reduction of the metal ion in the presence of complexes, and $[M_{free}(2)]$ and $[M_{Hg}(2)]$ are the values as before but again where complexes are formed.

The shift is potential, ΔE, caused by the formation of complexes is calculated as:

$$\Delta E = E(M_{free}) - E(M_{comp}) = \frac{RT}{nF} ln \frac{[M_{free}(1)][M_{Hg}(2)]}{[M_{Hg}(1)][M_{free}(2)]} \quad \text{(A2.3)}$$

Now the concentration of metal in the mercury electrode (which is due to the reduction of the metal ion at the surface of the electrode) is proportional to the peak or diffusion limited current. Thus the terms $[M_{Hg}(1)]$ and $[M_{Hg}(2)]$ can be substituted by $i(M_{free})$ and $i(M_{comp})$ which refers to the current in the absence and presence of complexes respectively. This gives:

$$\Delta E = E(M_{free}) - E(M_{comp}) = \frac{RT}{nF} ln \left(\frac{[M_{free}(1)]}{[M_{free}(2)]} \times \frac{i(M_{comp})}{i(M_{free})} \right) \quad \text{(A2.4)}$$

which can be rearranged as:

$$E(M_{free}) - E(M_{comp}) - \frac{RT}{nF} ln \frac{i(M_{comp})}{i(M_{free})} = \frac{RT}{nF} ln \left(\frac{[M_{free}(1)]}{[M_{free}(2)]} \right) \quad \text{(A2.5)}$$

A titration experiment is usually performed where, for example, a hydroxide solution is added to the original test solution (which contains the metal ion in an acid solution to which ligand was then added) such that current and potential data are determined from polarograms at each pH step. In doing so, the solution is diluted and this also needs to be accounted for.

The value of $E(M_{free})$ is independent of pH, but the value of $E(M_{comp})$ is pH-dependent as the type of complexes formed vary with the solution pH. To indicate pH-dependence the subscript (i) is included, where $E(M_{comp})_{(i)}$ implies the potential of the complexed metal ion at each pH step. The currents are affected by dilution and also complex formation if the diffusion coefficient for the free and complexed metal ion is different. Thus $i(M_{free})$ is calculated at each pH step by merely taking the dilution factor into account. The total metal ion concentration can also be calculated at each pH step by multiplying by the dilution factor. The resultant relationship as presented in Chapter 2 is therefore:

$$\{E(M_{free}) - E(M_{comp})_{(i)}\} - \frac{RT}{nF} ln \frac{i(M_{comp})_{(i)}}{i(M_{free})_{(i)}} = \frac{RT}{nF} ln \frac{[M_T]_{(i)}}{[M_{free}]_{(i)}} \quad \text{(A2.6)}$$

As discussed in Chapter 2, $[M_{free}]_{(i)}$ is determined by solving mass balance equations which contain the stability constants.

A2.2) Derivation of the expression for the half-wave potential[2]

Since the shift in the half-wave potential is so crucial in the use of polarography to determine the formation constants of complexes, it is important to understand the physical nature of the half-wave potential. This was clearly described by Lingane[2] by considering the reaction occurring at the electrode surface. For the reversible reduction of a simple (hydrated) metal ion at a mercury drop electrode to form the amalgam as follows:

$$M^{n+} + ne^- + Hg \rightleftharpoons M(Hg)$$

the working electrode experiences only concentration polarisation and the potential at the electrode can be described as:

$$E = E_a° - \frac{RT}{nF} \ln \frac{c_a \gamma_a}{c_o \gamma_s} \qquad \text{(A2.7)}$$

where $E_a°$ is the standard potential of the amalgam for the cell: RE $|$ M^{n+} (a = 1) $|$ M(Hg) (a = 1); c_a is the concentration of the amalgam on the mercury drop surface; c_o is the concentration of the metal ions at the surface of the electrode; and γ_a and γ_s are the activity coefficients of the metal in the amalgam and the metal ions in solution respectively. Under normal polarographic conditions, it can be assume that the amount of metal dissolved in the amalgam is negligible, so the value of γ_a is close to unity. When a high concentration of background electrolyte is present, diffusion is the main mass transport process (migration is negligible) and the concentration of metal ions in the bulk solution (c_B) and at the electrode surface can be related to the currents as:

$$i_d = Dc_B \qquad \text{(A2.8)}$$

and $$i = D(c_B - c_o) \qquad \text{(A2.9)}$$

where i is the current anywhere along the polarographic wave, i_d is the diffusion limited current and D is the diffusion constant. The concentration expression can be written as:

$$c_o = \frac{i_d - i}{D} \tag{A2.10}$$

and $$c_a = ki \tag{A2.11}$$

If the IR drop is assumed to be negligible (as would be the case for high concentrations of background electrolyte and small currents), the working electrode potential can be obtained by substituting Equations A2.10 and A2.11 into Equation A2.7 to give:

$$E = E_a^\circ - \frac{RT}{nF} ln \frac{\gamma_a kD}{\gamma_s} - \frac{RT}{nF} ln \frac{i}{i_d - i} \tag{A2.12}$$

The half-wave potential is the potential halfway up the wave where $i = i_d/2$ and since the log term is zero at this point, the potential at the mercury electrode is give as:

$$E = E_{1/2} - \frac{RT}{nF} \ln \frac{i}{i_d - i} \tag{A2.13}$$

where

$$E_{1/2} = E_a^\circ - \frac{RT}{nF} ln \frac{\gamma_a kD}{\gamma_s} \tag{A2.14}$$

A2.3) References

1) I. Cukrowski, Anal. Chim. Acta, 336 (1996) 23

2) J.J. Lingane, J. Am. Chem. Soc. 61 (1939) 2099

APPENDIX 3

Supplementary information for Chapter 3

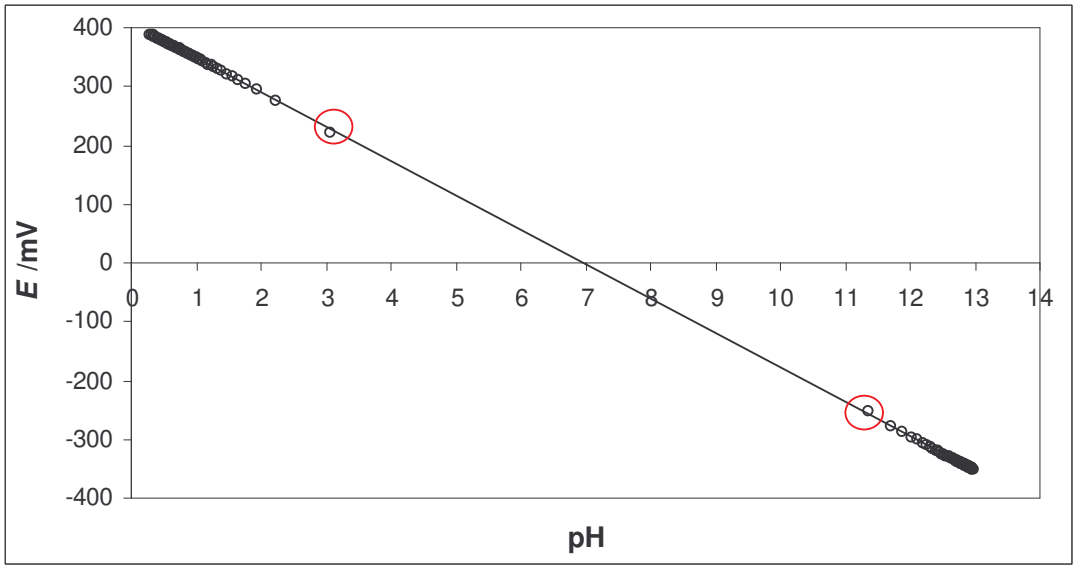

Figure A3.1: Calibration graph from a 0.5 M HNO_3–NaOH titration indicating data points closest to pH 7 deviating from the linear function (circled in red).

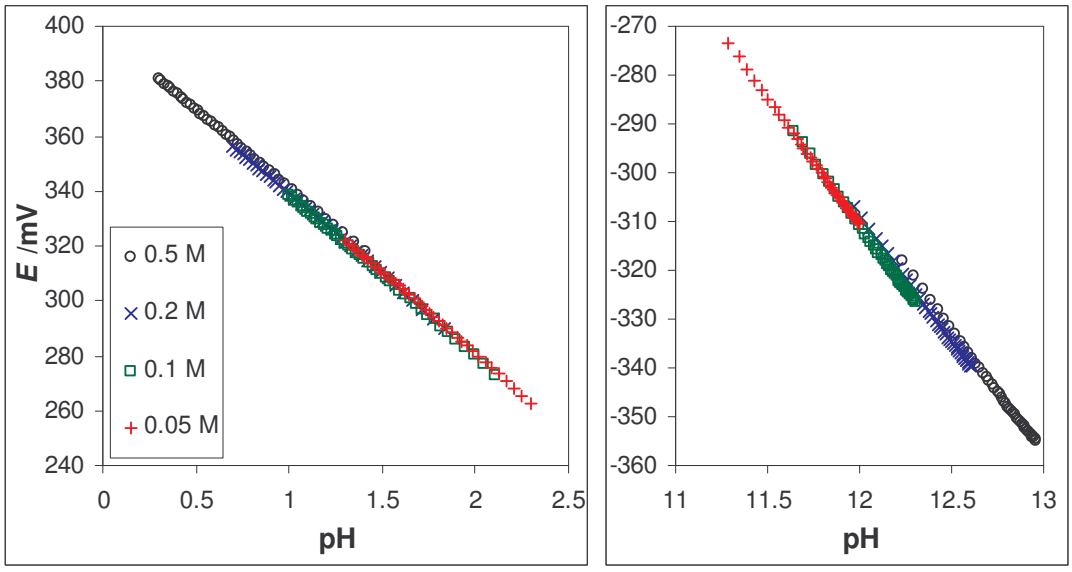

Figure A3.2: Comparison of calibration data using different concentrations of solutions, but where the HNO_3 and NaOH concentrations within a titration were the same.

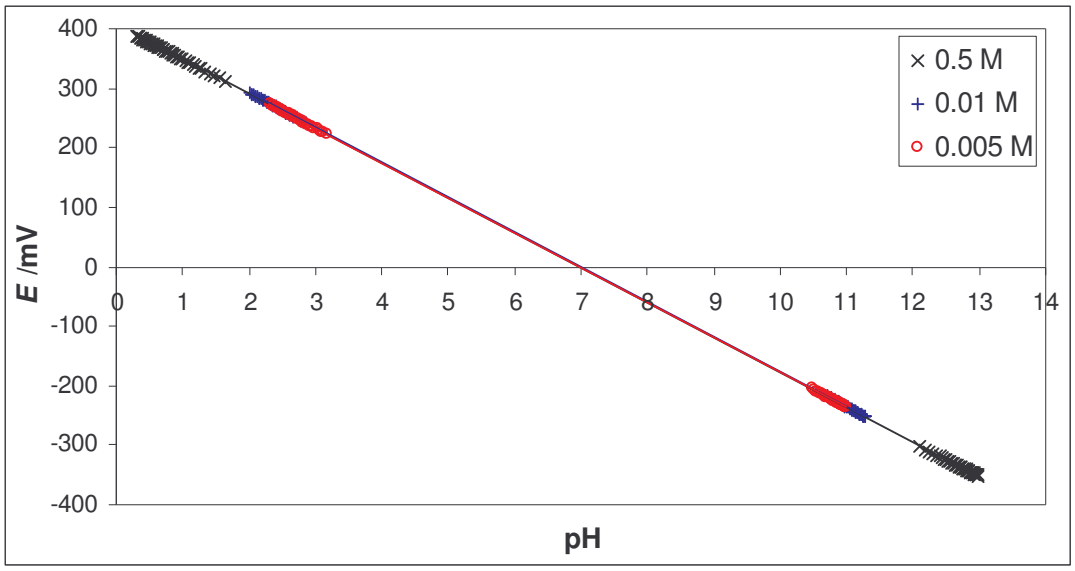

Figure A3.3: Comparison of calibration graphs obtained from HNO_3–NaOH titrations with different concentrations of solutions where [HNO_3] = [NaOH] within a titration and μ = 0.5 M.

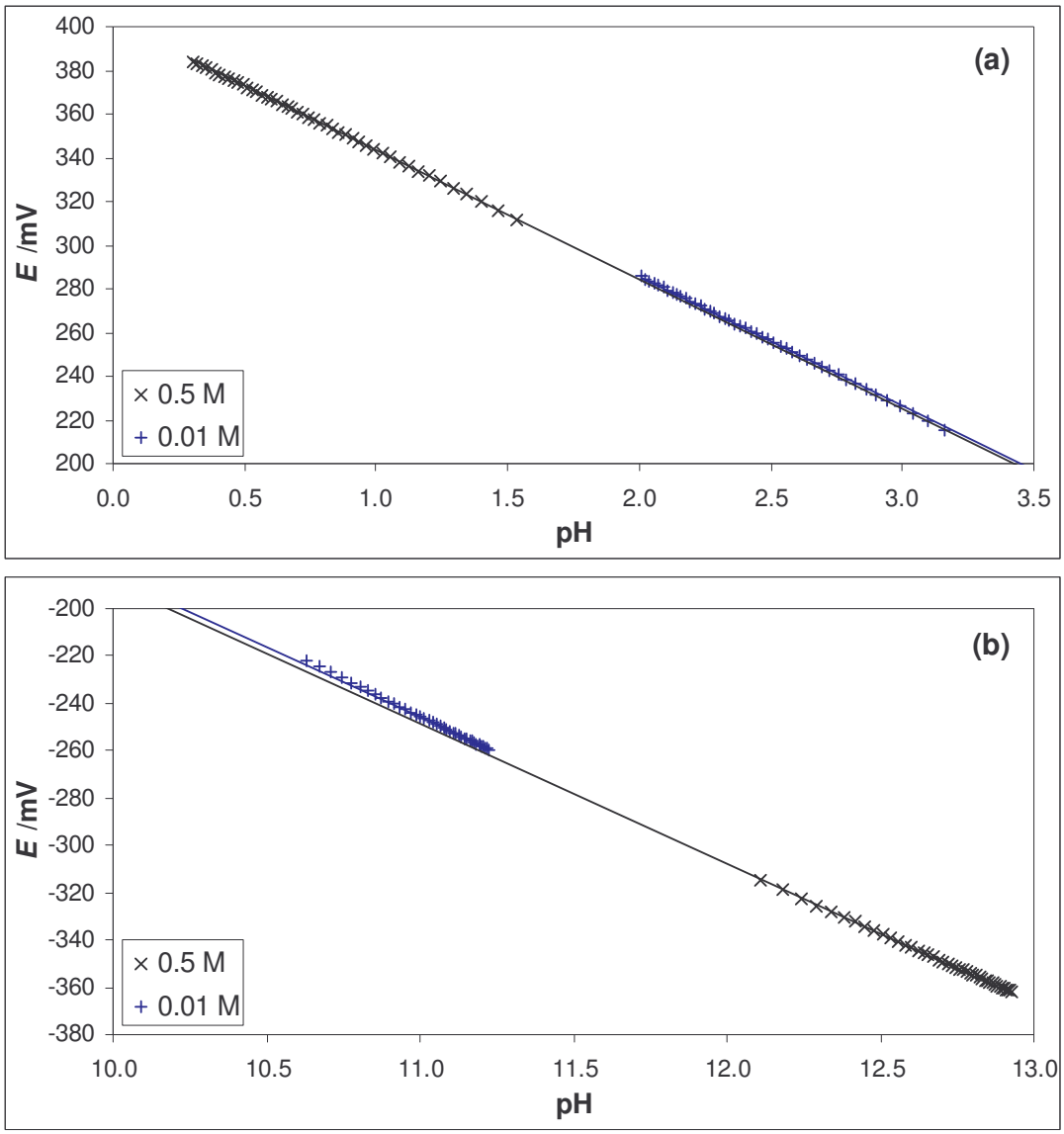

Figure A3.4: Comparison of (a) the acidic and (b) the basic regions of calibration graphs obtained from HNO_3–KOH titrations with different concentrations of solutions where $[HNO_3]$ = [KOH] within a titration and μ = 0.5 M.

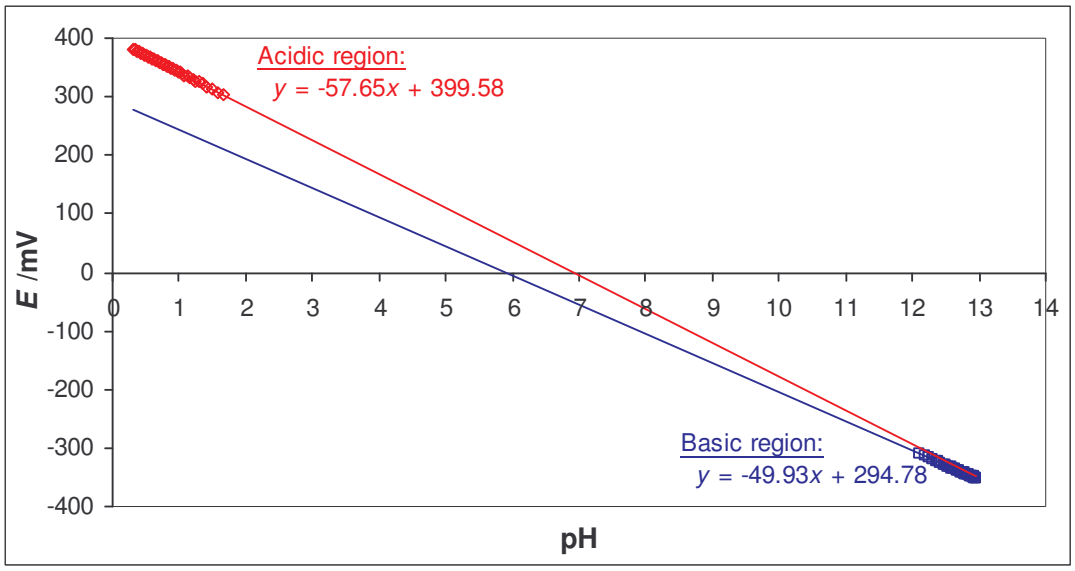

Figure A3.5: Differences in the separate linear correlations for the acid and base regions for a 0.5 M HNO_3–NaOH calibration using an old CGE.

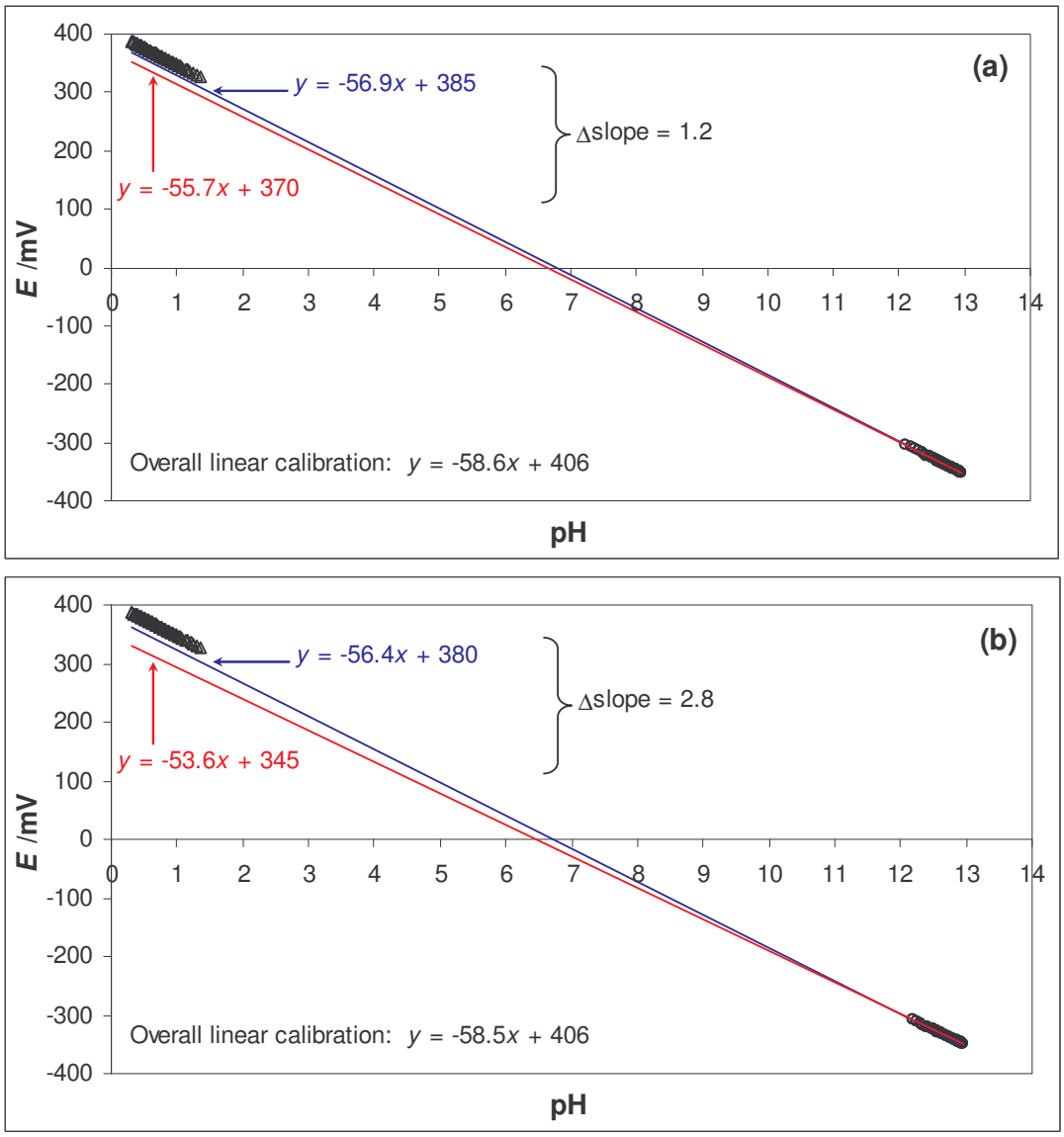

Figure A3.6: Testing the behaviour of (a) the new GE1 and (b) the well-used GE1 in a 0.5 M HNO_3–NaOH titration. Experimental data for the acidic (Δ) and basic (○) regions are shown. Two linear regressions are plotted for the basic region data: between pH 12.2 – 13.0 (red line) and between pH 12.2 – 12.8 (blue line).

Table A3.1: Methrohm's preset tolerances for standard GE tests.

	Excellent GE	Good GE	Passing GE
Streaming potential /mV	≤ 2.5	≤ 3.0	≤ 4.0
Total drift /mV	≤ 2.0	≤ 2.5	≤ 3.0
Slope, s /%	96.5 ≤ s ≤101	96 ≤ s ≤102	95 ≤ s ≤103
Response time /s	≤ 45	≤ 50	≤ 60
Offset potential, U_{off} /mV			-15 ≤ U_{off} ≤15

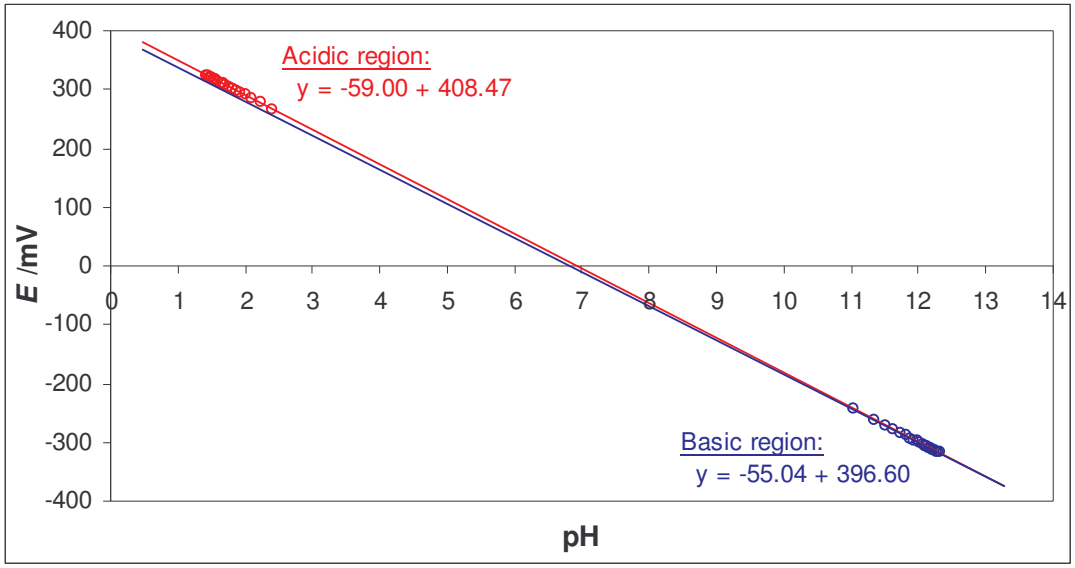

Figure A3.7: A combined calibration plot from Figure 3.13 with data points deviating from linearity omitted, to illustrate the near coincidence of the two graphs.

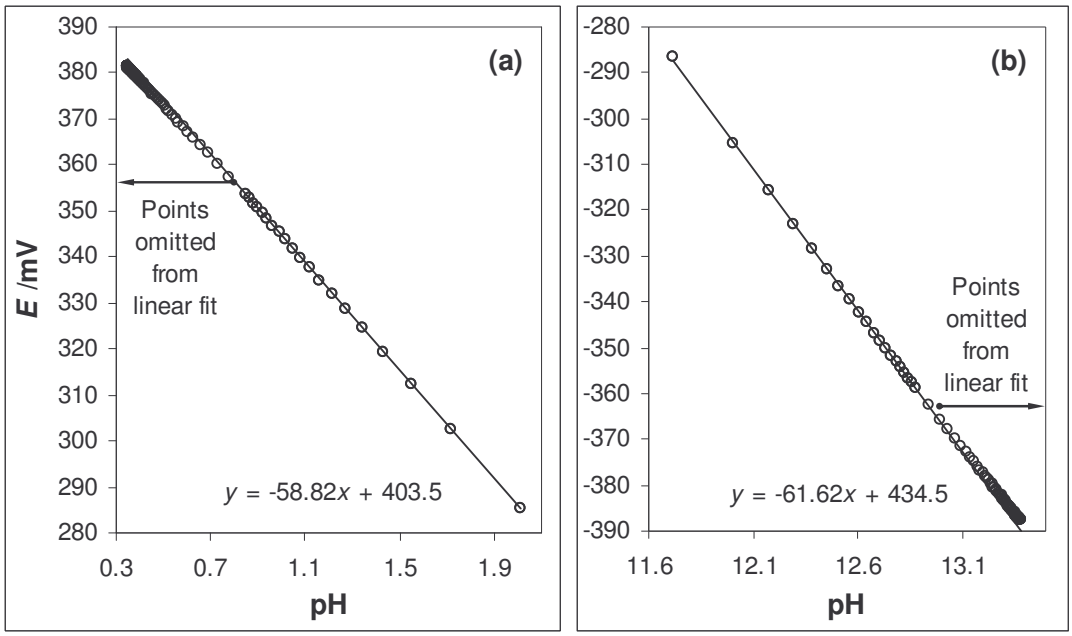

Figure A3.8: Calibration graphs from the titration of 0.5 M KNO_3 by (a) 0.5 M HNO_3 or (b) 0.5 M KOH. Data points deviating from linearity were omitted when the fitting the linear function as indicated.

APPENDIX 4

Supplementary information for Chapter 6

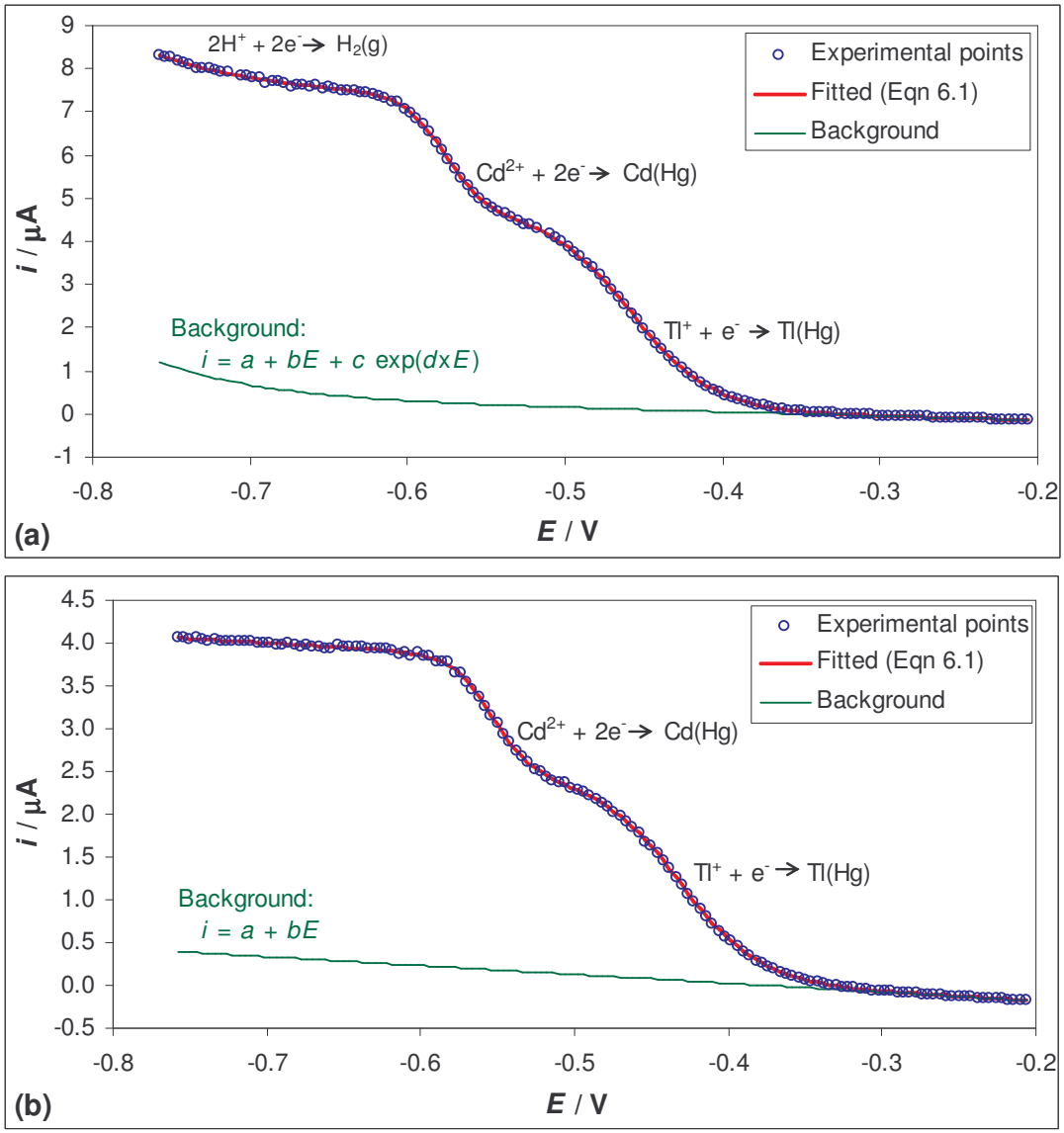

Figure A4.1: Fitting polarograms of the reduction of Tl(I) and Cd(II) in a NO_3^- solution at (a) pH 0.29 and (b) pH 1.67.

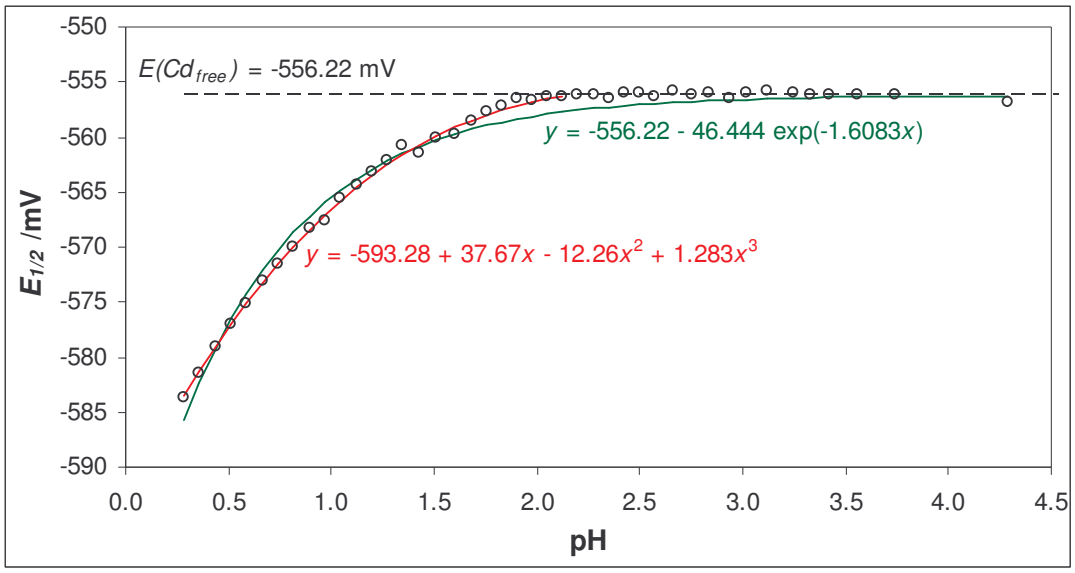

Figure A4.2: Experimental half-wave potentials (○) as a function of pH for Cd(II). Data was fitted with a third order polynomial (—) and the corresponding $E(Cd_{free})$ value is indicated by (---) (as in Figure 6.8), or an exponential function (—) where the value of "*a*" was fixed to $E(Cd_{free})$ determined previously.

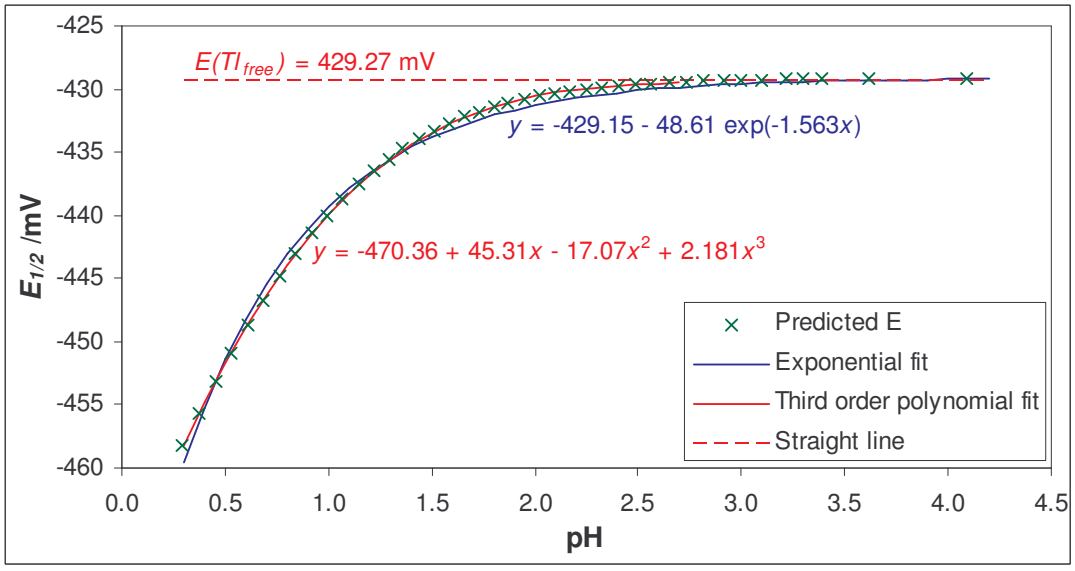

Figure A4.3: Fitting $E_{1/2}$ values predicted using the Henderson equation as a function pH. An exponential function (—) and a third order polynomial (—) together with horizontal line were used and the corresponding $E(Tl_{free})$ values are indicated.

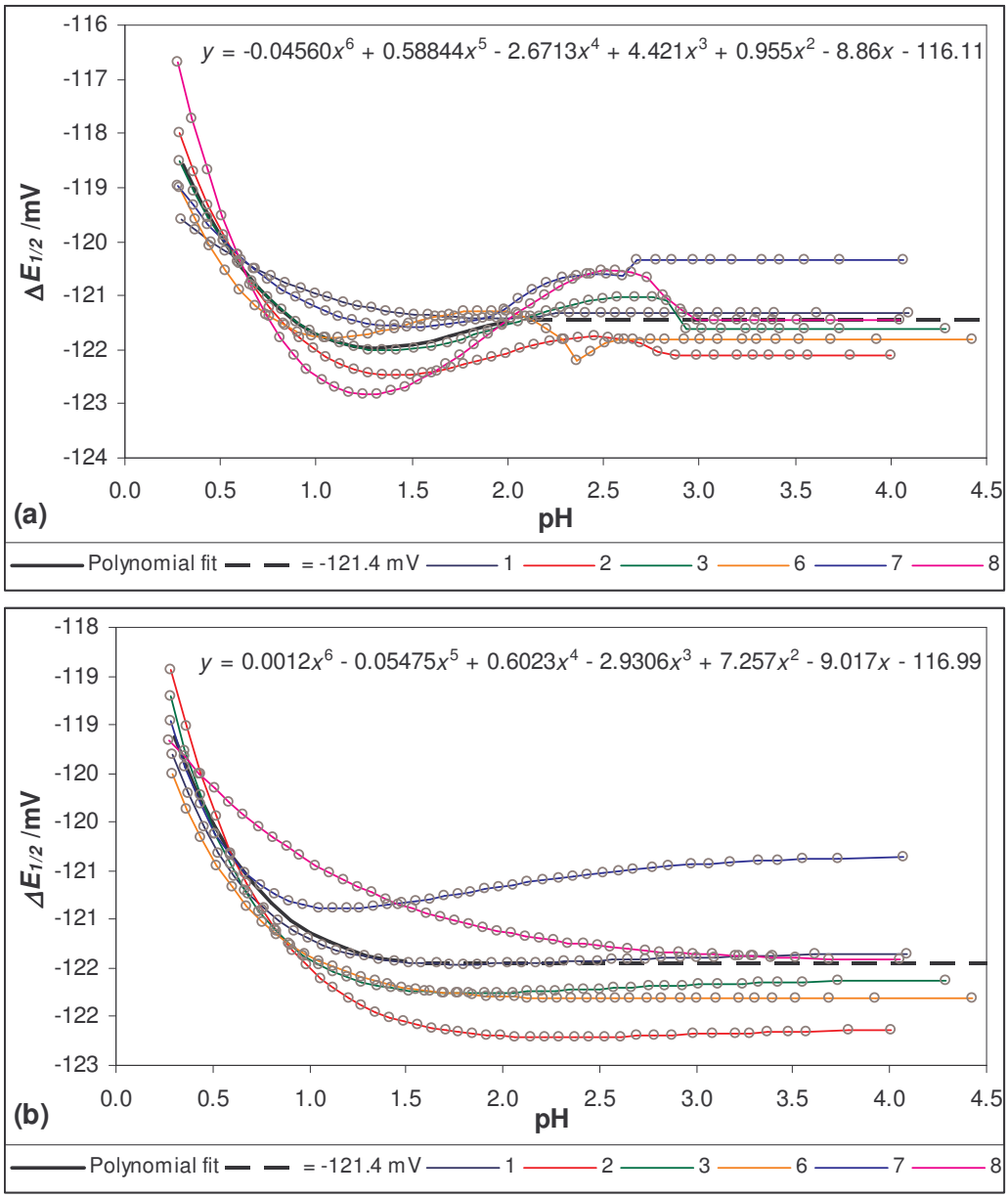

Figure A4.4: Sixth order polynomial fitted to the combined $\Delta E_{1/2}$ values versus pH. $E_{1/2}$ versus pH curves were fitted using (a) a third order polynomial and a horizontal line and (b) an exponential function where constant "*a*" was set equal to the value of the horizontal line. Above pH 2, $\Delta E_{1/2}$ was set to –121.4 mV. (The numbers in the legend refers to the experiment number.)

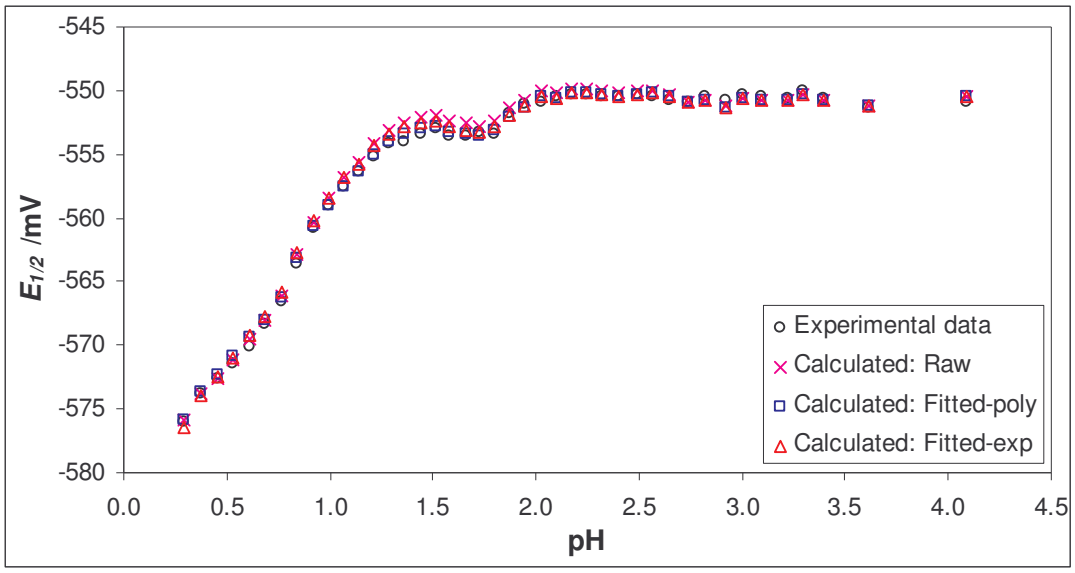

Figure A4.5: An example of a comparison of the experimental and predicted $E_{1/2}(Cd)$ values showing the same anomalous trend. The mE model was applied and the three different sixth order polynomials derived from raw or fitted data were used.

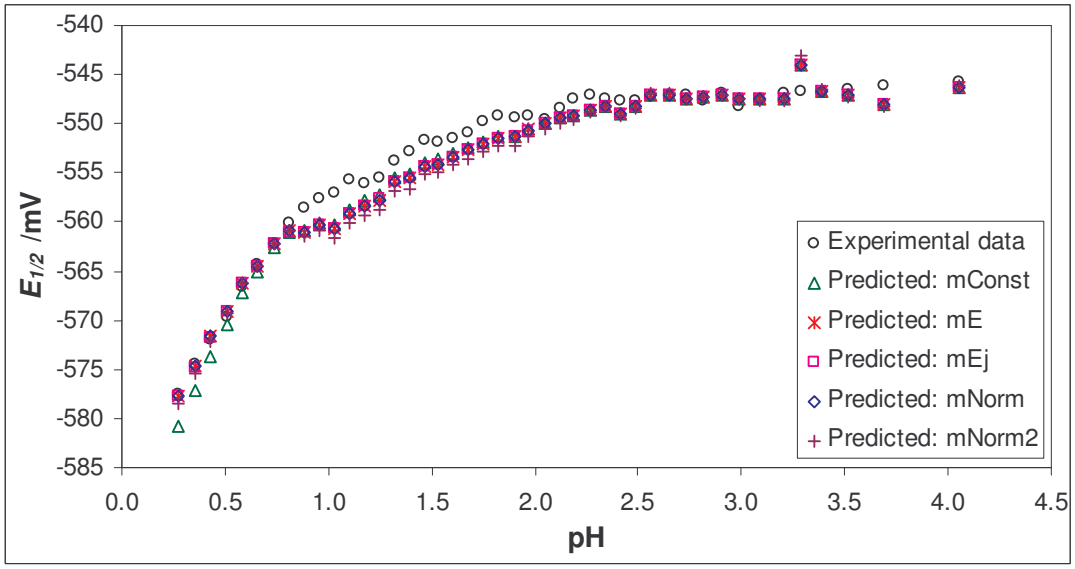

Figure A4.6: An example of a comparison of the experimental and predicted $E_{1/2}(Cd)$ values showing some discrepancies in the 0.8 – 2.4 pH region. The five different models derived from data fitted using the polynomial-straight line combination was used.

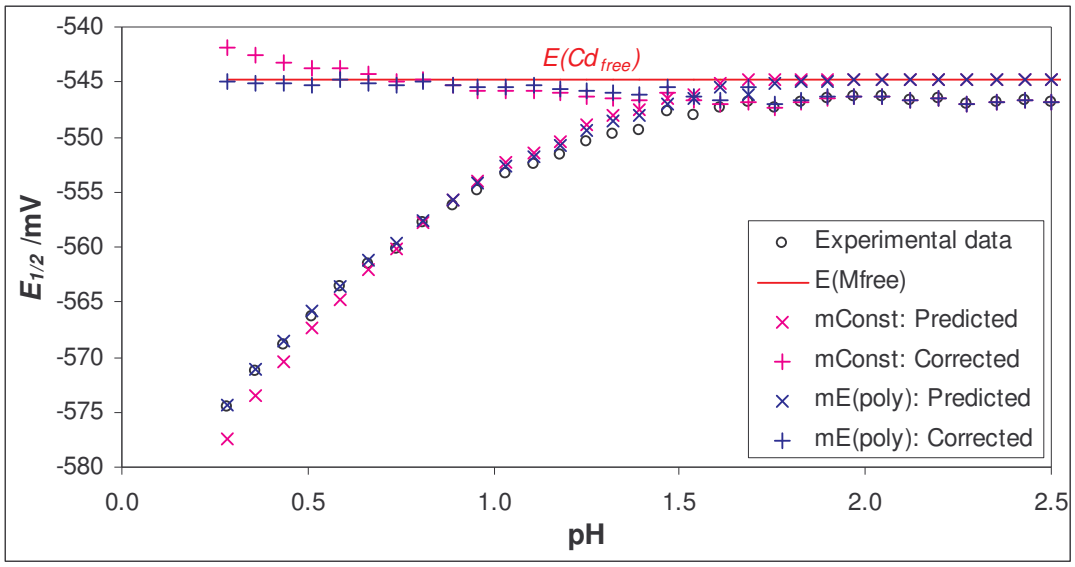

Figure A4.7: The difference between predicted Cd(II) potentials for uncomplexed Cd(II) when using the mConst and mE models and the corresponding corrected potentials for the complex formation experiment in the low pH region.

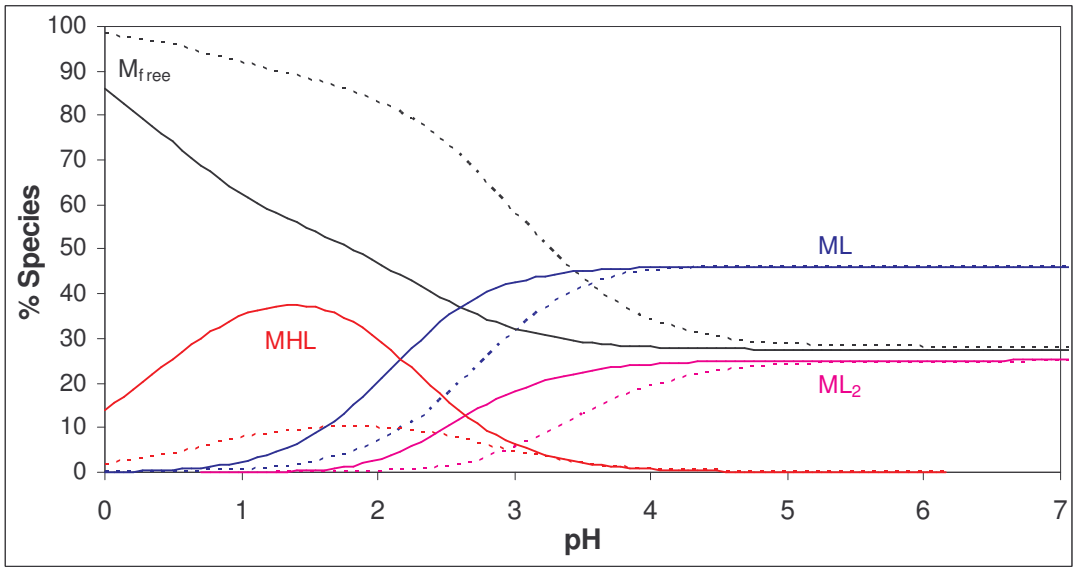

Figure A4.8: Species distribution diagrams determined using log β values derived in this work as given in Table 6.11. The $[PA]_T$:$[Cd(II)]_T$ = 1:1 and the four-fold increase in the percentage of CdHL in solution can clearly be observed when increasing the concentrations of both from 0.01 M (dotted lines) to 0.1 M (solid lines).

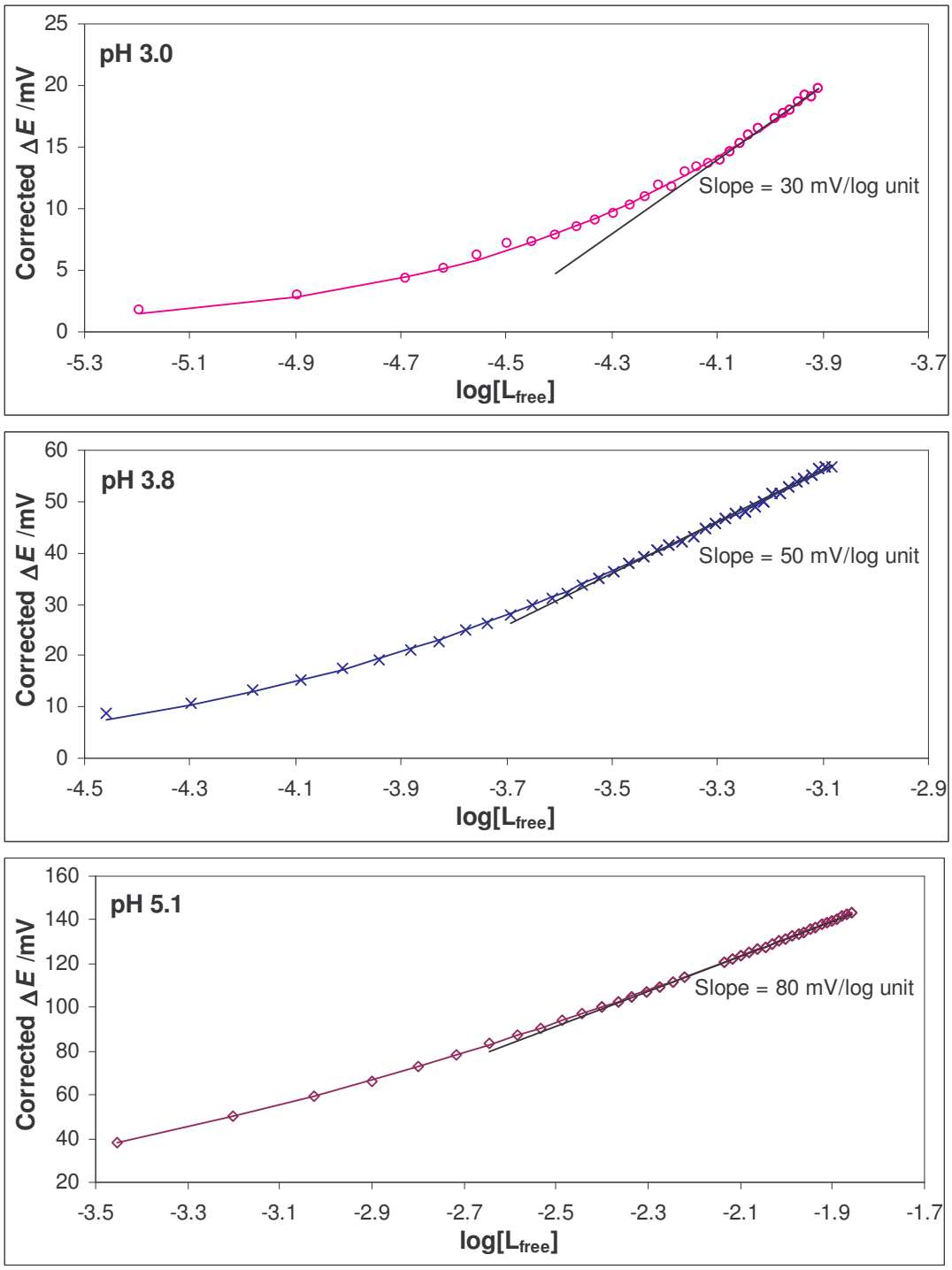

Figure A4.9: The ECFCs and CCFCs plotted separately for each ligand titration at the indicated pH values.

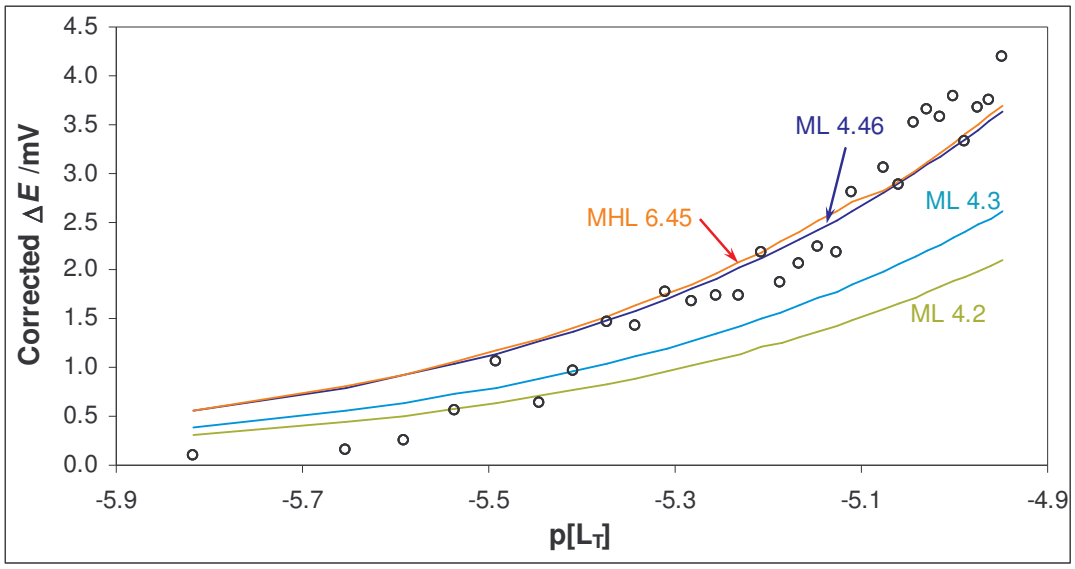

Figure A4.10: ECFC for the ligand titration at pH 2.0. Various CCFCs were calculated and the log β values are denoted next to the species type.

APPENDIX 5

Supplementary information for Chapter 7

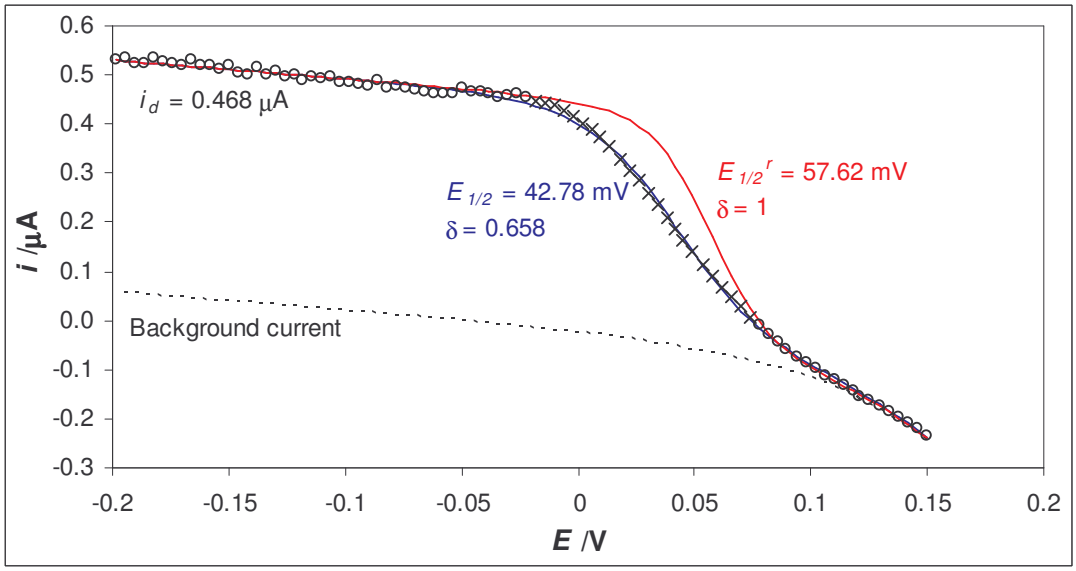

Figure A5.1: Polarogram for the reduction of Cu(II) at pH 3.05. The polarogram was fitted using the DC wave equation through all points (—) or only though the points indicated by ○ and fixing δ = 1 (—) to estimate $E^r_{1/2}$.

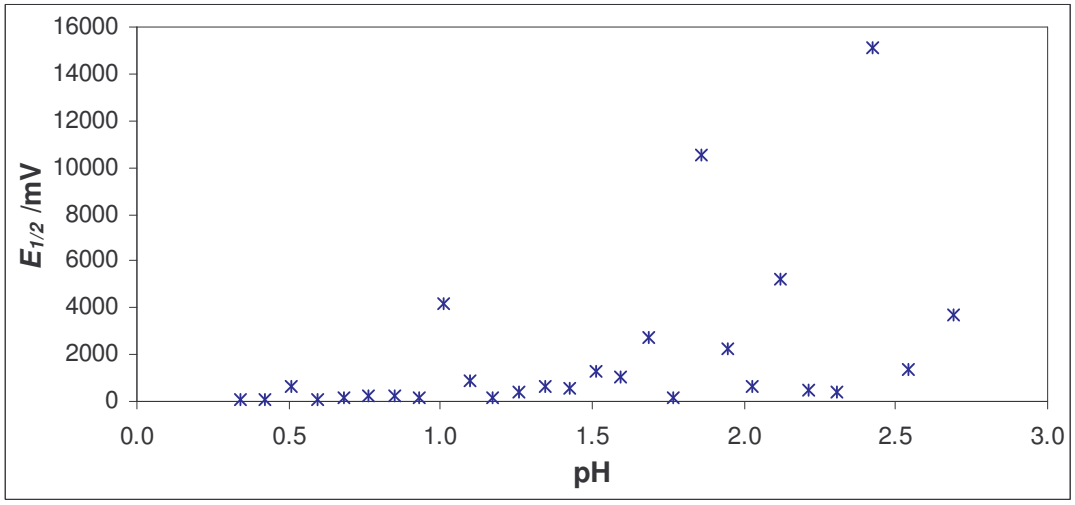

Figure A5.2: The $E^r_{1/2}$ values determined using the Ružić relationship (equation 7.15) were not physically meaningful values.

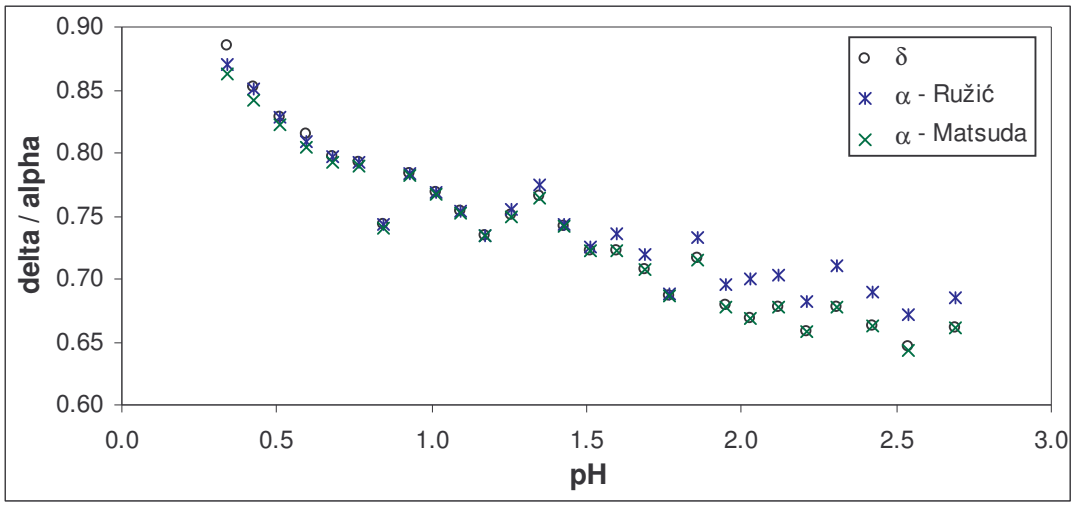

Figure A5.3: Comparison of the values of δ determined from fitting equation 2.15 and α from fitting equations 7.14 and 7.15 to Cu(II) reduction waves.

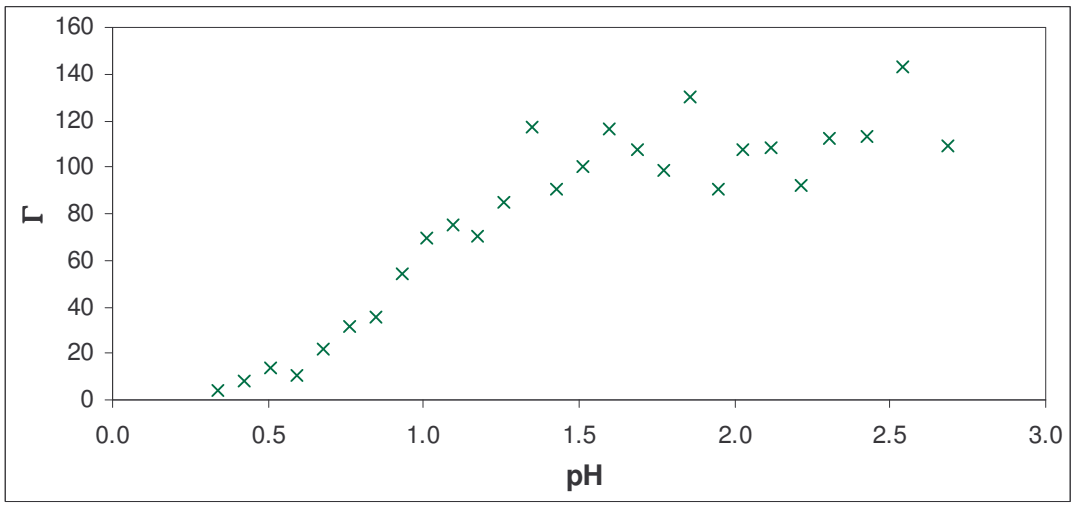

Figure A5.4: The value of Γ from the Matsuda and Ayabe relationship (equation 7.14).

APPENDIX 6

Supplementary information for Chapter 8

Table A6.1: Values for the parameters required for the automated DC polarogram VI. Values are specified for experiments run with two different Bi(III) concentrations.

Parameter	Settings used for ~5 × 10^{-5} M Bi(III)	Settings used for ~1 × 10^{-5} M Bi(III)
Potentiometric data:		
Equilibration time	15 s	300 s
Polarographic data:		
Initial potential	0.18 V	0.16 V
Final potential	–0.75 V	–0.70 V
Current integration time	60 ms	120 ms
pH step	0.07	0.1
Rest time	10 s	5 s

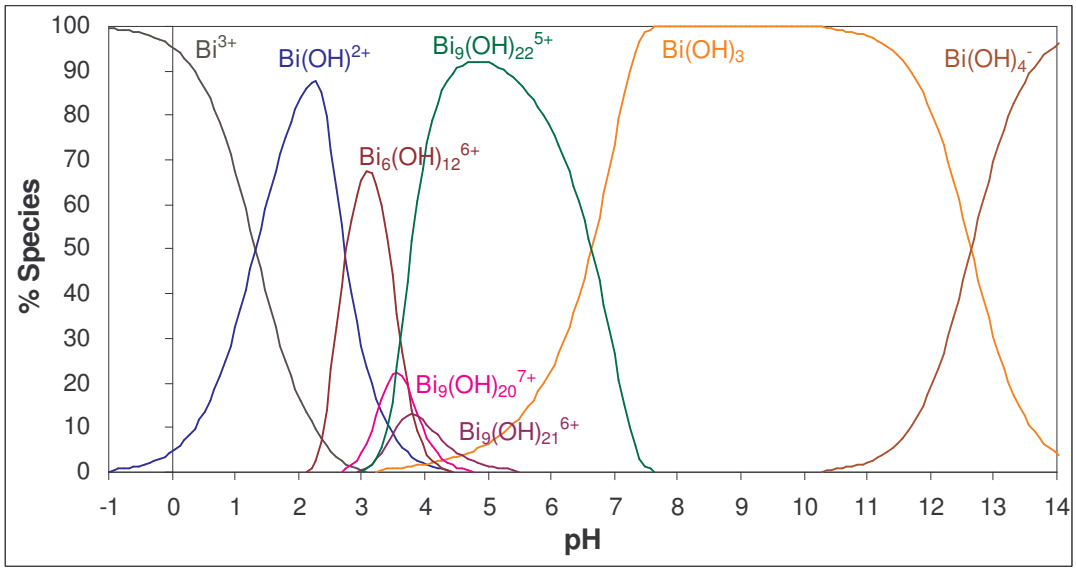

Figure A6.1: Species distribution diagram for [Bi(III)] = 4.99 × 10^{-5} M using log β values at 25 °C and 0.5 M ionic strength, assuming only $Bi_6(OH)_{12}^{6+}$ (and no $Bi(OH)_2^{+}$) is in solution.

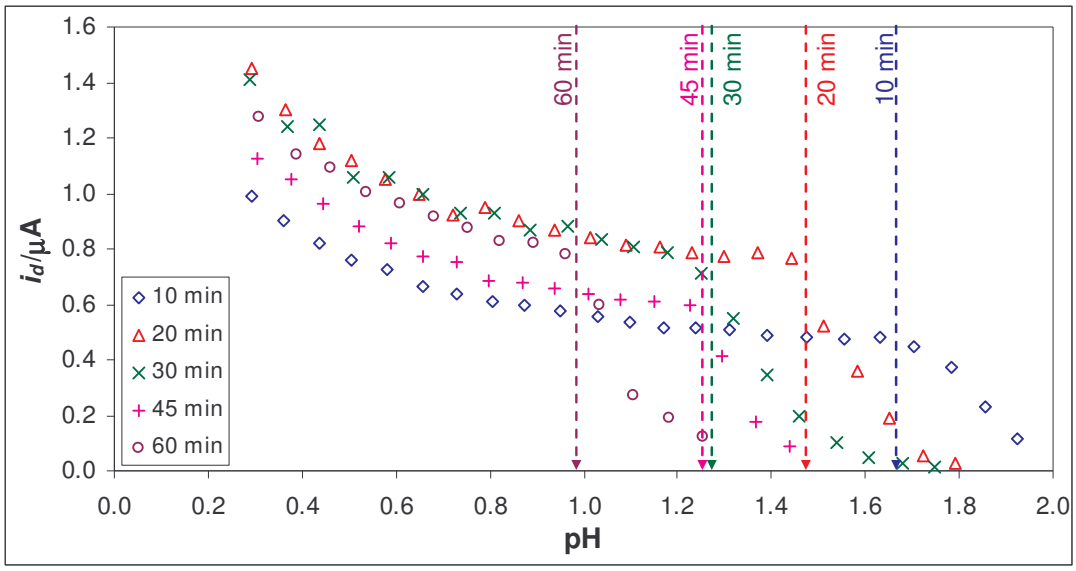

Figure A6.2: The diffusion limited currents for the reduction of Bi(III) (initial [Bi(III)] = 4.99×10^{-5} M) for titration experiments with varying time intervals (as indicated) between hydroxide addition and polarographic data collection. The approximate pH at which precipitation starts is also indicated by the arrows.

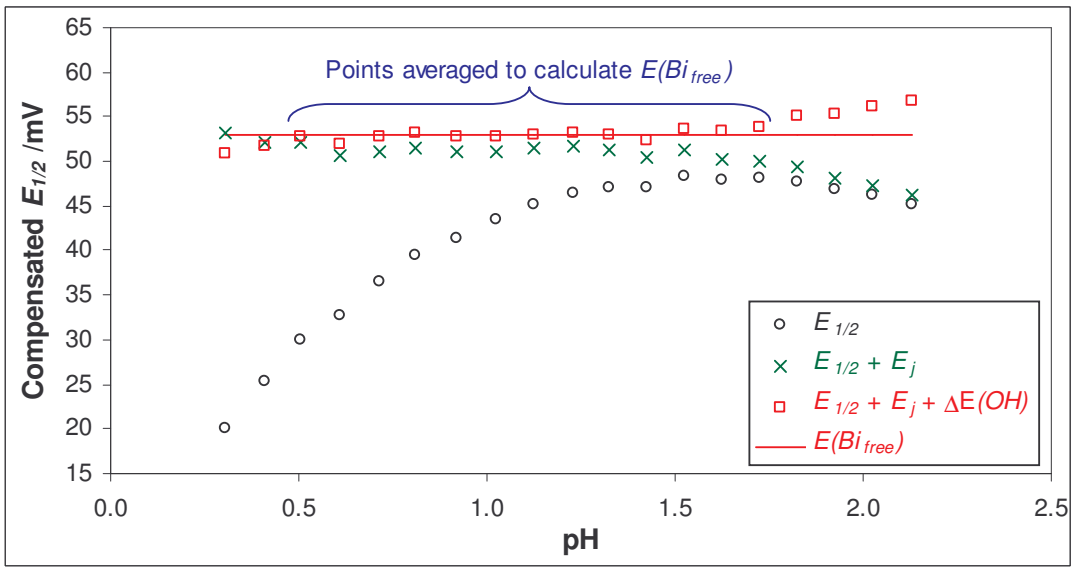

Figure A6.3: Compensated $E_{1/2}$ values showing points below and above the average value at the lowest and high pHs respectively. These points were neglected when calculating $E(Bi_{free})$. (Initial [Bi(III)] = 9.97×10^{-6} M)

APPENDIX 7

Supplementary information for Chapter 9

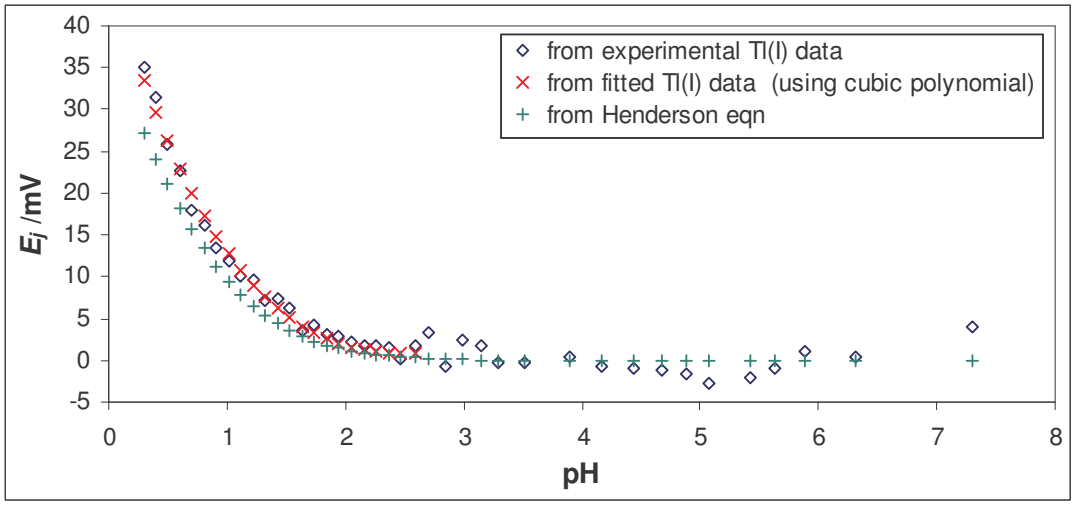

Figure A7.1: Comparison of measured and calculated E_j values. The fitted values are also shown.

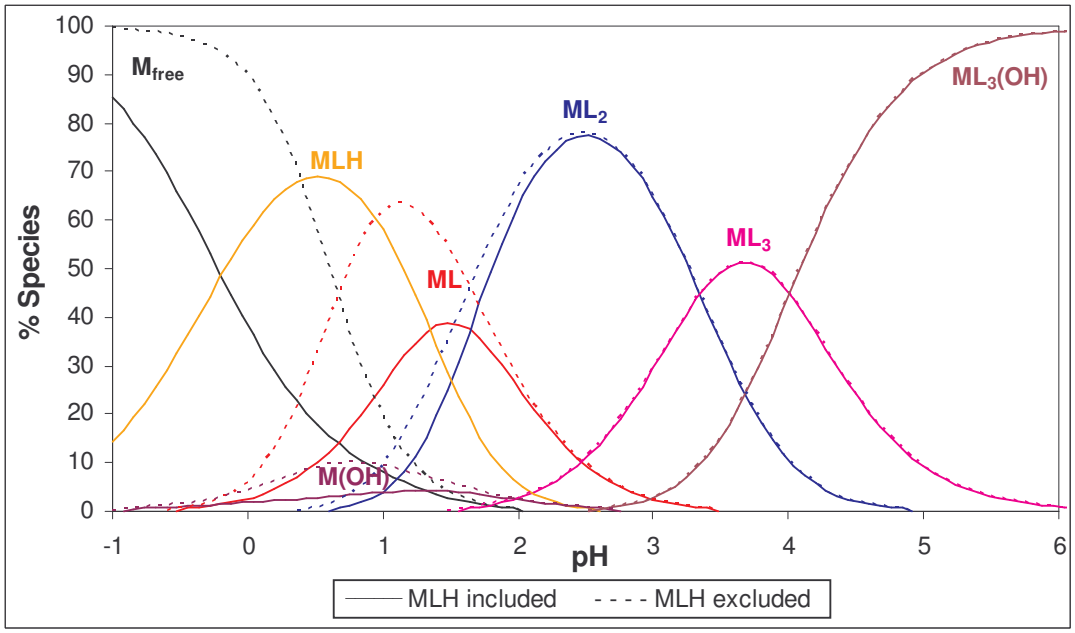

Figure A7.2: Species distribution diagrams for aqueous solutions of Bi(III)-PA using the average log β values in Table 9.2(a) where the MLH species is included or excluded. [Bi(III)] = 1×10^{-5} M and [PA] = 2×10^{-3} M.

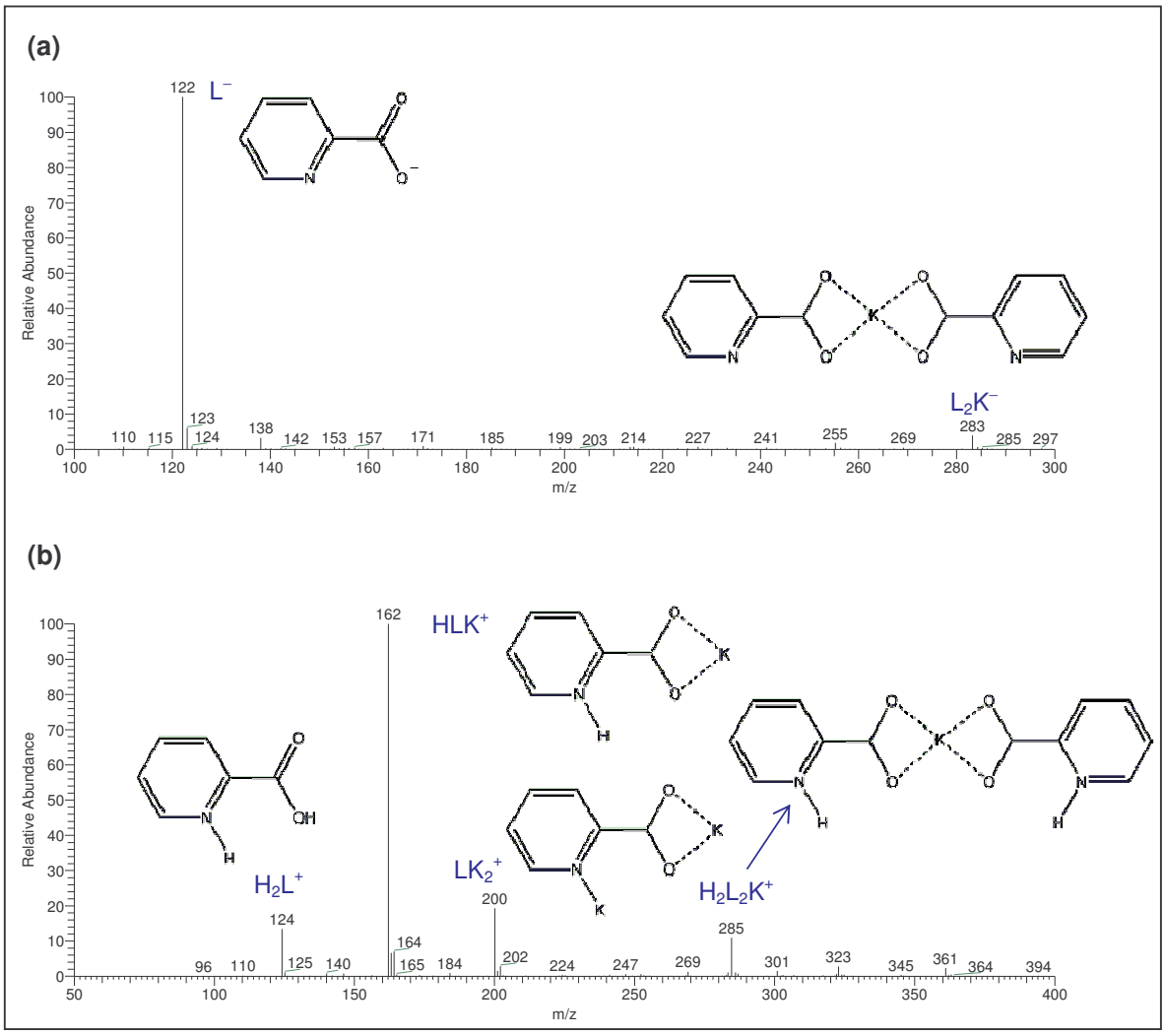

Figure A7.3: Mass spectra for (a) negative and (b) positive ions for 10^{-2} M PA at pH 4.

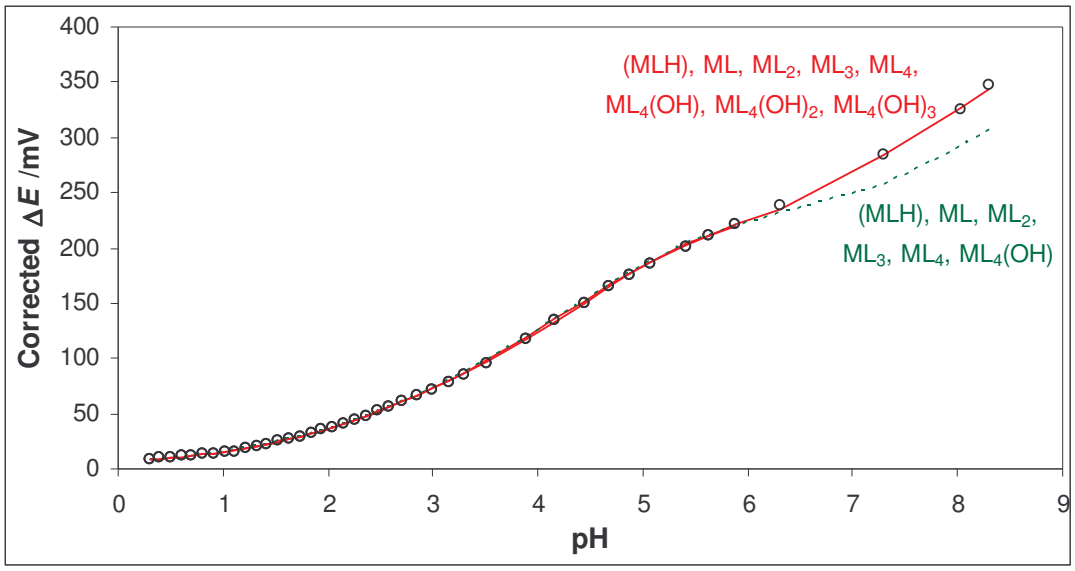

Figure A7.4: CCFC indicating the presence of $BiL_4(OH)_2^{3-}$ and $BiL_4(OH)_3^{4-}$ species at higher pH for $[PA]_T$:$[Bi(III)]_T$ = 197. The ECFC was to calculated using *E(Bi$_{free}$).*

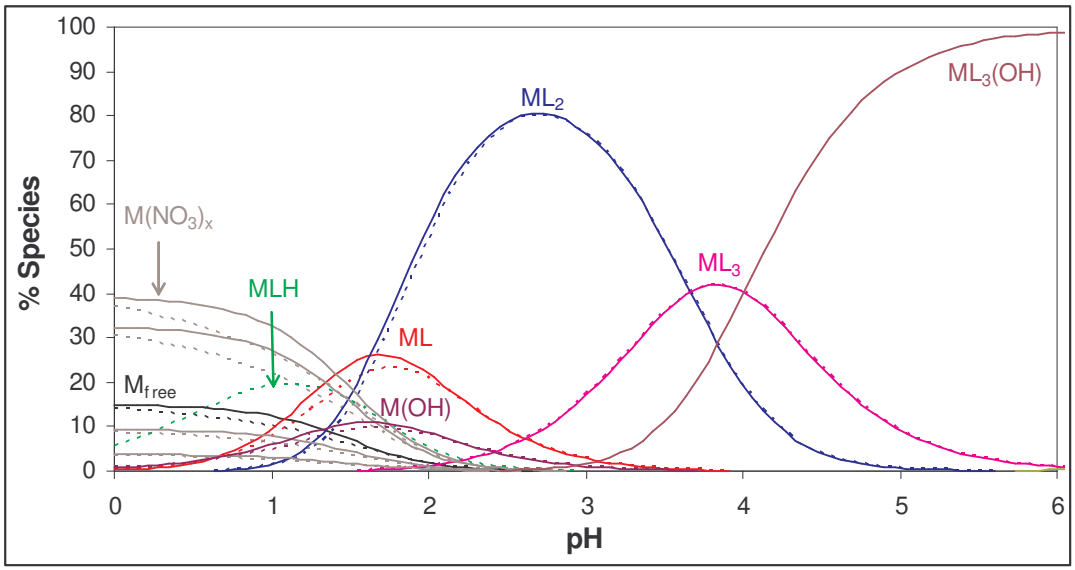

Figure A7.5: Species distribution diagram of the final log β values proposed for aqueous solutions of Bi(III)-PA (solid lines). The effect of incorporating MLH in the model is also shown (dotted lines). [Bi(III)] = 1×10^{-5} M and [PA] = 1×10^{-3} M.

Table A7.1: Typical entries in an ESTA file for the refinement of formation constants for Bi(III) PA species. The actual volumes of KOH and the *E(virt)* values (i.e. entries under “DATA”) are omitted.

```
TASK' 'OBJE'  '1  'PA-Bi+3-N'
'MODL' 0       'Bi+3'          'PA 0'          'N -1'          'H +1'/
'CPLX' 1*      -13.74          'H +1' -1/
'CPLX' 1*      5.16            'PA 0' 1        'H +1' 1/
'CPLX' 1*      6.02            'PA 0' 1        'H +1' 2/
'CPLX' 1*      -1.32           'Bi+3' 1        'H +1' -1/
'CPLX' 1*      -4.28           'Bi+3' 1        'H +1' -2/
'CPLX' 1*      -9.32           'Bi+3' 1        'H +1' -3/
'CPLX' 1*      -21.96          'Bi+3' 1        'H +1' -4/
'CPLX' 1*      -1.08           'Bi+3' 6        'H +1' -12/
'CPLX' 1*      -7.90           'Bi+3' 9        'H +1' -20/
'CPLX' 1*      -11.74          'Bi+3' 9        'H +1' -21/
'CPLX' 1*      -14.98          'Bi+3' 9        'H +1' -22/
'CPLX' 1*       0.72           'Bi+3' 1        'N -1' 1/
'CPLX' 1*      0.94            'Bi+3' 1        'N -1' 2/
'CPLX' 1*      0.7             'Bi+3' 1        'N -1' 3/
'CPLX' 1*      0.6             'Bi+3' 1        'N -1' 4/
'CPLX' '1  0'  7.4             'Bi+3' 1        'PA 0' 1/
'CPLX' '1  0'  13.9            'Bi+3' 1        'PA 0' 2/
'CONC'/
'VESL'    'IVOL'       25.075          0 0/
'VESL'    'H +1'       0.5082          0 0/
'VESL'    'Bi+3'       0.00000997      0 0/
'VESL'    'PA 0'       0.0009329       1 0/
'VESL'    'N -1'       0.3             0 0/
'BUR1'    'H +1'       -0.5183         0 0/
'ELEC'/
'ZERO'    'Bi+3'       174.6           1  0/
'GRAD'    'Bi+3'       19.71           0  0/
'DATA'/
```

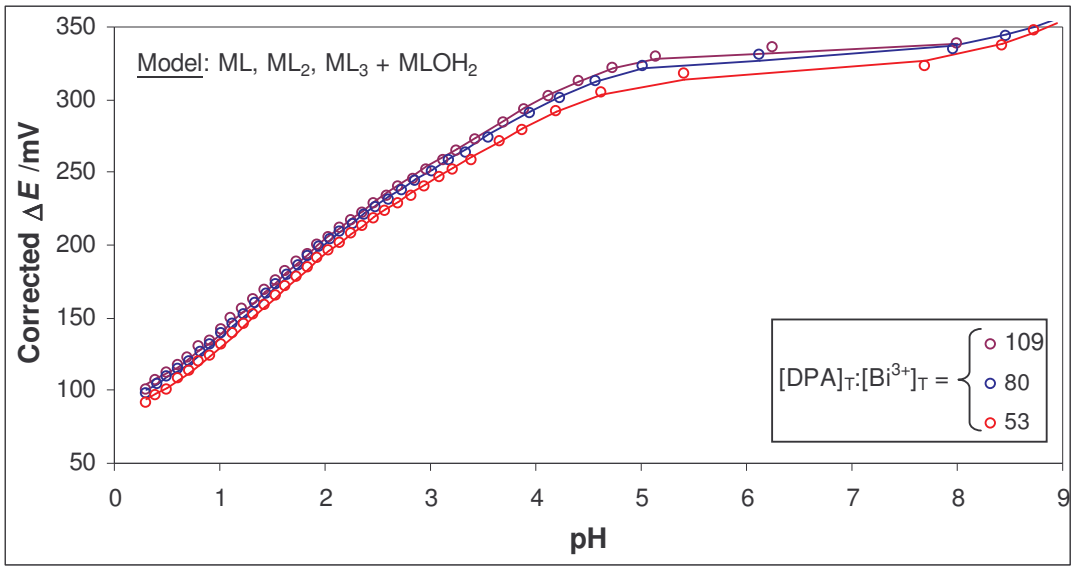

Figure A7.6: The ECFCs and CCFCs for the three DPA-to-Bi(III) concentration ratio experiments.

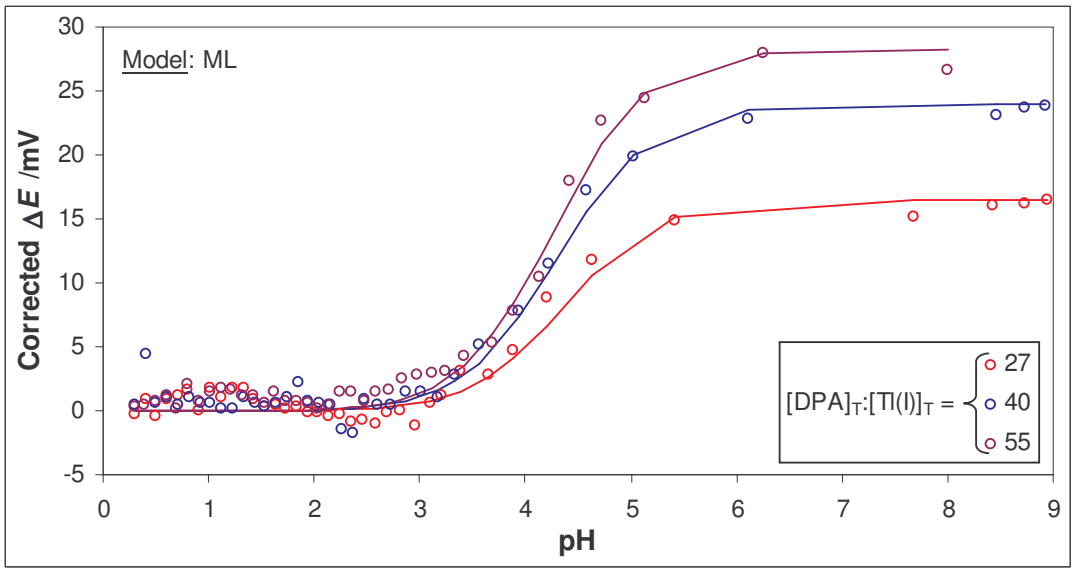

Figure A7.7: The ECFCs and CCFCs for the three DPA-to-Tl(I) concentration ratios.

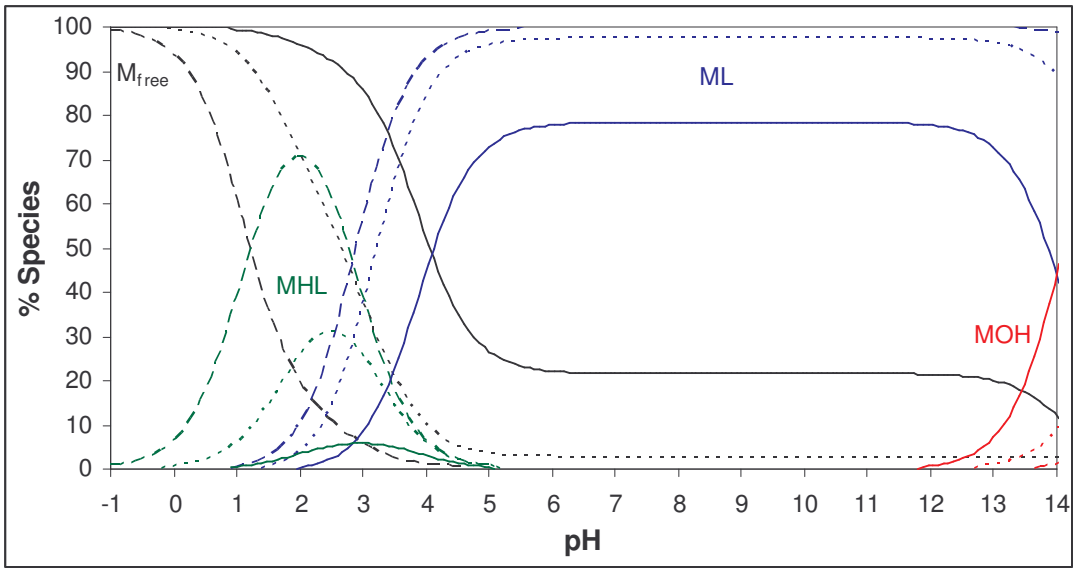

Figure A7.8: Species distribution diagrams for aqueous solutions of Tl(I)-DPA using average log β values in Table 9.12 and $[DPA]_T:[Tl(I)]_T = 50$. [Tl(I)] is varied as follows: 2×10^{-5} M (solid lines), 2×10^{-4} M (dotted lines) or 2×10^{-3} M (dashed lines).

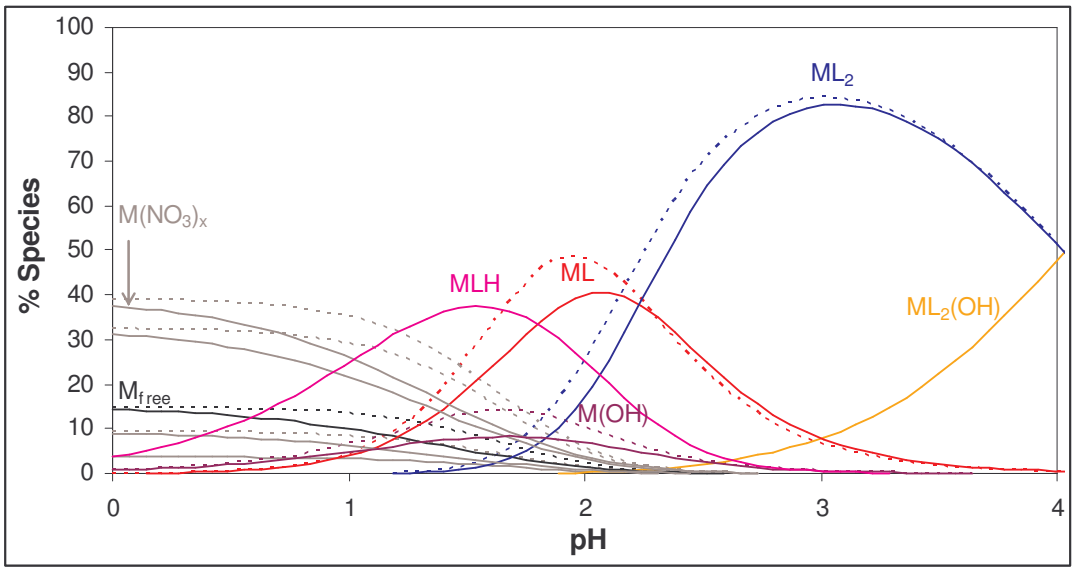

Figure A7.9: Acidic region of the species distribution diagrams showing the presence (solid lines) or absence (dotted lines) of the MLH species. $[QA]_T:[Bi(III)] = 100$, $[Bi(III)] = 1 \times 10^{-5}$ M and $[NO_3^-] = 0.5$.